Best
Available
Copy

AD-A284 293

'94 EDINBURGH

The International Conference on

OPTICAL COMPUTING

Technical Digest

R & D 7376-KK-02
N 68171-94-M-5839.

DTIC ELECTE SEP 0 8 1994 F

Sponsoring and Cooperating Societies:

International Commission for Optics
Optical Society of America
SPIE
IEEE/ Laser and Electro - Optics Society
The Japan Society of Applied Physics
European Physical Society
European Optical Society
IEE, U.K.
Institute of Physics, U.K.

This document has been approved for public release and sale; its distribution is unlimited.

94-29256
410pg

94 9 07 003 DTIC QUALITY INSPECTED 3

EDINBURGH CONFERENCE CENTRE
HERIOT-WATT UNIVERSITY
EDINBURGH, SCOTLAND

AUGUST 22 - 25, 1994

LOCAL ORGANISING COMMITTEE

The Department of Physics, Heriot-Watt University is pleased to provide the local organisation for OC'94.

Brian Wherrett	*Chairman*
Andy Walker	*Treasurer*
Mohammad Taghizadeh	*Coordinator (Publicity)*
Frank Tooley	*Coordinator (Registration)*
John Snowdon	*Conference Secretary*
Jimmy Smith	*Social Events Organiser*
Janice McClelland	*Committee Secretary*

Accesion For
NTIS CRA&I ☒
DTIC TAB ☐
Unannounced ☐
Justification .....
By form 50
Distribution /
Availability Codes
Dist | Avail and / or Special
A-1

Department of Physics
Heriot-Watt University
Edinburgh EH14 4AS
Scotland, U.K.

Tel: +44-(0)31-451-3027
Fax: +44-(0)31-451-3136

In addition to expressing our appreciation of the sponsorship provided by the Cooperating Societies, the organisers of OC'94 gratefully acknowledge the considerable support and financial assistance provided by the following organisations and companies:

Lothian and Edinburgh Enterprises Ltd.
The City of Edinburgh
The European Research Office of the US Army
BNR Europe Ltd.
Pilkington Technology Management Ltd.
Taylor & Francis Ltd.
Sharp Laboratories of Europe

The Proceedings of the Conference will be published by the UK Institute of Physics Publishing.

DTIC QUALITY INSPECTED 5

PROGRAMME COMMITTEES

General Chairman

Brian S. Wherrett	Heriot-Watt University, UK

International Advisory Committee

Pierre Chavel	Institut d'Optique, Paris, France (ICO representative)
Joseph W. Goodman	Stanford University, USA
Satoshi Ishihara	AIST, MITI, Japan
Fedor Karpushko	Academy of Sciences, Belarus
S. Desmond Smith	Heriot-Watt University, UK
Andrew C. Walker	Heriot-Watt University, UK

Technical Programme Committee Co-Chairs

Joseph W. Goodman	Stanford University, USA, (ICO representative)
Yoshiki Ichioka	Osaka University, Japan
S. Desmond Smith	Heriot-Watt University, UK

Members

J-L. de Bougrenet	ENST de Bretagne, France
Karl-Heinz Brenner	University of Erlangen, Germany
Vsevolod S. Burtsev	Academy of Sciences, Moscow, Russia
Pierre Chavel	Institut d'Optique, Paris, France
H. Scott Hinton	University of Colorado, USA
Kristina M. Johnson	University of Colorado, USA
Soo Young Lee	Korea Advanced Institute of Technology South Korea
Roger A. Lessard	Laval University, Canada
Chun-Fei Li	Harbin Institute of Technology, P.R. China
David A.B. Miller	AT&T Bell Labs., Holmdel, USA
John A. Neff	University of Colorado, USA
Alexander Sawchuk	University of Southern California, USA
Joseph Shamir	Technion, Israel
George Sinitsyn	Academy of Sciences, Belarus
Kunio Tada	University of Tokyo, Japan
Roger Vounckx	Vrije University of Brussels, Belgium
Toyohiko Yatagai	University of Tsukuba, Japan

Monday 22 August, 8.45 - 10.30 a.m.

8.45 a.m.
INTRODUCTION

B. S. Wherrett	*Heriot-Watt Univ*	*UK*
S. D. Smith	*Heriot-Watt Univ*	*UK*
C. Dainty	*Imperial College*	

Plenary
(Session Chair: S. D. Smith, Heriot-Watt Univ, UK)

9.00 a.m.
MA1 INVITED - Quantum Well Smart Pixels for Optical Switching and Processing, D.A.B. Miller, *AT&T Bell Labs, U.S.A.* A broad variety of experimental smart circuits with quantum well optical inputs and outputs has been fabricated for many users. Current status and future prospects for such large scale optoelectronic integration is summarized.

9.30 a.m.
MA2 INVITED - Large Scale Integration of LEDs and GaAs Circuits Fabricated Through MOSIS, A.C. Grot, D. Psaltis, K.V. Shenoy* and C.G. Constad, *California Inst. of Tech., U.S.A. (*MIT, Cambridge, U.S.A.).* We describe a new process to integrate LEDs with fully processed GaAs circuits using MBE regrowth. The bottom contact of the LED, grown in the dielectric vias, is made through the n+source/drain implant.

9.45 a.m.
MA3 INVITED - Parallel Algorithms for Optical Processors, P. Chavel, *Inst. d'Optique, Paris, France.* Fine grain parallel optoelectronic processors for dedicated tasks may deserve further consideration. The main case is vision machines; stochastic algorithms working on images considered as Markov fields are one possible approach to tackle real images.

10.15 a.m.
MA4 INVITED - Quantum-Statistical Restrictions on the Information Transmitting/ Processing Rate in Electronic and Photonic Channels, F.V. Karpushko, *DOPIT, Academy of Sciences of Belarus, Minsk, Belarus.* Quantum effects are shown to limit the information capacity of electronic channels by ~ 10^{12}bit/s. At higher rates the energy price for transmitting information is 2-4 order less in 1D-boson channels as compared with 1D-fermion ones. The 3D-optical channels are free of quantum restrictions up to information rates ~ 10^{19}nit/cm^{2}s.

10.30 - 11.00 a.m. Coffee Break

Monday 22 August, 11.00 - 12.30 p.m.
Plenary
(Session Chair: J. L. de Bougrenet, ENST de Bretagne, France)

11.00 a.m.
MB1 INVITED - Spatial-Light-Modulator Based Routing Systems, W.A. Crossland, R.J. Mears and S.T. Warr, *Univ. Cambridge, U.K.* This paper reviews the principles of SLM based free space photonic switch structures based on shadow logic and on dynamic holograms configured for optical fibre networks for parallel optoelectronic machines and highly parallel chip-to-chip interconnections.

11.30 a.m.
MB2 INVITED - Independently Addressable Vertical-Cavity Surface-Emitting Laser Diode Arrays, E. Zeeb, B. Möller, T. Hackbarth*, H. Leier* and K.J. Ebeling, *University of Ulm, Germany (*Daimler Benz Research Center, Ulm, Germany).* The fabrication of very uniform, planar 10 × 10 vertical-cavity surface-emitting laser diode arrays is reported. Individual elements show threshold currents around 4 mA, emit up to 300 μW single mode, and exhibit a 3 dB modulation bandwidth of 4.6 GHz.

11.45 a.m.
MB3 INVITED - The Scottish Collaborative Initiative on Optoelectronic Sciences - Devices and Demonstrators for Free-Space Digital Optical Processing, A.C. Walker, D.J. Goodwill, B.S. Ryvkin M. McElhinney,* F. Pottier*, B. Vogele*, M.C. Holland* and C.R. Stanley*, *Dept. Phys., Heriot-Watt Univ., Edinburgh, U.K. (*Dept. E&E Eng., Univ. Glasgow, U.K.).* 16 × 16 arrays of strained-InGaAs/GaAs S-SEEDs have been successfully operated with a diode-pumped 1064 nm laser. These, and other GaAs/GaAlAs devices, are being incorporated into digital parallel optical processing demonstrators. The status of this programme will be reviewed.

12.15 p.m.
MB4 INVITED - Smart Pixel Arrays: Challenges of Manufacturing and Testing, G. Livescu, L.M.F. Chirovsky, L.A. D'Asaro, S. Hui, R.A. Novotny*, A.L. Lentine*, M.W. Focht**, J.M. Freund**, K.G. Glogovsky**, G.D. Guth**, G. Przybylek** and R.E. Leibenguth**, *AT&T Bell Labs., Murray Hill, U.S.A. (*AT&T Bell Labs., Naperville, U.S.A., **AT&T Bell Labs., Breinigsville, U.S.A.).* Wafer level optical and electronic testing of smart pixel arrays is a must if a high yield technology is to be developed. Our results on GaAs FET-SEED based switching nodes show the uniformity and performance control levels achievable with today's technology, as well as its limits.

12.30 - 2.00 p.m. Lunch Break

Monday 22 August, 2.00 - 3.45 p.m.
Smart Pixels and SLMs
(Session Chair: J. Hegarty, Trinity College, Dublin, Ireland)

2.00 p.m.
MC1 Monolithically Integrated Optoelectronic Smart Pixels, U. Kehrli, D. Leipold, K. Thelen, H.P. Schweizer, P. Seitz and B.D. Patterson, *Paul Sherrer Institut, Zürich, Switzerland.* We describe a monolithically integrated optoelectronic smart pixel fabrication process using a GaAs/AlGaAs system. The smart pixels are realised with depletion type metal semiconductor field-effect transistors (MESFETs), high brightness light-emitting diodes (HBLEDs) and photodiodes (PDs).

2.15 p.m.
MC2 Optical Algorithmic and Electronic Considerations on the Desirable "Smartness" of Optical Processing Pixels, M.P.Y Desmulliez, J.F. Snowdon, J.A.B. Dines and B.S. Wherrett, *Dept. Physics, Heriot-Watt Univ., Edinburgh, U.K.* The performance gains associated with optical computing schemes must be traded off with the complexity of individual computing nodes in order to optimise the efficiency of an optical processor. We categorise the necessary trade-offs and provide examples of such optimisation.

2.30 p.m.

MC3 Low-Loss and High-Speed Optical Switching Modules for 1.3 μm Wavelength Using Active-Matrix Ferroelectric Liquid Crystal Devices, S. Shirai, T. Serikawa, S. Kohda, N. Kakuda, M. Okamura and N. Yamauchi, *NTT Interdisciplinary Research Labs., Tokyo, Japan.* A highly efficient optical coupling system using microlens arrays for free-space optical switching networks was proposed and demonstrated. High speed (< 100 μs) and high extinction ratio for 1.3 μm wavelength were obtained by a newly proposed ferroelectric liquid-crystal driving method.

2.45 p.m.

MC4 Dynamic Free Space Optical Interconnections Using Liquid Crystal Micro Optical Beam Deflectors, K. Hirabayashi, T. Yamamoto and M. Yamaguchi, *NTT Communication Switching Labs., Tokyo, Japan.* Micro-optical beam deflectors with a high transmittance of 95%, a large deflection angle of 15°, and with a structure of liquid crystals sandwiched by microprism plates are used in free-space optical interconnections and optical switches.

3.00 p.m.

MC5 Liquid Crystal Over Silicon Spatial Light Modulators, D.J. McKnight, K.M. Johnson, G.D. Sharp* and R.A. Serati*, *Optoelectronic Computing Systems Center, Univ. of Colorado, U.S.A. (*Boulder Nonlinear Systems, Colorado, U.S.A).* This paper describes our recent liquid crystal on silicon spatial light modulators. We will present the most recent results from our 256 by 256 binary reflection mode SLM and our 128 by 128 analog SLM.

3 .15 p.m.

MC6 Electronically Addressed Ferroelectric Liquid Crystal over Silicon Spatial Light Modulators, D.C. Burns, I. Underwood, A. O'Hara*, and D.G. Vass*, *Dept. of Elec. Eng., (*Dept. of Physics), Univ. of Edinburgh, U.K.* We discuss recent advances in the design and fabrication of electronically-addressed ferroelectric-liquid-crystal-over-silicon spatial light modulators. We summarise the prospects for further advances in the near future.

4.00 - 6.00 p.m. Poster Sessions

Analogue Processing	**MP1 - MP26**
Digital Optics	**MP27 - MP53**
Guided-Wave Devices and Processors	**MP54 - MP64**

Tuesday 23 August, 9.00 - 10.30 a.m.
Plenary
(Session Chair: T. Yatagai, Univ. of Tsukuba, Japan)

9.00 a.m.
TuA1 INVITED - Optical Detection Filters and Algorithm Fusion, D. Casasent, *Carnegie Mellon University, U.S.A.*. Detection of candidate object regions in a scene is step one in general scene analysis. New optical morphological, wavelet and Gabor transform filters for detection are presented and fusion is used to reduce false alarms.

9.30 a.m.
TuA2 INVITED - Space-Variant Filtering in Fractional Fourier Domains, H.M. Ozaktas, B. Barshan, D. Mendlovic* and H. Urey**, *Electrical Engineering, Bilkent Univ., Ankara, Turkey (*Faculty of Engineering, Tel-Aviv Univ., Israel, **Electrical Engineering, Georgia Institute of Technology, Atlanta, U.S.A.)*. Signals with significant overlap in both the space and frequency domains may have little or no overlap in a fractional Fourier domain. Spatial filtering in these domains may allow us to eliminate distortion components which cannot be eliminated in the ordinary Fourier domain.

9.45 a.m.
TuA3 INVITED - All-Optical Dynamic Memories, M.P. Petrov, *A.F. Ioffe Physical Technical Institute of Russian Academy of Sciences, St. Petersburg, Russia.* State-of-the-art review of all-optical dynamic memories and their crucial elements is given. It discusses the properties of all-optical regenerators of short optical pulses. Characteristics and properties of an optical dynamic memory operating through SRS in optical fibers are described.

10.15 a.m.
TuA4 INVITED - Parallel Information Recording and Processing using 1-D Hologram Technology, A.L. Mikaelian, *Russian Academy of Sciences, Russia.* 1-D hologram technology for parallel information recording and processing and some applications are considered. Among them are a two-layer neural net performing serial-parallel processing, and an associative memory using photothermoplastic material. Both the theoretical and experimental results are presented.

10.30 - 11.00 a.m. Coffee Break

Tuesday 23 August, 11.00 - 12.30 p.m. (Parallel Session)
Neural Networks
(Session Chair: D. Psaltis, California Inst. of Tech., USA)

11.00 a.m.
TuB1 Associative Memory for Rotation Pre-Processing and Projection Invariant Pattern Recognition, G. Lebreton, *GESSY, Université de Toulon, France.* New advances on invariant pattern recognition using associative optical memories, showing simulations and first experimental results, on 1) orientation detection of any object before identification, 2) pattern recognition invariant to scale and projections.

11.15 a.m.
TuB2 Optical Implementations of a Stochastic Neural System, W.A. Crossland, T.J. Hall*, J.S. Shawe-Taylor** and M. van Daalen**, *Dept. of Eng., Cambridge University, U.K. (*Dept. of E&E Eng., King's College, Univ. London, U.K., **Dept. of Comp. Sci., Univ. London, U.K.)*. The paper addresses the design of an optoelectronic implementation of a stochastic bit-stream neural system which operates by manipulating digital bit-streams to create emergent activation functions using extremely simple logic.

11.30 a.m.
TuB3 Dynamic Effects in Volume Interconnects with Feedback, C. Slinger, *ER1 Division, DRA Malvern, Worcs., U.K.* An attempt is made to exploit the inherently rich physics of volume holographic interconnects. The effects of crosstalk and nonlinearities are considered. When combined with a novel feedback configuration, complex, self-organising behaviour is seen to emerge.

11.45 a.m.
TuB4 Optical Lateral Inhibition Networks using Self-Linearised SEED's, P. Horan, *Hitachi Dublin Lab., Trinity College, Dublin, Ireland.* A family of lateral inhibition architectures which use the self-linearised SEED effect to implement optical subtraction are described, and the operation demonstrated in simulation.

12.00 noon
TuB5 Optical Spatial/Frequency Filtering and Adaptive Neural Networks Based on Fractional Fourier Transforms, S.-Y. Lee, *Dept. of Elec. Eng., KAIST, Taejon, Korea.* Based on fractional Fourier transforms a new optical architecture is developed to make compromise between shift-invariant (frequency) and position-dependent filterings, and its analogy to neural networks and corresponding learning algorithm are presented.

12.15 p.m.
TuB6 Experimental Realisation of an All-Optical Self-Organising Map, K. Hegarty, J. Duvillier and J.L. de Bougrenet de la Tocnaye, *ENST de Bretagne, Brest, France.* We present results obtained with an all-optical self-organising map neural network applied to digit recognition. The experimental system is built around two Ferroelectric Liquid Crystal Bistable Optically Addressed Spatial Light Modulators in a resonator configuration.

Tuesday 23 August, 11.00 - 12.30 p.m.
(Parallel Session - Lecture Theatre 4)
Digital Optic Devices
(*Session Chair: S. Ishihara, AIST, Tokyo, Japan*)

11.00 a.m.
TuC1 Optoelectronic Switch Operating with 0.2 fJ/μm^2 at 15 MHz, M. Kuijk, P. Heremans*, R. Vounckx and G. Borghs, *Vrije Universiteit Brussel, Belgium (* IMEC, Leuven, Belgium).* We present experimental data of a novel differential PnpN optical switch, showing a cycle time smaller than 60 ns and an optical switching energy of 0.2 fJ/μm^2.

11.15 a.m.
TuC2 AlAs/GaAs Multilayered Structures as Low Intensity Nonlinear Optical Media, S. Knigge, M. Wicke and D. Jäger, *Fachgebiet Optoelektronik, Univ. Duisburg, Germany.* The nonlinear optical properties of hybrid AlAs/GaAs Bragg reflectors are presented. Experimentally, optical bistability at optical intensities as low as 35 mWcm^{-2} is obtained when a bias voltage of 115 V is applied.

11.30 a.m.
TuC3 Dynamical Behaviour of Opto-Optical Logic Switching Devices Employing n-i-p-i-based Smart Pixels, M. Kneissl, P. Kiesel, P. Riel, K. Reingruber, K.H. Gulden, E. Greger, A. Höfler, B. Knüpfer, G.H. Döhler, X.X. Wu* and J.S. Smith*, *Inst. für Technische Physik, Univ. Erlangen-Nürnberg, Germany (*Dept. Elect. Eng. & Comp. Sci., Univ. California, Berkeley, U.S.A.).* We report on experimental results on the dynamical behaviour of n-i-p-i-based smart pixels. With switching energies of 2.4 fJ/μm^2 contrast ratios of 4:1 at 1.6 mW output power were achieved. The opto-optical gain is tunable from 10-10^6.

11.30 a.m.
TuC4 An Optical Set-Reset FlipFlop Semiconductor Laser with Two Mutually Complementary Outputs, M. Watanabe, S. Mukai and H. Yajima, *Electrotechnical Lab., Ibarakai, Japan.* Theory and experiment on crosscoupled-mode bistability in a twin-stripe laser is reported. The laser has two output ports complementary to each other, which is analogous to a set-reset flipflop in electronics.

11.45 a.m.
TuC5 Waveguide Type Rotating Phase Plate as Frequency Shifter on (110) GaAs Substrate, H. Inoue, S. Nishimura, S. Tanaka* and T. Kanetake**, *RWCP Optoelectronics Hitachi Lab., Tokyo, Japan (*Central Research Lab., Hitachi Ltd., Tokyo, Japan, **Advanced Research Lab., Hitachi Ltd., Saitama, Japan).* The fundamental modulation characteristics of waveguide type frequency shifter based on the rotating phase plate are demonstrated on (110) GaAs substrate as an optical device for multi-dimensional interconnection for the first time.

12.00 noon
TuC6 Asymmetric Light Bullet Dragging Logic, R. McLeod, S. Blair and K. Wagner. *Optoelectronic Computing Systems Center, Univ. of Colorado, U.S.A.* The asymmetric dragging interaction between three-dimensional optical solitons may allow cascadable, phase-insensitive, NOR gates with gain to be implemented at ultrahigh speeds in massively parallel three-dimensional bit-level systolic-array architectures.

12.30 - 2.00 p.m. Lunch Break

Wednesday 24 August, 9.00 - 10.30 a.m.
Plenary
(Session Chair: B. S. Wherrett, Heriot-Watt Univ, UK)

9.00 a.m.
WA1 INVITED - Architecture Design and Implementation Issues for Massively Parallel Processors, S. Nelson, *Cray Research Inc., U.S.A.* Dramatic improvements in microprocessor price/performance have challenged the supercomputer designer to achieve high levels of system performance by interconnecting hundreds or even thousands of processors. But to achieve high sustained computational rates it is imperative that designs be balanced with respect to processor speed, local and global memory bandwidth, input/output capability, and interprocessor synchronization primitives. This talk will discuss these criteria using examples from the recently announced CRAY T3D system.

9.45 a.m.
WA2 INVITED - Free-Space WDMA Optical Interconnects using Mesh-Connected Bus Topology, Y. Li, S.B. Rao, I. Redmond, T. Wang and A.W. Lohmann*, *NEC Research Institute, Princeton, U.S.A. (*University of Erlangen, Germany).* A mesh-connected bus networking topology is proposed for implementing the three-stage Clos network and is experimentally demonstrated using a WDMA technology.

10.00 a.m.
WA3 INVITED Design Issues for Free-Space Photonic Switching Demonstrators, F.B. McCormick, *AT&T Bell Labs., Naperville, U.S.A..* We discuss the issues involved in building demonstration systems integrating GaAs FET-SEED smart pixels, computer generated holograms, 2-D fibre bundles, high-power lasers, high resolution optics, and novel optomechanical packaging. A prototype 5 stage, 32×16 fabric operating at 155 Mb/s is described.

10.30 - 11.00 Coffee Break

Wednesday 24 August, 11.00 - 12.30 p.m. (Parallel Session)
Digital Optics Architectures
(Session Chair: Y. Ichioka, Osaka Univ, Japan)

11.00 a.m.
WB1 Demonstration of Optically Controlled Data Switching using Quantum Well Bistable Devices and Modulators, P. Koppa, P. Chavel, J.L. Oudar*, R. Kuszelewicz*. J.Ph. Schnell** and J.P. Pocholle**, *Inst. d'Optique, CNRS, Orsay, France, *France Telecom, CNET, Paris, France, **Thomson CSF, Orsay, France).* Experimental results on a 64 channel free-space photonic switching system are presented. Two control schemes are demonstrated: direct optical addressing with potential signal amplification and self-routing operation acting on data packets.

11.15 a.m.
WB2 Reconfigurable Architecture Based on Selective Enabling of Microlasers, M. Murdocca, J. Battiato*, D. Berger**, R. Bussjager* and T. Stone†, *Dept. of Comp. Sci., Rutgers Univ. New Brunswick, U.S.A. (*Rome Lab., Griffiss AFB, U.S.A., **Dept. of Comp. Sci., Univ. of California, U.S.A., †Wavefront Res. Inc., PA, U.S.A).* We report on a reconfigurable architecture that uses a static free-space optical interconnect. A two-dimensional array of microlasers controls a two-dimensional array of S-SEED optical logic modulators in a cascaded system.

11.30 a.m.
WB3 Optical Array Logic Network Architecture, J. Tanida and Y. Ichioka, *Dept. of Applied Physics, Osaka Univ., Japan.* A new concept called optical array logic network architecture (OAL-NA) is proposed for effective construction of optoelectronic hybrid computing system. With the help of optical array logic (OAL), not only data communication but also global data processing are implemented in the interconnection network.

11.45 a.m.
WB4 Cascaded Optical Data Transfer Through a Free Space Optical Perfect Shuffle, M.W. Derstine, S. Wakelin and K.K. Chau, *Optivision Inc., California, U.S.A.* We describe the design, fabrication and testing of an optical interconnect system constructed from a two dimensional array of symmetric self-electro-optic effect devices and a free space perfect shuffle module.

12.00 noon
WB5 Optical Circuitry for Data Transcription and Digital Optical Logic Based on Photothyristor Differential Pairs, H. Thienpont, T. Van de Velde, A. Kirk, W. Peiffer, M. Kuijk*, W. Stevens, J. Fernandez, I. Veretennicoff, R. Vounckx, P. Heremans* and G. Borghs*, *Applied Physics Dept., Vrije Univ. Brussels, Belgium (*Interuniv. Micro Electronics Center, Leuven, Belgium).* We present a novel technique for parallel optical data transcription and digital logic with high speed differential pairs of optical thyristors and demonstrate these vital operations with compact optical hardware circuitry.

12.15 p.m.
WB6 Optoelectronic Multiport Associative Memory for Data Flow Computing Architecture, V.B. Fyodorov, *Russian Academy of Sciences, Moscow, Russia.* New optical setups of multiport optical associative memory are suggested. Such a memory enables M users to execute a simultaneous and independent parallel associative data search and retrieval into memory N stored words by M search arguments, as well as a random-access writing of keys and data.

Wednesday 24 August, 11.00 - 12. 30 p.m.
(Parallel Session - Lecture Theatre 4)
Analogue Processing
(Session Chair: J. Caulfield, Alabama A&M Univ, USA)

11.00 a.m.
WC1 An Analog Retina for Edge Detection, C. Wang and F. Devos, *Inst. d'Elec. Fond., Univ. Paris Sud, Orsay, France).* We present a very simple optoelectronic analog retina which we constructed, using CMOS technology. The experimental results indicate that the system is capable of acquiring optical data of an image and detecting the edges.

11.15 a.m.
WC2 Theoretical Results on Accuracy Limitations in Analog Optical Processors, D.A. Timucin, J.F. Walkup and T.F. Krile, *Dept. of Electrical Engineering, Texas Tech Univ., U.S.A.* A complete statistical analysis and modelling of a generic three-plane optical processor is presented. Output signal statistics are determined for a number of interesting special cases, and the fundamental theoretical accuracy limitations are established.

11.30 a.m.
WC3 Time-Integrating Correlation Using a Fibre Optic Delay Line Processor, R.A. Athale and G.W. Euliss, *Dept. of Elec. & Comp. Engineering, George Mason Univ. Virginia, U.S.A.* A fibre optic tapped delay line correlator based on time-integration is proposed and demonstrated. Such a correlator will combine high bandwidth, large processing gain and ability to compute real-time autocorrelation functions.

11.45 a.m.
WC4 Experimental Implementation of a Joint Transform Correlator Providing Rotation Invariance, L. Bigué, M. Fracès* and P. Ambs, *ESSAIM, Univ. de Haute Alsace, France (*ONERA-CERT, Toulouse, France).* We optically experiment a joint transform correlator (JTC) where the input image is replaced by a synthetic discriminant function (SDF) filter. This latter allows us to ensure a practical invariance over a 10° range.

12.00 noon
WC5 Optimal Nonlinear Filtering for Pattern Recognition and Optical Implementation, Ph. Refregier, B. Javidi*, V. Laude and J.-P. Huignard, *Thomson-CSF, Orsay, France (*Dept. Elec. Eng., Univ. of Connecticut, U.S.A.).* An optimal processor for discrimination and noise robustness is developed for pattern recognition. It leads to a natural and attractive high speed optical implementation. Furthermore, it provides theoretical insight in previous heuristic nonlinear filtering techniques.

12.15 p.m.
WC6 Rotation Scale and Shift Invariant Real Time Pattern Recognition, E. Silvera and J. Shamir, *Dept. of Electrical Engineering, Technion-Israel Institute of Technology, Haifa, Israel.* An adaptive pattern recognition system is presented. Invariance is achieved by using two parallel channels, each dealing with a different distortion. The overall process is performed efficiently and can be executed in real time.

12.30 - 2.00 p.m. Lunch Break

Wednesday 24 August, 2.00 - 3.45 p.m.
Optical Interconnects/Integration
(Session Chair: K-H. Brenner, Univ. of Erlangen, Germany)

2.00 p.m.
WD1 Systems Partitioning and Placement in Optoelectronic MCM Design, J. Fan, S.H. Lee and C.K. Cheng, *Dept. of ECE, Univ. of California, U.S.A.* We discuss the CAD issues for partitioning between electrical and optical interconnects and physical layout in free-space optoelectronic MCM design. The results of a design example are also presented.

2.15 p.m.
WD2 Architecture of a Terabit Free-Space Photonic Backplane, T. Szymanski and H.S. Hinton, *Dept. of Elec. Eng., McGill Univ., Montreal, Canada.* The architecture of a "universal" photonic backplane is described. The architecture contains a large array of "programmable" smart pixels which can be configured into three states. By setting pixel states appropriately, any network can be embedded into the backplane.

2.30 p.m.
WD3 A Scalable Optical Interconnection Network for Massively Parallel Computers, A. Louri and H. Sung, *Dept. Elec. & Comp. Eng., Univ. of Arizona, U.S.A.* We present a new optical interconnection network, called an optical Multi-Mesh Hypercube, which is both size- and generation-scalable. It exhibits such properties as small diameter, fault tolerance, symmetry, constant node degree, and is highly amenable to optical implementations.

2.45 p.m.
WD4 Demonstration of a 3D-Integrated Refractive Microsystem, J. Moisel and K.-H. Brenner, *Inst. fur Angew. Optik, Univ. Erlangen-Nurnberg, Germany.* A 3D-integrated microsystem is presented which performs the overlay of data planes. Each channel of the microsystem consists of two gradient-index microlenses and two microprisms. The output plane is 500 μm squared and contains approximately 100 pixels.

3.00 p.m.
WD5 Integration of Free-Space Interconnects using Selfoc Lenses: Optical Properties of a Basic Unit, K. Hamanaka, K. Nakama, D. Arai, Y. Kusuda, T. Kishimoto and Y. Mitsuhashi, *Nippon Sheet Glass Co. Ltd., Ibaraki, Japan.* A vertical and horizontal integration technique of free-space interconnects using Selfoc lenses is described. A basic unit of the optical mother board has been fabricated by slicing a Selfoc rod of 4 mm in diameter.

3.15 p.m.
WD6 Fabrication of Fibre Arrays for Optical Computing and Switching Systems, J.M. Sasian, R.A. Novotny, M.G. Beckman, S.L. Walker, M.J. Wojcik and S.J. Hinterlong, *AT&T Bell Labs., Naperville, U.S.A.* We describe a technique for assembling fibre arrays as needed in optical computing and photonic switching. A 4 × 8 array was manufactured with fibre ends to within 1.5 μm from their ideal position and to a pointing precision of 30 arc-minutes.

4.00 - 6.00 p.m. Poster Sessions

Interconnects	**WP1**	**-**	**WP26**
Memory and Neural Networks	**WP28**	**-**	**WP45**
SLMs and Smart Pixels	**WP46**	**-**	**WP56**
Optical Switching	**WP57**	**-**	**WP71**

Thursday 25 August, 9.00 - 10.30 a.m.
Interconnection in Computers
(Session Chair: S.H. Lee, Univ. of California, San Diego, USA)

9.00 a.m.
ThA1 Experimental Results of a 64 Channel, Free-Space Optical Interconnection Network for Massively Parallel Processing, I. Redmond and E. Schenfeld, *NEC Research Inst., Princeton, U.S.A.* We report the experimental results of a 64 channel, high data rate, free-space interconnection network for massively parallel processing architectures. It uses VCSEL arrays, photodetector arrays and a passive optical routing network.

9.15 a.m.
ThA2 Performance of an Optical Free-Space Crossbar, H.J. White, G.M. Proudley, C. Stace, N.A. Brownjohn, A.C. Walker*, M.R. Taghizadeh*, B. Robertson*, C.P. Barrett*, W.A. Crossland**, J.R. Brocklehurst†, M.J. Birch+, M. Snook+ and D. Vass+, *BAe Sowerby Res. Centre, Bristol, U.K. (*Dept. of Physics, Heriot-Watt Univ., Edinburgh, U.K., **Eng. Dept., Univ. of Cambridge, U.K., †Thorn EMI CRL, Middlesex, U.K. +Dept. of Physics., Edinburgh Univ., U.K.).* Initial results on the performance of a 64 input 64 output free-space optical crossbar are reported. The components of the compact and ruggedised system are described.

9.30 a.m.
ThA3 A FET-SEED Based Optical Backplane Demonstrator, D.V. Plant, B. Robertson, H.S. Hinton, W.M. Robertson, G.C. Boisset, N.H. Kim, Y.S. Liu, M.R. Otazo, A.Z. Shang and L. Sun, *Dept. of Electrical Eng., McGill Univ., Montreal, Canada.* We demonstrate a representative portion of an optical backplane using free-space optical channels to interconnect printed circuit boards which employ FET-SEED based smart pixel arrays. Results of system demonstrator performance will be presented.

9.45 a.m.
ThA4 High Speed Parallel Switching of Symmetric Self-Electrooptic Effect Devices (S-SEEDs), D. Goodwill, D.A. Baillie and F.A.P. Tooley, *Dept. of Physics, Heriot-Watt Univ., Edinburgh, U.K.* An S-SEED switching experiment has been designed and constructed to investigate operation at 5-50 MHz using powers of 1 mW/device over a 512 device array. Details of the implementation and experimental results will be presented.

10.00 a.m.
ThA5 Arrays of Field Effect Transistor-Self Electrooptic Effect Device (FET-SEED) Differential Transimpedance Amplifiers for Two Dimensional Optical Data Links, R.A. Novotny, M.J. Wojcik, A.L. Lentine, L.M.F. Chirovsky*, L.A. D'Asaro*, M.W. Focht**, G. Guth**, K.C. Glogovsky**, R. Leibenguth**, M.T. Asom** and J.M. Freund**, *AT&T Bell Labs., Naperville, U.S.A. (*AT&T Bell Labs., Murray Hill, U.S.A., **AT&T Bell Labs, Breinigsville, U.S.A.).* Two dimensional (4 × 18) arrays of Field Effect Transistor-Self Electrooptic Effect Device transimpedance receivers have been fabricated for application in massively parallel optical data links. Up to 100Mbps/channel was demonstrated. Test results are discussed.

10.15 a.m.
ThA6 INVITED - The Optical Computing of National 863 High Technology Program in China, Y. Zhang, *Institute of Optoelectronic & Precision Engineering, Tianjin University, P.R. China.* Some of the achievements of National 863 High Technology Program in China are summarised.

10.30 - 11.00 Coffee Break

Thursday 25 August, 11.00 - 12.30 p.m.
Digital Optics Implementations
(Session Chair: H. S. Hinton, Univ. of Colorado, USA)

11.00 a.m.
ThB1 INVITED - Parallel Optoelectronic Processing Systems and Applications, M. Ishikawa, *Dept. Math. Eng. & Info. Phys., Univ. of Tokyo, Japan.* A parallel computing system using optical interconnection and its applications for visual information processing are shown. The system can be integrated into one chip by using VLSI technology.

11.30
ThB2 INVITED - Free Space Holographically Interconnected Counter, R.J. Feuerstein, D.C. O'Brien, A. Fedor, M.C. Chang and L.H. Ji, *Optoelectronic Computing Systems Center, Univ. of Colorado, U.S.A.* We have constructed a simple 4-bit counter using holographic interconnects, microlens arrays, vertical cavity lasers, and a CMOS detector array chip. Performance of this prototype system will be discussed.

11.45 a.m.
ThB3 INVITED - Versatile Compact Image Processor with Optical Feedback using Photopolymer and Ferroelectric Liquid Crystal on Amorphous Silicon, P. Cambon*, J. Sharpe and K.M. Johnson, *Optoelectronic Computing Systems Center, Univ. Colorado, U.S.A. (*GOSC, Télécom Bretagne, Brest, France).* An optical image processor with optical feedback and gray scale capability compactly organised around bistable binary amorphous silicon and ferroelectric liquid crystal devices and a one lens correlator using reflective multiplexed photopolymer hologram is presented.

12.00 noon
ThB4 INVITED - Digital Optical Computing Demonstration Systems, F.A.P. Tooley, S.M. Prince, D. Baillie, D. Goodwill, M. Desmulliez and M.R. Taghizadeh, *Department of Physics, Heriot-Watt University, Edinburgh, U.K.* Details of the implementation of two optical computer demonstrators will be presented: a 64-channel S-SEED, cellular logic image processor with a dynamic interconnect and a sorting module implemented by interconnecting smart pixels with a shuffle.

12.15 p.m. Closing Remarks

Pierre Chavel — *Institut d'Optique, Paris, France (ICO representative)*

Quantum Well Smart Pixels for Optical Switching and Processing

David A. B. Miller
Rm. 4B401, AT&T Bell Laboratories,
101 Crawfords Corner Road,
Holmdel, NJ 07733, USA

Abstract

A broad variety of arrays of experimental smart circuits with quantum well optical inputs and outputs has been fabricated for many users. Current status and future prospects for such large scale optoelectronic integration are summarized.

Quantum well optical modulator diodes have proved to be very useful devices for many optoelectronic information processing and switching systems experiments. They can be made in large numbers (e.g., 1000's) with usable yields, and can be used both as optical input devices (since they operate as good photodiodes) and optical output devices (operating as absorption modulators).[1,2] The devices themselves are low power, high speed, and apparently reliable. They have been used on their own in various configurations to perform optoelectronic logic and analog optical operations in the simpler of the so-called self-electrooptic-effect devices (SEEDs).

The diodes have also been successfully integrated with electronic devices in various ways. FET-SEEDs are monolithic integrations of quantum well diodes as detectors and as modulators together with GaAs field effect transistors.[3] They have also been successfully grown on silicon substrates,[4] and they have recently been integrated using a hybrid, solder-bump bonding onto silicon integrated circuits.[5] The integration with electronics brings two advantages: (i) the optical input energy needed can be reduced by the use of electronic gain - an important feature since the performance of large systems is usually limited more by available optical power rather than speed limits in the devices; (ii) the use of advanced electronic technologies allows much more complexity in the "nodes" or "smart pixels" - empirically it now appears that most potential applications need complexity in the nodes to perform the functions that the systems need.

The FET-SEED technology is currently the most advanced for practical applications. It has been run in a 5-stage switching system [6] at system speeds of 155 Mb/s, using chips with 400 transistors and 96 quantum well input or output diodes. Individual circuits have been run at 650 MHz or with input energies as low as 20-30 fJ. The simpler symmetric SEED (S-SEED) technology has been used in arrays of 2048 devices in multistage systems at slower speeds (e.g., 100 kHz) with up to 60,000 light beams in the system overall. The various integrations on silicon circuits are still at an earlier stage of device research, but are promising for integration with highly complex circuits; arrays of hybrid devices are being successfully fabricated now on silicon circuits.

In 1993, an experimental workshop was run in conjunction with the ARPA CO-OP program in the United States that trained users how to design in the FET-SEED technology and fabricated the chips designed by the users. The chips were delivered to users in early 1994. One goal of this workshop was to stimulate systems and applications research with parallel optoelectronic technologies, and users designed a broad variety of circuits in what may be the first multiproject optoelectronic wafer fabrication. The results of this workshop are currently being reviewed, but first indications are that this was a successful project and that there is demand for greater availability of this kind of service

for system research purposes. This will likely stimulate further such workshops or foundry services for optoelectronic arrays in this and other such technologies.

[1] D. A. B. Miller "Quantum-well self-electro-optic effect devices", Optical and Quantum Electronics, **22**, S61-S98, (1990)

[2] A. L. Lentine, and D. A. B. Miller, "Evolution of the SEED technology: bistable logic gates tooptoelectronic smart pixels", IEEE J. Quantum Electron. **29**, 655-69 (1993)

[3] L. A. D'Asaro, L. M. F. Chirovsky, E. J. Laskowski, S. S. Pei, T. K. Woodward, A. L. Lentine, R. E. Leibenguth, M. W. Focht, J. M. Freund, G. G. Guth, and L. E. Smith, "Batch fabrication and operation of GaAs-AlGaAs field-effect transistor-self-electrooptic effect device (FET-SEED) smart pixel arrays", IEEE J. Quantum Electron. **29**, 670-7 (1993)

[4] K. W. Goossen, G. D. Boyd, J. E. Cunningham, W. Y. Jan, D. A. B. Miller, D. S. Chemla, R. M. Lum, "GaAs-AlGaAs Multiquantum Well Reflection Modulators Grown on GaAs and Silicon Substrates" IEEE Photonics Tech. Lett., **1**, 304-306, (1989)

[5] K. W. Goossen, J. E. Cunningham, and W. Y. Jan, "GaAs 850 nm modulators solder-bonded to silicon", IEEE Photonics Tech. Lett. **5**, p.776-8 (1993)

[6] F. B. McCormick, T. J. Cloonan, A. L. Lentine, J. M. Sasian, R. L. Morrison, M. Beckman, S. L. Walker, M. J. Wojcik, S. J. Hinterlong, R. J. Crisci, R. A. Novotny, and H. S. Hinton, "Five-stage free-space optical switching network with field-effect transistor self-electro-optic-effect-device smart-pixel arrays", Applied Optics **33**, 1601-18 (1994)

Large Scale Integration of LEDs and GaAs Circuits fabricated through MOSIS

Annette C. Grot and Demetri Psaltis
California Institute of Technology
Pasadena, CA 91125 USA
818-395-3893

Krishna V. Shenoy and Clifton G. Fonstad, Jr.
Massachusetts Institute of Technology
Cambridge, MA 02139 USA
617-253-5165

Abstract

We describe a new process to integrate LEDs with fully processed GaAs circuits using MBE regrowth. The bottom contact of the LED, grown in the dielectric vias, is made through the n+ source/drain implant.

In this paper, we describe a process for integrating LEDs (Light Emitting Diodes) by Molecular Beam Epitaxial regrowth on high density GaAs MESFET (Metal-Semiconductor Field-Effect Transistor) circuits fabricated by Vitesse Semiconductor Corp. through the U.S. chip prototyping service, MOSIS (MOS Integration Service). The Vitesse process available through MOSIS offers enhancement-mode (V_T=0.25V) and depletion-mode (V_T=-0.6V) GaAs MESFETs (the minimum gate length is 0.8μm), optical FET and MSM (Metal-Semiconductor-Metal) photodetectors, Schottky diodes, and four levels of aluminum interconnect metalization. Each layer of interconnect metal is separated by a layer of SiO_2 dielectric. The total thickness of the dielectric stack is 4μm. The key features which allow the circuits to withstand (Al,Ga)As MBE (Molecular Beam Epitaxy) regrowth are that all of the metalization layers, i.e. the gate-metal, the source-drain ohmic contact, and the interconnect metal, are stable up to 500°C and none of the layers contain gold which would degrade the device performance.

The chip layout for the optoelectronic circuits is done using standard CAD tools. Figure 1 shows the cross-section of the Vitesse chip with the LED epitaxial layers regrown in the dielectric vias. In the areas where the LED material is later grown, an n+ source/drain implant is specified along with two overlapping dielectric etch layers, to specify the area where the dielectric covering the substrate should be removed. The dielectric vias for the LEDs have been made as small as 10μm x 10μm with vertical side walls. The n+ source/drain ion-implant under the LED provides the bottom n contact for the LED so that one terminal of the LED can be directly connected to the rest of the circuit without any post-processing. After receiving the chip from MOSIS with the MESFETs, interconnect circuitry, and the dielectric vias for the LEDs, the first step is to degrease the wafer and clean the GaAs surface with a buffered oxide etch. The chip is then loaded into an MBE chamber and a double heterojunction GaAs/AlGaAs LED structure is grown at 530°C. The total thickness is 4μm so that the top p+ GaAs layer is planar with dielectric stack. The superlattice at the bottom helps impede defects from the substrate surface from propagating upwards. After unloading the chip from the MBE chamber, the single crystalline LED material in the vias is masked off with photoresist so that the polycrystalline GaAs material, which forms over the rest of the chip, can be removed using a wet chemical etch. The final processing step is deposition of AuZn/Au for the top p+ contact.

Figure 2 is a photograph of part of a GaAs MOSIS chip after the MBE regrowth. The circuit surrounded by the 7 electrical pads is a 3 unit winner-take-all circuit. The function of the winner-take-all circuit is to determine the unit with the largest input signal. The LEDs, located to the right of the initials "AG JL dP", are the output signals for the circuit. The dimensions of the dielectric vias for the LEDs are 40μm x 40μm. The only LED which will be on will be the one with the largest optical input power. Optical FETs were used in this circuit as photodetectors because of their high responsivity (on the order of 1000A/W at 10nW input power levels). Figure 3 shows the output power of two competing units of the winner-take-all circuit. The optical power on unit 1 was fixed at 30nW while the power on unit 2 varied from 0 to 100nW. There was no input to the third unit so consequently its output remained off. The transconductance of the enhancement-mode MESFET after regrowth was 30mS/mm and the gate length was 1μm. The efficiency of the LEDs was 5 x 10^{-4}W/A, which is the one of the reasons for the low output power in the circuit. Another reason is backgating on the chip which reduces the output current and responsivity of the detectors. Improvements are expected with refined LED regrowth and processing techniques.

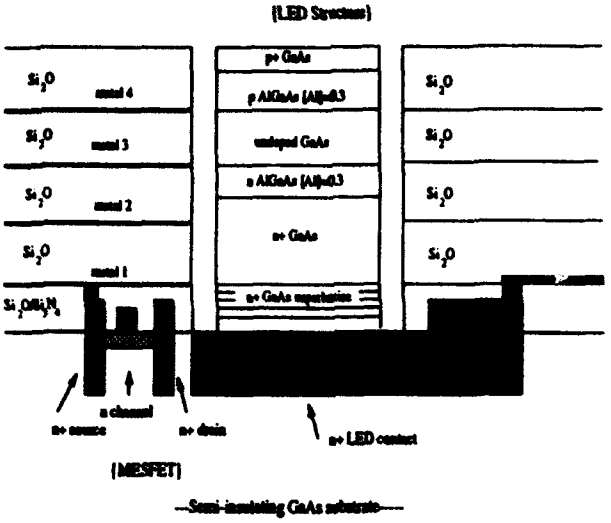


Figure 1 Cross-section of a Vitesse/MOSIS chip with LED grown in the dielectric via.

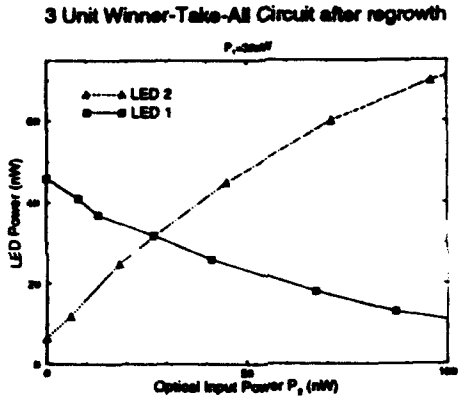


Figure 3 Output Power of Two Competing Branches of a Winner-Take-All Circuit

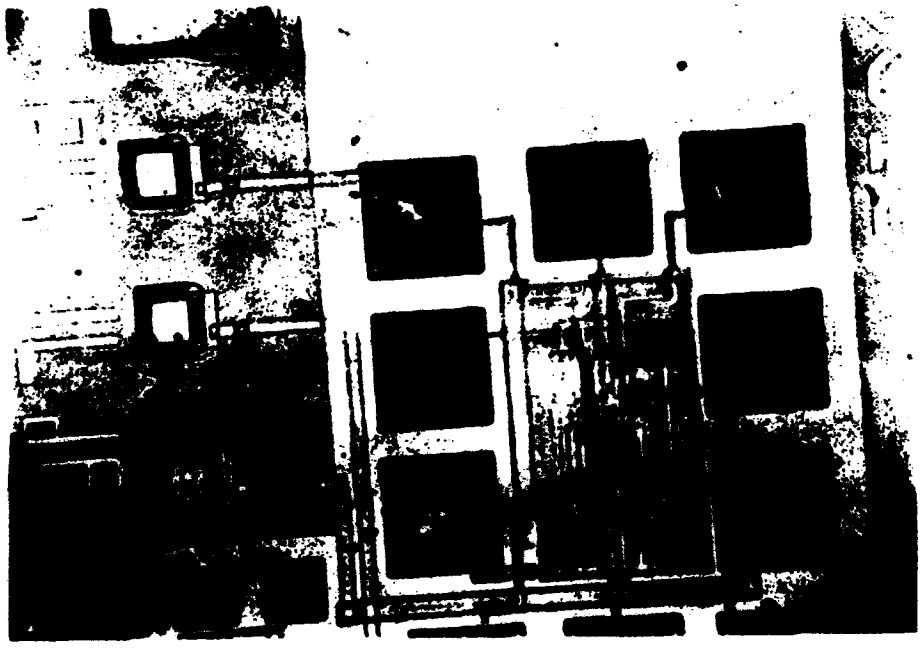


Figure 2 Photograph of a Vitesse/MOSIS chip with the LEDs grown in the dielectric vias.

Parallel Algorithms for Optical Image Processors

Pierre Chavel, Philippe Lalanne

Institut d'Optique (CNRS)
B.P. 147, 91403 Orsay cedex, France, tel. (1)69 41 68 41

Abstract Fine grain parallel optoelectronic processors for dedicated tasks may deserve further consideration. The main case is vision machines ; stochastic algorithms working on images considered as Markov fields are one possible approach to deal with real images.

Introduction

The processing of real images is one area where optical computing may come up with competitive solutions. The basic reason, as usual, is the number of interconnects that are needed before any sensible processing task on an image is completed ; the number of interconnects required is particularly large in parallel implementations, which is where free space optics is attractive. The word interconnect should be understood in a broad sense, including data input and output and the provision of various control signals to the processing elements as well as exchange of information among the processors themselves. We are interested in "optical scale" parallelism, where the processor consists in a number of processing elements (PE's) equal to the number of pixels in the image, typically at least 10^4 : this puts the heaviest weight on interconnects but alleviates considerably programme and data transfer control. For easy image format input, all PE's should fit together on a chip a few square centimetres on a side. But technology will allow to integrate only fairly weak PE's on such a small area. We are then faced with a double challenge : devise optoelectronic architectures that make the best use of optical interconnects to maximise the computing power and find algorithms that can use it for meaningful image processing tasks.

Convolutions

The simplest and most famous application of the above concept is the optical convolution, where the PE reduce to photodetectors and where weighted optical interconnects that define the impulse response do all the processing. The main application is pattern recognition. The double challenge then takes on the following form : can convolution be helpful in real pattern recognition problems and if yes, can optics implement such convolutions ? Progress on filter reprogrammability, adaptivity to the input signal and invariances will be reported in several papers in this conferences.

Optical Cellular Automata :

Convolution nevertheless shows only limited generality and it is important to seek broader classes of our image processors. The next simple case is cellular automata, that have been investigated in some detail for some years under various names, including symbolic substitution and mathematical morphology. Their operation cycle consists in the combination of one convolution and one point nonlinear operation. The main role of optics here is to implement the convolution part, while optoelectronic or nonlinear optical devices located at every pixel respond nonlinearly to its result. The invited communication by Casasent in this conference develops mathematical morphology applications for a number of image processing tasks.

Optimisation problems in image processing

One further step is to introduce optimisation problems into the realm of optical computing. In an optimisation problem, an energy function $E(\underline{x})$ is introduced as a measure of the departure of an image $\underline{x}$ from an ideal goal to be reached by the processing. The definition

of function E incorporates all relevant knowledge, i.e. the input data but also, for example, the sources of degradation to be removed, a priori information on the class of object, and the features of interest. The processing minimises the energy with respect to $\underline{x}$.

Previous algorithmic work, notably by Geman et al. who used the approach of Markov random fields to statistically describe the space of "real images", has demonstrated energy functions that can detect, for example, texture, edge or motion in fairly difficult situations. However, the computational load is usually extremely heavy because a small change in the image can generate a large change in the energy - the "energy landscape" is said to be wild - so that secondary minima will prevent simple gradient descent algorithms from reaching the desired minimum or even an acceptable suboptimal solution. As a consequence, it is not only impossible in practice to find the absolute minimum through exhaustive search in the $[\underline{x}]$ space, but even the efficient suboptimal procedures like simulated annealing are hardly practicable unless some way can be found to implement them in parallel : as we shall illustrate now, their parallelisation is where, in our opinion, optics may have a new role to play.

Optics for simulated annealing

In the simplest version of simulated annealing, the energy is first differentiated with respect to some variable ; here, the variable are the grey values x_{ij} of the pixels. If the result of changing x_{ij} to $x_{ij} + \delta x$ is an energy increment ΔE, a random test is made so that the change is accepted with a probability of order $\exp\left(\frac{-\Delta E}{T}\right)$, where T is an simulated "temperature". The process is then iterated and the temperature is decreased at some appropriate slow pace. Optical computing can provide three functions.

Firstly, energy functions can at least sometimes be constrained to quadratic variations in the x_{ij}. ΔE is then a convolution of the image, and we are back to the first section.

Secondly, the parallel generation of a large amount of random numbers of a good statistical quality can be best handled by a physical rather than digital approach, and we have demonstrated the use of speckle to provide around 10^{10} random numbers per second and project them onto a photodetector array, such as an array of "smart pixels". In particular, we have shown that speckle statistics can be easily moulded into exactly the required form of probability law, and that the simulated temperature can be controlled directly by the average speckle brightness, i.e. the laser power.

Finally, novel optoelectronic or nonlinear optical arrays such as SEEDs or pnpn photothyristors may be used to make the required decision.

For the simplest forms of the energy function, it may then be possible to devise an "all-optical" solution. In more elaborate cases, integrated circuits will be required to evaluate ΔE but the role of optics to provide the random numbers and possibly the convolution part of ΔE is still an important factor to open the way to compact, massively parallel integration of image processors for such algorithms.

Conclusion

The favourite operation of analogue optical processing, convolution, may provide a solution for a certain number of image processing problems. But we believe that it could well be combined with other readily available optical functions and with integrated circuit microtechnology into video-real-time systems for a significantly wider class of vision problems.

We acknowledge the contributions of F. Devos, P. Garda, G. Prémont D. Prévost and J.C. Rodier to the research leading to this work.

Quantum-Statistical Restrictions on the Information Transmitting/Processing Rate in Electronic and Photonic Channels

Fedor V. Karpushko

Division for Optical Problems in Information Technologies
Academy of Sciences of Belarus
P.O.Box No.1, 220072 Minsk Belarus
0172/39 58 82 (tel), 0172/32 45 53 (fax)
Email: dopit%bas02.basnet.belpak.minsk.by@demos.su

Abstract. Quantum effects are shown to limit the information capacity of electronic channels by ~ 10^{12}nit/s. At higher rates the energy price for transmitting information is 2-4 order less in 1D-boson channels as compared with 1D-fermion ones. The 3D-optical channels are free of quantum restrictions up to information rates ~ 10^{19} nit/cm^{2}s.

Because bosons and fermions obey the different statistics, the behaviors of the electronic and photonic information channels are expected to be essentially different in the cases when quantum-statistical effects take place. With use of the Fermi-Dirac distribution function we have derived the expressions for calculating the fermion information channel capacity and minimum energy required for transmitting one nit of information. The numerical estimates are compared with those of Lebedev and Levitin [1] for 1D-boson channels.

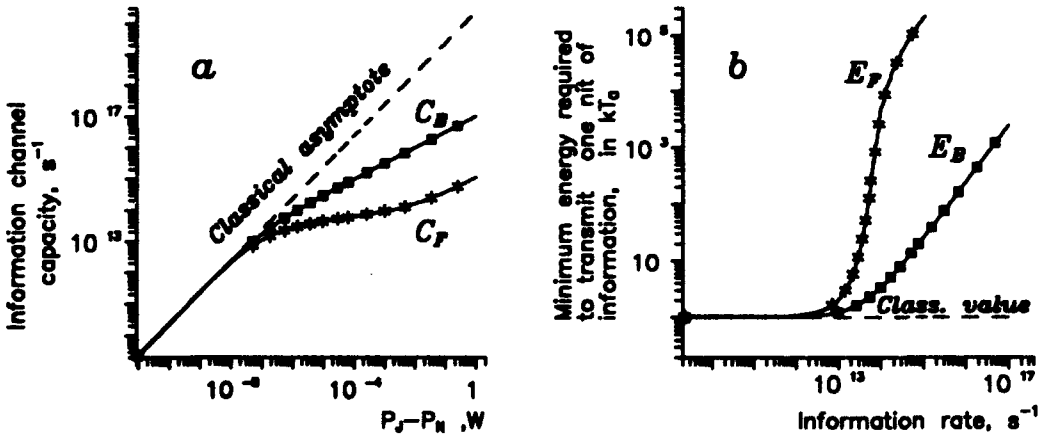


Fig.1. Information channel properties at 300 K. Indexes B and F correspond to 1D-boson(photon) and 1D-fermion(electron) channels respectively. (P_J - P_N) equals the boson signal power and gives the minimum estimate for the fermion signal power because of the statistical dependence of signal and noise fermions.

For both types of channels the quantum-statistical effects play an important but quantitatively different role when the power/energy of signals is effectively presented by the Fourier components with frequencies higher than the boundary thermal noise frequency $n_{noise} \sim kT_0/h$. It is seen from Fig.1, that for 1D-channel at room temperatures this corresponds to the information transmitting/processing rates of about 10^{12}nit/s. Below these rates both types of channels behave equally in agreement with the classical Shennon's theory.

At the information rates > 10^{13}nit/s the difference in behaviour of fermion and 1D-boson channels increases so much that the energy price transmitting the same information becomes 3-4 order of magnitude g er for fermion channels as compared with photon ones. It should be noted that transmitting and processing data will result in "nonlinear" distortions and losses of information at the conditions when information channel capacities are no longer the linear functions of the input signal powers.

Thus, the analysis of quantum-statistical restrictions in the information channels allows us to consider the value of information transmitting/processing rate of about 10^{12}nit/s as **the fundamental limit for electronic systems** (which are 1D-systems by the nature).

For 3D-photon channels a generalization of the Lebedev's and Levitin's formula [1] for the information channel capacity is obtained and it is shown (see, Fig.2) that such channels are free of quantum-statistical

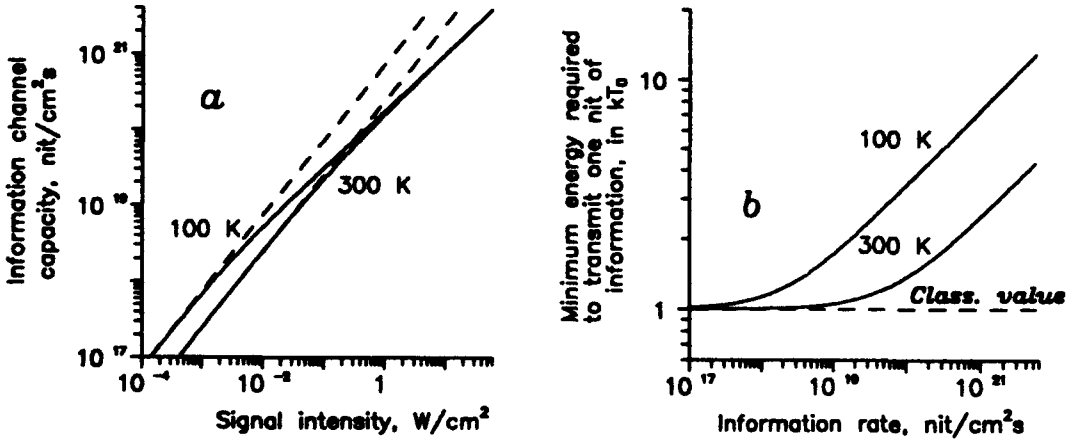


Fig.2. 3D-boson(photon) information channel properties. Dashed lines in (a) show the classical Shennon's asymptotes.

restrictions up to information transmitting rates of about 10^{19} nit/cm^2 s.

References

[1] D.S.Lebedev and L.B.Levitin, Information and Control, V.9, 1-22 (1966)

Spatial-Light-Modulator Based Routing Switches

W.A. Crossland, S.T. Warr, R.J. Mears, R.W.A. Scarr†

Department of Engineering, Trumpington St., Cambridge University, Cambridge, CB1 2PZ, (0223) 330264. †Consultant.

Abstract. Spatial light modulator based routing systems offer potential advantages over conventional electronic and waveguide-based systems. Integration of ferroelectric liquid crystal over silicon smart pixel modulators permits high levels of switch parallelism to be achieved.

1. Introduction

Free-space optical interconnection enables much greater fan-out and fan-in than can be accessed by electronics. These features make it appropriate to re-examine single-stage crossbar architectures. The purpose of this review is to summarise the technology of spatial light modulator (SLM) routing systems and to consider control and arbitration issues.

2. Device technology

The modulators in the systems proposed here are intended to be silicon integrated circuits with an overlay of chiral smectic liquid crystal [1]. The very large electro-optic effects that are observed enable high fan-out/fan-in switch structures to be constructed, and the electronic functionality of the silicon backplane, capable of electronically controlled mirrors and sensitive photodetectors, forms a powerful 'smart pixel' technology.

2.1. Matrix-matrix crossbar

An optical vector-matrix processor for fast Fourier transform calculations was proposed in 1978 [2], later identified as a single-stage, non-blocking space-switch, and then extended to the general matrix-matrix crossbar [3]. These architectures passively fan-out each optical input towards every output. The replications are then 'shadowed' by means of a reconfigurable shutter array and hence selective fan-in is achieved onto the output plane, *figure 1.*

Electrically addressed SLMs operating in a binary transmission mode are suitable high-speed switching arrays that can be used as the shutter plane. Each input replication must be optically resolved through a single shutter such that any arbitrary interconnection pattern may be formed, including broadcast, multicast and multiple-input fan-in. Reconfiguration of the switch simply involves closing any (single) shutters corresponding to completed calls and opening any new paths required.

2.2. Dynamic holographic crossbar

The generation and use of computer-generated holograms is well documented, e.g., [4]. The principle of operation of this architecture is the use of holograms to deflect as much optical power as possible, hence eliminating the need for the initial fan-out operation associated with the matrix-matrix architecture. Each routing area is filled with one from a set of base holograms which are stored in a non-volatile memory behind the interconnect plane, *figure 2.* Each hologram acts as an independent diffraction grating and also provide broadcast, multicast and fan-in capabilities [5].

Electrically addressed SLMs operating in a binary *phase* mode produce a more efficient system than amplitude mode devices, but both techniques lead to a redundant symmetry in the output plane. A means of breaking this symmetry without significantly increasing the system complexity or cost is proposed, [6]. Control of this switch involves periodically transferring im-

ages from memory onto the SLM display. A key scaling issue to be addressed is the number of pixels that are required per routing hologram.

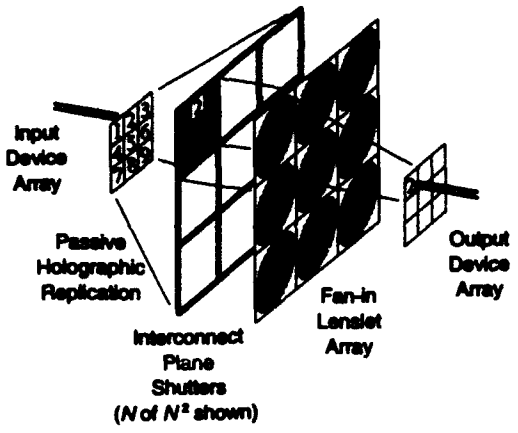


Figure 1: Matrix-matrix crossbar concept.

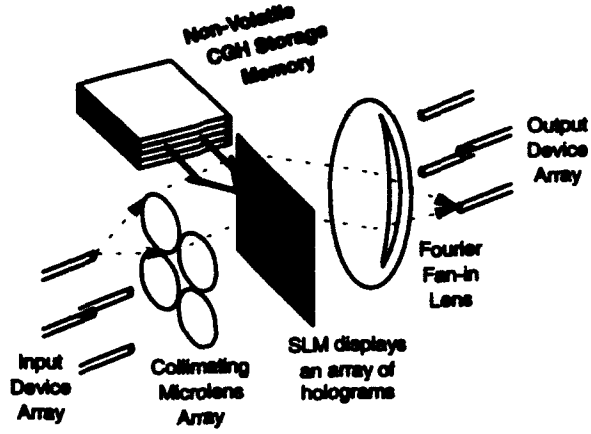


Figure 2: Holographic crossbar.

3. Data throughput, switch control and arbitration

The routing algorithms for non-blocking single-stage switches are very simple, all paths through the switch being mutually independent. The control information may be embedded in the main data paths using the existing free-space optics, or it may be separate from them.

The detection of contention external to the switch and the taking of the steps necessary to stop multiple channels being directed to the same port are also considerably simplified in these structures. Facilities for resolving contention can be built directly into the switch control electronics on the silicon backplane of the interconnect SLM.

4. Conclusions

The data throughput of optically transparent fibre optic switches is determined by the optical power budget and can be very high. The use of smart pixel systems therefore provides a viable switch technology. Results to be presented suggest that the matrix-matrix crossbar is not as critically dependent on SLM contrast ratio as is normally assumed. For both architectures, a significantly lower signal-to-noise ratio may still produce acceptable performance because of the single-stage nature of the switches. The holographic crossbar typically exhibits higher SNR and lower loss than the matrix-matrix architecture.

References

[1] N. Collings, W.A. Crossland, P.J. Ayliffe, D.G. Vass, and I. Underwood. Evolutionary development of advanced liquid crystal spatial light modulators. *Appl. Opt.*, 228(22):4720–4747, November 1989.

[2] J.W. Goodman, A.R. Dias, and L.M. Woody. Fully parallel, high-speed incoherent optical method for performing discrete Fourier transforms. *Opt. Lett.*, 2(1):1–3, January 1978.

[3] A.G. Kirk, W.A. Crossland, and T.J. Hall. A compact scalable free space optical crossbar. In *Proc. Third International Conference on Holographic Systems, Components and Applications*, pages 137–141, Edinburgh UK, 16th September 1991. IEE London. Cong Publication No. 342.

[4] M.P. Dames, R.J. Dowling, P. McKee, and D. Wood. Efficient optical elements to generate intensity weighted spot arrays: design and fabrication. *Applied Optics*, 30(19):2685–2691, July 1991.

[5] D.C. O'Brien, W.A. Crossland, and R.J. Mears. A holographically routed crossbar: Theory and simulation. *Optical Computing and Processing*, 1(3):233–243, September 1991.

[6] T.D. Wilkinson, S.T. Warr, and R.J. Mears. Holographic crossbar switch using asymmetric binary holograms. In *IEEE/LEOS Topical Meeting on Smart Pixels*, Lake Tahoe, Nevada, 11th July 1994.

Independently Addressable Vertical-Cavity Surface-Emitting Laser Diode Arrays

E. Zeeb[1], B. Möller[1], T. Hackbarth[2], H. Leier[2], K.J. Ebeling[1]
University of Ulm, Department of Optoelectronics, D-89069 Ulm, Germany[1]
Phone: +49/731/502-6050 Fax: +49/731/502-6049
Daimler Benz Research Center, D-89013 Ulm, Germany[2]

Abstract
The fabrication of very uniform, planar 10 × 10 vertical-cavity surface-emitting laser diode arrays is reported. Individual elements show threshold currents around 4 mA, emit up to 300 μW single mode, and exhibit a 3 dB modulation bandwidth of 4.6 GHz.

Independently addressable, two dimensional laser diode arrays have many applications for example in optical scanners, display technology, optical interconnects, high capacity switching systems, wavelength division multiplexing systems, or for the generation of high power coherent beams [1]. Using planar vertical-cavity surface-emitting lasers (VCSEL), such arrays with high packing densities are relatively easy to fabricate [2]. VCSELs allow single longitudinal mode oscillation, very low threshold currents, and alignment tolerant and efficient coupling into single mode fibers [3].

We have fabricated 10 × 10 independently addressable VCSEL arrays. The lasers were grown by molecular beam epitaxy. The active region contains 3 InGaAs quantum wells and is embedded between AlAs–GaAs Bragg reflectors. Lateral current confinement and insulation of the individual lasers is achieved by proton implantation with an energy of 300 keV and a dose of $5 \cdot 10^{14}$ cm^{-2}. The reflectivity of the upper Bragg reflector is improved with an additional Au layer on top. TiAu rings form the ohmic p-contacts. The 100 elements are connected to 25 bonding pads at either side of the 5 × 5 mm array chip by metallic TiAu feeding lines which are deposited on an insulating SiO layer. A schematic of the vertical structure and a top view of a full chip is depicted in Fig. 1. Individual lasers have active diameters of 12 μm and the pitch size of the array is 250 μm.

The processed arrays show a very good homogeneity of the output characteristics over the whole array size. A typical threshold current distribution is shown in Fig. 2. Almost all lasers exhibit threshold currents between 4.1 mA and 4.7 mA with an average value of 4.4 mA . Each laser has a maximum single-mode output power in the order of 300 μW. Above this value higher order transverse modes appear in the emission. By proper wedge shaping of the epitaxial layers during growth, a variation of the emission wavelengths, plotted in Fig. 3, was achieved, making the array very well suited for wavelength division multiplexing systems.

The small-signal response of a single bonded lasing element at different driving currents above threshold is shown in Fig. 4. A 3 dB modulation bandwidth of 4.6 GHz is measured for a driving current of 7.3 mA, corresponding to an output power level of 240 μW. This experiment, performed with a not yet optimized laser structure, shows the potential of the array for high bit rate data transmission. Operating all 100 elements in parallel, bit rates of several hundred Gbit/s can be obtained. Using laser arrays mounted on proper heat sinks with lower series resistances we expect still much higher output powers [4] and modulation bandwidths.

References:

[1] K. Iga, "Surface Operating Electrooptic Devices and Their Application to Array Parallel Signal Processing", in Proc. 16th European Conference on Optical Communication, Sept. 1990, Amsterdam, The Netherlands, pp. 895 - 931, (1990).

[2] D. Vakhshoori, J.D. Wynn, G.J. Zydzik, and R.E. Leibenguth, "8 × 18 top emitting independently addressable surface emitting laser arrays with uniform threshold current and low threshold voltage", Appl. Phys. Lett. **62**, pp. 1718 - 1720, (1993).

[3] T. Wipiejewski, K. Panzlaff, E. Zeeb, B. Weigl, and K.J. Ebeling, "Efficient Alignment Tolerant Coupling of Vertical-Cavity Lasers to Single-Mode Fibres", in Proc. 19th European Conference on Optical Communication, Sept. 1993, Montreux, Switzerland, pp. 333 - 336, (1993).

[4] E. Zeeb, T. Hackbarth, and K.J. Ebeling, "High Power Vertical Cavity Laser Diodes", in Proc. 23rd European Solid State Device Research Conference, Sept. 1993, Grenoble, France, (1993).

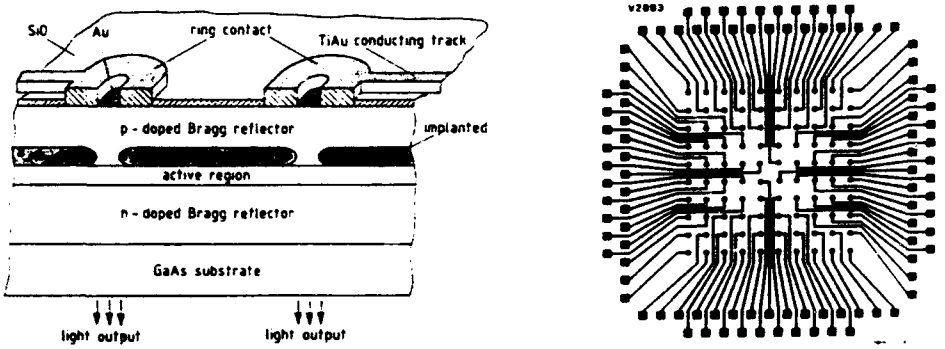


Fig. 1: Vertical structure and top view of an VCSEL array fabricated.

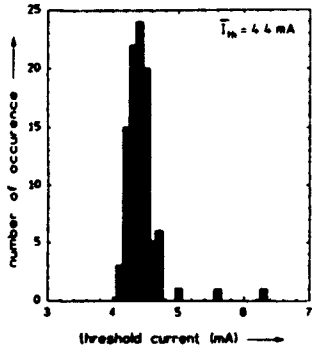


Fig. 2: Histogram of threshold currents.

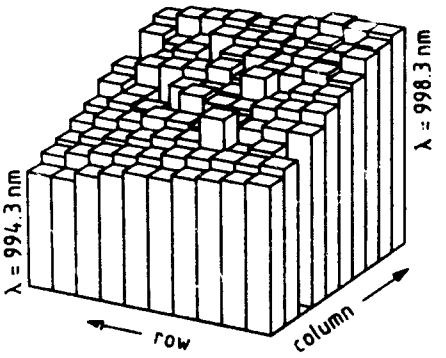


Fig. 3: Emission wavelength distribution.

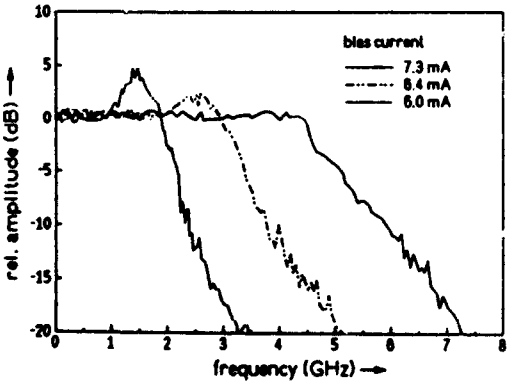


Fig. 4: Small-signal modulation characteristics.

The Scottish Collaborative Initiative on Optoelectronic Sciences – Devices and Demonstrators for Free-Space Digital Optical Processing

A.C. Walker, D.J. Goodwill, B.S. Ryvkin, *M. McElhinney, *F. Pottier, *B. Vogele, *M.C. Holland and *C.R. Stanley
Department of Physics, Heriot-Watt University, Edinburgh EH14 4AS, U.K.
*Department of Electrical and Electronic Engineering, University of Glasgow, U.K.

Abstract. 16×16 arrays of strained-InGaAs/GaAs S-SEEDs have been successfully operated with a diode-pumped 1064 nm laser. These, and other GaAs/GaAlAs devices, are being incorporated into digital parallel optical processing demonstrators.

The Scottish Collaborative Initiative on Optoelectronic Sciences (SCIOS) is a partnership between Heriot-Watt, Glasgow, St. Andrews and Edinburgh Universities that has been running since 1990. It has as its objectives:

(i) to pursue research into the physics, materials science, fabrication and packaging technologies underlying the development of optoelectronic devices, and

(ii) to combine the results of (i) with new system architecture concepts so as to realise free-space parallel optical computing and information processing demonstrators experimentally.

The SCIOS technology programme includes work on III-V semiconductor devices, diffractive optics, spatial light modulators and solid-state lasers. Recent emphasis has been on smart pixel arrays including hybrid silicon/InGaAs devices. In addition, new digital free-space system architectures are being explored and a range of novel demonstrators constructed.

SEED arrays [1] operating at 850 nm are proving to be effective as digital photonic logic planes in experiments on parallel optical processing and switching systems [2,3]. However, system speed can be limited by the degradation of SEED performance at the required high optical power [4,5] due to local heating, saturation and field screening. Woodward et al [6,7] showed that both the Joule heating associated with the photoresponse and the degradation in performance *at high irradiance* could be avoided by using material with a radically decreased non-radiative carrier lifetime τ in the electroabsorptive region. However, the ion-implantation method, used in Refs 6 and 7, broadens the exciton absorption peak and reduces the modulation performance. We have made MQW modulator structures [8] in which the carrier lifetime is already short in the as-grown structure, so that the finished device had both low photocurrent and good modulation performance. We have gone on to demonstrate how such MQW material may be used in a novel electroabsorptive optical switching device.

This device is based on vertically integrated modulator and detector elements, connected electrically in parallel. The non-QW GaAlAs detector (lower part) has unity quantum efficiency under reverse bias. The modulator diode (top part) consists of deep GaAs/AlAs quantum wells and has extremely low quantum efficiency (η=0.4% at 15V, η=1.4% at 25V) due to the long sweep-out time across the high barriers, coupled with a short non-radiative lifetime τ. In this case, the low value of τ was, we believe, produced by a deterioration in the MBE system at the time of growth, which fortunately did not broaden the exciton absorption feature. We hope to reproduce this effect controllably by growing at much lower temperatures.

At 851 nm, a combination of the quantum confined Stark effect in the MQW modulator and the Franz-Keldysh effect in the detector combine to give N-type negative resistance, leading to a factor of 3 decrease in the responsivity of the whole structure between 0V and 15V for 10μW incident optical power. This behaviour is maintained at intensities 8 times higher than for a conventional MQW SEED [4,5]. To show how this structure can be used to make a high performance reflection-mode SEED-type switch, we have recently made devices with optical output provided by a partial mirror (70% reflectivity) between the modulator and detector. A contrast ratio of 4 and a high state reflectivity of 40% are expected. Control of photo-response is likely to be an important factor in the design of future smart-pixel devices based on semiconductor modulators.

The clock-rates for demonstration parallel digital optical processing systems based on current-generation SEED arrays, operating at 850 nm wavelength, are limited by the diode laser power reaching the device array (milliwatts). The consequent demand for a better match to higher-power (> 1 watt) lasers, such as diode-pumped Nd:YLF and Nd:YAG, has prompted the development of strained InGaAs/GaAs multiple

quantum wells (MQW) grown by molecular beam epitaxy (MBE) for SEEDs operating at 1047-1064 nm. Previously reported devices in this materials system [9,10,11] had insufficient contrast ratio and too high operating voltage for use in switching systems. We have obtained enhanced device performance, compared to our previously reported device [11], by improved growth techniques, and have demonstrated for the first time operation of arrays of SEEDs at 1064 nm.

In our S-SEED, the *pin* MQW modulator is grown strain-balanced to a deliberately relaxed buffer layer of intermediate lattice constant, such that the InGaAs wells are in compression and balance the GaAs barriers in tension. Growth was by MBE on a [100] orientated semi-insulating GaAs substrate. To minimise the gliding of dislocations, and hence avoid broadening of the excitonic absorption peak, a low temperature was used with a low arsenic:group-III flux ratio to keep the mobility of the group-III atoms high. The buffer layer consisted of an *i*-InGaAs layer with 10-step grading of In composition from 0 to 13.5%, followed by an *i*-InAlAs/GaAs superlattice. The structure was designed to be completely relaxed at the top of the graded InGaAs layer, but X-ray diffraction measurements showed it was only 71% relaxed. The room temperature absorption peak occurred at 1061 nm rather than the design wavelength of 1047 nm. However, the variation in this wavelength was only ±0.2 nm across the central 1" of the 2" diameter substrate. The half-width half maximum on the low energy side of this peak was 6.0 meV (5.4nm), which is the best reported for this system. It is comparable to the figures of 6.8 meV for MOCVD-grown InGaAs/GaAsP [12] and 5.25 meV for gas-source MBE-grown InGaAs/InGaP [13], for both of which the MQWs are strain-balanced to the substrate. It also compares well to 4.5 meV for similar GaAs/GaAlAs MQWs [1].

For initial optical testing with a tunable laser, 200 μm diameter structures were fabricated by wet etching and metallisation. The front of the sample had a partial anti-reflection coating, the back was polished but uncoated. The photocurrent characteristics showed 98% quantum efficiency at 0V, 100% at 1V reverse bias. The transmission-voltage performance shows a contrast ratio of 2.0 between 0 and 10V at 1060 nm, which increases to 4.2 by the incorporation of a mirror.

S-SEED arrays, ranging in size from 16×16 (20 μm×20 μm windows) to 48×96 (9216 diodes with 7 μm windows), have been fabricated. The devices incorporate a metal mirror on the top for reflection-mode operation, with the light passing through the GaAs substrate and the temperature stabilised sapphire mount. Anti-reflection coatings have been applied at all interfaces. The whole package is compatible with our optomechanical system used for optical processing deminstrators [2]. Individual S-SEEDs show bistability with 3.0-4.2 contrast ration at 10V bias for wavelengths of 1059-1064 nm. Similar arrays with one bond-pad for each S-SEED have also been fabricated for flip-chip bonding to silicon CMOS to make a spatial light modulator.

We thank Y.P. Song, G. Mackinnon, G.S. Buller, N. Watson, N. Ross and M.R. Taghizadeh for help with fabrication of the SEEDs and holographic array generators. This work was supported by the UK Science and Engineering Research Council under the Scottish Collaborative Initiative on Optoelectronic Sciences (SCIOS). BSR acknowledges the support of an SERC Visiting Fellowship.

[1] A.L. Lentine, D.A.B. Miller, IEEE J. Quantum Electron, QE-29, 655 (1993) and references.
[2] F.A.P. Tooley, S. Wakelin, Applied Optics, 32, 1850 (1993).
[3] F.B. McCormick, T.J. Cloonan, A.L. Lentine, J.M. Saisan, R.L. Morrison, N.G. Beckman, S.L. Walker, M.J. Wojcik, S.J. Hinterlong, R.J. Crisci, R.A. Novotny, H.S. Hinton. Appl. Opt., 33, 1601 (1994).
[4] A.M. Fox, D.A.B. Miller, G. Livescu, J.E. Cunningham, W.Y. Yan, IEEE J. Quantum Electron QE-27, 2281 (1991).
[5] T. Sizer, R.E. LaMarche, T.K. Woodward, Appl. Phys. Lett. 61, 420 (1992).
[6] T.K. Woodward, B. Tell, W.H. Knox, J.B. Stark, Appl. Phys. Lett. 60, 742 (1992).
[7] T.K. Woodward, B. Tell, W.H. Knox, J.B. Stark, M.T. Asom, in *Quantum Optoelectronics Technical Digest*, 1993 (Optical Society of America, Washington, DC, 1993) Vol.8, p20.
[8] B.S. Ryvkin, D.J. Goodwill, A.C. Walker, C.R. Stanley, F. Pottier, M.C. Holland, Appl. Phys. Lett. 64, 117 (1994).
[9] T.K. Woodward, T. Sizer II, D.L. Sivco and A.Y. Cho, Appl. Phys. Lett. 57, 548 (1990).
[10] I.J. Fritz, D.R. Myers, G.A. Vawter, T.M. Brennan and B.E. Hammons, Appl. Phys. Lett. 58, 1608 (1991).
[11] D. Goodwill, A.C. Walker, C.R. Stanley, F. Pottier, M. McElhinney, Appl. Phys. Lett., 64, 1192 (1994).
[12] J.E. Cunningham, K.W. Goossen, M. Williams and W.Y. Jan, Appl. Phys. Lett. 60, 727 (1992).
[13] J.W. Kim, C.W. Chen, T.J. Vogt, L.M. Woods, G.Y. Robinson, D.L. Lile, IEEE Phot. Tech. Lett. 5, 987 (1993).

Smart pixel arrays: challenges of manufacturing and testing

G. Livescu. L.M.F. Chirovsky, L.A. D'Asaro and S. Hui
AT&T Bell Laboratories, Murray Hill, NJ 07974
R.A. Novotny and A.L. Lentine
AT&T Bell Laboratories, Naperville, IL 60566
M.W. Focht, J.M. Freund, K.G. Glogovsky, G.D. Guth, G. Przybylek and R.E. Leibenguth
AT&T Bell Laboratories, Breinigsville, PA 18031

Abstract

Wafer level optical and electronic testing of smart pixel arrays is a must if a high yield technology is to be developed. Our results on GaAs FET-SEED based switching nodes show the uniformity and performance control levels achievable with today's technology, as well as its limits.

The fabrication of monolithically integrated semiconductor microelectronics components with optical devices must be a high yield process in order to accomplish large scale manufacturing of smart pixel arrays for optical interconnects and switching. Smart pixels consist of optical input and output devices, whose performance is enhanced with logic and amplifying circuitry. We present here 4x4 arrays of 2x1 photonic switching nodes [1] made using the field-effect-transistor self electro-optic effect device (FET-SEED) technology [2,3]. Although simple circuits can switch as fast 200ps [4]. and fully functional individual nodes operating at 400Mb/s have been demonstrated [1,5], the speed of an *entire array* was only 155Mb/s, limited by the non-uniformity of the individual nodes. We have undertaken the task of systematically mapping the performance of the arrays at the wafer level, in order to identify failures and their origin.

A node is schematically shown in Fig.1. It consists of an optical receiver, an inverter, a control memory and a multiplexer/driver/transmitter. The electrical output A of the receiver becomes one of the inputs to the 2x1 multiplexer/driver located within the same node. The other input, B, comes from a receiver located in another node. Each mux/driver also has a pair of complementary electrical inputs (Q and $\overline{Q}$ in Fig.1), whose role is to control which one of the inputs A or B is regenerated as the optical output C. The control memory (set-reset latch) stores this control bit. An electrical control signal, V_{CC}, common to all the nodes in the array, is held either high, to enable writing of the memories with the control bits preceding the data bits, or low, to preserve the memory during the time the data are processed.

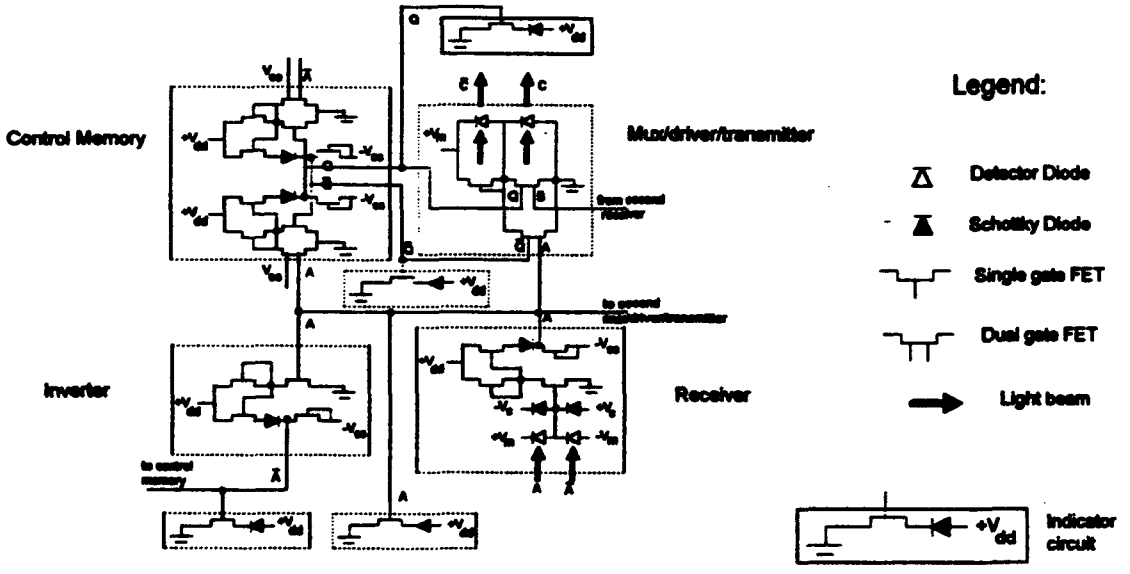


Fig.1. Schematic diagram of a single node. Notice the four "indicator lights" placed at the bottom left (the $\overline{A}$ and A), at the center ($\overline{Q}$), and the top right (Q).

The circuits contain quantum well p-i-n detector diodes, Schottky clamping diodes, single-gate and double-gate field-effect transistors. Single diodes, transistors, resistors and conductors are fabricated, adjacent to each array of smart pixels, for individual component characterization. By measuring their characteristics and mapping them over the area of the wafer we obtain the yields of individual devices, as well as the degree of uniformity. These yields are in general very high, of the order of 90% and better. An example of data mapping on a 3" wafer is shown in Fig.2, for threshold voltages V_{th} of FET's with 10μm long gates. The figure shows good uniformity. A variation of 100mV is observed within a 2" diameter, i.e. 50% of the useful area; the variation of V_{th} over the entire area is about 300mV. The pattern in Fig.2 is circular, which indicates that the variation is likely due to thickness and/or doping variation in the MBE growth, rather than to the subsequent processing.

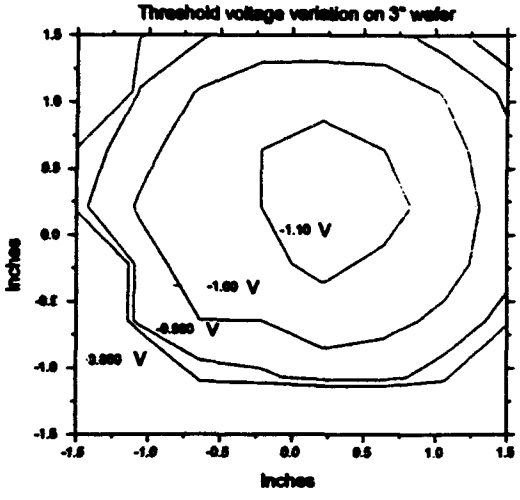


Fig.2 Mapping of threshold voltages on a 3" wafer.

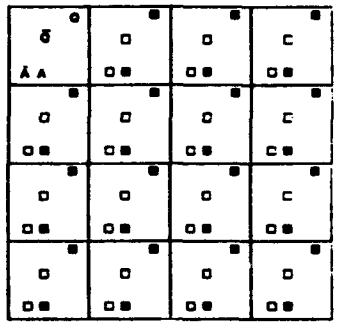


Fig.3. Optical functional testing of the entire 4x4 array. *The first cell illustrates the four* "indicators" which are monitored: the signal A from the receiver, the signal $\overline{A}$ from the inverter, the two control signals from the memory, $\overline{Q}$ and Q.

Testing the functionality of these nodes is a challenging task. Techniques typical to electronic testing of integrated circuits are useful, but insufficient: our circuits must perform optical functions as well. Thus the testing must address both optical and electronic functions. The implementation of such a technique for testing the receiver, inverter and the control memory is illustrated by the use of "indicators" in Figs.1 and 3. Each of the four "indicator circuits" in Fig.1 consists of a quantum well diode in series with a FET. When the FET is conducting, the diode is forward biased and emits light. The state of the FET is determined by the voltage on its gate. In Fig.1, the gate voltage on the indicators is determined by the $\overline{A}$ and A signals for the two lower left ones, and by $\overline{Q}$ and Q for the center and top left indicator. The A signals are simulated electrically. The Q signals are controlled by the voltage V_{ce}. A periodic sequence of high and low A signals is coincident in time with a periodic sequence of high and low V_{ce}. Since only the "high V_{ce}" allows changing the state of the memory, the rate at which $\overline{Q}$ and Q switch is half the rate at which the A signals switch. An infrared camera and a VCR are used to record the "indicator lights" switching. The "motion picture", a frame of which is illustrated in Fig. 3, contains the images of all the switching indicators for every array on the wafer. Similar optical measurements on the different types of nodes, as well as on especially designed "yield tester arrays" (consisting of indicator circuits only), have allowed us to assess the present functional yields. They vary from 5% to 50%, depending on the circuit. Our preliminary analysis of failures indicates that the vast majority of them are due to processing errors which can be avoided by using improved processing techniques.

REFERENCES

1. A.L Lentine et al., IEEE Topical Meeting on Smart Pixels, Santa Barbara, CA, August 1992, Paper PD1.
2. T.K. Woodward et al., IEEE Photon. Techn. Lett. 4, 614 (1992).
3. L.A. D'Asaro et al., IEEE J. Quant. Electron. 29, 670, 1993.
4. G. Livescu, G.D. Boyd, L.M.F. Chirovsky, R.A. Morgan and T. Mullally, CLEO 93, Paper CFF6.
5. F.B Mc Cormick et al., OSA Topical Meeting on Photonics in Switching, Palm Springs, CA, March 1993, Paper PD5.

Monolithically Integrated Optoelectronic Smart Pixels

U. Kehrli, D. Leipold, K. Thelen, H.P.Schweizer, P. Seitz, and B.D. Patterson
Paul Scherrer Institut, Badenerstr. 569, CH-8048 Zürich
Tel.: ++41-1-492 63 50, Fax.: ++41-111-491 00 07

Abstract

We describe a monolithically integrated optoelectronic smart pixel fabrication process using a GaAs/AlGaAs system. The smart pixels are realized with depletion type metal semiconductor field-effect transistors (MESFETs), high brightness light-emitting diodes (HBLEDs) and photodiodes (PDs).

Monolithically integrated optoelectronic "smart pixels" are of current interest in the field of parallel optical interconnects, early vision processing and optoelectronic neural networks [1,2].

We have developed a fabrication process where, in a flexible way different kinds of optoelectronic smart pixels can be realized in the GaAs/AlGaAs material system. The material is grown in a single step by metal organic chemical vapour deposition (MOCVD). On a n^+-doped GaAs substrate, we first grow a HBLED with a n-type $Al_{0.3}Ga_{0.7}As/Al_{0.8}Ga_{0.2}As$ distributed Bragg reflector of 30 pairs [3]. The PD/MESFET layers are grown on top of this structure. They consist of a 1 µm thick GaAs p^--buffer/absorber layer, a 200 nm thick $1 \cdot 10^{17}$ cm^{-3} n-doped GaAs channel, a 20 nm thick etch-stop layer of $Al_{0.3}Ga_{0.7}As$ and a GaAs n^+-contact layer. The p^-n-junction between the buffer/absorber layer and the channel of the MESFET is used as a PD (Fig. 1). The bandgap difference between the PD absorber and the HBLED emission is 127 meV. The light emitted by the HBLED is shifted to 790 nm using a $Al_{0.05}Ga_{0.95}As$ QW. Therefore the light can efficiently be detected by the PD. The etch-stop layer ensures a homogenous MESFET threshold voltage over a large area. The entire n-p-n layer structure is described in [4].

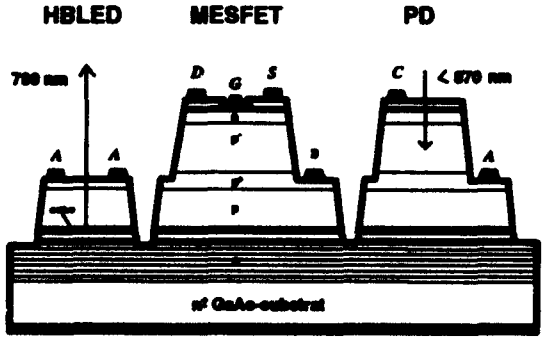


Fig. 1: Schematic layer sequence of an optoelectronic smart pixel.

The fabrication process requires eight photolithographic steps and is based on mesa isolation. The backside ohmic contact is formed first by a Ge-AuNiAu metallisation. This is the n^+-contact to all HBLEDs. For the ohmic contacts of the MESFETs and the PDs a NiGe-AuNiAuPt metallisation is evaporated and annealed at 440C°. Then the individual MESFETs and PDs are separated by magnetron enhanced reactive ion etching (MIE) of mesas. After the deposition of a Si_3N_4 dielectric film, contact areas to the ohmic contacts of the MESFETs and PDs on the n^+-side as well to the ohmic contact of the HBLEDs and the PDs on the p^+-side are opened by reactive ion etching (RIE). The gate areas are then also opened by RIE. The dielectric film is used as a mask for a selective, recessed wet-etch of the gate area. This etch removes the n^+-contact layer and produces an undercut of 200 nm under the dielectric film. The next metallisation (TiPtAu) forms the Schottky contact on the gate areas. This metallisation is also used as the p^+-contact of the HBLEDs and the PDs, and as a first wiring level. The HBLEDs are isolated by a second level of MIE mesa etching. The second wiring (TiAl) level is patterned by wet-etching on a dielectric film .

The fabricated devices are then characterised. The MESFETs, which have a threshold voltage of -1.75V, show a transconductance of 55 mS/mm (U_{gs}=0V, U_{ds}=4V) for a gate length of 1.5 µm and an effective gate width of 27 µm (Fig. 2). The current density per gate length is 66 mA/mm (U_{gs}=0V, U_{ds}=4V). The responsivity of the PDs is 0.56 A/W at a wavelength of 790 nm. This implies, for a practical optical input power of (1-5) µW, a photo current of (0.56-2.8) µA. An emission efficiency of 0.0095 W/A was measured for the HBLED. This implies, for HBLEDs of 25•25 μm^2 active area, a light output power of 95 µW at an input current of 10 mA, and a power dissipation of 22 mW. The mean emission wavelength is 792 nm.

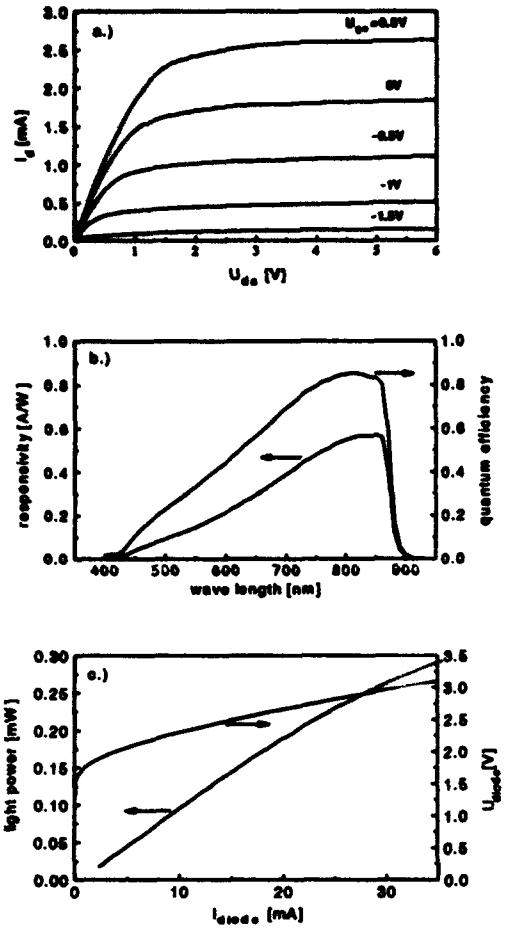


Fig. 2a) The drain I-V characteristic of a MESFET with a gate length of 1.5 μm and an effective width of 27 μm, b) the quantum efficiency and responsivity vs. wavelength for a PD with an active area of 100×100 μm^2, c) the optical output power and diode voltage vs. injection current of a HBLED with an 25×25 μm^2 active area.

We have used HPSPICE to simulate an optoelectronic smart pixel. The GaAs MESFET level 1 model of HPSPICE is serving for the simulation of the MESFET. The pn-junction model of HPSPICE is extended to include a parallel resistance to simulate the reverse current of the PD. The same model is used for the simulation of the HBLED. The MESFET model is also extended to include a PD, which lies under the MESFET. The backgating effect on the MESFET is simulated by a voltage-controlled voltage source placed between the internal gate node and the gate terminal. The PD is connected by the p^+-layer to the parasitic HBLED. To obtain accurate fits to the measurements, all these parasitic devices must be implemented in the models.

We have simulated a simple threshold circuit in which all the parasitic devices are implemented (Fig. 3). The HBLED can be turned off by increasing the light input power P_{in}. The threshold can be controlled by changing the gate voltage V_{TH} of the MESFET M1. The output current is balanced, i.e. the current flows either through the HBLED or through the MESFET M2. The MESFET M3 serves as a current source and limits the HBLED current. The simulated data predict an average optoeletronic gain of 260 for a contrast ratio of 10. The threshold circuit is realised on a chip area of approximately 250×250 μm^2 implying a maximum pixel density of 450 per cm^2.

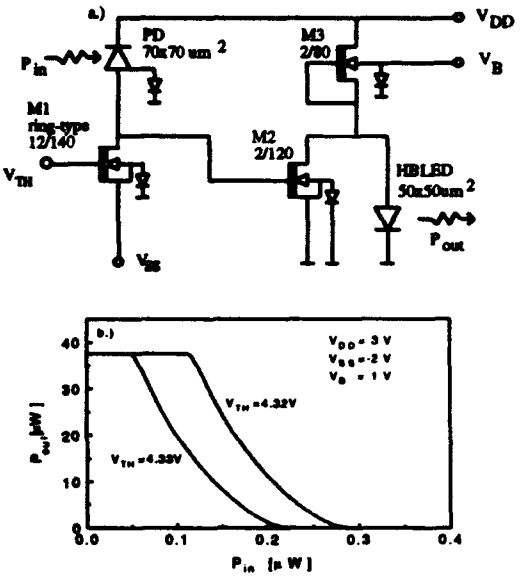


Fig. 3a) The circuit diagram of the simulated threshold circuit, b) the simulated optical output power vs. optical input power.

Based on these results, we are designing and fabricating different types of optoelectronic smart pixels, in particular optoelectronic neurons for optoelectronic neural networks.

References

[1] Julia J. Brown, J. T Gardner, and Stephen R. Forrest, "An Integrated, Optically Powered, Optoelectronic "Smart" Logic Pixel for Interconnection and Computing Applications," IEEE J. Quantum Electron., vol. 29, nr. 2, pp. 715-726, 1993.

[2] Steven Lin, Annette Grot, Jiafu Luo, and Demetri Psaltis, "GaAs optoelectronic neuron arrays," Appl. Opt., vol. 32, pp. 1275-1289, 1993.

[3] E. F. Schubert, Y.-H. Wang, A. Y. Cho, L.-W. Tu, and G. J. Zydzik, "Resonant cavity light-emitting diode", Appl. Phys. Lett., vol. 60, no. 8, pp. 921-923, 1992.

[4] D. Leipold, U. Kehrli, B. Delley, K. Thelen, and B. D. Patterson, "An AlGaAs/GaAs OEIC structure for the integration of LEDs, MESFETs and photodetectors", Materials Science and Engineering, vol B21 pp. 300-303, 1993.

Optical, algorithmic and electronic considerations on the desirable "smartness" of optical processing pixels

Marc P.Y. Desmulliez, John F. Snowdon, Julian A.B. Dines and Brian S. Wherrett

Department of Physics, Heriot-Watt University,
Riccarton, Edinburgh, EH14 4AS, Scotland,UK
Tel : UK 31 451 3068 E-mail : marc@phy.hw.ac.uk

Abstract

The performance gains associated with optical computing schemes must be traded off with the complexity of individual computing nodes in order to optimise the efficiency of an optical processor. We categorise the necessary trade-offs and provide examples of such optimisation.

Introduction

The recent advent of VLSI compatible optically interconnected electronic devices has triggered a tremendous interest in the use of such components at a system level. Few studies, however, have focussed on the numerous trade-offs, benefits and limitations which are offered by the combination of the competing technologies (electronics and optics) [1]-[3]. To recognize whether a task is worth being performed in an opto-electronic form constitutes probably the first stage of the investigation. A definite answer to such a question assumes however that all trade-offs have already been fully quantified. Some tasks are nevertheless recognized as a priori more efficient if optically implemented by algorithms whose possible mappings take benefit of the advantages of non-local optical interconnections. For example, the two-dimensional sorting can be achieved with the bitonic sort algorithm which uses the folded perfect-shuffle [4, 5]. It is the purpose of this paper to carry out a complexity analysis of the opto-electronic implementation of such functions on optical, algorithmic and electronic grounds.

Algorithmic considerations

Previous studies showed that a bonus factor of at least two orders of magnitude is expected for the 8-bit sorting if the computational time of the sorting is reduced [6]. In other words, the degree of smartness of the pixel impacts on the number of processing steps required for sorting. Performance metrics of some algorithms, which all perform the sorting, will be presented. They differ by the minimum required intelligence or smartness at the nodes of the multi-stage interconnection network (MIN). For example, the powerful bitonic sort algorithm demands the presence of complex exchange-bypass modules [5]. In that respect, it is expected that such an algorithm provides a large bonus factor compared to its electronic counterpart. The algorithms are implemented within the Extended-Cellular-Logic-Image-Processor (EX-CLIP) architecture [6].

Optical considerations

The algorithmic analysis ignores the feasibility of large scale implementation in the optical

and electronic domain. In the optical domain, the limitations on the upscaling possibilities originate from fundamental properties or practical constraints. For example, the aberration and diffraction of the imaging devices and the space-variant nature of the optical interconnections impose an upper limit on the space-bandwidth-product available. Technical limitations encompass the micro-mechanical alignment and the stability of the optical implementation.

The highly partitioned feature of an opto-electronic array arises from placing the electronic circuitry of each pixel around their regularly distributed transceivers. This conventional layout eases also the design of the synthetic diffractive elements (DOEs) traditionally used as fan-out and interconnection optical units [7]. A pixel density can be then defined which is directly related to the degree of smartness of the pixel. A multichip configuration [8] increases the throughput rate at the expense of a larger field of view of the imaging devices. The resulting increased space bandwidth product is moreover rarely fully utilized because of the low density of transceivers. In other words, the pixel density is limited by the scaling possibilities of the optical hardware. Solutions have been proposed to overcome that limitation such as the use of hybrid optical components [9] or the topological separation of the transceivers from their circuitry [10]. The possibility to scale up the architecture will be analysed for the different available arrays.

Electronic considerations

The type of technology and the logic family used for the electronic circuitry impacts on the throughput rate through different forms. The area taken by the logic circuitry, while depending on the ability of the electronic designer, provides higher bounds on the pixel density. These bounds can be further modified if the power-delay product of the logic gates and/or the energy dissipated by the transceivers prevent efficient off-chip heat dissipation . Comparisons based on area and power consumption will be made in the cases of GaAs S-SEEDs, L-SEEDs, FET-SEEDs arrays [11] as well as hybrid arrays which involve SEEDs transceivers flip-chip bonded on silicon based CMOS circuits. These arrays exhibit the functionalities required for the different algorithms explained above.

Conclusion

Tabulating various device/architecture/algorithm combinations under the considerations mentioned above allows the optimisation of such combinations in terms of the pixel complexity. Examples of the optimisation of sorting and other transforms will be presented in this context at the conference.

References

[1] F.E. Kiamilev et al., 1991, *J. Light. Techn.*, Vol. 9, **12** , 1674.
[2] D.T. Lu et al., 1992, *Opt. Quantum Electron.*, **24** , S379.
[3] T.J. Cloonan, 1993, *IEEE J. Quantum Electron.*, Vol. 29, **2** , 619.
[4] H.S. Stone, 1971, *IEEE Trans. Computers*, Vol. C-20, **2** , 153.
[5] C.W. Stirk and R.A. Athale, 1988, *Appl. Opt.*, Vol. 27, **9** , 1271.
[6] B.S. Wherrett et al., 1992, *SPIE Proceedings on Optical Computing*, Vol. 1806, 333.
[7] M.R. Taghizadeh and J. Turunen, 1992, *Optical Computing and Processing*, Vol. 2, **4** , 221.
[8] P. Lall and S. Bhagath, 1993, *Solid State Technology*, 65.
[9] S. Prince et al., 1994, *submitted to Optical Computing OC94, Edinburgh.*
[10] M.P.Y. Desmulliez and B.S. Wherrett, 1994, *submitted to Optical Computing OC94, Edinburgh.*
[11] A.L. Lentine and D.A.B. Miller, 1993, *IEEE J. Quantum Electron.*, Vol.29, **2** , 655.

Low-Loss and High-Speed Optical Switching Modules for 1.3 μm Wavelength Using Active-Matrix Ferroelectric Liquid Crystal Devices

Seiiti Shirai, Tadashi Serikawa, Shigeto Kohda, Nobuhiko Kakuda,
Masamichi Okamura and Noriyoshi Yamauchi

NTT Interdisciplinary Research Laboratories
3-9-11, Midori-cho, Musashino-shi, Tokyo 180 Japan
Tel: +81-422-59-2942, Fax: +81-422-59-3870

Abstract

A highly efficient optical coupling system using microlens arrays for free-space optical switching networks was proposed and demonstrated. High speed(<100 μs) and high extinction ratio for 1.3 μm wavelength were obtained by a newly proposed ferroelectric liquid-crystal driving method.

1. Introduction

Two dimensional optical switching devices consisting of liquid-crystal cell arrays and birefringent plates have many advantages for use in large-scale and transparent optical switching networks. We have demonstrated the successful operation of an 8-stage optical concentrator using 1024-input-ports optical beam shifter modules for visible light.[1],[2] To use this type of module for optical communication networks, good performance for long-wavelength, highly efficient fiber-to-fiber coupling and high speed switching operation are required. This paper describes the new optical design for low-loss interconnection and a new method of driving high speed ferroelectric liquid-crystals(FLC).

2. Optical design for fiber interconnection

Figure 1 shows an example of N×N optical switching network.[3] The distance between input and output fiber arrays is several tens of centimeters because the system consists of the cascaded optical beam shifter modules. The beam expansion due to diffraction results in very large increases of the coupling loss and limits the size of switching networks.

Figure 2 shows the newly proposed configuration of lenses for low-loss propagation. Figure 2(a) shows the confocal lens system, which consists of a very short focal length lens and a long focal length lens, to obtain long collimation distances. Figure 2(b) shows the relay lens with long focal length for compensating beam expansion. The number of relay lenses depend on the size of switching system. Relay lenses can compensate the beam expansion. Figure 3 shows the changes of beam radius along the propagation direction in Fig.2(a) using a ball lens(f=0.57 mm) and sputter-liftoff microlens(f=25 mm) in Fig.4. Microlenses was fabricated by sputter deposition using a shadowing effect.

Figure 5 shows the experimental configuration of a polarization independent switching system. On the input side, an input beam is separated into two components, an ordinary-ray and an extraordinary-ray. These beams go through the two adjacent cells in each optical beam shifter. At the final stage, the polarization of each beam is controlled and the beams are combined into one non-polarized beam. Optical beam shifter modules with 990 μm cell size and 350 μm aperture radius are used. Two long focal length lenses, ML1(f=150 mm) and ML2(f=25 mm), are very effective for highly efficient optical coupling between an input fiber and an output fiber array.[4] Very low total insertion-loss of 8.7 dB was obtained for four output ports. This value proves the accurate coupling to output fibers in spite of very long propagation span of 424 mm.

3. High speed optical switch for 1.3 μm using FLC

Ferroelectric liquid-crystal is a very attractive material for high speed operation, which is two to three orders higher than that of twisted-nematic liquid-crystal. But, there are two main problems to solve in adapting it to optical switching devices for long wavelengths. To obtain the high extinction ratio, the cell gap is required to be two times thicker than that for visible light. This thicker gap reduces the FLC memory effect. The ordinary bipolar driving method is not adequate for optical switching because of short break of optical signal by reset pulse.

To overcome these problems, we developed a new driving method for FLC optical switch. An active-matrix driving method with the voltage waveforms shown in Fig. 6 was used. The unipolar data driving pulse can prevent a short signal-break. The low voltage part of the pulse can sustain the cell data without losing reliability and the high voltage part of one pulse results in high speed switching and high extinction ratio. In Fig.7, high extinction ratio (>30 dB) and low insertion-loss(<1 dB) were obtained at 1.3 μm wavelength. High speed switching operation(<100 μs) was confirmed. This value is two orders faster than that of twisted-nematic liquid-crystal.

4. Conclusions

We proposed a new configuration microlens system for high optical coupling and experimentally demonstrated low propagation loss. An FLC driving method for optical switch in optical communication networks was newly proposed. High speed operation and high extinction ratio were obtained using this new method. These optical switching modules are applicable to large scale free-space optical switching networks.

(1)S.Shirai et.al.;PS'92,2A6,Minsk,1992.
(2)M.Yamaguchi et.al.;PS'92,1A5,Minsk,1992.
(3)M.Yamaguchi et.al.;NTT REVIEW,5,p62,1993.
(4)K.Koyabu et.al.;OFC/IOOC'93 Tech. Dig.,TuB2,1993.

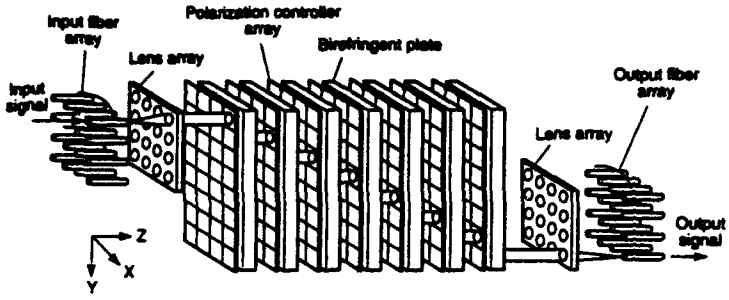


Fig.1 N × N free-space optical switching network.

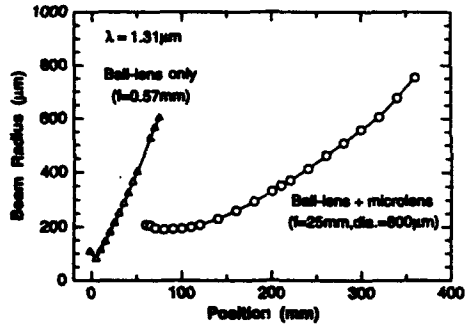
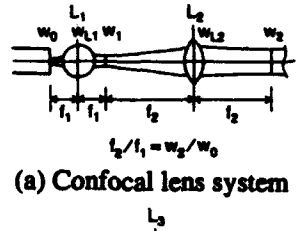
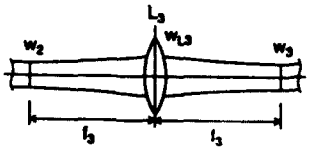


Fig.3 Propagation profiles for collimation lens system.



(a) Confocal lens system



(b) Relay lens

Fig.2 Microlens configuration for long-span beam propagation.

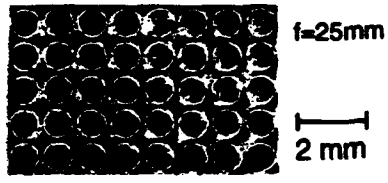


Fig.4 Photograph of sputter-liftoff microlens array.

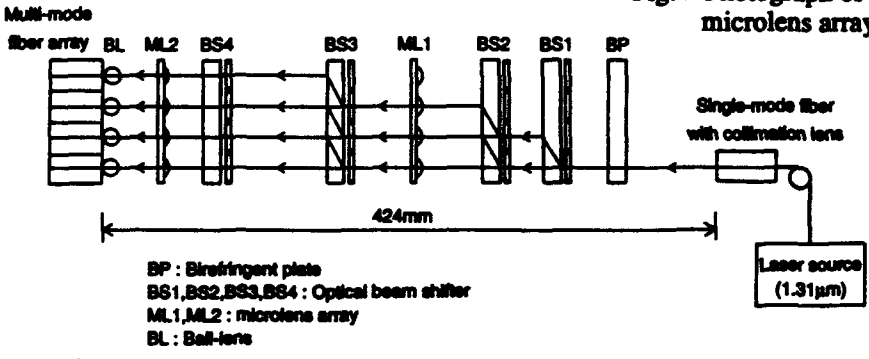


Fig.5 Experimental set-up for fiber-to-fiber coupling using 1× 4 optical switching network.

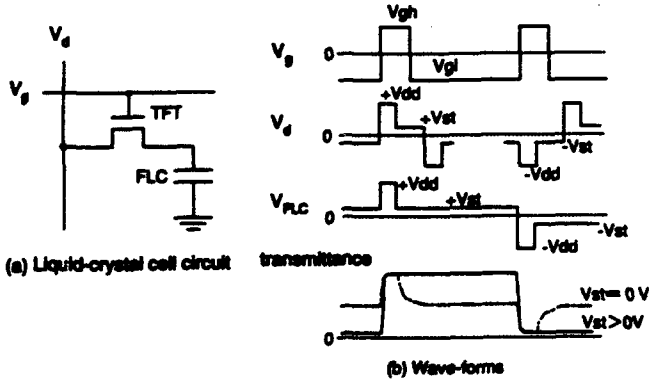


Fig.6 New driving method for ferroelectric liquid-crystals.

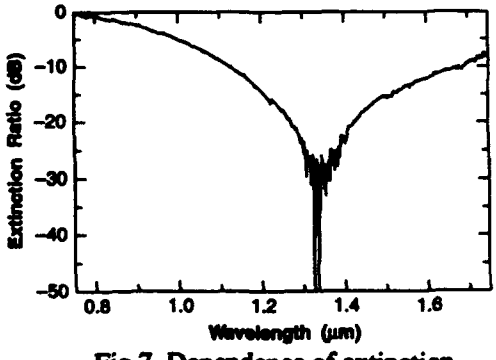


Fig.7 Dependence of extinction ratio on wavelength.

Dynamic Free Space Optical Interconnections Using Liquid Crystal Micro Optical Beam Deflectors

Katsuhiko Hirabayashi, Tsuyoshi Yamamoto and Masayasu Yamaguchi
NTT Communication Switching Laboratories
9-11, Midori-cho 3-chome Musashino-Shi, Tokyo 180 Japan
TEL:+81 0422-59-4812, FAX:0422-59-2473

Abstract

Micro-optical beam deflectors with a high transmittance of 95%, a large deflection angle of 15° , and with a structure of liquid crystals sandwiched by microprism plates are used in free-space optical interconnections and optical switches.

Introduction

Various kinds of optical beam deflecting devices such as holographic diffraction cells[1-3] have been developed for dynamic free space optical interconnections. However they have the drawbacks of low efficiency, low beam steering angle, undesired high order diffraction peaks and the limited wavelength range. The liquid crystal (LC) microprism array, which is an LC cell sandwiched between substrates that have notches, was originally developed by Sato et al[4]. We have improved these for microbeam optical interconnections, and achieved high transmittance of 95% and high deflection angle of 15 degrees. We have also developed optical interconnections and free-space optical switches that use these interconnection. .

Device structure and principle of beam deflection

The structure of the LC microprism array is shown in Fig. 1. It is a homogeneously aligned nematic LC cell. Micro prisms with a pitch of 250 μm are fabricated on one transparent plate, which is then covered with a transparent indium tin oxide (ITO) electrode. The input optical beam is refracted at the prism plane according to Snell's law. When voltage is applied, the LC molecules are realigned and the refractive index varies from n_e to n_o. Thus the deflection angle changes with applied voltage. Larger deflection angle can be obtained by using an LC with larger refractive anisotropy. The dependence of beam deflection angle on applied voltage is shown in Fig. 2. For the apex angle ϕ of 40° the deflection angle was 15 ° The transmittance was 95%, independent of the applied voltage.

Reconfigurable optical interconnections

We used the LC microprism array beam deflectors in optical interconnections between 2-D optical switches as shown in Fig. 3(a). We used 2-D fiber arrays (8x8) with a pitch of 250 μm for the input and a CCD camera for the output. The results for crossing optical beams are shown Fig. 3(b).

Free-space optical switch

Two crossed LC microprism arrays, between which a λ/2 plate is inserted, can also be used as a free-space optical switch as shown in Fig. 4(a). 1x9 switching is demonstrated in Fig. 4(b). The optical beam can be deflected to any point within an area of 5 mm x 3.8 mm on a plane 30 mm from the LC microprism deflectors.

Summary

Micro optical beam deflectors (LC microprism arrays) were developed for reconfigurable free-space optical interconnection and electrical alignment of optical beams. These devices can deflect closely spaced optical beams individually to any position with high transmittance of 95%, high deflection angle of 15° and low voltage of 3V. Reconfigurable optical interconnections and various optical networks can be achieved simply by changing the voltage applied to each miroprism array. Furthermore the LC microprisms were also shown to be useful for large-scale free-space optical switches.

Acknowledgments

The authors wish to thank Dr. Susumu Sato of Akita university for providing the cells and helpful discussions.

References

1. F. B. McCormick, T. J. Cloonan, F. A. Tooley, A. L. L. Lentine, J. M. Sasian, J. L. Brubaker, R. L. Morrison, S. L. Walker, R. J. Crisci, R. A. Novotny, S.J. Hinterlong, H. S. Hinton and E. Kerbis, Appl. Opt., 32, pp.5153-5171,(1993)
2. G. Paullat, J. P. Herriau, A. Delboulbe, G. Roosen, and J. P. Huignard, J. Opt. Soc. Am. B2, 306-314 (1986).
3. E. Tervonen, A. T. Friberg, J. Westerholm, J. Turunen, and M. R. Taghizadeh, Opt. Lett., 16, 1274-1276 (1991).
4. S. Sato T. Nose, R. Yamaguchi and S. Yanase, Liquid Crystals, 5, 1435-1442 (1989).

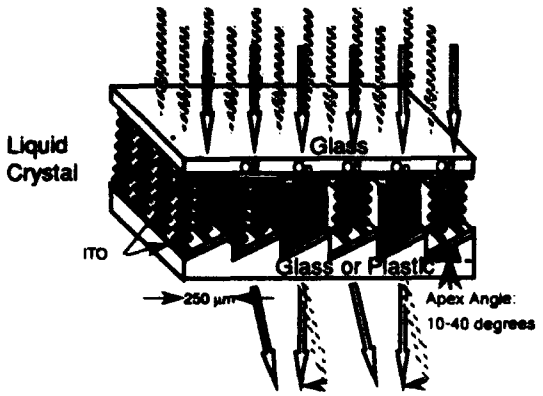


Fig. 1 Structure of the LC microprism array

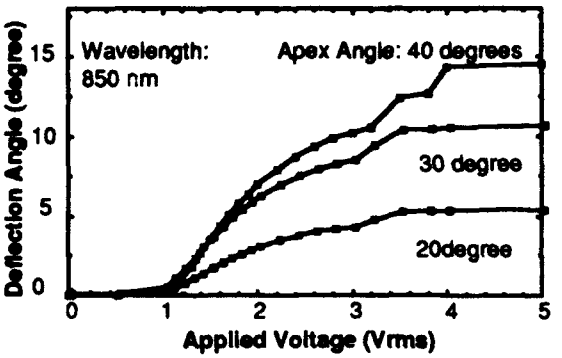
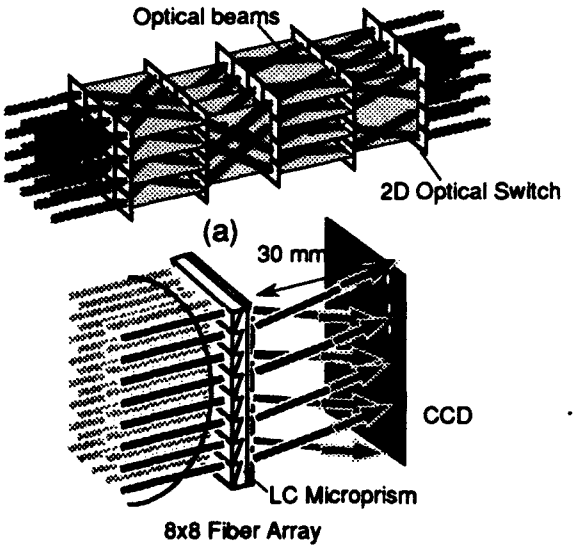
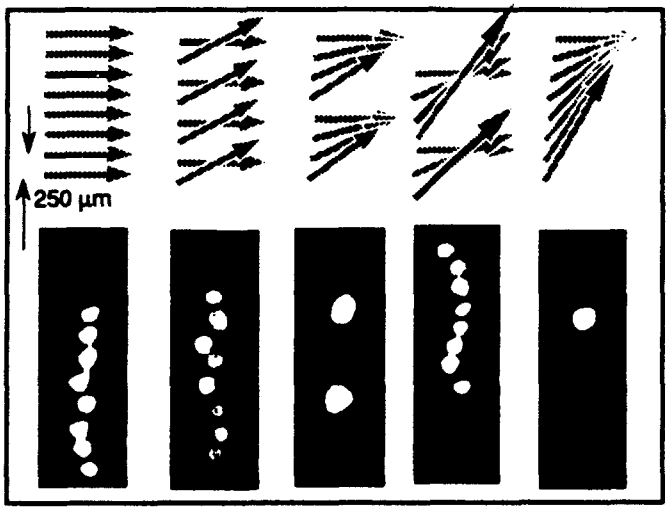


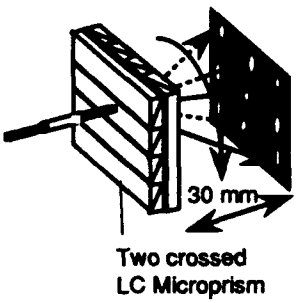
Fig. 2 Dependence of the deflection angle on applied Voltage



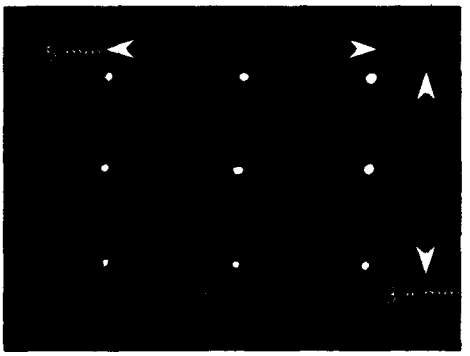


(b)

Fig. 3 Optical interconnection by the LC microprism array



(a)



(b)

Fig. 4 Optical beam switching by the LC microprism

Liquid Crystal Over Silicon Spatial Light Modulators

Douglas J. McKnight,[1] Kristina M Johnson
Optoelectronic Computing Systems Center,
University of Colorado at Boulder
Optoelectronic Computing Systems Center
Engineering Building
Campus box 525
Boulder, Colorado 80309-0525
(303) 492 0958

Gary D Sharp and Roylnn A Serati
Boulder Nonlinear Systems
1898 South Flatiron Court
Boulder, Co.

Abstract

This paper describes our recent liquid crystal on silicon spatial light modulators. We will present the most recent results from our 256 by 256 binary reflection mode SLM and our 128 by 128 analog SLM.

Introduction

Liquid crystal on silicon spatial light modulators are made by placing a thin layer of liquid crystal directly on top of a silicon chip. For a recent review of this technology see, for example, reference [1]. We have constructed a 256 by 256 binary SLM for application in an optical correlator which uses a ferroelectric liquid crystal as the light modulating layer. We are also in the process of constructing an analog SLM.

The 256 by 256 binary SLM

The SLM is based on a 7mm by 7mm CMOS die fabricated by US2 under a 1.2 micron design rule. The active array area is a square approximately 5.53mm on a side. Each pixel in the array is addressed by a row select wire and a column data wire. The row wire activates the pixel transistor gate and the column wire presents a binary data signal to the pixel. On activation of the gate wire the data on the column wire is written to the pixel, where it is capacitively stored. The resulting electric field between the pixel mirror and a transparent electrode on a piece of cover glass drives the liquid crystal into the desired state.

Data are transferred to the SLM over 32 parallel lines under the control of a master clock and a frame sync signal. We have demonstrated the addressing of the SLM with a master clock frequency of 48MHz which gives an image refresh rate of 23.5kHz. This is data rate of 1.6Gb/s from the driver board to the SLM. To achieve these data rates the SLM backplane utilised on-chip clock and control signal generation and data pipelining.

The most important design criteria for the correlator application were the optical efficiency and the frame rate. In a correlator which uses identical SLMs in the input and Fourier planes, the amount of power in the output is proportional to the fourth power of

[1]Currently a visiting scholar from Heriot-Watt University, Edinburgh, Scotland

the flat fill-factor. The use of minimum geometry polysilicon wires for the pixel gates helps maintain the fill-factor, but requires us to take account of the relatively slow propagation of gate signals across the array. The control circuits within the chip are designed to start activating the gate line for a row simultaneously with the data input for that row. This data is then maintained on the column data wires while simultaneously the gate line is taken low, the new data is loaded into the shift register and the next gate line is driven high. This scheme allows us to present the frame of data as a continuous stream without interruptions to wait for the gate lines to switch.

Results

The fabricated chips have been packaged and bonded. Electrical testing shows that the shift registers and clock generation circuits function as designed. A cover-glass was fixed over the pixel array, spaced with polyimide balls, and the gap filled with BDH SCE13 liquid crystal by capilliary action under vacuum. The liquid crystal was aligned by means of a rubbed PVA layer on the cover glass. Measurements of the optical properties of the SLM show that the optical switching speed of the liquid crystal is 50μs (10% to 90% and 90% to 10%) and the zero-order contrast ratio is 70:1. The imaged contrast ratio was measured to be 10:1. The device specifications are summarized in the table below.

Two of these SLMs have been used in an optical correlator as input and Fourier plane devices operating in a binary phase mode. The system was operated at 1000 correlations per second, i.e. a positive input and filter pattern were written for 500μs, followed by their inverses for 500μs. The camera shutter was set at 1ms to capture the output from both true and inverse frames. On and off-axis inputs consisting of small targets that used 0.6were used. With the laser producing approximately 5mW the correlation peaks in the output were able to saturate the camera and yield a signal to noise (pk/rms) of greater than 10dB for most of the images.

Array size	256 by 256
Pixel Pitch	21.6μm
Fill-factor	79%
Flat fill-factor	60%
Diffraction efficiency	15%
Throughput into zero order	3.4%
Demonstrated frame load time	43μs
Simulated frame load time	27μs
Contrast ratio	70:1 (10:1 imaged)
LC switching time	50μs

The 128 by 128 analog SLM

We are in the process of constructing an analog SLM with a 40μm pixel pitch. Results from this device will be presented at the meeting.

References

[1] K.M. Johnson, D.J. McKnight and I. Underwood. "Smart Spatial Light Modulators using Liquid Crystal on Silicon". Journal of Quantum Electronics, special issue on Smart Pixels, Vol. 29 No. 2 p699 Feb. 1993

Electronically Adressed Ferroelectric Liquid Crystal over Silicon Spatial Light Modulators

D.C. Burns, I. Underwood, A. O'Hara† and D.G. Vass†

Department of Electrical Engineering († Dept of Physics)
The University of Edinburgh, Edinburgh EH9 3JL, UK.
tel +44 31 650 5652, fax +44 31 650 6554, email slm@uk.ac.ed.ee

Abstract

We discuss recent advances in the design and fabrication of electronically addressed ferroelectric liquid crystal over silicon spatial light modulators. We summarise the prospects for further advances in the near future.

BACKGROUND

The Spatial Light Modulator (SLM) is a key component in many optical computing systems. The SLM technology of Ferroelectric Liquid Crystal over Very Large Scale Integrated (FLC/VLSI) silicon has matured considerably over the past few years. Electronically Addressed SLM's (EASLM's) of medium resolution (128^2 pixels or more) have been reported by several labs [1]; systems containing multiple devices have been reported [2]. We are now designing custom devices with system-specific performance characteristics.

INTRODUCTION

FLC/VLSI SLMs are produced by sandwiching a thin layer of FLC between a custom designed silicon backplane and a cover glass coated on the inside with a transparent conductive electrode. Most EASLM backplane designs are based on a pixel circuit consisting of one active element - a Metal-Oxide-Semiconductor Field Effect Transistor (MOSFET) which acts as a switch to control the amount of charge stored on a capacitive storage element - a small metal mirror on the surface of the silicon. The voltage thus generated produces an electric field which alters the state of a thin overlying layer of FLC to produce a binary phase or amplitude modulation in an incident wavefront.This scheme provides the smallest possible pixel and thus the highest density of pixels; it is analogous to the purely electronic Dynamic Random Access Memory (DRAM) cell. This type of pixel suffers from light induced charge leakage which is manifest as a reduction in contrast ratio with incident light intensity thus limiting the maximium light level at which it can be operated. There is also a limit to the spontaneous polarization, P_s, of the FLC material which can be used - the pixel capacitor must store enough charge to switch it. The drive to reduce the pixel size is compromised by the need to maintain an optically-flat metal area to act as the reflective aperture (or mirror). Underlying circuit elements such as transitors or interconnect cause undulations in the overlying part of the mirror; these can cause non uniform optical contrast across a mirror, losses due to scattering and, in coherent systems, phase variations. A flat fill factor (flat mirror area / pixel area) of around 25% has become a de facto minimum.

CURRENT DESIGNS

We have previously reported a 176 x 176 DRAM-type pixel array [3] .The frame rate was limited by the RC time constant of the relatively high resistance polysilicon row access lines. A 512 x 512 pixel array based upon the original 176 x 176 device has been designed. The primary modification has been the use of aluminium to replace the polysilicon row access lines within the pixel array. The finished design has been fabricated by Austria Mikro System and is undergoing electrical testing.

An alternative to the single transistor pixel design above is based around an enhancement of the six transistor Static RAM (SRAM) cell. The enhancement involves inserting a simple logic gate between the memory and the mirror. This allows some of the addressing requirements of the FLC to be met more easily. The SRAM design overcomes all of the above disadvantages of the DRAM pixel at the expense of increased transistor count leading to increased pixel area and decreased chip yield. In particular it maintains its state indefinitely, allows the use of the fast-switching, high P_s, FLC materials and shows no variation of contrast ratio with incident light intensity over a wide range of input intensity. We have demonstrated a fully working 256 x 256 pixel array built in 1.2um CMOS technology. We have also demonstrated the principle of grey scale on this binary device by means of temporal multiplexing of sequential frames.

SILICON FABRICATION ISSUES

We have succesfully applied a post-processing backplane planarisation technique to the 176 x 176 DRAM device which has allowed a flat mirror to be placed on top of the existing circuitry. The technique involves the deposition of a thick dielectric layer which is subsequently polished flat; this allows the deposition of a further metal layer which forms a flat mirror covering almost the entire pixel. The planarisation technique is described in detail elsewhere [4]. LC cell construction has been carried out succesfully on planarised backplanes. The increased flat fill factor of the backplane increases the light throughput of the finished SLM and reduces the stray light reaching the substrate.

SUMMARY AND FORWARD LOOK

Table 1 summarises the current situation. High resolution devices, based on both DRAM and SRAM pixels, have been demonstrated. The pixel designs lend themselves to use in different applications areas. The planarisation process, which significantly enhances device performance, has been demonstrated on one design. It is, in principle, equally applicable to all of the devices of Table 1. (Clearly, to be optically useful, the 512 DRAM device requires to be planarised.)

Given the current (minimum feature size and maximum die size) limitations of using commercial silicon vendors it should be possible to pursue the DRAM technology to 1024 x 1024 and the SRAM to 512 x 512 with frame rates comparable to, or better than, those of Table 1. Beyond that there is a likely need for access to specialised memory fabrication processes.

Device	176 DRAM	512 DRAM[1]	16 SRAM[2]	50 SRAM	256 SRAM
Date	1989	1994	1986	1988	1994
Silicon process	3μmCMOS	3μmCMOS	2μmCMOS	1.5μm nMOS	1.2μm CMOS
Pixel pitch (μm)	30	30	200	72	40
Nominal Mirror size (μm^2)	235 (not square)	145 (not square)	110 x 110	40 x 40	19 x 19
Mirror size (μm^2) after planarization	26 x26	26 x26	196 x 196	NA	36 x 36[3]
Flat fill factor[4] (%) before / after planarisation	26 / 75	16 / 75	30 / 96	31 / NA	23 / 81
Approx electronic address time (μs)	250	1000	1	NA	85
Frame rate (Hz)	1000	250[5]	5[6]	20[6]	4000

[1] undergoing electronic testing at time of writing
[2] currently undergoing re-design from NMOS to CMOS
[3] planarization not yet completed
[4] does not include deductiond for contact or via holes
[5] predicted from SPICE simulations
[6] measured using slow nematic liquid crystal

Table 1. Summary of silicon backplanes for FLC/VLSI EASLM's

REFERENCES

1. K.M. Johnson, D.J. McKnight, I. Underwood, "Smart spatial light modulators using liquid crystals on silicon", IEEE Journal of Quantum Electronics, Vol 29, 699-714, 1993.
2. R. Turner, D.A. Jared, G.M. Sharp and K.M. Johnson, "Optical correlator using very-large-scale integrated circuit / ferroelectric liquid crystal electrically adressed spatial light modulators", Appl. Opt. Vol 32, 3094-3101, 1993
3. I. Underwood, D.G. Vass, R.M. Sillitto, G. Bradford, N.E. Fancey, A.O. Al Chalabi, M.J. Birch, W.A. Crossland, A.P. Sparks, S.G. Latham, "A high performance spatial light modulator", Proc. S.P.I.E., Vol 1562, 107-115, 1991
4. A. O'Hara, J.R. Hannah, I. Underwood, D.G. Vass and R.J. Holwill, "Mirror quality and efficiency improvements of reflective mode spatial light modulators by the use of dielectric coatings and chemical-mechanical polishing", Appl. Opt., Vol 32, 5549-5556, 1993.

Application of Optical Multiple-Correlation to Recognition of Road Signs

Katsunori Matsuoka, Masaki Taniguchi, and Yoshiaki Mokuno

Osaka National Research Institute, AIST,MITI
1-8-31 Midorigaoka, Ikeda, Osaka 563, Japan
Phone:+81-727-51-9534 FAX:+81-727-51-9631

Abstract

Two kinds of optical pattern recognition methods based on multiple correlations are applied to actual scenes. The ability of those methods to locate multiple objects is discussed. The results of computer simulations are also presented.

Summary

Optical system based on a optical correlator has the ability to perform fast pattern recognition and such fast operation is just needed in machine vision system. To evaluate the ability of optical system for machine vision, we have attempted to apply optical multiple correlation methods to some actual scenes.

Pattern recognition, we intend, is described in the three steps; locating all multiple objects in the input, zooming one of the object images up to the appropriate size, and understanding the meaning of zoomed object. We focus here on achieving the first step, locating objects, by optical correlators, which step is important and basic for other steps.

Two procedures, monochromatic processing and color processing, were applied to some actual scenes obtained around the street crossings. These test scenes have individually different image complexities in their backgrounds. One of them is shown in Fig.1 (a). In these scenes, the objects are road signs. To perform shift-invariant and size-invariant processing, we made the procedures based on multiple correlation by using the well-known correlation filters such as a synthetic discriminant function (SDF) filter[1] and a minimum average correlation energy (MACE) filter[2] as described in the following. They can be realized optically by using optical multiple-correlator.

1. Monochromatic Processing

Both of SDF filters and MACE filters have been applied to actual scenes. The filters are designed to discriminate 6 kinds of road signs by using 33 training patterns and to catch 14 different sizes of objects. Each of filters catches one kind of road sign with two different sizes. The processing procedure is described as follows: the input image is firstly correlated with all filters by the multiple-correlator; the correlation patterns are binarized to pick out the correlation peaks by a threshold device; and finally they are added. Bright spots in the final image denote the locations of objects.

The result of computer simulation by applying MACE filters to the scene of Fig.1 (a) shows that all three objects inside the scene can be picked up but many false signals are produced by

background image such as trees. In other results, all objects could not perfectly detected in many cases and many false signals appeared.

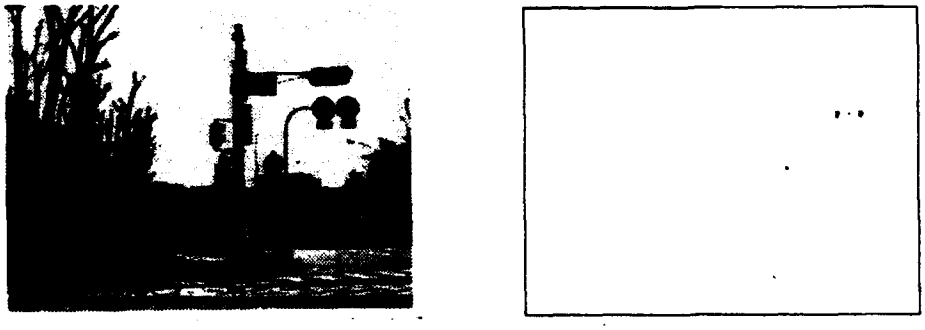
2. Color Processing

To improve the above procedure, we introduced a color processing, which achieves individual spatial filtering on red (R), green (G), blue (B), and gray (W) components of original polychromatic image. We choose the color components in the domain of chromaticity coordinates as a vector (2, -1, -1) for R component, (-1, 2, -1) for G, (-1, -1, 2) for B, and (1,1,1) for W. It can be realized optically to separate an input image to the color components.

In this processing, the filters designed for each color component of object are applied to the corresponding color component of input image (component processing) in the same manner as in the monochromatic processing. Final result is obtained by executing AND operation on all results from component processings, that means final signals denoting the object locations will appear only when all component processing detect objects in the same locations of the inputs.

Figure 1 (b) shows the result of computer simulation by applying this processing to the image of Fig.1 (a). The SDF filters are used and they are designed in the same condition as described in monochromatic processing except for using the color components as the training images. Three objects are perfectly located without false signals in this case.

Other simulations denotes the color processing yielded always good results compared with the case of monochromatic processing. But the color processing also produced false signals when the background of input image has heavy complexities and it is a large drawback to be overcome now.



(a) (b)

Fig.1 Results of computer simulation to locate the road signs: (a) shows original scene and (b) is the result obtained by color processing. The brightness of (b) is reversed.

References

1) D.Casasent, "Unified synthetic discriminant function computational formula," Appl. Opt. 23, 1620(1984).

2) A.Mahalanobis, B.V.K.Vijaya Kumar, and D.Casasent, "Minimum average correlation energy filters," Appl. Opt. 26, 3633(1987).

Parametric Design of Correlation Filters for Multiple-object Discrimination

Masaki Taniguchi and Katsunori Matsuoka

Osaka National Research Institute, AIST, MITI
1-8-31 Midorigaoka, Ikeda 563, Osaka, JAPAN
TEL: +81-727-51-9534 FAX: +81-727-51-9631

Abstract

We propose a new algorithm to design multiple-object discriminant correlation filters. This technique makes it possible to control the sidelobe levels of the filter with considering the dynamic range of recording medium.

Summary

The technique of using optical correlators for optical pattern recognition has been well studied. To obtain high performance of recognition, it is necessary to use optimum correlation filters suitable for an object of recognition. We studied an algorithm to design correlation filters for pattern recognition in the presence of distortions or for multiple-object pattern discrimination. As this type of correlation filters, the Synthetic Discriminant Function[1] (SDF) filters are well known. The main feature of SDF is that we can specify the correlation values for training patterns used to calculate the function. Some filters, which can be regarded as modifications of SDF, are proposed to suppress sidelobes and produce sharp correlation peaks.

However, the output correlation values for the sidelobe-suppress filters are very sensitive to distortion of input patterns. The request for sharpness of correlation peaks and the distortion invariance may conflict. Therefore we should be paid attention to the equilibrium of them.

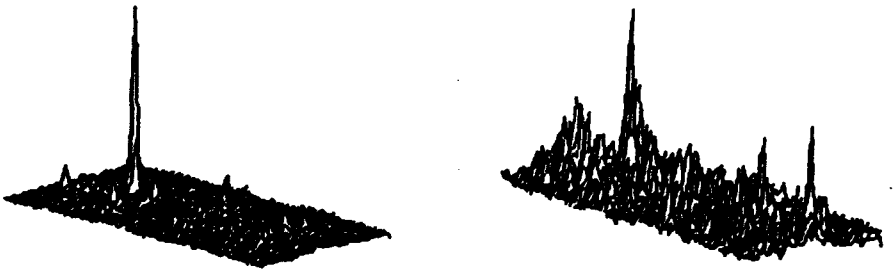
In addition, the filters have wide range and gentle gradation, in general. So, it is difficult to record the filter function correctly on a medium. The incorrect recording may detract from the correct discrimination.

To solve these problems, we have tried to calculate the correlation filter functions parametrically by using the optimization algorithm. We set up a cost function, which is a weighted summation of some feature values calculated from the filter function. As the feature values, we use the correlation energy, squared error between correlation value and specified one at the origin, and variance of filter function values. We regard these values as the sidelobe level, the accuracy of specification of correlation values, and the tolerance for distortion of input pattern, respectively. By adjusting the weight coefficients, it can be possible to control the characteristics of filter. The dynamic range of recording medium is

used as the constraint in optimization. By using an optimization algorithm, the filter function which gives the minimum value of the cost function can be obtained.

As the optimization algorithm, we have introduced the Simulated Annealing (SA) algorithm. We studied the case of recording multiple-object discriminant correlation filters as Lohmann type Computer Generated Holograms (CGHs) with discrete values of amplitude and phase components.

A computer simulation was performed to estimate the performance of the filter. We compared the filter to some other filters, such as SDF, the Minimum Average Correlation Energy[2] (MACE) filters, and their phase-only versions[3]. Figure 1 shows the example of simulation results. Figure 1 (a) is the cross-correlation pattern of the filter calculated by SA with a priority of suppressing sidelobes. The amplitude and phase components of filters are represented with 5 and 4 levels, respectively. It shows that the sharpness of the peak is excellent. Figure 1 (b) is of the MACE filter which components are quantized to the same levels. Computer simulation results shows that the algorithm makes it possible to obtain multiple-object discriminant correlation filters, which gives expected correlation response, on a discrete type recording medium. In addition, the correlation responses of the filters can be controlled parametrically.



(a) (b)

Figure 1. Typical correlation plane for (a) a filter by SA (b) a quantized MACE filter.

References

1. D. Casasent, "Unified synthetic discriminant function computational formulation," Appl. Opt., 23, 1620-1627 (1984).
2. A. Mahalanobis, B. V. K. Vijaya Kumar and D. Casasent, "Minimum average correlation energy filters," Appl. Opt., 26, 3633-3640 (1987).
3. J. L. Horner and P. D. Gianino, "Applying the phase-only filter concept to the synthetic discriminant function correlation filter," Appl. Opt., 24, 851-855 (1985).

Optoelectronic implementation of a phase-retrieval Vander-Lugt correlator.

Santiago Vallmitjana, Arturo Carnicer, Estela Martín-Badosa and Ignacio Juvells.
Universitat de Barcelona, Laboratori d'Optica, Dep. de Física Aplicada i Electrònica,
Diagonal 647, E-08028 Barcelona, Spain. Tel. +34-3-4021202.

An implementation of a Vander-Lugt correlator, which operates with a single spatial light modulator is proposed. Optical phase-retrieval manipulation, based on the simmetrization of the information, is required. Some experimental results are also presented.

In recent years, some authors have proposed the same compact correlation architecture[1-3] for different purposes. These setups are based on the use of a spatial light modulator (SLM) to introduce and display information; a Fourier lens system, a video-camera (CCD) to register light distributions and a computer that controls the whole system (see Figure 1). If the setup performs as a joint transform correlator, both the scene and the reference are displayed on the SLM and the CCD in the Fourier plane registers the joint interferences between them. This power spectrum is processed by a computer and displayed again on the same SLM. A second optical Fourier transform is obtained and the correlation is recorded by the CCD.

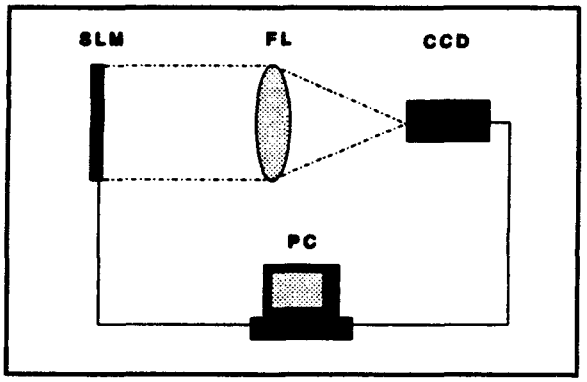


Figure 1: Single SLM architecture.

Kotzer et al. proposed in 1991 the use of the same architecture to implement Vander-Lugt correlators. The scene is shown on the modulator and its power spectrum is recorded by the CCD. To recover the phase, they obtained the joint interferences between the object and a plane wave. By processing these light distributions the phase can be retrieved. In a second step, the reference is handled in the same way. As a consequence, the correlation between the scene and the target is obtained.

In this communication we present an alternative to Kotzer's idea that simplifies the experimental procedure without lack of recognition capability. The idea of retrieving the phase lost in the recording process is based on the symmetrization of the images used (see Figures 2a and 2b). The images should be placed as close as possible, without superposition, in order to take advantage of the spatial bandwidth of the modulator. Let s(x,y) be the scene, and let $|S(u,v)|\exp(i\phi(u,v))$ be its Fourier transform; a is the separation between the original image and its symetric and f is the focal of the lens. In the conditions of Figure 2a, we obtain in the Fourier plane the following distribution:

$$S_F(u,v)=\left| |S(u,v)|\exp(i\phi(u,v))\exp(-i2\pi au/\lambda f) + |S(u,v)|\exp(-i\phi(u,v)\right|^2 \quad (1a)$$

We present two alternatives for performing pattern recognition. The first method consists in registering the power spectrum $|S(u,v)|^2$ and then computing digitally the subtraction $S_F(u,v)-2|S(u,v)|^2$. Finally, the result is binarized, which is equivalent in a first approximation to $S_b(u,v)=\cos(2\phi-2\pi au/\lambda f)$. The reference r(x,y) can be processed in a similar way and in the Fourier plane, the light distribution can be written as

$$R_F(u,v)=\left| |R(u,v)|\exp(i\theta(u,v)) + |R(u,v)|\exp(-i\theta(u,v)\exp(-i2\pi au/\lambda f)\right|^2 \quad (1b)$$

where $|R(u,v)|\exp(i\theta(u,v))$ is the Fourier transform of r(x,y). Recording $|R(u,v)|^2$, computing $R_F(u,v) - 2|R(u,v)|^2$ and binarizing we obtain $R_b(u,v)=\cos(2\theta+2\pi au/\lambda f)$. Finally, the product $S_b(u,v)R_b(u,v)$ is obtained,

$$S_b(u,v)R_b(u,v)=2\cos2(\phi+\theta) + 2\cos2(\phi-\theta+2\pi au/\lambda f) \quad (2)$$

If $\phi-\theta=0$, the second cosinus will perform two Delta-distributions in the correlation plane at points $x=2a$ and $x=-2a$.

A further simplification (method #2) can be obtained by binarizing the intensities (1a) and (1b) considering as threshold the median values of $S_p(u,v)$ and $R_p(u,v)$ and then computing the product of these binary distributions.

Figures 2a and 2b show the scene and the reference used as a test. Figures 3 and 4 show the optical detection of the reference using the architecture described in Figure 1. Figure 3 has been obtained following the first method and the correlation of Figure 4 corresponds to binarize equations (1a) and (1b) using the median value of these distributions.

As a conclusion, the use of single SLM architectures allow the simultaneous implementation of Vander-Lugt and joint transform correlators with similar recognition capabilities.

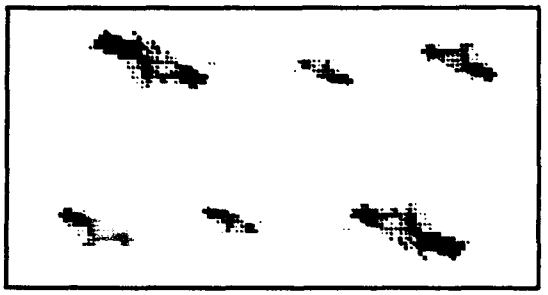


Figure 2a: Scene $s(x-a,y) + s(-x,-y)$.

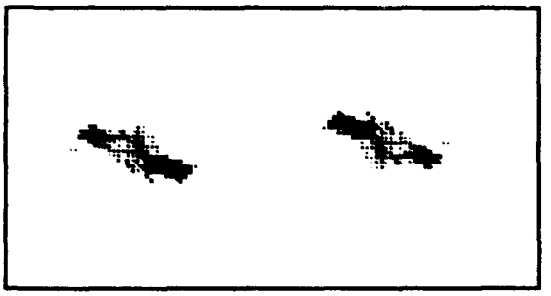


Figure 2b: Reference $r(x,y) + r(-x+a,-y)$.

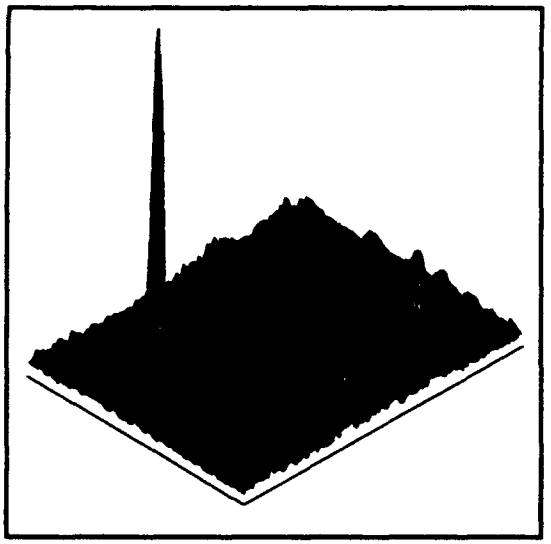


Figure 3: Optical correlation (method #1).

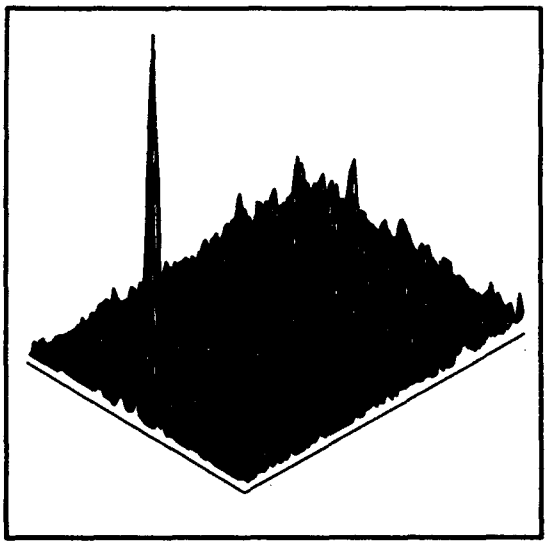


Figure 4: Optical correlation (method #2).

This paper has been supported in part by the Spanish CICYT (Comisión interministerial de Ciencia y Tecnología) project No. ROB91-0554.

1. B. Javidi and J. Horner, "Single spatial light modulator joint tranform correlator", Appl. Opt 28, 1027-1032 (1989).
2. T. Kotzer, J. Rosen and J. Shamir, "Phase extraction pattern recognition", Appl. Opt. 31, 1126-1137 (1992).
3 T. Kotzer, J. Rosen and J. Shamir, "Multiple-object input phase extraction correlation", Appl. Opt. 32, 1919-1932 (1993).

Performance Of An Acousto-Optic Joint Transform Correlator

C D REEVE
School of Electronic, Communication and Electrical Engineering
University of Plymouth
Drake Circus
PLYMOUTH, PL4 8AA 0752-232330

A W HOUGHTON
Department of Electrical and Electronic Engineering
Royal Naval Engineering College, Manadon
PLYMOUTH, PL5 3AQ 0752 553740 ext 81320

ABSTRACT

A joint transform correlator is described whose input is provided by two acousto-optic devices. It is shown that the system is capable of detecting and direction finding signals which are more than 10 dB below the noise level.

SUMMARY

A schematic diagram of the system is shown in Figure 1. It is a standard joint transform correlator [1] in which the inputs are provided by two acousto-optic (AO) cells and the square law detector is a spatial light modulator such as a liquid crystal light valve (LCLV). The lenses and spatial filter required to extract the first order light from the AO cells have been omitted for clarity.

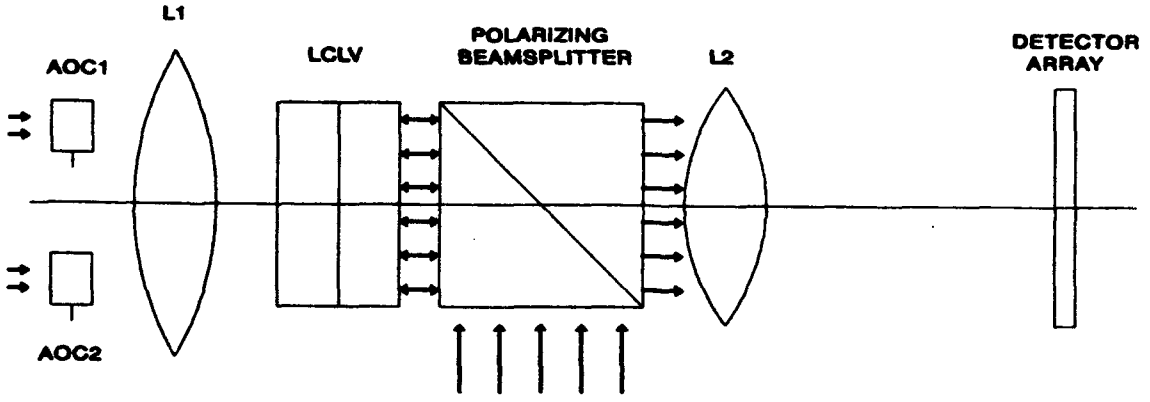


Figure 1. The acousto-optic joint transform correlator - schematic.

Taking the first order diffracted light from the AO cells as the input to the system the input function is of the form

$$o(x,t) = f(x-a-Vt) + g(x+a-Vt) \quad (1)$$

where f(t) and g(t) are the signals applied to the AO cells, V is the acoustic velocity in the cells and the separation of the cells is 2a. It is straightforward to show that if the Fourier transforms of f(x) and g(x) are written as $|F(u)|\exp\{j\varphi(u)\}$ and $|G(u)|\exp\{j\phi(u)\}$ respectively then the response of the square law detector at a given instant in time will be

$$|O(u)|^2 = |F(u)|^2 + |G(u)|^2 + |F(u)|\cdot|G(u)|\cos\{2ua + \varphi(u) - \phi(u)\} \quad (2)$$

Since the two signal are propagating at the same acoustic velocity the extra phase term due to the terms Vt in equation (1) will cancel out. The final term in equation (2) represents a set of sinusoidal fringes of spatial frequency 2a, amplitude modulated by the amplitude of the cross spectral density (CSD) of f(x) and g(x) and phase modulated by the phase of the CSD. Taking the Fourier transform of this fringe pattern optically from the read side of the spatial light modulator output enables us to obtain the cross correlation function of f(t) and g(t). The performance of the system has been modelled on the assumption that the inputs to the AO cells are from two independent receivers, a distance D apart, that receive the same signal but the noise in the two receivers is uncorrelated. Figure 2 shows a sample cross correlation output from the model. The time window of the AO cell was 50 μs, and the signal tested was a chirp of length 100 μs, with a centre frequency of 10 MHz and a bandwidth of 10 MHz. The noise bandwidth was 20 MHz and the signal to noise ratio was -12.5 dB. The cross correlation function was computed after integrating the cross spectral density on the spatial light modulator for 100 μs. The position of the correlation peak gives a measure of the time difference of arrival of the signal at the two receivers so that direction finding is possible as well as detection. The performance of the system is examined in detail and results are presented from a practical system.

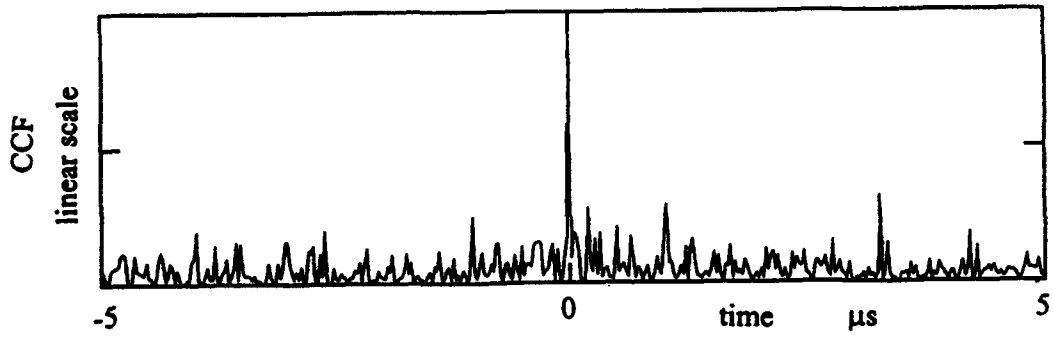


Figure 2. Sample cross correlation output from the model

Reference.

1. C.S. Weaver and J.W. Goodman. "A Technique for Optically Convolving Two Functions" Appl. Opt. 5, 1248 (1966).

A zeroth order non-hetereodyning space integrating acousto-optic correlator

A W Houghton Msc MIEE CEng,
Department of Electrical and Electronic Engineering, Royal Naval Engineering College, Manadon, Plymouth, PL5 3AQ, Tel: 0752 553740 ext. 81320

C D Reeve PhD MIEE CEng,
School of Electronic Communication and Electrical Engineering, Smeaton Building, University of Plymouth, Drake Circus, Plymouth, Tel: 0752 232330

Abstract

Both a theoretical analysis and practical results are presented for a non-heterodyning acousto-optic correlator that uses the zeroth diffraction order to produce a true correlation function containing both amplitude and phase information.

Summary

The structure of the zeroth order non heterodyning space integrating acousto-optic correlator is as shown in figure 1.

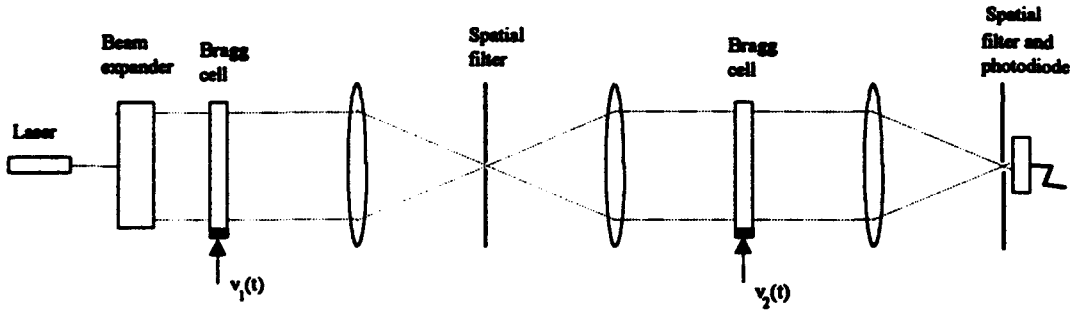


Figure 1. Physical structure of zeroth order space integrating acousto-optic correlator

The basic architecture is similar to many correlators previously described in the literature [1,2], but there are two important differences. The spatial filters select all or part of the zeroth diffraction order. Most correlators use the first order and some papers assume that the zeroth order contains no information. In reality, the zeroth order contains as much information as all the other orders put together, but it can be difficult to access due to large optical power incident on a photodetector causing saturation or excessive shot noise. However, it can be shown that the zeroth diffraction order has sub orders that can be used very effectively [3]. The second important difference lies in the way the signals are introduced into the acousto-optic cells. A common technique is to insert the signals as double sideband suppressed carrier modulation of a carrier at the centre frequency of the acousto-optic cell. The modulation used here is double sideband large carrier; the difference is crucial.

The operation of this correlator is as follows. One of the two signals to be correlated is inserted into the first acousto-optic cell as double sideband large carrier modulation of a carrier (For the TeO_2 cells used in the correlator built by the authors the carrier frequency is 45 MHz). At the optical output of the first acousto-optic cell the optical wavefront is phase modulated by the acoustic wave in the acousto-optic cell. The Fourier transform of this wave function is formed at the first spatial filter which

passes all of the zeroth diffraction order from the first cell onto the second acousto-optic cell. The combination of the spatial reversal of the first signal through the imaging process and time reversal of the second signal before injection into the second acousto-optic cell leads to the counter propagation of the signals required for correlation. The final lens forms the Fourier transform of the output from the second acousto-optic cell at the final spatial filter which selects out the first sub order of the zeroth diffraction order. It can be shown [4] that the photodetector, acting as a spatially integrating square law detector, then forms a true correlation function, containing both amplitude and phase information, which can be fed through a simple highpass filter directly to (e.g.) an oscilloscope.

The autocorrelation function for a linear chirp pulse, sweeping from 4.25 MHz to 5.75 MHz in 15 μs (BT = 22.5) using the correlator shown in figure 1, is shown in figure 2.

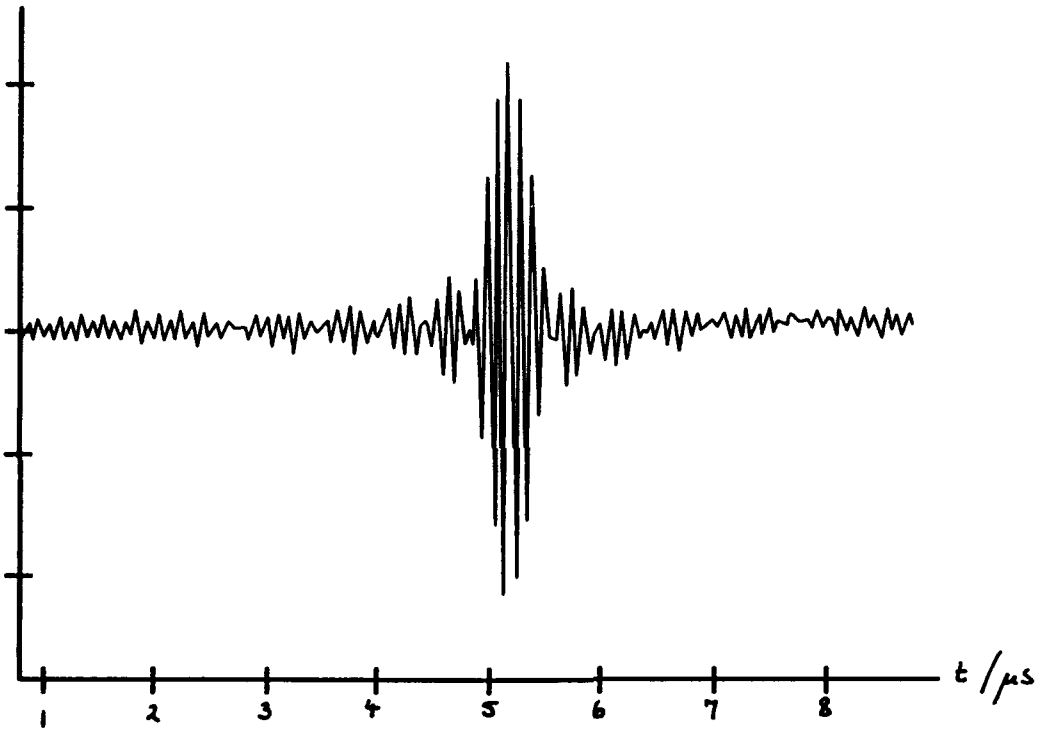


Figure 2. Autocorrelation of a linear chirp pulse produced by the correlator shown in figure 1.

References

1. Lee, J.N. and VanderLugt, A.: "Acoustooptic signal processing and computing", Proc. IEEE, Vol. 77, No. 10, October 1989.

2. Reeve, C.D. and Wombwell, J.F.: "Novel space-integrating acousto-optic correlator: amplitude and phase information from intensity only measurements", Proc. IEE, Vol. 136, Pt. F, No. 4, August 1989.

3. Houghton, A.W. and Reeve, C.D.: "The Raman-Nath acousto-optic interaction: information in the zeroth diffraction order", Royal Naval Engineering College Research Report No. 92033, December 1992.

4. Houghton, A.W. and Reeve, C.D.: "The theory of one dimensional space integrating acousto-optic correlators", Royal Naval Engineering College Research Report No. 93026, July 1993.

Edge Enhancement In Photorefractive Joint Transform Correlators

Olivier Daniel, Jean-Michel C-Jonathan and Gérald Roosen

Institut d'Optique Théorique et appliquée - Unité Associée au CNRS n° 14
Centre Universitaire d'Orsay, Batiment 503,
BP. 147, 91403, ORSAY CEDEX -FRANCE

Abstract

We show that edge enhancement is inherent to the photorefractive recording. Its effect in Joint Transform Optical Correlators is demonstrated and a computational model, valid for most input images, is given .

Summary

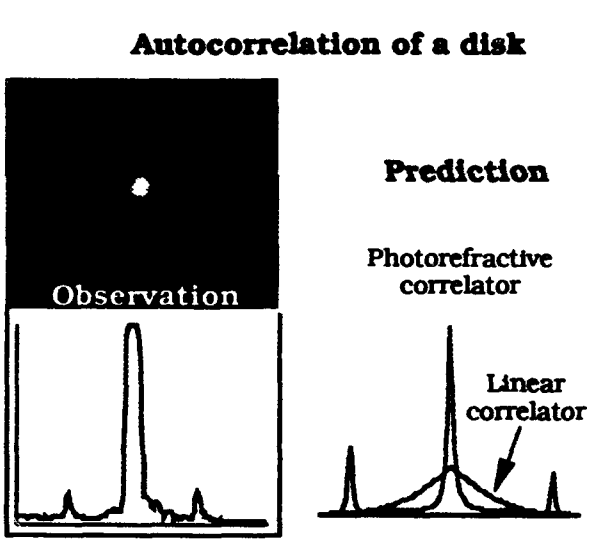
The improving availability of liquid crystal Spatial Light Modulators, and sensitive photorefractive materials makes possible the implementation of effective optical correlators using low energy laser sources. The Joint Transform Correlator (JTC) is well adapted to applications where the size of the correlator is an issue [1]. The purpose of this paper is to demonstrate some specific properties introduced by the response of the photorefractive crystal used in the Fourier plane, and to present a model that predicts their response in those particular experimental conditions.

The geometry of our experimental set-up is directly derived from that described by Rajbenbach & al [2]. The object to be recognized and the scene where it is expected are introduced in the input plane using a TFT nematic liquid crystal spatial light modulator illuminated by the collimated beam of a diode pumped doubled YAG laser. Their Fourier transforms o and s are formed by the same lens. The resulting distribution of intensity is recorded as a modulation of refractive index by a BSO crystal. It is observed using the 670 nm beam of a laser diode incident from the back at an angle adjusted to fulfill the Bragg condition. At that wavelength, the sensitivity of the BSO crystal is considered as negligible compared to that at the writing wavelength (532 nm), so that reading and writing may take place simultaneously . The Fourier transform of the amplitude distribution diffracted by the photorefractive grating is observed in real time in the correlation plane P_C, using a CCD camera.

Conventional models describe the build-up of the photorefractive effect under illumination by a one dimensional sinusoidal interference pattern of average illumination I_0 , modulation depth m and wave vector k. Assuming a uniform Io and a weak m, a space charge field is predicted whose steady state value E_{SC} does not depend on I_0 and is proportional to m . Through linear electrooptic effect, an index grating is formed with a modulation proportional to E_{SC}. For objects much smaller that their separation, the model still applies to the joint transform correlator. At steady state, the induced index modulation and the diffracted

amplitude are found to be proportional not to $o(r')s^*(r')$ as expected from a linear holographic recording but to $m(r')=o(r')s^*(r')/\left(I_d+|o(r')|^2+|s(r')|^2\right)$ where the term I_d describes the effect of the crystal's dark conductivity and stray light. This non linearity is typical of the Joint Transform Correlator. In a Vander Lugt correlator one of the terms would describes the reference plane wave. The value of its fluence would be chosen either to restore the linearity of the correlator or to cause edge enhancement[3]. This non linearity is illustrated by the correlation of two identical slits. The shape of the object only affects the local intensity I_0 that only determines the speed of the effect, while m equals unity all over the crystal. A quasi-uniform diffraction efficiency is then expected, that generates a sharp correlation peak located at the maximum of the correlation function and periodical side peaks caused by the zeros of the $sinc^2$ function. This non linear response causes amplification of the spatial frequencies of weak amplitude in the objects. In most cases, this gives rise to edge enhancement. However it is moderated by noise and the reading beam. Experimental evidences will be presented.

The model for the photorefractive effect fails when the spatial distribution of illumination varies rapidly on the crystal or is two-dimensional. It also fails to describe the case where the modulation of one grating locally becomes close to unity. A "whole beam method" has been recently proposed [4]. We show that it provides a simple analytical steady-state solution of the equations in the experimental conditions of the joint Fourier Transform correlator. It fully describes the edge enhancement in the correlator, including the effect of the reading beam which affects the width of the correlation peaks. It provides an accurate simulation of the correlator that will be illustrated.



These results are part of a contribution to the NAOPIA II Project, funded by the Commission of the European Community under the ESPRIT Programm for Research and Development.

References

[1] B. Loiseaux, G. Illiaquer, J.P. Huignard, Optical Engineering, Vol 24, n°1, pp.144-149, (1985).

[2] H. Rajbenbach, S. Bann, P. Réfrégier, P. Joffre, J.-P. Huignard, H.-S. Buchkremer, A.S. Jensen, E. Rasmussen, K.H. Brenner, G. Lohman, Appl. Opt.Vol 31,n°26. pp.5666-5674, (1992).

[3] J. Feinberg, Optics Letters, Vol 5, N°8, pp.330-332, (1980)

[4] M. Cronin-Golomb, Optics Communications 89 , pp. 276-282, (1992)

Optical matrix multiplication and its application in pattern recognition

Yansong Chen, Dehua Li, Shihai Zheng, Yuhe Zhang, Chengxinag Li

Institute of Physics, Chinese Academy of Sciences
Beijing 100080, China
Tel: 86-1-2559131x257, Fax: 86-1-2562605

Abstract

A 4*f*-type optical system for matrix multiplication is presented, and with the system the hybrid optical image processor is constructed for recognizing Roman letters, Arabic letters and some airplanes. The experiments are successful in the case of above input images undergoing shift and rotation.

Summary

Optical matrix multiplication is a basic optical computing operation, which is widely utilized in optical image processing and artificial neural network. In this paper, based on the study of optical general transformation, a 4*f*-type optical system for matrix multiplication is presented and with this system a hybrid optical image processor is designed and set up for pattern recognition. The system, shown in Figure 1, is consisting of two Fourier lenses and a holographic mask, by which the matrix inner-product multiplication proceeds in a nongearing manner and many matrix multiplication can be achieved by connecting several such systems in series. As an example, the inner products of 4×8 and 8×4 matrices are calculated, yielding results that are in agreement with theoretical values.

A hybrid optical processor constructed by the matrix multiplicator is designed for computing invariant moments of images in real time. Taking six capital Roman letters (C, F, G, H, J, L) as the input image the processor is tested for recognizing them. The experimental results show that a letter is of approximate values of invariant moment for its undergoing translation and rotation, and the moments of different letter are distinct enough for one to recognize them. Therefore an input letter can be recognized by extracting its invariant moments with the processor even if the letter taking shift and rotation.

With the matrix multiplicator the hybrid character recognition system is also designed and set up, which is composed of two parts, the image feature extractor and the inner-product correlator. The feature extractor draws 32 bits' information forming a vector from an input image and the correlator carries out inner-product of the vector with storage memory matrix. Ten Arabic figures from 0 to 9 and eight various airplanes as the input images are tested by the system. The experimental results show that, for printing Arabic figures and the eight airplanes, that are permitted to rotate an angle of 15°, the recognized ration reaches 100%, and for hand-writing Arabic figures about 70% of their recognition may be reached.

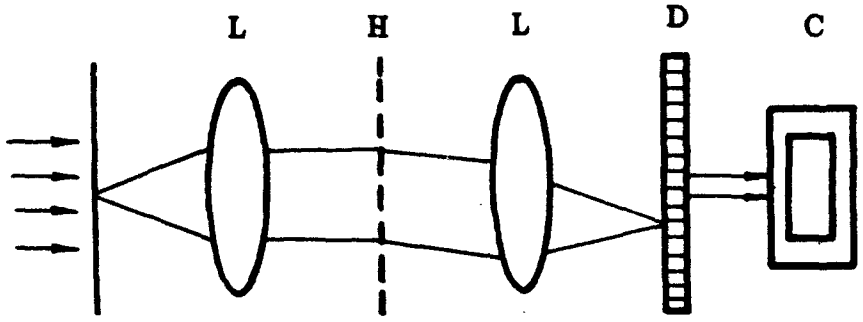


Figure 1 The schematic of non-gearing inner-product matrix multiplicator
L--lens, H--holographic mask, D--CCD, C--microcomputer

Precision optical correlator for the analysis of large format images with the computer processing of the results.

Korolkov A.V., Mosyakin Y.S., Pronkin G.I.
Science researce institute "KVANT"
125438 Moscow, Russia

We described the experimental results about construction and application the precision optical correlator for analysis of large format images with the computer processing of output fields for fast and precess determination of correlation maxima coordinates.

For the structural analysis of highly informative images, for example, astro- and aerial photography, we effectively use optical correlators /1/. For the solution of the task in precess determination of coordinates of correlation maxima for the analysis of large format images (180*180 mm) we have developed precision coherent optical correlator according to the scheme of Wander Lugt on the basis of optical Fourier processor with aperture 500 mm and resolution to 100 lin/mm, holographic registrator type HRS 1001 with the working area 40*40 mm and resolution to 1500 lin/mm, scanning photoreceiving units Eikonix 1000 (Kodak Co.) with the resolution of elements 4096*4096, conjugated with the computer IBM PC AT.

The output image of the correlation function, formed by the Fourier processor, is read by the scanning unit, digitized with the gradation number 256 and put into the computer for the digital processing. Realized so, algorithms permit to automatically determine the location of correlation peaks, increasing given by the operator threshold, independently of their dimensions and form and with regard for unevennes of the background, on which images are optically formed. Algorithms are optimized according to fast activity and permit to analyse one correlation field with information capacity 4096*4096*8 bit for the time during five minutes and writing results into the file and the possibility of depicting the map of location of detected correlation maxima and fragments of read image in pseudocolours on the monitor of the compu-

ter.

In the report we describe the peculiarities of mounting, methods of conducting investigations, and also we give experimentally received estimates of maximum possibilities for the analysis of large format highly informative images. The usage of the described automated correlator permits to significantly shorten the time of analysis of images and ensure high precission and reliability of received results.

We shall presents also the results about using of 2-D thin field optical bistable devices for the analysis of coherent images, which forms by optical correlator with very high speed. The unit, which make this analysis, consists of one 2-D optical bistable device, two multielement linear photosensors and one cubic beamspletter /2/. This unit provided a good signal/noise relation. The 2-D optical bistable devices had 30 mm diameter and made in the Devision of Optical Problem of Informatics (Academy of Sciences of Belarus).

REFERENCES:

1. "Applications of Optical Fourier Transforms"- Edited by H. Stark: Academic Press (1982).

2. Korolkov A.V., Fast correlator on the basis of optical bistable elements. Technical Digest ICO Topical Meeting on Optical Computing'92, paper 29E36 (1992).

Optical Coordinate Transformations; A New Architecture

Ronglong Tian, Masahide Itoh, and Toyohiko Yatagai
Institute of Applied Physics, University of Tsukuba
Tsukuba, Ibaraki 305, Japan
Tel: +81-298-53-5334
Fax: +81-298-53-5205

Abstract:
A new architecture for optical coordinate transformations with two phase filters employed is proposed, which is described by the Wigner distribution function. A precise theory and experimental results are presented.

Many attempts for optical coordinate transformations are based on the coherent optical Fourier transformation.[1-3] We propose here an alternative approach, in which two phase-only filters are used and the input plane and the output plane are conjugate each other, as shown in Fig. 1. Two phase-only filters $\exp[\Phi_1(r)]$ and $\exp[\Phi_2(r)]$ are positioned at a distance of z from the input plane and at the Fourier transform plane of a lens L_1, respectively. The Fourier transform of the first filter is obtained in the second filter plane. The final output is the Fourier transform of the transmitted light from the second filter. In terms of paraxial approximation, the optical system is generally described by the following double Wigner distribution function;[4]

$$K(r_o,a_o,r_i,a_i)=\frac{1}{\lambda^2}\iint h\left(r_o+\frac{r_o'}{2},r_i+\frac{r_i'}{2}\right)h^*\left(r_o-\frac{r_o'}{2},r_i-\frac{r_i'}{2}\right)\exp\left[-jk\left(a_o.r_o'-a_i.r_i'\right)\right]dr_o'dr_i' \tag{1}$$

where $h(r_i;r_o)$ denotes the point spread function of the system. Equation (1) gives a relationship between heights r and angles α in the input and the output planes. In the particular case of Fig. 1, the optical system is represented by

$$\begin{aligned}K(r_o,a_o,r_i,a_i)=\iiiiiiiii\ &\delta(r_1-r_i-z\,a_i)\delta(a_1-a_i)\delta(r_i'-r_1)\delta\left[a_1'-a_i-\frac{1}{k}\frac{d\Phi_1(r_1)}{dr_1}\right]dr_1da_1\\ &\delta(r_2-fa_1')\,\delta\left(a_2+\frac{r_1'}{f}\right)dr_1'da_1'\delta(r_2'-r_2)\delta\left[a_2'-a_2-\frac{1}{k}\frac{d\Phi_2(r_2)}{dr_2}\right]dr_2da_2\\ &\delta(r_o+fa_2')\delta\left(a_o-\frac{r_2'}{f}\right)dr_2'da_2'\end{aligned} \tag{2}$$

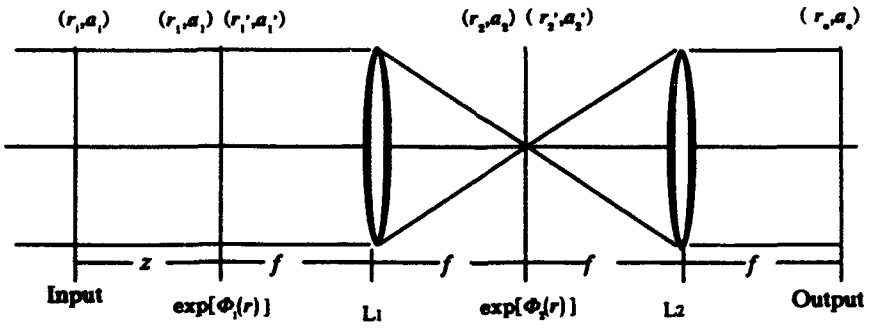


Fig. 1 Optical system for coordinate transform.

Suppose the phase of the second filter is written by the following form;

$$\exp[\Phi_2(r_2)]=\exp\left[\left(-\frac{jk}{f}\right)\int S\left(\frac{r_2}{f}\right)dr_2\right] \tag{3}$$

We have the double Wigner distribution function written by;

$$K(r_2', a_2', r_1, a_1) = \delta(r_2' - r_2)\,\delta[a_2' - a_2 - \frac{1}{k}\frac{d\Phi_1(r_1)}{dr_1}] = \delta(r_2' - r_1)\,\delta[a_2' - a_2 + \frac{1}{f}S(\frac{r_1}{f})] \tag{4}$$

We generally consider here the following coordinate transformation;

$$r_2 = g(r_1) \tag{5}$$

Then we have final phase distributions of filters as follows;

$$\Phi_1(x,y) = k\{\int R_x(x_i,y_i)\,dx_i + \int [R_y(x_i,y_i) - \frac{\partial}{\partial y_i}\int R_x(x_i,y_i)\,dx_i]\,dy_i\} \tag{6}$$

$$\Phi_2(x,y) = -\frac{k}{f}\{\int g_x[x_i(\frac{x}{f},\frac{y}{f}),y_i(\frac{x}{f},\frac{y}{f})-x_i(\frac{x}{f},\frac{y}{f})]\,dx + \int [g_y[x_i(\frac{x}{f},\frac{y}{f}),y_i(\frac{x}{f},\frac{y}{f})-x_i(\frac{x}{f},\frac{y}{f})] - \frac{\partial}{\partial y}\int g_x[x_i(\frac{x}{f},\frac{y}{f}),y_i(\frac{x}{f},\frac{y}{f})-x_i(\frac{x}{f},\frac{y}{f})]\,dx\}\,dy\} \tag{7}$$

As an typical example, we consider the following coordinate transformation;

$$g_x(x_i,y_i) = \eta \ln(x_i) \tag{8}$$

$$g_y(x_i,y_i) = \xi y_i \tag{9}$$

The phase distributions of the filters are given by

$$\Phi_1(x,y) = -\frac{k}{Z}[\frac{x^2}{2} - \frac{x^3}{6\eta} + qx + (1-\frac{1}{\xi})y^2] + c \tag{10}$$

$$\Phi_2(x,y) = -\frac{k}{f}\{\eta[(x+\frac{qf}{z})\ln(\sqrt{1+\frac{2zx}{\eta f}+\frac{2q}{\eta}}-1) + x\ln(\eta)] - \frac{\eta f}{4z}(\sqrt{1+\frac{2zx}{\eta f}+\frac{2q}{\eta}}+1)^2 - x + \frac{\eta f}{3z}(\sqrt{1+\frac{2zx}{\eta f}+\frac{2q}{\eta}})^3] + \frac{qf}{z}\ln(\sqrt{1+\frac{2zx}{\eta f}+\frac{2q}{\eta}}-1) - (\frac{\xi z}{2f})y^2\} + c' \tag{11}$$

We have made the phase-only filters with the computer-generated hologram technique. Figure 2 shows an input pattern example (a) of the grating whose pitches are exponentially changed. Because of the logarithmic coordinate transformation system, we have the output (b) of an equi-spaced grating image.

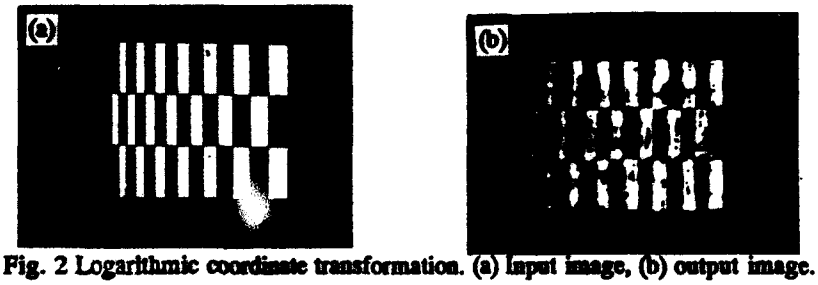


Fig. 2 Logarithmic coordinate transformation. (a) input image, (b) output image.

We have proposed a new architecture of the optical coordinate transformation using a pair of phase-only filters and derived the analytical solution of the filters. Optical experiments with computer-generated filters verifies the analytical solution for logarithmic coordinate transformation. Features of the architecture are discussed in comparison with Bryngdahl Fourier transform method.

References

1. O. Bryngdahl, J. Opt. Soc. Amer., 64, 1092-1099 (1974).

2. Y. Saito *et al*, Opt. Commun., 47, 8-11 (1983).

3. H. Bartelt *et al*, Opt. Engr., 22, 497-500 (1983).

4. M. J. Bastiaans, Opt. Commun., 30, 321-326 (1979).

Breaking Symmetry in the Binary Phase Only Matched Filter

T. D. Wilkinson and R. J. Mears
Cambridge University Engineering Dept,
Trumpington St, Cambridge CB2 1PZ
Tel + 44 223 332600

Abstract

A new means of breaking symmetry in binary phase only matched filters is reported. A randomly pixellated diffractive element is combined with a dynamic binary filter to produce a pseudo four-level phase matched filter.

The Binary Phase Only Matched Filter (BPOMF) has been well researched to ensure such features as invariance robustness. A much less publicised feature of the BPOMF is the inherent rotational symmetry due to the binary phase levels of 0 and π. The symmetry means that when an object appears either correctly or rotated by 180° in the input, the corresponding correlation peaks will be identical. In an application such as road sign recognition, this is an undesirable property, as triangular signs have very different implications for each orientation, hence an asymmetric BPOMF is desirable. Symmetry can be broken by increasing the number of phase levels, but this requires another binary Spatial Light Modulator (SLM) for the filter[1]. We suggest a system which produces a pseudo four level phase system, not total quaternary phase, but sufficiently flexible to break the BPOMF symmetry.

The correlator is the classical $4f$ Vander Lugt BPOMF constructed using binary ferroelectric liquid crystal SLMs as the modulation devices. Included with the second SLM (in binary phase mode) is a pixellated diffractive element (random phase array) to create the four level system. The random phase array has the same pixel pitch as the filter SLM and is aligned pixel to pixel with the SLM. Each pixel on the random phase array is set to either 0 or $\pi/2$ and is fixed. Ideally, the phase array would be physically etched onto the glass surface of the SLM, but for initial demonstration, we have constructed a photoresist pattern on a $\lambda/10$ optical flat to generate the $\pi/2$ phase step.

The SLMs used are 128x128 pixel devices from THORN EMI CRL. The pixel pitch is 220μm, so a chrome on glass mask was made containing the random phase array pattern. The initial random phase array was made by spinning, exposing and developing Shipley S1400-31 photoresist onto a $\lambda/10$ glass optical flat, but this gave too large a step in the photoresist. Shipley S1400-17 photoresist was then tried giving a step size of 320nm (247nm required for $\pi/2$ at $\lambda = 633$nm). However, if the wavelength of 780nm is used, then the phase step will be 1.65rad which is close enough to $\pi/2$.

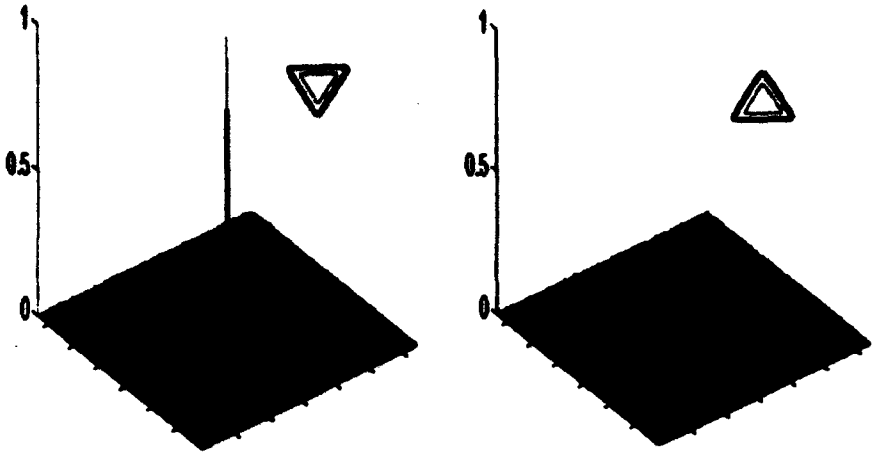


Figure 1: Simulation of the pseudo four phase level system applied to a triangular road sign

Extensive simulation of the effects of the random phase array have been completed. Figure (1) shows the effect of the random phase array ($\pi/2$ delay) for a triangular road sign. The BPOMF was generated by a simulated annealing algorithm[2] which was adapted to include the random phase array in the calculation. The suppression of the symmetric order was 16dB and there was no increase in signal to noise ratio (26.5dB). For the constructed random phase array with a delay of 1.65rad, the symmetric suppression was reduced to 15.1dB but the signal to noise ratio remained at 26.5dB.

We have presented a new means of suppressing the symmetric correlation peaks in the BPOMF without requiring an extra SLM or penalising the signal to noise ratio of the correlation peak. An experimental evaluation will be presented at the conference.

References

[1] M.A. Neil and E.G.S. Paige. Breaking of inversion symmetry in 2-level, binary, Fourier holograms. In *Proc IEE Holographic Systems, Components and Applications 4, Switzerland*, page 6, 1993.

[2] T.D. Wilkinson, D.C. O'Brien, and R.J. Mears. Scale invariant matched filter generation by simulated annealing. In *OSA Annual Meeting Tech. Dig. V16*, page 221, 1993.

Adaptive Space-Variant Coordinate Transformations, Their Applications and Optical Implementation

Y. B. KARASIK
Computer Science Department, Tel Aviv University, Tel Aviv, Israel
e-mail: karasik@math.tau.ac.il

Abstract

We introduce the notion of space-variant coordinate transformations, consider some of their applications in computer science and show how they can be implemented optically.

1 Definition of Space-Variant Coordinate Transformations

The optical implementation of coordinate transformations has received much attention in optical literature since the publication of O. Bryngdahl's classical paper in 1974 [B].

However, both O. Bryngdahl and all subsequent researchers have been concerned with optical implementation of coordinate transformations

$$\begin{cases} u = f(x,y); \\ v = g(x,y), \end{cases}$$

such that both f and g are expressed in elementary functions and these expressions do not vary across the plane. We call such coordinate transformations "Space-Invariant".

For example, the polar mapping

$$\begin{cases} u = \sqrt{x^2+y^2}; \\ v = \tan^{-1}(\frac{y}{x}) \end{cases}$$

is a space-invariant coordinate transformation because all points on the plane are transformed due to the same law:

$$(x,y) \longrightarrow (\sqrt{x^2+y^2}, \quad \tan^{-1}(\frac{y}{x})),$$

whereas the following coordinate transformation

$$\begin{cases} u = \sin x; \quad v = \cos y, & \text{if } x^2+y^2 \le 9; \\ u = x^3; \quad v = \ln y, & \text{if } x > 4; \\ u = \sqrt{y}; \quad v = e^x, & \text{if } y > 4 \& x < 4; \\ u = 0; \quad v = 0, & \text{otherwise} \end{cases}$$

is space-variant because it cannot be represented in the form

$$\begin{cases} u = f(x,y); \\ v = g(x,y), \end{cases}$$

where f and g are elementary functions invariant across the plane.

A space-variant coordinate transformation

$$\begin{cases} u = f_i(x,y); \quad v = g_i(x,y), & \text{if } (x,y) \in D_i, \\ u = 0; \quad v = 0, & \text{otherwise} \end{cases}$$

is called adaptive if domains D_i are not known in advance and are determined in the course of the solution of a problem.

Adaptive space-variant coordinate transformations play an important role in the various problems of computer science as a whole, and pattern recognition, in particular. One of these applications is considered in the section that follows.

2 An Application

Consider the problem of recognising all cross-roads in a photograph of the land, such that the angle between roads is exactly $\pi/2$.

With the help of space-variant coordinate transformations, this can be done as follows.

Step 1. Let I_1 be the image of a photograph and let $\{(x_i, y_i)\}_{i=1}^N$ be the coordinates of cross-roads which are easily recognised with the help of other techniques. Apply to this image the following space-variant coordinate transformation

$$\begin{cases} u = (x - x_i), \quad v = (y_i - y), & \text{if } \sqrt{(x-x_i)^2 + (y-y_i)^2} \le r; \\ u = 0, \quad v = 0 & \text{otherwise,} \end{cases}$$

where r is a sufficiently small radius (significantly less than the minimum distance between points $\{(x_i, y_i)\}_{i=1}^N$ which can easily be computed optically in constant time using the algorithm described in [KS].)

As a result, we obtain a new image I_2 which concides with I_1 only in the vicinity of those cross-roads which have angle $\pi/2$ because the above coordinate transformation rotates each cross-road by $\pi/2$ with respect to the corresponding (x_i, y_i) and, hence, only those cross-roads which have angle $\pi/2$ remain invariant after the rotation.

Step 2. Having now subtracted I_2 from I_1, we obtain a new image $I_3 = I_1 \setminus I_2$ containing only those cross-roads whose angles are not equal to $\pi/2$.

Step 3. Compute $I_4 = I_1 \setminus I_3$. Obviously, image I_4 contains the desired cross-roads only.

3 Optical Implementation

Let $H_{invar}(x, y)$ be the transmittance distribution of a CGH for space-invariant coordinate transformation

$$\begin{cases} u = f(x, y); \\ v = g(x, y). \end{cases}$$

Then space-variant coordinate transformation

$$\begin{cases} u = f(x - x_i, y - y_i); \quad v = g(x - x_i, y - y_i), & \text{if } \sqrt{(x-x_i)^2 + (y-y_i)^2} \le r; \\ u = 0; \quad v = 0, & \text{otherwise,} \end{cases}$$

which is adaptive to points $\{(x_i, y_i)\}_{i=1}^N$ can easily be implemented optically using CGH whose transmittance distribution is described as follows:

$$H_{var}(x, y) = (H_{invar}(x, y) \cdot A_r(x, y)) * \sum_{i=1}^{N} \delta_{x_i, y_i},$$

where

$$A_r(x, y) = \begin{cases} 1, & \text{if } \sqrt{x^2 + y^2} \le r; \\ 0, & \text{otherwise.} \end{cases}$$

Thus, the CGH for an adaptive space-variant coordinate transformation can be obtained on a photo-addressed SLM in constant time from the CGH for the corresponding space-invariant transformation (which is assumed to be known) using an optical convolver. Hence, the transformation itself can also be performed optically in constant time.

References

[B] O. Bryngdahl, Optical map transformations, *Optics Communication*, 10(2), 164-168 (1974).

[KS] Y. Karasik, M. Sharir, Optical algorithms in geometry, *The Fifth Topical Meeting on Optical Computing, technical digest of papres, volume 7*, Palm Springs, CA, USA, 1993, pp. 164–167.

Constant Time Optical Algorithm for Extracting Regions of Maximum/Mimimum Intensity From a 2-dimensional Image.

Y. B. KARASIK
Computer Science Department, Tel Aviv University, Tel Aviv, Israel
e-mail: karasik@math.tau.ac.il

Abstract

We present an optical algorithm for extracting regions of minimum/maximum intensity from an image. Time-complexity of the algorithm is $O(1)$.

1 Introduction

Extracting regions of maximum/minimum intensity from an image, as well as thresholding an image at a given level of intensity, are important operations in image processing [NR].

Even though thresholding has received considerable attention from the optical engineering community [WT, SMLBTSSC], little work has been done on the optical implementation of the maximum/minimum operation. The only exception is [GCHHZY] which, however, deals with the computing maximum/minimum entry of a 1-dimensional array of light beams rather than a 2-dimensional image.

The point is that extracting the above regions cannot be performed in a purely engineering manner (as is the case for thresholding), but requires a somewhat algorithmic approach.

In this paper we present an optical algorithm which extracts regions of maximum/minimum intensity from an image and does it in constant time.

2 The Zero-Crossing Approach and Its Drawbacks

It may appear that the simplest way to solve the above problem is to make use of spatial differentiation of an image that can be readily implemented optically. Indeed,

$$\left.\frac{\partial I(x,y)}{\partial x}\right|_{x=x_{\max},y=y_{\max}} = \left.\frac{\partial I(x,y)}{\partial y}\right|_{x=x_{\max},y=y_{\max}} = 0,$$

if $I(x_{\max}, y_{\max}) = \max\limits_{(x,y)} I(x,y)$, where $I(x,y)$ is the intensity of an image at the point (x,y). Hence, computing $(x_{\max}, y_{\max})$ can be performed optically by determining regions of zero intensity of the differentiated image.

However, this approach does not allow one to distinguish between minimum intensity and maximum intensity, or between local extremum and global extremum, not to mention its sensitivity to noise in the input data.

To avoid these drawbacks, we propose an optical algorithm for computing minimum/maximum of the bivariate function $I(x,y)$ using θ–modulation (or frequency modulation).

3 θ−modulation approach to maxima operation

It is well known that θ−modulation of an image followed by a Fourier transform, maps a point (x, y) of the image to the point $(\cos I(x, y), \sin I(x, y))$, where $I(x, y)$ is intensity of the image at (x, y) [AL]. Hence, regions of minimum intensity are mapped to the point closest to the X-axis, whereas regions of maximum intensity are mapped to the point furthest from the X-axis.

These points can be extracted optically in constant time as follows:

Step 1. Project points $\{(u, v) | u = \cos I(x, y), \quad v = \sin I(x, y)\}$ obtained as a result of the θ−modulation of the intensity distribution $I(x, y)$ to the Y-axis. Obviously, this can be readily done with the help of CGH which performs the coordinate transformation

$$\begin{cases} u = 0; \\ v = y. \end{cases}$$

As a result we obtain a set of points $P = \{(0, \sin I(x, y))\}$.

Step 2. Compute the vector sum $P + Ray$ of the points P with the *Ray* emanating from the origin of coordinates upward along the Y-axis (obviously, it can be done optically in constant time with the help of an optical convolver.)

As a result, we obtain an image where the point $(0, \sin(\min_{(x,y)} I(x, y)))$ has unit intensity whereas other points have higher intensity. Hence this point can be extracted by thresholding as follows:

Step 3. Threshold the image obtained at Step 2 at the unit level of intensity and extract thereby the point $(0, \sin(\min_{(x,y)} I(x, y)))$.

Step 4. Demodulate the point $(0, \sin(\min_{(x,y)} I(x, y)))$ and obtain thereby the region of minimum intensity of the input image.

An algorithm for extracting the region of maximum intensity of an image is the same up to substituting the vector sum $P + Ray$ at Step 2 by the vector difference $P - Ray$.

References

[AL] J. D. Armitage, A. W. Lohmann, Theta modulation in optics, *Applied Optics*, 4(4) 339–403 (1965).

[GCHHZY] C. Gu, S. Campbell, J. Hong, Q. He, D. Zhang, P. Yeh, Optical thresholding and maximum operations, *Applied Optics*, 31(26), 5661 - 5665 (1992).

[NR] Y. Nakagawa, A. Rosenfeld, A note on the use of local min and max oerations in digital ppicture processing, *IEEE Transactions on Systems, Man, And Cybernetics*, Vol. SMC-8, No. 8, 632 - 634 (1978).

[SMLBTSSC] B. H. Soffer, J. D. Margerum, A. M. Lackner, D. Boswell, A. R. Tanguay, Jr., T. C. Strand, A. A. Sawchuk, P. Chavel, Variable Grating Mode Liquid Crystal Device for Optical Processing and Computing, *Mol. Cryst. Liq. Cryst.* **70**, 145–161 (1981).

[WT] C. Warde, J. Thackara, Operating modes of the microchannel spatial light modulator, *Optical Engineering*, 22(6), 695-703 (1983).

UNIVERSAL COMPUTATION AND OPTICAL CORRELATORS

M. Montes-Usategui, I. Juvells, J. Campos(*) and J. R. de F. Moneo

Universitat de Barcelona, Departament de Física Aplicada i Electrònica, Laboratori d'Optica.
Diagonal, 647. E-08028 Barcelona. Spain.
(*) Universitat Autònoma de Barcelona, Departament de Física. E-08193 Bellaterra. Spain.

Abstract: We show the possibility of implementing the LIFE game by means of an optical correlator. Since this cellular automaton is an universal computer there is no inherent limitation in the information processing capabilities of correlators.

Optical correlators are probably the most popular and well-studied devices used in optical pattern recognition. They are applied to a wide variety of problems including those requiring multiple invariances. However, there is no guarantee that a particular problem can be solved by means of an optical correlator, and therefore it is a legitimate question whether they can be considered as general purpose classifier devices.

In this communication we show that it is possible to implement the game of LIFE by means of correlation and a simple nonlinear postprocessing of the resulting correlation plane. This procedure is very similar to that used in optical pattern recognition, although the nonlinear function is slightly different (we need a rectangle function instead of the threshold function).

Cellular automata are usually described as a regular infinite array of cells that can take one of several allowed states. The automata evolve in discrete time steps (generations) governed by deterministic rules. The state of a given cell in the generation k+1 is a function of its previous state (that at generation k) as well as of the states of its neighbors (also at generation k). The updating of the cells is performed synchronously, that is all at a time. Some of these cellular machines exhibit a behavior complex enough to support universal computation[1]. They are called class-IV automata and LIFE is one of them[2]. The possibility of being implemented by correlation leads to the conclusion that a correlator is as powerful, in its information processing capabilities, as the most powerful machines known (or for those who accept the Church-Turing thesis as the most powerful machines that can exist), namely universal computers.

The cells of LIFE can be in one of the two possible states, dead or alive. The transitions between these two states are controlled by the states of its eight neighboring cells following these basic rules:

- A cell that is alive at time k continues living at time k+1 if and only if it has 2 or 3 living neighbors.
- A cell that is dead at time k becomes alive at time k+1 if it has exactly three living neighbors.

From these rules it is evident that the state of any cell is determined by the total sum (assuming one for live cells and zero for the dead ones) of the values of its neighbors, and not depends on their individual values. This property is called totalistic and enables the optical implementation. By correlating an input LIFE pattern with the 3x3 filter:

$$\begin{bmatrix} 1 & 1 & 1 \\ 1 & 0.5 & 1 \\ 1 & 1 & 1 \end{bmatrix}$$

and processing the output intensity distribution by the function f(x) =rect (x/10 - 1) we obtain the next generation.

As an example of the computing capabilities of the automaton we show the construction of an AND gate. The correlation was simulated by using the Fast Fourier Transform (FFT) algorithm over an array of 128x128 cells. The input pattern is that shown in Fig. 1 where the two inputs are labelled by A and B. The signals are carried by patterns formed by five cells called gliders (labelled

with ones) which move one position diagonally each four generations. The presence or absence of a glider represents the bit 1 or 0 respectively. The structure at the bottom left corner is a glider gun, a periodic pattern that emits a glider after 30 generations. With the proper timing and alignment the collision (indicated by C) of two gliders produces a vanishing reaction which annihilates both patterns, as shown in Fig. 2. The logic operation is based on these collisions. When there is a glider in both channels (A and B) the collision of one of them opens a hole in the stream produced by the glider gun, which is profited by the second to pass through (Fig. 3). When there is only one glider it is eliminated by the stream (Fig. 3) and therefore by detecting the presence or absence of gliders at the position indicated in Fig. 4 at predetermined times we obtain the output of an AND gate. The rest of the stream produced by the glider gun is eliminated by the eater (the collision C shown in Fig. 4).



Figure 1. Initial pattern.

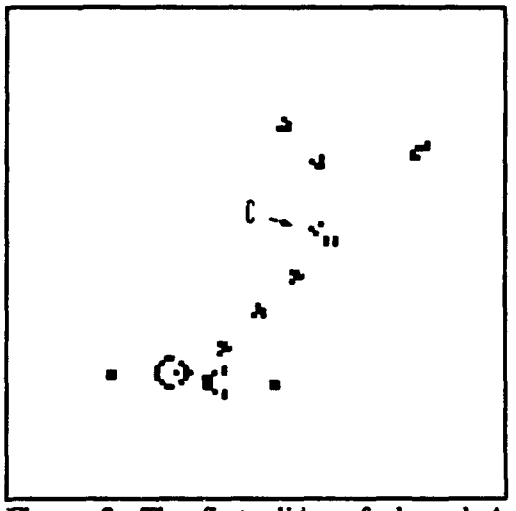


Figure 2. The first glider of channel A opens a hole in the stream.



Figure 3. The first glider of channel B pass while the solitary second glider of channel B is destroyed.

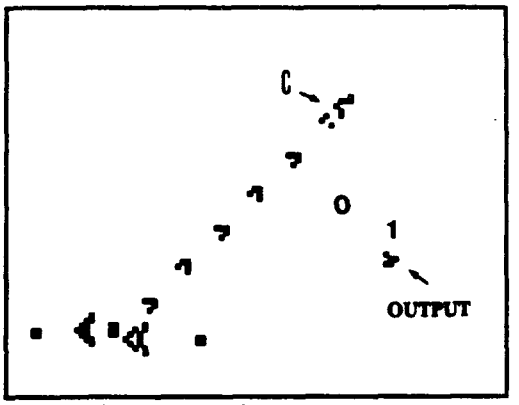


Figure 4. Final result

This work was supported in part by CICYT projects ROB91-0554 and TAP93-0667-C03-01.

References:

1. S. Wolfram. "Universality and Complexity in Cellular Automata". Physica D 10, 1-35 (1984).
2. E. R. Berlekamp, J. H. Conway, and R. K. Guy. *Winning Ways for Your Mathematical Plays.* Academic Press. New York (1982).

A Filter Design to Improve the Recognition of Defocused Images

J. Sallent, M. Montes-Usategui, J. Campos(*), S. Bosch

Universitat de Barcelona, Departament de Física Aplicada i Electrònica, Laboratori d'Optica. 08028 Barcelona, Spain.
(*) Universitat Autònoma de Barcelona, Departament de Física, Laboratori d'Optica. 08193 Bellaterra, Barcelona, Spain.

Abstract. The use of Minimum Average Correlation Energy Filters for the recognition of defocused images is studied. We propose to adapt the filter simultaneously to the original and to the blurred images to improve the recognition process. In this way the value of the correlation peak is stable for a wide range of blurring in the input image.

The input image in an optical correlator may be degraded by different sources of blurring. A common degradation is defocus. The theoretical performances of several correlation filters have been previously studied[1]. The filter was designed from the original image (non defocused). As expected, the autocorrelation peak decreases as the blurring increases, and the discrimination capability decreases similarly. In Ref. 1 the study was done with the Classical Matched Filter, Phase Only Filter, and Inverse Filter. Recently a similar study was carried out for a joint transform architecture[2]. One possibility to improve the performance of the correlation method is the use of Minimum Average Correlation designs as the MACE and MINACE filters[3]. With these designs it is possible to control the correlation at the origin with different input objects (called the training set). This allows to include the blurred images as part of this training set and therefore to obtain defocusing invariant filters. We show that this is a useful technique to improve the performance of a MACE or MINACE filter for a wide range of defocused scenes with as few as one blurred image for each target pattern.

Figure 1 shows the original object to be detected and two blurred versions. We show also the two other objects to be rejected. The butterflies are 54x64 pixels in size zero-padded to a total of 128x128 pixels. The point spread functions of the blurring are approximated by circles of diameter d=1(non defocused), 4.16, and 20.8 pixels respectively.

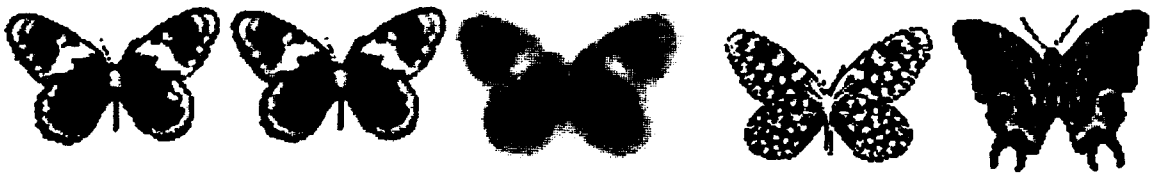


Figure 1

Figure 2, and 3 represent the values of the correlation peaks obtained with different filter designs as a function of the defocus. Fig.2 corresponds to MACE filters and Fig.3 corresponds to MINACE filters. In both figures, lines A correspond to a filter designed to give a central correlation value 1 with the non-defocused target and 0 with the two non-targets. A1 is the autocorrelation line and A2, and A3 to the crosscorrelations peaks. Although the discrimination capability is good, we see that the correlation value decreases rapidly as the defocus increases, being the MACE less resistant than MINACE.

This lack of resistance to defocusing in the MACE design when no blurred images are included in the training set is due to the high values of the filter components corresponding to frequencies of low energetic content in the training images. Since it can be assumed with wide generality that these low-

energy components are those of high frequency, the MACE filter will be very sensitive to even small changes in the high frequency components of the input images. On the other hand, the defocus of an image mainly affects to its high frequency components (the effect can be approximated to a low-pass filter) being the error largely amplified and thus producing significative variations in the correlation peaks. The MINACE filter, although designed with the noise resistance in mind, performs better due to the limitation imposed to the maximum value of a filter component corresponding to a low-energy frequency. A better understanding of this behavior may be used to design more robust filters in the future.

Since the MACE and MINACE filter design methods allow multiple target correlation conditions, we can use a defocused object as one of the targets and we can impose that the central correlation value with the non-defocused and with the defocused target to be the same. Curves labeled B correspond to the use a defocused (diameter=4.16) object together with the non-defocused one. B1 corresponds to the autocorrelation and B2, and B3 to the crosscorrelation. Curves C show similar results when using the most defocused object (diameter= 20.8) in the filter design. Of course the autocorrelation values with the objects included in the design are the same. The interesting feature is that when the most defocused image is used in the filter design, the autocorrelation values for intermediate values of defocusing also take almost the same value. The discrimination capability is high and the same for all defocusings, and the absolute intensity of the autocorrelation peak is still quite high.

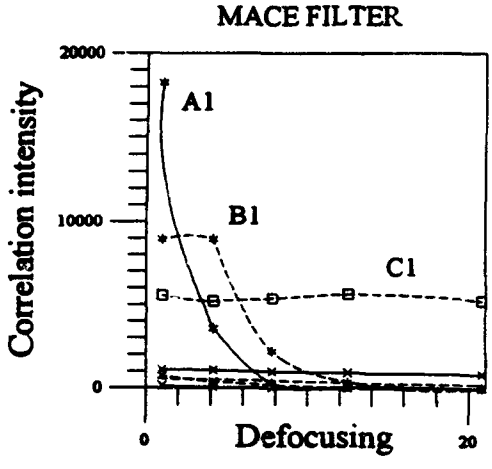


Figure 2

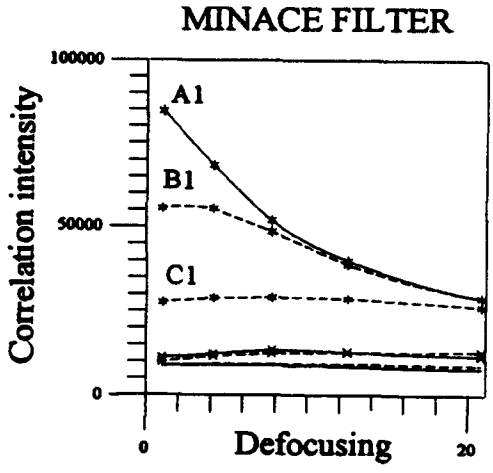


Figure 3

Acknowledgements
This work was supported in part by the CICYT project ROB91-0554.

References

1.- J. Campos, S. Bosch, and J. Sallent, "Optical pattern recognition in defocused images using correlation filters," Opt. Commun. 82, 370-379, (1991).
2.- B. K. Karch, M. A. Karin, and D. L. Flannery, "Binary joint transform correlation of defocused images", Opt. Eng. 32, 2709-2719 (1993).
3.- G. Ravichandran and D. Casasent, "Minimum noise and correlation energy optical correlation filter," Appl. Opt. 31, 1823-1833 (1992).

Optical Haar wavelet transform using a time-division-multiplexed shadow casting system

Ju-Seog Jang and Shin Il Jeong

Department of Telematics Engineering
National Fisheries University of Pusan
599-1 Daeyun-Dong, Nam-Gu, Pusan, Korea
TEL 82-51-620-6475; FAX 82-51-628-7433

Abstract

An optical system for the Haar wavelet transform of binary images based on a time-division-multiplexing technique is described. We show that a simple image differentiator can handle the bipolar wavelet function efficiently in the system.

Recently, various optical architectures of the wavelet transform have been investigated to get fast transform results by taking advantage of parallelism of optics[1]. Following Yang *et al.*[2], we performed experiments on the optical Haar WT using a shadow casting system. To handle bipolar nature of the wavelet functions, Yang *et al.* used a polarization encoding technique in their shadow casting system with a coherent light source. Through a properly rotated analyzer, the phase difference between the lights from the positive and negative parts of the wavelet function becomes π, by which the amplitude subtraction is obtained in their experiment. However, we could not obtain good amplitude subtraction results because the sum of two coherent beams with a phase difference π still interfered constructively at higher-order positions in the output focal-plane.

To represent bipolar images in incoherent systems, area encoding, wavelength multiplexing, and time division multiplexing (TDM) techniques have been commonly used[3–5]. In these schemes, an additional subtraction process is required after the two outputs of different signs are obtained. Here we adopt the TDM technique and show that a simple parallel image differentiator[6] can be used efficiently for the subtraction.

The Haar WT of a 2-D image $s(x,y)$ is mathematically described by

$$W(p,q,a,b) = \frac{1}{\sqrt{ab}} \int\int s(x,y) h\left(\frac{x-p}{a}, \frac{y-q}{b}\right) dxdy \qquad (1)$$

where $h(x,y)$ is the mother Haar wavelet function, a and b are dilation factors, and p and q are shifting factors. Let us denote the positive and negative parts of the wavelet function $h^+(x,y) = \mathrm{rect}(x-0.5, y-0.5) + \mathrm{rect}(x+0.5, y+0.5)$ and $h^-(x,y) = -\mathrm{rect}(x+0.5, y-0.5) - \mathrm{rect}(x-0.5, y+0.5)$, respectively. Thus $h = h^+ + h^-$. The Haar WT by TDM means that h^+ and $|h^-|$ are presented alternately during $2jt_o \le t < (2j+1)t_o$ and $(2j+1)t_o \le t < (2j+2)t_o$, respectively. $j = 0, 1, 2, \cdots$, and t_o is a time duration. Thus the TDM version of Eq. (1) can be written as

$$\begin{aligned} W_{TDM}(p,q,a,b,t) &= W^+(p,q,a,b) \sum_j [u(t-2jt_o) - u(t-(2j+1)t_o)] \\ &\quad + W^-(p,q,a,b) \sum_j [u(t-(2j+1)t_o) - u(t-(2j+2)t_o)] \end{aligned} \qquad (2)$$

where $W^{\pm}(p,q,a,b) = (1/\sqrt{ab}) \int\int s(x,y)|h^{\pm}((x-p)/a,(y-q)/b)|dxdy$ and $u(t)$ is the Heaviside step function. Note that W_{TDM} is always unipolar if $s(x,y)$ is a unipolar function. To obtain W, $W^+ - W^-$ should be executed. We can get this subtraction by differentiating W_{TDM} of Eq. (2), *i.e.*,

$$\frac{\partial W_{TDM}}{\partial t} = W^+(p,q,a,b)\delta(t) + \sum_{k=1}^{\infty}(-1)^k[W^+(p,q,a,b) - W^-(p,q,a,b)]\delta(t-kt_o) \quad (3)$$

where $\delta(t)$ is the Dirac delta function. Practically, $k = 1, 2$ is enough. Eq. (3) implies we can get $W^+ - W^-$ by detecting the pulse amplitude after $t > 0$.

Our system that implements Eq. (2) and (3) is shown in Fig. 1. The first part that calculates W_{TDM} is a shadow casting system whose structure is similar to that in Ref. 2. The patterns for h^+ and $|h^-|$, which are flipping alternately, are represented by the light transmittance of a spatial light modulator (SLM1). A sequence of discrete shifting factors (p_m,q_n) is represented by the positions of the point sources. Thus for a given size of the wavelet pattern, a and b, $W_{TDM}(p_m,q_n,t)$ is detected and fed to SLM2 in the image differentiator[6] (or novelty filter[7]). Both the two-beam coupling and four-wave mixing differentiators[6,7] detect only the magnitude of $|W(p_m,q_n)|$, because they produce only unipolar light pulses whenever W_{TDM} changes. To detect both the sign and magnitude of W, we used a beam-fanning differentiator[6,8], which produces positive light pulses only when W_{TDM} increases. If the pulses are generated at $t = kt_o$ of even (odd) k, W is positive (negative). The photorefractive crystal ($BaTiO_3$) is placed near the image plane of W_{TDM} so that the beam fanning can occur independently for every beam spot of (p_m,q_n). An experimental output of the beam-fanning differentiator when $W^+(p_m,q_n) \neq 0$ and $W^-(p_m,q_n) = 0$ is shown in Fig. 2.

References

1. See, for example, *Opt. Eng.* **31**, 1823-1898 (1992).
2. X. Yang, H. H. Szu, Y. Sheng, and H. J. Caulfield, *Opt. Eng.* **31**, 1846 (1992).
3. E. A. Trabka and P. G. Roetling, *J. Opt. Soc. Am.* **54**, 1242 (1964).
4. D. Psaltis, D. Casasent, and M. Carlotto, *Opt. Lett.* **4**, 348 (1979).
5. X. Yang, T. Lu, and F. T. S. Yu, *Appl. Opt.* **29**, 5223 (1990).
6. M. Cronin-Golomb, A. Biernacki, C. Lin, and H. Kong, *Opt. Lett.* **12**, 1929 (1987).
7. D. Z. Anderson and J. Feinberg, *IEEE J. Quantum Electron.* **25**, 635 (1989).
8. M. Cronin-Golomb and A. Yariv, *J. Appl. Phys.* **57**, 4906 (1985).

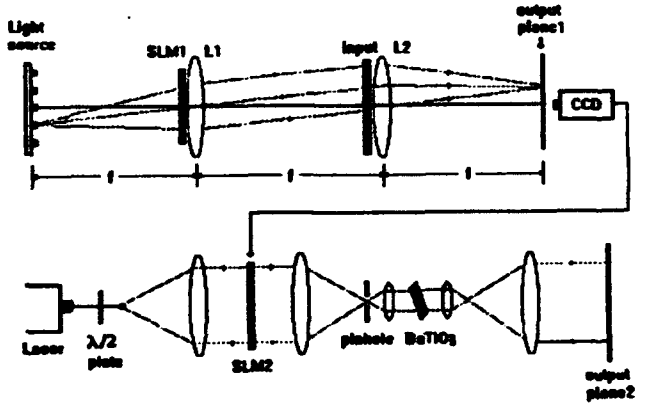


Fig. 1. The optical Haar WT system.

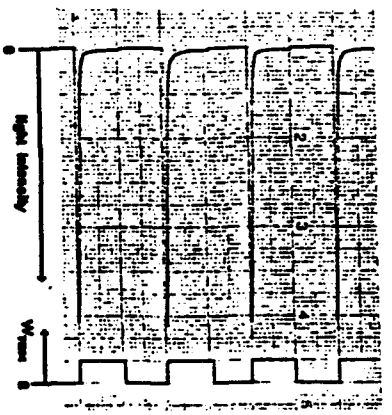


Fig. 2. An experimental result.

Generalized Fourier Transforms, Imaging Systems and Correlators

Luís M. Bernardo, Francisco J. Marinho, Olivério D. D. Soares
CETO, Centro de Ciências e Tecnologias Ópticas
Faculdade de Ciências, Universidade do Porto
4000 Porto, Portugal (ph.: 351-2-2001653; fax: 351-2-319267)

Generalized Fourier transforms of integer, fractional and imaginary degrees can be implemented by lenses. Optical units which realize such basic transformations are shown to be useful in the implementation of more complex optical systems such as imaging systems and correlators.

Very recently, Lohmann[1] has shown that generalized Fourier transforms (GFT's), defined on the basis of Wigner functions, can be optically implemented by lenses, after generalizing the usual geometries used for the implementation of the conventional Fourier transform. Figures 1(a) and 1(b) show those geometries. For the configuration shown in figure 1(a), the GTF of order p, $F^{(p)}$, (p>0), can be written in the form:

$$F_{x_f,y_f}^{(p)}\{o(x,y)\} = \iint o(x,y)\, e^{i\frac{k\cos\phi}{2f\sin^2\phi}\left[(x^2+x_f^2)+(y^2+y_f^2)\right]} e^{-i\frac{k}{f\sin^2\phi}(xx_f+yy_f)}\,dx\,dy \tag{1}$$

where
$$\sin\phi = \frac{1}{f}\sqrt{z_1(2f-z_1)}\ ; \qquad \cos\phi = \frac{f-z_1}{f} \tag{2}$$

and $\phi=p\pi/2$. When collimated illumination is used:

$$z_1 = z_2 = f(1-\cos\phi) \tag{3}$$

For the configuration of figure 1(b), the expression of $F^{(p)}$ takes the form:

$$F_{x_f,y_f}^{(p)}\{o(x,y)\} = \iint o(x,y)\, e^{i\frac{k\cos\phi}{2f(1-\cos\phi)}\left[(x^2+x_f^2)+(y^2+y_f^2)\right]} e^{-i\frac{k}{f(1-\cos\phi)}(xx_f+yy_f)}\,dx\,dy \tag{4}$$

and
$$d = f(1-\cos\phi) \tag{5}$$

The inverse GFT's $F^{(-p)}$ can be obtained from equations (1) and (4) after substituting there *i* by *-i*. The implementation of inverse GFT's is also realized with the geometries of figure 1, after substituting there the positive lenses by negative lenses and interchanging the object and the transformation planes. The object and the transform distributions are in this case virtual. According to equation (2), GFTs may have imaginary degrees for certain ranges of z_1.

An important parameter, associated to any GFT $F^{(p)}$, is the so called standard focal length, f_1. The expressions of f_1, for the single-lens configuration and for the two-lenses configuration, are respectively:

$$f_1 = f\sin\phi\ ; \quad f_1 = f\frac{1-\cos\phi}{\sin\phi} \tag{6}$$

Transforms $F^{(\beta)}$ with the same parameter $|f_1|$ belong to the same family, meaning that, when they are implemented and cascaded in tandem, they satisfy the properties of the GFT's expressed by the relationship:

$$F^{(\alpha)}\left\{F^{(\beta)}\left\{f(x,y)\right\}\right\} = F^{(\beta)}\left\{F^{(\alpha)}\left\{f(x,y)\right\}\right\} = F^{(\alpha+\beta)}\left\{f(x,y)\right\} \tag{7}$$

Now, the meaning of standard focal length f_1 becomes clear. It represents the scale of $F^{(1)}$, resulting from the application, in tandem, of other GFT's belonging to the same family.

Exact imaging optical systems and correlators, showing no phase curvatures in the planes of interest, can be realized by cascading basic units which implement fractional Fourier transforms of the same family. Particularly, $F^{(\alpha+\beta)}$ may represent a conventional Fourier transform of an object distribution if $\alpha+\beta=1+4n$ (n is an integer), an inverted image if $\alpha+\beta=2+4n$, or an erect image if $\alpha+\beta=4n$. Figure 2 shows two examples of imaging systems based on fractional GFT's of the same family. The single lens configuration units are used in figure 2(a) with lenses with the same focal length, and two-lenses configuration in figure 2(b). In this last case, it happens that the exact conventional Fourier transform $F^{(1)}$ is formed in plane π; the system is therefore a correlator of focal distance $f_1 = f/\sqrt{3}$.

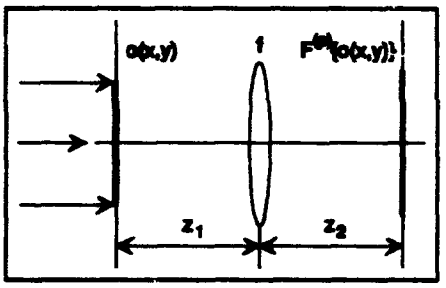


Figure 1(a) Single-lens configuration.

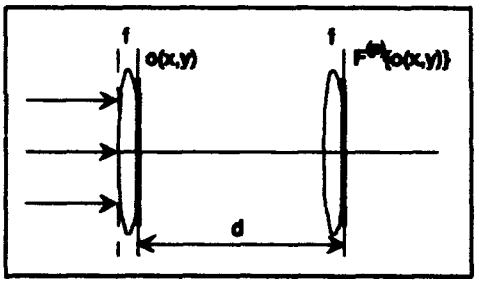


Figure 1(b) Two-lenses configuration

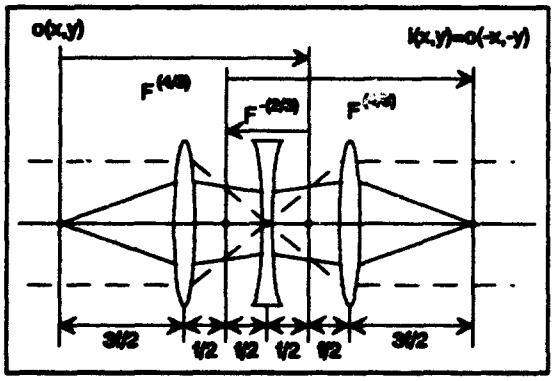


Figure 2(a) Exact imaging system.

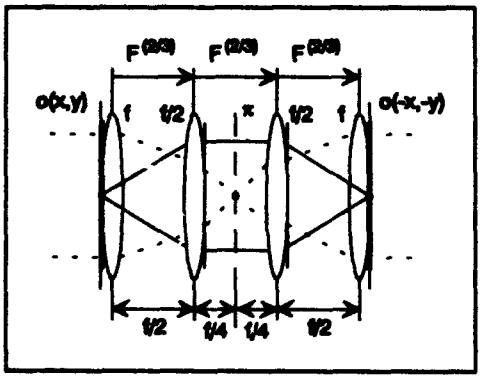


Figure 2(b) Exact imaging system and correlator.

[1] A. W. Lohman, "*Image rotation Wigner rotation and the fractional Fourier transform*", J. Opt. Soc. Am. A, 10, 2181-2186 (1993).

Programmable 2-D optical wavelet transform in space domain

Dong-Xue Wang and Ju-Wei Tai,(Institute of Automation, Academia Sinica, B.O. Box 2728, Beijing 100080, PRC)

Abstract:
In the paper, a new architecture of optical wavelet transform (OWT) system with a lenslet array is proposed, and its optical performance and optical limits are analyzed.

1. Optical Wavelet Transform System

1.1 Wavelets Arrangement

For the fixed dilation factor (a_j, a_l), wavelets can be represented by h_{xyik}:

$$h_{xyik} = h[\frac{(x-x_i)}{a_j}, \frac{(y-y_k)}{a_l}] \qquad ①$$

It can be considered as a 4-D matrix, and the wavelet matrix(WM) can be arranged with a 2-D array (indexed by i,k) of 2-D submatries (indexed by x,y). These wavelets are displayed on a high resolution color video monitor or a LCTV addressed by a CRT monitor according to the space arrangement(Fig.1).

1.2 lenslet array

An optical device to provide optical connection between input image and wavelets displayed on video monitor is needed in OWT. We have designed an array of lenslet with N*N lenses, and each lens images a specific wavelet submatrix onto the input image which is a SLM with N*N binary pixels, thus the submatrix of wavelets can be superposed to the input image, and the transmitted beam from the SLM are collected onto the output plane to form a N*N pixel array which represents N*N products of the 2-D wavelet submatries with a 2-D processed image (Fig.2 ~~and Fig.3~~). In the output plane, each of pixel indexed by the translation factor (x_i, y_k) corresponds to a WT of the input image under one wavelet indexed by the same translation factor and a specific dilation factor.

For the wavelets with both positive and negative values, we need a subtraction implemented by computer to obtain optical results.

2. Optical limits of the OWT system

Since the OWT system is designed on the basis of geometrical optics, the diffraction and aberration of lenslet array must be considered when the SLMs with large space-bandwidth product(SBW) are used to be represented the wavelet mask and input pattern in the optical system; and SBW of WM affects the number of lens in the lenslet array which is the one of the most valuable factors for evaluating performance of the OWT system.

In Ref.5, Dr. Sakano et al. analyzed optical limits for one kind of lenslet array used for optical interconnections, the general method can also be used in describing the limits of our OWT system.

Because off-axis state lenses are used. In this case astigmatic aberration is dominant. Thus we analyze the astigmatic aberration; on the other hand, the diffraction limits have to be considered.

Let λ and D represent the wavelength of light and the diameter of lens, N_{max} denotes the upper limit of the number of lens in lenslet array, and n denotes the refractive index of the lens. The following condition is satisfied:

$$N_{max} \leq 0.468\left(\frac{D}{\lambda \cdot I}\right)^{\frac{1}{3}}$$

$$N_{ef} \leq 0.468 I^{-\frac{1}{3}} \qquad (2)$$

$$I = \frac{3n+1}{4n}$$

The condition implies that N_{ef} is determined by geometric factors of lenses.

References:

1. Harold Szu, Y. Sheng and J. Chen," Wavelet transform as a bank of the matched filters," Appl. Opt. 31, 3267(1992).
2. X. Yang, H.Szu, Y. Sheng and H.J. Caufield, " Optical haar wavelet transforms of binary images," Opt. Eng. 31, 1846(1992).
3. D.-X. Wang, J.-W. Tai, Y.-X. Zhang and Y. Ma, " Programmable 2-D optical wavelet transform," Submitted to Opt. Comm.
4. Y.-X. Zhang, D.-X. Wang and G.-G. Mu, " The optical implementation of tensor interconnection for a 2-D Programmable neural networks," in Annals of optoelectronics in high Tech.(Beijing, 1991)
5. T. Sakano, K. Noguchi and T. Matsumoto, " Optical limits for spatial interconnection networks using 2-D optical devices," Appl. Opt. 29,1094(1990).

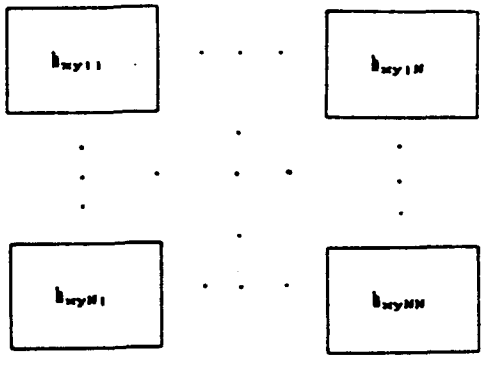


Fig.1

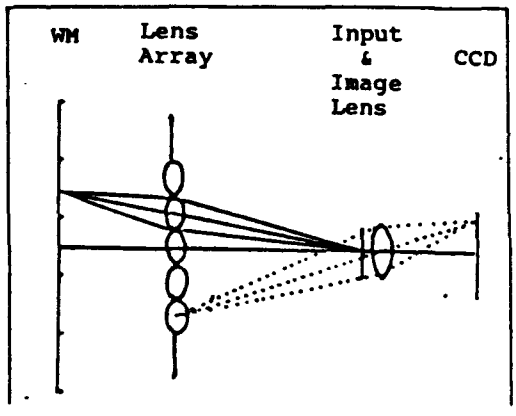


Fig.2

Spatial Filtering of Light Fields at Phase Conjugation

V.N.Ben, E.V.Ivakin, A.S.Rubanov

Institute of Physics, Academy of Sciences of Belarus
F.Scorina Ave.,70, Minsk 220072, Belarus
Tel.: 7-0172-394977, fax: 7-0172-393131
E-mail: ifanbel%bas03.basnet.belpak.minsk.by@demos.su

The method is suggested of conjugated wave formation with controlled contrast inversion of images of 2-D binary optical matrices. The optimum conditions for realization of phase filtration of object field are established.

By means of computer simulation methods the peculiarities are considered of light field transformation at phase filtering of Fourier spectrum in the scheme of DFWM wavefront conjugation.

Phase conjugation mirror constitutes a key element of optical setup under consideration [1] which consists of a nonlinear layer as photosensitive matter together with counterpropagating pump beams and a phase filter just behind the layer. Phase filter is inserted into one of the pump beams and there is a small central zone on it which shifts an appropriate pump field by some arbitrary phase with respect to remainder parts of the field. An object beam is formed by plane wave illumination of amplitude transparency. A resulting beam comes through a positive lens which is set at an arbitrary distance from the transparency and then is focused on the nonlinear layer placed at the focal plane of the lens.

At the moment of three beams action a conjugated beam is generated by DFWM which propagates into opposite direction. The resulting field in the plane just before transparency is described by the expression

$$E_c(\vec{\rho}) = (\lambda f)^{-2}\iint t(\vec{\rho}_T)\Phi(\vec{\rho}_N)\exp\{-ikf^{-1}(\vec{\rho}-\vec{\rho}_T)\vec{\rho}_N\}d^2\vec{\rho}_N d^2\vec{\rho}_T. \qquad (1)$$

Function $t(\vec{\rho}) = t_0+\tau(\vec{\rho})$, where $\tau(\vec{\rho})$ is a variable part relative to the average value, describes the amplitude transmittance of the transparency; $\Phi(\vec{\rho})=\Phi_0+(1-\Phi_0)\Pi(\vec{\rho})$, where Φ_0 is phase delay $\exp(i\varphi)$, describes the Π-form phase filter; f is the focal length of the lens; $k = 2\pi/\lambda$ is the wave number.

If $\varphi = \pi$ (sign of the field amplitude is inverted in a limited region near the optical system axis), the expression (1) describes contrast inverted image

$$E_c(\vec{\rho}) = t_0-\tau(\vec{\rho})+S(\vec{\rho}). \qquad (2)$$

$S(\vec{\rho})=2[\tau(\vec{\rho})*\Im\{\Pi(\vec{\rho})\}]$ is an additional term , which depends on the filter as well as on the object configuration. An efficiency of transformation is depicted in Fig.1. For values of t_0 less than 0,25 a contrast inversion is not obtained because it is an intensity (not amplitude) of inverted input matrix that is recorded in the trasparency plane.

Under certain conditions when Fourier plane of the lens doesn't coincide with the PCM plane a partial contrast inversion of object image may be obtained. In this case conjugated field in the object plane is described by the expression

$$E_c(\vec{\rho}) = Const\,\Im\{\iint G(\vec{\rho}-\vec{\rho}_N, d)\,\Phi(\vec{\rho}_N)\,G^*(\vec{\rho}_F-\vec{\rho}_N, d)\,\Im^*\{t(\vec{\rho}_F)\}d^2\vec{\rho}_N d^2\vec{\rho}_F\}.$$

where $G(\vec{\rho}_1-\vec{\rho}_2, d) = (i\lambda d)^{-1}\exp\{(ik/2d)^{-1}|\vec{\rho}_1-\vec{\rho}_2|^2\}$ is Fresnel transmittance of free space, d - distance between PCM and Fourier plane of the lens, symbols C, N and F mark the planes of image, phase conjugating mirror and phase filter respectively.

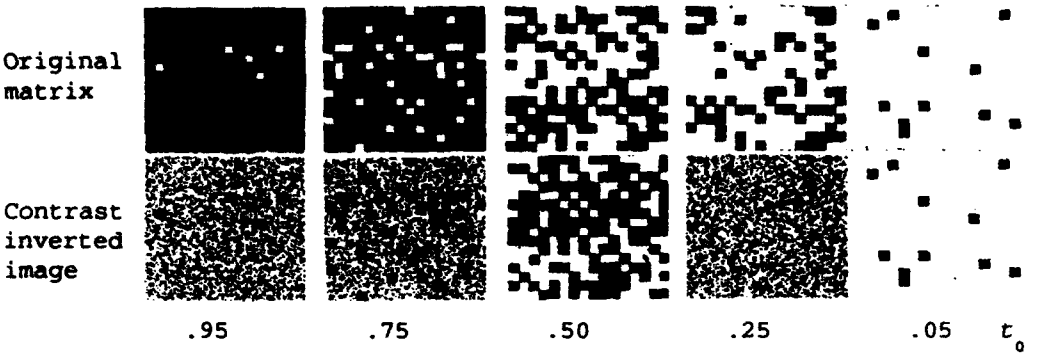


Fig.1. Efficiency of contrast inversion transformation vs spatially averaged value of input matrix transmittance t_0.

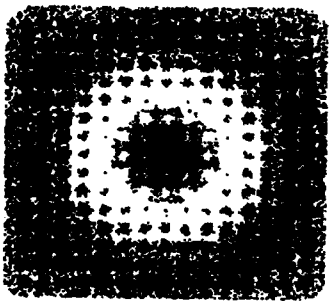


Fig.2. Partial contrast inversion of the conjugated image.

Calculation of field in the object plane (Fig.2) has been carried out using the model of NxN matrix of 2-D Gaussian profiles with the following values of parameters: N=15, f=25 cm, d=10 cm, halfwidth of the filtering zone b=250 μm, halfwidth of Gaussian function a=50 μm, period - h=150 μm. As it is seen from Fig.2, the inverted image in the initial matrix image is only partially saved. Dimensions of the inverted region depend upon the distance between PCM and Fourier plane of the lens, whereas its position on the image depends on the transverse filter shift. There is some transitory annular zone in Fig.2 which corresponds to gaussian function of the phase filter.

The method of contrast inversion in conjugated wave corresponds to logical NOT operation in binary matrices of optical signals processing. By the same way using four-wave mixing for realization of light fields multiplication together with phase filtering gives the opportunity to form conjugated fields, which to the action of logical operator AND.

1.V.N.Ben, E.V.Ivakin, A.S.Rubanov. "Contrast inversion of DFWM conjugated wave by phase modulation of the pump" Tech.Digest of Conf. on Wavefront Conjugation, Minsk, 1987, pp. 131-138 (In Russian).

Low Resolution Fresnel Encoded Lenses Applied to Pattern Recognition

E. CARCOLÉ, I.JUVELLS
Universitat de Barcelona, Departament de Física Aplicada i Electrònica, Laboratori d'Optica, 08028 Barcelona
J.CAMPOS
Universitat Autònoma de Barcelona, Departament de Física. 08193 Bellaterra, Spain.

Abstract:
The frequency response of Low Resolution Fresnel Encoded Lenses is calculated in terms of all parameters that characterizes these lenses and possible applications to pattern recognition are discussed.

1. PSF of Low Resolution Fresnel Encoded Lenses

When a Fresnel Lens with focal length f for a wavelength λ is encoded in a pixelated low resolution device, with a center to center pixel distance given by Δx, Δy, infinite new focal regions appear at the coordinates (kX,lY) where $X = \lambda f/\Delta x$ and $Y = \lambda f/\Delta y$ where k,l are arbitrary integers[1]. A low resolution fresnel encoded lens (LRFEL) seems an array of lenses with a size given by XY. Then, if the device has NxM pixels with a rectangular pupil of dimensions $L_x = N\Delta x$ and $L_y = M\Delta y$, the number of lenses appearing in the device is given by $W_x = L_x/X$ and $W_y = L_y/Y$. In Fig.1 we can see a LRFEL with $W_x = W_y = 3$.

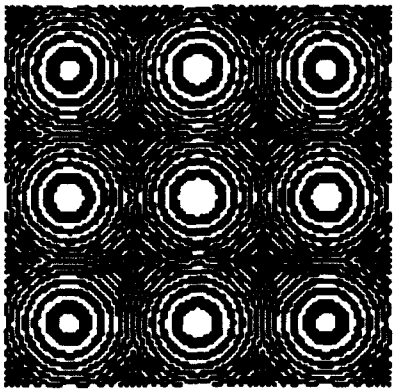


Fig.1. LRFEL with $W_x = W_y = 3$.

The amplitude distribution at a k,l focus for a plane wave illumination is given by (Eq. 20 of Ref.[1]):

$$U_{k,l}(x_i,y_i) = \frac{1}{i\lambda f}\frac{L_xL_y}{\Delta x\Delta y}\left[sinc\left(\frac{L_xx}{\lambda f},\frac{L_yy}{\lambda f}\right)\exp\left[i\frac{2\pi}{\lambda f}(x.kX+y.lY)\right]\right]*rect\left(\frac{x}{\Delta x'},\frac{y}{\Delta y'}\right) \quad (1)$$

The sinc function comes from the Fourier transform of the rectangular pupil of the device and the rect function defines the pixel of dimensions $\Delta x'\Delta y'$. Another useful parameters are $c_x = \Delta x'/\Delta x$ and $c_y = \Delta y'/\Delta y$.

2. Coherent transfer function for a (k,l) focus

In order to calculate the frequency response we must perform the Fourier transform of Eq.1.Taking as a natural unity of length the pixel size we obtain:

$$H_{k,l}(g_x,g_y) = \frac{\lambda f c_x c_y}{i}rect\left(\frac{g_x-k}{W_x},\frac{g_y-l}{W_y}\right)sinc(c_x.g_x,c_y.g_y) \quad (2)$$

For a (k,l) focus, the rect function is shifted k in the g_x direction and l in the g_y direction. In a general case (any shape of the pupil or the pixel) it will happen the same, we will have the integral of the Fourier transform of the pixel function multiplied by the shifted pupil function. Now, let us study some different cases:

First we consider (k=l=0). In this case the cut-off frequency is determined by the rect function at the frequency (in pixels^{-1}) $g_{c,x} = W_x/2$, $g_{c,y} = W_y/2$. The first zero for $W_x > 2/c_x$ or $W_y > 2/c_y$ of H is given by $g_{0,x} = 1/c_x$ $g_{0,y} = 1/c_y$. If $W_x < 2/c_x$ or $W_y < 2/c_y$ then $g_{0,x} = g_{c,x}$ or $g_{0,y} = g_{c,y}$. For smaller values of the focal length H take negative values and inversions of contrast may happen. For $c_x \to 0$ and $c_y \to 0$ we obtain H corresponding to the infinite resolution case (with a diffraction

diffraction efficiency tending also to zero). Then the limitations imposed for the low resolution condition is a function of c_x, the ratio between the pixel size and the center to center pixel distance.

We can now make general considerations for different k,l. When $c_xW_x/2$, $c_yW_y/2 >> 1$ then the rect function is large compared with the sinc function and his effect will not be appreciable for $k<W_x/2-1/c_x$ and $l<W_y/2-1/c_y$. In that conditions each focal region verifying the inequalities will replicate near the same information. This situation is sketched in Fig 2 for $W_x=W_y=40$ and $c_x=c_y=1$. Note that the inequalities can be verified for the particular case of a short focal lens with $c_x,c_y \sim 1$, or a large focal length with $c_x,c_y << 1$. When $c_xW_x/2$, $c_yW_y/2 << 1$, then the rect function is thinner than the sinc function, for k,l>0 H has the aspect of Fig. 2.a. The H for each k,l corresponds only to a little window of frequencies. In such case each focus will concentrate information corresponding to a certain range of frequencies. If W_x, $W_y = 1$ then the windows are the ones sketched in Fig 3 In this case each focus replicates different information but all information is replicated.

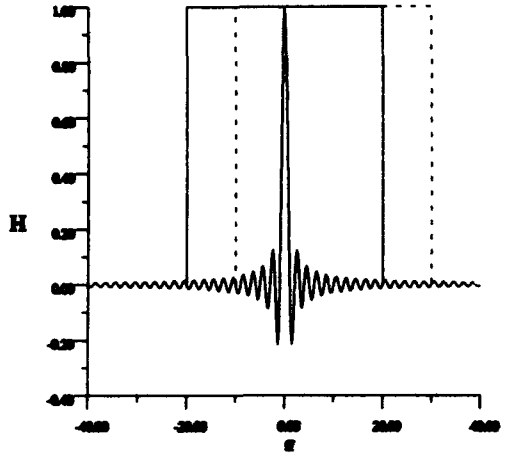


Fig.2 H for $W_x = 40$ and $c_x = 1$.

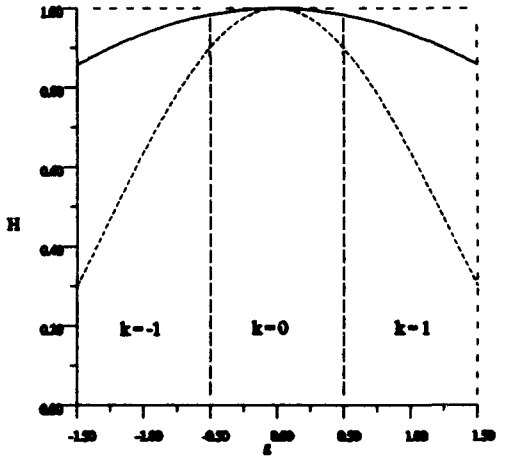


Fig.3 H for $W_x = 40$ and $c_x = 0.3$ (Dashed) and 0.2 (Solid)

4. Application to pattern recognition

We have seen that in certain conditions each focus can replicate different information of the object. The central focus can replicate the information corresponding to a window of low frequencies and the others ones can replicate windows corresponding to high frequencies. This will permit to compare separately the information corresponding to high and low frequencies and different kind of filters can be used in order to process appropriately this information.

We have also seen that for short focal length encoded each focus replicates near the same information. This opens the door to apply different types of filters for the same image in order to improve the recognition process.

Acknowledgments

This work has been financed by CYCIT (Comisión Interministerial de Ciencia y Tecnología). Project TAP93-0667-C03-01 and ROB91-0554

Bibliography

[1] E. Carcolé, J. Campos, S. Bosch, "Diffraction Theory of Fresnel Lenses encoded in low resolution devices" Appl. Opt. (In Press).

Region of suport to improve discrimination of Phase Only Filter

E. Ahouzi, J. Campos and M.J. Yzuel.

Physics Department, Autonomous University of Barcelona 08193 Bellaterra, Spain.
e-mail: ifop1 at cc.uab.es.

Abstract We propose a Phase only filter with maximum discrimination capability. The zero modulation state is introduced to block certain region in spatial frequencies which equalize the phase difference histogram. The discrimination capability is increased significantly compared with the POF.

The discrimination capability (DC) is one of the most important parameter to evaluate the performance of a filter for pattern recognition. Different kinds of filters have been proposed to increase this parameter: The Phase Only Filter (POF)[1], Optimal Filter[2] and other techniques [3]. In [4] B.V.K.V. Kumar and Z. Bahri introduced the notion of optimal support function for a Phase Only Filter (OPOFs) in the sense of maximising the signal to noise ratio SNR The support function indicates which pixels in the filter have magnitudes of 1 and which pixels have zero magnitudes. Other support functions to optimize different criteria or multicriteria have been proposed [5]. In all of these designs the support functions are calculated taking into account the amplitude distribution. As we will see the phase distribution plays a crucial role in the discrimination capability and, in consequence, we propose a support function to optimize the DC based on the phase information.

In this contribution we propose a method that optimizes the discrimination capability by using a POF with a support function. The procedure is based on modification of phase difference histogram by blocking some frequencies. We investigate the DC with computer simulation and we show the improvement in DC obtained with this method.

We denote by t(x,y) and d(x,y) the target and nontarget respectively, when the target (t(x,y)) is present at the origin, and the nontarget d(x,y) is placed in the scene at coordinates that the maximum of the cross-correlation is at the origin. Let $T(u,v) = |T| \exp(i\phi_t)$ and $D(u,v) = |D| \exp(i\phi_d)$ be their Fourier transforms. When the POF is used the cross-correlation function in Fourier domain is given by:

$$C_D(u,v) = |D(u,v)| \exp[\, i\,\Delta\phi(u,v)\,]$$

where $\Delta\phi(u,v) = \phi_d(u,v) - \phi_t(u,v)$ is the phase difference. The discrimination capability, DC, is a parameter that measures the ability of the correlator to discriminate between two very similar input objects, and it is defined as:

$$DC = \left| \sum_{u,v} |D(u,v)|\, e^{i\Delta\phi(u,v)} \right|^2 \Big/ \left| \sum_{u,v} |T(u,v)| \right|^2$$

Let us divide the 2π phase interval in N steps of width $\delta\phi = 2\pi/N$. Let S_j be the set of pixels (u,v) for which the phase difference $\Delta\phi$ is in the interval $\Delta\phi_{j-1} < \Delta\phi \le \Delta\phi_j$, where $\Delta\phi_j = j.\delta\phi$. Let us define the weighted phase difference histogram as:

$$P_j = \sum_{(u,v)\in S_j} |D(u,v)|$$

we approximate the phase difference of those pixels which belong to S_j by $\Delta\phi_j$, the DC can be written as:

$$DC = \left| \sum_{j}^{N/2} (P_j - P_{\frac{N}{2}+j}) \, e^{i\Delta\phi_j} \right|^2 / \left| \sum_{j}^{N} T_j \right|^2$$

The DC is optimized if we equalize $P_j = P_{N/2+j}$, j=1...N/2. This can be made by blocking some frequencies.

Figure 1 shows the input scene, the target is the letter F, and the object to be rejected is the letter E (letters F is contained in letter E). In figure 2a and 2b, we show the original and the modified phase difference weighted histogram, with N equal to 100. The corresponding correlations are shown in figure 3a and 3b. By comparing these figures it is shown that the algorithm proposed in this paper, enhances clearly the discrimination capability of the POF.



Fig.1. Input scene.

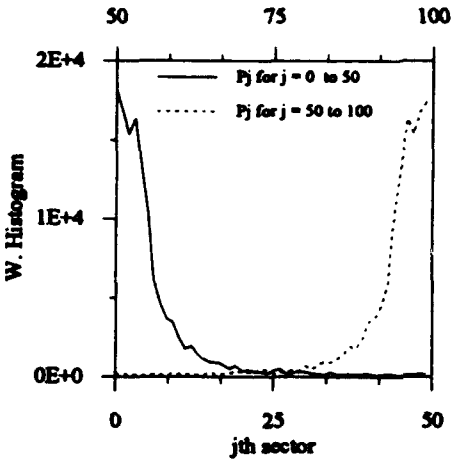


Fig. 2a. The original Weighted Phase Diffrenece Histogram.

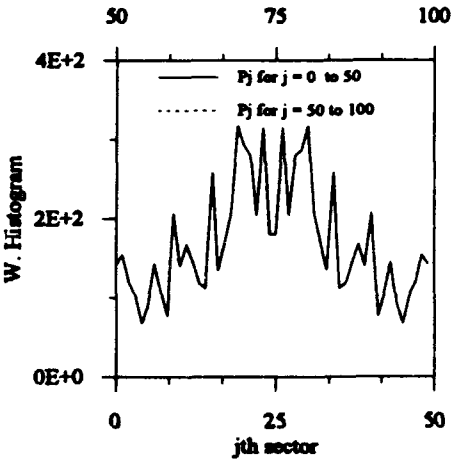
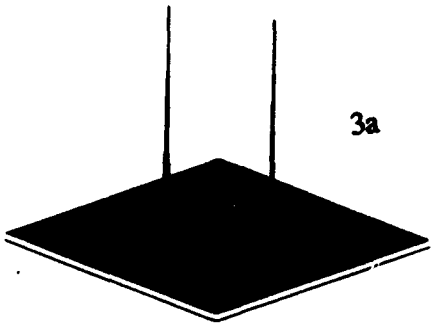


Fig. 2b. The modified Weighted Phase Diffrenece Histogram.



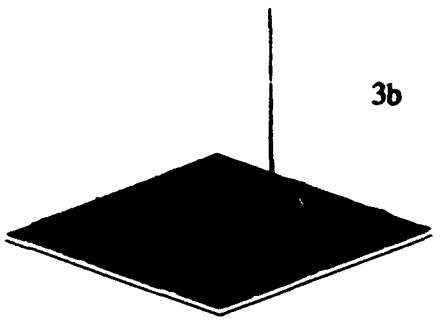


Fig. 3. Correlation planes. a) With conventional POF. b) With POF and DC optimization.

Acknowledgments

This work has been financed by CICYT(Comision Interministerial de Ciencia y Tecnologia). Project: TAP 93-0667-C03-01.

References

[1] J.L. Horner and P.D. Gianino, Appl. Opt., 23, (1984) 812.

[2] J. Campos, F.Turon, L.P. Yaroslavsky, and M.J. Yzuel, Int J. Optical Computing 2, 341-365 (1993).

[3] H. Zhou, F. Zao, F.T.S. Yu, T.H. Chao, Opt. Eng 32, 2720-2725 (1993).

[4] K.V. Kumar and Z. Bahri, Appl. Opt. 28, 250-257 (1989).

[5] Ph. Réfrégier, B.V.K. Vijaya Kumar, and Hendrix, J. Opt. Soc. Am. A9, 2118-2125 (1992).

Multi-distance, Multi projection, parallel projection method

T. Kotzer, N. Cohen and J. Shamir
Department of Electrical Engineering
Technion—Israel Institute of Technology
Haifa 32000, Israel

With the increasing demands and complexity of signal processing systems, renewed interest emerged in the set theoretic formulations [1] applied to optimization problems such as signal synthesis in pattern recognition [2, 3, 4], Computerized Tomography [5], constrained deconvolution [6], Image restoration [7, 8] etc. The task is, usually: "Given some a priori, corrupted, signal, h^o, which is known to, supposedly, have satisfied N constraint sets, try to restore it to a signal which will satisfy the constraint sets". The framework is quite similar if the task is to design a signal which is to satisfy N constraints.

Projection methods have been suggested for this task. A projection of an arbitrary element, h, onto a Closed Convex Set C_i is that unique element in the set ,h', closest to h, where "close" is measured by some distance function d_i. Namely,

$$P_{C_i}^{d_i}(h) = h' \quad \text{if and only if } \inf_{h_1 \in C_i} d_i(h_1, h) = d_i(h', h); \quad h' \in C_i$$

. Given N sets C_i one usually constructs operators of the form $T^{n+1} = \sum_{i=1}^{N} w_n(i) P_{C_i}^{d_i}$ where $w_n(i)$ is some, iteration dependent, weight function. This leads to a sequence $h^{n+1} := T^{n+1}(h^n)$. One strives to show that the sequence generated converges to a solution satisfying all constraint sets which means that $\lim h^n \in C_0 := \bigcap_{i=1}^{N} C_i$. The results known to date are basically composed of the following: if $C_0 \neq \emptyset$ and d_i are constant for all sets involved and all sets C_i are convex then under some general conditions the algorithm converges.

However, what happens if the constraints are inconsistent i.e. $C_0 = \emptyset$ (which is a frequent occurrence due to detection error, slight mis-characterization of the set etc.)? Is there convergence at all and if so to what? Also, how will one project onto a constraint when the constraint is given indirectly (implicitly)? This may be transformed in many instances to projection onto an explicit set but then the distance function is modified ([4]) and thus not all distance functions are uniform, what then? Finally, in many Image recovery problems more than 2 constraints exist (when one is non convex) - Can't we indeed use a projection base algorithm for this case (classically [8] we are limited to 2 sets if one is non convex)?

Fortunately, all of the above problems may be solved by use of a very special parallel projection method. It amounts to performing projections of the current estimate onto all N sets involved and then taking a very special average of these projections. More specifically:

1. Even if C_0 is empty, the algorithm converges. Moreover, it converges to the best solution possible i.e. that minimizing its distances (squared) from all sets involved.
2. Projections onto individual sets may be performed w.r.t **different** distance functions and yet convergence is assured to an Element in C_0, or to the closest one to it. Thus many implicit constraint problems may be converted to explicit constraints with various distance functions which can be handled by this method.
3. The algorithm converges for an **arbitrary** number of non convex constraints (the SDER property introduced by Stark *et al* [8] is maintained). Although convergence is not necessarily to C_0, and it may get stuck at some "trap" point. In most cases, however, convergence is to C_0. In any event it should be realized that the traps are a result of the non-convex constraints, not the projections algorithm.

References

[1] P. L. Combettes, *Proc. IEEE* **81**, p. 182 (1993).

[2] J. Rosen and J. Shamir,*Opt. Lett.*, **16**, p. 752 (1991).

[3] J. Rosen, *Opt. Lett.*, **18**, p. 1183 (1993).

[4] T. Kotzer, N. Cohen and J. Shamir, EE Pub. No. 900, Technion, I.I.T., November 1993.

[5] G.T. Herman, *Image reconstruction for projections: The fundamentals of computerized tomography*, Academic, NY 198.

[6] H.J. Trussell and M.R. Civanlar, *IEEE Trans. on Acou. Spe. and Sig. Proces.*, **ASSP-32**, p. 201 (1984).

[7] D.C. Youla and H. Webb, *IEEE Trans. Med. Im.*, **TMI-1**, p. 81 (1982).

[8] A. Levi and H. Stark, *JOSA A* **1**, p. 932 (1984).

Discrete incoherent Shadow–Casting: theoretical investigation

V. Laude[1], P. Chavel[2] and Ph. Réfrégier[1],
[1]: Laboratoire Central de Recherches
Thomson-CSF 91 404 Orsay cedex France. Tel.: 33 1 69 33 91 56
[2]: Institut d'Optique, B.P 147,
Orsay cedex, France.

January 25, 1994

Abstract

Diffraction effects and photometric non–uniformities of the spatially incoherent shadow–casting architecture are investigated when the input and output planes are pixelized. The acceptable geometrical configurations are then derived precisely.

Shadow–casting systems have been known since a long time, and were first used to analyse crystal lattices [1,2]. They provide a very simple way to obtain the convolution or correlation of bi-dimentional positive functions directly in object space [3]. They have also been used for implementing optical logic [4] and image morphology [5] operations, as well as symbolic substitution [6]. The simplest shadow–casting system is depicted in fig. 1, and is composed of three planes. The first one is a diffuse plane source which can consist for example of a CRT, or a Spatial Light Modulator (SLM) followed by a diffuser illuminated by a primary source. In a second plane at a distance d is another SLM, and in a third plane at a distance p is a screen or an array detector. The distance d between the SLMs is always positive, but the distance p between the second SLM and the detector can be either positive or negative, in which case the third plane has to be observed with an additional lens.

The basic system of fig. 1 can be generalized [7,8,3] by incorporating a lens (or lenses) between the source and intermediate planes, and between the intermediate and detector planes.

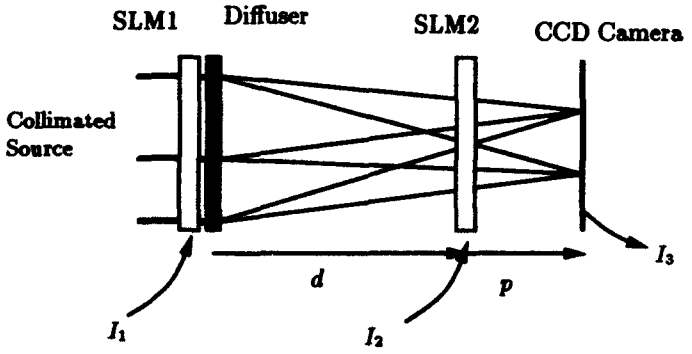


Figure 1: lensless shadow–casting architecture.

The first plane being a diffuse source, it is spatially incoherent, and the system is generally assumed to behave approximately according to geometrical optics (depending on ratios of caracteristic lengths in the set-up to the wavelength(s) used). Even with that assumption, the optical distances are different for horizontal or tilted rays between the SLMs. This phenomenon has important consequences on the correlation operation since, due to photometric effects, the optical flux is dependent on the tilting of the rays. The consequence may be a loss of translation invariance, and a degradation of the measured correlation in comparison with the mathematical

correlation operation. This point is in general emphasized by the imperfect diffuser placed after the first SLM. Taking into account this aspect leads to a first domain for the acceptable values of the geometric scaling of the architecture.

A second domain for the acceptable values of the geometric scaling of the architecture is obtained if diffraction effects are analyzed. Indeed, the geometrical optics description is a first approximation, and diffraction needs to be taken into account. Previous analyses [9, 10] of the effect of diffraction on resolution did not describe precisely the behavior of a shadow–casting system in presence of discrete elements such as the pixelized SLM.

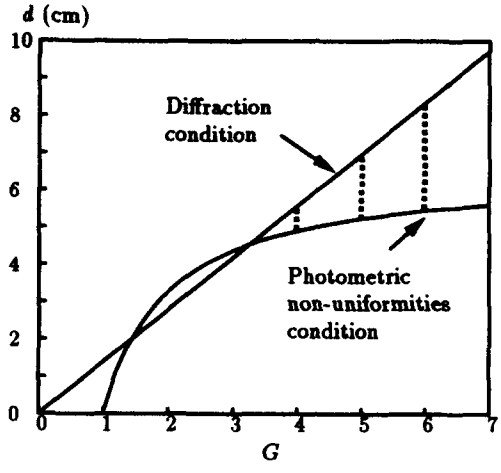


Figure 2: definition of acceptable domain for the geometrical parameters of the shadow–casting architecture.

Furthermore, if a CCD is used in the output plane, the continuous output is as well sampled. Then the system is an image processor, for which there exist discrete relations between output and input images.

The results of our theoretical analysis of diffraction and photometric effects will thus be provided as a transformation between discrete images (the inputs and the output). The acceptable choices of the geometric scaling of the architecture are then rigourously defined. This acceptable domain is shown in fig. 2, where the ratio G is defined by: $G = |d + p|/|p|$. The influence of diffraction, which was only addressed previously with rough estimations, had led to pesssimistic predictions as will be shown in the presentation. Finally we will discuss the practical implications on the architecture of these considerations in relation with realistic applications. Indeed, it will be shown that classical situations in which the reference image is smaller than the input image are favorable.

Acknoledgements The authors acknoledge fruitfull discussions with D. Broussoux and G. de la Forest, and partial support in this study by the Direction des Recherches Etudes et Techniques under contract 92/352.

References:

[1] M. M. Robertson, Nature **152**, 411 (1943).
[2] L. Bragg, Nature **154**, 69 (1944).
[3] G. L. Rogers, (Wiley, New York, 1977).
[4] Y. Ichioka and J. Tanida, Proc. IEEE **72**, 787–801 (1984).
[5] Y. Li, A. Kostrzewski, D. H. Kim, and G. Eichmann, Opt. Lett. **14**, 981–983 (1989).
[6] A. Louri, Appl. Opt. **14**, 3264–3267 (1989).
[7] P. L. Jackson, Appl. Opt. **6**, 1272–1973 (1967).
[8] M. A. Monahan, K. Bromley, and R. P. Bocker, proc. of IEEE **65**, 121–129 (1977).
[9] E. L. Green, Appl. Opt. **7**, 1237–1239 (1968).
[10] D. Raj, D. W. Prather, R. A. Athale, and J. N. Mait, Appl.Opt. **32**, 3108–3112 (1993).

Fourier Optics and Holography of Temporal Signals

Yu.T.Mazurenko
S.I.Vavilov State Optical Institute, 199034, St.Petersburg, Russia
Phone:(812) 2180949, Fax:(812) 3509993,
E-mail: MAZUR@SOI.SPB.SU

Abstract

The principles of time-domain holography of short laser pulses based on wave interactions in spectrally nonselective medium are considered. Using these principles the system of methods may be proposed for flexible controlling and processing fast optical signals.

Summary

We review the principles underlining the possibilities of recording and reconstruction of time-dependent radiation (wave packets), while using, as the normal holography, interference and diffraction of waves, and spectrally nonselective recording media. These principles allow to develop the system of methods for flexible controlling and processing fast optical signals ranging in duration from femtoseconds to nanoseconds.

From the methods proposed the most promising one is the holography of time-varying signals based on spectral decomposition of light (spectral holography). In this case we use interference and diffraction of waves formed during spatial spectral decomposition of short light pulses (spectral decomposition waves) by a normal spectral device.

Recording interference pattern of spectral decomposition waves of two optical pulses (a signal and a reference pulse) allows to store the temporal optical signal (the signal pulse) in the form of a spectral hologram. The reconstruction of the stored signal in the form of its real replica occurs by diffraction of the spectral decomposition wave of a reference

pulse from the spectral hologram. It is also possible to obtain a time-reversed replica of the stored signal.

Spectral holography serves the basis for time-domain Fourier optics that can be developed using the analogies with the normal Fourier optics and Fourier transform holography.

The possible applications of spectral holography are analysis, synthesis, time-reversal, recognition, optimal filtering, and optimal compression of short temporal optical signals.

The methods of dynamic spectral holography and spectral nonlinear optics are also proposed. Spectral decomposition waves of several light pulses may be superimposed in a common dynamic light-sensitive medium (optical nonlinear medium). That makes possible the nonlinear interaction of spectral decomposition waves and, also, the interaction of spectral decomposition waves with inhomogeneous monochromatic waves. As a consequence, various real-time transformations of ultrashort temporal signals become possible. In particular, it is possible to mix spatial and temporal signal and, using such mixing, to obtain fast space-to-time and time-to-space signal conversions.

Methods of dynamic spectral holography and spectral nonlinear optics may be used for highly parallel processing of optical data streams. In particular, dynamic space-time conversions may be used for for time- and code-division multi/demultiplexing of broad-band data streams and fast optical vector-matrix multiplications in communication and computing systems.

The experimental results on recording, reconstruction, time-reversal, and holographic recognition of ultrashort optical pulses by spectral holography methods are presented. Also presented are the experimental results on real-time conversion of ultrashort optical pulses into the spatial signals using three-wave nonlinear interaction of spectral decomposition waves and monochromatic waves.

See also: Yu.T.Mazurenko, Opt. Eng., V. 31, 739-749 (1992).

"Spatial Brightness Amplification" for Increasing Signal-to-Noise Ratio in 2D Optical Information Processing

George V.Sinitsyn, Sergey P.Apanasevich,
Fedor V.Karpushko, and Andrew V.Lyakhnovich

Division for Optical Problems of Information Technologies,
Academy of Sciences of Belarus
P.O.Box 1, 220072 Minsk, Republic of Belarus
phone: (0172) 39-58-82; fax: (0172) 32-45-53
e-mail: dopit%bas02.basnet.belpak.minsk.by@demos.su

Abstract. The concept of "spatial amplification" based on transverse effects in optical bistability is proposed. The possibility is shown experimentally to detect with the help of "spatial amplifier" weak optical signals with the power that is 10^7-10^8 times less than the power of noise.

In present contribution the concept is proposed for increasing the signal-to-noise ratio in 2D optical information processing systems which is based on application of transverse effects in optical bistability. This concept allows to develop the technique for identification of separate information pixels in wide-aperture 2D systems for information processing.

The basic idea of the above concept is to provide the favorable conditions for the rise and propagation of switching waves in optical bistable layers if the switch-on threshold has been exceeded at least in one local area. This leads to a many-fold increase of output light power up to the highest value which corresponds to the total switching of the whole bistable layer.

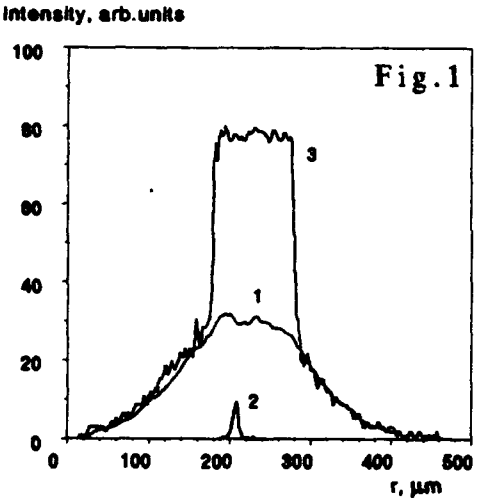
In a number of algorithms for optical information processing one needs to detect the presence or absence of information at least in one pixel of wide-aperture matrix. Since the "0"-level signal in optical systems is not equal to zero, the power of background signal coming from the whole matrix is many times higher than the power of information signal in an only separate pixel.

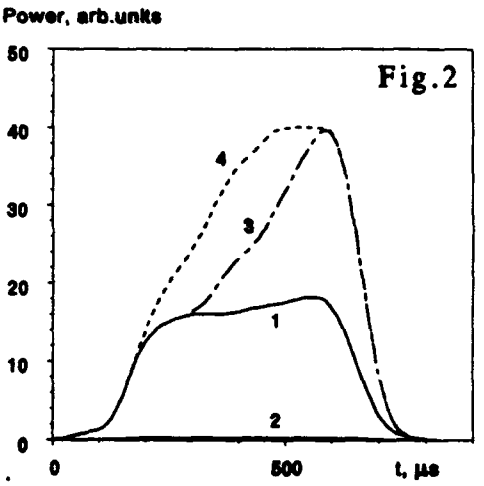
Using OB-matrix formed on an optically uniform nonlinear layer one can switch on not only the specified pixel but its nearest surrounding as well, and thus the resulting output signal to be registered can be increased many-fold.

The estimates of the gain factor of such a "spatial brightness amplifier", defined as the ratio of the output light power change to the power of the optical information signal that has caused this change, give the values of 10^7-10^8.

The technique proposed has been proved by modeling the "spatial brightness amplifier" experimentally using a thin-film bistable ZnS-interferometer. Basic results are presented on Figures 1,2.

Fig. 1 shows background light distribution of the whole illuminated area (1), intensity profile of the signal beam (2), and the output intensity profile (3) which gives the evidence of the signal somewhere within the switched area. On Fig. 2 time dependencies are plotted for the power of output light beam when there is only background and no signal (1), for the power of the signal beam to be detected on the above





background (2), and power of the output beam while detecting local signal with the maximum intensity that makes up 10% (3) and 20% (4) of the background. The experimentally obtained gain factor of our "spatial brightness amplifier" of about 5 10^3 has been limited by the power of the laser available.

The concept of "spatial brightness amplification" has been applied also to analyze output light fields of the coherent correlation processor.

Optical Heterodyning Noise-Protected with Stochastic Resonance

M.I. Dykman (010-1-415-723-3783)
Department of Physics, Stanford University, Stanford, CA 94305, USA,
G.P. Golubev, E.A.Jukov, I.Kh.Kaufman, D.G. Luchinsky (010-7-095-135-7540)
VNIIMS, Andreevskaya nab. 2, Moscow, 117965, Russia
P.V.E. McClintock, N.D. Stein, and N.G. Stocks (0524-65201)
School of Physics and Materials, Lancaster University, Lancaster, LA1 4YB, UK.

Abstract A new form of heterodyning in an all-optical bistable system, related to stochastic resonance, in which a heterodyne signal can be *enhanced* by adding noise, is reported.

The phenomenon of stochastic resonance (SR) in which a signal-to-noise ratio (SNR) can be increased by adding noise, [1] has attracted much attention recently (see [2]) . Most of the data have been obtained for bistable systems driven by noise and by a low-frequency periodic force. However, the noise-induced increase of the SNR, and also the frequency-selective response of bistable systems, make it interesting to apply the idea of SR to heterodyning in which two high-frequency fields (an input signal and a reference signal) are mixed nonlinearly to generate a heterodyne signal at the difference frequency.

In this paper we report and discuss a new form of the phenomenon, *noise-enhanced optical heterodyning*. The *enhancement* rather than suppression by noise of the heterodyne signal has been investigated theoretically, experimentally and by means of analogue electronic simulation.

We are investigating a double-cavity membrane system (DCMS) which displays all-optical bi- and multistability [3]. To a reasonable approximation [3(a)] the dynamics of the DCMS driven by two modulated laser beams at different wavelengths is described by a Debye relaxation equation for the phase gain ϕ

$$\dot{\phi} + \frac{1}{\tau}(\phi - \phi_0) = (I_0 + I_{in}\cos(\omega_0 + \Omega)t + \delta I(t))M(\phi) + I_{ref}(\cos\omega_0 t + 1) \qquad (1)$$

where ϕ_0 is the phase of the DCMS in the "dark"; $\delta I(t)$ is a zero-mean random term in the modulated light intensity; and I_{ref} and I_{in} are the amplitudes of the periodic modulation of the beams. The frequency detuning is assumed to be small, $|\Omega| \ll \tau^{-1} \ll \omega_0$. The function $M(\phi)$ determines the nonlinearity of the response of the DCMS. It is convenient to rewrite (1) in the form

$$\dot{x} + U'(x) = I_{ref}F(x)\cos\omega_0 t + I_{in}\cos(\omega_0 + \Omega)t + \delta I(t) \qquad (2)$$

$$x = \int_0^{\phi(x)} d\phi M^{-1}(\phi); \qquad U(x) = I_0 x + \int_0^{\phi(x)} d\phi(I_{ref} + (\phi - \phi_0))M^{-2}(\phi), \qquad (3)$$

($F(x) \equiv M^{-1}(\phi(x))$). Eq. (2) is a stochastic differential equation for the variable x driven by multiplicative reference ($\propto I_{ref}$) and additive input ($\propto I_{in}$) signals. It is the signal at frequency Ω that is to be revealed via heterodyning.

In view of the possible applications we will allow for a zero-mean Gaussian noise $\delta I(t)$ in (1) that consists of two independent components, at low- and high-frequencies respectively:

$$\delta I(t) = f_{lf}(t) + f_{hf}(t), \quad f_{hf}(t) = \mathrm{Re}\left(\tilde{f}_{hf}(t)\exp(-i\omega_0 t)\right), \tag{4}$$

where both $f_{lf}(t)$ and $\tilde{f}_{hf}(t)$ have a cut-off frequency $\omega \sim \omega_c \gg \tau^{-1} \equiv U''(x_{1,2})$ ($x_{1,2}$ are the stable states of the system in the absence of noise and periodic drive).

For $\omega_0 \gg \tau^{-1}$ the motion consists of fast oscillations at frequency ω_0 superimposed on a slower motion, and the heterodyning can be characterized by the low-frequency signal at the output, $x^{(sl)}(t) = \overline{x(t)}$ (the overbar stands for averaging over the period $2\pi/\omega_0$). In the spirit of [4], to first order in ω_0^{-1} the slow part of the coordinate is given by

$$\dot{x}^{(sl)} + U'(x^{(sl)}) = A\frac{\partial F}{\partial x^{(sl)}}\sin\Omega t + f^{(0)}(t), \quad A = \frac{I_{ref}}{2\omega_0} I_{in} \tag{5}$$

The predictions of this theory have been tested quantitatively by analogue simulation for the simplest nontrivial case of overdamped motion in the symmetric Duffing potential, for $F(x) = x$. In this simulation *noise-enhanced heterodyning* has been demonstrated for both types of noise, in good agreement with theory. The SNR dependence on I_{in}^2, I_{ref}^2, ω_0^{-1} and Ω were investigated for white noise.

The DCMS consists of a thin GaSe semiconductor film separated from a dielectric mirror by a metal diaphragm. The incident radiation from the Ar laser providing the input signal is propagated normally to the mirror and is modulated by superimposed random and periodic (at frequency $\omega_0 \pm \Omega$) signals with an electro-optical modulator. It had been shown previously that this system exhibits standard SR for $\omega_0 \ll \tau^{-1}$, $\Omega = 0$ [5].

We have now shown experimentally that, in the presence of additional radiation from a HeCd laser modulated by a chopper to induce periodic heating of DCMS at the frequency of reference signal ω_0, this system displays *noise-enhanced optical heterodyning* for $\omega_0 \gg \tau^{-1} \gg \Omega$. It has been found in particular that there is a range of noise intensity where the SNR of the heterodyne signal at Ω is strongly increased by adding noise. Below and above this range the SNR decreases with the increasing noise intensity D. This behaviour coincides with that observed in standard SR, cf. [5].

A semiquantitative description of this new phenomenon is provided by Eqs. (1)-(5), with an absorption coefficient in the form given in [3(a)]. A more detailed comparison with the theory will require computer simulation of the dynamics of the DCMS.

The work was supported by the Science and Engineering Research Council, by the European Community, by the Royal Society (London), and by the Gosstandart of Russia.

References

1. R. Benzi, A. Sutera and A. Vulpiani, *J. Phys. A* **14**, L453 (1981); C. Nicolis, *Tellus* **34**, 1 (1982); R. Benzi, G. Parisi, A. Sutera and A. Vulpiani, *Tellus* **34**, 10 (1982).

2. Special issue of the *J. Stat. Phys.* **70**, no.1/2 (1993)

3. (a) A.L.Velikovich, G.P.Golubev, V.P.Golubchenko, and D.G.Luchinsky *Opt. Commun.* **80**, 444 (1991); (b) M.I. Dykman, G.P.Golubev, D.G.Luchinsky, A.L.Velikovich, and S.V.Tsuprikov, *Phys. Rev. A* **44**, 2439 (1991).

4. L.D. Landau and E.M. Lifshitz, *Mechanics*, 3rd edition (Pergamon, Oxford, 1978).

5. M.I. Dykman, G.P.Golubev, D.G.Luchinsky, A.L.Velikovich, and S.V.Tsuprikov, *JETP Lett.* **53**, 193 (1991).

Creative Uses of Redundancies in Optical Computing

H. John Caulfield
Alabama A&M University, Normal, AL 35762, U.S.A.

Abstract

Information is related to unexpectedness and nonredundancy. Efficient processing of information should use minimum redundancy. I show that fanin/fanout can minimize computational load for algorithms whose touch complexities are less than their computational complexities.

Summary

There are many algorithms for most complex operations such as solving Ax = b. The bases for preference in digital computing are usually computational complexity and match to the available hardware. For analog optical computing we should ask the same questions of its algotecture/archirithms.

In conventional digital computing, only the computational complexity of algorithms is considered. For instance, Ax = b solution is an $O(N^3)$ problem. Doubling the size of A requires eight times more calculations.

Recently computer scientists have started to attend to the match of algorithm to computer. This has led to the concept of "touch complexity". This is a measure of how many times we must go to the memory to get the information needed for a given algorithm. For some algorithms and some problems, the touch complexity is less than the computational complexity. For example, the touch complexity for some Ax = b solvers is $O(N^2)$.

I now propound a thesis which I have not proved but whose probable truth I will argue by showing several examples. It is this: "The space-time complexity of an analog optical processor can always be driven to the touch complexity".

The way we do this is with fanin/fanout. That is the datum to be used multiply is represented as an SLM pixel (or its equivalent) and all operations on that datum are performed simultaneously. I will illustrate this with two special cases, leaving the proof of the thesis to others or for me at a later time.

First, I consider Ax = b: a problem of $O(N^3)$ computational complexity and $O(N^2)$ touch complexity. I will show that this can be solved in analog optics with

$$S = O(N^2) \text{ spatial complexity},$$

$T = O(N^0)$ temporal complexity and ,

$ST = O(N^2)$ space-time complexity .

The other O(N) comes from fanin/fanout.

Second, I consider matrix-matrix multiplication: a problem of $O(N^3)$ computational complexity and $O(N^2)$ touch complexity. Yet, I can solve it by analog optics with

$S = O(N^2)$,

$T = O(N^0)$, and

$ST = O(N^2)$.

The remaining O(N) comes from fanin/fanout.

My hope is that this work can give us insight into which problems are best suited for analog optical computation.

Optoelectronic Implementation of Tomographic Sorting

Pericles A. Mitkas and Leo J. Irakliotis

Optoelectronic Computing Systems Center and the Department of Electrical Engineering
Colorado State University, Fort Collins, CO 80523
Tel. 1-303-491-7481

Abstract

A parallel sorting algorithm and its implementation on a 3-D multistage optoelectronic sorting network are presented. The network operates on bit-slices of words and combines regular structure and simple interconnections between stages.

Introduction

Tomographic (bit-sliced) sorting is a parallel pipelined algorithm that can be mapped directly on a 3-D computer architecture that uses optical interconnections to propagate data and control bits from one processing plane to another. The algorithm is a combination of the odd-even transposition sort and the standard radix sort [1]. In this paper, we describe the algorithm and the structure and functionality of the 3-D sorting network. We also discuss how this network can be implemented as a multistage architecture similar to the 3-D optoelectronic computer under development at the Optoelectronic Computing Systems Center in Colorado. Tomographic sorting can serve as a test application for this computer.

Hardware Description

The 3-D optoelectronic computer under development comprises multiple 2-D stages of electronic processing element arrays, stacked in a 3-D formation (Figure 1). Each element in a 2-D array can accept optical input on a phototransistor. process the incoming signal electronically, and generate an optical output by driving a vertical-cavity surface-emitting laser (VCSEL). The VCSEL's output becomes input for the next stage. Computer-generated holograms can implement the interconnection patterns required for each operation.

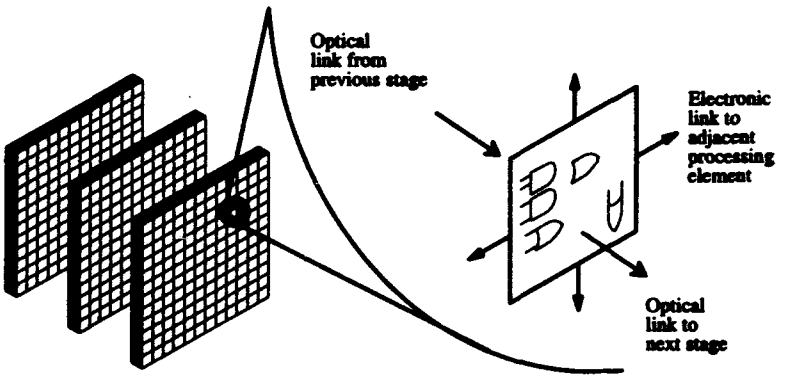


Figure 1. Schematic of the 3-D optoelectronic architecture

The tomographic sorting network (TSN) operates on a list of N words with M bits each and has M processing stages. A 2-D version of a TSN is shown in Figure 2. The N words are stored as M bit slices with the k-th slice containing the k-th significant bit of every word. All the bit slices are pipelined into the network, and remain there for a fixed number of clock cycles until they are sorted and ready to be transferred out and into a buffer. Sorting is performed by rearranging bits on the same slice so that, eventually, words are reshuffled and end up in ascending order from top to bottom. After the bit slices are loaded into the sorting unit, only control signals are transmitted from one stage to another to indicate any necessary bit exchanges. Two types of cells are present in the TSN: data and control cells. Each cell contains a flip-flop to hold the value of a bit. Rows of data cells are interleaved with rows of control cells as shown in Figure 2. The control cells are basically bitwise compare-and-exchange modules with some additional control lines. Optical signals propagate along the horizontal direction, while electronic signals traverse along the vertical direction.

A column of data and control cells constitutes a stage. The data cells in every stage will receive and hold the contents of the corresponding bit slice. Notice that all signals flow from left to right and that the stages are numbered in descending order from M to 1 (from left to right) to coincide with the bit order in a word. The number of data cells on each stage is equal to N, while the number of control cells is $N-1$. The number of stages that are required is equal to the length of each word in bits. The interconnection pattern between any pair of stages is a straightforward one-to-one mapping. As we are going to show later, the 3-D version of this sorting network retains these regular interconnections which can be realized optically using lenslet arrays between two stages. Another characteristic of this network is its regular structure which also contributes to a simple implementation and permits easy scaling up to accommodate larger sets of words.

Sorting Algorithm

As mentioned earlier, the sorting algorithm is a combination of the odd/even transposition and the radix sort algorithms. The process is initiated by looking at the most significant bit slice and trying to partition it into two groups: the 0-group at the top and the 1-group at the bottom. Every pair of adjacent bits that are not equal allows a decision on the relative magnitude of two words to be reached. If the two words must be exchanged, the process is completed in a pipelined fashion with an unconditional exchange control signal gradually forcing all the lower significance bits of the two words to exchange positions. If a decision cannot be reached at the MSB slice because the two bits under consideration are equal, the decision is deferred to the next most significant bit slice by sending a conditional exchange control signal to the next stage. This will force the next control cell to perform a bit comparison to determine the relative magnitude of the two words. While an unconditional or conditional exchange signal ripples through all the stages of the network, a new set of tests can be initiated at the MSB slice. The outcome of these tests and the subsequent execution of any action required will not affect the completion of the previously initiated exchanges that may still continue to occur towards the final stages of the pipeline.

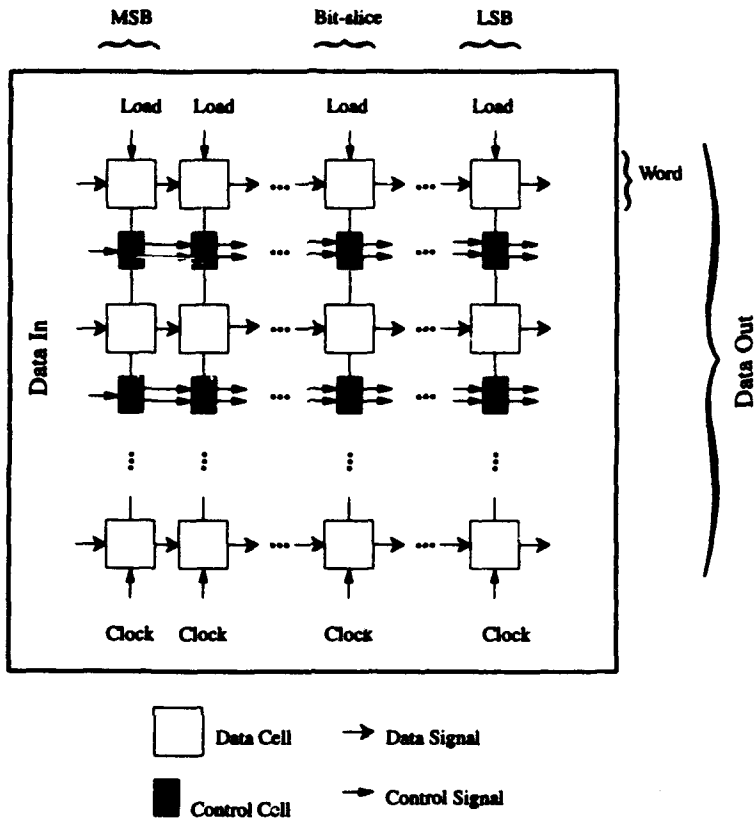


Figure 2. Block diagram of the 2-D tomographic sorting network

Three distinct phases are present in the tomographic sorting operation: (i) data loading, during which the bit-slices are pipelined into the sorting stages; (ii) sorting, and (iii) data unloading, during which the bit slices of sorted words exit the pipe.

Discussion

Despite the fact that special purpose numerical sorting processors and networks have relaxed the burden of sorting, when the size of these networks becomes large, the latency of the data input/output process and the complexity of the interconnections between stages become serious bottlenecks that render their implementation impractical. An optoelectronic sorting network such as the one we presented in this paper, using straight pass optical interconnections for interstage communications, allows for a simpler implementation. Although the TSN is somewhat slower when compared with other sorting networks such as the bitonic sorting network, it is simpler to implement. The optical bitonic sorting network [2] becomes prohibitively complex as the number of words to be sorted increases. The reduced space complexity of the TSN is its main advantage over other sorting networks.

We plan to design and fabricate a 2-D tomographic sorting unit in a VLSI chip and experiment with a smaller version of a 3-D architecture using arrays of VCSELs as sources and heterostructure phototransistors as detectors.

Acknowledgment

This work was partially supported by NSF-ERC grant ECD9015128, the Optoelectronic Computing Systems Center, the Colorado Advanced Technology Institute, and the Colorado Commission for Higher Education.

References.

[1] S. G. Akl, *Parallel Sorting Algorithms*, Academic Press Inc., Orlando, 1985.

[2] C. W. Stirk and R. A. Athale, "Sorting With Optical Compare-and-Exchange Modules," *Applied Optics*, Vol. 27, No. 9, pp 1721–1726, May 1988.

Sorting with an Optoelectronic Recirculating Architecture

F. R. Beyette, Jr., P. A. Mitkas, S. A. Feld, and C. W. Wilmsen

Optoelectronic Computing System Center
and the Department of Electrical Engineering
Colorado State University
Fort Collins, CO 80523, USA
Tel. 1-303-491-7577

Abstract. An optoelectronic implementation of bitonic sorting is presented which uses a recirculating architecture to reduce the required number of stages to two. This architecture decreases the mechanical complexity at the cost of system capacity.

While a wide variety of sorting algorithms have been explored for implementation in both hardware and software,[1] only the implementation proposed by Stirk and Athale[2] utilized the parallelism associated with optoelectronic processing arrays. Their pipelined architecture was based on the bitonic sorting network shown in figure 1. Each stage of the sorting network was comprised of latching compare-and-exchange (C&E) modules which performed a bitwise comparison on two input words. The stages were connected with optical perfect shuffle interconnection networks. Since the number of processing stages required to implement a pipelined sorting system is dependent on the number of words to be sorted, the realization of a large capacity pipelined sorter may be limited by a maximum achievable mechanical complexity (defined by Cheng et al. as the work required to build an optoelectronic system).[3]

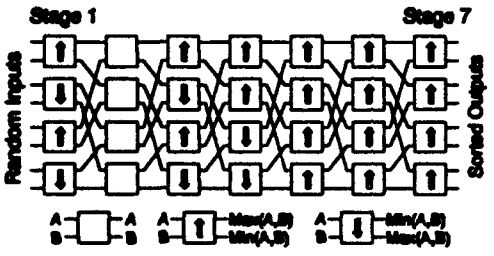


Figure 1. Bitonic sorting network.

This paper proposes an optoelectronic sorting implementation which reduces the number of required stages to only two and thus the system has a low mechanical complexity. Figure 2 shows the system layout of this sorter which is comprised of the two stages on opposite sides of a beam splitter. This arrangement is compact and the beam splitter provides a means for convenient optical input and output. Each stage of this recirculating system consists of C&E modules which compare adjacent elements of the input set. The optical outputs of one stage provide optical inputs for the other stage. Thus, the data can be transmitted optically between the processing stages through the same interconnection network used to implement the pipeline architecture.

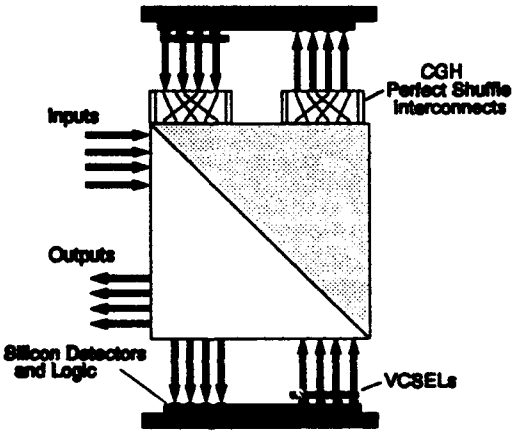


Figure 2. Recirculating bitonic sorter.

We are presently fabricating a 4 x 4 demonstration of this sorting implementation which will be presented at the conference. The bitwise C&E modules in each stage are based on the hybrid integration of silicon photodetectors, CMOS logic, and vertical cavity surface emitting lasers (VCSEL). In addition, this paper discusses fabrication reliability, capacity and mechanical complexity issues.

This recirculating architecture requires that each array hold all of the data bits for each of the words to be sorted. Thus, the data are available for word-wise C&E modules. However, the simplicity of bitwise C&E modules, which operate on pairs of input bits, is desirable. In order to compare m-bit words with bitwise C&E modules, m-bitwise C&E modules are electrically chained together on a single chip. These electrical connections are used to communicate control signals such as the exchange status and exchange criteria.

While the proposed recirculating architecture reduces the number of required processing stages to two, the system capacity (the number of words that can be processed in parallel) is also reduced unless the size of each stage is increased. Thus, there is a hardware trade off between the pipelined and recirculating architectures. The former requires many stages while the latter requires two large stages.

Figure 3 plots the system capacity as a function of array size for both architectures. As expected, the pipeline architecture exhibits significantly larger system capacity due to the n^2 dependence associated with the bit serial data flow. The capacity of the recirculating architecture is dependent on the word length, m. Figure 3 shows the capacity for m = 8, 16, 32, and n .

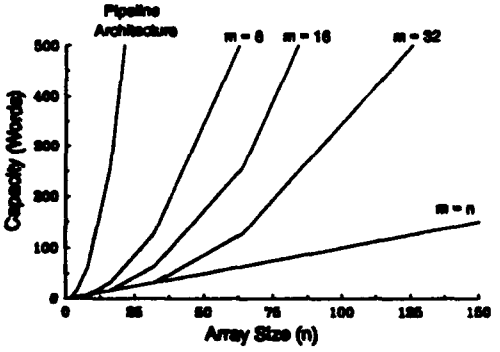


Figure 4. Capacity of recirculating sorter.

While it is possible to increase system capacity by utilizing larger arrays, available fabrication technology will set a maximum achievable limit on array size. In order to overcome this limitation on system capacity, it is possible to implement each stage of the recirculating architecture with multiple arrays. However, this increases the mechanical complexity of the system.

Figure 4 plots the number of arrays required to implement a bitonic sort as a function of maximum array size (and sorter capacity) for both architectures. For comparison it is assumed that system capacity is the same for both architectures. The shaded portion of figure 4 indicates the region where the recirculating architecture requires fewer arrays than the pipeline architecture. Note that for word lengths shorter than 64 bits, the number of arrays required for the recirculating system is always less that the number required for the pipeline system.

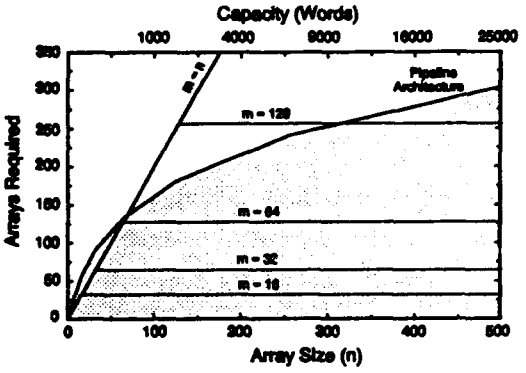


Figure 3. Arrays required to implement bitonic sorter.

Summary

We have presented an optoelectronic sorter based on a recirculating architecture. Since the recirculating architecture requires only two processing stages, the mechanical complexity of this implementation is lower than pipeline implementations. Each stage of the recirculating system is comprised of bitwise C&E modules which use electrically transmitted control signals and optical data transmission. We are presently fabricating a demonstration system which will sort four 4-bit words. The bitwise C&E modules used in this demonstration will be based on hybrid integration of silicon and VCSEL technologies.

Acknowledgments

This work was funded partially by NSF-ERC grant ECD9015128-the Optoelectronic Computing System Center and the Colorado Advanced Technology Institute.

References

1. S. G. Ak., *Parallel Sorting Algorithms*, Academic Press, Inc., Orlando FL, 1985.
2. C. W. Stirk and R. A. Athale, "Sorting with Optical Compare-and-Exchange Modules," Appl. Opt., Vol. 27, No. 9, pp. 1721-1726, May 1988.
3. L. Cheng, J. M. Wang, and A. A. Sawchuk, "Design of Space-Multiplexed Three-Dimensional Omega Networks and Their Optical Implementation," Appl. Opt., Vol. 32, No. 32, pp. 6482-6492, Nov. 1993.

Optoelectronic parallel processing system with reconfigurable diffractive interconnections

Andrew Kirk*, Tomohira Tabata, Takayuki Ishida and Masatoshi Ishikawa

Department of Mathematical Engineering and Information Physics, Faculty of Engineering, University of Tokyo, Bunyo-ku, Tokyo 113, JAPAN. Tel. +81 3 3812 2111 ext 6901

*Department of Applied Physics, TW-TONA, Vrije Universiteit Brussel, B-1050, Brussel, BELGIUM Tel. +32 2 641 3613

Abstract

The experimental implementation of an optoelectronic parallel processing system is described. A reconfigurable computer generated hologram is used to provide a programmable interconnection kernel and simple cellular processing operations are demonstrated.

Optical interconnections offer an attractive solution to the interconnection bottleneck which is encountered within high-speed parallel processing systems. In the case of single instruction multiple data (SIMD) architectures the interconnection mapping between the processing elements is shift-invariant. This has led to interest in the use of Fourier plane holograms to perform this operation. We have previously described the design of an optoelectronic processing system in which a programmable interconnection is obtained by the use of a reconfigurable computer generated hologram (CGH) [1]. In this paper we demonstrate simple cellular processing operations.

The structure of the optoelectronic cellular processing system is shown in Fig. 1. The processing plane consists of an array of optoelectronic processing elements (PEs), each of which receives optical input via a photodetector (PD) and provides an optical output via a light emitting diode (LED). The design of the processing elements is based upon that recently described by Ishikawa et al [2]. Each PE can perform simple bit-serial 8-bit addition and logic operations. The PEs are interconnected optically through the use of a reconfigurable Fourier plane CGH. The output from the LED array is imaged onto the photodetector array via the two lenses L. These form a 4-f optical system and the reconfigurable CGH is placed in the Fourier plane. The interconnection kernel is determined by the state of the CGH.

In the experimental system the PE array has been simulated with an array of LEDs together with a CCD camera. The reconfigurable CGH has been implemented by displaying a binary CGH pattern on a liquid crystal display (LCD) screen (containing 640 x 400 pixels). This is then optically reduced onto an optically addressed spatial light modulator (OASLM). This is a parallel aligned nematic liquid crystal (PAL) SLM manufactured by Hamamatsu Photonics K.K. and has a resolution of 50 lp/mm [3], allowing pixel sizes of 10-20 μm to be obtained.

Several simple feature detection operations have been demonstrated with this system. A binary CGH was designed by use of the simulated annealing algorithm [4]. This encoded a

convolution kernel which was designed to give a maximum response to groups of three isolated pixels in the input plane. Bipolar interconnection weights were achieved by using alternative rows in the output plane to represent positive and negative values. Ever... ...y this operation may be performed by the use of an array of bipolar photodetectors. In the experimental system this was emulated by measuring and subtracting the intensities in alternate rows of the output plane with a CCD camera. Several input patterns were presented via the LED array and it was found that the system was able to reliably differentiate groups of three isolated pixels as requir... ...he interconnection accuracy was found to be ±21% for this operation. This errror was dominated by the relatively large non-uniformity (16%) of the LED array intensites at the exit plane. The remaining 5% was due to errors in the CGH.

By updating the hologram pattern on the LCD the interconnection kernel may be modified, thus allowing a programmable SIMD processing system to be obtained. Further work is required to reduce the interconnection errors in the experimental system and to improve the high insertion loss. This is caused by the small hologram aperture together with the long focal lengths (2m) of the Fourier transform lenses and the Lambertian nature of the LEDs. We will present techniques by which the performance of this system may be improved and will consider issues of scalability. We will also demonstrate that analogue interconnection weights may be achieved by the use of this approach.

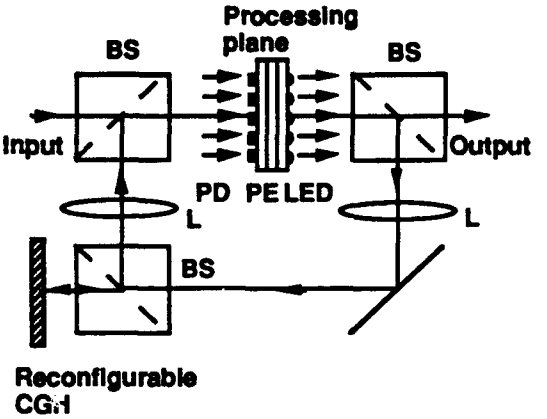


Figure 1. A looped optoelctronic cellular processing system:(PD - photodetector, PE - processing element, BS - beam splitter, L - Fourier transform lens).

1. A G Kirk , T Tabata, M Ishikawa, 'Design of an optoelectronic cellular processing system with a reconfigurable holographic interconnect', *Appled Optics* 1994 (to appear).
2. M Ishikawa, A Morita, N Takayanagi, 'Massively parallel processing system with an architecture for optical computing', in *Optical Computing Technical Digest 1993*, (OSA) 7 272-275.
3. N Yoshida, N Mukohzaka, T Hori, H Toyoda, Y Koboyashi, T Hara, 'Optically addressed liquid crystal phase only modulating spatial light modulator' in *Spatial light modulators and applications Technical Digest, 1993* (OSA) 6 p 97.
4. M R Feldman, C C Guest, 'Iterative encoding of high efficiency holograms for generation of spot arrays' , *Opt Lett* 14, 479-481, 1989.

Digital Optical Computing Architectures for Compute Intensive Applications

Peter S. Guilfoyle, Richard V. Stone, John M. Hessenbruch
OptiComp Corporation
P.O. Box 10779
Zephyr Cove, Nevada 89448
702-588-4176

ABSTRACT

Two digital optical computing architectures are being developed for compute intensive applications. A 32-bit digital optical processor has been implemented in hardware. Development efforts are underway to design miniature high performance optoelectronic computing (HPOC) modules.

INTRODUCTION

Two digital optical processor designs are being developed for hardware implementation. A second generation, 32-bit, digital optoelectronic computer (DOC II) prototype has been demonstrated at peak speeds of up to 10^{12} binary operations per second. DOC II is fully programmable and operates in a UNIX environment running RISC microcode. The 64 channel prototype operates at the 5000 photon per gate level, which is equivalent to 1.2 femtoJoules (fJ) per bit.

HPOC modules are being developed which exploit the same optical principles as DOC II. This new architecture integrates III-V technology with global (multi-dimensional) free space "Smart" optical interconnects. These low power modules are designed to operate at speeds up to 10^{14} operations per second. It is anticipated that each module will be less than 10 cubic centimeters and will yield 1 million optical interconnects.

DOC II

The hardware consists of two primary assemblies (Figures 1 and 2): the illumination assembly (Train A) and the modulation relay assembly (Train B). Both trains, which are optimized for maximum throughput at 837 nm, are positioned on a 36" x 48" optical table which is packaged in a optoelectronic cabinet.

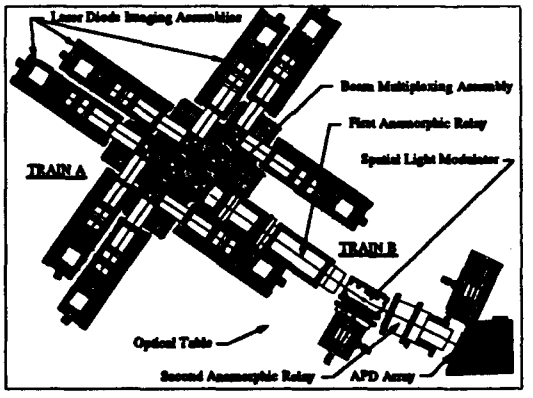


Figure 1: DOC II layout

The system architecture is based on a N^2 1x1 parallel interconnect topology. At the microcode level, each instruction can be written as a series of parallel combinatorial functionals. Data re-use at the control mask is achieved by operating on the data several times within one instruction. Up to 128 selections (logical functionals) of 64 input signals can be computed every 10 nsec. The selection occurs by use of a control mask which is clocked into the spatial light modulator (64 x 128 input control data matrix). Thus, the processor can achieve an optical data carrier fan-out of 1:128 and a control logic fan-in of 64:1.

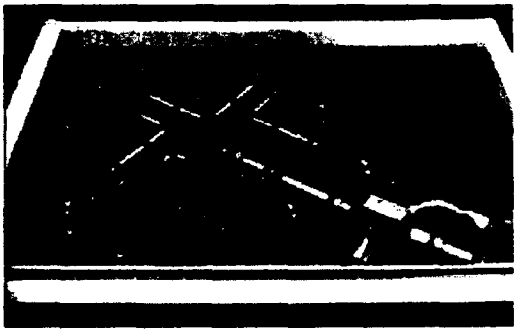


Figure 2: Photograph of DOC II layout

Current compute intensive applications include RISC emulation, full text data searches, and multimedia database development.

HPOC Modules

HPOC modules are being developed to provide a high speed, low power inter-module enhancement to GaAs logic families. The architecture exploits optical interconnect technology [1-2], and capitalizes on the advantages of "Smart" global interconnects which include high fan-outs and fan-ins, low power consumption, high algorithmic efficiency, and high noise margin. Because of the high fan-out /fan-in capability and high clock rates (100 MHz+), wide word processing is realized. This is accomplished by increasing the number of multi-input gates thereby decreasing the number of gate delays.

Figure 3 is an example of a "Smart" interconnect where the fan-in is N bits wide. When an arbitrary digital wide word is represented in its complemented form, the detector acts as an OR gate, literally performing a Boolean summation on the wide-word. After electronic inversion and laser emission, the output light represents the N-bit AND product of the input bits. Consequently, a single gate delay with 64-bit AND gates is possible. These structures may be arbitrarily expanded to any digital function required such as wide word addition, counting and floating point multiplication structures.

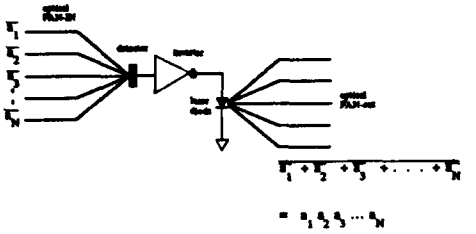


Figure 3: Simple example of "Smart" interconnect which demonstrates DeMorgan's theorem on free space optical interconnects to achieve a wide input AND function

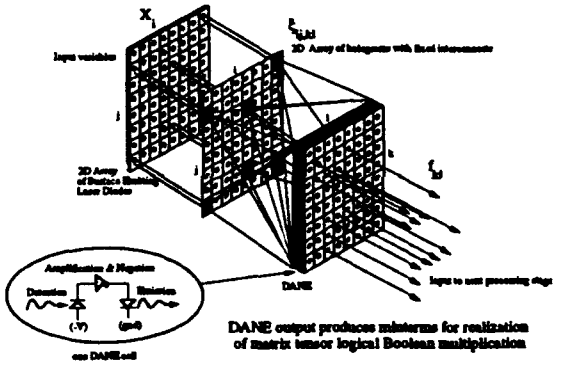


Figure 4: Single stage global free space "Smart" interconnect module utilizing DANE switching devices to form arbitrary minterms

Each interconnect module consists of an array of 2-dimensional GaAs DANE (Figure 4) cells and a diffractive optical interconnect element (DOIE). "DANE" is an acronym that refers to a "Smart" pixel which [1] detects light, [2] amplifies the result, [3] negates the result (inversion) and [4] emits the Boolean value through the output laser. DOIEs selectively image each element on the DANE array to predetermined positions on the next DANE detector plane. The logical functions performed by the combination of DANE and "Smart" interconnects are Shannon's minterms (functionals) at the photodetector array and the summation of minterms or complete instructions at the logical summation of the laser array.

In Figure 4, it is possible to expand both the ξ input arrays to two dimensions and the linear DOIE arrays to two dimensions. The DOIE arrays are performing a 4 dimensional interconnect. The input is written X_{ij}, the control mask is $\xi_{ij,kl}$ and the output may be written f_{kl} where a two dimensional array of minterms is generated. Each minterm generated in the output array can consist of up to i*j Boolean variables. Equation 1 summarizes the 4 dimensional interconnect scheme:

$$f_{kl} = \overline{\sum_{i=1}^{I}\sum_{j=1}^{J} x_{ij}\,\xi_{ij,kl}} = \prod_{i=1}^{I}\prod_{j=1}^{J} \overline{x_{ij}\,\xi_{ij,kl}} \qquad (1)$$

HPOC modules are being designed to solve compute intensive algorithms for applications such as data compression, data encryption, artificial intelligence, high speed switching, numerical analysis and finite element analysis. MCM communications applications are also being pursued because the global technology allows for increased fan-in and interconnect density.

[1] J. W. Goodman, F. Leonberger, H. Kung & R. Athale, "Optical Interconnects for VLSI Systems", Proc. IEEE Vol. 72, 1984.
[2] J. W. Goodman, "Optics as an Interconnect Technology" in H. H. Arsenault, T. Szoplik, B. Macukow, "Optical Processing and Computing", 1989 Academic Press Inc., Boston.

The Physical Design of an Optical Content-Addressable Parallel Processor [1]

Ahmed Louri and James A Hatch Jr.
Department of Electrical and Computer Engineering
The University of Arizona
Tucson, AZ 85721
Phone: (602) 621 - 2318, Fax: (602) 621 - 8076

Abstract - This paper presents the physical design and demonstration of an optical content-addressable parallel processor (OCAPP). We present the optical implementation of our laboratory prototype and discuss the experimental results of a representative string search.

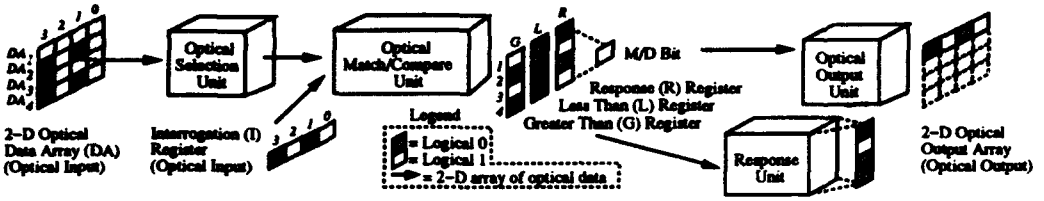


Fig 1: Structural organization of OCAPP.

Summary - The demand for high-speed parallel processors, stimulated by applications such as real-time control systems and database processing, encouraged researchers to seriously consider the use of optics for solving the problems experienced by conventional architectures. Our original research in this area led to the development of a new architecture called Optical Content-Addressable Parallel Processor (OCAPP)[1]. The architecture is designed to exploit optics advantages fully in interconnects and high-speed operations. This paper discusses the physical implementation of an experimental prototype version of OCAPP. that we are constructing in our Optical Computing and Parallel Processing Laboratory at the University of Arizona. We begin by first presenting a brief overview of the architecture, which is then followed by the layout of the optical system and photographs of the system's experimental results.

Architectural description of OCAPP:

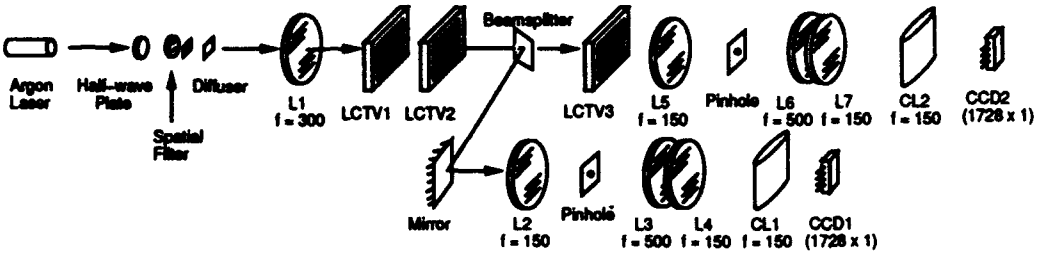


Fig 2: The optical system for the experimental OCAPP.

Fig. 1 illustrates the structural organization of OCAPP. The architecture consists of the *selection unit, match/compare unit (MCU), response unit, output unit,* and *control unit*(not illustrated). The selection unit is an $n \times m$ bit storage array loaded in parallel from optical memory. Word and bit-slice selection logic allow the enabling/disabling of words and/or bit-slices as required. The output of the selection unit is processed by the MCU where the parallel matching of the storage array and the $1 \times m$ interrogation register (I) occurs. The I register stores the comparand(s) of a search. The processing capability of OCAPP relies on the results of equivalence and threshold comparisons between the I register and a multi-element data set known as the 2-D optical data array. An equivalence comparison determines if two words are equal or not equal while a threshold comparison determines the relative magnitude of an inequality. Three $n \times 1$ bit output registers; R, G, and L result from the MCU operation. A one in the R register denotes the equivalence of the I register with the corresponding row of the enabled storage array. Accordingly, ones in the G(L) register indicate words of the storage array that are greater(less) than I. Meanwhile, the match/detector bit signifies that at *least* one word of the storage array matches I. Extended versions of the architecture make use of the single-iteration thresholding algorithm [2] to process threshold searches in constant time. Based upon the contents of the R, G, and L registers, the desired words of the data set are transferred to the output array by the output unit.

[1]This research was supported by an NSF grant No. MIP 9113688.

Optical Implementation of OCAPP: Our system uses a mixture of electronics and optics. To begin, all of the electronics are controlled by a Motorola M68HC11 microcontroller board. The spatial light modulators (SLMs) are active-matrix liquid crystal televisions (LCTVs). Instead of using frame grabbers to write the LCTVs, we interfaced video generation ICs to the microcontroller to generate a composite video signal of the pattern. After the patterns are written to the LCTVs, linear CCD arrays detect the result which is then digitized by in-house circuits.

A detailed illustration of the optical system appears in Fig. 2. The system is sourced by an Argon laser. The beam passes through a half-wave plate that aligns the light polarization with the liquid crystals in LCTV1. The diffuser makes the intensity variation of the data beam more uniform while also reducing the double-slit interference effects due to the pixel apertures. Lens L1 collimates the source beam. The combination of the first two LCTVs forms a vector-matrix multiplier. The I register is loaded into each row of LCTV1 while the 2-D optical data array is loaded into LCTV2. Multiply writing the LCTV1 pattern eliminates the beam expansion optics necessary for vector-matrix multiplication. The result is then split into two paths. The path reflecting off the beamsplitter is spatially filtered and imaged onto CCD1 by lenses L2, L3, L4 and CL1. This branch performs equality searches and reports its results in the R register (CCD1). In the other path, the bit-slice and word disabling functions of the selection unit are provided by LCTV3. The result is spatially filtered and imaged onto CCD2 by lenses L5, L6, L7, and CL to form the G register. The L register was not implemented because it does not demonstrate any more functionality than the G register does.

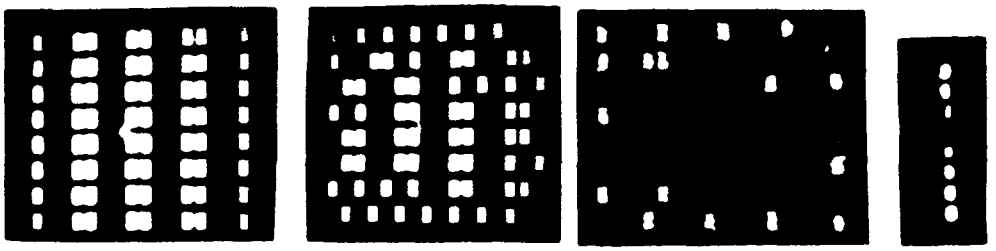


Fig 3: Physical demonstration of the parallel search capability of OCAPP.

Experimental Results: The data in our initial experiments is encoded using a dual-rail spatial encoding scheme [3]. In this scheme, both a binary value and its complement represent a single bit, requiring two pixels per bit. The optical matching operation is performed by superimposing the patterns written to LCTV1 and LCTV2 with the incident laser beam. Two input bits are logically equivalent if both pixels of the result are dark. Illumination present in either pixel of a result bit indicates the mismatch of the two input bits. Two words are equivalent if there is no light in any bits of the result.

Words are mapped onto the SLMs by partitioning the LCTV display areas into eight rows of sixteen squares to demonstrate an 8 x 8 data array. We load the comparand 10101010 into each of the eight rows of LCTV1. Meanwhile, the patterns 00000000, 01001010, 10101111, 00101010, *10101010, 10101011, 00001010, 11111111 are written to rows one through eight of LCTV2. Notice that the word in row 5, highlighted by the asterisk, matches the comparand while the words in rows 4 and 6 differ by only a single bit. These three rows ultimately determine the system's success since the digital thresholding of the result must be capable of distinguishing perfectly matching entries from those with at least a single mismatch.

Experimentally-obtained photographs of the data planes are shown in Fig. 3. The input patterns written to LCTV1 and LCTV2 are shown in Fig. 3(a) and Fig. 3(b), respectively. In Fig. 3(c), we report the results of the optical matching operation. We see that row 5 is completely dark because of the perfect match between the comparand and the fifth entry. A single pixel is illuminated in rows 4 and 6, indicating a single mismatch between these array entries and the comparand. Furthermore, the photograph in Fig.3(d) illustrates the output of the horizontal summing of Fig. 3(c). Note that the column vector is vertically inverted due to the spatial filtering operation. Overall, the results display a high contrast level and successfully demonstrate the system's ability to perform optical parallel string searches. The CCD detects the result and reports it to the microcontroller. A new set of patterns are generated and the feedback is completed. Please note that the architecture is not limited to parallel string searches. There are a wide variety of applications such as knowledgebase processing, parallel sorting, etc. that are excellent candidates for implementation on OCAPP. More details and results will be provided at the Meeting.

References

1. A. Louri, "Optical Content-Addressable Parallel Processors: Architecture, Algorithms, and Design Concepts," *Applied Optics*, vol. 31, no. 17, pp. 3241 - 3258, June 10, 1992.

2. A. Louri and J. A. Hatch Jr., "Optical implementation of a single-iteration thresholding algorithm with applications to parallel database/knowledgebase processing," *Optics Letters*, vol. 18, pp. 992 - 994, 1993.

3. S. Akyokus and P. B. Berra, "Optical Content Addressable Memories for Data/Knowledge Base Processing," in *Proceedings of the 5th International Symposium on Parallel Processing held in Anaheim, CA.*, pp. 202 - 207, 1991.

Phototransistor/Surface Emitting Laser Array Implementation of an Optoelectronic Data Filter

R. D. Snyder, F. R. Beyette, Jr., S. A. Feld, K. M. Geib,
L. J. Irakliotis, P. A. Mitkas, and C. W. Wilmsen

Optoelectronic Computing System Center
and the Department of Electrical Engineering
Colorado State University, Ft. Collins, Colorado 80523
1-303-491-7301

Abstract: An optoelectronic database filter demonstration using arrays of phototransistors and surface emitting lasers connected as AND and XOR gates will be presented.

Introduction:

Optoelectronics can have an advantage over electronics in database operations if the parallelism of optics is employed. Utilizing massively parallel optical signals from memories such as parallel read-out optical disks, volume holograms, and 3-D two-photon memories, large sets of records in a relation can be simultaneously compared against a search argument [1]. In the past much effort has been spent in developing either devices for optoelectronic systems or systems for optoelectronic devices but very little effort on integration of the devices with the systems. The database filter affords the opportunity to create a system with modern devices which can utilize massive parallelism in an application where electronics cannot realistically compete. Previously [1,2] we have reported optoelectronic architectures that function as a data base filter. Figure 1 shows the current architecture, which requires 2-D arrays of AND and XOR logic gates. We have shown that these smart pixels can be realized with a combination of heterojunction phototransistors (HPTs) which serve as photodetectors, amplifiers, and logic switches; and vertical cavity surface emitting lasers (VCSELs) which are efficient optical output devices that have a low divergence angle. This paper describes the implementation of a database filter types of devices.

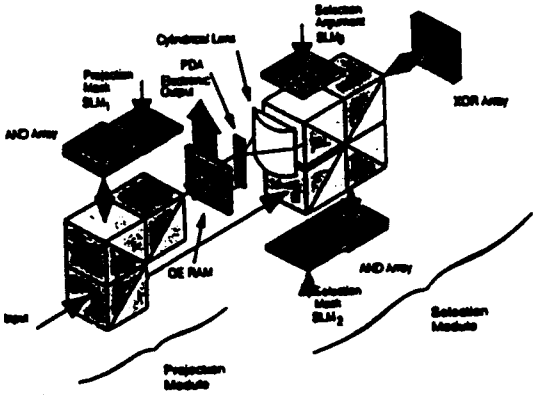


Figure 1: The optoelectronic data filter showing optical signal flow [1].

In the initial implementation, the logic gate arrays will utilize a hybrid interconnection of HPTs and VCSELs, each in separate packages. The AND and XOR gate arrays have been demonstrated as single pixels [3].Optical gains of these hybrid devices have been measured to be approximately 3 and are expected to increase to over 5 in the near future [3], which is sufficient to overcome the losses introduced by the beam splitters between successive stages of the filter. VCSEL arrays (Figure 2) have been fabricated and the mask set for the AND and XOR arrays have been designed and fabricated. The layout designs for the XOR arrays (Figure 3) required special consideration of the interconnects and traces for the bonding pads in order to minimize array area while maximizing the input window area of the phototransistors. This increases the gain efficiency of the detector and allows easy optical coupling of the input signals. An important characteristic of the XOR configuration is the fact that the series connected HPTs must be

able to conduct twice as much current as the parallel HPTs when both inputs are "ON" (logic 1), which enables the current through the VCSEL to fall below I_{th} and the output to be "OFF" (logic 0) [3]. This has been accomplished by reducing the input window of the parallel connected HPTs with an opaque metal mask. This method requires that the input spot be not smaller than the input window. The HPT arrays are being fabricated from InGaP/GaAs layers grown by gas source molecular beam epitaxy as described previously [4]. This choice of material system allows for dependable processing which will improve device uniformity across the wafer, as well as provide cascadability. The VCSELs were fabricated from AlGaAs/GaAs layers grown with MBE. The hybrid arrays will be packaged in DIP packages and optics will be used to direct and focus the optical signals. The system will be constructed on an optical table complete with an interface to an electronic computer to monitor operation and aid in obtaining results.

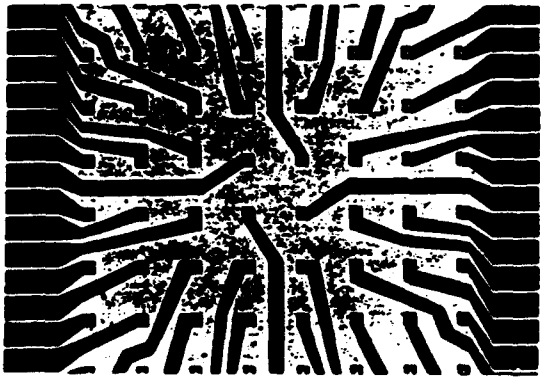


Figure 2: Photograph of 8 X 8 VCSEL array for hybrid smart pixels

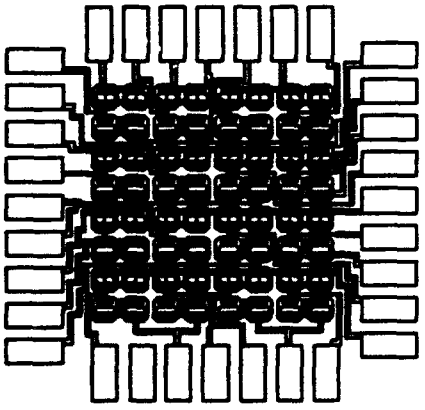


Figure 3: Layout of mask for XOR array

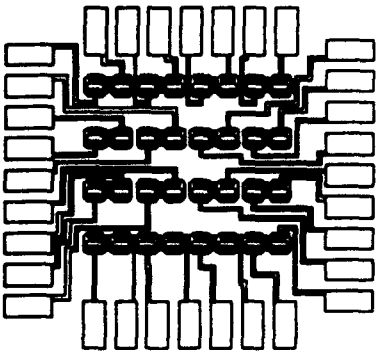


Figure 4: Layout of mask for AND array

References:

[1] P.A. Mitkas, L. J. Irakliotis, F. R. Beyette, Jr., S. A. Feld, and C. W. Wilmsen, "An optoelectronic data filter for selection and projection", to appear in *Applied Optics in Optical Computing*, (1994).

[2] P. A. Mitkas, and P. B. Berra, "Phoebus: An optoelectroinc database machine based on parrallel optical disks", *J. Parallel and Distributed Computing*, vol. 17, pp. 230-244, 1993.

[3] F. R. Beyette Jr., K. M. Geib, C. M. St. Clair, S. A. Feld, and C. W. Wilmsen, "Optoelectronic Exclusive-OR Using Hybrid Integration of Phototransistors and Vertical Cavity Surface Emitting Lasers", *Photonics Technology Lett.*, vol. 5, pp. 1322-1324, June 1993.

[4] C. M. St. Clair, S. A. Feld, M. J. Hafich, K. M. Geib, X. An, F. R. Beyette, Jr., G. Y. Robinson, and C. W. Wilmsen, "InGaP/GaAs Light Amplifying Optical Switch", Proceedings of Conf. on Lasers and Electro-optics, Baltimore, Maryland, p. 378, May 1993.

Fault-Tolerant Design in Digital Optical Computing

Kelvin Wagner
Optoelectronic Computing Systems Center, Dept of ECE, box 425
University of Colorado, Boulder CO 80309-0425 USA
1-303-492-4661 kelvin@boulder.colorado.edu

Abstract

Fault tolerance can be incorporated in digital optical computers using a distributed redundancy technique called quadding, at an expense of quadruplicating the hardware, and fan-in and fan-out increasing to 4.

A key requirement in a practical digital optical computing scheme is the ability to recover from transient and permanent device faults and signal errors. This is especially critical when using emerging technologies such as optical switch arrays which are bound to have large numbers of device errors, and for optically interconnected systems which may suffer transient errors such as that due to dust particles floating through the optical beams. Redundancy is the most common technique utilized to endow a system with a limited degree of fault tolerance and increase the system reliability beyond that given by the product of the probabilities of correct operation of the components. However, in many redundant systems, a voter is required to resolve conflicts between the redundant components, but a fault in the voter still produces erroneous outputs. Although multiply redundant voters can be incorporated, a mechanism must be included that eliminates and replaces faulty elements from the circuits, or else errors can propagate. These techniques can become quite complex and may be inappropriate for optical implementation. Another approach is to distribute the voter throughout the circuit using the technique of quadded logic.[1-3] In quadded logic, 4 copies of the circuit are produced, then interconnected in a permuted fashion that allows isolated errors within a quadded block of elements to be detected and corrected within the next few layers. This is often considered an expensive approach to fault tolerance, since it multiplies the hardware by a factor of 4, and doubles the fan-out and fan-in of the elements. However, the optical implementation of quadded logic in a regularly interconnected system has some attractive features as shown in Figures 1 and 2. The depth of the circuit is not increased, just the width, so no additional delay or speed penalties are imposed. The interconnections between the quadded circuits are reasonably regular and may be amenable to optical implementations. These interconnection topologies are reminiscent of optical crossovers, and might be implemented with a similar technique. One possibility is to interleave the original circuits on rows separated by 4, and interleave the quadded duplicates at the intervening positions. The same basic architecture of shuffles or crossovers within the rows can be performed, and holographic interconnections within a quadded set of 4 rows might not overly increase the system complexity.

The operation of a quadded system based on a regular logical structure is illustrated in Figure 1. Device errors are indicated as signals in boldface type. For example $x = 1$ should be represented at the input with four 1's, however the last input is in error. The quadded interconnects in the first layer mix the signals from the first two and last two redundant inputs, represented as (12,34). This corrects the NOR gate subcritical error $1 \rightarrow 0$ in one step. On the other hand, the input error for $\bar{x}$ is a critical $0 \rightarrow 1$ NOR error, which is converted by the first layer quadded interconnect to two subcritical errors, shown in italics. As long as the next layer of quadded wiring mixes the correct and erroneous signals, these subcritical errors will be corrected in the next layer, and this is accomplished by mixing the odd redundant signals and the even redundant signals, represented as (13,24). Similarly, errors introduced throughout the logical structure can be corrected, unless they appear too close to another error. As a result error free outputs are produced.

The regular, layered structure of the conventional digital optical computer interconnects is eminently suited for quadding without the complexities encountered in random logic. In addition, the quadded interconnects take advantage of the capabilities of the optical interconnects to accommodate complex wiring topologies. The isomorphism between the (12,34) and (14,23) quadding patterns with crossover interconnects should allow efficient implementation of quadding in crossover networks, and in these regular structures only two alternating quadded patterns are needed. Alternatively, by placing the redundant quadded logic devices in a sparse topology then a shift-invariant interconnection can be utilized. The example shown in Figure 3 shows that the (12,34) and (13,42) quadding patterns can be implemented with a fanout of 3, light efficiency of 66% and device packing densities of 66% and 50% respectively, while the quadding pattern (14,23) requires a fanout of 5, and achieves a light efficiency of only 40% and a packing density of only 44%. Quadding as 2 by 2 blocks allows 2-D shift invariant interconnections with 44-50% packing density. For these shift invariant topologies the (12,34) and (13,42) quadding patterns should be alternated.

This approach to redundant fault tolerant digital optical computing may allow the utilization of devices with increased probabilities of failure without an unacceptably large system reliability penalty. Such an approach may be required in order to make practical and reliable digital optical computers out of simp' arrays of unreliable switching elements.

The author acknowledges support of the NSF young investigator program ECS 9258088.

References

1. J. G. Tyron, Quadded Logic, in R. H. Wilcox and W. C. Mann, Eds., *Redundancy Techniques for Computing Systems*, Spartan Books 1962.
2. W. H. Pierce, *Failure-Tolerant Computer Design*, ch 5 Academic 1965.
3. Z. Kohavi, *Switching and Finite Automata Theory*, ch 8.6, Mcgraw-Hill 1970.

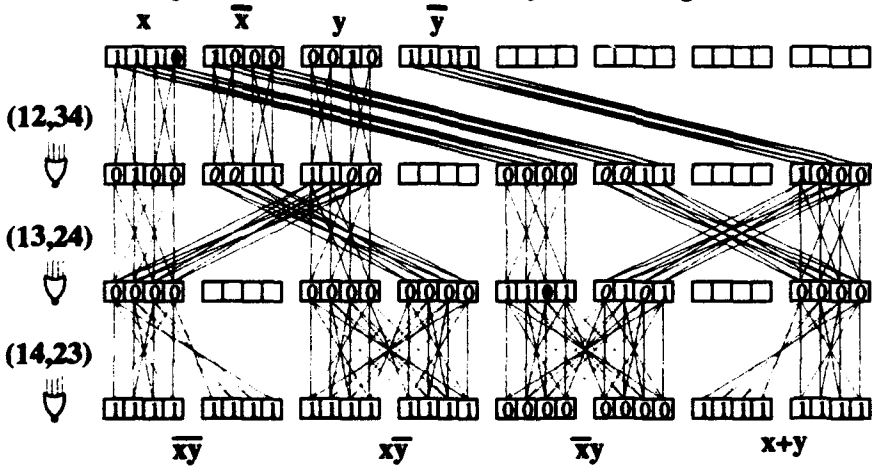


Figure 1: Error correction operation of a quadded regularly interconnected system.

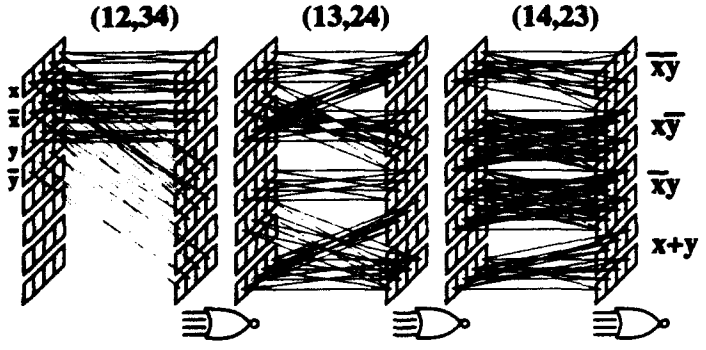


Figure 2: One possible 3-D topology of quadded regular interconnections.

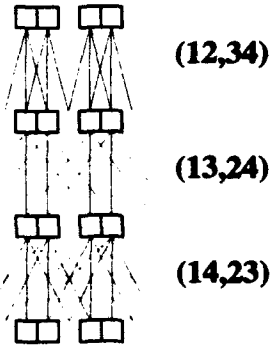


Figure 3: Sparse device layout for shift invariant quadding.

The need for a duality between algorithms and optical implementations

J.Ph. Heer, P. Pellat-Finet
École Nationale Supérieure des Télécommunications de Bretagne
Département d'optique
B.P. 832, 29285 Brest cedex, France.
Email:heer@gosc.enst-bretagne.fr

Abstract:

Considerations on number representation are introduced to make use of the advantages of optics in computer architectures. Specific optical systems are proposed for CORDIC algorithms and for discrete transforms.

The recent developments of bistable or fast switching optical components (S-SEED, combination of laser diodes and photodiodes) do not alone imply that optics could be an alternative technology for high speed parallel computers.

Generally the need for a duality between algorithms and optical implementations is not considered. In this paper we focus on number representations and give some examples of optical processing architectures. We distinguish two well known number representations: the position number representation and the residue number representation.

One of the most widespread position number representations is the binary number representation used in electronic digital computers. This number representation is imperfectectely suited to optical implementation because of the sequential nature and of the limited spatial representation which reduce the advantages of optical implementations. The signed digit number representation, introduced by Avizienis [1], is a possible alternative. This representation permits carry free parallel processing with a number of steps independent of the length of the number representation. If pattern recognition method is left aside, it is then possible to implement efficient algorithms based on elementary operations. CORDIC algorithms [4] are initially developped for binary number representation and need only additions and shifts. We demonstrate that CORDIC algorithms were also adaptable to modified signed digit number representation. We then propose an optical implementation which takes advantage of an incoherent illumination, spatial optical number encoding, parallel processing and low cost devices. A 25 MHz operating frequency is expected for an all optical comparator of modified signed digit numbers.

CORDIC-like algorithms could be written for higher radices which allows a more suitable spatial encoding for an optical processor. The position number representations are not optimal because they do not take full advantage of the parallelism of optics and optically addressed component arrays.

The residue number system [2] reduces the operation complexity by dividing the number representation into small independent integers. In this way, the quadratic residue number system allows computations on complex numbers. The spatial positions

of spots of light could be a possible optical representation. An operation is then easily obtained in one step by looking up the result in an optical memory. This addressing method permits parallel processing for all residues. We implement this number representation in butterfly structure for discrete transform computations [3]. The regular aspect of optical interconnections in butterfly structures is the most attractive property of a passive and parallel optical network. Each node of this network is made of an optical lookup table structure which performs computations on complex numbers.

For each mathematical number representation, specific algorithms are developped and benefit from the properties of optics. From our point of view, it is advisable to use only optical codings which are based on the binary intensity modulation of light. In this way, optical implementation could bring, for example, solutions to problems of interconnection in electronic parallel computers

1 Avizienis,A., Signed-digit Number representations for fast parallel arithmetic. *IRE Transactions on electronic computers*, **EC-10** (Septembre 1961), 389-400

2 Huang, A., Tsunoda, Y., Goodman, J.W., Ishihara, S., Optical computation using residue arithmetic*Applied Optics*, **18**, 2 (15 Janvier 1979), 149-162.

3 Truong, T.K., Chang,J.J., Hsu,I.S., Pei,D.Y.,Reed,I.S., Techniques for computing the discrete Fourier transform using the quadratic residue fermat number systems *IEEE Transactions on Computers*, **C-35**, 11 (Novembre 1986), 1008-1012.

4 Volder, J.E. The CORDIC Trigonometric Computing Technique. *IRE Transactions on electronic computers*, **EC-8**, 3 (Septembre 1959), 330-334.

Design of symbolic substitution systems for micro integration

C. Passon, K.-H. Brenner and W. Eckert, Universität Erlangen-Nürnberg, Physikalisches Institut, Angewandte Optik, Staudtstraße 7/B2, 91058 Erlangen, Germany,
Tel. +49 9131 858377, Fax. +49 9131 13508, e-mail: chris@ao.physik.uni-erlangen.de

Abstract: The design of micro optical systems has to consider features of the micro optical components. We introduce design concepts for micro optical systems exemplified at a system for symbolic substitution.

Introduction: Systolic arrays represent a concept for developing highly parallel computer systems using regularly interconnected simple processor arrays [1]. We have recently demonstrated that systolic arrays can be easily mapped to symbolic substitution rules [2] and thus can be implemented optically. We have constructed an optical pipeline adder based on systolic arrays, which was realised with macroscopic optical components.

This adder consisted of an array of 8x8 half adders, performing a full addition of 8-bit, dual rail coded numbers in a pipeline within 8 iterations. The active array consisted of 16x16 pixels. From space-bandwidth considerations one can derive that the imaging of an such an array requires only lens-diameters of a few hundred microns. Consequently the size of the whole system can be reduced into the submillimeter range using micro optical components. A concept for such a miniaturising of free-space optical systems was recently presented [3,4]. With this stacked approach, the packing density and the connectivity of three-dimensional optical systems can be utilised better that with planar integrated optics.

Design Concepts: Here we try to build on this integration concept in order to conceptually first realise a miniaturised version of the optical pipeline adder and then to generalise this architecture to implement general systolic array architectures. The concept takes the features of micro optical components into account and is thus compatible with fabrication constraints.

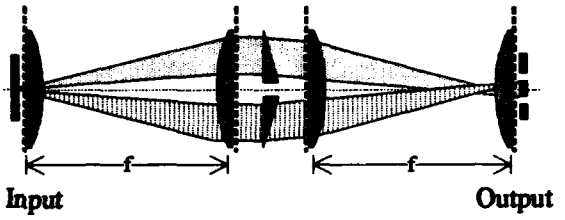


Fig. 1: Multiple imaging system

The optical pipeline adder consists of a recognition and a substitution part. Each part is realised by a sequence of two multiple imaging systems (MIS). Active components (NOR- and OR-gate arrays) are located at the exit of each part. Each MIS (fig. 1) consists of two Fourier transform stages, which are constructed as light pipes, because this configuration offers best light efficiency and resolution [5].

The complete sequence of components, needed to realise a substitution system is shown in fig. 2. This stretched out version could in principle be realised by a stack of optical components.
There are, however, a series of issues that have to be addressed

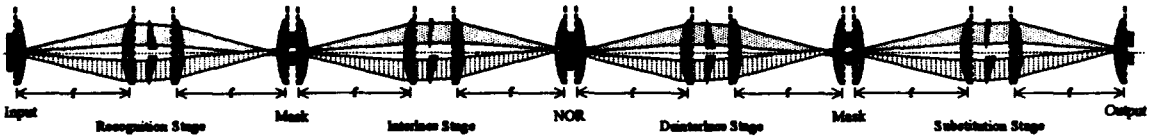


Fig. 2: Complete symbolic substitution stage

First, the number of layers, to be stacked, is very large in this version. This may cause problems in aligning the system.

Second, the active device in the centre of this sequence would have to be realised in transmission mode, which is undesirable both for thermal and for connectivity reasons. A more realistic design should place the active components at the ends of the stack. Thus a folding of the system is necessary.

The first version of folded systems, shown in Fig. 3 is a straight forward step from the multilayer approach to fewer layers, since the deflecting mirrors perform both functions, the folding of the system and splitting and shifting of data planes. The space between the light pipes, needed for the deflecting mirrors, requires a pupil between the mirrors to prevent vignetting. This is not compatible with a layered structure, since the pupil would have to be oriented perpendicular to the substrate surface, in order to be located in the centre between the mirrors.

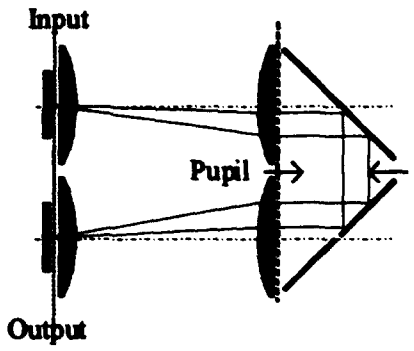


Fig. 3: Fourier folded MIS

Another limitation of this configuration is that the location a of the pupil has to satisfy the condition $D \leq a \leq f/2$. The largest numeric aperture (N.A.) is achieved for minimal a. Thus the best configuration $D = a = f/2$ results in a maximum N.A. of 0.5.
The light efficiency is determined by the diameter of the pupil, which is given by $Wp(a) = D(1-a/f)$.

In our second approach (fig. 4) we insert the mirrors into the light pipes. Here all components are arranged in separate layers and no vertically oriented components are necessary. In this approach, we move the image plane away from the input data plane. The N.A. is also limited by the increased distance resulting from the double mirror reflection. The minimum distance between lenses is 2D, resulting in a maximum N.A. of 0.5. Here beam splitters are necessary, which can be implemented by the LIGA technique [6].

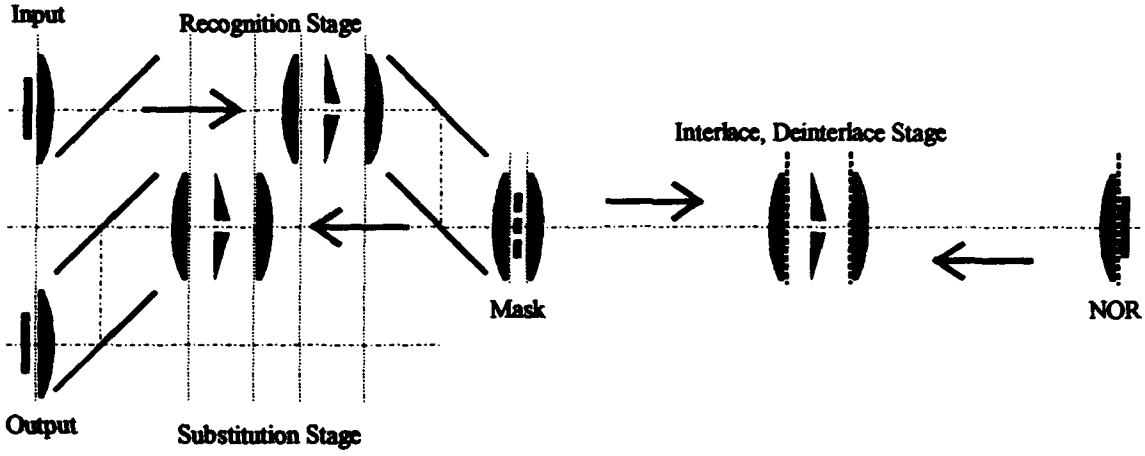


Fig. 4: Full folded substitution, with active components at the ends of the layer structure

In a next step we can exploit the fact that the required shifts in two successive stages are identical. Thus the same hardware can be used in the forward and in the backward direction, if a reflective array is placed between these stages (fig. 4, right side). This scheme can be replicated infinitely above and below. Thus the initially stretched out system can be arbitrarily cascaded to achieve complex systems and also make full use of the available substrate area.

[1] W. Erhard, D. Fey *Parallele digitale optische Recheneinheiten*, B.G.Teubner, Stuttgart, 1994
[2] D. Fey, K.-H. Brenner *Digital optical arithmetic based on Systolic Arrays and Symbolic Substitution Logic*, Optical Computing 1, 153-167, 1990
[3] K.-H. Brenner, Techniques for integration of 3D-optical systems, SPIE Proc. Vol 1544, Miniature and Micro-Optics, San Diego, p. 263-270, 1991
[4] K.-H. Brenner *Three dimensional microoptical integration techniques*, SPIE Vol. 1806, Proc. of the 16th Congress of ICO 1992, Topical Meeting on Optical Computing, Minsk, p. 98-104, 1992
[5] K.-H. Brenner, W. Eckert, C. Passon *Demonstration of a systolic array optical adder based on symbolic substitution*, Optics & Laser Technology, accepted Jan. 1994
[6] K.-H. Brenner, M. Kufner, S. Kufner, S. Moisel, J. Müller, A. Sinzinger, S. Testorf, M. Göttert, J. Mohr *Applications of LIGA components in three-dimensional microoptics*, Appl. Optics, 32 No. 32, 6464-6469, 1993

Optical thyristor based stochastic elementary processor

Guy Prémont, Philippe Lalanne, Pierre Chavel
Institut d'Optique Théorique et Appliquée, CNRS URA 14, BP 147, 91403 Orsay Cedex, France
Tel: (33-1) 69.41.68.41 Fax: (33-1) 69.41.31.92

Paul Heremans, Maarten Kuijk
IMEC, Kapeldreef n°75, B-3001 Leuven, Belgium
Tel: (32-16) 28.15.21 Fax: (32-16) 28.15.01

Abstract

Differential pairs of *pnpn* photothyristors, which behave as comparators with optical inputs and outputs, can be used with laser speckle to implement sigmoid updating probability processors and thus used in stochastic information processing.

Introduction

In optimisation techniques, the simulated annealing algorithm is widely used. It is based on the iterative procedure of an elementary stochastic operation which provides acceptance or rejection with sigmoid updating probability

$$P(F) = 1/\left[1+\exp(-F/T)\right] \qquad (1)$$

where the parameter T is called the temperature and should decrease slowly over time (annealing) to reach energy minimisation. F is called the force and is related to energy gradient. We will show that, when combined with speckle illumination, a simple processing element (namely a *pnpn* photothyristor) can perform this stochastic operation.

Optoelectronic elementary processors arrays are essential to the development of reliable high-speed parallel stochastic processing units. Many different optoelectronic devices could conceivably be used in the elaboration of new algorithms: SEEDs, optically activated VCSEL, etc. *Pnpn* photothyristors are particularly well-suited for these applications. These devices, first introduced by Jacques Pankove[1] and his co-workers, associate rapid and easy operation with high sensibility by combining light detection and emission in a single unit. The basic *pnpn* photothyristor acts as a simple light activated diode. This GaAs device has two stable operating points: when OFF, the impedance is high and no light is emitted, and when ON the photothyristor conducts and emits light. The *pnpn* photothyristors are most useful when two of them are combined in a differential pair[2]. This mode of operation is obtained by connecting two photothyristors in parallel. The voltage source applied to the pair is a three-step voltage sequence corresponding to reset, light detection and light emission. The differential pair of photothyristors can be viewed as a simple comparator; the photothyristor which has detected the highest intensity turns on.

Differential detection of random speckle

Laser speckle, as a means of generating high volumes of random numbers for parallel processing, offers great flexibility and easy implementation[3]. By differential detection of two speckle intensities, a random signal of zero mean is created and thus an easier implementation of a symmetric output probability function is allowed.

We illuminate a differential pair of *pnpn* photothyristors with an homogeneous random speckle pattern. As usual, the photothyristor detecting the most intense speckle will switch on. We can calculate this switch-on probability by relating it to the speckle probability function. The speckle intensity I on a detector can be statistically described by a gamma probability function where the only parameters are the mean intensity of the speckle field and the number of degrees of freedom of the detected speckle[4]. To simplify the analysis in this paper, we will reduce the gamma probability functions to gaussian ones. This approximation is valid when the number of degrees of freedom is large - in practice greater than 10. The switch-on probability is simply the probability that the first incident speckle intensity I_1 is larger than the second one I_2. We also implement the force F of Eq. 1 by illuminating the first photothyristor of the pair with an additional laser beam. The resulting switch-on probability $P(F)$ of the first photothyristor is given by

$$P(F) = p(I_1 + F > I_2) = p(I_2 - I_1 < F) \qquad (2)$$

The random variable $(I_2\text{-}I_1)$ is the difference of two known gaussian random variables having the same statistical parameters. The probability distribution of the new random variable will be a gaussian probability distribution of zero mean and double variance. Therefore, the probability that the *pnpn* where the additional force F is applied will switch on is

$$P(F) = \frac{1}{\langle I \rangle}\sqrt{\frac{M}{4\pi}} \int_{-\infty}^{F} \exp\left[-M(x/2 < I >)^2\right] dx, \quad (3)$$

which is simply an Erf function. This Erf function is equal to the sigmoid of Eq. 1, with a high degree of accuracy, provided that

$$T = \langle I \rangle \sqrt{\frac{\pi}{4M}}. \quad (4)$$

This temperature is found by fitting the slopes of the sigmoid and of the Erf function for F=0. Consequently, a differential pair of photothyristors illuminated with a speckle pattern should implement the stochastic updating operation of Eq. 1.

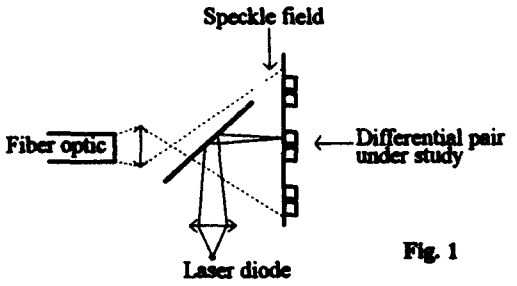


Fig. 1

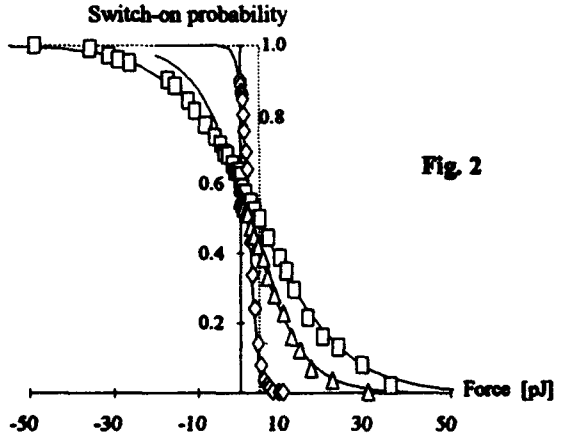


Fig. 2

Experimental results

The first tests of the differential operation described above were made with the experimental set-up shown on Fig. 1. The two photothyristors of the differential pair used were identical squares of 50x50 μm^2 separated by 15 µm. Two laser illuminations were used. First, a speckle pattern created by the modal noise of a step index fibre was used to randomly illuminate the pnpn integrated circuits. The successive generation of time independent speckles was ensured by a rotating diffuser inserted between the laser source and the fibre input. Then, a laser diode was imaged onto one of the photothyristor of the pair, thus acting as the force on one of the photothyristor.

Light emission was recorded by imaging onto a photodiode the photothyristor which was not illuminated by the force. We synchronised the detection with the voltage alimentation of the pair. The data points are computed switch-on probabilities, each corresponding to the average of 5000 intensity measurements. Experimental results are shown on Fig. 2. Three sigmoid updating probability curves, corresponding to three different temperatures, are shown. According to Eq. 4, these three curves were obtained with three different values of the mean speckle intensity $\langle I \rangle$. Since the temperature determines the amount of randomness in the updating operation, large values of T correspond to large values of $\langle I \rangle$. To show the obvious sigmoid characteristic of the response curves, the sigmoid updating probabilities of Eq. 1 were fitted to the experimental data points. Note that all the sigmoid curves are shifted to the right. This shift corresponds to the smallest energy required for the correct switch-on operation to take place and was caused by intrinsic asymmetry of the pair. It corresponds to an energy of about 5 pJ.

Processor architecture using this stochastic operation for low level image processing with arrays of pnpns will be discussed at the conference.

---

[1] J. I. Pankove et al. *A pnpn optical switch*, SPIE vol. 963, p. 191, Optical Computing 88, 1988.
[2] P. Heremans, M. Kuijk, R. Vounckx, G. Borghs, *Fast and sensitive two-terminal double-heterojunction optical thyristors*, Microelectronic Eng., 19, p.49, 1992.
[3] P. Lalanne et al., *2-D generation of random numbers by multimode fiber speckle for silicon arrays of processing elements*, Opt. Comm., 76, p. 387, 1990.
[4] J.W. Goodman, "Statistical Properties of Laser Speckle Patterns", in *Laser Speckle and related phenomena*, J.C. Dainty, ed., Chap. 2 (1975).

Multistage Interconnection Network with Wide Format Optoelectronic Switches and Optical Control for Massively Parallel Processing.

Valentin N. Morozov

Optoelectronic Computing Systems Center

University of Colorado at Boulder,

Boulder, CO 80309-0525, USA, Tel. (303) 492-0478

Abstract

Massively parallel processing (MPP) requires interconnection schemes for switching entire computer words in parallel. A wide format switch, based on free-space global interconnects and optoelectronic ExOR gates and capable of switching computer words in parallel under optical control is proposed. Distributed and centralized routing control is discussed and hardware realization is proposed.

Summary

I. Objective

Massively parallel processing requires highly parallel communications, and such communications has become a bottleneck with conventional electronic implementations because of the technological limitations of electrical interconnection in terms of area, latency, and power dissipation [1,2]. There are many efforts in developing free-space interconnection systems [3]. As a rule, these efforts are best suited to telecommunication applications but not to the computer area. In computer applications entire computer words consisting of 64-128 bits should be switched in time simultaneously. This requires the design of a wide-format-switch (WFS) with the minimal number of switching and processing elements to achieve minimal latency and the highest possible bit rate transmission.

II. Approach to the Solution of the Problem

The basic building block for multi-stage interconnection networks (MIN) is the 2x2 crossbar switch. If A and B are inputs, the outputs of a cross-bar switch are: $D = AC + B\overline{C}$ and $E = BC + A\overline{C}$, where C is the control signal. If $C = 1$, the outputs are $D = A$ and $E = B$ (bar state), but if $C = 0$, then $D = B$ and $E = A$ (cross state). There are many ways to implement the cross-bar switch function through complete logic function sets. For example, a wide-format-switch (WFS) for cross-bar switching could be implemented through an optoelectronic ExOR gate array and free space interconnects. An 8x2 WFS implementation for two 8 bit computer words is shown in Fig.1. The interconnection pattern for two digits is shown only. For an even number of MIN stages, input and output words will be in the same representation system - no additional complementing will be needed. Notice that the control signal C is applied to all of the bits in two computer words, thus achieving switching of the entire words simultaneously and in parallel. Major advantageous of optics, such as - significantly larger fan-out than in electronics and less power for long, off-chip runs, are used in this design.

III. Control Issues

A Multistage Interconnection Network is a practical compromise to create an interconnection mechanism that allows each processor to connect to only one other processor at a

time, but this interconnection pattern should be dynamically reconfigurable. The routing control for multistage networks can be centralized or distributed [2], and both of these techniques could be implemented in a MIN with WFSs. In distributed control the destination address propagates in parallel to the message, thus eliminating latency associated with address decoding. At each step only part of the destination address is decoded. In centralized control, paths are established via a controller which knows "a priori" the most efficient switch setting for a given permutation. An optoelectronic controller that could be used for the centralized control of a MIN has already been proposed by us [4]. In the holographic ROM, which serves as the interconnect path memory, routing paths are pre-recorded, and the desired paths are selected by the input OP Code. There is an internal feed back loop in the controller which gives rise to the possibility of reconfiguring the path routing automatically in accordance with the programs stored in the holographic memory and in the MPP executing routine.

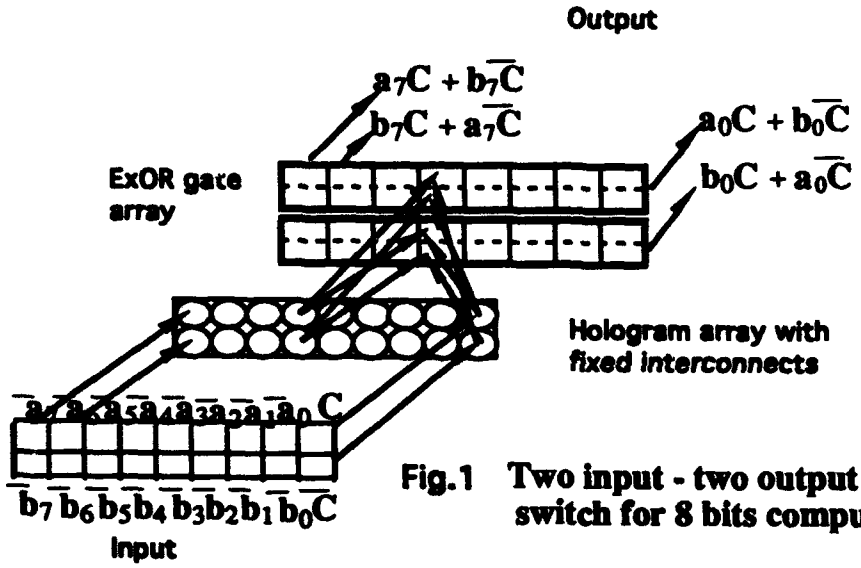


Fig.1 Two input - two output cross - bar switch for 8 bits computer words

IV Hardware realization.

As far as practical implementation is concerned, the proposal for hardware realization, based on an ExOR smart pixel array and holographic interconnects will be discussed. The important issue is mean-time-between-failure of the newly proposed interconnecting scheme. Factors affecting the BER in this free-space interconnected scheme will be considered.

Support for this work was provided by the University of Colorado Optoelectronic Computing Systems Center.

References:

1. H.J.Siegel "Interconnection Networks for Large-Scale Parallel Processing" Lexington Books, 1985.

2. T. Mark Pinkston "The GLORY Strategy for Multiprocessors: Integrating Optics into the Interconnects Architecture", Technical Report: CSL-TR-92-552, Stanford University, December 1992.

3. H. Scott Hinton, "Architectural Consideration for Photonic Switching Networks", IEEE J. on Selected Areas in Communications, 6, 1209 - 1225 (1988).

4 V. Heuring, V. Morozov "An Optically Controlled Digital Optical Matrix Processor", Proc. Soc. Photo-Instr. Eng. 1992 Int'l Symp. on Optical Science and engineering, 19-24 July, 1992, V. 1773, pp. 201 - 206.

Simulation and benchmark of a new algorithm for the Optical Cellular Image Logic Processor

Marc P.Y. Desmulliez, Brian R. Gillies, John F. Snowdon and Brian S. Wherrett

Department of Physics, Heriot-Watt University,
Riccarton, Edinburgh, EH14 4AS, Scotland,UK
Tel : UK 31 451 3068 E-mail : marc@phy.hw.ac.uk

Abstract

A shortest path hunt algorithm is simulated for the Optical Cellular Logic Image Processor. Its efficiency is compared with its serial implementation.

In 1961, Lee developed a maze algorithm capable of finding the shortest connections between two given points within a rectangular grid filled with obstacles [1]. For this algorithm, the nearest neighbours of the starting point are marked. The labelling is repeated in increasing order to the next nearest neighours until the finish point is reached. The shortest path is then found by tracing back the increasing sequence of the labels generated by the expansion process (figure 1a).

The shortest path hunt algorithm was later derived for single instruction multiple data (SIMD) computers within the logic image algebra formalism [2, 3]. The optical implementation necessitates however, at certain stages, a fan-out corresponding to the number of elements of the grid. The new version presented here utilizes a four-nearest neighbour interconnect such as in the optical cellular logic image processor (O-CLIP) [4]. The O-CLIP implementation of this algorithm has been simulated by a distributed array processor (DAP). Results of this simulation and benchmark to the serial Lee routine version will be presented.

A schematic of the O-CLIP architecture adapted to the algorithm is shown in figure 2. All the information as to the labelling of the elements can be held on just three label planes, which greatly eases the programming of the O-CLIP. Three different labels are in fact the minimum number needed to trace the shortest path from the finish point back to the starting point (figure 1b).

References

[1] C. Lee, "An algorithm for path connections and its applications", *IRE Trans. Electron. Comput.*, **EC-10** , 346-365 (1961).

[2] M. Fukui and K. Kitiyama, "Image logic algebra and its optical implementations", *Appl. Opt.*, vol. 31, **5** , 581-591 (1992).

[3] M. Fukui and K. Kitayama, "Applications of image logic algebra : wire routing and numerical data processings", *Appl. Opt.*, vol. 31, **23** , 4645-4656 (1992).

[4] B.S. Wherrett and J.F. Snowdon, "Prospects for optical computing devices based on bistable and logic plates", *SPIE Optical Computing 88*, Vol. 963, 15-22 (1988).

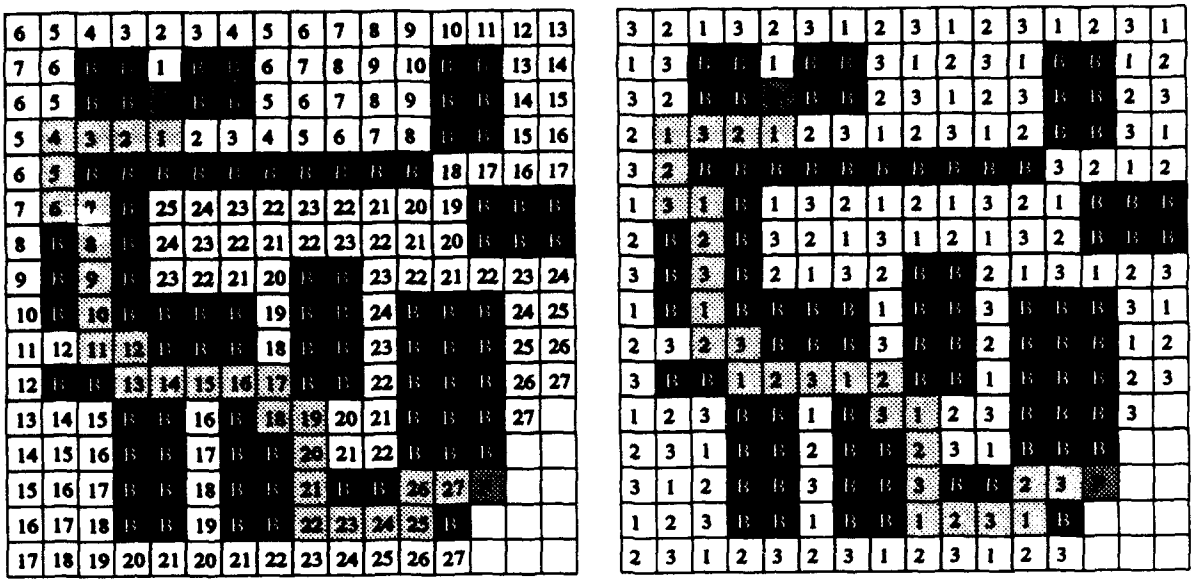


Figure 1: Lee and revised Lee routines

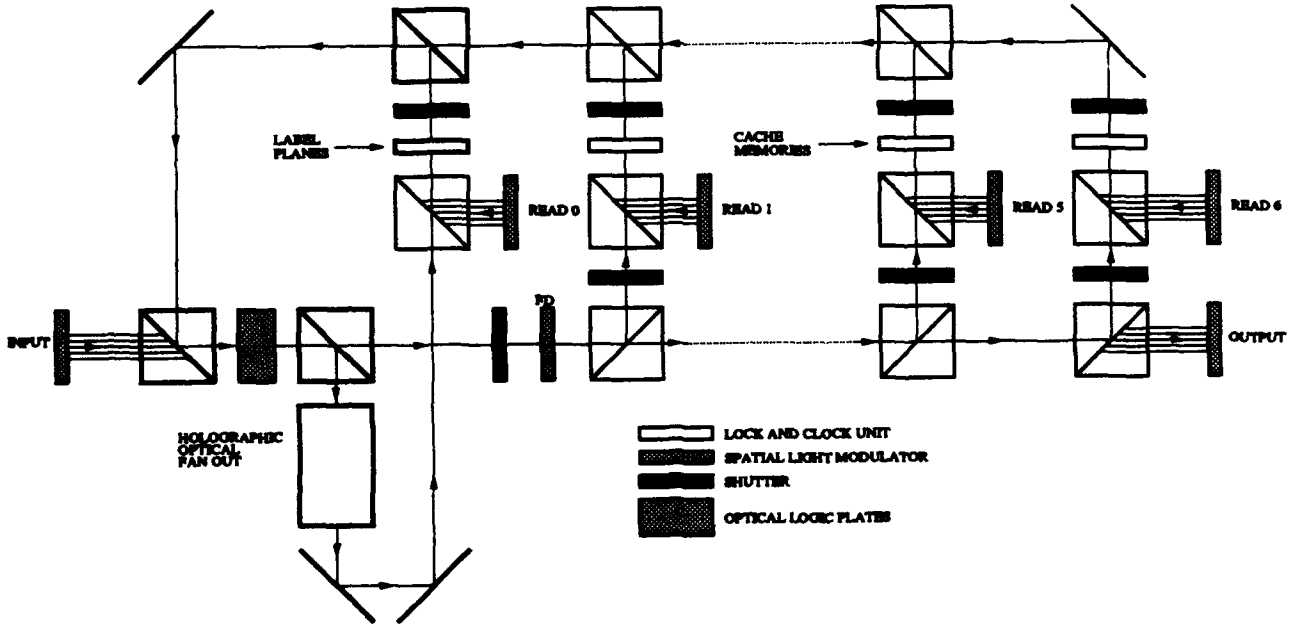


Figure 2: Layout of O-CLIP

An Optoelectronic Hybrid Parallel Multiprocessor System

Yimo Zhang, Wenyao Liu, Ge Zhou, Yong Wang, Dongjun Sun, Xiaoqing He

Institute of the Optoelectronic and Precision Engineering
Tianjin University, 300072, Tianjin, P.R.China

Abstract: In this paper the architecture of a 3D O-E hybrid multiprocessor is proposed. And the O-E hybrid interconnection network is used for this system.

1. The architecture of the optoelectronic hybrid parallel multiprocessor system

A optoelectronic hybrid parallel multiprocessor system is building up in our laboratory; in which there are three stages' processor arrays (2DPA); the optical interconnections are employed between these arrays, as shown in Fig. 1[1,2]. Its architecture is the 3D pipeline.

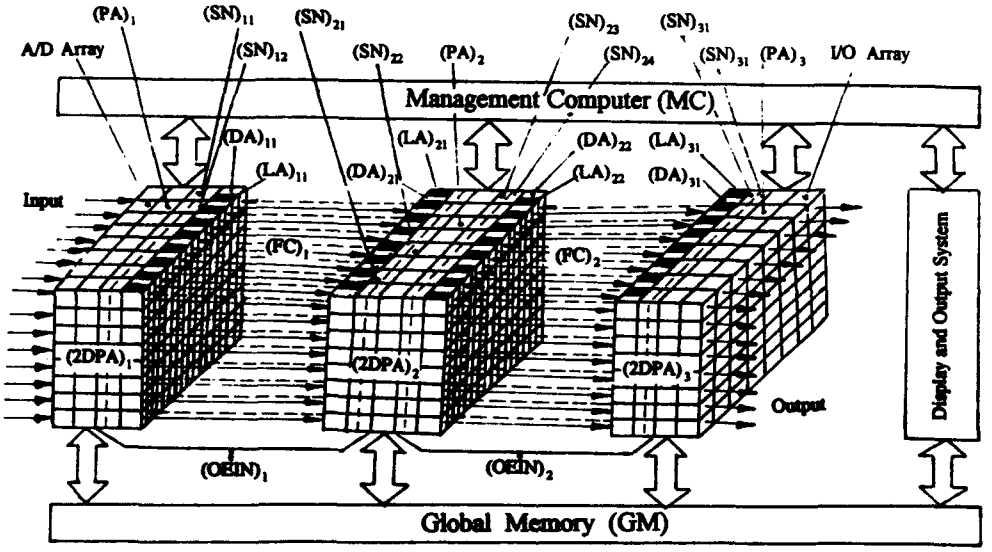


Fig. 1 The scheme of O-E hybrid parallel multiprocessor system

(2DPA)—2D Processing Elements Array; (PA)—Processing Elements Array; (SN)—Switch Network; (LA)—LEDs Array; (DA)—PINs Array; (FC)—Fiber-optic Channel; (OEIN)—O-E hybrid Interconnection Network.

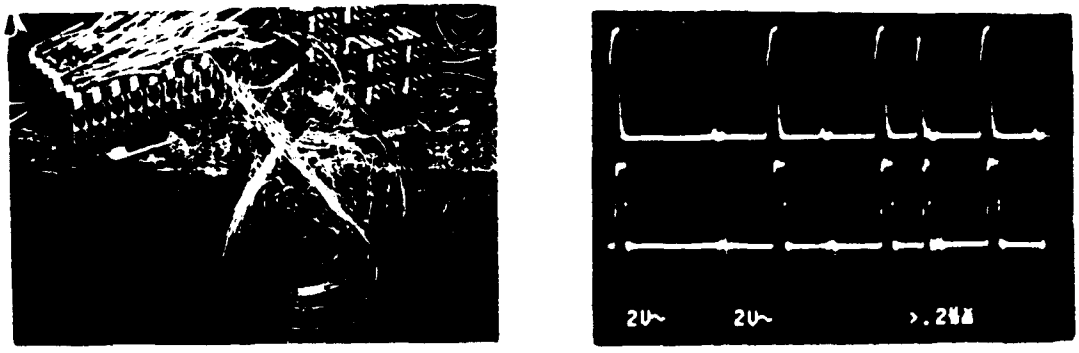
Every two dimensional O-E hybrid processor array (2DPA) comprises N×N processing elements (PEs). The interconnection in 2DPA is electronic. It can be easily reconfigured into various topologies.

2. O-E hybrid interconnection network

The optical interconnection provides the communication of two PEs located at two 2DPAs, respectively, in the third dimension. Then it can be described as follows:

$$(2DPA)_n\,(PE_{ij}) \Leftrightarrow (2DPA)_m\,(PE_{kl})$$

where n,m=1,2,3 and i,j,k,l=1~8. This is an O-E hybrid interconnection network, showing in Fig. 2: a) the photo of emitting array, fiber-optic channels and receive array; b) the photo of data transmission.



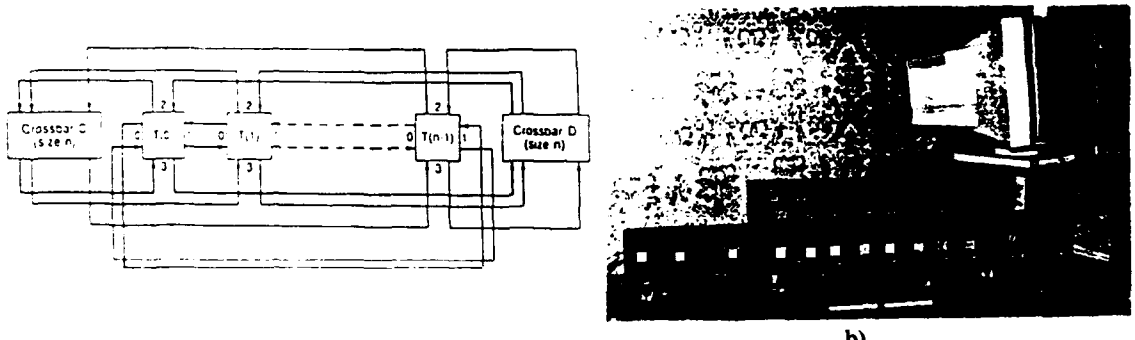
a) b)

Fig. 2. a) The photo of Emitting Array,Fiber-optic Channel and Receive Array
b) The photo of data transmission

3. Implementation of topological reconfiguration

The implementation of the topological reconfiguration relays on an electrically addressing device, that is an M×M (I/O) crossbar switch. In this system a 2M×2M(I/O) crossbar device is needed. So the extended complexer of the crossbar has to be developed with 3n crossbars mentioned above. As n=2, 6 crossbars with M×M (I/O) are used to obtain a crossbar complexer with 2M×2M (I/O). It can be easily programmed to determine which input connect to which output by instructions.

In 2DPA, the PEs with four pairs of input/output links are interconnected each other by using the two extended complexer of crossbars with 2M×2M (I/O). By programming such two crossbars, various topologies such as mesh, tree and hyper cube, etc., could be reconfigured. Fig. 3 shows: a) the scheme of the interconnection network; b) the photo of (2DPA).



a) b)

Fig. 3、 a) The scheme of the Interconnection network; b) The photo of (2DPA)

4. Conclusion

1) A O-E hybrid multiprocessor system is accomplished.
2) A O-E fiber-optic interconnection network is used in this system successfully.

Reference

[1] Y. M. Zhang, W.Y. Liu, SPIE Vol. 1983, 1993/429-431
[2] Y. M. Zhang, et al, Proc. of LEOS' 93, 1993, 73

Cellular Processing For Multilevel Edge Detection In A Hybrid Optical Shadow-casted Architecture

A. K. Datta and M. Seth

Department of Applied Physics
University of Calcutta
92, Acharya Prafulla Chandra Road
Calcutta 700 009, India

Abstract

A cellular image processing technique to detect edges of gray-image in an optical shadow-casted architecture is described. Coding of image is done for different preselected threshold levels and edges are obtained in a single operation.

Summary

For achieving parallel gray-image cellular processing [1] each cell I_{ij} of the image is assigned to a coded spatial pattern, termed as virtual processing element V_{ij}. The coded spatial patterns are generated for conversion of gray-image I to binary virtual image V, from gray pixels of the original image, the size of which is dependent on the number of gray levels selected. In terms of image logic algebra (ILA) [2] the output edge-detected state of V can be obtained by the following operations:

$$O|M;N| = V|M;N| \,.\, (\partial_{1,0}\overline{V|M;N|} + \partial_{0,1}\overline{V|M;N|} + \partial_{-1,0}\overline{V|M;N|} + \partial_{0,-1}\overline{V|M;N|})$$

where $O|M;N|$ is the output edge detected state of V. M and N are the number of horizontal and vertical cells in the image respectively and therefore i varies from 1 to M and j varies from 1 to N. $V|M;N|$ and $\overline{V|M;N|}$ are the input virtual image and its inverted forms respectively. ∂_{xy} is a shift operation by x cells horizontally and y cells vertically over an image. '+' and '.' are the logical OR and AND operations respectively.

To detect edges in a shadow-casted optical architecture the input virtual image V is inverted and optically shifted through one V_{ij} cell in four directions and logically OR-ed. Subsequently the AND operation between the resultant image and the input image V_{ij} is obtained by optical parallel array logic (OPAL) processing [3]. After proper sampling of the processed image, the edges are obtained for the virtual pattern. The processed virtual output image is then decoded to give the edge detected image at multiple pre-selected levels.

The proposed experimental set-up (fig.1) consists of a pair of four LED sources where operational kernels are selected by proper on-off states of the LEDs for desired logic operation. A rule is proposed for multiple level coding of gray-level image which converts I to V. Results obtained for a simple gray object in the actual set-up proves the validity of the method. A computer simulated edge detection based on the proposed technique for a tomoscan picture (fig.2a) is presented with four and eight intensity levels in fig.2b and fig.2c respectively.

References:

1. J. Taboury, J. M. Wang, P. Chavel, F. Devos, P. Garda, Appl. Opt. 27, 1643-1650 (1988).

2. M. Fukui and K.Kitayama, Appl. Opt. 31, 581-591, (1992).

3. S. Kakizaki, J. Tanida and Y. Ichioka, Appl. Opt. 31, 1093-1102 (1992).

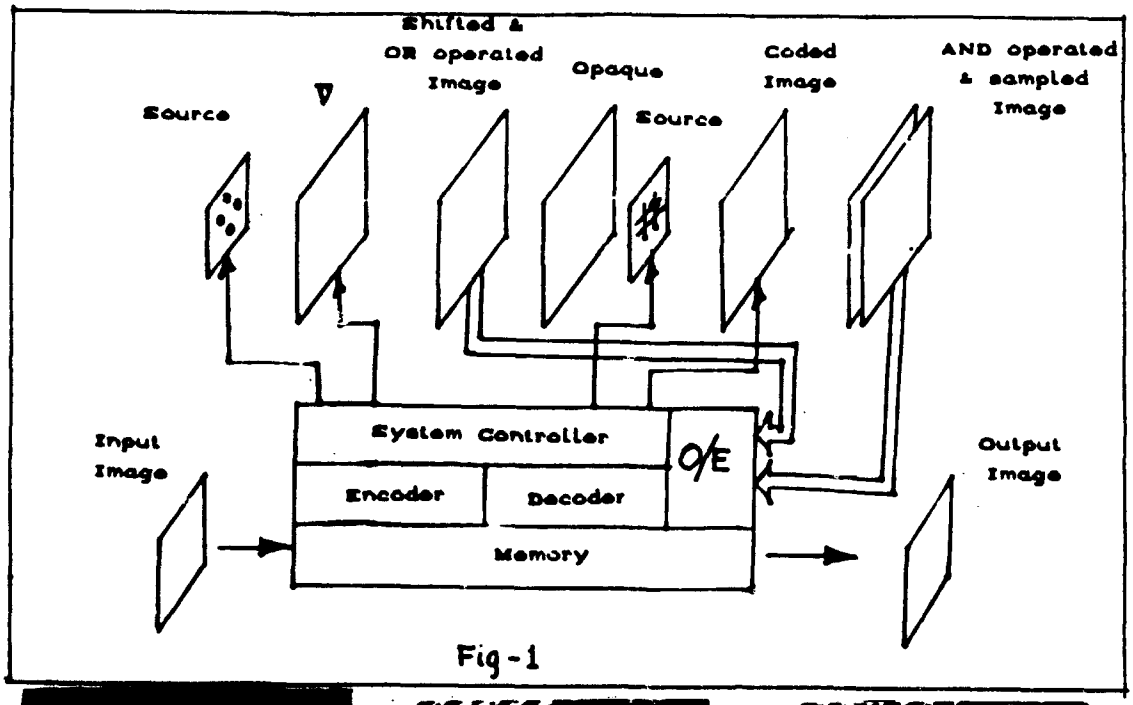
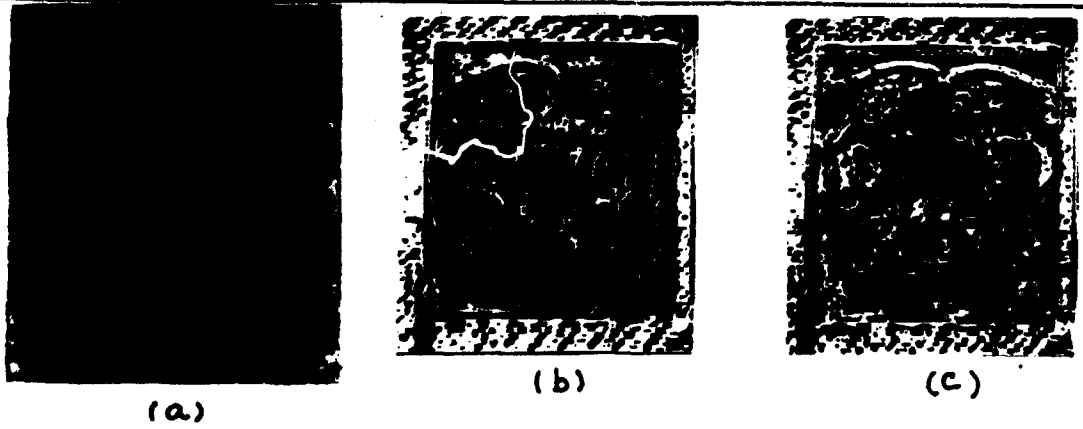


Fig-1



(a) (b) (c)

Fig-2

Image Processing by System Based on a Optoelectronic Active Medium with Controlled Connections.

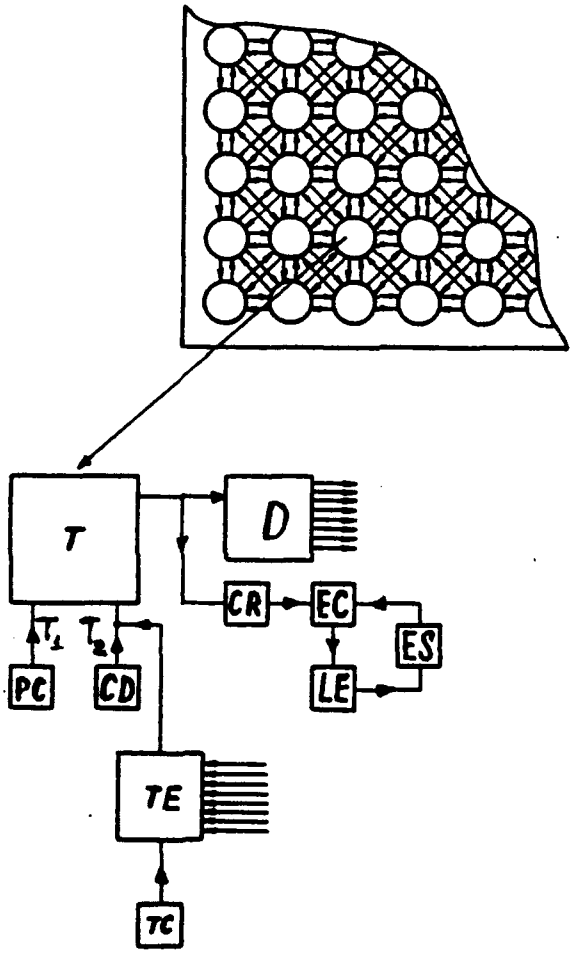
Yuri I. Balkarey, Mordukh I. Elinson.

Institute of Radio Engineering and Electronics,
Russia Academy of Sciences,
11 Mokhovaya St., Moscow, 103907, Russia.
Tel: (095) 462 1031; Fax: (095) 203 8414
E-mail: LAB191@IRE.UUCP.FREE.MSK.SU

ABSTRACT

New abilities of image processing appearing from introduction of controlled local connections between cells in optoelectronic trigger medium are discussed.

1. An optoelectronic memory usually consists of independent electronic cells with optical inputs and outputs. We consider new abilities of optoelectronic memory arising from local connections between cells. With specific types of connections memory medium is able to extract (process) the informative features of recorded images. Resolution and memory capacity are determined by the microelectronic technology possibilities. We will refer to a memory medium with connected cells as CMM.



2. Consider the binary optoelectronic memory. Every cell comprises trigger T with an optical input and output. The projected onto medium image is percepted by photocell PC, and is recorded by flip- over from state T_1 to state T_2 ($T_1 \Rightarrow T_2$). The circuits (photocells) for reading (CR) and destroying (CD) are switched off during recording.

Uniform illumination of all CR turns on light emitters (LE); it restores recorded images (when the photocells CR and CD are turned off).

The picture is destroyed by flip- over $T_2 \Rightarrow T_1$ by uniform illumination of all CD.

Every cell is connected with its nearest eight neighbors. The connections are of inhibitory type; they block up connected cells, i.e. prevents $T_1 \Rightarrow T_2$ flip-over. A special threshold element (TE) (coupled with CD to the arm of trigger T_2) combines all connections from

neighboring cells. The threshold control unit (TC) sets the number of connections (N) necessary for a signal to appear at the TE output. This signal switches the memory cell off ($T_2 \rightarrow T_1$) in the same way as CD signal does. The system also includes a connection distributor (D) and light emitter control unit (EC). When LE is turned on, after the delay time the ES unit switch the LE off for the whole image analysis cycle.

The main feature of CMM with the inhibitory connections is that the memory state of the chosen cell depends only on the number of illuminated neighbor cells which prevent to $T_1 \rightarrow T_2$ flip- over by their connections. Of course, there is also a back inhibitory effect of the chosen cell on its neighbors.

3. We discuss the possibilities of CMM for image processing. We assume that the minimal size of a picture element is of the same order as of a cell size and the distance between cells is substantially smaller than the linear cell size.

When N = 1, the memory records only isolated elements of a size of the order of a cell, with at least a one cell spacing. It is not possible to record another picture elements, because even one inhibitory connection prevents this. The addition of a new neighboring illuminated element leads to local information destruction.

When N = 2 the memory extracts both 1- cell and arbitrary 2- cell spots. If N = 3 it is also possible to record 3- cell spots and arbitrary lines and contours of a one cell thickness; then the neighboring elements are connected only by two inhibitory connections. With the increasing of N the minimal size of recorded spots is increased, and cells in off state can appear inside illuminated spots.

Large- pattern contours can be extracted when $N \geq 5$: inner cells are inhibited, whereas contour cells (which have no illuminated neighbors outside the pattern) are not inhibited.

Analysis of pictures, maps etc. is best carried out by "step by step" cycle increasing N from 1 to 8 with exclusion of fragments extracted at the (N - 1)th step. In fact CMM can be used for decomposition of the initial picture into fragments: small spots, contours of large spots, lines, lines crossings, angles, etc.

4. An important possible application is extraction of moving fragments. The initial picture is projected onto the CMM and then all corresponding LE are turned off by unit ES. Then the initial picture with shifted elements is projected again. Obviously, only emitters of the cells corresponding to recorded shifted elements are turned on. The subsequent projecting operations make it possible to determine the directions and velocities of moving elements. This method is also suitable for extraction of motionless but distinct parts of patterns.

5. The possible applications of CMM are expanded if every cell is connected not only to the nearest cells or not only by inhibitory connections. Activating excitatory connections (with inhibitory connections switched off) for certain time it is possible to enlarge the size of extracted spots and the width of lines, and to spline indented edges.

Parallel Image Processing by Media of Resonantly Excited Oscillators

Yuri I. Balkarey, Alex S. Cohen, Walter H. Johnson, Mordukh I. Elinson, Michael G. Evtikhov, Polievkt I. Perov.

Institute of Radio Engineering and Electronics,
Russia Academy of Sciences,
11 Mokhovaya St., Moscow, 103907, Russia.
Tel: (095) 404 6175; Fax: (095) 203 8414
E-mail: LAB191@IRE.UUCP.FREE.MSK.SU

Abstract

A system of oscillators with optical inputs and outputs transforms a projected image into spatial distribution of oscillator frequencies. Resonant excitation of different groups of oscillators is discussed as a new method of image processing.

1. The main idea of the discussed approach is the following [1]. Suppose there is a matrix of identical quasiharmonic noninteracting oscillators with optical inputs and outputs. The image I(X,Y) is projected onto the matrix and it leads to the change of oscillators' frequencies ω_0:

$$\omega_0 \Rightarrow \omega_{loc} \equiv \omega_0 + \alpha I(X,Y)$$

Hence the image is encoded into the spatial distribution of frequencies.

Then the homogeneous pumping is projected onto the medium through a wide aperture modulator with a harmonic regime of modulation (frequency Ω). The pumping excites only such parts of medium which correspond to the condition: $\omega_{loc}(X,Y) \approx \Omega$. The parametric resonance can be used by the same way. Therefore varying Ω we can provide the parallel extraction of regions of equal intensity. If oscillators' inputs are sensitive with respect to light wavelength it is possible to extract regions of certain color.

Example of a problem which can be solved by the proposed method. A sheet of paper contains a set of patterns drawn with different intensities (or colors). Projecting the sheet onto the medium and using a set of appropriate Ω it is possible to extract every pattern.

2. We have studyed different modifications whereas th additional elements are used: passage of analyzing pictures through a modulator; periodic shift of picture along the medium; usage of background light pump distribution in the form: $I_B(X,Y) = I_0 + F(X,Y)$, where, for example, $F(X,Y) = F_0(X^2 + Y^2)$. Such complications allows us to realize the following procedures: extraction of certain parts of picture; removing small scale distortions from patterns; extraction of contours, points of extrema; correlative comparison of images; determination of common and distinct parts of images, moving elements, etc.

3. Media of oscillating elements can be realized by the several ways.

a) Matrices of microcavity lasers.

There are structures in which every microcavity laser is integrated with a photocell for noncoherent light [2]. Informative light flow is percepted by the photocells and changes the frequency ω of laser electron- photon resonance ($\omega \sim 10^9$ s^{-1}). Existing electrooptical modulators can excite this resonance by modulation of pumping light. So we only have to find the fact of lasers' modulation.

Matrices of microcavity lasers without photocells can also be used when the coherent informative light flow is used.

b) Matrices of passive optical bistable elements in regime of optical oscillations [3] can be used by the same way.

c) Analog microelectronic matrices containing oscillating circuits with optical inputs and outputs are convenient too.

References

1. Yu.I. Balkarey, A.S. Cohen, W.H. Johnson, M.I. Elinson, M.G. Evtikhov, P.I. Perov. (1994). Homogeneous neuron- like microelectronic media from oscillating elements for image processing. Russian Microelctronics, v. 24, no. 3.

2. W.K. Chan, J.P. Harbison, A.C. von Lechmen, L.T. Florez, G.K. Nguen, S.A.Schwarz. (1992). Optically Controlled Surface- Emitting lasers. Appl. Phys. Lett., 58, 2342- 2344.

3. K. Ikeda, O. Akimoto. (1982). Instability Leading to Periodic and Chaotic Self- Pulsations in a Bistable Optical Cavity. Phys. Rev. Lett., 48, 617- 620.

Planar - Free Space Optical Circuits Based On The "Transverse Lock-And-Clock" Architecture

George V. Sinitsyn, Fedor V. Karpushko

Division for Optical Problems in Information Technologies
Academy of Sciences of Belarus
P.O.Box No.1, 220072 Minsk Belarus
0172/39 58 82 (tel), 0172/32 45 53 (fax)
Email: dopit%bas02.basnet.belpak.minsk.by@demos.su

Abstract. An approach of "transverse interconnection optical processor architecture" is proposed which allows flexible optically programmable data exchange between individual beam channels without changing their relative dispositions.

Using the light as information carrier implies usually that the direction, in which data are transported in free space or in waveguide, coincides with the light beam direction. However, there are a number of nonlinear optical phenomena such as transverse effects in optical bistability that allow to direct the information flow perpendicularly to the light beam. When studying such nonlinear transverse phenomena it has been found that there are different steady profiles of the output beam/image intensity for the same distribution of input light interacting with a bistable interference layer. The selection of a desired profile as well as transitions between them can be easily controlled optically. It gives a basis, for instance, for all-optical implementation of 2D-data shift. In this method all the stages of the information transfer are performed in the plane of matrix of optical elements. It provides an opportunity for organizing the interconnections and information exchange between neighbour logic elements/pixels within 2D-array leading to new optical computer architectures.

In this paper the method of "transverse lock-and-clock" processing [Ref.] is extended to a "planar - free space" optical interconnections and circuits. The basic idea of the "planar - free space" architecture is to combine the parallel data transfer between sequentially located (within loop parallel processor) matrices of switching/bistable elements and planar transverse interconnections and processing within the plane of each matrix.

In such an approach an ensemble of light beams (a digital image) preserves the topology of their relative disposition (with no shuffle, etc.) when propagating in free space between two sequentially located nonlinear matrices, in contrast to other flexible interconnection architectures. The flexibility of the information connections between different parts of the image is reached due to the optically programmable transverse transport and redistribution of the different logical states of transmission/reflection within the matrices of nonlinear elements. As a result, the data in different individual channels are exchanged without changing the spatial positions of the beams that carry the data along the processor loop.

The examples of design and experimental modeling of all-optical serial-parallel and parallel-serial data convertors, stack and associative memory, multiplexor-demultiplexor, non-blocking crossbar, planar loop circuits and regular networks are given (Fig.) using 2D bistable thin-film Fabry-Perot interferometer with optical aperture of 40mm.

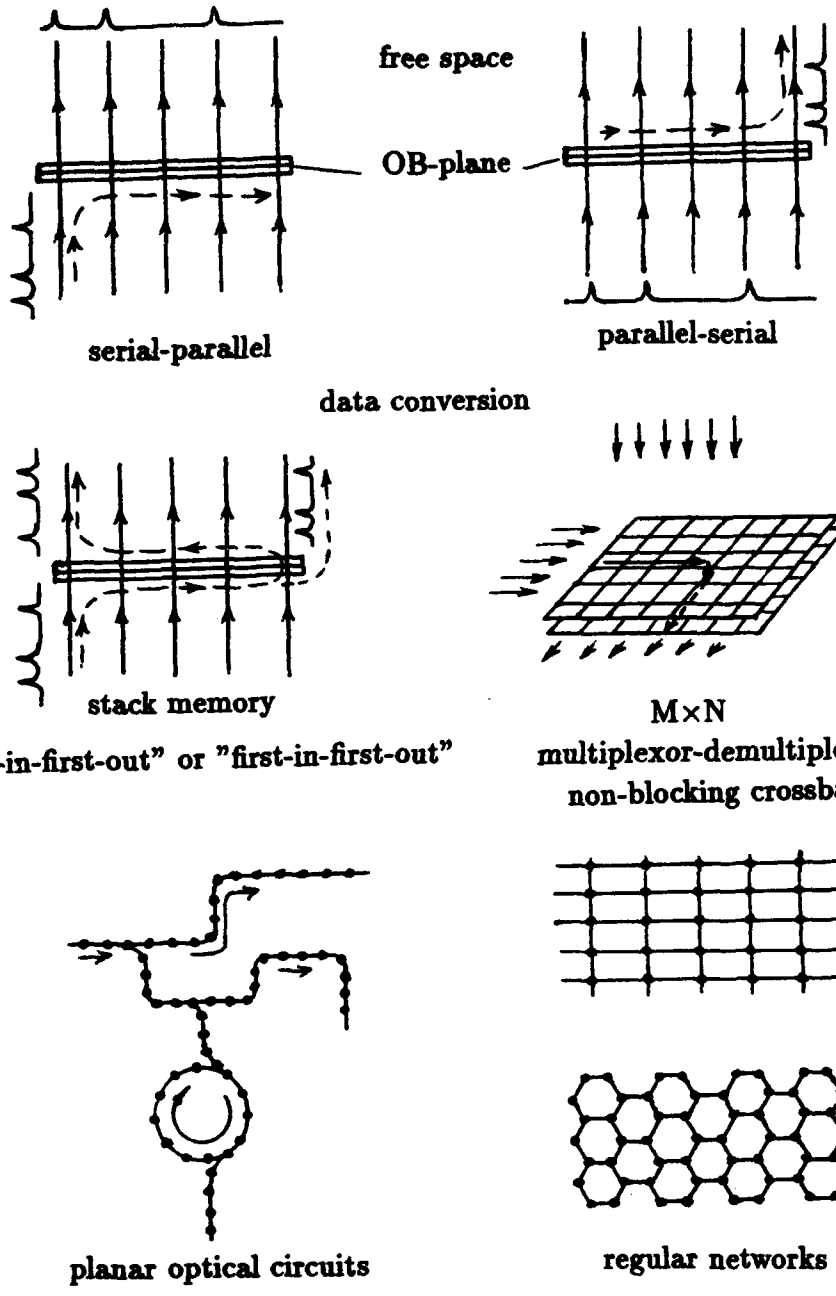


Fig. Optical "planar - free space" logic circuits

Reference:
G.V.Sinitsyn, S.P.Apanasevich, A.V.Lyakhnovich, F.V.Karpushko "All-optical implementation of information shift on the base of transverse effects in optical bistability" in *Optical Computing*, A.M.Goncharenko, F.V.Karpushko, G.V.Sinitsyn, S.P.Apanasevich, Editors, Proc.SPIE 1806, 559 (1993).

2D All-Optical Shift Registers: Numerical Simulation

Sergey P.Apanasevich, Andrew V.Lyakhnovich and George V.Sinitsyn

Division for Optical Problems of Information Technologies,
Academy of Sciences of Belarus
P.O.Box 1, 220072 Minsk, Republic of Belarus
phone: (0172) 39-58-82; fax: (0172) 32-45-53
e-mail: dopit%bas02.basnet.belpak.minsk.by@demos.su

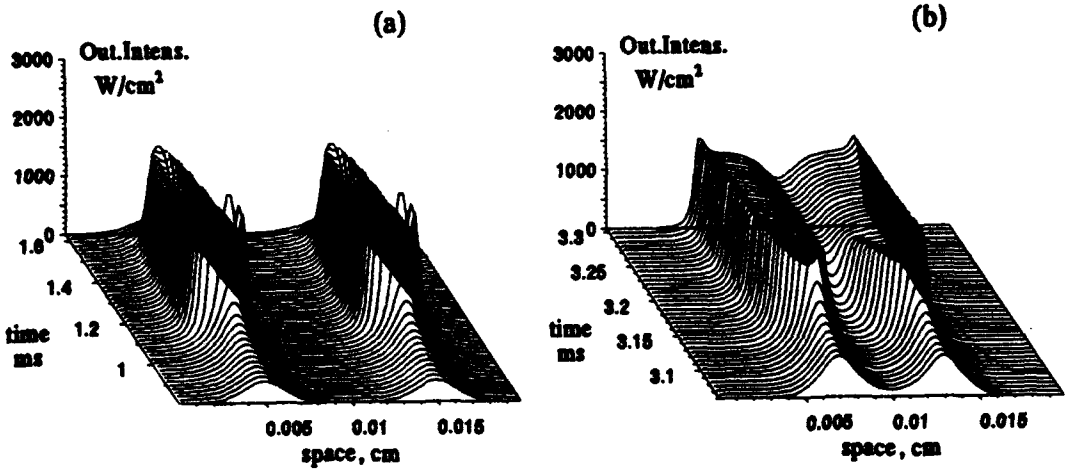
Abstract. Operation of shift register based on propagation of switching waves in distributed nonlinear media is studied by numerical simulations. Comparison with experimental results is also presented.

The concept of lock-and-clock architecture for optical data processing has been recently modified to take into account two transverse degrees of freedom and all-optical shift register based on this concept has been demonstrated experimentally [Ref]. Information shift in the register takes place in the plane of matrix of optical bistable elements. For further development of this concept an adequate theoretical description would be useful.

In present contribution we describe theoretical model of a planar all-optical chip consisting of an array of bistable elements that could be coupled using transverse interconnections. Analysis of the model is based on solving coupled equations for light field in nonlinear interference layer and equations that describe phenomenologically diffusion of medium's nonlinear parameters. Light and heat energy balance in the system "bistable layer - substrate" is taken into account. The approach can deal with various types of nonlinearity, such as band-filling or free carrier generation. In particular, we use heat transfer equations for substrate and layer, that is necessary when behavior of TFI with thermal nonlinearity is simulated.

Results are presented for switching dynamics of bistable elements at a transition from one logical state to the other. The shift of binary data in the chip's plane by means of optically controlled switching waves is also modeled numerically. Temporal, spatial and power parameters have been

investigated that allows to optimize 2D lock-and-clock data processing using bistable matrix. The above parameters define rates of data transfer and processing, spatial resolution and information capacity of matrix devices, error rate, life time etc., and are important for architecture development. Most of the obtained results agree well with the previous experimental data. The rate of data transfer in intra-chip interconnections and in shift registers is estimated.



By way of illustration profiles of transmitted intensity for two bistable pixels with no influence on each other (a) and with distinct degree of coupling (b) are presented. It can be seen, that in second case, when pixels are placed closer, conditions for transverse transfer of information signal are met.

Reference:

G.V.Sinitsyn, S.P.Apanasevich, A.V.Lyakhnovich and F.V.Karpushko, 'All-Optical Implementation of Information Shift on the Base of Transverse Effects in Optical Bistability', SPIE, v.1806, p.559.

ALL OPTICAL DIGITAL DATA PROCESSING BASED ON THE PHOTON ECHO PHENOMENON

E.A.Manykin,
Russian Research Center "Kurchatov Institute",
123182, Moscow, Kurchatov Square, Russia
Phone: (095) 196-91-07, Fax: 7-(095) 196-59-73
S.M.Zakharov,
Scientific Computer Center of the Russian Academy of Sciences,
117334, Moscow, Leninsky prospect, 32A, Russia
Phone: (095) 938-56-89, Fax: (095) 938-58-84

ABSTRACT

Principles for optical digital data processing based on photon echo phenomenon in a resonant media are considered. The various schemes of optical processors realization with the pixel structure and of holographic type based on using of the digital multiplication by analog convolution (DMAC) algorithm are suggested. Manners of optical data flow switching of informational channels on the basis of photon echo phenomenon are discussed.

SUMMARY

The Photon Echo (PE) phenomenon at present is not only the method of kinetic relaxation processes studing in a resonant media, but also is the mean of multifunctional processing of optical images, formed by the excitation pulses at different time moments. Primary proposals of PE using concerned in the main of analog processing methods [1-3]. These methods are characterized by very high-speed processing and can be used in the problem of pattern recognition [4]. However there is interest in the development of optical information processing methods based on the PE phenomenon for the realization of digital data processing and of optical digital processors design.

Here we analize the optical processing for realization of vector and vector-matrix algebra operation as a intrinsic (scalar) and external vector product calculations, vector-matrix and matrix-matrix multiplication.

As a main principle of optical digital information processing the *digital multiplication by analog convolution* (DMAC) algorithm is usually used [5,6]. We consider two types of optical schemes with using of this algorithm in time-domain and space-domain fields.

In the first case the binary representation of the multipled numbers is accomplished in the form of temporal sequential code and the processing takes place in the independent space structural regions (pixels). In each pixel of resonant medium the convolution or correlation functions corresponding of two pulses in time are calculated. On the whole, the spatial-temporal light modulator (SLM) has to form different images, the number of which is equal to the significant digit of using representation for under the time action either of exciting light pulses. The adding operation of the different components is accomplished by cylinder lens.

In the second case (so-called the scheme of holographic type) all numbers are introdiced in parallel code and DMAC algorithm is realized in space. A compound optical scheme accomplishes one-dimensional Fourier transformation on one coordinate and other coordinate forms optical image and compensates the phase distortion. In this case the resonant medium is a spectral plane of multichannel dynamic hologram with the one-dimensional filtering of spatial frequencies. As a result, the data of products of different vector components A_iB_i in the mixed binary representation is formed in output plane. The cylinder lens executes the addition operation and the signal that is proportional to the scalar multiplication of two vectors **A** and **B** is arrised on the linear array of photodetectors.

By the particular case of digital data processing the data flow switching may act as a control data transmission, that is information channel switching.

Data flow switching can be easily implemented on the principle of vector-matrix multiplication. In the first scheme, called by the scheme with the pixel spatial structure, the setting of vector components is initiated by the specification of images with identical rows and column numbers being equal vector dimension, and addition operation is accomplished by the cylinder lens.

In the scheme of holographic type each image, formed by the spatial-temporal light modulator represents the vector with the component number on one coordinate equal to dimension of defined vector and with number of binary digit on other coordinate. Thus so far as matrix **A** defines under the time action of one of light pulses in a view of M images (that corresponds of definition of M vectors or data matrix), that is in a view of different vector sequence in time than the channel numeration on input must correspond to definition of number sequence in time.

Thus, the digital data processing principle is based on filtering in a resonant medium usually time frequencies in processor with the pixel structure and in processor of holographic type - on multichannel one-dimensional filtering of spatial frequencies.

REFERENCES

1.S.M.Zakharov, E.A.Manykin. In: "Problemy kvantovoi optiki" (OIYaI, Dubna, 1988), pp.44-48 [in Russian].
2.E.A.Manykin, S.M.Zakharov. Izv.Ak.Nauk SSSR, ser.fiz., 53, 2281 (1989).
3.E.Y.Xu, S.Kroll, D.L.Huestis, R.Kachru, M.K.Kim. Opt. Lett., 15, 562 (1990).
4.X.A.Shen, R.Kachru. Opt. Lett., 17, 520 (1992).
5.W.R.Babbitt, Y.S.Bai, T.W.Mossberg. Proc. SPIE, 1986, v.639, p.240-247.
6.D.Manganaris, P.Talagala, M.K.Kim. Appl.Opt., 31, 2426 (1992).

Optical self-routing complex-valued neural network using mixed negabinary numbers

Liren Liu, Lan Shao, and Guoqiang Li

Shanghai Institute of Optics and Fine Mechanics, Academia Sinica, P.O.Box 800-211, Shanghai 201800, P.R.China

A general neural unit with a complex-valued matrix depicting integrated synaptic connection and lateral interaction is proposed. Various connections can be self-programmed by a complex routing code pair contained in the input. Based on the mixed negabinary number system, an optical and parallel neural architecture of incoherent optical correlation and spatial coding is developed.

Various artificial neural net models were suggested to simulate the biological behaviors[1], in which neurons were usually considered to have a set of two real states. In this paper, we suggest a new concept that neurons have complex-valued states, which stimulate a combination of synaptic connection and lateral interaction. On this basis, a general neural unit with only a complex-valued matrix is proposed to organize the integrated synaptic connection and lateral interaction. Thus, various connection functions can be self-programmed by the routing code contained in the input stimuli. Based on the mixed negabinary number system, an inner-product algorithm for complex matrix-vector multiplication necessary for the neural unit is developed. The features are: no carriers, no signs and simple pre-processing and post-processing. An optical architecture of incoherent correlation with spatial coding of data are suggested. The required complex matrix-vector multiplication can be realized optically in parallel in a single optical channel with a high accuracy.

The model of complex-valued general neural unit is shown in Fig.1. The states of the input stimuli are denoted by a complex-valued column vector, $[v_j(K_1+jK_2)]$ where $[v_j]$ is the bipolar input stimuli and $K_1, K_2 \in \{1, 0, -1\}$ assemble the routing code pair. The complex-valued interconnection matrix is divided into the real part and the imaginary part as $[T^R_{ij}]+j[T^I_{ij}]$. A matrix-vector multiplication will result in a real part and an imaginary part as

$$\begin{aligned} [v_i^R] &= K_1[T_{ij}^R][v_j] - K_2[T_{ij}^I][v_j], \\ [v_i^I] &= K_1[T_{ij}^I][v_j] + K_2[T_{ij}^R][v_j]. \end{aligned} \tag{1}$$

Thus, the access of different routing codes will yield various connection functions.

We can now establish the rule to learn the complex-valued matrix from the matrix for synaptic connection, $[T^{sy}_{ij}]$ (NxM, M≥N), and the matrix for lateral interaction, $[T^{la}_{ij}]$ (NxN):

$$\begin{aligned} [T_{ij}^R] &= [T_{ij}^{sy}], \\ [T_{ij}^I] &= ([T_{ik}^{la}] - [1])[T_{kj}^{sy}]. \end{aligned} \tag{2}$$

The negabinary number system has the radix of -2[2]. A positive

or negative real number can thus be represented in a form of the mixed negabinary number:

$$a = \sum_{n=0}^{N-1} a_n (-2)^n \qquad (a_n \geq 0). \tag{3}$$

For the neural complex matrix-vector multiplication, the nth real digit at the ith row of the resulting column vector can be reached by the inner-product algorithm:

$$v'^{R}_{n}(i) = \sum_{j} K_1 \boldsymbol{T}^{R}(i,j) \cdot \boldsymbol{v}_n(j) - K_2 \boldsymbol{T}^{I}(i,j) \cdot \boldsymbol{v}_n(j),$$

$$\textit{substraction conversion}: \quad -\boldsymbol{a} \cdot \boldsymbol{b}_n = \frac{1}{2} \boldsymbol{a} \cdot \boldsymbol{b}_{n-1}. \tag{4}$$

It should be noted that a substraction can be converted to an addition operation by a shift operation.

To implement the complex matrix-vector multiplication by optics, an incoherent optical correlation and spatial coding architecture is suggested as shown in Fig.2. The coding format of the vector and the matrix are indicated. The image of the light array represents the output digits in the mixed negabinary system.

This work was supported by the National Natural Sciences Foundation of China.

References:

1. R.P. Lippmann, IEEE ASSP Magazine, April 4-22(1987).
2. M. P. de Regt, Comput. Design, 6, 53-60(1967).

Fig.1. Complex valued general neural unit.

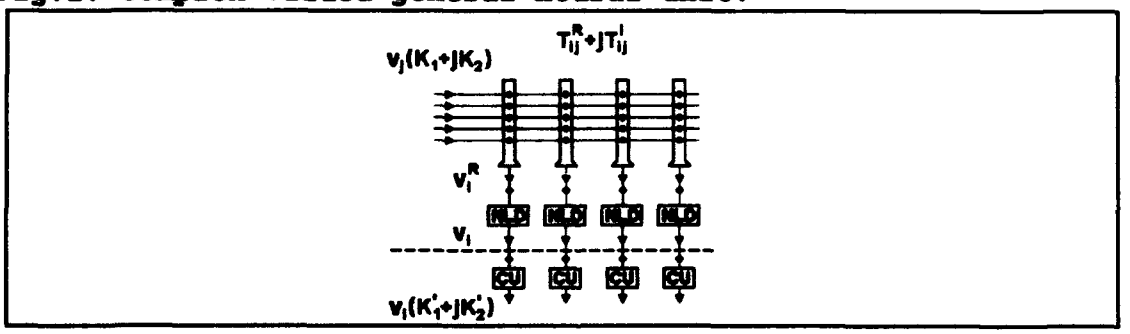
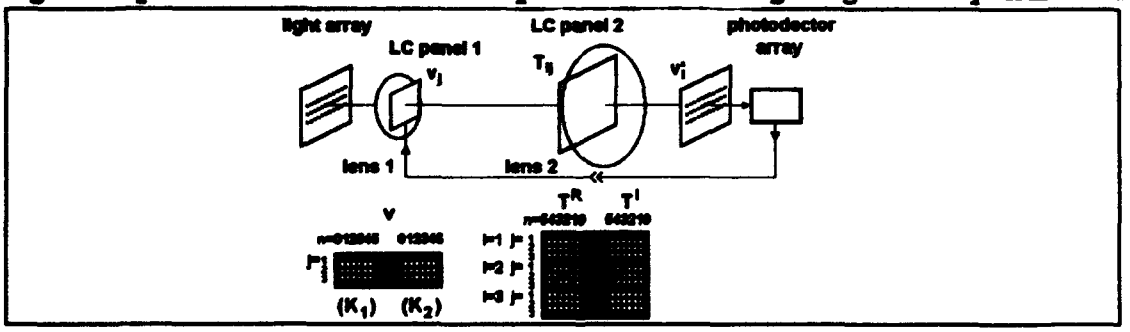


Fig.2. Optical matrix-vector processor using negabinary numbers.



Polarisation-optical stacked integrated module of cellular logic two-layer image processor

Liren Liu, Haifeng Peng, and Yaozu Yin

Shanghai Institute of Optics and Fine Mechanics
Academia Sinica, P.O.Box 800-211, Shanghai 201800, P.R. China

A 3-D polarization-optical stacked integrated module of cellular logic image processor is developed, which is the optical cascade of a parallel binary logic gate and a morphological dilation processor. The system is very compact and effective.

Cellular logic image processors[1] is an important architecture for optical computing. The recently reported optical cellular image processors include: The optical implementation of the cellular logic image processor (CLIP) architecture[1] by using S-SEED devices[2] and BEAT devices[3]; A digital optical cellular image processor based on binary image algebra with the use of light valve[4]; An optical cellular two-layer logic image processor based on one-operation image algebra using dual-rail spatial coding and electronic thresholding[5]. In these suggestions, however, the optical interconnections were realized in the free space. A quite distant light path should be utilized, so that the optical system is large. In this paper, we develop a new optical module scheme using 3-D stacked integration of polarization elements. It can been seen that the suggested optical cellular image processor module is compact in configuration, effective in performance, and insensitive to environment.

Fig.1 shows schematically the cellular architecture, which consists mainly of a CPU of a parallel binary logic processor followed by a morphological binary dilation processor and a feedbacking manager. The threshold device and sum gate are used to deal with gray-tone images. It was proven that all the possible binary and gray-tone image processing functions can be executed by programming the logic operations in the iterations[5].

The packaged design of the optical CPU module is shown in Fig.2. The calcite plates (CP) are used to split an incident beam into two spatially separated beams with polarizations orthogonal to each other, the quartz plates (PR) to rotate the polarization of beam by 45°, the input masks or the PLZT SLMs (IM) to display the two input images in a dual-rail spatial coding manner, the ML mask to control the logic operations, and the MS masks to stop the undesired beams.

The optical elements from the IM_1 to the beamsplitter (BS) constructs the parallel logic processor, and the following elements constitute the morphological processor. On the lower part of the figure, the path routing of beams in a coding area of cell is illustrated. It is seen that the output pattern from the logic processor at the BS is a combination of four equivalent maxterm of two input images. The selection of the ON/Off states (k_1-k_4) of the four apertures in each coding area of the ML mask can result in all the sixteen binary logic operations. In the morphological processor, a beam is splitted into four spots in its nearest neighbors. The structuring element S is a set of {(1,0),(-1,0),(0,1),(0,-1)}. Using a photodetector array with electronic max thresholding, the dilation can be obtained.

The polarization-optical stacked module has been developed: the dimension 20mmX20mmX140mm and the possible image pixels 1 X10. Some primary experimental results were obtained.

This work was supported by the National Natural Sciences Foundation of China and the Bureau of High Technique of China.

References:

1. K. Preston, et al, Proc.IEEE 67, 826(1979).
2. F.A.Tooley and S.Wakelin, Appl.Opt. 32, 1850(1993).
3. R.G.A. Craig, et al, Appl.Opt. 30, 2297(1991).
4. K.-S. Huang, et al, Appl.Opt. 32, 166(1993).
5. L. Liu, X. Zhang, and 3. Zhang, Appl.Opt. (to be published).

Fig.1. Cellular logic image processor architecture.

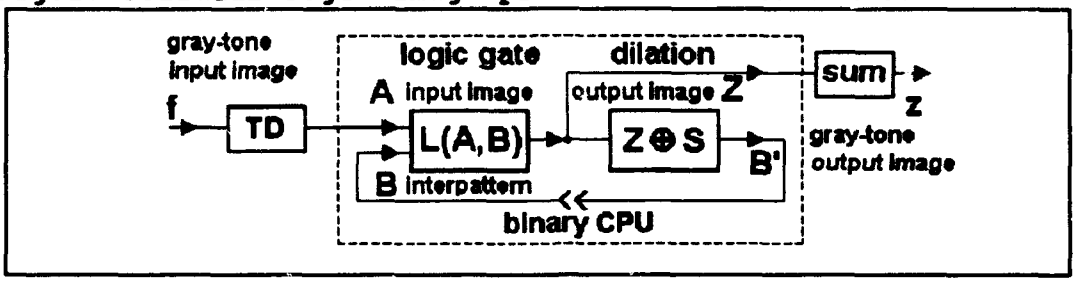
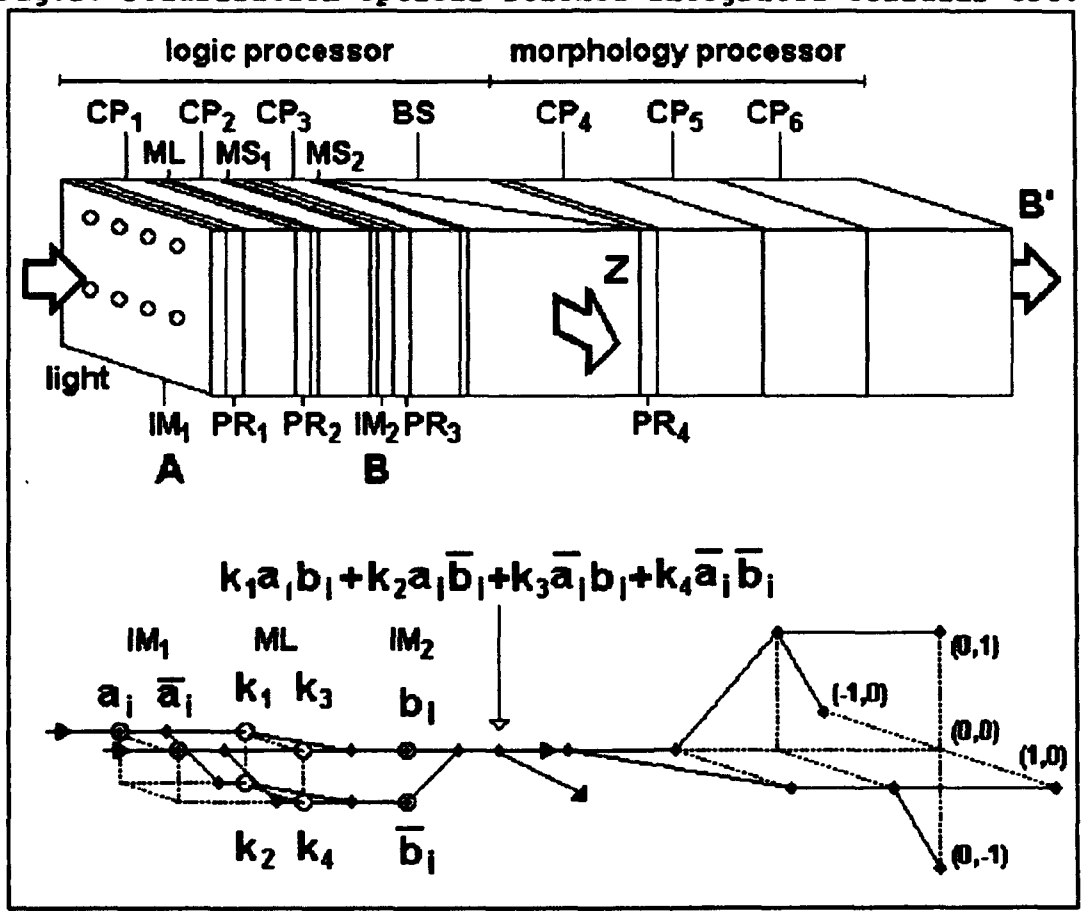


Fig.2. Polarization-optical stacked integrated cellular CPU.



Direct Twos Complement Parallel Array Multiplication: Algorithm and Optical Implementation

Guoqiang Li, Liren Liu and Zhhijiang Wang
Shanghai Institute of Optics and Fine Mechanics,
Academia Sinica. P.O. Box 800-211, Shanghai 201800, P.R.China.

Abstract: A direct 2's complement array multiplication architecture is proposed, and for higher radix system, it also applies. Based on complex partition, a two-stage array is constructed for complex operation. In correspondence, an optical configuration is put forward.

Twos complement encoding has been widely used in optical matrix operation, but the conventional algorithm has several fatal defects[1], such as the limitation on the bit number of the operands and the severe waste of space bandwidth product(SBWP). The modified version[1] needs much sign decision and postprocessing, and the convolutional result is still unable to be directly weighted and summed. In the following, another modified direct 2's complement array multiplication algorithm is advanced and applied to complex operation.

In 2's complement, assume either of the two N-bit operands a and b takes the form $\{x_{N-1}x_{N-2}\cdots x_1x_0\}$. With the help of mixed 2's complement number system, the bitwise addition is conducted without carries and subtraction is changed to addition according to the additive inverse representation of the subtrahend. For multiplication, the below equation can be derived[2]:

$$p=1\cdot(-2^{2N-1})+(1+\bar{a}_{N-1}\bar{b}_{N-1})\cdot 2^{2N-2}+\sum_{i=0}^{N-2}\sum_{k=0}^{N-2}a_ib_k\cdot 2^{i+k}+\sum_{i=0}^{N-2}(a_{N-1}\bar{b}_i+b_{N-1}\bar{a}_i)\cdot 2^{i+N-1}+(a_{N-1}+b_{N-1})2^{N-1}. \quad (1)$$

The above product can be formed with a parallel array architecture as shown in Fig.1. Compared with the original algorithm, the direct array multiplication eliminates the limitation on the bit number of the operands, use the SBWP more efficiently, and the result is represented in mixed 2's complement straightly. Furthermore, the algorithm can be extended to higher radix system.

For complex operation, the preceding array architecture applies. Let $a=a_1+ja_2$, $b=b_1+jb_2$, in which a_1, a_2, b_1, and b_2 are real numbers and are encoded by N bits, then their product $p=p_1+jp_2$, where $p_1=a_1b_1+(-a_2b_2)$, $p_2=a_1b_2+a_2b_1$. Therefore, a two-stage array architecture consisting of four subarrays is established in Fig.2.

The two-stage array architecture has been verified by experiment. The optical construction is shown in Fig.3, which comprises three parts. The first imaging part forms the product array; The second multiple-imaging system[4] carries out addition of the relevant subarrays; The incoherent correlator[5] integrates the diagonal elements to get both real and imaginary parts of the result. The system is interfaced with a PC computer for pre- and post- processing.

The work is supported by the National Natural Science Foundation of China.

References:
1. R.Bocker, S.Clayton and K.Bromley, Appl. Opt. 22, 2019(1983).
2. B.Taylor and D.Casasent, Appl. Opt. 23, 4095(1984).
3. C.Baugh and B.Wooley, IEEE Trans. on Comput. C-22, 1045 (1973).
4. L.Liu and X.Liu, Opt. Commun. 82, 446(1991).
5. L.Liu, Opt. Lett. 14, 482(1989).

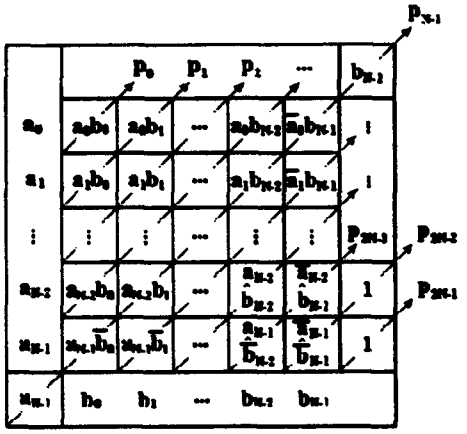


Fig.1 Parallel array multiplication scheme.

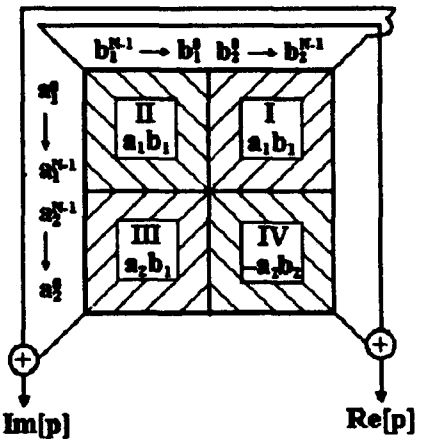


Fig.2 An array complex unit.

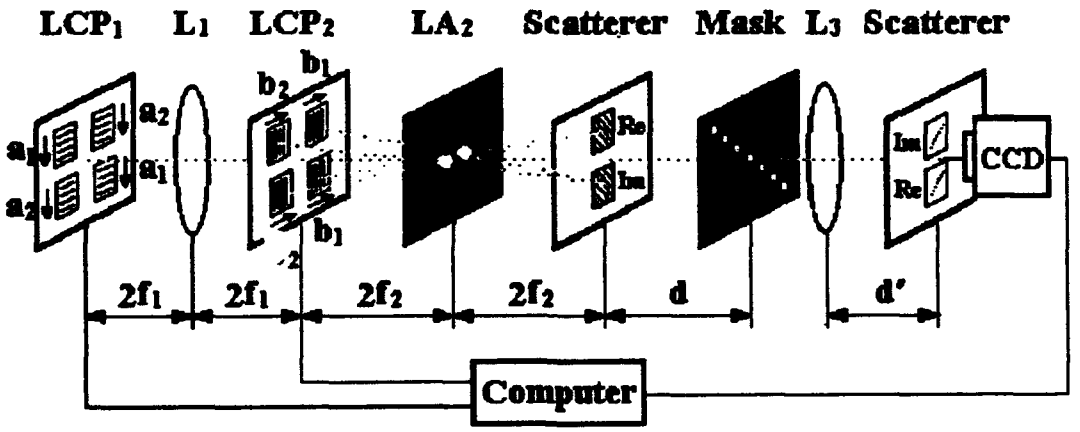


Fig.3 Configuration for two-stage array complex multiplier.

Optical Parallel Arithmetic Using Recoded Trinary Signed-Digit Number System

M. S. Alam
Purdue University, Department of Engineering, Fort Wayne, IN 46805-1499
Voice: 219-481-6020, Email: alam@sunsinger.ipfw.indiana.edu

ABSTRACT

A new technique for high-speed recoded trinary signed-digit arithmetic using optical symbolic substitution is presented. This technique performs multi-bit carry-free addition and borrow-free subtraction in constant time using the minimum number of minterms.

SUMMARY

The problems of achieving massively parallel optical computing have been investigated by many authors using the residue number system, signed-digit number system, and recoded signed-digit number systems [1-3]. Using residue number system, one can perform parallel arithmetic in constant time using symbolic substitution [4], but the size of the truth table required increases rapidly with the increase of the operand length. The redundant signed-digit number system [5] allows parallel arithmetic with fewer carry propagation steps. For example, the modified signed-digit (MSD) number system confines the carry propagation to two adjacent digit positions [5]. This property of the MSD number system permits carry-free addition and borrow-free subtraction of two arbitrary length numbers in parallel which makes it suitable for optical architectures. However, the information storage density of the MSD number system is limited which may result in complex circuits and may increase the severity of the interconnection bottleneck [6]. Higher radix signed-digit number systems allow higher information storage density, less complexity, fewer system components, and fewer cascaded gates and operations. Among the higher radix number systems, the trinary signed-digit number system appears to be the most promising in terms of storage density and processing elements [6].

Carry-free addition using n-step [7], three-step [8], two-step [1], and one-step [9] optical symbolic substitution have already been reported. The number of symbolic substitution rules usually decreases as the number of computational steps increases. Recently, a two-step symbolic substitution technique for trinary signed-digit arithmetic has been reported [6]. This technique performs carry-free addition and borrow-free subtraction by checking a pair of reference digits from the next lower order digit position and requires 58 four-variable minterms for each output digit. Later on, a higher-order trinary signed-digit symbolic substitution technique has been designed [1] which enhances the computation speed but excessively increases the number of minterms per output digit.

Parhami [10] recently proposed a simpler carry-free addition scheme where the MSD numbers are recoded before performing the addition. Awwal [2] implemented the recoded MSD arithmetic technique using an opto-electronic implementation which requires sixteen four-variable minterms per output digit. Thus, in any symbolic substitution scheme, the most important objective is to minimize the number of minterms (substitution rules) and computational steps while incorporating the optimum information in fewer digits. To achieve these objectives without sacrificing the processing speed and parallelism of optics, we propose herein the recoded trinary signed-digit system for multi-digit carry-free addition and borrow-free subtraction.

The proposed trinary signed-digit technique is memory efficient since it reduces the substitution rules by more than 50% when compared to the most recently reported trinary signed-digit arithmetic technique [6]. Moreover, only three two-variable minterms are required for the addition stage of the proposed technique while six-variable [1] and four-variable [6] minterms are required for the addition stage of the previously reported schemes. The proposed technique can be implemented using a single-stage opto-electronic implementation where the recoding operation is performed electronically and the addition is performed optically using a content-addressable memory (CAM). An all-optical CAM-based implementation involves two processing steps since both recoding and addition must be performed optically. In either implementation technique, the minimized minterms are stored using a holographic or nonholographic CAM. A holographic CAM usually suffers from its inconvenient recording problems. On the other hand, a nonholographic CAM provides faster processing speed, ease of alignment, and programmability. Since a few minterms is required in the proposed technique, therefore, a nonholographic CAM may be used for storing the minimized minterms.

In this paper, we presented an efficient technique for parallel trinary signed-digit arithmetic. The proposed technique performs parallel carry-free addition and borrow-free subtraction in a constant time in two steps independent of the operand length. This technique requires the minimum number of minterms when compared to the previously reported trinary signed-digit arithmetic techniques [1, 6]. Also, in this technique, more information can be incorporated in fewer digits, thereby reducing the system size and complexity. Finally, a CAM based optical implementation is suggested for the proposed scheme.

REFERENCES

1. M. S. Alam, M. A. Karim, A. A. S. Awwal and J. J. Westerkamp, "Optical processing based on conditional higher-order trinary modified signed-digit symbolic substitution," Appl. Opt., Vol. 31, pp. 5614-5621, 1992.
2. A. A. S. Awwal, "Recoded signed-digit binary addition-subtraction using opto-electronic symbolic subetitution," Appl. Opt., Vol. 31, pp. 3205-3208, 1992.
3. G. A. De Baise and A. Massini, "Redundant binary number representation for an inherently parallel arithmetic on optical computers," Appl. Opt., Vol. 32, pp. 659-664, 1993.
4. A. Huang, "Parallel algorithms for optical digital computers," Proceedings of the 10th International optical Computing Conference, IEEE Computer Society, Los Angeles, pp. 13-17, 1983.
5. A. Avizienis, "Signed-digit number representation for fast parallel arithmetic," IRE Trans. Electron. Comp., EC-10, pp. 389-400, 1961.
6. A. A. S. Awwal, M. N. Islam and M. A. Karim, "Modified signed-digit trinary arithmetic by using optical symbolic substitution," Appl. Opt., Vol. 31, pp. 1687-1694, 1992.
7. K. H. Brenner, A. Huang and N. Streibl, "Digital optical computing with symbolic substitution," Appl. Opt., Vol. 25, pp. 3054-3060, 1986.
8. A. K. Cherri and M.A. Karim, "Modified signed-digit arithmetic using an efficient symbolic substitution," Appl. Opt., Vol. 27, pp. 3824-3827, 1988.
9. M. M. Mirsalehi and T. K. Gaylord, "Logical minimization of multilevel coded function," Appl. Opt., Vol. 25, pp. 3078-3088, 1986.
10. B. Parhami, "Carry-free addition of binary signed-digit numbers," IEEE Trans. Comput., Vol. 37, pp. 1470-1476, 1988.

A Methodology for Optical Architectures Modeling

Mohsen Guizani
Computer Engineering Department
King Fahd University of Petroleum and Minerals
Box 1969, Dhahran 31261, Saudi Arabia.
e-mail: FACY015@SAUPM00.Bitnet
Fax: (966 3) 860-3306

Abstract

We devise a methodology for optical architectures. We present the general description of the multi-port optical components. Then use flow graph analysis for these components to analyze optical architectures before the implementation phase. It illustrates the behavior of the optical data signal at any point of the optical system.

Summary

Development of optical components have witnessed great interest in the last few decades [1]. These components were successfully used in optical computing. Experimental results for this success are available in the literature [2] and [3]. As far as we know, very few researchers have discussed modeling of these optical components in a classical manner [4]. A methodology for a special purpose optical architecture has been developed by Murdocca [5].

Our objective is to develop a new methodology to include the most widely used optical components such as Fabry-Perot interference filter. Then we extend this method to complete optical architectures. We discuss first the general aspects of these modeling techniques. Then we apply these techniques to optical architectures that widely use some of these components [2].

In practice there are three generic classes of optical network architectures. Those that use fiber-optic interconnects (fiber-optic networks), others that use waveguides (integrated-optic networks), and third that use free-space interconnects (free-space optic networks).We expect that this methodology will be suitable for all these categories.

The analysis and the methodology that is presented follow the analysis of the microwave networks. the similarities stems from our concern with the travelling waves, in

which the so-called *scattering parameters* are useful. These parameters constitute the *S-matrix* (scattering matrix) [4]. Similarly, with optical components, we can talk about the S-matrix. Except that when we have optical components we should introduce two single virtual ports instead of each physical port.Therefore, our optical scattering matrix is composed of elements of 2x2matrices rather than regular numbers. The S-matrix of some common optical devices such as the one-port, two-port components and directional couplers are presented.

Usually virtual ports have to be introduced for the optical components in addition to the existing physical/real ports. This is necessary in order to account for the reflections or losses of these optical components. Signal flow graphs can be used to simplify the results.They are also used to represent the proper equations describing the components.

We have developed a new methodology that can be used to model optical architectures based on some widely used optical components such as the Fabry-Perot interference filter. Extension of this methodology to large optical architectures is simple. The objective is to provide a tool to the experimenter to deal with the architecture before its implementation. The next step for this methodology is validation. We expect to validate the steps of this methodology soon.

References

[1] F. B. McCormick, F. A. P. Tooley, T. J. Cloonan, J. L. Brubaker, A. L. Lentine, L. R. Morrison, S. J. Hinterlong, M. J. Herron, S. L. Walker, and J. M. Sasian, "Experimental Investigation of Free-space Optical Switching Network by Using S-SEED", *Appl. Opt.*, Vol. 31, No. 26, 1992, pp. 5431-5446.

[2] M. Guizani, "Picosecond Multistage Interconnection Network Architecture for Optical Computing", *Appl. Opt.*, Special Issue on *Optical Computing*, 1994.

[3] V. P. Heuring, H. F. Jordan, and J. P. Pratt, "A bit Serial Architecture for Optical Computing",*Appl. Opt.*, Vol. 31, No. 23, 1992, pp.3213-3224.

[4] Weissman, *Optical Network Theory*, Artech House, 1992.

[5] M. Murdocca, *A Digital Design Methodology for Optical Computing*, The MIT Press, 1990.

A System for the Computer Aided Design of Optical Architectures

Adel O. Lafi and Subbarao Ghanta
Department of Information & Computer Science
King Fahd University of Petroleum and Minerals
Dhahran — 31261, Saudi Arabia
e-mail: facp07a@saupm00.bitnet or facp026@saupm00.bitnet
Fax no: +966-3-860-2174

Abstract

Optical computing is an emerging field that makes use of light as a carrier of information. During the last decade numerous architectures have been proposed to solve problems ranging from special purpose image processing to general purpose optical computers. The advantages such as high connectivity, non-interference of signals, high spatial and temporal bandwidths, low signal dispersion, electromagnetic immunity, massive inherent parallelism, combined with analog / digital computational capabilities make optical computing an attractive area.

Despite the aforementioned features, the discipline of optical computing remains an ad hoc one. One of the primary reasons for that is the lack of significant design tools that help automate the design process which is ad hoc in nature. Tools will also promote reusability of building blocks in different optical systems.

As part of an ongoing project, we have been looking into the various aspects of design automation. We are primarily interested in developing an overall design automation system for optical systems to assist system architects.

In this paper, a design for a Computer Aided Optical Design system (CAOD) is presented. A sketch of the status of implementation is also presented.

1 Summary

The Computer Aided Optical Design CAOD system:

1. is a workbench of software tools with clearly separated functionalities and well designed interfaces. This promotes independent evolution of these tools
2. allows optical systems designers to fully exploit and use the special characteristics of optics
3. provides a language-centric view to the designer
4. provides unified semantics across different interaction paradigms
5. promotes object-oriented design methodologies for the development of optical architectures
6. does not over burden physicists with excessive programming details
7. does not over burden system architects with the theoretical foundations of optics

Figure 1. shows the CAOD system. It consists of a number of software tools (represented by boxed items). These tools interact by reading from and writing to a number of files (represented by elliptic shaped items). An architect describes the optical system under study/development using either PLOADS (a language representation) or using an interactive 3-D graphics editor. The *translator* tool takes the description in PLOADS and produces a detailed representation of the architecture. The 3D graphics editor produces a detailed representation as well. The *simulator* uses the detailed representation to conduct simulation and produce results. The *design rule checker* verifies user defined constraints and reports the outcome of different analyses. The *optical layout tool* takes the specification of a verified architecture and translates that into a detailed manufacturable setup: its importance is expected to grow with large integrated systems.

The *component database* contains detailed information about optical components. The *component library* is a collection of implementations for the methods that model the behavior of various optical components types. *Mathematica* is a general purpose algebraic, numerical, and symbolic computation package. Mathematica is included in the CAOD system to simplify the implementation of complex computations that arise in several parts of the CAOD system. Whenever any sophisticated computation is required, services from the commercial package Mathematica are sought. With this overall view of the CAOD system in picture, subsequent sections discuss the details of the different CAOD tools.

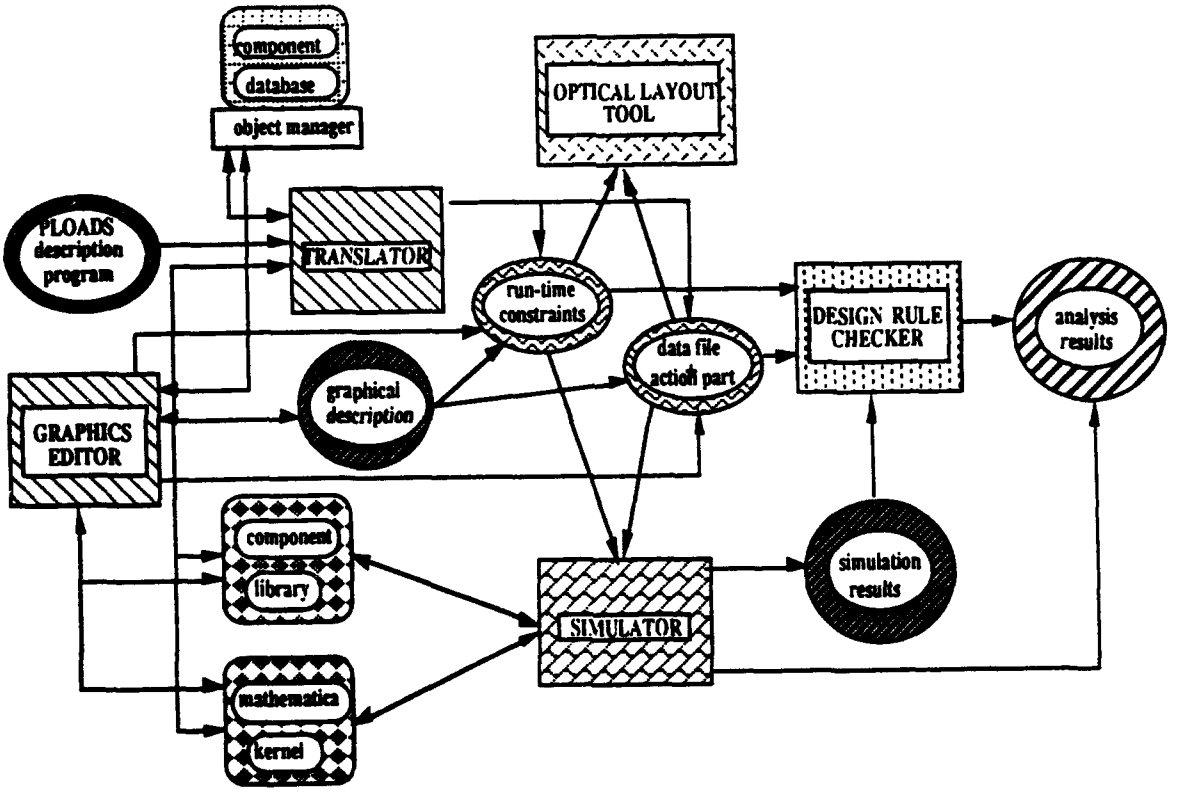


Figure 1. The overall CAOD system

Fractal Dimension as a new method of the precision evaluation on a Non-Linear Device

Ana González-Marcos
E.T.S.I. Telecomunicación
Ciudad Universitaria
28040 - Madrid
Spain
Telephone: +34-1-336 73 04
Fax: +34-1-336 73 19

ABSTRACT

A new method able to evaluate the behaviour of an optical non-linear device, used as logic gate, based on fractal dimension tools, is reported. A real example is shown.

SUMMARY

It is already well know that using an optical bistable device as a logic gate, we have four possible configurations. Each one of them give us a different logic function.
This logic function will be obtained from two binary input data. A bias signal will allow to control the decision level of the non-linear characteristic[1].

One of the most important parameters of a logic gate are margin tolerances of the different signals. They let the logic gate to operate correctly on the sense of the expected function. These parameters are difficult to define for an optical non-linear device due to the device dependence on wavelength, temperature and others. We propose a method to know the precision level of data and bias signals on an specific logic gate, by two measurements of every one of the possible outputs. This method will be described in this work.

As an example of precision measurement by fractal dimension we are going to analyze one of the most complicated configurations of an optical bistable device as a logic gate (Fig. 1). Its difficult comes from the output characteristics. It corresponds to the output characteristic of a SEED.

The method is based in the generation of a data chart that indicates the various logic functions that can be obtained. The y-axis corresponds with the bias signal values and the x-axis with the expected value of the decision level D_i normalized by:

$$\Delta = \frac{D_i}{\left(\frac{i}{I}\right)}$$

where I is the intensity normalized value of a bit "1" at the input. i is the total intensity at the input (sum of the two data signals plus the bias signal).

The total chart for all the possible outputs has been presented as part of the result of an Optically Programmable Processing Element and it has been reported previously [2]-[3]. We just present here an small area of the total chart, fig.2. This figure has been obtained by computer simulation of the ideal characteristic shown in figure 1.c. In this example we have considered that the distance between the different decision levels are the same. So $D_i = d$, but it can be taken any other value.

Figure 2 shows the logical function obtained with a precision level of the bias signal of 0.1 and a decision level of 0.01. On figure 3, the precision level of each axis has been increased separately: a) 0.01 - 0.01; b) 0.1 - 0.001. Figure 4 shows the result for a better precision on both axis: bias signal - 0.01; decision level - 0.001. These figures show how the image is repeated as the precision gets higher. It corresponds with the type of fractales that can be found in the nature.

The fractal dimension calculated by box-counting method, for the different charts shown in figures 2-4, can be summarized on the table.

TABLE I.- Parameter values for fractal dimension.

	S	u	d
A	0.01/0.001	554	0.9145
B	0.01/0.01	58	0.8817
C	0.1/0.01	7	0.8451

In this table we can see the direct relation between the precision level of the data on each axis and the value of the fractal dimension. So if two data charts of a logic gate function are obtained by direct measurements of input and output signals, the fractal dimension will give the precision of the logic gate. And this precision would be better as nearest the value is to one.

REFERENCES

(1).- "Optical Computing", Ed. B.S. Wherrett and F.A.P. Tooley. SSUSP (1989).
(2).- Martín-Pereda, J.A. & A. González-Marcos, **LEOS'92** pp. 374-5. (1992).
(3).- González-Marcos, J.A. & J.A. Martín-Pereda, **SPIE.** Vol 2038, pp. 67-77 (1993).

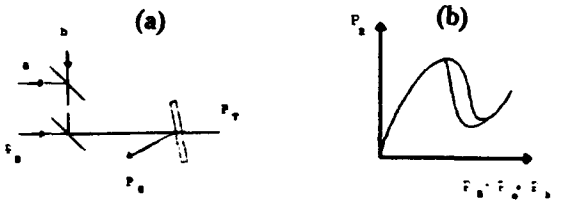


Figure 1

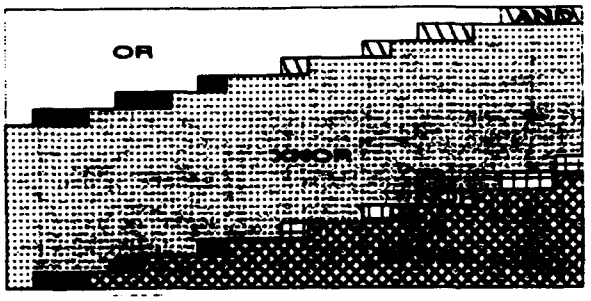


Figure 2

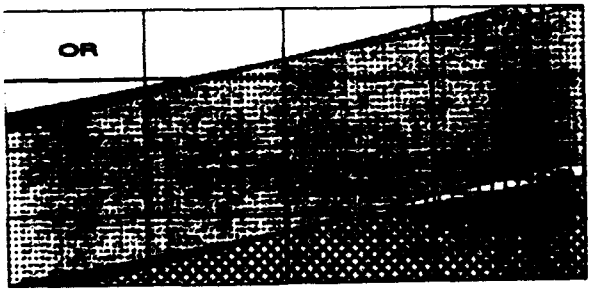
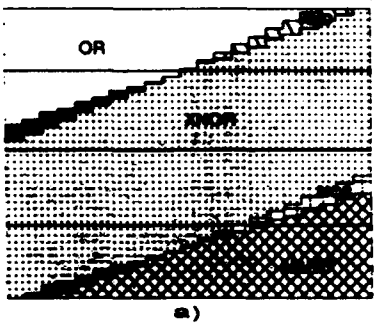


Figure 4



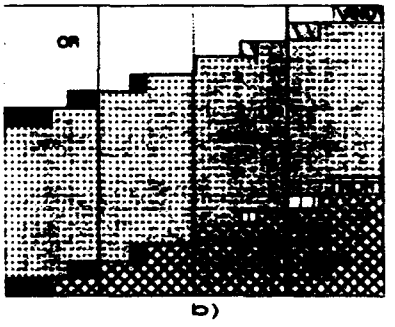


Figure 3

Sequences of bifurcations and transition to Chaos in an Optically-Processing Element

Ana González-Marcos & J.A. Martín-Pereda
E.T.S.Ingenieros de Telecomunicación.
Universidad Politécnica de Madrid
28040 Madrid. Spain
Telephone: +34.1.336.7304
Fax: +34.1.336.7319

ABSTRACT

Digital chaotic behaviour in an Optically-Processing Element is reported. It is obtained as the result of processing two fixed train of bits. Period doublings in a Feigenbaum scenario have been obtained.

SUMMARY

The employed optically-programmable digital circuit has been already reported in (1)-(2) as a Programmable Logic Gate. A brief description on its method of operation, as well as the way it has been implemented, can be fund there.

Our circuit is composed by two optical devices, P and Q, (see Figure) with a non-linear behaviour. The output of each one of them corresponds the two final outputs, O_1 y O_2, of the cell. The possible inputs to the circuit are four. Two of them are for the input data, I_1 e I_2, and the other two, g and h, for control signals. The corresponding inputs to the non-linear devices are based on these signals plus some other coming from inside the own cell.

The practical implementation we have carried out of the processing element has been based on an optoelectronical configuration. Lines in Figure represent optical multimode fibers. The indicated blocks, placed in order to combine the corresponding signals, are conventional optical couplers. In this way, the inputs arriving to the individually devices are multilevel signals.

Moreover, for the results we are going to report here, a computer simulation has been carried out.

The main difference of our present circuit with respect to previous similar logical circuits is the presence of additional delays and feedbacks.

The first difference has been the introduction of a feedback from one of the two possible outputs to one of the system inputs. Moreover, according to previous studies in this field, the introduced feedback should have some delay. An internal delay has to be taken into account because the response time of the optoelectronic devices. In this case, an oscillatory behaviour could be the normal output of the system. But, under some conditions, this is not always true. The output, as we will shown, is not periodic for some parameters of the system. Some of these situations will be shown in this paper.

In order to chose the more adequate feedback, two are the possibilities. Because the P-device output has more possible different functions depending on its control signal than the Q-, we have used this output for feedback. The input is the control signal g of device P. The figure shows the employed circuit.

If we consider an inner delay time, owing to the switching time of internal device, plus a feedback delay time, we find different results depending on the rate between both delays. In all cases, we find an asymptotic behaviour of the circuit. Some of the obtained results have been achieved by experimental methods and some others by computer simulation. Optoelectronic cells simulate P and Q devices.

The first analysis that we have performed considered null delay times. This situation has not an algebraic solution and no data were obtained. The circumstances are strongly different if we introduce finite delay times, namely, internal and external delays.

According to previous studies, the situation with more probability to give a periodic or even chaotic solution is when internal time delay is shorter than the external one. In any case, input has been a regular train of pulses. The input to the non-linear device is a multilevel signal corresponding to the addition of the two inputs. The period of this signal corresponds to a time of 14 milliseconds.

If the ratio between internal delay time and external delay time is smaller than 1, we obtain a periodic situation. The period of this signal is strongly dependent on the ratio value. In the particular case, where external time delay is 200 ms and internal delay are 2, 4 and 12 ms, obtained results are summarized

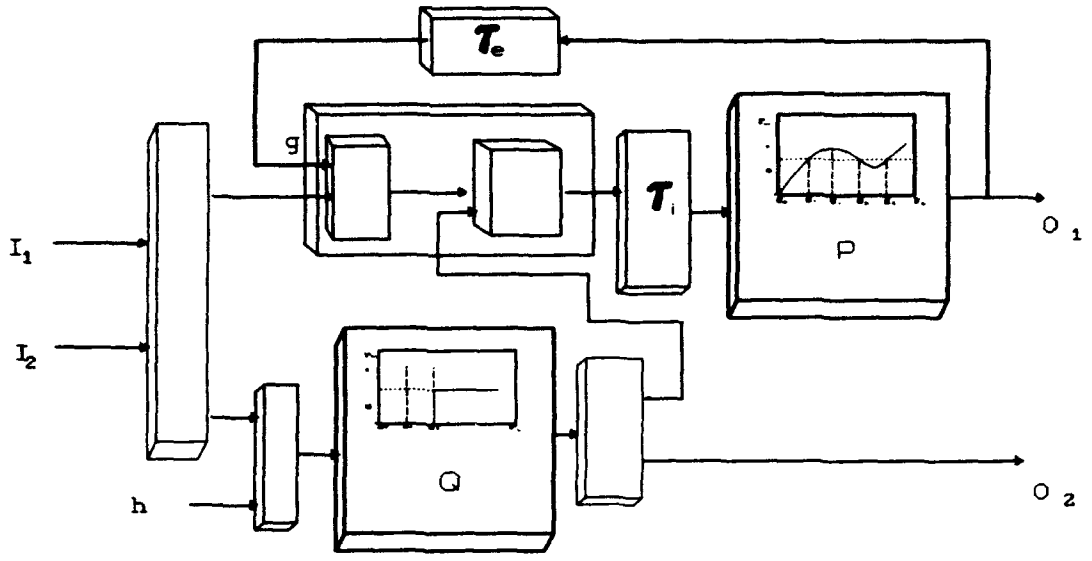


Figure.- Optical-Programable Logic Circuit with Feedback.

in Table I. An interesting result is the duplication in period time when the ratio between delays get smaller. It goes from 70 to 280. Hence, we have obtained frequency doubling. And this is one of the best indications of the route to chaos.

TABLE I.- Characteristics of the output signals, according to the delay times.

t_p	τ_e	τ_i	τ_i/τ_e	Period
14	200	2	0.01	280
14	200	4	0.02	140
14	200	12	0.06	70

Values given at Table I do not correspond to the transition points between different periods. They are in a range where period remains constant. If we calculate the equivalent to the Feigenbaum ratio for the indicated values we obtain 4.

But if higher order transition points are taken into account, a number, closer to 4.6692, has been have been obtained.

As it is can be seen in Table I, as internal delay time goes to smaller values, the period of the output signal get higher and, eventually, becomes chaotic. This situations has been just obtained by computer simulation with internal delay time zero. Experimentally, we have not been able to obtain it.

The above facts show that optically processing elements are good candidates as pulse generators with controlled periods and, if the computer results are obtained experimentally, a random sequence of optical pulses can be achieved.

REFERENCES

1.- J.A.Martín-Pereda and A.González-Marcos, SPIE, Vol. 2038. pp. 67-77. (1993)

2.- A.González-Marcos, PhD Thesis. 1993.

Architectures for Photonic Space-and Wavelength-Switching Using Collinear guided-wave Acoustooptics.

Proklov V.V., Bashlakov A.U. and Birjukov V.A.

Institute Radio Engineering and Electronics of the Russian Academy of Sciences, Moscow, 103907, Mochovaya 11, GSP-3, Russia

telephone:(095)-526 91 92

Fax: (095)-203 84 14

E-mail: bys324@ire216.msk.SU

Abstract

This work presents a new approach for algorithms and architectures for photonic switching in mixed space-wavelength domains by means of collinear guided-wave acoustooptic interaction. We investigate a few most advanced schemes and proposed capabilities for $LiNbO_3$ guided-wave implementations in optical computation and associative memory devices.

Summary

There were known a different wavelength - division - multiplexing and space-division-multiplexing systems to perform the optical switching with increased transmission capacity and system flexibility (see, for example [1]). In each mentioned case it has been used a specific property of required devices - the wavelength selectivity or the spatial resolution.

In this paper, we investigate an improvement of the guided-wave photonic switching devices by means of utilizing of the combined space-wavelength divisions multiplexing. The principal idea is based on earlier demonstrated switching capability of the multifrequency acoustooptic (AO) interaction of the light guided modes with collinear propagated surface acoustic waves (SAW) in planar Ti-diffused waveguide in YX-$LiNbO_3$ that results in the radiative substrate mode with

90^0 -rotation of light plane polarization [2]. Fig. 1 shows the scheme of this kind of single channel planar AO cell with estimated switching capability in space-wavelength divisions about ~ 10^{11} switch./sec.

In this paper we consider a few possible architectures and algorithms for 1D and 2D photonic switching in space-wavelength domains based on the mentioned multifrequency and multichannel planar AO cells. It gives also detailed analysis experimentally achieved and potential (extrapolated) characteristics of this technology for aims of optical computing and optoelectronic associative memory systems (with estimated capability ~ 10^{14} switch./sec for one chip device similar to shown in Fig. 2).

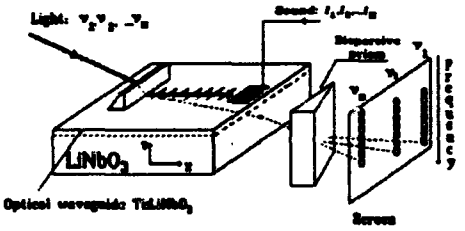


Fig.1. Single channel planar AO cell based on Ti:$LiNbO_3$ with collinear wave interaction.

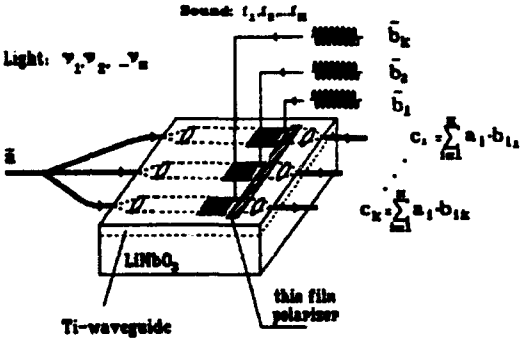


Fig. 2. Scheme of multifre quency/multichannel planar AO cell for associative memory system.

References

[1]. Technical Digest of International Topical Meeting on Photonic Switching, April 12-14, 1990, Kobe, Japan.

[2]. Proklov V.V., Bashlakov A.U., Technical Digest of International Conference on Optical Information processing, p.7, August 2-7, 1993, St.Petersburg, Russia.

A Bi-Cell Diode Acousto-Optic FM Demodulator

P BROOKS
Royal Naval Engineering College
Manadon
PLYMOUTH, PL5 3AQ 0752 553740 ext 81505

C D REEVE
School of Electronic, Communication and Electrical Engineering
University of Plymouth
Drake Circus
PLYMOUTH, PL4 8AA 0752-232330

ABSTRACT

The use of a bi-cell photodiode detector in an acousto-optic FM demodulator is described. Theory is developed showing that the system is capable of up to 57 dB AM rejection and practical results are presented to support the theory.

SUMMARY

The acousto-optic FM demodulator [1,2] is a conceptually simple and yet highly sensitive system for real-time demodulation of narrow band FM signals at carrier frequencies up to around 2 GHz. The basic system is shown in Figure 1. The system depends upon the frequency dependent deflection ($\delta\theta$) of a laser beam (wavelength λ) by an acousto-optic cell (acoustic velocity V_a), given by

$$\delta\theta = \frac{\lambda}{V_a}\delta f \qquad (1)$$

where δf is the change in frequency.

In the original system a single detector is used and the deflected spot of light scans across a knife edge so that, as the frequency changes, so does the amount of light reaching the detector. This system is highly sensitive to any AM content in the signal and also to any variations in the intensity of the laser. The AM content can be removed by hard limiting but the laser intensity noise remains a problem.

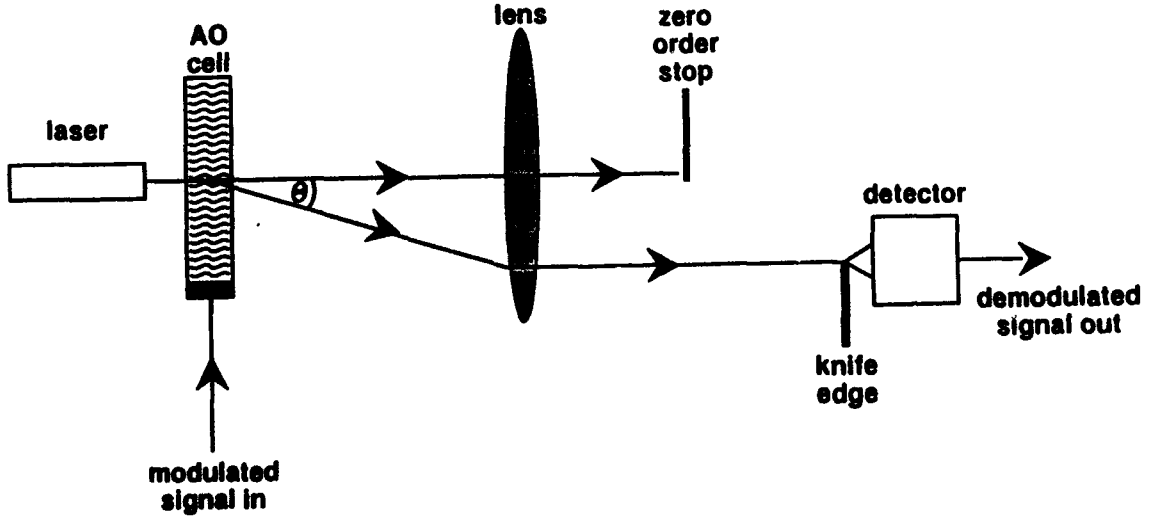


Figure 1. The Acousto-Optic FM Demodulator - Schematic

In the new system the knife-edge/single detector assembly is replaced by a bi-cell detector comprising two photodiodes with a very small inactive strip between them. This strip is perpendicular to the direction of beam deflection so that the edge of each diode acts as a knife edge. For small deviations of the gaussian beam ($\leq$ half the standard deviation) the optical power reaching the two detectors is

$$P_+ = \frac{P_1}{2}(1+K) \qquad \text{and} \qquad P_- = \frac{P_1}{2}(1-K) \tag{2}$$

where P_1 is the power in the first order diffracted beam and K is the ratio of the signal power (P_s) due to the movement of the beam to the background power ($P_1/2$). It should be noted that it is the quantity K that gives the frequency modulation since it may be shown that

$$K = \sqrt{2\pi}\frac{d}{V_a}\delta f \tag{3}$$

where d is the $1/e^2$ laser beamwidth at the AO cell.
Taking the difference of P_+ and P_- we obtain an output proportional to P_1K. Since, for linear response, $K << 1$ we can see that variations in the diffracted optical power P_1 have a far larger effect upon the output of the single detector system (P_+) than on the output of the bi-cell system. The AM rejection of the bi-cell system relative to the single detector system may be shown to be

$$\frac{1+K}{2K} \approx \frac{1}{2K} \qquad \text{for } K << 1 \tag{4}$$

Using d = 0.5 mm and V_a = 617 m/s, we find that the AM rejection of the bi-cell system is

$$57 - 10\log(\delta f) \text{ dB} \tag{5}$$

Clearly the AM rejection is very good for small values of δf. Even at the limit of the linear range of this system (δf = 200 kHz), the AM rejection is 4 dB. Theoretical predictions of this model are presented and compared with experimental results and are found to be in good agreement. Although the performance of the system falls off as the frequency deviation increases, its main advantage lies in its simplicity. The AM effects discussed arise from both the AM content of the signal and any laser intensity variations. If this technique is combined with a hard limiter on the input signal the resulting system performance is found to be significantly better than the knife edge/single detector system. An alternative technique, which would completely remove the AM content, is to split the diffracted beam. One portion goes to the knife edge/single detector and the other to a detector which measures only the AM content. Dividing the first signal by half the second yields the FM signal. However with currently available AO cells the system is capable of operating at modulation bandwidths up to 10 MHz; at these frequencies analogue dividers do not perform well.

References

1. Poon T C and R J Pieper. 'An acousto-optic FM receiver demonstrating some principles of modern signal processing.' IEEE Transactions on Education, E-28, 1, 11-17 (1985).
2. Reeve C D. 'An acousto-optic FM demodulator: computer modelling and experimental results.' Proceedings of the Optical Society of America Annual Meeting 1989.

Integrated-Optic Commutator for High-Speed Local Communication Network with Cross-Talk Minimization in Optical Directional Couplers

Igor G.Voitenko and Toyohiko Yatagai*

Institute of Applied Optics, Byelorussian Academy of Sciences
212793 Mogilev, Belarus

*Institute of Applied Physics, University of Tsukuba
Tsukuba, Ibaraki 305 Japan
Tel: +81-298-53-5334
Fax: +81-298-53-5205

Abstract

The performance of an 8x8 polarization-independent $LiNbO_3$ switch matrix formed by directional couplers for the local area network is described. The cross-talk of the coupler is precisely estimated and its minimization is discussed.

We report the performance of a 8x8 polarization-independent $LiNbO_3$ switch matrix on the base of a directional coupler with its full complement of the local area network. The objective of this work was to provide an MgO:Ti:$LiNbO_3$ switch array on the base of a new type directional coupler for use as a photonic center stage switch in the architecture switching network.

In designing such schemes the problem of cross-talk minimization holds. In the given work a dependence of the switch cross-talk on the adjusting section parameters is analyzed. An adjusting section scheme which permits to eliminate the cross-talk is proposed. We investigate the device on the basis of diffused channel waveguides where modes of the waveguides are described approximately by the scalar equation

$$\frac{\partial^2 \Psi}{\partial x^2} + \frac{\partial^2 \Psi}{\partial y^2} + \frac{\partial^2 \Psi}{\partial z^2} + k_0 \Psi(x,y,z) = 0$$

where Ψ denotes the light amplitude in the waveguide and k_0 the wave number. This equation is solved for $y<0$ with the boundary condition $\Psi|_{y=0}=0$.

The optical modulators used in the experiment are high-speed waveguide electro-optic directional couplers. The fabrication

parameters for the single-mode waveguides: titanium stripe width 4μm and coupler length L-8mm. For this device more than 80% efficiently was obtained (wavelength is 1.3μm and 12V switching voltage, -29dB "bar" state crosstalk and -19dB "cross" state crosstalk). The insertion loss, when coupled to input and output single-mode fibres, is 2.6dB for the TE0-mode, including 0.4dB reflection loss.

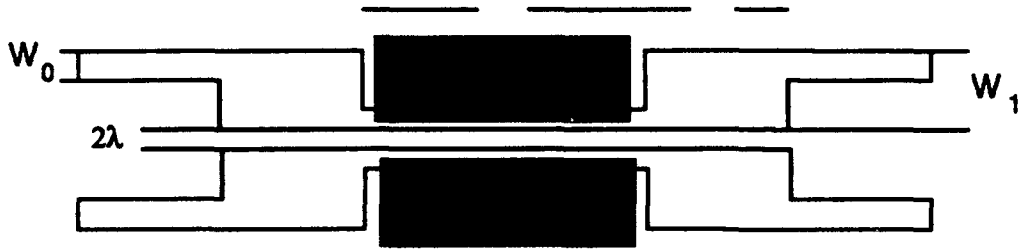


Fig. 1 Structure of a new type of a directional coupler.

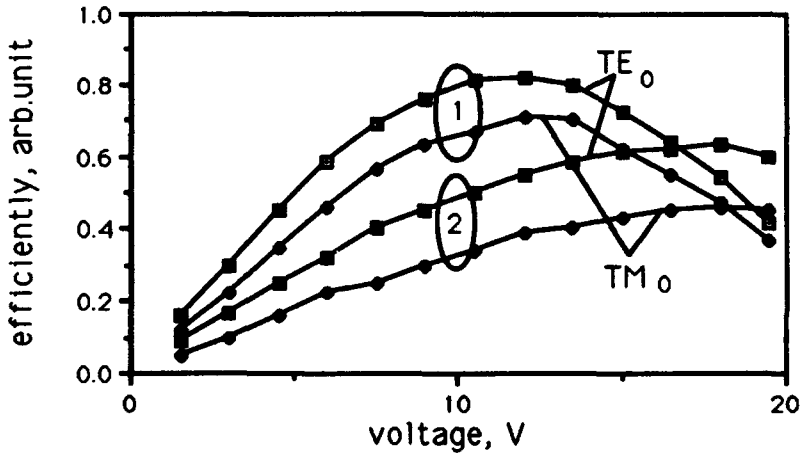


Fig. 2 Optical output power of the directional coupler vs. input voltage.

Optical Characteristic of Photorefractive Three-Dimensional Waveguides in Lithium Niobate

Kazuyoshi Itoh, Osamu Matoba, Yoshiki Ichioka
Osaka University, Department of Applied Physics,
2-1 Yamadaoka, Suita, Osaka, 565, Japan
Tel. 81-6-877-5111 ext. 4664

ABSTRACT

Various near field patterns of a photorefractive waveguide fabricated in a lithium niobate crystal are compared with those of numerical analysis using a waveguide model to evaluate the optical characteristic of photorefractive waveguides.

SUMMARY

We present in this paper experimental and numerical analysis of a novel approach to optical interconnections for neural networks. The approach is to fabricate waveguide structures in photorefractive media by simply focusing and scanning a laser beam (see Fig. 1). Resultant waveguides with variable index profiles may be used for the optical dynamic interconnections. We believe in the possibility that high-density optical interconnections with a self-organization ability be realized by this approach. Experimental evaluation of simple photorefractive waveguides has been made[1,2]. In this paper, optical characteristic of a photorefractive waveguide in a lithium niobate (LN) crystal is studied experimentally and numerically. Comparison between the results of the experiment and numerical analysis showed[4] that the maximum photorefractive change of refractive index is as large as 1×10^{-3}. Results of modal analysis will also be presented.

The experimental setup is briefly outlined. A linearly polarized Ar-ion laser beam whose electric field vector and propagation direction are perpendicular to the c-axis of a LN crystal is focused by a microscope objective lens to fabricate the waveguide structures in the LN crystal. A He-Ne laser beam whose electric field vector is polarized along the c-axis is also provided. This beam causes a negligible photorefractive effect and is used to excite the guided modes in the fabricated waveguides. The longitudinal position of the focus of the fabrication beam can be controlled by a translator. A microscope objective is placed behind the LN crystal for observation of near field patterns on the rear face of the crystal. The near field patterns are observed by a CCD image sensor.

We observed the lateral profile of refractive index change around the waveguide[1,2]. To evaluate the refractive index change within the crystal, we have made a model of photorefractive index distribution within the crystal. In this model, the maximum refractive index change is an unknown parameter. We observed also the near field patterns across the rear face of the crystal[1,2]. We have calculated the variation of intensity distribution of guided beams along the waveguide (Figs. 3 and 4) and near field patterns across the rear face of the crystal. Comparison between the experimental and numerical results made us possible to estimate the maximum value of refractive index change[4].

In this paper, we compare the results of a more-detailed experiment with

those of numerical analysis to estimate precisely the refractive index distribution within the crystal by using more realistic model for the refractive index change. We also observe the variation of near field pattern when the amplitude distribution of the excitation beam across the entrance of the waveguide is changed. Such observation gives us the information about the propagation characteristic of the waveguide. Comparison of these observations with the numerical results will improve the accuracy of estimation of index distribution and optical characteristics of the waveguide. Examples of the side views of the calculated intensity distribution along a curved waveguide are shown in Figs. 3 and 4. The maximum values for the refractive index change are assumed to be 1.2×10^{-3} and 0.9×10^{-3}, respectively.

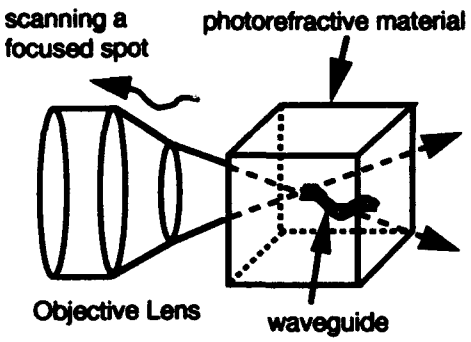


Fig. 1 Fabrication of 3-D photorefractive waveguide.

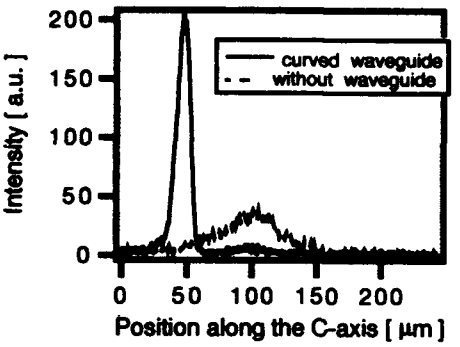


Fig. 2 Near field pattern across the rear face of the crystal.

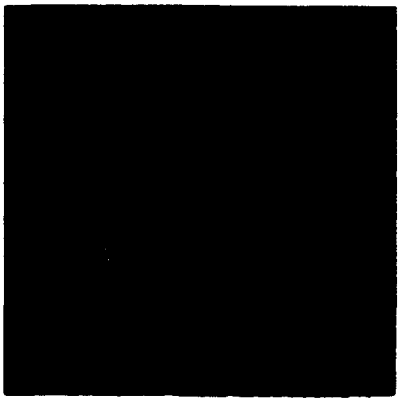


Fig. 3 Side view of the guided beam intensity; $\Delta n=1.2\times10^{-3}$.

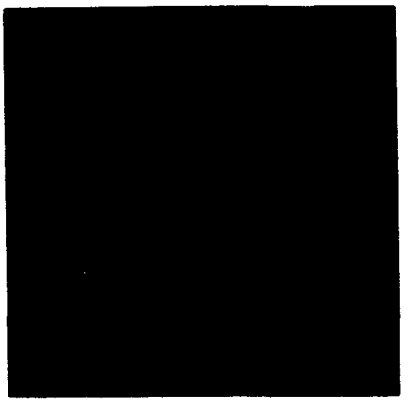


Fig. 4 Side view of the guided beam intensity; $\Delta n=0.9\times10^{-3}$.

References

1. K. Itoh, O. Matoba, and Y. Ichioka, "Fabrication of photorefractive three-dimensional waveguides in lithium niobate," Opt. Lett., submitted.
2. O. Matoba, K. Itoh, and Y. Ichioka, "Photo-induced waveguide for optical dynamic 3-D interconnections in $LiNbO_3$," Proceedings of 1993 International Joint Conference on Neural Networks, Nagoya, Vol. 1, 825-828, (Oct. 25-29, 1993).
3. M. D. Feit and J. A. Fleck, Jr., "Light propagation in graded-index optical fibers," Appl. Opt. 17, 3990-3998 (1978).
4. O. Matoba, K. Itoh, and Y. Ichioka, "Analysis of photo-induced waveguide in lithium niobate crystal," ICO Topical Meeting 1994, submitted.

Photorefractive Channel Waveguide Structures for Optical Computing Applications

Vladymir M. Shandarov
Laboratory of Acoustooptoelectronics
State Academy of Control Systems and Radioelectronics
40 Lenin Ave., Tomsk 634050, Russia
Phone: 007-(3822)-496278, Fax: 007-(3822)-223262

Abstract

Characteristics of channel optical waveguide structures, formed in lithium niobate by photorefractive impurity diffusion, have been investigated, and two - dimension matrix of such waveguides for optical computing devices has been proposed.

Summary

Besides bulk photorefractive crystals, recently some investigations of photorefractive effects in fiber - shape samples and planar waveguides on the base of such crystals have been performed [1 - 3]. They showed some advantages of similar fiber and waveguide elements compared with bulk materials because of the high optical energy density within them and easier changing of their photorefractive properties. It resulted, in particular, in proposal to use the photorefractive fiber bundles as the two -dimension matrix in optical storage devices and pixel - by - pixel image processors [1]. Because channel optical waveguides and optical fibers have many similar features, the photorefractive channel waveguide structures can be used in such a manner as well. In this work some technological features and photorefractive properties for lithium niobate single - mode and multi - mode channels were investigated and the one of possible channel structure configurations for optical computing has been proposed.

1. Fabrication of channel waveguides.

The single channels and channel arrays were formed both on the Y and Z cut $LiNbO_3$ substrates. To increase the photorefractive sensitivity of $LiNbO_3$, the Fe diffusion and the sequential Ti and Cu (or Fe and Cu) diffusion were used (because Cu diffusion only results in a negative change of $LiNbO_3$ refraction index). To provide more symmetric depth profile of channels, some of them were formed by the counterdirected Fe diffusion in the substrates with thickness 0.1 mm. The initial film thicknesses of doping impurity films on the substrate surface made up 20,0 - 30,0 nm for single - mode and up to 200,0 nm for multi - mode channels. The diffusion process was carried out in the air atmosphere at 900 - 1000° C for time period from 2 up to 40 hours. The width of metal strips was changed within the range from 5,0 mcm up to 0,1 mm for single - mode and multimode waveguides, respectively. To use samples obtained in experiments, their input and output end faces were polished with optical quality. As waveguide, as photorefractive characteristics of channel structures were tested at the light wavelenght 633 nm (He - Ne laser).

2. Channel element characteristics.

The waveguide parameters of channels formed were determined from modal characteristics inspected by a prism coupling method for multi - mode elements and from near field distributions for single - mode ones. Their photorefractive characteristics were investigated by hologram recording in the common two - beam setup (Fig.1).

Characteristics of waveguides produced considerably depended on doping impurity kind and channel waveguide geometric parameters. Thus, the best result (combination of optical quality, photorefractive sensitivity and time response

characteristics) for single - mode channels was obtained for only **Fe** diffusion. The refractive index change at the waveguide boundary was measured in this case 0.005 - 0.007 and the waveguide depth was close to its width value 5,0 mcm. The typical time response at photorefractive grating recording and erasure made up about 1 s for such waveguides. The main feature of multi - mode $LiNbO_3$:**Fe** waveguides is the inhomogeneity of **Fe** distribution in the channel cross section, that results in the strong dependence of photorefractive grating recording and erasure characteristics on the input light field space structure. These characteristics were improved in waveguides produced by the counterdirected **Fe** diffusion in 0,1 mm **Z** cut substrates. The **Fe** films with thicknesses from 100,0 up to 200,0 nm were used in this case. It should be noted the different conditions for light definition in such waveguides in the horisontal and vertical directions, that has to be taken into attention for image processing in such elements.

3. Applications of channel photorefractive waveguide structures in optical computing.

Like the fiber photorefractive elements, the channel structures discussed have some advantages compared with bulk crystals. They allow nonlinear interactions of light beams at low optical powers, easy to control the photorefractive characteristics of separate elements in the whole structure and their spatial configuration. Besides, many wafers with channel arrays can be stacked in the 2D matrix for optical storage devices and other processors (Fig.2) with possibility to provide any required dependence of photorefractive properties in the cross section of such an artificial "bulk photorefractive cell".

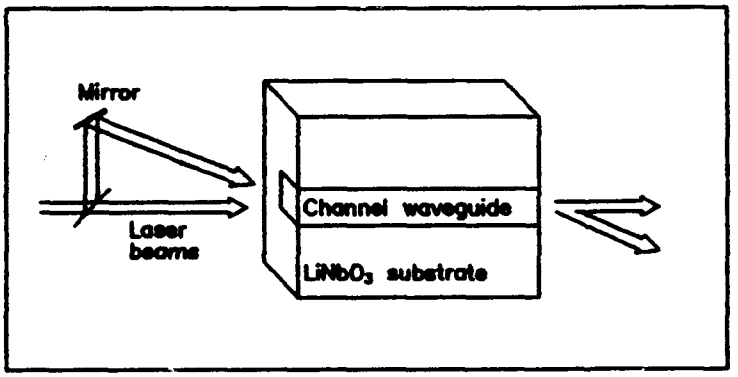


Fig.1 Experimental setup for inspections of photorefractive characteristics in channel waveguides

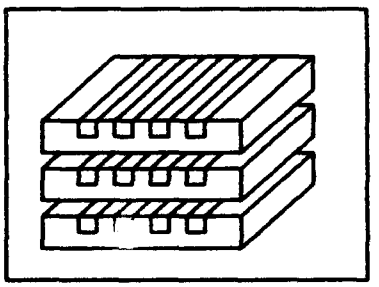


Fig.2. Schematic of 2D matrix from channel waveguide arrays

References

1. L. Hesselink. Intern. Journ. of Optoelectronics, 1990, Vol.5, No.2, pp. 103 - 124.

2. A.Kamshilin, R.Silvennoinen, T.Jaaskelainen, C.Lima, M.Andreeta, V.Prokofiev. Opt. Lett., Vol.18, No.9, 1993, pp. 690 - 692.

3. Glazov G., Itkin I., Shandarov V., Shandarov E., Shandarov S. J.Opt.Soc.Amer. B/Vol.7, No. 12, December 1990, pp.2279 - 2288.

Fiber-optical Loop Memory Structure for Optoelectronic Computer

V.A. Pilipovich, A.K. Esman, I.A. Goncharenko,
V.S. Posedko, I.F. Solonovich

Institute of Electronics, Academy of Sciences of Belarus,
22 Lagoiski Trakt, Minsk-90, 220841 Republic of Belarus
Tel. (0172) 65 61 12, Fax. (0172) 65 25 41

Abstract.

The method of structural organization of fiber-optical memory device (FOMD) is proposed which allows effective solutions to the problems of data addressing, control and correction taking the peculiarities of FOMD's into account. By this purpose two contrary-directed circulation channels - main and built-in additional ones - are organized in a single-fiber FOMD loop.

A number of features peculiar to fiber-optical memory devices[1,2], namely, high signal circulation rate, incontrollability of signals in optical channel, dependence of their time position on various destabilizing factors, hamper the use of conventional methods of data synchronization, addressing and control employed in other memory types.

This paper presents a method of structural organization of fiber-optical memory loop which allows effective solutions to the problems of data addressing, control and correction taking the peculiarities of FOMD's into account.

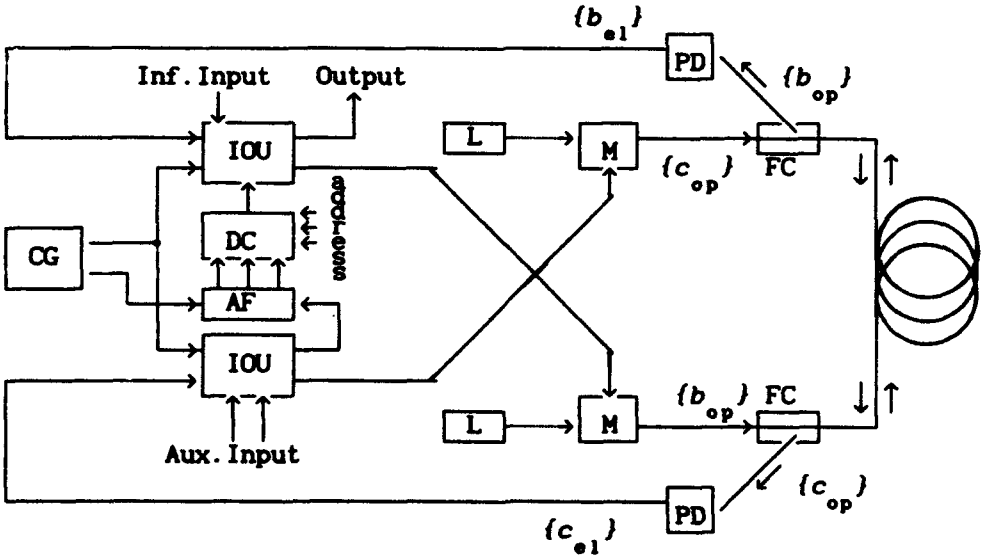


Figure 1. PD - photodetector, M - modulator, L - laser, IOU - input/output unit, FC - fiber coupler, CG - clock generator, AF - address former, DC - digital comparator.

In accordance with the method proposed, two contrary-directed circulation channels - main and additional ones - are organized in a single-fiber FOMD loop by using fiber couplers. Information signal sequence circulates in the main channel, while the additional channel can be used to transmit various auxiliary signals (verifying, synchronizing and addressing signals).

To ensure a reliable access to any segment of circulating information sequence and to improve its storage security, the additional channel can be used as an addressing channel. In the writing mode (see figure 1), the information sequence $\{b_{el}\}$ and the addressing sequence $\{c_{el}\}$ are written into the loop memory be feeding them synchronously to the information (inf.input) and auxiliary (aux.input) input terminals of the input/output unit (IOU), respectively, and further to control input terminals of the corresponding electrooptical modulators. As the addressing sequence circulates in closed loop, its segments (address words) are also synchronously written into an n-bit address former (AF) thereby forming the address of a coming information sequence. Synchronous circulation of signal flows along identical channels allows simultaneous feeding of the IOU input terminals independent of any external influences.

Access to the required information signal (rewriting, retrieval) is realized through setting appropriate address on the address inputs of a digital comparator (DC). When the contents of the AF coincides with the set address during the next passage of the address sequence along the circulation loop, the DC generates a control signal used to strobe information signals.

In order to reduce error probability in forming address words, it is advantageous to use a pseudo-random sequence (PRS) as address sequence. The PRS length is $M = 2^N - 1$, where N is the PRS-generator bit capacity, and is determined by the memory information capacity; the address former represents an n-bit shift register, where n is not less than N. In case a redundant length of the PRS address words is used, i.e. for $n > N$, addressing is free of errors even if the received address word has several incorrect ("spoilt") bits.

Transmission of verification and synchro signals in the additional channel results in enhanced reliability of data storage owing to correction of possible errors and elimination of mistiming in synchronous detection of signals[3]. In addition, by using non-linear optical effects it is possible to realize operating mode ensuring compensation of attenuation of information signals in the optical fiber.

REFERENCES

1. M.I. Belovolov, N.I. Golovin, T.N. Golovina, E.M. Dianov et al. Dynamic random-access memory based on fiber-optic guides. // Kvantovaya Elektronika. - 1985. - Vol. 12, N 1. - P. 214-216 (in Russian).
2. V.A. Pilipovich, A.K. Esman, I.A. Goncharenko, V.S. Posedko, I.F.Solonovich . Contrary-directed circulation of signals in dynamic fiber-optical memory loop // Doklady Akademii nauk Belarusi. - 1994. - Vol. 38, N 1. (in press) (in Russian).
3. V.A. Pilipovich, A.K. Esman, I.A. Goncharenko, V.S. Posedko, I.F. Solonovich . In: ISFOC'93 - Conference Proceedings. - Information Gatekeepers Inc., 1993, p. 97-100.

NEW TYPES OF OPTICAL SOLITON-LIKE STRUCTURES AND THEIR POSSIBLE APPLICATIONS TO OPTICAL COMPUTING

A.V.Fedorov, S.V.Fedorov, G.V.Khodova,
N.N.Rosanov, V.A.Smirnov, and N.V.Vyssotina

S.I.Vavilov State Optical Institute
St.Petersburg, 199034, Russia

Basic properties and possible applications to optical computing of new types of spatial and spatiotemporal solitons and their bound structures are considered in the following nonlinear optical schemes: (a) medium with nonlinearity of refractive index; (b) wide-aperture nonlinear interferometer; (c) wide-aperture laser with saturable absorption; (d) optical fiber with sections of gain and absorbing media.

Soliton-like light structures of different types (spatial and spatiotemporal optical solitons) can be formed in a wide spectrum of nonlinear optical systems: passive and active, with and without feedback. A number of their properties promising for optical computing differ noticeably from the case of "traditional solitons" observed, for instance, in single-mode fibers with Kerr nonlinearity. In the present communication we present results of theoretical investigations and computer simulations of basic properties of soliton-like structures in four different nonlinear optical systems and consider their possible applications for processing of optical information and optical computing.

In transparent medium with saturable nonlinearity of the refractive index, formation of different kinds of spatial solitons is possible, including solitons with different topological charges (vortices). Single spatial solitons are characterized by azimuthal (topological charge) and radial integer indexes, and by the propagation constant, which can vary continuously in some interval. As a result, there is a set of solitons with continuous variation of their characteristics (*e.g.*, maximum intensity). In the case of copropagation of a pair of solitons, depending on characteristics of single solitons, initial distance between them (in the transverse direction), angle between axes of propagation and phase difference, the following regimes can be realized: oscillations of the transverse distance between solitons with increase of the longitudinal coordinate, elastic and inelastic collision (with transfer of power), decay of solitons into fragments; merging of solitons into one with larger power. Dynamics of interaction of laser beams, initial profile of which differs from a spatial soliton, depends on the degree of nonlinear distortions of these beams before their collision in the medium.

In passive wide-aperture nonlinear interferometers excited by homogeneous coherent external radiation, a wide set of spatial solitons (diffractive autosolitons) and their bound states can exist. In contrast to "traditional solitons" which have continuous spectrum of widths and amplitudes, diffractive autosolitons have discrete set of

widths and a certain value of amplitudes. Bound states of diffractive autosolitons are also characterized by a discrete set of distances between them. Transverse (with respect to the direction of the wave vector of radiation) motion of solitons and their symmetric structures is possible only with oblique incidence of radiation on the interferometer. The property of asymmetric structures of bound diffractive autosolitons to propagate along the interferometer aperture even with normal incidence of radiation on the interferometer gives wide opportunities to use these structures in transverse transmission of information and performing different arithmetic operations.

In a wide-aperture laser with hard excitation of lasing, soliton-like structures - laser autosolitons - can be excited. Their type is intermediate with respect to the two cases considered above. Really, the presence of the characteristic level of intensity (the intensity of stationary transversely homogeneous lasing) prohibits arbitrary change of maximum autosoliton intensity. This makes the properties of the laser autosolitons close to the properties of the autosolitons in passive interferometers. However, the absence of external radiation injection allows excitation of single autosolitons moving in the transverse direction. Another specific feature of the laser autosolitons is the shift of lasing frequency caused by diffractive and nonlinear effects. Characteristics of single laser autosolitons and dynamics of their interaction are described.

In single-mode optical fibers in the range of anomalous dispersion with quasiperiodic location of elements with saturable gain and absorption, the temporal soliton-like structures similar to the laser autosolitons can be formed. With a certain choice of parameters, cw-radiation with low intensity is damped out (thus weak noises are suppressed), and radiation with high intensity is stabilized at a certain level. Analogs of switching waves and laser autosolitons can be realized for pulsed radiation. Pulses of fixed self-sustained form, with certain value of peak intensity and pulse width, can be transmitted in this fiber system.

The types of soliton-like structures considered above have potential interest in the problems of optical information processing and optical computing. Spatial solitons in transparent medium with saturable nonlinearity of the refractive index can be used for optical switching and performing a number of other elementary operations. Diffractive autosolitons in wide-aperture nonlinear interferometers allow to perform a number of operations within the discrete-analogous method of optical computing, e.g. in shift registers or multi-digit full adders. Laser autosolitons can be used in the schemes of information storage. Soliton-like pulses in single-mode optical fibers with elements with saturable gain and absorption are characterized by high contrast, high signal-to-noise ratio, and stability of power characteristics, thus being promising for information transmission.

Analysis of an Alternative Approach for Constructing a Parallel All-Optical Data Transmission Line

A. Dreischuh, E. Eugenieva, S. Dinev

Department of Physics, Sofia University
5 J. Bourchier Blvd., BG-1126 Sofia, Bulgaria
Fax: (359-2) 463 589 Tel: (359-2) 62 561/ext:611

We propose and analyze an alternative approach for constructing a parallel all-optical data transmission line. Control laser beams can form intermediate channels in which pulses of information could be guided without a cross-talk.

The solitons in optical fibers are proposed as highly suitable carriers of information. Unfortunately, the changes of the femtosecond soliton characteristics at long propagation distances may limit their use. In this work we propose an alternative approach for constructing a parallel all-optical data transmission line. CW control beams copropagate in a planar optical waveguide and form intermediate nonlinear channels in which pulses of information could be guided (Fig.1). To ensure a reasonably extended transmission distance, the control beams should propagate in the form of noninteracting fundamental bright spatial solitons. The signal waves experience the influence of the control beams only. This induced action originates in the spatial refractive index change along/across the nonlinear medium caused by the control beams.

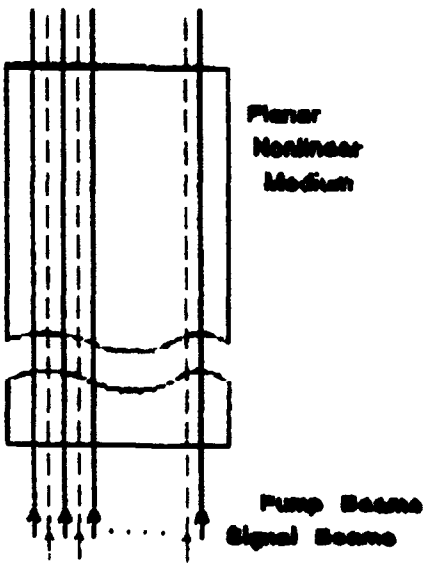


Fig. 1

The evolution of the control- and the signal (information)- waves is analyzed using the split-step Fourier method. For 5 control beams of equal radii a and intensities we obtained stable propagation at a beam-to-beam distance $\Delta x=1.75a$. Fig.2 represents the spatial evolution of the signal pulses in such a situation. The initial spatial profiles of the signal waves are assumed to be Gaussian. Periodic spatial oscillations of the signals along the nonlinear medium without a cross-talk between the information channels are clearly expressed.

In the configuration proposed a stable spatial guiding of the information pulses should be expected even at control-beam intensity fluctuations within 10%. The signal waves behavior is almost the same as under perfect initial conditions (Fig.2). Fig.3 shows the spatial evolution of the information pulses when they are not perfectly aligned with respect to the centers of the nonlinear channels (maximum initial deviation within 25% the channel half-width). The nonlinear waveguide induced by the control beams "reflects" back the signal wave preventing the information-channel cross-talk.

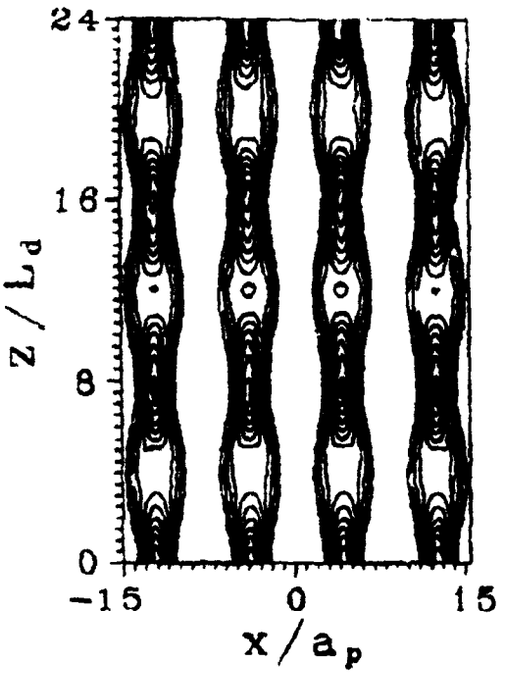


Fig. 2

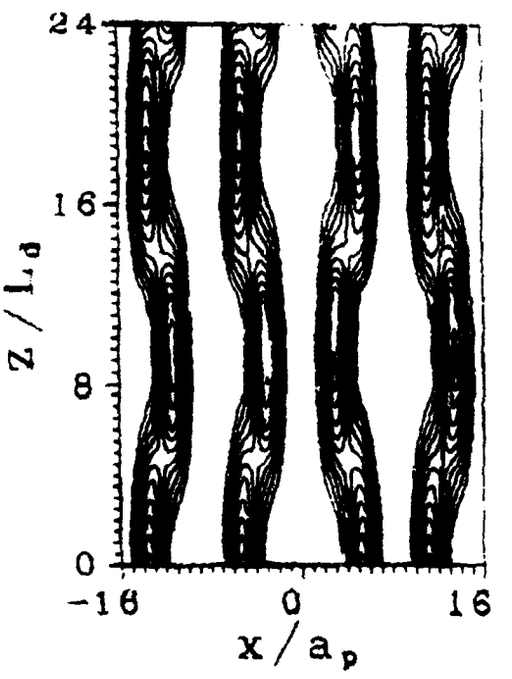


Fig. 3

The performance of the parallel all-optical data transmission line proposed seems encouraging. Further analyses are under way in order to evaluate the restriction on the maximum bit-rate of the parallel data transmission scheme proposed.

This work was done with the financial support of the National Science Foundation, Bulgaria, under a contract F-206.

All-Fiber Optical Adder Based on Symbolic Substitution Algorithm

N.A.Khilo

Division for Optical Problems in Information Technologies
Academy of Sciences of Republic of Belarus
P.O.Box No.1, Minsk, 220072, Belarus

All-fiber optical schemes are promising for high-speed information processing. Due to fiber broadbanding their clock frequencies in these schemes may achieve to the value of $f_T \sim 10^{12}$ Hz and more. In real, however, operation rate restrictions appear due to insufficient switching rate of logical elements. As important branch to win through the restrictions is the transition to speed-of-light latchless architecture [1,2]. Fiber elements serve here both for information transformation and for its storage. Particularly, operations of switching may be realized on the base of nonlinear directional couplers or fibers with nonlinear ellipse rotation, where speed non-resonance nonlinearities are used. Functional abilities of schemes based on speed-of-light latchless architecture essentially depend on the number of algorithms realized in them.

In the study reported as an example of adding operation it is shown that symbolic substitution algorithm may be realized on the base of speed-of-light latchless architecture approach.

The scheme of adder is presented at the figure 1.

For number representation two orthogonally polarized modes of A and B fibers are used. At the fiber inputs clock pulses from laser power source are entered with polarization, corresponding, for example, to zero. To switch the polarization to "one" state the control signals from feedback line or input block are used. The switching is fulfilled by means of nonlinear ellipse rotation.

Then output from the fibers signals are multiplied in couplers and are entered to the interconnection block input. A signal of a high level is being formed at the one of four outputs of this

block depended on input signals combination and is entered then to a feedback line in accordance with symbolic substitution algorithm. A portion of energy of signals is directed to output. In a feedback line additional one-bit time delay is fulfilled and owing to this carry operation is realized. After m+1-th cycle, where m is digit capacity, the result of calculation is formed at the output. One can easily examine that under condition of signals relative coherency in interconnection block crosstalk level in the feedback line and at the output is about 25% of a valid signal. The processing power of the adder is determined as $w = \frac{f_T}{(m+1)^2}$

At $f_T = 10^{11}$, $m = 3$ w is equal to $6.25 * 10^9$ operations/sec.

References

[1] V.P.Heuring, H.F.Jordan, T.Main, R.Feuerstein, J.Feeher, L.Ji, in *Optical Computing* 1992, Technical Digest, Minsk. p.30F1.

[2] V.P.Heuring, *Opt.Eng.*, v30(2),1931-1935 (1991).

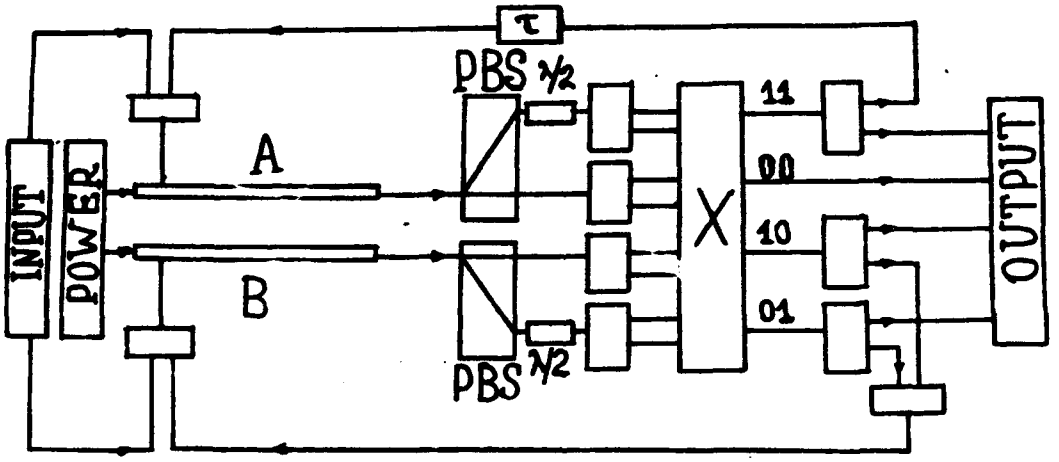


Fig.1. The all-fiber adder based on simbolic substitution algorithm scheme.

Optical Fiber Parallel Logic Processor

M.R. Wahiddin and S. Abdul Halim

Department of Mathematics, University of Malaya
59100 Kuala Lumpur, Malaysia.

Tel : 603 - 7555466 Ext. 341
Fax : 603 - 7566343

Abstract

We propose an optical logic processor using wavelength division multiplexing in a single optical fiber.

During the past decade, many attempts have been made to realize optical parallel binary and multiple-valued logic processing based on digital logic theory - see for example [1-4]. In this paper we propose a novel optical method based on wavelength division multiplexing in a single optical fiber to perform parallel binary logic. Our system essentially operates very much like a single-hop local lightwave network. This clearly needs wavelength - agile optical transceivers for the purpose of dynamic coordination, and an efficient protocol; we propose the Receiver Collision Avoidance Protocol. The method involves coding parallel pairs of data channels with a '0' or a '1' in packets in an N data channel system with one

control channel which is encoded with a stream of '0' (for 'off') and '1' (for 'on') to match the number of pairs of data channels used. The encoded control channel would then alert the receivers (detectors) operating in pairs to manipulate the output for corresponding pairs of inputs. In Table 1 and Table 2 below we illustrate respectively the AND function and XOR function involving just a pair of data channels for true logic. Note that identical pairs of segments in the control channel are such that both on (off) means output is 1 (0).

A	B	1st Segment of Control Channel	2nd Segment of Control Channel	Output
0	0	off	off	0
0	1	on	off	0
1	0	off	on	0
1	1	on	on	1

Table 1

A	B	1st Segment of Control Channel	2nd Segment of Control Channel	Output
0	0	off	off	0
0	1	off	on	1
1	0	on	off	1
1	1	off	off	0

Table 2

References

1. H. Bartelt, A.W. Lohmann and E.E. Sicre, J. Opt. Soc. Am. A1 (1984) 944.

2. J. Tanida and Y. Ichioka, J. Opt. Soc. Am. 73 (1983) 800.

3. M.T. Fatehi, K.C. Wasmundt and S.A. Collins Jr., Applied Optics 20 (1981) 2250.

4. Y. Fainman, C.C. Guest and S.H.Lee, Applied Optics 25 (1986) 1598.

All Optical Arithmetic Operations By Means Of Spatial Solitons Interaction

M.BERTOLOTTI, F.GARZIA, C.SIBILIA

Dipartimento di Energetica, Universita' degli Studi di Roma, "La Sapienza"

Via A. Scarpa 14, 00161 Roma, Italy, GNEQP of CNR, and INFM

Tel.+39-6-49916541

Fax+39-6-44240183

ABSTRACT

We have studied the possibility of realizing all optical arithmetic operations using spatial solitons and their interaction properties. A nonlinear planar waveguide geometry has been considered.

SUMMARY

Our scheme is based on a couple of two propagating spatial solitons in a nonlinear waveguide, under the hypotesis of transverse confinement realized by a third order nonlinear medium, and where the relative phase is properly varied, so that the interaction properties of solitons can be utilized to perform the required process.

Our analysis starts from an adimensional nonlinear Schroedinger equation[1]:

$$i\frac{\partial u}{\partial Z} = -\frac{1}{2}\frac{\partial^2 u}{\partial X^2} - |u|^2 u. \qquad (1)$$

Under proper conditions the propagation is described from the following system of coupled differential equations[2]:

$$q_z = -4\exp(-2q)\cos(2\Phi)$$

$$\Phi_z = 4\exp(-2q)\sin(2\Phi) \qquad (2)$$

where q=q(z) is the relative distance, along the propagation direction, at the generically z coordinate, and Φ is the relative phase of solitons.

In Ref.[3] the influence is studied of the change of relative phase of two input solitons, of equal input intensity, on the intensity of the soliton whose phase has not been changed. The intensity is found to vary according to the law:

$$I_0 = k_I \Phi \qquad (3)$$

where k_I is a constant depending on initial distance with respect to the other soliton.

This means that the phase information carried by a pulse can be transferred to the intensity of another pulse after propagation (intensity modulation by change in phase).

By the help of this property all arithmetic operations can be realized. For example the adder can be realized when two soliton beams enter in the same waveguide with a relative phase equal to zero and their interaction in the first part of propagation is avoided by means of a proper shield. A beam of intensity I_1 propagated normally to the soliton path, changes via a nonlinear interaction the refractive index of a lenght L of the soliton path (see Fig.1), inducing a phase-change equal to $k_\Phi L I_1$. A second beam of intensity I_2 interacts with the same soliton

for the same length L inducing a further phase change equal to $k_\phi L I_2$. The total phase change is $k_\phi L(I_1+I_2)$. If now we let the two solitons to interact, they interfere according to the intensity modulation effect, and the intensity of one soliton becomes $I_0 = k_i k_\phi L(I_1+I_2)$, that is proportional to the sum of intensities of input beams, realizing an optical addition.
In a similar way it is possible to realize an optical subtraction. In fact if we consider the same structure of the adder where the zone interested by the second beam I_2 is composed by a negative nonlinear refractive index coefficient, the phase change induced over the soliton beam is equal to $-k_\phi L I_2$. The intensity of soliton after interaction becomes: $I_0 = k_i k_\phi L(I_1-I_2)$.
The division is made in a quite similar way by using only a beam of intensity I_1. If we reduce the length L by a factor N, the phase change induced over the soliton is equal to $k_\phi I_1 L/N$, and the output intensity becomes $I_0 = k_i k_\phi I_1 L/N$. This process is quite critical since it depends of our capability of reducing the length L properly.
The multiplication is made by increasing N times the length L, so that the output intensity becomes $I_0 = k_i k_\phi L N I_1$.

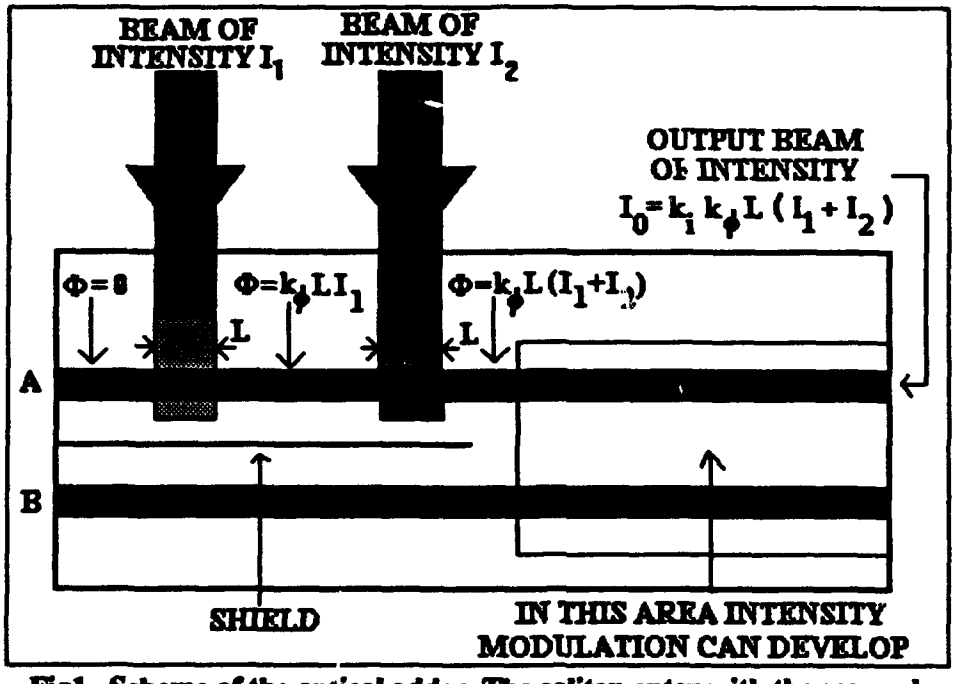


Fig1. Scheme of the optical adder. The soliton enter with the same phase.

References

[1] V.E.Zakharov, A.B. Shabat, Sov.Phys. JETP, 34, p.62, (1972).
[2] J.P. Gordon, Opt. Lett., 8, No.11, p.596, (1983).
[3] F.Garzia, C.Sibilia, M.Bertolotti, in print on Optics Communications.

Optical Detection Filters and Algorithm Fusion

David Casasent
Carnegie Mellon University, Center for Excellence in Optical Data Processing
Department of Electrical and Computer Engineering, Pittsburgh, PA 15213
Telephone (412) 268-2464; Fax (412) 268-6345; e-mail marlene@young.ece.cmu.edu

Abstract

Detection of candidate object regions in a scene is step one in general scene analysis. New optical morphological, wavelet and Gabor transform filters for detection are presented and fusion is used to reduce false alarms.

Optical image processors must fulfill a variety of different functions if they are to find widespread use in scene analysis, pattern recognition and product inspection. The first three operations performed in general image analysis are: detection (location of candidate object regions), reduction of false alarms and image enhancement.

We consider three algorithms for detection: morphological wavelet transforms (MWTs), macro Gabor filters (MGFs) and the hit-miss transform (HMT). These are shown in block diagram form in Figure 1. All algorithms are realizable on the same optical correlator architecture using different filter functions and nonlinear input and output operations. Each algorithm will be highlighted and initial results shown.

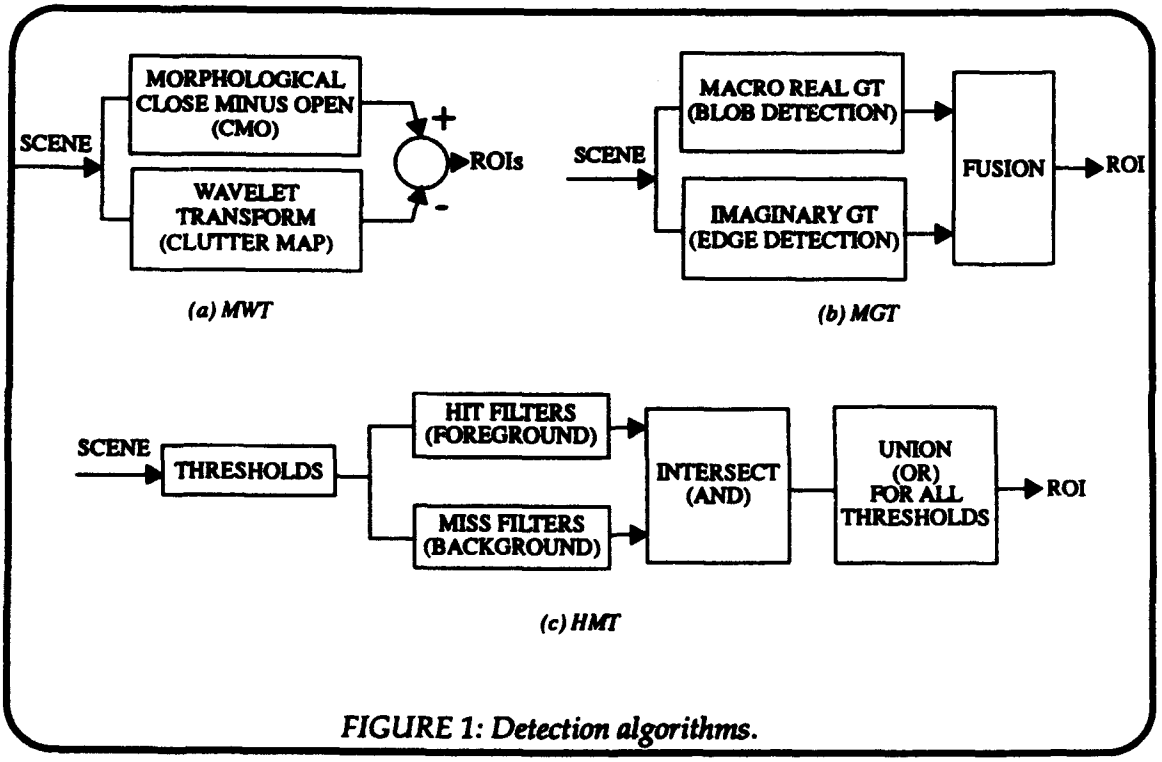


FIGURE 1: Detection algorithms.

Detection of multiple classes of objects independent of 3-D distortions and object contrasts in the presence of clutter is a formidable problem. Thus, we expect a number of false alarms in these detection outputs. To reduce these, we employ algorithm fusion as shown conceptually in

Figure 2. The concept is to produce all three output detection planes and to AND etc. them. This is expected to reduce false alarms, since only false alarms present in the same pixel location in all three outputs will be present in the final fused result. Data showing a significant reduction in false alarms will be presented.

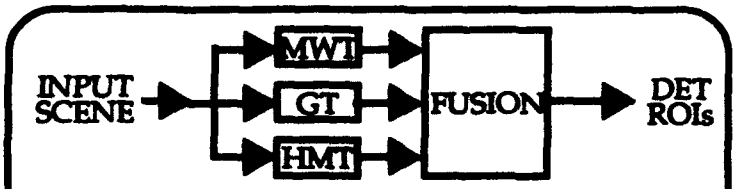


FIGURE 2: Algorithm fusion to reduce false alarms.

Once candidate regions of interest have been located, they are now analyzed further to identify the object present in each region. Prior to this, image enhancement is performed. The morphological portion of the MWT algorithm removes large clutter regions, the wavelet portion of this algorithm removes clutter with small particle sizes and produces a clutter map. We also employ morphological operations to enhance each such scene region. A new fast and very efficient optical gray-scale morphological algorithm and architecture are used. The architecture (Figure 3) is quite attractive as it only requires binary light modulators. This algorithm and architecture will be described and initial results will be presented.

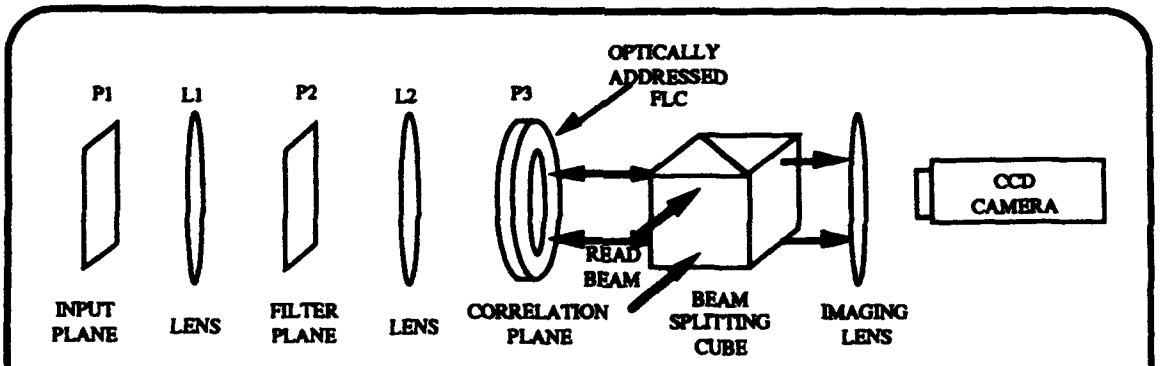


FIGURE 3: Optical gray-scale threshold decomposition architecture for image enhancement.

Space-variant filtering in fractional Fourier domains

Haldun M. Ozaktas, Billur Barshan
Electrical Engineering, Bilkent University, 06533 Bilkent, Ankara, TURKEY
David Mendlovic
Faculty of Engineering, Tel-Aviv University, 69978 Tel-Aviv, ISRAEL
Hakan Urey
Electrical Engineering, Georgia Institute of Technology, Atlanta, GA 30332, U.S.A.

Abstract

Signals with significant overlap in both the space and frequency domains may have little or no overlap in a fractional Fourier domain. Spatial filtering in these domains may allow us to eliminate distortion components which cannot be eliminated in the ordinary Fourier domain.

1 Introduction

Space-invariant filtering may be performed by multiplying the Fourier transform of the input signal by the Fourier transform of the impulse response. Recently we have discussed how various space-variant operations can be performed by multiplying with a filter function in a fractional Fourier domain [1]. These operations can be realized optically, because the fractional Fourier transform can be realized optically. One approach is based on the use of quadratic graded index media [2, 3], whereas another is based on the use of bulk lenses [4]. The graded index approach is closely connected to the definition of the fractional Fourier transform in terms of its spectral decomposition, whereas the bulk implementation is closely connected to its definition in terms of its linear transform kernel [1].

The many mathematical properties of the fractional Fourier transform, its relation to the Wigner space-frequency distribution, wavelet transforms, and chirp basis expansions, its applications to signal processing, and issues relating to its optical implementation are discussed in the references. Due to limited space, we will here content ourselves with the presentation of two examples of how space-variant filtering can be achieved by applying simple binary masks in fractional Fourier domains. Among the many things we cannot mention, of particular interest is correlation in fractional Fourier domains and its application to pattern recognition.

2 Definition of the fractional Fourier transform

The ath order fractional Fourier transform of a function $f(\cdot)$ is denoted by $\mathcal{F}^a[f](x)$ and may be defined as:

$$(\mathcal{F}^a[f])(x) = \int_{-\infty}^{\infty} \frac{e^{i(\pi\hat{\phi}/4-\phi/2)}}{|\sin\phi|^{1/2}} \exp[i\pi(x^2\cot\phi - 2xx'\csc\phi + x'^2\cot\phi)]\, f(x')\, dx', \qquad (1)$$

where $\phi = a\pi/2$ and $\hat{\phi} = \mathrm{sgn}(\sin\phi)$. Some of its properties are: i.) linearity; ii.) $\mathcal{F}^0$ and $\mathcal{F}^4$ correspond to the identity operation; iii.) $\mathcal{F}^1$ corresponds to the conventional Fourier transform; iv.) $\mathcal{F}^{a_1}\mathcal{F}^{a_2} = \mathcal{F}^{a_1+a_2}$.

One of the most important properties states that performing the ath fractional Fourier transform operation corresponds to rotating the Wigner distribution by an angle $\phi = a(\pi/2)$ in the clockwise direction. We are unable to discuss the Wigner distribution here, although it is important to fully understand the filtering examples discussed below. The reader is encouraged to consult [1] and the references given there. Roughly speaking, the Wigner distribution of a function $f(\cdot)$, denoted by $W_f(x,\nu)$, can be interpreted as a function that indicates the distribution of the signal energy over space x and frequency ν. Defining the rotation operator $\mathbf{R}_\phi$ for two-dimensional functions, corresponding to a counterclockwise rotation by ϕ, the property mentioned above can be expressed as $W_{\mathcal{F}^a[f]}(x,\nu) = \mathbf{R}_{-\phi}W_f(x,\nu)$. Another version of this property [6] is $\mathcal{R}_\phi[W_f(x,\nu)] = |\mathcal{F}^a[f]|^2$, where the operator $\mathcal{R}_\phi$ is the Radon transform evaluated at the angle ϕ. The Radon transform of a two-dimensional function is its projection on an axis making angle ϕ with the x axis.

3 Filtering examples

Consider the signal $\exp[-\pi(x-4)^2]$ distorted additively by $\exp(-i\pi x^2)\mathrm{rect}(x/16)$. The magnitude of their sum is displayed in part a., on the left hand side of the figure. These signals overlap in the frequency domain as well. In part b., we show their $a = 0.5$th fractional Fourier transform. We observe that the signals are separated in this domain. The chirp distortion is transformed into a peaked function which does not exhibit significant overlap with the signal transform, so that it can be blocked out by a simple mask (part c.). Inverse transforming to the original domain, we obtain the desired signal nearly perfectly cleansed of the chirp distortion (part d.).

Now we consider a slightly more involved example in which the distorting signal is also real. The signal $\exp(-\pi x^2)$ is distorted additively by $\cos[2\pi(x^2/2-4x)]\mathrm{rect}(x/8)$, as shown in part a., on the right hand side of the figure. The $a = 0.5$th transform is shown in part b. One of the complex exponential chirp components of the cosine chirp has been separated in

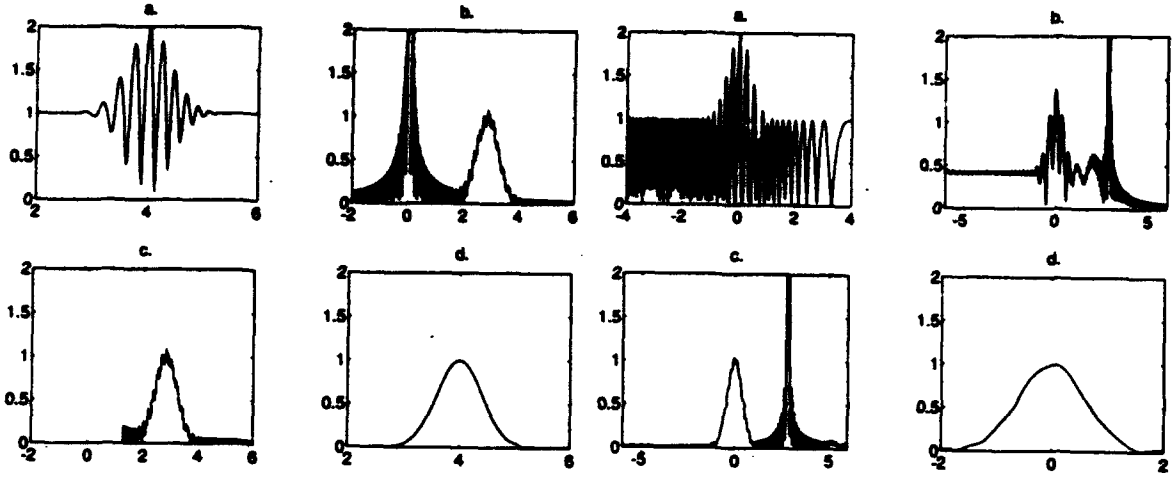


Figure 1: Example 1 (left) and example 2 (right)

this domain and can be masked away, but the other still distorts the transform of the Gaussian. After masking out the separated chirp component (not shown), we take the $a = -1$st transform (which is just an inverse Fourier transform) to arrive at the $a = -0.5$th domain (part c.). Here the other chirp component is separated and can be blocked out by another simple mask. Finally, we take the 0.5th transform to come back to our home domain (part d.), where we have recovered our Gaussian signal, with a small error.

The examples above have been limited to chirp distortions which are particularly easy to separate in a fractional Fourier domain (just as pure harmonic distortion is particularly easy to separate in the ordinary Fourier domain). However, it is possible to filter out more general types of distortion as well. In some cases this may require several consecutive filtering operations in several fractional domains of different order [1]. There is nothing special about our choice of Gaussian signals other than the fact that they allow easy analytical manipulation. Also, there is nothing special about the 0.5th domain. It just turns out that this is the domain of choice for the examples considered above.

In the above examples we have demonstrated that the method works, but did not discuss what led us to transform to a particular domain and what gave us the confidence that doing so will get rid of the distortion. This becomes very transparent once one understands the relationship between the fractional Fourier transform and the Wigner distribution. This relationship, as well as the general philosophy behind such filtering operations is discussed in [1].

4 Conclusion

What we know as the space and spatial frequency domains are merely special cases of fractional domains. These domains are indexed by the parameter a. The representation of a signal in the ath domain is the ath fractional Fourier transform of its representation in the $a = 0$th domain, which we define to be the space domain. The representation in the $a = 1$st domain is the conventional Fourier transform. If we set up a two-dimensional space, called the Wigner space, such that one axis (x) corresponds to the $a = 0$th domain (the conventional space domain) and the other (ν) to the $a = 1$st domain (the conventional spatial frequency domain), then the ath domain corresponds to an axis making an angle $\phi = a\pi/2$ with the x axis.

A desired signal and noise may overlap in both conventional space and frequency domains, but not in a particular fractional domain. Even when this is not the case, spatial filtering in a few fractional domains in cascade may enable the elimination of noise quite conveniently. It is possible to implement these operations optically.

It is a pleasure to acknowledge the contributions of A. W. Lohmann of the University of Erlangen-Nürnberg in the form of many discussions and suggestions.

References

[1] H. M. Ozaktas, B. Barshan, D. Mendlovic, and L. Onural. *J. Opt. Soc. Am. A*, early 1994.

[2] H. M. Ozaktas and D. Mendlovic. *Opt. Comm.*, 101:163–169, 1993.

[3] D. Mendlovic and H. M. Ozaktas. *J. Opt. Soc. Am. A*, Part I: 10:1875–1881, 1993, Part II: late 1993/early 1994.

[4] A. W. Lohmann. *J. Opt. Soc. Am. A*, 10:2181–2186, 1993.

[5] A. C. McBride and F. H. Kerr. *IMA J. Appl. Math.*, 39:159-175, 1987.

[6] A. W. Lohmann and B. H. Soffer. *Technical Digest of the 1993 Annual Meeting of the OSA*, 109, 1993.

All-Optical Dynamic Memories

M. P. Petrov

A. F. Ioffe Physical Technical Institute of Russian Academy of Sciences, 194021, St. Petersburg, Polytechnicheskaya str. 26, tel. (812) 515 67 65

ABSTRACT State-of-the-art review of all-optical dymanic memories and their crucial elements is given. It discusses the properties of all-optical regenerators of short optical pulses. Characteristics and properties of an optical dynamic memory operating through SRS in optical fibers are described.

SUMMARY An all-optical dymanic memory (AODM) is designed to store information in the form of optical pulses. AODM is needed in optical digital computers, telecommunication systems, for signal coding and decoding devices etc.

To be competitive, AODM should operate with rather short pulses ($\tau_p = 10^{-11}$-10^{-12} s) and provide almost unlimited storage time (τ_m). In the simplest case of moderate storage times ($\tau_m < 10^{-5}$ s) AODM can be simply an optical fiber delay line. However, at long τ_m that is achieved by circulating pulses through a fiber ring, AODM must include an amplifier to compensate for optical losses and a nonlinear threshold element to restore the shape and time position of pulses, i.e., to provide the functional stability of the scheme. Such a nonlinear element that has to suppress a weak signal and form a required standard level of a high output signal provides a necessary signal/noise ratio, the ratio between logic one and zero, and also a precise pulse timing. In essence, this element is a regenerator of light pulses.

Since a large bandwidth is required in AODM ($\Delta f = 10^{12}$-10^{13} Hz) it is most suitable to use fiber optic logic or switching elements of the type of nonlinear Mach-Zendner or Sagnac interferometers, and elements based on the Kerr effect, soliton interaction or SRS as regenerators. A typical drawback

of fibre elements, i.e. a long latency time, does not play an important role in AODM. As an example of a regenerator with high parameters a nonlinear Sagnac interferometer [1] can be mentioned. Its parameters are: clock frequency 5 Gbit/s, $\tau_p \geq 10$ ps, signal peak power - as low as 0.74 W, interferometer loop length - 5 km, and switching contrast - 15 db. Nevertheless in spite of evident progress in various particular elements constituting AODM there are little published data on the experimental investigation of AODM as a whole. This report will consider the main principles of operation of optical regenerators and will consider in detail the experimental model of AODM developed at A.F.Ioffe Physical Technical Institute [2]. The AODM scheme uses a logic invertor operating through SRS [3] as a regenerator and amplifier simultaneously. The parameters of the scheme are as follows [2]. Storage time is almost unlimited, memory capacity - 500 bit, clock frequency - 100 MHz, pump wavelength - 1.06 μm, average energy consumption - 2.5 W, pulse duration - 70-100 ps, ratio between logic one and zero levels - 50-100.

Another approach of great interest are the schemes using solitons. Here the pulse shape is preserved on signal propagation along a large fiber length. Therefore increase of the memory capacity and storage time can be achieved sometimes in a more economical way [4].

To summarize, a fiber AODM is one of those optical devices that are of great scientific interest and can find practrical use.

References

1. M. Jinno and M. Abe. Electr. Lett., v. 28, 1350 (1992)

2. V. I. Belotitskii, E. A. Kuzin, M. P. Petrov, and V. V. Spirin. Electr. Lett. v. 29, 49 (1993)

3. M. P. Petrov and E. A. Kuzin, In: "Optical Processing and Computing", Academic Press , p. 33 (1988)

4. H. A. Haus and A. Mecozzi, Opt. Lett. v. 17, No. 21, 1500 (1992).

Parallel Information Recording and Processing Using 1-D Hologram Technology

A.L.Mikaelian

Russian Academy of Sciences, Institute of Optical Neural Technologies
App.55, 44-2 Vavilov Str., Moscow 117333 Russia
Phone: (095) 135-5551, Fax: (095) 925-5972 box K-03

ABSTRACT

1-D hologram technology for parallel information recording and processing and some applications are considered. Among them are a two-layer neural net performing serial-parallel processing, and an associative memory using photothermoplastic material. Both the theoretical and experimental results are presented.

SUMMARY

A disk memory system using 1-D hologram technology and some applications for information processing are discussed.

One of applications is an optoelectronic neuroprocessor using 1-D hologram technology. The neuroprocessor processes information in a serial-parallel way, which allows implementation of a high-capacity neural network with up to 10^{10} interconnections, the number of real neurons being small. This is achieved by means of serial accumulation of signals during continuous disk rotation.

The artificial neuron used comprises a pair of photodiodes and an electronic scheme with thresholding. Signals are accumulated in time using capacitors. That means the summation of signals weighted with weights T_{ij}.

Interneuron connections are implemented by recording a 1-D microhologram array on the disk. The structure of interneuron connections can be changed by using different tracks corresponding to the different models of neural networks. The disk can also be replaced, if necessary.

The holographic neuroprocessor having 200-mm disk with more than 1 Gbyte capacity provides the transfer rate of 16 Mbit/s, RPM being equal to 150. This allows implementation of neural networks having 10^5 neurons in each layer or 5000 different neural nets T_{ij} having 1000 neurons in each layer. In this case the processing time of one layer is equal to 120 ms. Note that one has an opportunity to increase the processing rate by 1 or 2 orders of magnitude by increasing RPM, laser power and the sensitivity of the photodetector array.

Another application relates to a holographic associative memory wherein 1-D information is recorded on photothermoplastic material. Information is recorded in the bipolar form using separation by polarization. Two version of the memory have been investigated: with angularly superimposed holograms and with spatially separated ones.

Linear electrooptic 32-channel light modulators were used to form both information arrays and reference sources in the process of recording and correlation retrieval. The arrangement of modulators and linear photodetector arrays minimizes the overlapping of correlation signals. 1-D information recording is performed sequentially, each information array being recorded with a separate reference beam, using a separate channel of a reference modulator.

When the correlation analysis is performed, a key array is fed to the signal modulator for associative search. The retrieved correlation signals

are detected by photodetectors of correlation signals. Electric correlation signals are then processed to determine the number of the array which corresponds most of all to the key array according to one or another criterion.

To retrieve information of the selected array, the signal modulator is turned off and the respective channel of the reference modulator is turned on. The beam restores the selected information array on the signal photodetectors.

In the experiment ten information arrays were recorded in the holographic associative memory with spatially separated holograms. Each area of the photothermoplastic was charged and developed separately. The diffraction efficiency of holograms was in the range of 5-7%. The associative search was investigated by feeding parts of the recorded arrays to the modulator. The probability of an array selection error versus number of bits in the key array after 100 recording/erasing cycles was determined. As has been found, the scheme with spatial separation is more preferred in case photothermoplastic holographic media are used.

ACKNOWLEDGEMENTS

This work was financially supported by the Russian Fundamental Research Foundation, Grant No. 93/012/921.

REFERENCES

1. A.L.Mikaelian, E.H.Gulanyan, B.S.Kretlov, V.A.Semichev and L.V.Molchanova, "Superposition of 1-D Holograms in Disk Memory System", Int. J. of Optical Memory and Neural Networks, vol.1, No.1, pp.15-19, 1992.

2. D.E.Okonov, B.S.Kiselyov, B.A.Novoselov, "Optoelectronic Holographic Associative Memory Based on Photothermoplastic", Int. J. of Optical Memory and Neural Networks, vol.2, No.2, pp.1993.

Associative memory for rotation pre-processing and projection invariant pattern recognition .

Guy Lebreton, GESSY, Université de Toulon
B.P.132, 83957 La Garde cedex, France

Abstract

New advances on invariant pattern recognition using associative optical memories, showing simulations and first experimental results, on
1) orientation detection of any object before identification,
2) pattern recognition invariant to scale and projections.

Summary

To increase the computing efficiency with moderate data flow (Video rate typical), the original idea of the hybrid neural network architecture (modified Hopfield type), is to utilise a non-linear optical amplifier between two cascaded optical correlators, the first one giving the weights (inner product with central correlations), the second yielding the weighted memory output for electronic thresholding and feed-back to the optical processor. In the implementation proposed at OC'92 [1], the high capacity programmable optical memory was a photothermoplastic plate, and the non-linear amplifier was a BGO crystal with phase conjugation. It was shown that a high non-linearity (to the order 4 at least) maintains the dominant influence of the $\Gamma(0)$ peak in an extended window required for shift invariance [2]). The progresses presented here do not concern the non-linear optical layer, but the algorithms of the process, and should be also of interest for electronic computing.

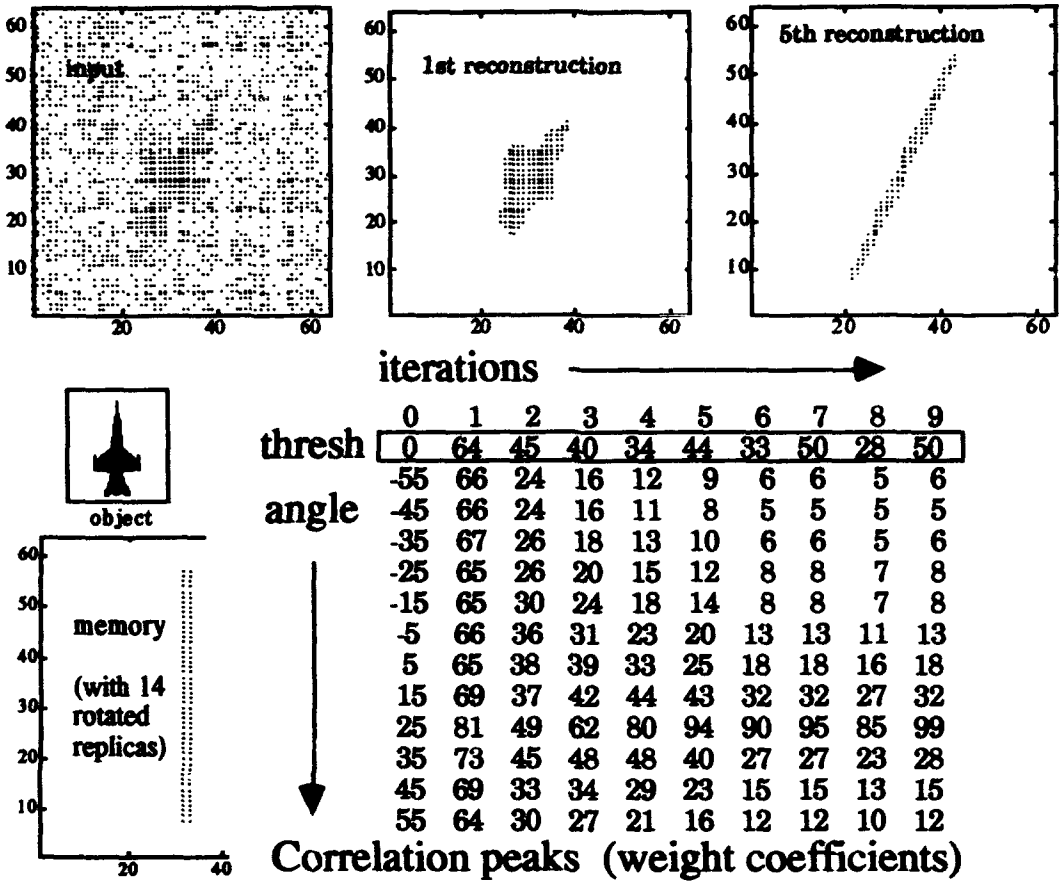
The main improvement for the convergence is an adaptive thresholding. In a standard Hopfield model, the threshold plane is the correlation plane, which cannot be accessed here. Thus one utilise the Parseval Theorem, saying that the correlation peak amplitude equals the energy of the signal. Our threshold criterion is then the sum of the output plane. Simulations show that the best convergence is obtained with an adaptive threshold coefficient, to increase the gain when the competition is low between the output modes.

Previously, the memory content for orientation detection had to be selective of one class of object, with limited tolerance to distortions, and worked only on contours with low optical efficiency. Now, excellent results have been obtained for any type of filled objects, using as memory a simple line with rotated replicas. An example is shown on Figure 1.The selectivity, tested with ellipses as input, reaches a 1 dot difference in the discrete image.

After this pre-processing, a full invariance in pattern recognition has been obtained with a new Log-Log single harmonic filter (2-D Mellin transform). Invariant to projections on both axes, it does dot require a Mellin transform on the real-time input as in previous implementations [3]. Its discrimination capability is illustrated on Figure 2.

Simulations for the associative memory with this filter are on progress and will be shown at the conference, so as the optical experiments for rotation pre-processing.

Associative memory for rotation pre-processing and projection invariant pattern recognition .



thresh / angle	0	1	2	3	4	5	6	7	8	9
0	64	45	40	34	44	33	50	28	50	
-55	66	24	16	12	9	6	6	5	6	
-45	66	24	16	11	8	5	5	5	5	
-35	67	26	18	13	10	6	6	5	6	
-25	65	26	20	15	12	8	8	7	8	
-15	65	30	24	18	14	8	8	7	8	
-5	66	36	31	23	20	13	13	11	13	
5	65	38	39	33	25	18	18	16	18	
15	69	37	42	44	43	32	32	27	32	
25	81	49	62	80	94	90	95	85	99	
35	73	45	48	48	40	27	27	23	28	
45	69	33	34	29	23	15	15	13	15	
55	64	30	27	21	16	12	12	10	12	

Fig.1 - Associative memory : detection of the orientation of an unknown input object

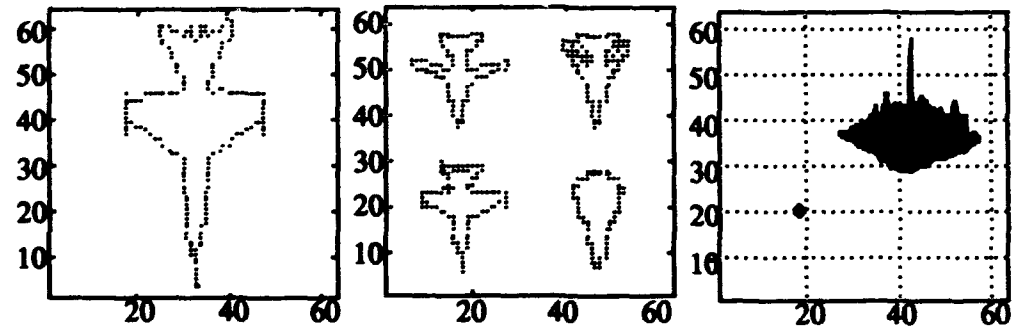


Fig.2 - Correlation with a Log-Log single harmonic filter (invariant to projections on both axes)

References : 1) G.Lebreton et al.,"Invariant pattern recognition and hybrid neural network",SPIE Proceed.Vol.1806, 1993, pp.305-312; 2) D.Psaltis, J.Hong, "Shift-invariant optical associative memories", Opt. Eng. 26/1, 1987, pp.10-15; 3) D.Mendlovic, E.Marom, N.Konforti, "Scale and projection invariant pattern recognition", AO 28/23, Dec.1989, pp.4982-4986.

Optical Implementations of a Stochastic Neural System

W.A. Crossland, Dept of Engineering, (0223 330264)
Trumpington Street, Cambridge, CB2 1PZ
T.J. Hall, Dept of Electronic and Electrical Engineering, (071 873 2151)
King's College, University of London, Strand, London WC2R 2LS
J.S. Shawe-Taylor and M. van Daalen, Dept of Computer Science, (0784 443421)
Royal Holloway, University of London, Egham, Surrey TW20 0EX

Abstract

The paper addresses the design of an opto-electronic implementation of a stochastic bit-stream neural system which operates by manipulating digital bit streams to create emergent activation functions using extremely simple logic.

This paper investigates the possible strategies for implementing a stochastic neural network design [6] making use of the latest opto-electronic technologies [3, 4]. The network design operates by manipulating digital bit streams to create an emergent activation function using extremely simple logic. The neural design and implementation strategy will potentially yield a number of impressive benefits.

- The optical connections have a very high bandwidth which can overcome the I/O bottleneck in VLSI implementations of the stochastic neural design [5].
- The stochastic approach introduces real values through a precisely controlled probabilistic technique, which makes possible a complete and exact mathematical description and simulation of the network functionality.
- In contrast to analogue implementations, digital networks can be combined without introducing further uncertainties in the accuracy of the computation. Hence implementations can be scaled up without major modifications.
- Both the speed and the digital nature of the basic operations will mean that effective on-chip learning may be incorporated into the design, by exploiting the stochastic properties of the network operation.

A standard neural design involves a network of neurons each processing its inputs through a weighted sum and calculating a sigmoid-like function on the result. Hence, one of the fundamental problems inherent in a massively parallel implementation of a neural architecture is how to multiply together the real inputs and their corresponding weights without resorting to cumbersome bit-parallel digital circuitry. The analog solution to this problem incurs a number of difficulties, including relatively low resolution, cross-chip variations in component performance, and the resulting problems in constructing large-scale reliable systems.

The stochastic bit-stream approach combines the benefits of digital circuitry and analog simplicity. In this approach a real value v in the range $[-1, 1]$ is represented by a sequence of bits [2] in which the probability of each bit being set to 1 is $(v + 1)/2$. The bit stream created by the bit-wise XOR of the weight and input streams computes a stream representing their product. One bit of each of these individual weighted input streams are summed and compared with a threshold value to determine a bit of the output stream. The interaction of the probability distributions of the sum and the thresholds creates a sigmoid-like functionality, which can be precisely described [5]. The design of a single neuron is, therefore, extremely simple, making it possible to map a large network onto an established implementation technology. The functionality of the neuron will, however, be demonstrated with simulations of the application of the Mean Field Annealing algorithm to the graph bisection problem. The quality of solution and number of iterations is comparable with standard neurons, though if the neurons were implemented in massively parallel technology large graphs could be processed in real time using the bit stream technique.

In this paper we will present two opto-electronic implementations of the neural architecture. They are illustrated in figure 1. One design is fully spatially multiplexed (maximally parallel), whilst the other introduces the extra dimension of time multiplexing. A neuron in a time multiplexed system receives the first bit from each connection in turn and only delivers an output bit when all have been processed. This considerably simplifies the design of the neurons, but at the expense of their operational speed. It also simplifies the beamlet optics for a given number of neurons when compared to the fully spatially multiplexed design.

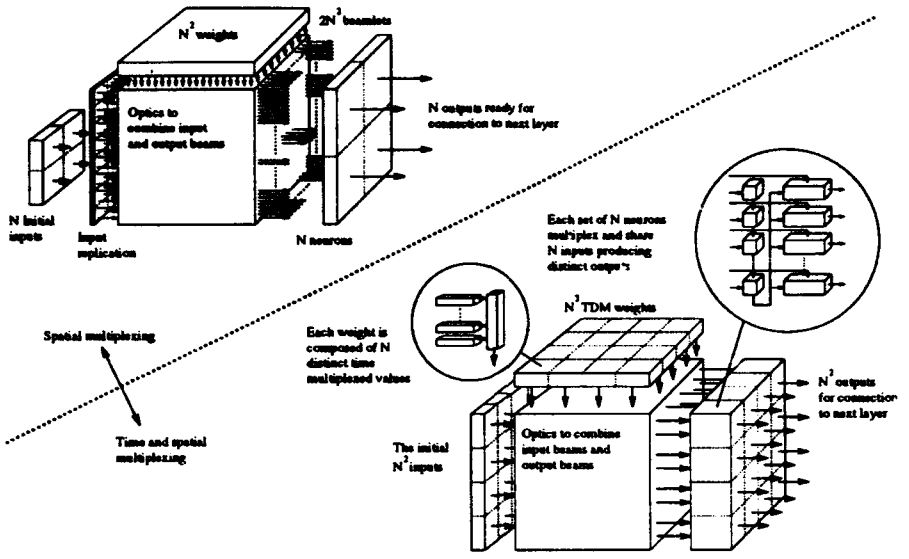


Figure 1: *The spatial/time multiplexing scale of implementations*

Both of the optical implementations require image replication and beam handling optics. Image replication has been demonstrated [4] using computer generated holograms in conjunction with bulk lense systems to produce output arrays consisting of up to 1000×1000 beamlets. Beam detection is achieved by the use of silicon/GaAs photodetectors, and modulation is possible through the use of various opto-electronic devices. Modulation is most easily achieved with liquid crystal spatial light modulators, but only at relatively slow speeds in the region of 10 MHz may be realised. We will therefore incorporated faster devices such as LED based photothyristors [1] featuring switch off times less than 10ns, or arrrays of individually addressable surface emitting semiconductor lasers [3] operating at speeds up to 1 GHz. The choice of detectors and modulators will depend of the overall system architecture. For example, the time multiplexed designs will contain high speed subsystems, that will require the use of the faster opto-electronic devices.

References

[1] P. Heremans, *et, al.*, 'Image transcription between arrays of N-p-n-P optoelectronic switches', IEEE Transactions on Electron Devices, **39**(10), 1992, pp. 2248-2253.

[2] P. Jeavons, D. Cohen and J. Shawe-Taylor, Generating Binary Sequences for Stochastic Computing, to appear in IEEE Transactions on Information Theory.

[3] J. L. Jewell, *et al*, 'Vertical-cavity surface-emitting lasers: design growth, fabrication, characterisation', IEEE J. Quantum Electron., **27**, 1991, pp. 1332-1346.

[4] A.G. Kirm, S. Jamieson, H. Imam and T.J. Hall, Experimental implementation of an opto-electronic matrix-matrix multiplier which incorporates holographic multiple imaging, Optical Computing and Processing, 2 (1992) 293–304.

[5] John Shawe-Taylor, Pete Jeavons and Max van Daalen, Probabilistic Bit Stream Neural Chip: Theory, Connection Science, 3 (3) (1991) 317–328.

[6] M. van Daalen, Peter Jeavons and John Shawe-Taylor, A Stochastic Neural Architecture that Exploits Dynamically reconfigurable FPGAs, IEEE Workshop on FPGAs for Custom Computing Machines, pp.202–211, April 5–7, 1993, Napa CA.

Dynamic Effects in Volume Interconnects with Feedback

Chris Slinger
ER1 Division, DRA Malvern, St Andrew's Road, Great Malvern, Worcestershire, WR14 3PS, UK
44-(0)684-895670 (phone), 44-(0)684-894146 (fax), slinger@signal.dra.hmg.gb

Abstract

An attempt is made to exploit the inherently rich physics of volume holographic interconnects. The effects of crosstalk and nonlinearities are considered. When combined with a novel feedback configuration, complex, self-organising behaviour is seen to emerge.

Summary

Volume holographic interconnects represent one way of applying optics in connectionist approaches to signal processing. They combine the usual advantages of optical interconnects, together with high storage capacities (>10^9 weighted connections cm^{-3}) and offer the possibility of weight update during training [Paek et al].

However, when used in the 'conventional' way, several factors constrain their performance. These include effects such as diffracted amplitudes being a nonlinear function of grating strength; cross gratings and multiple grating interactions giving crosstalk; the recording of modifying of gratings invariably changing the strengths of other gratings in the hologram and nonlinearities introduced by the recording process itself. All the foregoing limit the use of volume interconnects, even when the training process takes account of these factors [slinger]. An alternative approach is to attempt to use these phenomena to good advantage - in effect, to exploit more fully the rich physics of this dynamic, multiple grating system. This may enable it to perform useful information processing tasks in its own right. To investigate this idea, it is necessary to study the regimes of behaviour of the interconnect in various configurations.

One such novel system is shown schematically in figure 1. A single mode fibre has been added to the conventional volume interconnect arrangement. This fibre feeds light from one output, back into input 1, via a beamsplitter of reflectivity *R*.

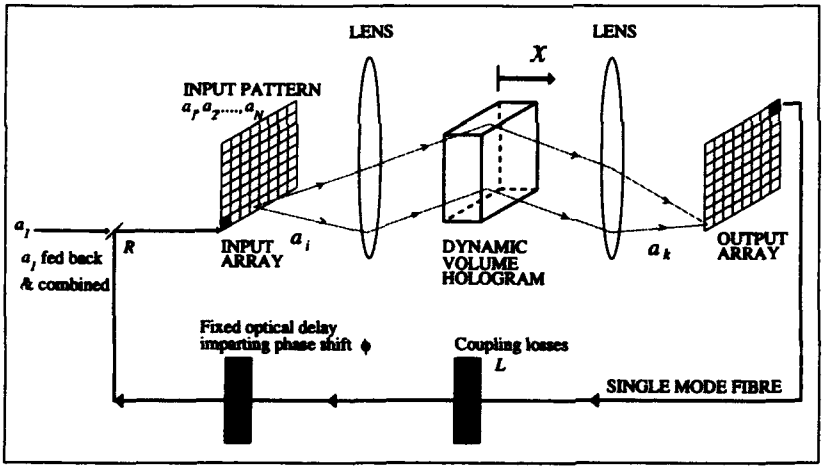


Figure 1. Schematic of the fibre feedback modification to the usual volume interconnect arrangement. Note the dynamic holographic material (e.g. a liquid crystal cell or a photorefractive) and the absence of a training array.

The governing equations can be written as :

$$\left\{\frac{n}{c}\frac{\partial}{\partial t} + \frac{\partial}{\partial x}\right\} a_m + \frac{j\gamma}{\cos\theta_m}\sum_{\substack{n=1 \\ m \neq n}}^{N} G_{mn}\, a_n = 0 \qquad (1)$$

$$\frac{\partial G_{mn}}{\partial t} = -A\, G_{mn} + B\, a_m\, a_n^* \qquad (2)$$

where n is the bulk refractive index of the hologram material, c is the velocity of light, θ_m is the angle of propagation of wave m, amplitude a_m. G_{mn} is the mn th grating strength. γ, A and B are material constants. Equations (1) are coupled wave equations describing the diffraction of the waves as they propagate through the hologram, whilst equations (2) describe the grating formation in the hologram - for the case shown, a photorefractive type response is assumed. The boundary conditions can be written as :

$$a_m(x=0,t) = a_{m0}, \qquad \text{for } m \neq 1$$

$$a_1(x=0,t) = a_{10}(1-R) + R(1-L)\, a_1(x=d,t)\exp(j\phi) \qquad (3)$$

The feedback from the fibre, combined with the time dependant nature of the gratings in the hologram, endows the system with very rich and varied behaviour. In particular, for certain system parameters, the output of the interconnect can exhibit multiple fixed point, limit cycle and strange attractor behaviour. These arise as the system essentially performs a N dimensional complex mapping :

$$\underline{a}(x)_{t+1} = f\left(\underline{a}(x)_t,\ \underline{G}(x)_t\right) \qquad (4)$$

where $\underline{a}(x)_t = [a_1(x,t),\ a_2(x,t),.....,a_N(x,t)]^T$ is the vector representing the diffracted wave amplitudes, $\underline{G}(x)_t$ is the matrix of the G_{mn} grating strengths (m,n=1,2,3,..N), at hologram depth x and time t. $\underline{a}(0)_t$ can be regarded as an input pattern presented to the system. This pattern input, together with the material and other system parameters, determines the time evolution of the system output.

Figure 2, for example, shows a bifurcation diagram resulting from varying the loss factor L in the fibre feedback loop. The figure indicates the variety of complex behaviour possible with this system, by changing a single, easily modifiable, parameter.

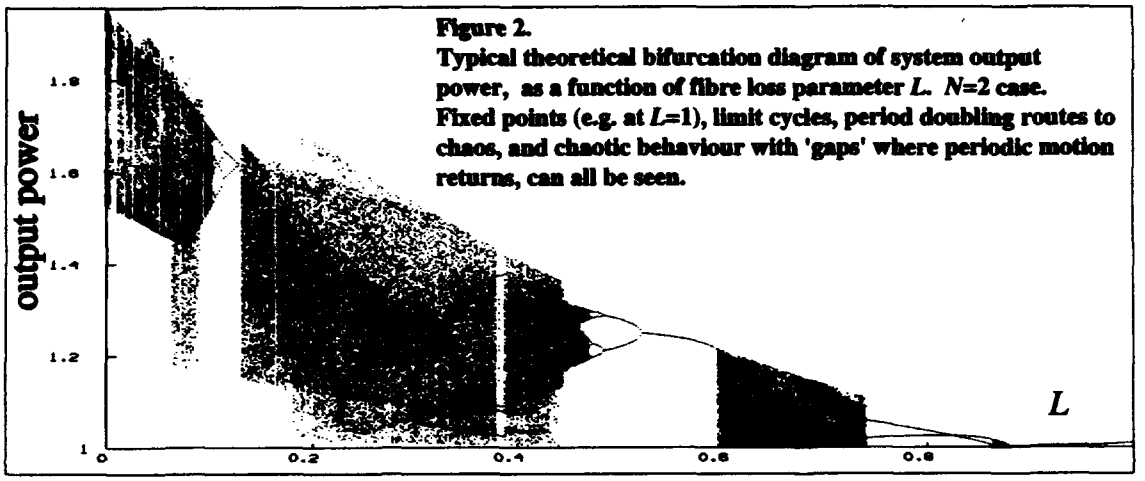


Figure 2.
Typical theoretical bifurcation diagram of system output power, as a function of fibre loss parameter L. N=2 case. Fixed points (e.g. at L=1), limit cycles, period doubling routes to chaos, and chaotic behaviour with 'gaps' where periodic motion returns, can all be seen.

Such complex modes of behaviour are being increasingly viewed as advantageous in pattern processing. For example, the ability of a system to change its dynamics during a search task has been demonstrated to give superior classification performance [Nara et al]. Additionally, complex dynamics in a classifier can also give it advantages in noisy environments. The volume interconnect system described here also has direct equivalence to many features of the coupled map lattice paradigm [Kaneko]. Looked at in a slightly different way, the iterative processing, generated by the feedback, endow the system with properties not obtained with layered networks of comparable size.

Self organisation in pattern processing can be useful as a preprocessing stage of a pattern recognition system (e.g. as in Kohonen's self organising feature maps). The interconnect described here also has its own self organising features. In particular, it is able to associate input patterns with different attractors at its output. Inputs that differ slightly can be classified to give rise to the same attractor. In this way, the system performs classification and clustering without external supervision.

In conclusion, a system has been formulated that exploits, more fully, the complex physics available in the volume interconnect. This includes the use of many processes conventionally regarded as detrimental to interconnect behaviour. Unusual, and possibly beneficial, modes of behaviour result.

References

Kaneko K (ed) "Theory and applications of coupled map lattices", Wiley, Nonlinear Science Series, (1993).

Nara S, Davis P. Totsuji H, "Memory search using complex dynamics in a recurrent neural network model", *Neural Networks*, 6, (1993), p.963-973.

Paek E G, Wullert J R, Patel J S, "Holographic implementation of a learning machine based on a multicategory perceptron algorithm", *Optics Letters*, 14, no.23, (1989), p.1303-1305.

Slinger C W, "Weighted volume interconnects for adaptive networks", *Optical Computing and Processing*, 1, no.3, (1991), p.219-232.

Optical Lateral Inhibition Networks using Self-Linearised SEED's

Paul Horan
Hitachi Dublin Laboratory,
O'Reilly Institute, Trinity College, Dublin 2, Ireland.
Tel +353-1-6798911 Email <paulh@hdl.ie>

Abstract

A family of lateral inhibition architectures which use the self-linearised SEED effect to implement optical subtraction are described, and the operation demonstrated in simulation.

Introduction.

Lateral inhibition networks, where nodes within a processing layer inhibit one another, form a very important class of networks. They are not amenable to processing on conventional serial machines, since they require some type of iterative self-consistent solution. But it is this property that makes such networks suited to parallel implementation, and the dense, recurrent nature of the interconnection suggests an optical approach.

The essence of any inhibition network is that the activity level of an individual node must decrease in response to increasing input from neighbouring nodes *i.e.* subtraction, which is difficult to do optically. One approach has been to use an optically coupled *pnpn* light emitter and an *npn* phototransistor.[1] An alternative possibility is to use the Self Linearised SEED effect, observed in a serial photodiode-SEED modulator combination.[2,3] Feedback provided by the common current causes the modulator reflectivity to decrease as the light falling on the photodiode increases. The small range of modulation can be improved by incorporating the SEED device in a resonant optical cavity.[4] This combination is made more attractive when we consider that the SEED is, itself, a *pin* diode, allowing the possibility that the detector and modulator can be made together in the same integrated process. However, certain difficulties are experienced using the quantum well diode as a photodiode, as it is not voltage independent. Miller has suggested 3 ways of circumventing this problem.[3]

Having established that we have a good optical subtraction technology, we will go on to investigate architectures in which this effect can be utilised.

Simple lateral inhibition.

The simplest lateral inhibition optical system we can conceive of is shown in figure 1 in a one-dimensional format, although this can be extended to a two dimensional computing surface. Each node consists of a detector-modulator pair, and receives an external input which is incident on the modulator. A portion of the reflected signal is redirected to the detectors of neighbouring nodes in some manner, which defines the lateral interconnection function $g(x)$. The node does not inhibit itself. The optical element is not specified and may be reflective, refractive, diffractive, or holographic. Thus, the reflectivity of a given modulator is dependent on the total inhibitory signal received from neighbours, and decreases linearly in response to it. A point to note is that the internal state of the node, which we identify with the modulator reflectivity, is determined purely by the neighbours, and is not dependent on the input to that node, although the final output is. This single pass geometry effectively results in a convolution of the input with the lateral interconnection function. Figure 2 shows the results of a typical simulation with flat lateral inhibition ±3 nodes. A periodic boundary condition is imposed to avoid edge effects. This network performs a simple edge-enhancement function. The response of the system reflects the essentially linear nature of the device. While still linear, the state of the node can be made positively dependent on the input, as well as inhibited by neighbouring nodes, by using a differential pair of detectors, following the example of Miller.[3]

Lateral inhibition with feedback

By introducing a nonlinear, recurrent feedback of the output to the input winner-take-all (W-T-A) behaviour can arise. This can be done by using a second modulator array for input, as shown in figure 3. The modulator array is uniformly illuminated and the external inputs presented. The modulated beams are then directed to the laterally connected layer as before. However, if the output is monitored and used to control the input modulator array a recurrent loop is established.

All that is required is that the input is presented for a sufficient time for the feedback loop to be established, thereafter the input is removed and the system converges to a stable state. Again, this is a one-dimensional example of a possibly two-dimensional surface.

Cheng & Wan have shown that there must be gain, however small, in the feedback loop; if not, all signals will decay to zero.[5] More importantly, from an optical point of view, they have examined the situation of limited lateral inhibition. Global interconnection, leading to a single winning node, is not feasible in an optical system, as finite optical power can only be distributed to a limited neighbourhood. They have shown that in a finite interconnection network a winner will arise in a neighbourhood defined by the range of interconnection.[5] Thus, there are local winners where the width of each competing cell is roughly determined by the lateral interconnection distance. A point not stressed by Cheng & Wan is that each cell must have a winner, even if the input in that area is perfectly uniform. Small spurious variations arise during the iteration process, and these become amplified, eventually giving a "winner". Figure 4 shows an example of an input and the final result that the simulation converged upon. As can be seen, local maxima are located, but a spurious peak also occurs (around node 22). Such a system could form the heart of a self-organising network, when prefixed by a Hebbian network.[6]

A further nonlinearity is introduced in shunting networks where the lateral inhibition signal is modulated (multiplied) by the value of the node. [7] In the context of this work an optical implementation can be envisaged whereby the inhibition optical signal is reflected from the node modulator before detection. This would necessitate a more complex optical arrangement. It should be noted that this would not correspond directly to the conventional shunting network as, in this case, the inhibition signal is being multiplied by the modulator reflectivity rather than the single state variable generally used.

References.

1 Y. Nakano, M. Ikeda, W. Kawakami, and K. Kitayama, "Internal light-coupled optical device array", Appl. Phys. Lett., 58, 1698-1700 (1991).

2 D. Miller, D. Chemla, T. Damen, T. Wood, C. Burras, A. Gossard, and W. Wiegmann, "The quantum well self-electrooptic effect device: optoelectronic bistability and oscillation, and self-linearized modulation" IEEE J. Quant. Electron QE-21, 1462-1475 (1985).

3 D. Miller, "Novel analog self-electrooptic-effect devices", IEEE J Quant. Electron 29, 678-698 (1993).

4 B. Shoop, B. Pezeshki, J Goodman and J. Harris, "Noninterferometric optical subtraction using reflection-electroabsorption modulators", Opt Lett 17, 58-60, (1992).

5 Y. Cheng and Z Wan, "Distribution of winners in local lateral inhibition", Proc. of the Intl. Joint Conf on Neural Networks, Baltimore, Maryland, 7-11 June 1992 (IEEE 92 CH 33114-6, 1992) pp III-456 - III-460.

6 T. Kohonen, "The self-organising map", Proc. IEEE, 78, 1464-1480 (1990).

7 S. Grossberg, "Nonlinear neural networks: principles, mechanisms, and architectures", Neural Nets, 1, 17-61, (1988).

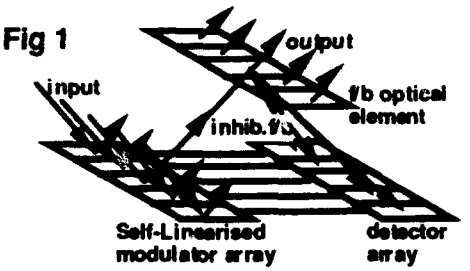


Fig 1

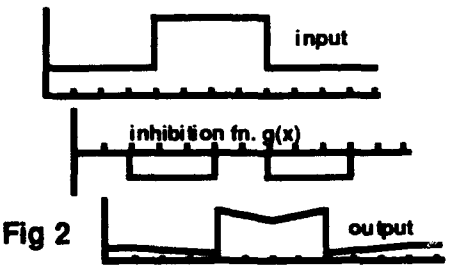


Fig 2

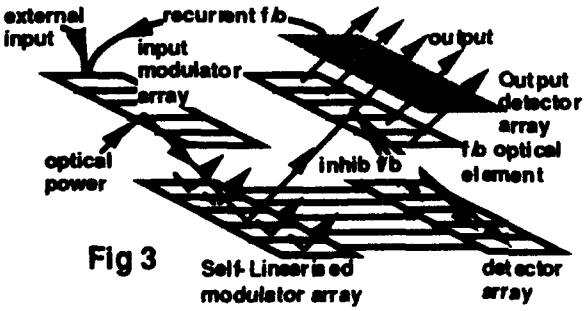


Fig 3

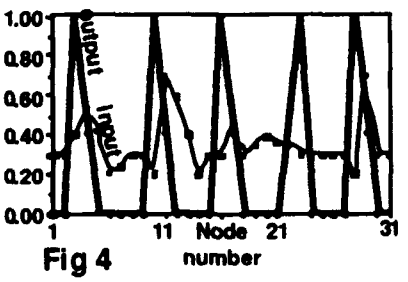


Fig 4

Optical Spatial/Frequerncy Filtering and Adaptive Neural Networks based on Fractional Fourier Transforms

Soo-Young Lee
Department of Electrical Engineering
Korea Advanced Institute of Science and Technology
373-1 Kusong-dong, Yusong-gu, Taejon 305-701, Korea (South)
Tel: +82-42-869-3431 / Fax: +82-42-869-3410 / E-Mail: sylee@ee.kaist.ac.kr

Abstract: Based on fractional Fourier transforms a new optical architecture is developed to make compromise between shift-invariant (frequency) and position-dependent filterings, and its analogy to neural networks and corresponding learning algorithm are presented.

1. Introduction

Recently Fourier transform of fractional order and their optical implementation had been developed. [1,2] Unlike the ordinary Fourier transform, i.e. the fractional Fourier transform with order 1, the fractional Fourier transforms extract features which combine both spatial and spatial-frequency charactersitics of the original images. One may easily expect that the fractional Fourier transformed image is something between the original image and full Fourier transformed image. The fractional Fourier transform may be optically implemented by quadratic graded index (GRIN) media, which provide rotation in Wigner [2] or Quasiparticle [3] distribution function. Much simpler optical architectures with only single lens or double lenses with proper spacing were also reported. [2] In this paper we present a new optical architecture for shift-invariant (spatial frequency) and position-dependent filterings based on 2 fractional Fourier transforms, and develope analogy between this architecture and neural networks. Adaptive learning algorithm to design the filters or neural networks is presented.

2. Optical Spatial and Spatial-Frequency Filter based on Fractional Fourier Transforms

The fractional Fourier transform of order $p=1/N$ performs ordinary Fourier transform when applied N times sequentially. Its shifting rule is worth noticing. Assuming the fractional Fourier transform of order p for the $u(x)$ is $F^p(u(x))=U(k)$, $|F^p(u(x-b))|$ becomes $|U(k - b\cos\phi)|$ where $\phi=p\pi/2$. [1] For ordinary Fourier transform, i.e. $p=1$, $|F^1(u(x-b))|$ is $|U(k)|$ to result in shift invariance. For fractional Fourier transforms this shift invariance is somewhat destroyed and position-dependent information is maintained. When input image is filtered at Fourier plane in the *4-f* matched filter, only spatial-frequency filtering is performed and results in convolution integral. This space-invariant input-to-output mapping is useful for target localization and tracking, but not desirable for many classification or associative memory of many images. Slight local shift invariance is usually enough and preferred.

We substitute the ordinary Fourier transforms in the *4-f* matched filter into fractional Fourier transforms with orders p_1 and p_2. Following Ref.[2], we adopt simple one thin-lens architecture and explicit integral formula for a fractional Fourier transform. Within the approximations input-output mapping relationship of the p_1-p_2 filter is now newly derived, and the result for the most interesting case ($p_1+p_2=2$) becomes

$$v(x) = \int u(z)\, h\left(\frac{x+z}{\sin\phi_1}\right) \exp\left[\frac{i\pi}{\lambda f_o}\frac{z^2-x^2}{\tan\phi_1}\right] dz\,, \qquad (1)$$

where $u(z)$ and $v(x)$ are input and output, respectively, and $\phi_1 = p_1\pi/2$ and $\phi_2 = p_2\pi/2$. The $h(.)$ is the ordinary Fourier transform of the filter $H(k)$ between the two fractional Fourier transforms. Compared with the *4-f* matched filter, Eq.(1) now has scaling factor ($\sin\phi_1$) in the filter function. Also, additional exponential modulation, which emphasizes spatial points near $x=z$, is introduced. This exponential term destroys the shift-invariance, and provides position-dependent classificastion with slight local shift-invariance. The relative importance of the shift-invariant (frequency) filtering and position-dependent classification is controlled by the $\phi_1 = p_1\pi/2$. Character, image, and speech recognitions might be useful applications of this optical filters.

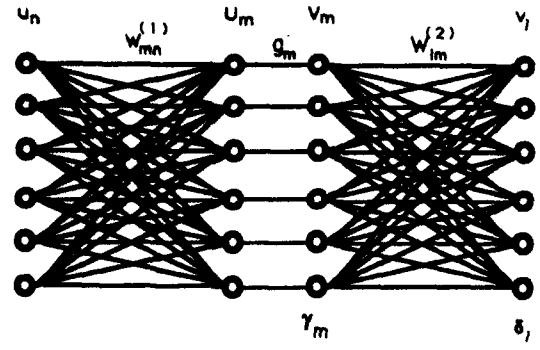


Fig.1 Neural network analogy of the spatial/frequency filters based on fractional Fourier transforms.

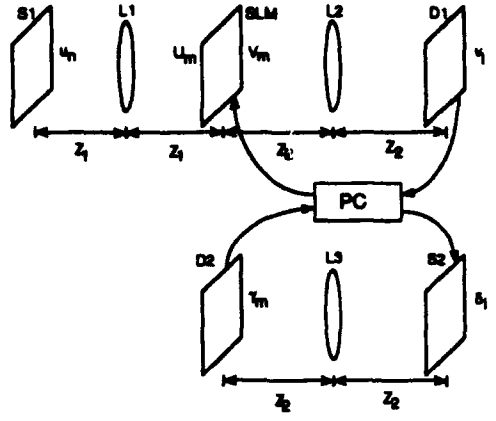


Fig.2 Optical architecture of the neural networks based on fractional Fourier transforms

3. Neural Networks based on Fractional Fourier Transforms

In Fig.1 the neural network analogy of the fractional Fourier transform and the spatial/frequency filters are shown, where the u_n and v_l are input and output, respectively, and U_m and V_m are corresponding fractional Fourier and inverse transforms. The fractional Fourier transform operations are now substituted by 2 synaptic weights, $W_{mn}^{(1)}$ and $W_{lm}^{(2)}$, and linear summation at U_m and v_l. For classification problems additional Sigmoid function $S(.)$ may be followed. The g_m's are filter transmissions between the two fractional Fourier transforms and adaptively trainable. This architecture with fixed global synapses and adaptive local control gains is similar to the TAG (Training by Adaptive Gain) model [4], and the popular error back-propagation learning rule is still applicable. With proper definition of total output error one can update the g_m propotional to $-Re[U_m\gamma_m]$, where the γ_m is back-propagated error from δ_k. Optical architecture for this neural networks with error back-propagation learning is shown in Fig.2.

4. Conclusion

In this paper we present a new optical architecture for spatial/frequency filtering and adaptive neural networks based on fractional Fourier transforms. The developed learning algorithm for the neural networks is also applicable to design of the filters. The optical architecture is similar to 4-f matched filters, and requires only 2 lenses for filters and 3 lenses for single-layer adaptive neural networks with back-propagation learning rule. Extension to multi-layer neural networks is straight-forward, and the error back-propagation algorithm and optical architecture are still valid. With this simple architecture and devices large-scale optical implementation of adaptive neural networks becomes feasible.

Acknowledgements: The basic idea on this paper was initiated during the author's sabbatical leave at the University of Erlangen-Nürnberg as a Humboldt Research Fellow hosted by Prof. Gerd Häusler. The author also would like to express his thanks to Prof. Adolf Lohmann for introducing him to the subject of fractional Fourier transforms.

References

[1] David Mendlovic and Haldun M. Ozaktas, "Fractional Fourier transforms and their optical implementation: I", J. Opt. Soc. Am. A, 10, 1875-1881 (1993)

[2] Adolf W. Lohmann, "Image rotation, Wigner rotation, and the fractional Fourier transform," J. Opt. Soc. Am. A, 10, 2181-2186 (1993)

[3] Soo-Young Lee and Nathan Marcuvitz, "Quasiparticle description of wave propagation and reflection in inhomogeneous media," IEEE Trans. Ant. Prop., AP-34, 613-625 (1986)

[4] Hyuek-Jae Lee, Soo-Young Lee, Sang-Yung Shin, and Bo-Yun Koh, "TAG : A neural network model for large-scale optical implementation," Neural Computation, 3, 135-143 (1991)

Experimental realization of an all-optical self-organizing map.

K.Heggarty, J.Duvillier and J.L. de Bougrenet de la Tocnaye.

Département Optique, ENST de Bretagne, BP 832, 29285 Brest Cedex, France.
Tel +33 98001205, Fax +33 98001025, Email heggarty@gosc.enst-bretagne.fr

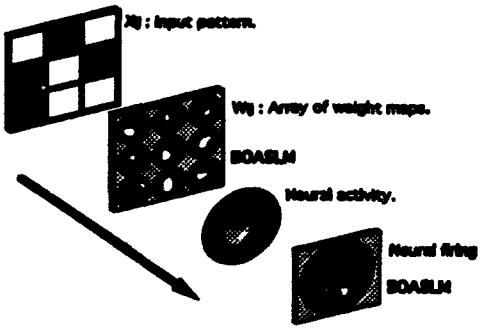
Abstract

We present results obtained with an all-optical self-organizing map neural network applied to digit recognition. The experimental system is built around two Ferroelectric Liquid Crystal Bistable Optically Addressed Spatial Light Modulators in a resonator configuration.

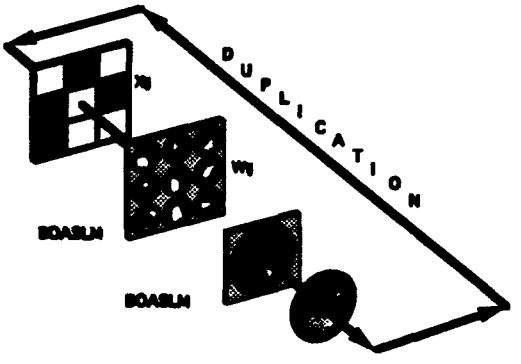
Summary

The neural network we implement has a conventional structure with an input layer of neurons connected via the synaptic weights to a second layer or "map" of neurons. The system is based on Kohonen's self-organizing map [1] where the spatial neighbourhood of the active neurons is taken into account during learning process to produce a topological organization of the activity: similar inputs produce similar map-layer activities. The implementation is all-optical in that electronics (in the form of a personnal computer) are used only for system synchronization and modification of learning parameters, all calculations, thresholding, weight updating etc are performed in parallel in optics.

The key devices in the optical setup are two Ferroelectric Liquid Crystal Bistable Optically Addressed Spatial Light Modulators (FLC-BOASLMs). If such a valve is illuminated with a given pattern and an electrical pulse is applied to the electrodes, the pattern can be binarized and stored on the valve for subsequent rereading. One valve is used in this way to perform the thresholding of the neural activity. Although the BOASLMs are intrinsically bistable, by operating them near the threshold voltage and using spatial integration techniques they can be made to show a grey-level behaviour [2]. A second valve is used in this manner to store and update the synaptic weights.



(a) Creation of the neural activity.



(b) Weight updating.

The basic operation of the system is shown above. The input pattern, X_{ij}, is presented to the system with an electrically addressed SLM. This pattern is imaged onto the array of weight maps, W_{ij}, (first BOASLM) thus activating the corresponding weight maps. An optical crossbar, consisting of a lenslet array and a collimating lens, then images the activated weight maps onto the second BOASLM thus realizing the required sum $\sum X_{ij}W_{ij}$. The resulting neural activity is binarized and stored on the second BOASLM. The neighbourhood function is introduced by varying the height and duration of the voltage pulse sent to the BOASLM to dilate or erode the neural activity pattern.

This activity is read with a plane wave, duplicated with a Dammann grating and fed back, through the input image, to the weight map BOASLM where it is added to the active weight maps and subtracted from the inactive ones. The effect is to reinforce the connections between active input neurons and active zones in the neural map, while at the same time weakening non-productive connections. In this way a Hebbian-type learning rule is implemented.

Computer simulations which take the limits of the optical system into account, have confirmed the feasibilty of the approach; the network correctly learning and classifying a set of test input images as well as demonstrating generalization capabilities [3]. The experimental system has already been shown to correctly recognize the different input classes when initialized with a weight map array obtained from the simulations. Our present work is concentrated on the demonstration of optical learning, the most recent results in this direction will be presented at the conference.

References

[1] T. Kohonen, "The Self-Organizing Map", IEEE Proceedings, **78**, 1464-1480 September (1990).

[2] M. Killinger, J.L. de Bougrenet and P. Cambon, "Controlling the Grey-Level Capacity of a Bistable FLC Spatial Light Modulator", Ferroelectrics **122**, 89-99 (1991).

[3] J.Duvillier, M.Killinger, K.Heggarty, K.Yao and J.L. de Bougrenet de la Tocnaye, "All optical implementation of a self-organizing map: a preliminary approach", *accepted for publication in Applied Optics.*

Optoelectronic Switch Operating with 0.2 fJ/μm² at 15 Mhz

Maarten Kuijk*, Paul Heremans*, Roger Vounckx*, Gustaaf Borghs*

* Vrije Universiteit Brussel, Appl. Phys. Dept. (TONA)
Pleinlaan 2, B-1050 Brussel, Belgium, tel: 32 - 2 - 6412990

* Interuniversity Micro Electronics Center (IMEC)
Kapeldreef 75, B-3001 Leuven, Belgium, tel: 32 - 16 - 281521

Abstract: *We present experimental data of a novel differential PnpN optical switch, showing a cycle time smaller than 60 ns and an optical switching energy of 0.2 fJ/μm².*

III-V optical *PnpN* devices (also variously called DOES, VSTEP,...) are promising optoelectronic switches. Very good optical sensitivity (400 fJ or 0.07 fJ/μm²) has been reported for a differential pair of optical *PnpN* devices [1]. However, the repetition speed of the operation cycle is very slow due to the long switch-off time (of the order of 0.1 to 10 ms). The switch-off is governed by the slow decay of excess free carriers stored in the center *p* and *n* layers of the element of the pair which was in its on-state in the previous cycle. For correct operation of the pair, the light-generated carriers must exceed the excess left-over carriers of the previous operation cycle. Therefore, for operation above kilohertz, the optical input energy is large. In other words, the trade-off between cycle speed and optical sensitivity is poor.

We solved this trade-off problem by making monolithic differential pairs using the *PnpN* devices described in the abstract of Heremans et al. [2]. The devices are specially designed such that the center *p* and *n* layers can be completely depleted of free carriers in nanoseconds by application of a negative anode-to-cathode voltage pulse ("carrier-extraction phase") prior to giving the optical input. The area of the thyristors of a pair is 30 x 40 μm².

An operation cycle consists of 3 phases. First, a carrier-extraction pulse (20 ns), to reset the thyristors of the pair; then, a light input phase (the shortest time for this phase was 3 ns); third, a switch-on phase, during which the thyristor which has received the optical input switches on and emits light (20 ns). The total cycle time is thus smaller than 60 ns (limited by our apparatus). Such cycles can be pasted without dead time in between. Therefore, the operation cycle frequency of our switch is at least 15 MHz. Figure 1 shows the measured relationship between the duration of the optical input pulse and the optical input power necessary for correct switching in a sequence LRRLLRRL (L meaning switch-on of the left element, and R of the right element in the pair). The figure shows that 0.25 pJ is sufficient for correct switching. This corresponds to 0.2 fJ/μm². Figure 2 demonstrates the necessity to use the carrier-extraction pulse: the optical input energy increases with 2 orders of magnitude when the amplitude of the carrier-extraction pulse is not sufficient for completely depleting the *PnpN* devices of the pair during the first phase of the operation cycles. It should be noted here that all *PnpN*-based optoelectronic switches published so far have a layer structure which does not permit complete carrier extraction by an extraction pulse.

Figure 3 gives a general overview of the performance of acknowledged optoelectronic switches, including S-SEED, FET-SEED, HPT+LED, VSTEP, PNPN. Two figures-of-merit are plotted: the required optical switching energy per unit area and the achievable cycle frequency. Our switch shows the largest sensitivity-bandwidth product, despite the fact that we have performed no optimisation as to its speed (10-fold improvement should be achievable). Additional advantages are the non-critical operation voltages and input wavelength, simple and short epitaxial growth and relaxed lithographic constraints.

[1] K. Hara, K. Kojima, K. Mitsunaga and K. Kyuma, IEEE J. Quant. Electr., vol. 28, no5, 1992.
[2] P. Heremans, M. Kuijk, R. Vounckx and G. Borghs, "The completely depleted *PnpN* optoelectronic switch", abstract sent in to Optical Computing '94, Edinburgh, August 1994.

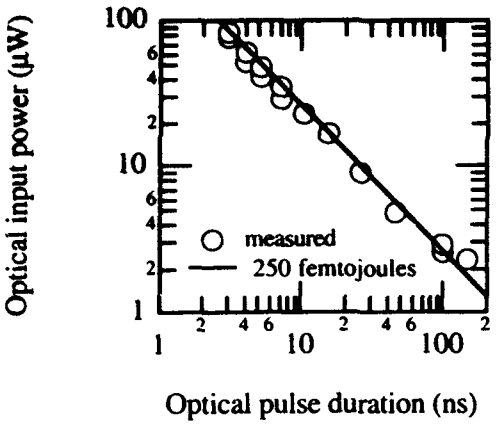


Figure 1: Measured external optical switching energy of 0.25 pJ/1200 μm^2

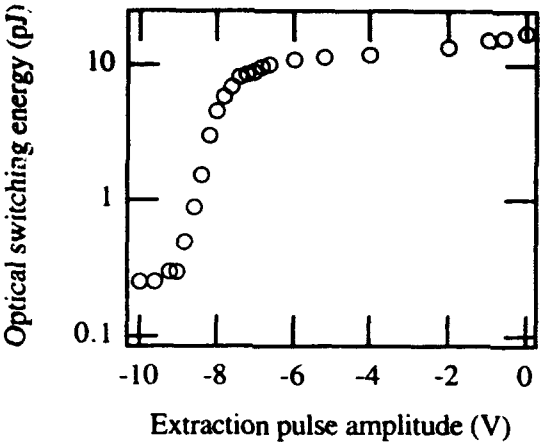


Figure 2: The necessity of the carrier-extraction pulse: insufficient carrier extraction results in 2 orders of magnitude larger optical input energy

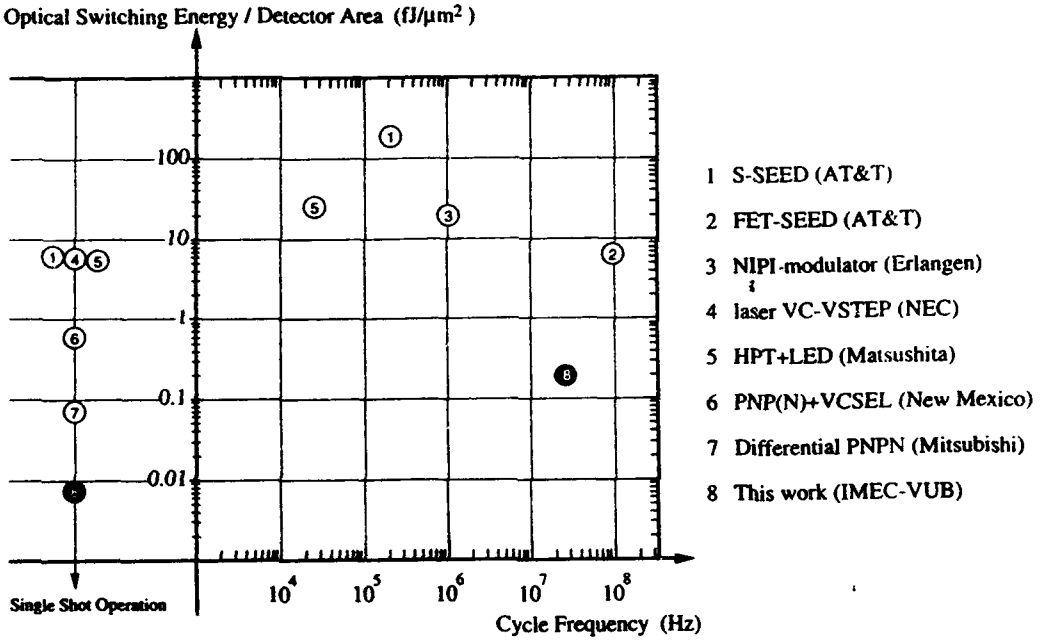


Figure 3: Optical switching energy per unit detector area versus cycle frequency of optoelectronic switches. The reports not mentioning a cycle frequency have been grouped under "single shot operation"

AlAs/GaAs Multilayered Structures as Low Intensity Nonlinear Optical Media

Steffen Knigge, Markus Wicke, and Dieter Jäger

Fachgebiet Optoelektronik, Universität Duisburg, FB 9,
Gebäude Kommandantenstr. 60, 47048 Duisburg, Germany,
phone +49 (203) 379 - 2409, fax. +49 (203) - 3400.

Abstract

The nonlinear optical properties of hybrid AlAs/GaAs Bragg reflectors are presented. Experimentally, optical bistability at optical intensities as low as 35 mWcm^{-2} is obtained when a bias voltage of 115 V is applied.

Summary

In 1992 Cada et al. [1] observed optical nonlinearity in a periodically layered III-V semiconductor structure consisting of pairs of optically linear (AlAs) and nonlinear (GaAs) layers and optical bistability was found at optical intensities I_{in} of about 10 KWcm^{-2}. In the same year, optical bistability was achieved by the authors in a hybrid multilayered AlGaAs structure at optical intensities of merely 1.4 Wcm^{-2} at a wavelength of 885 nm using a bias voltage applied perpendicular to the layers [2]. And a physical model for this hybrid case has been developed recently using a phenomenological approach [3]. Moreover, Ivanov and Haug [4] formulated analytical equations for this hybrid case leading to optical intensity levels of less than 1 Wcm^{-2}. Additionally, they predicted switching times in the order of 100 ns giving characteristic energy densities smaller than 100 nJcm^{-2}.

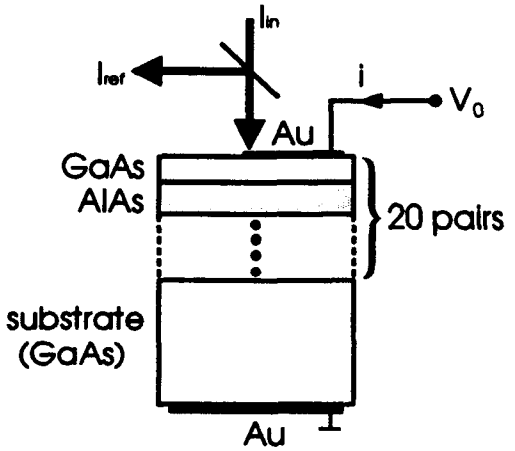


Fig. 1: Sketch of the hybrid multilayered structure.

In this paper, a hybrid Bragg reflector is investigated consisting of 20 pairs of GaAs and AlAs layers with nominal thicknesses of 58 nm and 69 nm, respectively (Fig. 1). In a first experiment, the reflection is measured as a function of the incident optical intensity I_{in} at a wavelength λ of 879.5 nm and using an impressed voltage V_0, see Fig. 2. Obviously, starting at low intensities the reflection first decreases with increasing I_{in}. Further, at

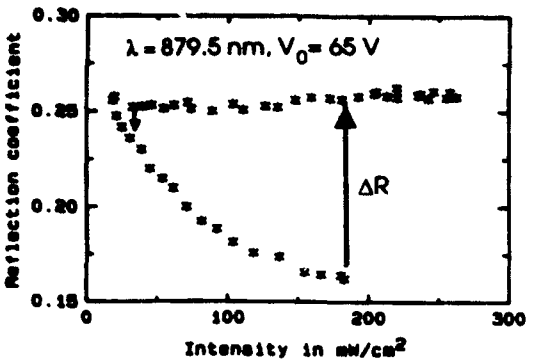


Fig. 2: Optical bistability measured at room temperature.

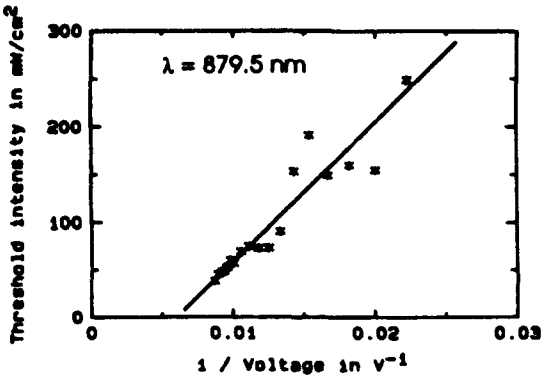


Fig. 3: Intensity for the switching between lower and higher reflection state versus reciprocal externally applied voltage.

a threshold intensity I_{th}, in this case 180 $mWcm^{-2}$, the reflection switches to a higher state. As can be depicted from Fig. 2, the reflection contrast ratio is 2.0 dB. Lowering the optical intensity again, the reflection remains almost constant at the higher level. At I_{in} = 32 $mWcm^{-2}$ the reflection switches back to the first state and a hysteresis loop is formed. As a key result, the optical nonlinearity is enhanced by an order of magnitude as compared to the results of 1.4 Wcm^{-2} in [2].

In a further experiment, the threshold intensity I_{th} is determined as a function of the external voltage V_0. From the plot in Fig. 3, it is concluded that I_{th} is proportional to $1/V_0$ + *const*. As can be seen, optical bistability can be found at optical intensities as low as 35 $mWcm^{-2}$ at a bias voltage of 115 V. Consequently, using a spot diameter of 20 μm an optical threshold power of 440 nW is expected for bistability. Hence, an array of 100 * 100 elements can easily be switched using a laser diode with an optical power of only 10 mW.

In summary, it is shown that hybrid multilayered semiconductor structures exhibit huge optical nonlinearities leading to potential applications for low intensity optical computing devices.

References

[1] M. Cada, J. He, B. Acklin, M. Proctor, D. Martin, F. Morier-Genoud, M. A. Dupertuis, and J. M. Glinski. All-optical reflectivity tuning and logic gating in a GaAs/AlAs periodic layered structure. *Appl. Phys. Lett.* **60**, 404–406 (1992).

[2] S. Knigge, S. Zumkley, G. Wingen, O. Humbach, C. Chaix, and D. Jäger. Experiments on optoelectronic bistability in distributed AlAs/GaAs-Bragg reflectors. *Microelectronic Engineering* **19**, 52–56 (1992).

[3] S. Knigge, H. Pint, M. Wicke, G. Wingen, S. Zumkley, F. Bugge, C. Chaix, and D. Jäger. Nonlinear hybrid AlAs/GaAs Bragg reflectors for photonic switching applications. In *Proc. International Conference on Optical Information Processing*, St. Petersburg, Russia, SPIE Vol. 2051 (in press).

[4] A. L. Ivanov and H. Haug. Modelling of a low-intensity electro-optical semiconductor switching device. *Appl. Phys. Lett.* (submitted).

Dynamical behaviour of opto-optical logic switching devices employing n-i-p-i-based smart pixels

M. Kneissl, P. Kiesel, P. Riel, K. Reingruber, K.H. Gulden, E. Greger, A. Höfler, B. Knüpfer, G.H. Döhler

Institut für Technische Physik, Universtät Erlangen-Nürnberg, Erwin-Rommel-Str.1, 91058 Erlangen, Germany (Phone +49-9131-858318, Fax +49-9131-857293)

X.X. Wu, J.S. Smith

Department of Electrical Engineering and Computer Sciences, University of California, Berkeley, CA 94720, USA

We report on experimental results on the dynamical behaviour of n-i-p-i-based smart pixels. With switching energies of 2.4 fJ/μm^2 contrast ratios of 4:1 at 1.6 mW output power were achieved. The opto-optical gain is tunable from 10-10^6.

Lately we have demonstrated a new smart pixel concept [1] composing of a photoconductive switch with high electrical gain [2] and a high contrast electro-optic n-i-p-i modulator [3]. A schematic picture of our smart pixel concept is shown in figure 1. One advantage of such a hybrid concept is that both elements (switch and modulator) can be optimized separately. Therefore the switches can have high responsivity and high photoconductive gain and the modulators can have high contrast and low insertion loss. Due to the high photoconductive gain of the switch only a small optical input P_{sw} is necessary to controll the much larger output power of the n-i-p-i modulator. So pure opto-optical logic devices with high optical gain are realized requiring only a dc voltage for operation. By choosing a suitable design of the switch one can obtain a high electro-optical gain and extremely low switching energies. We minimized the capacitance of the switch by using a sophisticated sample design with a small detection area and a spatially separated large absorption area, which doesn't contribute to the device capacitance [4]. In figure 2 experimental results on the dynamical switching behaviour of the photoconductive switch are shown. With an optical power P_{sw} of 880 μW a switching time in the n-layer of 1.9 ns was achieved. This corresponds to a switching energy of 1.7 pJ (= 2.4 fJ/μm^2 referring to the area of this device (Ø = 30 μm)). For this low switching time the opto-electrical gain is still 40.

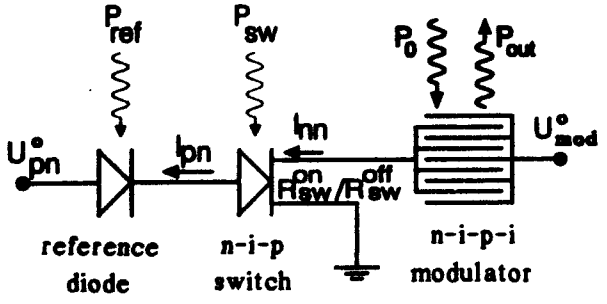


Figure 1 : Schematic picture showing our smart pixel concept composing of an opto- electrical switch, a reference diode and a high contrast electro-optical n-i-p-i modulator. In this circuit the large modulator output power P_{out} is controlled by the small input power P_{sw} on the switch.

By combining the photoconductive switch with a high contrast n-i-p-i modulator, as described in Ref. 3, we obtained opto-optical switching. Depending on wether the switch is in the high or low resistance state the voltage U^{o}_{mod} (see figure 1) drops either across the switch or the modulator. If the voltage drops across the switch, the modulator is in its transparent state and then the optical output signal P_{out} is high. The opto-optical switching behaviour for various reference power P_{ref} is shown in figure 3. In this case the optical output signal jumps from 400 μW to 1.6 mW corresponding to an on/off ratio of 4:1. By changing the reference power the switching point can be adjusted externally. Depending on the switching power an opto-optical gain from 10 to 10^6 has been achieved.

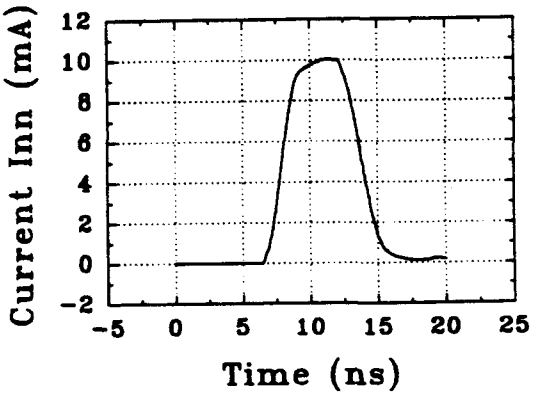


Figure 2: Dynamical switching behaviour in the n-layer current I_{nn} of the photoconductive switch. In this case the optical switching power P_{sw} was 880 μW and the switching time τ_{sw} was 1.9 ns, corresponding to a switching energy of 1.7 pJ for this Ø = 30 μm device.

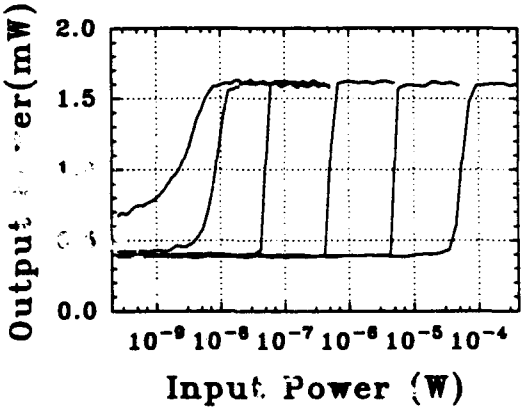


Figure 3 : Opto-optical switching with the smart pixel. For various optical power levels P_{ref} on the reference diode the diagram shows the output power of the n-i-p-i modulator controlled by the input power on the photoconductive switch.

[1] P. Kiesel, K.H. Gulden, A. Höfler, M. Kneissl, B. Knüpfer, P. Riel, X.X. Wu, J.S. Smith, and G.H. Döhler, "Bistable opto-optical switches with high gain based on n-i-p-i doping superlattices", Appl. Phys. Lett. 62 (25), 3288-3290 (1993)

[2] A. Höfler, K.H. Gulden, P. Kiesel, M. Kneissl, B. Knüpfer, P. Riel, G.H. Döhler, "Low power (bistable) opto-electrical switches with high gain based on n-i-p-i doping superlattices", Appl. Phys. Lett. 62 (26), 3400-3402 (1993)

[3] P. Kiesel, K.H. Gulden, A. Höfler, M. Kneissl, B. Knüpfer, N. Linder, P. Riel, X.X. Wu, J.S. Smith and G.H. Döhler, "High speed and high contrast electro-optical modulators based on n-i-p-i doping superlattices", Superlattices and Microstructures 13 (1), 21 (1992)

[4] P. Riel, P. Kiesel, M. Ennes, T. Gabler, M. Kneissl, G. Böhm, G. Tränkle, G. Weimann, K.H. Gulden, X. Wu, J.S. Smith, and G.H. Döhler, SPIE Proc. 1675, 242-264 (1992)

An optical set-reset flipflop semiconductor laser with two mutually complementary outputs

Masanobu Watanabe, Seiji Mukai, and Hiroyoshi Yajima

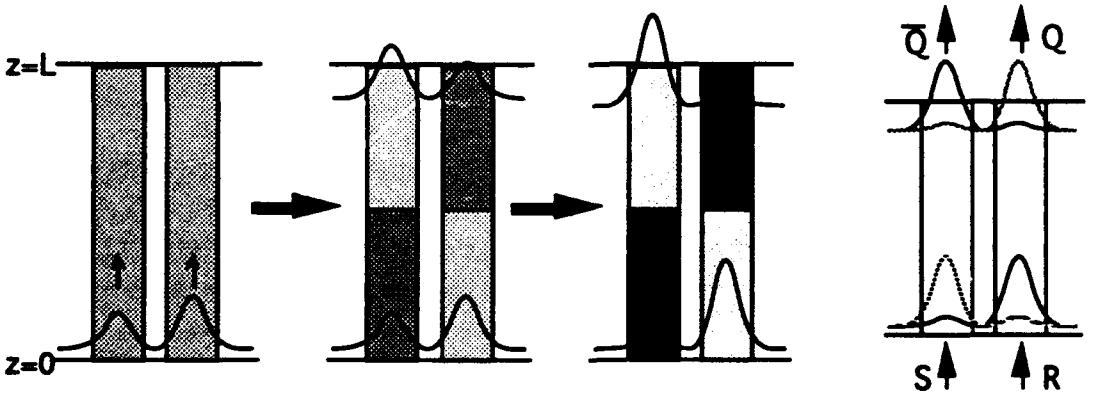
Optical Information Section, Electrotechnical Laboratory,
Umezono, Tsukuba, Ibaraki, 305 Japan : Phone 81-298-58-5620 Fax 81-298-58-5627

Abstract
Theory and experiment on crosscoupled-mode bistability in a twin-stripe laser is reported. The laser has two output ports complementary to each other, which is analogous to a set-reset flipflop in electronics.

Theory

Fig.1 illustrates top views of a twin-stripe laser to show how a cross-coupled mode [1] buiilds up [2-4]. Assume that the light power and the carriers are mainly in each of the two waveguides under the stripes, the current is *uniformly* injected into the stripes, and the cavity length is near to the coupling length of the twin waveguide. The explanation starts with symmetric light pattern at both facets. Suppose a fluctuation which leads to a slightly asymmetric pattern near a facet (z=0) as shown in Fig.1(a). This field pattern changes during one-way propagation to the other facet (z=L), where it becomes nearly the mirror image (left and right is reversed) of the light pattern at z=0, as shown in Fig.1(b). During this propagation, this light consumes more carrieres at the right-lower and left-upper regions of the twin waveguide than at the other regions. We should now examine how the resultant diagonal carrier distribution react to the light field in the next step.

Intuitively, one may expect that the carrier distribution will enhance the light power at the regions with high carrier density, which makes the light pattern return to the symmetric shape because of negative feedback. On the contrary, however, it was theoretically shown that the diagonal carrier distribution enhances the light power at the regions with *low* carrier density and makes the original light pattern more asymmetric, if the cavity length is shorter (longer) than the coupling length for twin-stripe lasers with low (high) inter-stripe gain [2-4]. This happenes because of both lateral and longitudinal resonance, and the light confinement difference between the modes. The light and the carrier distributions enhance the asymmetries of each other due to the positive feedback and finally, both have substantially asymmetric patterns as illustrated in Fig.1(c). If the original light fluctuation is such that the left peak (instead of the right peak as shwon in Fig.1(a)) becomes larger at z=0, then another stable state with mirror images of the light and the carrier distributions shown in Fig.1(c) is obtained.



(a) Fluctuation leads to slightly asymmetric pattern at a facet

(b) After one-way propagation

(c) Final stable state

(d) Set-reset flip-flop

Fig. 1

Thus, there are two stable states drawn in Fig.1(d) in solid and broken curves, respectively. The laser can be switched from a crosscoupled state to the other by light injections. The operation is similar to a set-reset flip-flop in electronics particularly in that the laser has two mutually complementary outputs, while bistable semiconductor lasers reported so far have usually only one output and hence require an additional inverter to get the complementary output. Thus, twin-sripe lasers in crosscoupled-mode operation should be useful for optical switching and logic operation.

Experiment

The lasers made for measurement has a similar structure with that in [5]. It has an ordinary double heterostructure with a 0.1 μm thick GaAs active layer sandwiched by two $Al_{0.35}Ga_{0.65}As$ cladding layers. Two 2-μm-wide stripe anodes with 4 μm spacing were formed on 4-μm-wide mesas made by wet etching. The wafer was cleaved to make lasers with typical cavity length of 500 μm which is estimated to be near to the coupling length.

Fig.1(a) and (b) show near-field patterns measured with the left and right currents fixed at 90mA and 95mA, respectively. They show the two crosscoupled modes whose patterns are the mirror images of each other. When we measured the field patterns with pulse drive, Fig.1(a) was obtained at some pulses and (b) was obtained at the other pulses. This shows bistability between two crosscoupled modes.

Cavity length limitation

The cavity length should be near to the coupling length of the twin waveguide to give a highly asymmetric light patterns. To reduce the laser length for crosscoupled mode generation, the coupling between the two waveguides should become stronger. The strongest limit is that the two waveguides are combined into one. Therefore, the possibly shortest laser length can be estimated by the propagation constant difference between the fundamental and first order lateral modes of a single waveguide. For GaAs-AlGaAs doublehetero structure, it is estimated as short as a few micrometers.

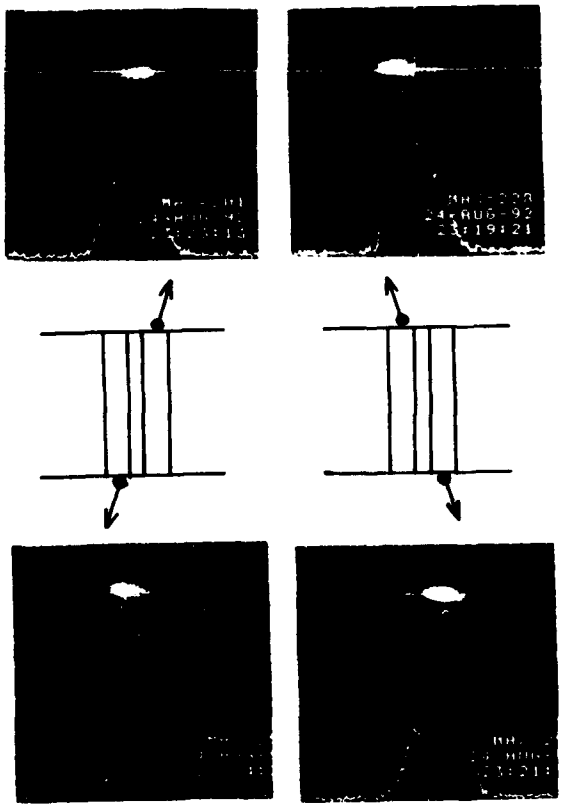


Fig.2 Measured near-field patterns

References

[1] I.H. White and J.E. Carroll, Electron. Lett., vol.19, pp.337-339, 1983.
[2] M. Watanabe, I.H. White, and J.E. Carroll, IEEE J. Quantum Electron., vol.QE-26, pp.1942-1953, 1990.
[3] M. Watanabe, I.H. White, and J.E. Carroll, IEEE J. Quantum Electron., vol. QE-28, pp.395-399, 1992.
[4] M. Watanabe, S. Mukai, K. Matsubara, and H. Yajima, to be published in IEEE J. Quantum Electron., vol.QE-29, no.12.
[5] M. Watanabe, S. Mukai, H.Itoh, and H. Yajima, J. Appl. Phys., vol.68, pp.2599-2605, 1990.

Waveguide Type Rotating Phase Plate as Frequency Shifter on (110) GaAs Substrate

Hiroaki Inoue, Shinji Nishimura, Shigehisa Tanaka* and Tatsuo Kanetake**

RWCP Optoelectronics Hitachi Laboratory,
*Central Research Laboratory, Hitachi, Ltd.,
Kokubunji, Tokyo 185, Japan
Tel:+81-423-23-1111

**Advanced Research Laboratory, Hitachi, Ltd.,
Hatoyama, Saitama 350-03, Japan

Abstract
The fundamental modulation characteristics of waveguide type frequency shifter based on the rotating phase plate are demonstrated on (110) GaAs substrate as an optical device for multi-dimensional interconnection for the first time.

A large number of activities on 2 dimensional optical devices for free space optical interconnection have been done in order to attain a large interconnection through-put for optical computing. In addition to the space domain processing, frequency domain data processing can realize the larger through-put by means of a multi-dimensional interconnection technology.

Here, a frequency shifter would be one of the most important devices, because it may realize the multi-dimensional interconnection as well as the FDM crossconnect technology in communication network. Some frequency(wavelength) conversion devices such as semiconductor optical amplifiers utilizing FWM effect and bistable laser diodes are reported so far. These have advantageous features of high conversion efficiencies(>0dB) and large frequency(wavelength) shift(>10nm). However, there are also drawbacks of limits on signal bandwidth(<~GHz) and signal modulation code(only applicable to intensity modulated signal). Rotating half-wave plate[1], in principle, can realize bit-rate free and modulation code free frequency conversion since it stands on Doppler shift.

In this paper, we report the fundamental modulation characteristics of waveguide type frequency shifter based on the rotating phase plate for the first time. We successively demonstrate parallel and perpendicular phase modulation characteristics for the effective azimuth control of the phase plate.

Figure 1 shows the principle of the frequency shifting of the rotating half-wave plate. The angular frequency of right(left) circularly polarized incident light(ω) is converted to ω-ω_p on the rotating phase plate in clockwise(couter clockwise) due to Doppler shift. Here, ω_p denotes the angular frequency of the rotaing phase plate. If the phase plate is a half-wave plate, the output light becomes the left(right) circularly polarized light with the angular frequency of ω-$2\omega_p$. This process does not depend on the signal bit-rate and the modulation code of incident light. Therfore, the optical devices based on this principle can be applicable to the bit-rate free and the modulation code free(not only to intensity modulated, but also to FSK or PSK coded signals) frequency shifter. The rotating phase plate could be realized by applying the rotating electric field to EO material effectively.

A schematic view and a cross sectional view of the fabricated device are shown in Fig.2. The waveguide was formed by RIBE, after successive growth of $Al_{0.3}Ga_{0.7}As$ lower clad, GaAs guide and $Al_{0.3}Ga_{0.7}As$ upper clad layers on a (110) GaAs substrate being 6° off towards (111)A. All layers were undoped and grown by MBE. Because the light propagation direction should be in the 3-fold axis of GaAs(<111>), the waveguide was designed to be S-shaped, which was inclined to $(1\bar{1}0)$ cleaving facets by 35°. 3

Schottky electrodes(Cr/Au), one of them being on the waveguide and two of them being besides the waveguide, were evaporated to apply the rotating electric field to the waveguide. Figures 3 and 4 show a photograph and an example of the phase modulation characteristics of the device, respectively. A DFB laser diode(λ=1.3μm) was used as the input light source. Both of TE and TM modes were launched to evaluate the phase modulation characteristics induced by the parallel and the perpendicular field respectively. As shown in Fig.4, obtained V_π values for the parallel and perpendicular field were 10V and 13V, respectively. Therefore, by applying sinusoidal electric fields to the electrodes with adequate phases, the effective rotating azimuth of the phase plate can be induced as the waveguide frequency shifter based on Doppler shift. These V_π values are so high to attain the large frequency shift because of neccessity of the high voltage and high frequency electric driver. However, by introducing large EO effect by quantum size effect such as QCSE[2], we beleive the issue can be overcome.

In conclusion, the fundamental modulation characteristics of waveguide type frequency shifter based on the rotating phase plate have been repoted as an optical device for multi-dimensional interconnection for the first time. Demonstrated parallel and perpendicular phase modulation characteristics for the effective azimuth rotation of the phase plate indicated the possibility of the bit-rate and modulation code free frequency shifter in practical.

References

1) C.F.Buhrer, D.H.Baird and E.M.Conwell, "Optical frequency shifting by electro optic effect', Appl. Phys. Lett., vol.1, p.46, 1962

2) S.Nishimura, H.Inoue, H.Sano and K.Ishida, "Electrooptic effect in an InGaAs/InAlAs multiquantum well structure', IEEE Photon. Technol. Lett., Vol. 4, p.1123, 1992

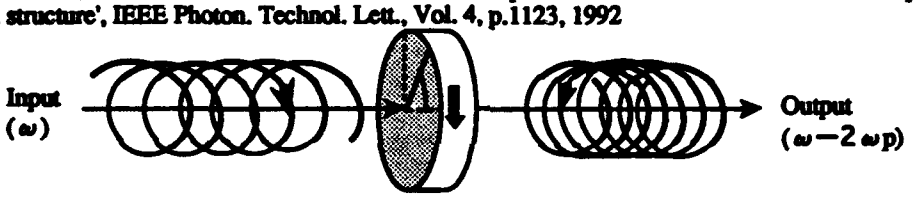
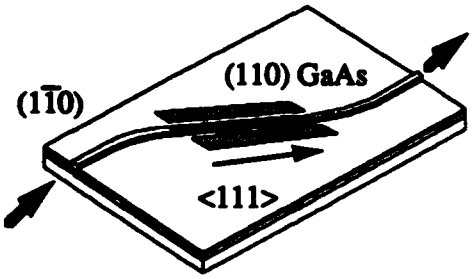


Fig.1 Principle of frequency shifting by rotating half-wave plate, which is equivalent to Doppler shift.



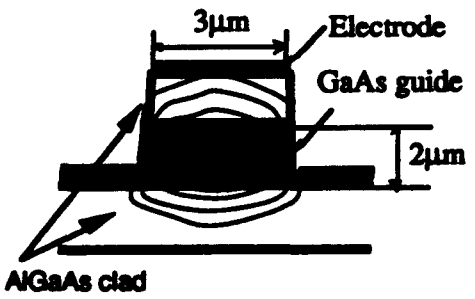


Fig.2 Schematic and cross sectional views

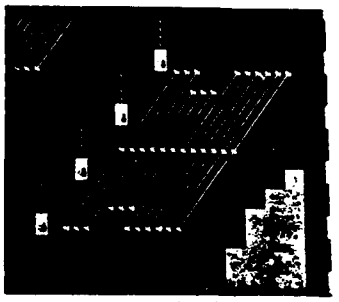


Fig.3 Photograph of fabricated device

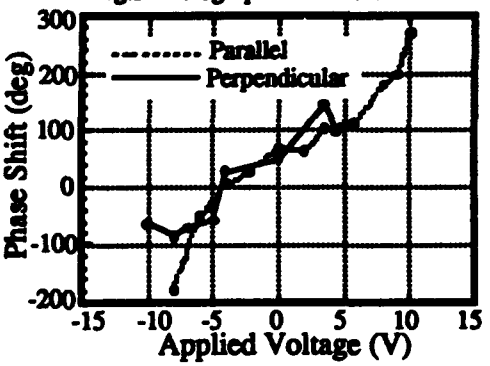


Fig.4 Phase modulation caracteristics

Asymmetric Light Bullet Dragging Logic

Robert Mcleod, Steve Blair, and Kelvin Wagner
Optoelectronic Computing Systems Center
University of Colorado, Boulder CO, 80309-0425
1-303-492-4661 kelvin@boulder.colorado.edu

Abstract
The asymmetric dragging interaction between three-dimensional optical solitons may allow cascadable, phase-insensitive, NOR gates with gain to be implemented at ultrahigh speeds in massively parallel three-dimensional bit-level systolic-array architectures.

In media that have both a self-focusing nonlinearity ($n_2 > 0$) and negative group velocity dispersion, a pulse can collapse in both space and time forming a stable "light bullet" in 3+1 dimensions.[1-2] These collapsed optical pulses have high peak powers but small total energies, making them attractive for nonlinear optics applications. These three dimensional solitons can be made to interact to produce a logic gate in the same way that one-dimensional spatial (or temporal) solitons do. We are investigating the asymmetric interaction between two orthogonally polarized solitons brought into coincidence both spatially and temporally at the boundary of a nonlinear medium and propagating at slightly different angles. This geometry permits a weak signal to drag a strong pump by well over a beam width, allowing them both to be blocked by a spatial aperture.[3] This results in a phase insensitive inverter with gain that can be cascaded to implement a high contrast NOR gate that transmits an uncorrupted pump through the aperture if the signals are not present, and drags the pump out of the spatial aperture so that it is blocked if they are present. Simultaneous multidimensional dragging by two signals is possible for light bullets, allowing the single stage implementation of NOR gates. A beam propagation simulation of an asymmetric light-bullet dragging interaction is shown in Figure 1. This shows a dragging of a $6\mu m \times 6\mu m \times 11\mu m$ 3.3pJ pump (I_p=140MW/cm^2) by a .7pJ signal (I_s=20MW/cm^2) in about 1.5mm of propagation distance using a rather large saturating nonlinearity of $n_2^E = 10^{-16}\text{m}^2/\text{V}^2$.

In order to optimize these light bullet dragging gates without the huge computational overhead of the 3+1 dimensional beam propagation simulations, we are examining the properties of 1D asymmetric spatial soliton dragging interactions, as illustrated in Figure 2. As an example we illustrate the output contrast ratio (wrt the fundamental soliton power) in a two-level system saturating nonlinear medium (in this case I_{sat} is 4 times the nonsaturated fundamental soliton peak intensity), as a function of interaction angle, propagation distance and pump-to-signal beam ratio in Figure 3.

Layered sandwiches of nonlinear media, aperture arrays and linear media suggest the possibilty of computing in 3-D with asymmetric light bullet dragging gates. But getting the signals and pumps to the desired interaction sites without disruption by unwanted signals may be difficult. It may be necessary to systolisize at the bit level in 3-dimensions by pulsing the clock pumps and signals so that they pass through each other in intervening layers of linear media until arriving at the desired dragging logic site, and to program the functionality of the array of logic gates by the presence and absence of clock pumps in the space-time lattice of possible light bullet locations. An example of a 1-D spatial soliton dragging logic cascaded majority logic circuit is illustrated in Figure 4, demonstrating that more complex functions than simple NOR gates can be implemented without intervening interconnections.

Ultrafast, massively parallel, low latency, all optical NOR gates with gain, cascadability, input-output isolation, and phase insensitivity have been proposed, numerically demonstrated and parametrically optimized. This optical switching interaction opens up new architectural possibilities for computing in 3+1 dimensions that may allow the realization of volume parallel digital optical computers.

The authors acknowledges support of the NSF young investigator program ECS 9258088.

References

1. Y. Silberberg, Collapse of optical pulses, *Opt. Lett.*, vol. 15(22), p 1282, 1990.
2. J. E. Rothenberg, Space-time focusing, *Opt. Lett.*, vol. 17(19), p 1340, 1992.
3. K. Wagner and B. Mcleod, Spatial Soliton Dragging Gates and Light Bullets, OSA Topical Mtg. on Optical Computing, Palm Springs CA, March 1993.

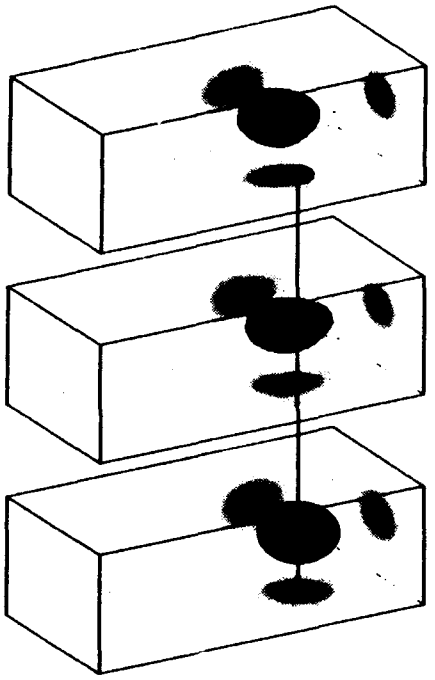


Figure 1: Light bullet dragging by more than a beam width. The two orthogonally polarized light bullets are represented with a mesh and a solid surface thresholded at .1% of the peak pump intensity, and are propagating vertically with an initial 1 degree angle.

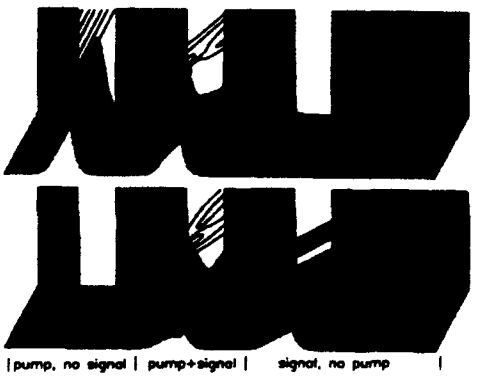


Figure 2: Asymmetric 1-D spatial soliton dragging, showing pump output through the aperture as an inversion of the signal input.

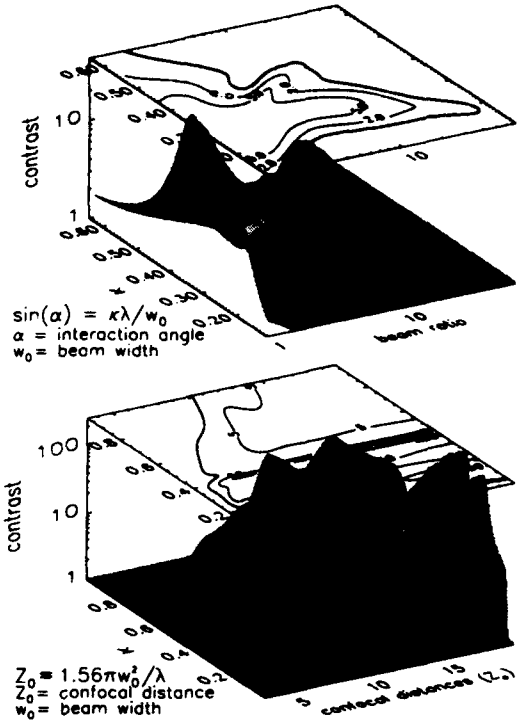
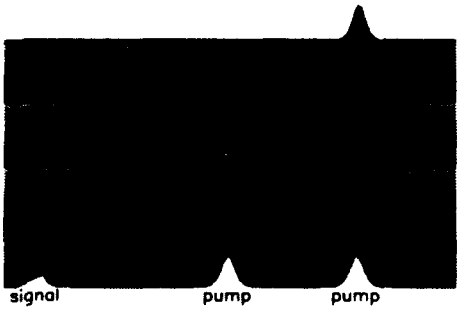


Figure 3: Output contrast versus interaction angle and pump-to-signal ratio for a propagation distance of 5 confocal distances, and contrast versus interaction angle and propagation distance for a beam ratio of 5.



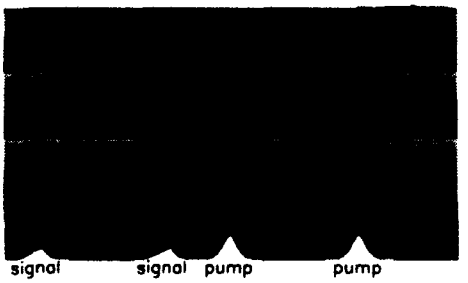


Figure 4: Cascaded 3-level simulation of majority logic circuit showing that the first pump implements a NOR that is blocked by either signal, and the second pimp is only blocked when 2 or more off-axis signals are present.

Architecture Design and Implementation Issues for Massively Parallel Processors

Steve Nelson
Cray Research, 900 Lowater Road, Chippewa Falls, WI, U.S.A.

ABSTRACT

Dramatic improvements in microprocessor price/performance have challenged the supercomputer designer to achieve high levels of system performance by interconnecting hundreds or even thousands of processors. But to achieve high sustained computational rates it is imperative that designs be balanced with respect to processor speed, local and global memory bandwidth, input/output capability, and interprocessor synchronization primitives. This talk will discuss these criteria using examples from the recently announced CRAY T3D system.

It has been more than twenty years since the supercomputer industry was more or less defined by the CRAY-1. Very significant technological changes have occurred since then. Most compelling are the great advances in integrated circuit density and speed. These advances have spawned multiple generations of microprocessors and inexpensive semiconductor memory. In fact, the latest microprocessors now challenge the performance claims of the original CRAY-1 but at small fraction of the cost. There is naturally a strong incentive to try to achieve high processing rates across large numbers of these relatively inexpensive microprocessors. However, realizing the aggregate potential performance of such a system has proven to be quite challenging.

First, the problem and selected algorithm must be highly parallel. As is well known, Amdahl's law observes that for practical problems, the total execution time will consist of a parallel portion parceled out to a collection of processors plus a serial portion. If large numbers of processors are frequently forced to wait for the computation of data coming from a single processor in the system plus the additional time required to distribute the data, the actual benefit of the large numbers of processors will be reduced. At some point, adding more processors is no longer cost effective in reducing the time to solution. Even for a problem which is 95% parallel, one can not expect speedups beyond 20 for even an arbitrarily large number of processors. Massively parallel (or MPP) systems of hundreds of processors require problems that are more than 99% parallel.

Second, the problem should exhibit high algorithmic efficiency. Each calculation should effectively move the calculations toward the final solution. A high sustained floating point operation rate is diminished in value if the algorithm demands many more intermediate results than a competing algorithmic choice. Such false achievements that do not contribute to reducing the time-to-solution have caused a great deal of confusion in the marketing of competing MPP systems.

Third, it must be possible to efficiently move dependent data to requesting processors. This communication overhead can have the same effect as the serial portion of the computation. Algorithms of choice require only modest amounts of interprocessor communication or else allow mechanisms in the hardware to effectively make the latency transparent when coupled with software prefetching techniques.

There are two distinct architectural choices for which cooperation among large numbers of processors might be enforced. The Single Instruction Multiple Data (or SIMD) model causes each processor to operate in lock step with all other processors in the partition but with different, parallel data sets.

The Multiple Instruction Multiple Data (or MIMD) model allows each processor to follow its own control flow, executing from distinctly different instruction streams.

SIMD designs are a good match for data parallel programming models and can be somewhat simpler to program. But these suffer from inefficiencies when, for example, sparse matrix data is being manipulated in rather naive ways with lots of multiplications or additions of zero operands. Although the operation count may be high, the algorithmic efficiency is low. MIMD systems provide many more degrees of freedom with, conceptually, each processor operating from distinctly different, optimized control stores. Whereas synchronization is implicit for the SIMD model with all parallel calculations occurring simultaneously, it is necessary in the MIMD case to manage more explicitly the limited interaction among processors. Although somewhat more difficult to program, the opportunity for increased hardware utilization has caused a shift in essentially all recent MPP designs toward the MIMD domain.

Uniform access memory sub-system have worked effectively for vector supercomputers but do not scale well to large number of processors because the required number of independent data paths grows exponentially. The non-uniform physically distributed memory model provides a more scalable solution with each processor located physically nearby a set of memory devices. The processors can then have preferential access (that is, lower latency and/or higher bandwidth) to the nearby memory. The non-uniform memory access model can provide a much more cost effective solution for parallel algorithms that emphasize a high degree of local computation and only moderate amounts of global data movement. Whereas the high degree of connectivity in the uniform access memory system may actually be under utilized a significant part of the time.

Whether the memory is physically shared or distributed, there is another significant architectural choice: the *logical* addressing mechanism among processors determining whether the system is a multi-computer or a true multi-processor. Many MPP systems are designed as multi-computers with interprocessor communication depending upon explicit I/O based requests. Data moving from one processor to another must pass through the I/O ports of the processors. This usually requires the use of processor interrupt mechanisms and even intervention by the operating system. The target processor must decode or interpret via software techniques the address tag and the purpose of the message to determine the exact source or destination for the payload. This results in significant increases in latency for the interprocessor communication process. A multi-processor on the other hand provides direct paths to each memory location within the entire processor-pool partition. Addressing is managed through a single global address space. On the target end of the transfer, the data communication mechanism does not interrupt the processor, but proceeds directly via hardware support to that processor's local memory.

Interprocessor synchronization must be fast and scalable. Typical RISC microprocessor designs anticipate only very moderate numbers of processor working together within a workstation. Techniques used are often bus-based, such as the popular bus snooping protocol technique. Due to very real physical constraints, these schemes do not scale well beyond about a dozen processors. Software and I/O based synchronization protocols used in workstation cluster organizations may scale to large numbers but fall far short of the goal for providing single microsecond or less global synchronization latency. Much more effective techniques providing barrier, atomic swap, pre-fetch, and message queuing approaches are possible and provide for more efficient hardware utilization within critical regions of code execution.

Free-space WDMA Optical Interconnects Using Mesh-connected Bus Topology

Yao Li, Satish B. Rao, I. Redmond, Ting Wang
NEC Research Institute, Princeton, NJ 08540, U.S.A.

Adolf W. Lohmann
Angewandte Optik, University of Erlangen
Erlangen, Federal Republic of Germany.

ABSTRACT

A mesh-connected bus networking topology is proposed for implementing the three-stage Clos network and is experimentally demonstrated using a WDMA technology.

We consider networks for interconnecting parallel computers that are parameterized by their diameters (number of switching stages) and degree (fan-out) of switches which are used to build the network. Clos used switch fan-out to describe a family of networks that range from the complete network that has maximum fan-out and minimum switching diameter to the "Benes" network with nearly minimum fan-out and larger networking diameter. Electronic networks tend towards the small fan-out/large diameter end of the spectrum due to limitations on the fan-out of electronic switches. The fan-out of systems of optical switches is anticipated to be significantly higher than electronic switches. Thus, it has been suggested that optics can be used to build the complete network which is the most desirable of Clos's family of networks. Even optics, however, has practical limits on the fan-out of switches in any given configuration. Thus, in this paper, we describe an implementation of a network with significantly smaller degree and slightly larger network diameter than the complete network. The network that we implement is called the mesh-connected bus network. We remark, however, that it is essentially an implementation of the second most desirable network in the family of networks defined by Clos, which is widely referred to as the Clos network.

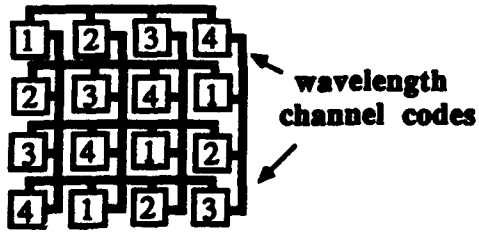


Fig.1: A 16 node WDM MCB network layout.

The Clos network is often depicted in its linear node distribution format. We remap this 1D format to a 2D linking topology (see Fig.1 for N=16 nodes) which can be referred to as the mesh-connected bus (MCB) topology where the three switching stages are embedded into a permutation along a row, followed by along a column, and finally along a row in a grid structured 2D node array. It can be shown depending on the number of switches used in each row and column, the MCB offers at least a rearrangable non-blocking switching environment. We also summarize other important embedding, off-line as well as on-line communication features of the MCB network.

To optically implement the MCB interconnect, we propose to use the wavelength-division multiple access (WDMA) concept which is commonly used in fiber communication community. However, in our approach, free-space optical components such as cylindrical optical lenses, mirrors, or 1D gratings, etc. for routing optical signals are adopted [1]. We will show various ways of realizing the proposed optical WDMA MCB network and analyze the corresponding fundamental and technological limits.

The proposed system concepts are experimentally verified through routing both low (10 MHz) and high (1.25 GHz) bandwidth optical signals (see Fig.2 for our system connection diagram) [2]. In the low bandwidth situation, some base-band video, audio and RS-232 data

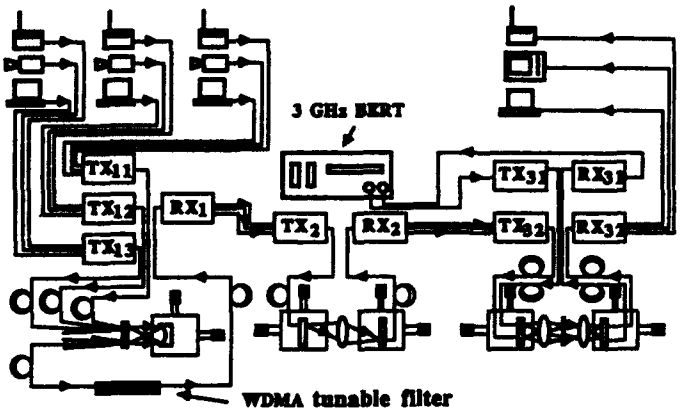


Fig.2: Experimental setup for the 3-stage WDMA MCB interconnect.

are multiplexed to fill up the 10 MHz bandwidth. Conventional Fabry-Perot lasers operating in the range of 1290 - 1340 nm were used. Our power measurement confirmed that a fan-out to as many as 36 channels could be established along each bus making a network linking 1,296 nodes power-wise possible. Through 3-stages of free-space routing and associated electric-to-optical and optical-to-electric conversions, an overall 49 dB signal-to-noise ratio for video signal reception was still maintained. The images shown in the four quadrants of Fig.3 are the

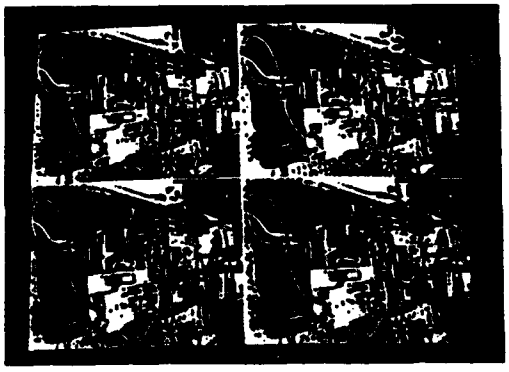


Fig.3: Experimental results of three-stage routing.

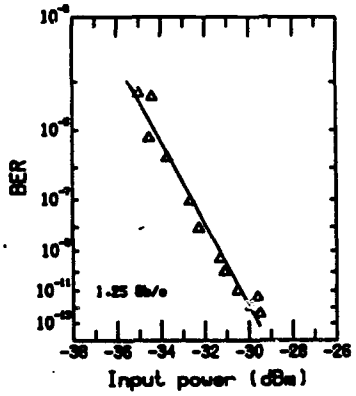


Fig.4: Bit-error-rate test results of 1.25 Gb/s bus link.

original camera image of our setup, and the received images at the first through the last stages of our network. Our high bandwidth experiment involved using high-quality DFB lasers operating around 1310 nm. The corresponding optical system power measurement illustrates that at the transmission rate of 1.25 Gb/s, our WDM bus array can accommodate 16 channels per bus or equivalently 256 nodes in the network with a guaranteed receiving bit-error-rate of lower than 2×10^{-13} (see Fig.4 for the bit-error rate measurement results).

[1] Y. Li, A. W. Lohmann, and S. B. Rao "Free-space optical mesh-connected bus networks using wavelength-division multiple access" Appl. Opt. 32 (1993) 6425-6437.

[2] Y. Li, A. W. Lohmann, Z. G. Pan, S. B. Rao, I. Redmond and T. Wang, "Optical multiple-access mesh-connected bus interconnects," submitted for publication.

Design Issues for Free-Space Photonic Switching Demonstrators

F. B. (Rick) McCormick
AT&T Bell Laboratories
Room 2F-231, 263 Shuman Blvd.
Naperville, IL 60566 USA
voice: 708-713-5442, email: fmac@iexist.att.com

Abstract:
We discuss the issues involved in building demonstration systems integrating GaAs FET-SEED smart pixels, computer generated holograms, 2-D fiber bundles, high-power lasers, high resolution optics, and novel optomechanical packaging. A prototype 5 stage, 32x16 fabric operating at 155Mb/s is described.

Summary:

An exciting new trend in free-space photonic switching and computing systems is the use of smart pixel device arrays which combine the processing power of electronics with the interconnection and communication advantages of optics. A recent system prototype (Fig. 1) implements a 32-input, 16-output multi-stage switching fabric using 5 stages of 4x4 FET-SEED "smart pixel" (2,1,1) node arrays, and Banyan interconnections.[1,2] The first experiments with this system achieved 50 Mb/s operation of the 5 stages with 15 active inputs and outputs, and 155 Mb/s operation of 2 stages with 8 of the 15 active nodes functioning correctly along their "straight" routing paths. This talk presents the critical design and testing issues for this system, including recent modifications enabling operation of 5 stages at 155 Mb/s, with 32 active inputs and 16 active outputs.

Each stage's optical power supply combined a high power semiconductor laser diode with an external cavity grating for frequency stabilization and a computer generated binary phase grating (BPG) to form the non-uniformly space array of equal power spots required to address the FET-SEED modulators. The lasers [3] supply 60 mW of optical power at 850 +/-0.1nm. The BPGs have a measured efficiency of 73% (neglecting Fresnel losses) and a power uniformity of 93%. A custom beam combination assembly, consisting of 2 polarizing beam splitters is used to combine the power supply and signal beams onto the node array by creating input and output ports for the single f/1.5 Fourier transform lens at each stage. [4] Each FET-SEED switching node consists of a differential optical receiver, a control memory to store a routing bit extracted from the data stream, and a multiplexer/modulator driver. The first stage array has 11x11 μm^2 detector windows, and 2 differential optical receivers per node separated by 120 μm. Tested individually, the node circuits operated up to 400 Mb/s with 80 fJ of incident optical signal energy. The interconnections between stages were initial performed by 1x3 BPGs between stages. System inputs are generated by 810nm laser diodes attached the input fibers, which are arranged in an 8x4 bundle on a 500 μm pitch. This fiber matrix is imaged onto the first node array through a dichroic beam combination system similar to the PBS assemblies of the other stages, except that PBS_1 has $\lambda/4$ retarders and dichroic mirrors (transmit 850nm, reflect 810nm) attached so that the unpolarized light from the input fibers is directed onto the first node array. A custom mounting plate similar to our previous system [5] is used to mount and align all system components. The laser units, PBS assemblies, and the input and output fiber bundles are mounted on kinematically registered sub-mounts for easy assembly and replacement.

Several system modifications have been made for the second experiment. Design and processing modifications have increased FET currents and uniformity. The areas of the modulators have been increased to 10x10 μm^2 from 7x7 μm^2 (detector areas remain at 7x7 μm^2), and the node pitch increased from 210 μm to 240 μm. The Banyan interconnections between stages are realized by metallization on the node arrays rather than by binary phase gratings (BPGs), providing 4 times more optical signal power at each FET-SEED receiver. The use of non-separable BPGs rather than multi-level suppressed order phase gratings for spot array generation provided increased light efficiency. Population of all 32 input fibers enabled testing of all 512 paths through the fabric. The use of 1300 nm SM fibers in an actively aligned fiber bundle eased the alignment of the data input lasers, but since they support 4 modes at 810nm, a -2.2dB modal noise tradeoff was introduced. Fabrication errors in the input beam splitter assembly have been corrected by the addition of a birefringent wedge arrangement.

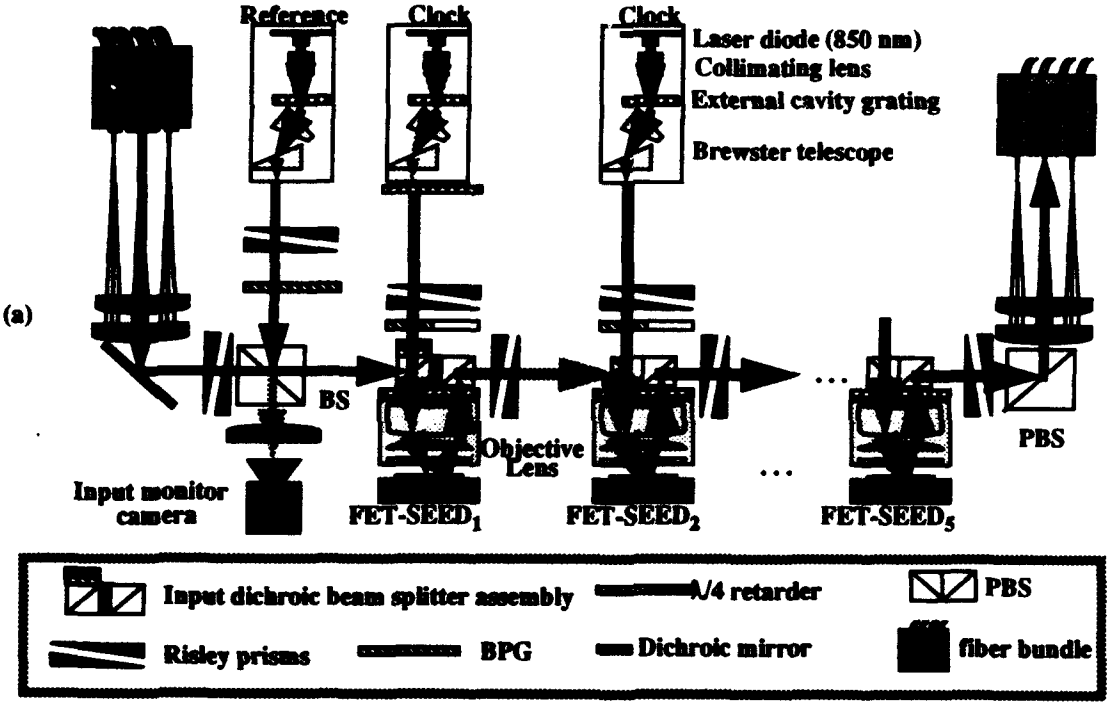
An automated call-load generation system was developed to test all 512 paths through the 5-stage network. At 155 Mb/s, 45% of the paths were functional due to 3 non-functional pixels and 1 low-powered input fiber. The system maintained this functionality within our lab (+/-1° C, Newport table) for over 8 weeks. *The development of this prototype would not have been possible without the combined efforts of the authors listed in the references.*

References:

1. F. B. McCormick, T. J. Cloonan, A. L. Lentine, J. M. Sasian, R. L. Morrison, M. G. Beckman, S. L. Walker, M. J. Wojcik, S. J. Hinterlong, R. J. Crisci, R. A. Novotny, and H. S. Hinton, "A 5-Stage Free-Space Optical Switching Network Using FET-SEED Smart Pixel Arrays," accepted by Applied Optics, Information Processing, special issue on Optical Computing, 1994
see also: Photonics in Switching Technical Digest, 1993, (Optical Society of America, Washington, D.C., 1993), post-deadline

paper PD-5.
2. A. L. Lentine, T. J. Cloonan, H. S. Hinton, L. M. F. Chirovsky, L. A. D'Asaro, E. J. Laskowski, S. S. Pei, M. W. Focht, J. M. Freund, G. D. Guth, R. E. Leibenguth, L. E. Smith, G. D. Boyd, and T. K. Woodward, "4x4 arrays of FET-SEED embedded control 2x1 switching nodes," Postdeadline paper, IEEE LEOS Summer topical meeting on Smart Pixels, 1992.
3. J. M. Sasian, R. L. Morrison, T. J. Cloonan, M. G. Beckman, M. J. Wojcik, and S. J. Hinterlong, "Frequency control, modulation, and packaging of an SDL (100 mW) laser diode," in Technical Digest of OSA Topical Meeting on Optical Design for Photonics, March 22, 1993.
4. J. M. Sasian, F. B. McCormick, R. Webb, R. J. Crisci, and K. O. Mersereau, "Design, assembly, and testing of an objective lens for a free-space photonic switching fabric," Optical Engineering, 32 (6), 1871-1878, (1993).
5. F. B. McCormick, F. A. P. Tooley, J. L. Brubaker, J. M. Sasian, T. J. Cloonan, A. L. Lentine, R. L. Morrison, R. J. Crisci, S. L. Walker, S. J. Hinterlong, and M. J. Herron, "Design and Tolerancing Comparisons for S-SEED-based Free-Space Switching Fabrics" Optical Engineering, 31(12), 2697-2711 (1992).

(a)



(b)

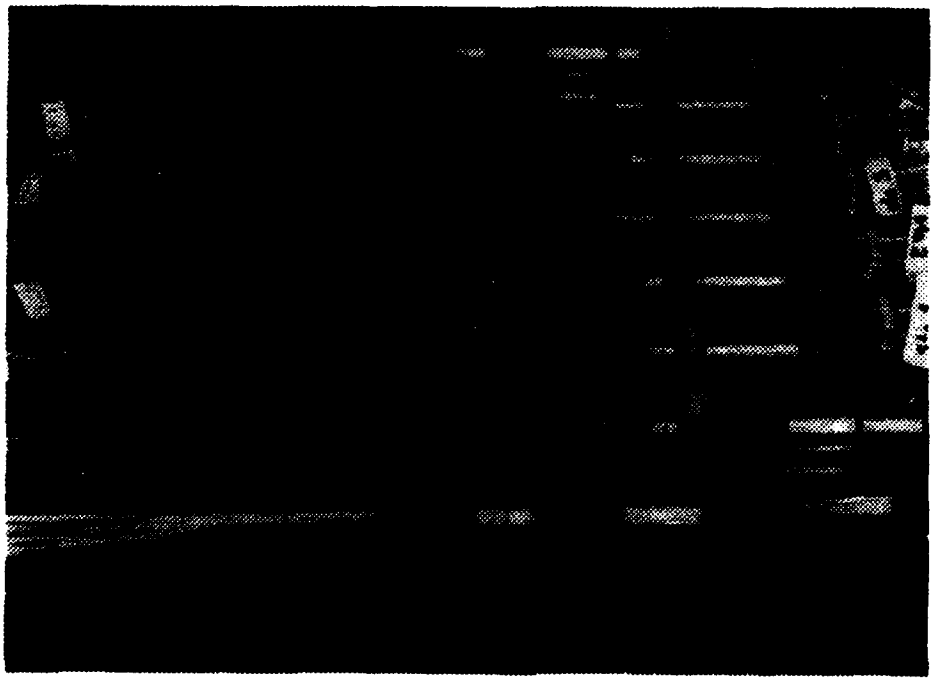


Fig. 1. Prototype free-space switching network: (a) Optical schematic (b) Photograph

Demonstration of optically controlled data switching using quantum well bistable devices and modulators

P. Koppa, P. Chavel (Institut d'Optique-CNRS, BP.147 - 91403 Orsay Cedex, France)
J.L.Oudar, R. Kuszelewicz (France Telecom , CNET Paris-B, BP.107 - 92225 Bagneux Cedex, France)
J.Ph. Schnell, J.P. Pocholle (Thomson CSF. LCR, Domaine de Corbeville, 91404 Orsay, France)

Abstract:
Experimental results on a 64 channel free-space photonic switching system are presented. Two control schemes are demonstrated : direct optical addressing with potential signal amplification and self-routing operation acting on data packets.

We present a 1 to 64 free-space optical switch which can be operated both in packet switching and circuit switching environments. The system associates a spatial light modulator (1) (SLM) and an optical bistable device array, both based on GaAs/GaAlAs Multiple Quantum Well (MQW) structures. The SLM is an 8x8 array of individually addressable transmission type electro-absorption modulators. The optical bistable device (2) consists of a non-linear Fabry-Perot etalon. The 8x8 bistable pixels are simply defined by separated light spots incident on the same cavity. When maintained in the bistable region of operation by a holding beam array, the devices exhibit a two state memory effect for about 1 ms (fig.1/a). With a slight modification of the detuning from the Fabry-Perot resonance, this hysteresis loop can be transformed into a simple thresholding curve (fig. 1/b).

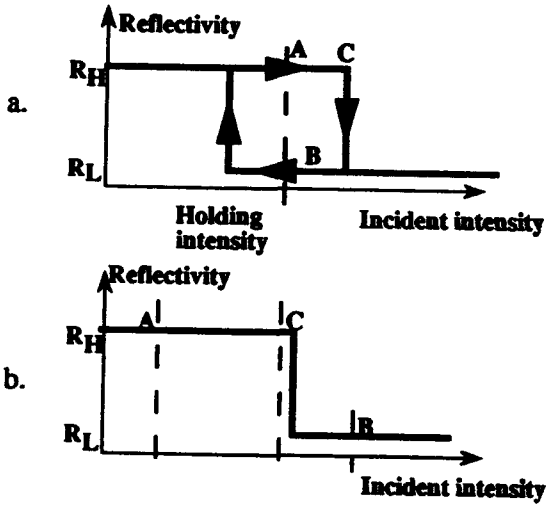


Fig.1. : Bistable device response curves. a.: bistable, b.: simple thresholding operation

In the packet switching mode, self-routing commutation is implemented by optical decoding of the header address preceding each data packet. This address decoding (3) consists in fanning-out the signal into 64 channels, comparing bit by bit the address of the packet to the address of each output channel, and switching off all channels where the identification of one or more bits fails. A two bit coding technique is used to code the binary addresses : each bit is followed by its complementary value, so bit one is coded by a high-low sequence, bit zero by a low-high. By the use of this code, address comparison becomes a simple bitwise multiplication of the packet address by the inversely coded channel address, introduced as the modulated transmission of the SLM pixel. Any mismatch between the two addresses is turned into the transmission of a high level address pulse by the modulator element.

This pulse then switches down the corresponding bistable element in its blocking state (point B on fig 1/a), from its initial reflective state (point A). Consequently, the only bistable element staying in reflective state will be that of the destination channel, where address matching is perfect. After the data packet has passed through this channel, all bistable devices are reset to the initial high reflection state to receive the next packet.

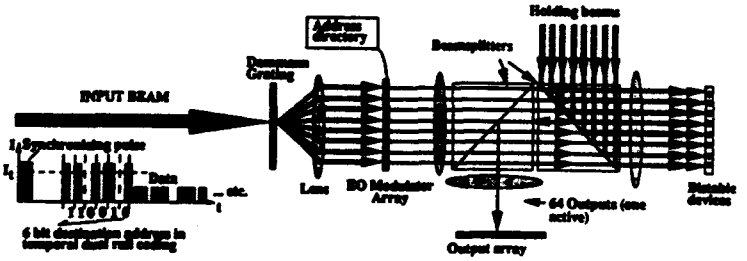


Fig.2. : Operation scheme (arrows indicate data flow not geometrical optics rays)

Figure 3 shows output signals obtained by single channel operation of the system. The first oscilloscope trace shows a packet addressed to the observed output : there is no high level pulse due to address mismatch, so data are transmitted by the system. The last three traces represent packets with different addresses which do not match the address of this output. We can distinguish the high level address pulse which immediately switches off the bistable device. The bistable devices used in this experiment have a contrast ratio of about 2:1, so theoretically blocked packets are attenuated, but still visible at the output. The data rate in this experiment is 20 Mbit/s and total input intensity is about 15 mW. System operation is demonstrated for packet lengths up to 8 kbits, with a typical error rate of 1%.

In circuit switching mode holding beams are directly used to control bistable device reflectivity. To achieve this functionality, holding and signal beams are interchanged compared to figure 2, so that we can modulate independently each holding beam. (denoted as control beams in this case.) Bistable devices are set to non-bistable thresholding mode (fig. 1/b).

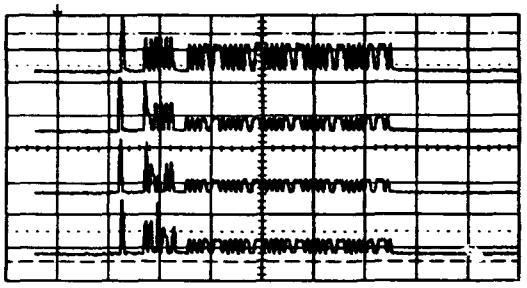


Fig.3 : Output signals of the self-routing operation

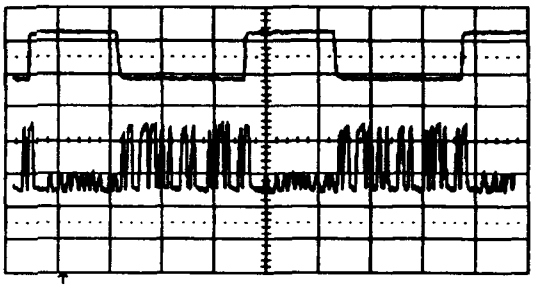


Fig. 4 :Output obtained by direct addressing

Figure 4 shows one channel operation in that mode : when the control beam is off (point A of figure 1/b), the bistable device is reflective, so the signal is routed to the output ; when the control beam is on, the device is in the low reflection state, so the signal beam is mostly absorbed. In this operation mode the contrast ratio can be improved up to a value of 4:1, while the total input intensity is lower than 5 mW. The switching threshold is about 1 mW, as opposed to 3.5 mW in the bistable mode .

This operation mode can be transformed into active switching, by setting the control beam intensity to point C of figure 1/b (i.e. very close to the switching threshold). If the additional signal intensity exceeds the threshold, the device is switched by each data bit change, so modulation of the signal is transmitted onto the control beam. As the control beam is in general more intense then the signal beam, data amplification can be obtained. The actual gain depends on device response curve and signal to noise ratio. In our system an amplification factor of nearly two was obtained, but with other bistable devices higher gains have also been demonstrated[4]. This operation scheme presents the advantages of data reshaping and amplification, but it requires data-rate switching of the bistable element, limiting the data rate by its operation speed. (Rise- and fall-times of the order of 10 ns were observed for our actual devices, with 3mW input on 200 µm.) In self-routing operation and passive circuit switching modes, the data-rate is not limited by the device speed, since the set-up is transparent to data bits.

In conclusion, single channel operation of the 1 to 64 free-space optoelectronic switch was presented both in packet switching and in circuit switching mode. Further results on parallel operation of the system will be given, as well as a study of system limitations due to crosstalk, uniformity and noise effects.

This work is supported by the French Ministry of Research under the project MOTS/OSTI 91.

References :

1. J. Ph. Schnell, J. Raffy, J. P. Pocholle, A. Delboulbe, G. Dutrey, J. Lehoux, M. Werner, M. Papuchon, J. P. Huignard ; Technical Digest of Spatial Light Modulators 1990, Vol.14, pp 60-64
2. J. L. Oudar , R. Kuszelewicz , B. Sfez, D. Pellat, R. Azoulay; Superlattices and Microstructures, 12, p.89 (1992)
3. P.Chavel, P.Koppa, J.Taboury, J.L.Oudar , R. Kuszelevicz, J .Ph. Schnell, J. Raffy, J.P. Pocholle, M. Papuchon ; Topical Meeting on Spatial Light Modulators, Palm Springs, California, 1993, OSA 1993 Technical Digest Series Volume 6, p.81
4. B. Sfez, J. L. Oudar, R. Kuszelewicz, J.C.Michel, R. Azoulay ; Appl. Phys. Lett. 57, p.1849 (1990)

Reconfigurable Architecture Based on Selective Enabling of Microlasers

Miles Murdocca†, James Battiato*, David Berger††, Rebecca Bussjager*, and Thomas Stone**

ABSTRACT

We report on a reconfigurable architecture that uses a static free-space optical interconnect. A two-dimensional array of microlasers controls a two-dimensional array of S-SEED optical logic modulators in a cascaded system.

1. INTRODUCTION

In previous experiments at Rutgers University, a property known as **functional locality** [1] was observed for a mix of programs executing on a SPARC processor. The concept behind functional locality is that only a fraction of the hardware in a processor is used for a given interval of time, and that there is repetition within that interval. If we consider implementing just 10% of the SPARC instruction set, then we observe a hit ratio on the order of 80%. That is, 80% of the instructions are executed from only 10% of the code over a lengthy period of time.

As a result of this finding, the development of a **function cache** [1] is proposed in which the most recently used hardware is kept in the form of interconnection patterns in a high speed section of a processor. A processor that supports functional locality must provide for gate-level reconfiguration, which motivates our development of an optically reconfigurable architecture.

A model for a reconfigurable optical architecture that was demonstrated in the Photonics Center at Rome Laboratory in September 1993 is illustrated in Figure 1. The architecture consists of an array of active optical logic devices (S-SEEDs) that are interconnected in free space. The architecture is customized by selectively enabling channels with electrically controlled vertical cavity surface emitting lasers (VCSELs) that provide optical setup power for the S-SEEDs, and can ultimately provide readout power for the S-SEEDs as well. The free-space interconnect has a regular pattern implemented as a simple split-and-shift.

2. DISCUSSION

A **smart pixel** is an electronic component with optical input and output ports. The complexity of a smart pixel is typically on the order found in a small programmable logic array (PLA), which may be a few logic gates or a few dozen logic gates.

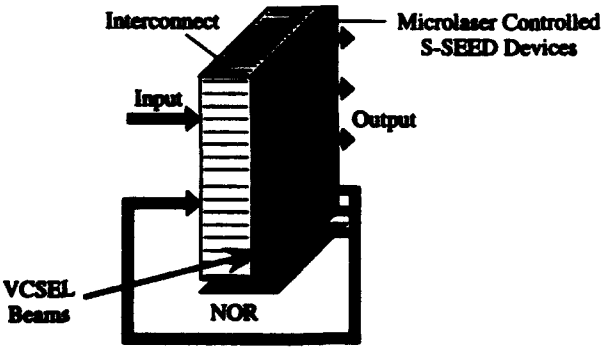


Figure 1: *Architectural model for the demonstration processor.*

†Dept. of Computer Science, Rutgers Univ., Hill Center, New Brunswick, NJ 08903, murdocca@cs.rutgers.edu
††Dept. of Computer Science, Evans Hall, Univ. of California, Berkeley, CA 94720, dvberger@cs.berkeley.edu
*Rome Laboratory/OCPB, Griffiss AFB, Rome, NY 13441-5700, battiatoj@lonex.rl.af.mil
**Wavefront Research, Inc., 1605 Main St., Bethlehem, PA 18018, tstone@cs.rutgers.edu

We consider the use of smart pixels as the basis for a reconfigurable processor, in which a static free-space interconnect (a perfect shuffle for this example) is customized to perform specific functions. Figure 2 illustrates a simple version of this scenario, in which the interconnects among full adders in a conventional ripple-carry adder are forced into a single stage of a perfect shuffle.

We know from permutation theory that a set of N inputs can be arbitrarily permuted at the outputs of a shuffle-exchange network of depth $3\log_2 N-1$. In Figure 2b, N=16 and so the depth of such a permutation network for the general case is 11. The example shown in Figure 2c is significant because it shows that the interconnects for at least one circuit can be forced into a *single* stage of a perfect shuffle structure, rather than the theoretical upper bound of $3\log_2 N-1$, and so no depth penalty is incurred with this approach. We were concerned that this mapping might only have been possible because the example is so small, and so we doubled the width of the adder, and found a mapping that still required only a single perfect shuffle stage. Two irregularly structured mappings were also investigated, involving the interconnection of PLAs for a 12-bit section carry lookahead (SCLA) adder, and a 16-bit SCLA. The interconnects are irregular, the PLAs have different sizes as measured by the varying numbers of inputs and outputs, and there is fan-out within the interconnect. These mappings were also successfully made using only a single stage of a perfect shuffle.

In summary, we have an opportunity for reconfiguring a static free-space interconnect to implement a variety of circuits simply by selectively enabling connections and appropriately labeling the PLAs. Little or no depth penalty is incurred despite the forced regularity.

3. REFERENCES

[1] Murdocca, M. J. and V. Gupta, "Architectural Implications of Reconfigurable Optical Interconnects," *Journal of Parallel and Distributed Computing*, vol. 17, no. 3, pp. 200-211, (Mar. 1993).

This work was jointly supported by the Air Force Office of Scientific Research and the Office of Naval Research under grant N00014-90-J-4018. The initial exploration that led to the function cache work was supported by the Strategic Defense Initiative Office under contract F49620-91-C-0055, which was administered through the Air Force Office of Scientific Research. The work reported in Section 2 was supported by Rome Laboratory through the SBIR program under contract F30602-91-6-0101.

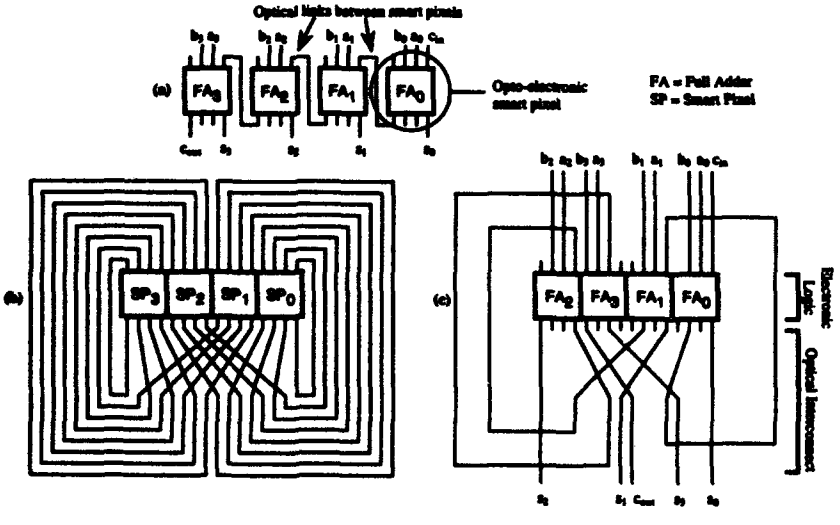


Figure 2: *Interconnects of a 4-bit ripple-carry adder (a) are mapped onto a single perfect shuffle. Generic interconnection topology (b); and customized interconnect for the adder (c).*

Optical Array Logic Network Architecture

Jun Tanida and Yoshiki Ichioka
Osaka University, Department of Applied Physics
2-1 Yamadaoka, Suita 565, JAPAN
Phone: +81 6 877 5111
Fax: +81 6 877 2900

A new concept called optical array logic network architecture (OAL-NA) is proposed for effective construction of optoelectronic hybrid computing system. With the help of optical array logic (OAL), not only data communication but also global data processing are implemented in the interconnection network.

I. Introduction

Digital optical computing is one of promising schemes for massively parallel computation in near future because of the common foundation with the current computer science. According to the concept, a lot of techniques including optical array logic (OAL)[1] have been proposed. However, quantitative estimation on processing capability suggests that a processing style in which all operations are executed by optical methods is inefficient and difficult to achieve processing capability comparable to electronic computing systems. Current electronic computers offer tremendous computational power, so that massive parallelism and ultra fast operation must be exploited in optical computing systems to overcome the electronic ones. Considering current status of researches on optical computing, we conclude that at least in near future optoelectronic hybrid optical computing systems are promising and practical. However, even for hybrid optical computing system, sophisticated architecture is required to fully utilize capabilities of optical computing techniques. In this paper, we propose a concept of optoelectronic hybrid computing system, in which OAL is used for high functional interconnection network.

II. Concept of OAL-NA

Optical array logic network architecture (OAL-NA) is a conceptual architecture of optoelectronic hybrid computing system. Essentially, multiple electronic processors execute arithmetic and logical operations in parallel and they communicates each other through optical interconnection network. The most important feature of the OAL-NA is that the optical interconnection network is implemented by OAL processor and provides high functionality: data communication, data search, data test, command delivery, and so on.

Figure 1 shows a schematic diagram of an example system of OAL-NA. In the system, multiple processing elements (PEs) with local memories are located on one plane (PE array) and a set of a global sharing memory and input/output processors are arranged onto another plane (MIO array). The two arrays are connected by an OAL processor with symmetric data flow. Export signals from one array are used as inputs of the following OAL processor and the output of the OAL processor is transferred to the other array. Electronic modules on the array complete encoding required in OAL and generate a coded image by composition of individual elements of the modules. Once the coded image is generated, the export signals from the electronic modules are processed by OAL. For the reversal data transfer, the same procedure is adopted. For inter-PE communication, round-trip routing is established. Specifying the OAL processor, we can achieve versatile functions.

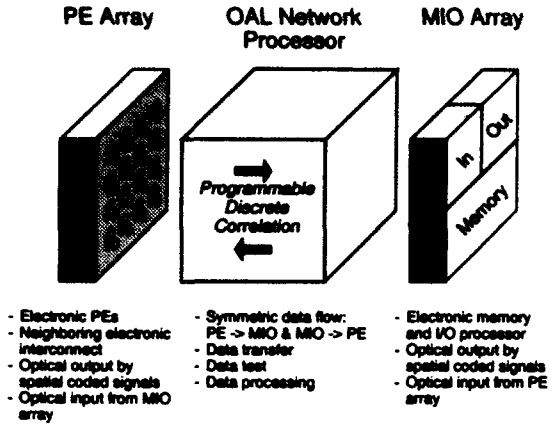


Fig. 1 Schematic diagram of OAL-NA

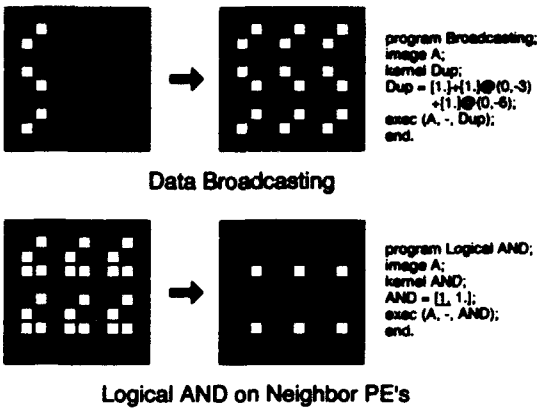


Fig. 2 Example operations in OAL-NA

III. Advantages of OAL-NA

OAL-NA has various advantages with respect to system construction and system capability. Use of highly developed microprocessor and smart pixel technologies for PEs is practical and matches with current trend of massively parallel architecture in computer science. It has been pointed out that optical interconnection in interchip level is advantageous over electronic one. In addition, merging interconnection with processing, the key idea of OAL-NA, is expected to provide more effective communication and system operation than conventional simple optical interconnection. OAL implements single instruction stream multiple data stream (SIMD) type of parallel processing, which is suitable for global search and test on the export data from PEs, memory, and input/output processors. In terms of processing complexity, global search and test are appropriate for OAL scheme and the advantages of OAL, *i.e.*, large processing capability and flexibility, can be effectively utilized. Although an encoding device must be prepared even for a simple OAL processor, the encoding process can be combined into each electronic modules and no additional device is required in OAL-NA.

IV. Operations on OAL-NA

OAL-NA provides various operations in the interconnection level. Typical operations are 1) data transfer (parallel data shift, broadcasting, exchange, token propagation[2]), 2) data test (conditional search, validity check), 3) data processing (differentiation, logical AND/OR for same/neighbor PE's), and so on. These operations are achieved by programming of OAL. Figure 2 shows the examples and corresponding OAL programs. Accumulated resource in OAL research can be fully utilized for OAL-NA.

V. Summary

In this paper, we have proposed a new concept called optical array logic network architecture for effective construction of optoelectronic hybrid computing system. With the help of optical array logic, not only data communication but also global data processing are implemented in the interconnection network. As a result, effective data communication and system operation can be expected.

References

1) J. Tanida and Y. Ichioka, Int. J. Opt. Comput. **1**, 113 (1990).
2) M. Iwata, J. Tanida, and Y. Ichioka, Appl. Opt. **31**, 5604 (1992).

Cascaded Optical Data Transfer Through a Free Space Optical Perfect Shuffle

M.W. Derstine, S. Wakelin and K.K. Chau

Optivision, Inc.
4009 Miranda Ave
Palo Alto, CA 94304

We describe the design, fabrication and testing of an optical interconnect system constructed from a two dimensional array of symmetric self-electro-optic effect devices and a free space perfect shuffle module.

The perfect shuffle has been proposed as an efficient interconnect that optics can do well[1]. However, to our knowledge, no free space optical system has been constructed that tests the operation of a shuffle between optical logic elements. Most previous work has focused on the development of the perfect shuffle optics without regard to interfacing to the optical logic elements.

An optical system designed to be used to implement sequential logical processing has been fabricated and used to demonstrate transfer of optically encoded data from an optical logic array though a pertect shuffle interconnect and back onto the logic array. An array of self-electrooptic effect devices (S-SEEDs) [2] serve as the logic array and the perfect shuffle is similar to that developed at Heriot-Watt University [3].

The basic architecture is shown in Figure 1. The input, output and power supply optics are not shown. The primary optical circuit is implemented in a loop. The S-SEED array is divided up so that each column corresponds to one stage of the interconnect. The output of the S-SEED array is routed through a one-dimensional perfect shuffle module and then imaged back onto the S-SEED array displaced by one column. This produces a multistage interconnect with perfect shuffles between each stage.

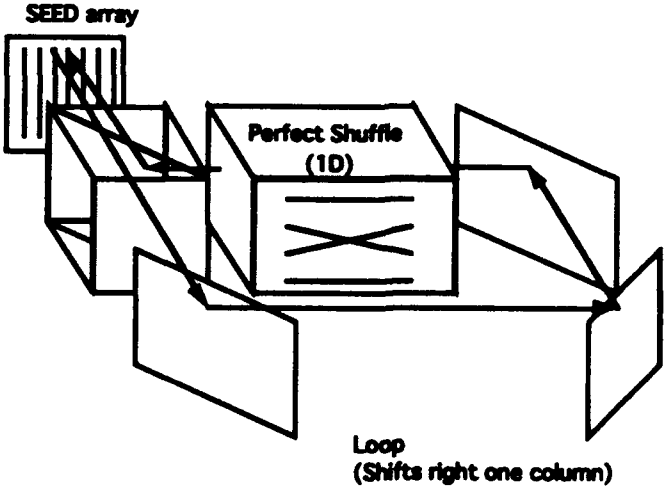


Figure 1. Interconnect architecture

The S-SEED array is arranged to so that it is used as 8 columns of 16 devices each. This size was selected to match the field of a commercial 7.78 mm laser objective used to image the S-SEED. Spots to read out the array are generated by two lasers, one for the even columns and one for the odd columns. The necessary spot pattern is generated by a binary phase diffractive element.

The perfect shuffle employs the basic split-and-shift approach to implement a theoretically lossless interconnect [3]. Its other major advantages are that it can be constructed from readily

available components, it could be aligned in stages, it has identical loss (theoretically zero) for all the beams through the system, it could be enhanced to provide internal fanout, and would work with data in differential representation. Another important advantage is that it could be designed to maintain telecentric imaging through the shuffle and anamorphic optics.

The cascaded input of data is provided by an electrically addressed linear array of vertical cavity surface emitting lasers (VCSEL). It is used to set the first column of S-SEEDs. The VCSEL array is directly driven with an open-collector TTL circuit that is also used to sequence the column and programming lasers.

Figure 2 shows a schematic of the basic system. Light from the even and old column laser is combined and then the array of spots is generated. These spots are then directed through a beam combining system and focused onto the S-SEED array. The reflected light from the S-SEED is shuffled and then has the spot pitch corrected by an anamorphic telescope before being combined and imaged onto the S-SEED array. The entire system is doubly telecentric for improved alignment tolerance, except at the intermediate focus of the anamorphic telescope. The system was constructed using the milled baseplate approach [4].

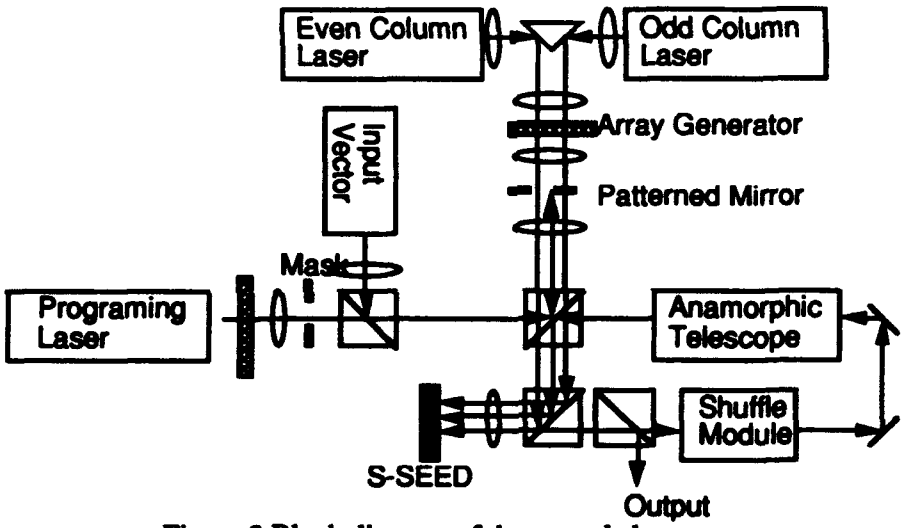


Figure 2 Block diagram of the cascaded system.

The system has been assembled and aligned and demonstrated cascaded data transfer at 10 kHz. The design and alignment process have uncovered issues relating to cascading of devices, operation of the perfect shuffle and free space optical system design.

In conclusion, we have demonstrated the first, to our knowledge, free space optical system that cascades light through a perfect shuffle. This system was constructed using bulk optics and employed a 16x8 array of S-SEEDs.

We wish to thank Robert A. Morgan of AT&T for providing the laser array. This research is supported by the Advanced Research Projects Agency of the Department of Defense and was monitored by the Air Force Office of Scientific Research under Contract No. F49620-92-C-0050. The United States Government is authorized to reproduce and distribute reprints for governmental purposes notwithstanding any copyright notation hereon.

References

1. A.W. Lohmann, W. Stork, G. Stucke, Applied Optics, Vol. 25, No. 10, May 1986.
2. A.L. Lentine and D.A.B. Miller, IEEE J. Quant. Electron. **29**, 655-669 (1993).
3. S.Wakelin, "Design and construction of a free-space digital optical information processor," Ph.D. Thesis, Heriot-Watt University (1992).
4. J. Brubaker et al., Proc. SPIE **1533** (1991) 88-96.

Optical circuitry for data transcription and digital optical logic based on photothyristor differential pairs

Hugo THIENPONT[1], Thierry VAN DE VELDE[1], Andy KIRK[1], Werner PEIFFER[1], Maarten KULIK[2], Wouter STEVENS[1], Jesús FERNANDEZ[1], Irina VERETENNICOFF[1], Roger VOUNCKX[2], Paul HEREMANS[3], Gustaaf BORGHS[3]

1) Free University Brussels, Applied Physics Department (TW/TONA), Lab for Photonic Computing and Perception, Pleinlaan 2, B-1050 Belgium
tel 0032-2-6413569 (629 from 1/5/94) fax 0032-2-6413450 (629 from 1/5/94)
2) Free University Brussels, Applied Physics Department (TW/TONA), Lab for Microelectronics and Technology, Pleinlaan 2, B-1050 Belgium
3) Interuniversity Micro Electronics Center, Kapeldreef 75, B-3001 Leuven, Belgium

Abstract

We present a novel technique for parallel optical data transcription and digital logic with high speed differential pairs of optical thyristors and demonstrate these vital operations with compact optical hardware circuitry.

Summary

Among the very promising elements for digital parallel optical information processing are differential pairs of PnpN optical thyristors. It has been shown very recently that these optical detector-regenerator type of devices can be switched-on in very short times (typical 10 ns) with very low switching energies (typical 40fJ of absorbed optical energy), while the problem of slow switch-off times, causing unpractical cycle times, was tackled using a double-heterojunction structure that can be completely depleted by means of a simple negative anode-to-cathode low voltage pulse. In this way PnpN thyristors with switch-off times of 10 ns became available [1].

First , we will propose in this paper a novel approach to perform two vital functions in digital optical computing using these high speed differential pairs of optical thyristors, namely *optical data transcription* and *digital optical logic*. We therefore use a differential pair with a particular electrode configuration such that each thyristor of the differential pair (i.e. T_a and T_b) has two topelectrodes (see Fig1). This makes it possible to control electronically the position of the optical output of the activated thyristor. For example, if thyristor T_a wins the competition with thyristor T_b, the two topelectrodes of T_a allow for three different light output combinations, depending on the voltages applied (see Fig2). Our conventions to represent the logic 1 and a logic 0 states are depicted in Fig3. Moreover, these topelectrodes can be normally-connected or cross-connected. We show that cascading one cross-connected and two normally-connected differential pairs of optical thyristors in the proper sequence, and providing them with the correct and synchronized voltage sequences allows the performance of AND, OR, NAND and NOR logic functions.

Next, we will present an optical hardware circuit, for cascading and interconnecting these differential pairs, such that both digital optical logic and optical data transcription become possible. The optical hardware consists of quarter pitch GRIN lenses and cube splitters; components that can be easily packaged with the thyristor chips into very compact and stackable optical processing modules.

Finally, we show videotaped experimental results of optical data transcription and digital optical logic, and we discuss operation speed as a function of the optical energy transfer efficiency of the optical hardware circuitry.

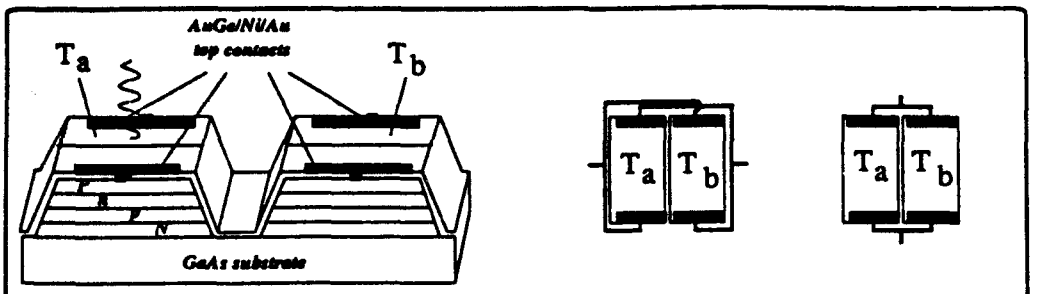


Fig. 1 : Differential pair of optical thyristors, in the cross-connected and normally connected configurations

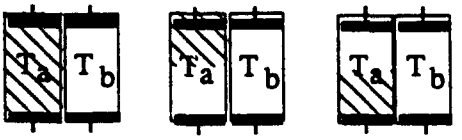


Fig. 2 : Joint and separate turn-on of thyristor Ta

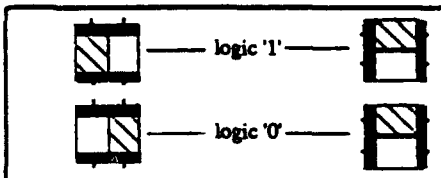
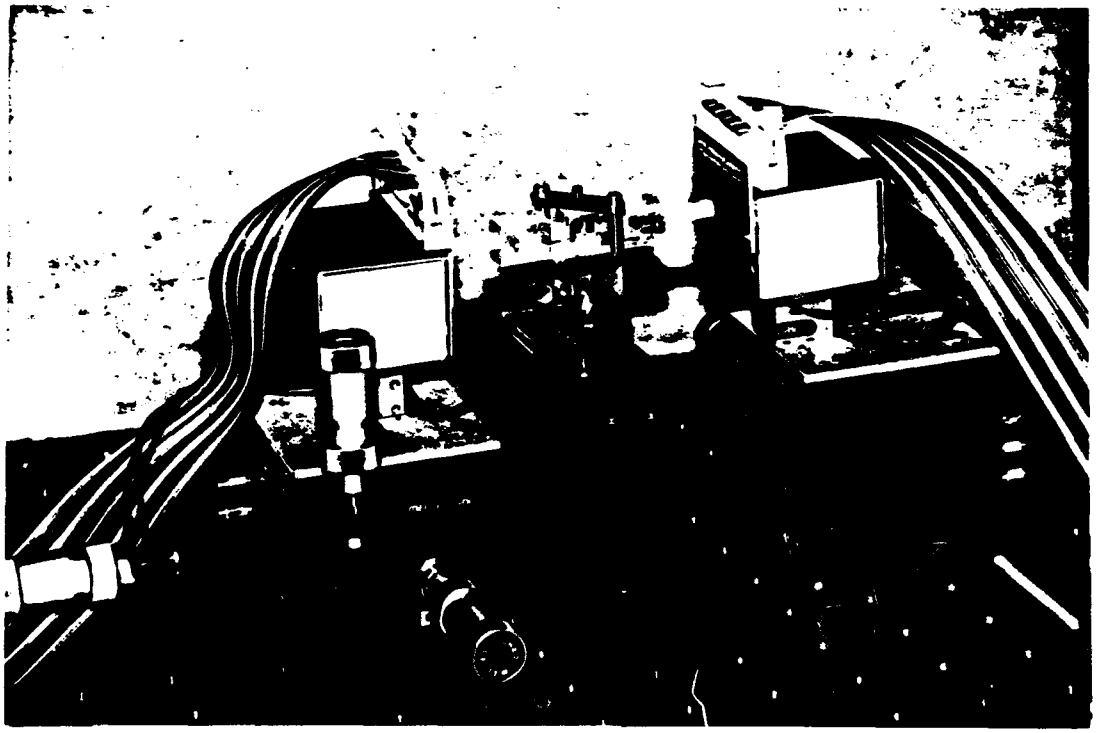


Fig. 3 : Logic convention



Reference: [1] P. Heremans, M. Kuijk, D.A. Suda, R. Vounckx, R.E. Hayes and G. Borghs, "Fast turn-off of two-terminal double heterojunction optical thyristors", *Appl. Phys. Lett.*, **61**(11), pp. 1326-1328, 1992.

Optoelectronic Multiport Associative Memory for Data Flow Computing Architecture

V.B. Fyodorov

Scientific Computer Centre, the Russian Academy of Sciences, Leninsky pr. 32 A, Moscow, 117334, Russia. Tel: (7-095)938-6646. Fax: (7-095)938-6986.

An associative memory is of primary importance in data flow digital computers [1]. Such a memory searches by special code (key) coming out of processing unit (PU) for a data set to be transferred to the next operation for an execution. A high-speed, high-capacity optoelectronic associative memory (OAM) implemented of K one-port OAM modules, where K is the number of PUs [2,3] requires using in data flow computing architecture the high-performance reconfigurable rearrangeable nonblocking interconnection networks of size KxK. Its realization is highly conjectural nowadays.

In this report, the new optical setups of multiport OAM are suggested. The OAM enables M users to execute a simultaneous and independent parallel associative data search and retrieval into memory N stored words by M search arguments, as well as a random-access writing of keys and data. The exploitation of such a multiport associative memory in data flow digital computers is illustrated by the block diagram in Fig. 1. The circuit diagram that explains the principle of the optoelectronic multiport memory with the parallel optical associative M key search for M=4, L=4, and N=16, as examples, is shown in Fig. 2. Spherical lenses are employed in the setup only. The hybrid memory board (HMB) is a 2-D memory cell array, where each memory cell consists of the light modulator and MOS-transistor-based trigger placed near it and electrically connected to the light modulator and with key information stored into electronic semiconductor memory. The address writing of keywords in the HMB, encoding and decoding of memory cell physical addresses and data associated keywords is accomplished by the electronic devices that include in the semiconductor memory. The stored keywords are registered as transparent and nontransparent areas corresponding to 1 or 0 of the binary bit b_{ln}. The functions of masked search argument registers are accomplished by the light source arrays. The availability or absence of light beam corresponds to 1 or 0 in the binary bit a_{lm} of search argument. The physical coincidence addresses c_{mn} are fixed by photodetector arrays which serve as threshold optical invertor arrays. The OAM scheme represented in Fig. 2 ensure an associative search in the HMB in light transmission mode. However, if light polarization plane modulators are employed for the HMB it can be modified to operate reflected light by using polarizing beam splitter cube placed before the lens of the hybrid memory board.

The data search process for such an OAM consists of the following. The binary bits a_{1m}, a_{2m} ... a_{Lm} of all (m = 1,2. ... M) search arguments produced are encoded by a dual-rail code and binary bits b_{1n}, b_{2n} ... b_{Ln} of all (n = 1,2, ... N) keywords are stored in an inverse dual-rail code. The optical system projects each search argument image onto the keys stored on the HMB and the result of coincidences (i.e. ight absences) are fixed by threshold optical invertor arrays. As seen in Fig. 2 the optical invertor with the numbers m and n fixes the fact of coincidence of the mth search argument with the nth key.

In the report, a same variants of the optical scheme for the multiport optoelectronic memory with associative data search are suggested. The method for enhancing the memory size and write rate based on combining the K multiport OAM modules into the whole system is considered. It is shown that such a mulimodule OAM can provide a simultaneous and independent M key search for the number of ports M=100 with an associative data access time

of ~10 *ns* and overall peak write and readout rate of 10^{10} words into memory of overall capacity of up to KN = 10^7-10^8 words with 50-bit dual-rail coded keys The possibility of creating the multiport OAM is discussed.

1. Burtsev V.S., *Optical Computing & Processing*, 1, 1991, no. 4, p. 269.
2. Burtsev V.S. and Fyodorov V.B., *Optical Computing & Processing*, 1, 1991, no. 4, p. 275.
3. Burtsev V.S. and Fyodorov V.B., *Optical Computing & Processing*, 2, 1992, no. 3, p. 161.

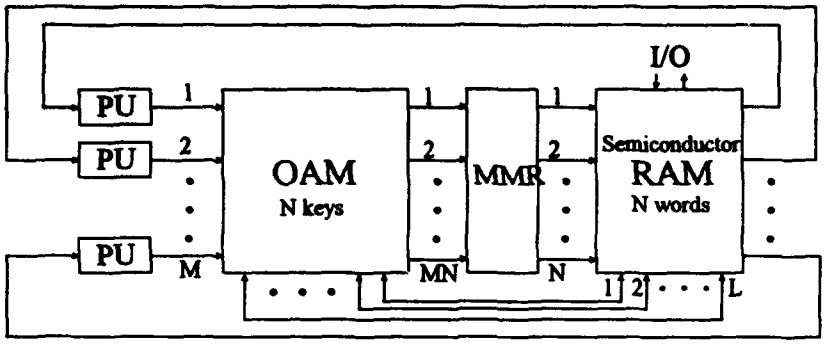


Fig. 1. A simplifyed block diagram of the data flow computer based on the multiport associative memory: PU-processing unit, I/O-input and output, MMR-multiple-march resolver and encoder.

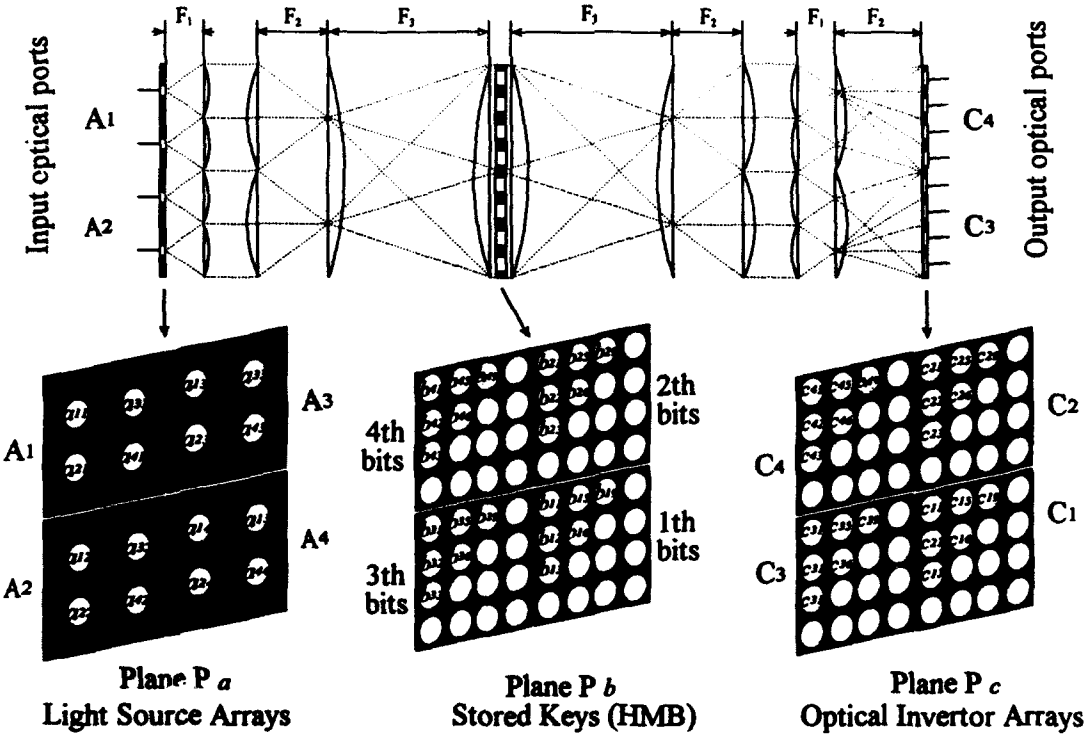


Fig. 2. The optical scheme of the optoelectronic multiport memory with parallel associative M key search: a_{lm} is the lth binary bit (l=1,2, ... L) of the mth search argument word (m=1,2, ... M), $_{ln}$ is the lth binary bit of the nth stored keyword (n=1,2, ... N), c_{mn} is the physical address of the coincidence of the mth search argument with the nth keyword.

AN ANALOG RETINA FOR EDGE DETECTION

Chunyan WANG, Francis DEVOS
Institut d'Electronique Fondamentale, Bat.220, Université Paris Sud
91405 Orsay Cedex FRANCE
Tel. 33-1-69416574

Abstract

We present a very simple optoelectronic analog retina which we constructed, using a CMOS technology. The experimental results indicate that the system is capable of acquiring optical data of an image and detecting the edges.

Summary

Each basic cell in this retina contains only 21 transistors (surface : 4.9 mm²). When connected to the photodiodes it is able to do the data acquisition, optical-electric signal transformation, calculation for edge detection and data shifting. The retina is expected to be formed by 128*64 such cells.

The algorithm implanted in the circuit is based on the "Roberts" differential detection(Fig.1-a and Fig.1-b). Compared to the "classic Roberts" detection four supplemental operators are introduced into the template impulse response arrays in order to improve the sensitivity of edge orientation (S3, S4, S5, S6 on Fig.1-a). The complixity of the circuit for such an improvement remains the same.

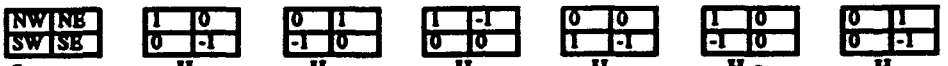


Fig.1-a H_{R1} H_{R2} H_{S1} H_{S2} H_{S3} H_{S4}

H_{R1}, H_{R2} : classic Roberts differentiators $H_{S1}, H_{S2}, H_{S3}, H_{S4}$: supplemental differentiators



F(m,n) : original image
Hi(m,n) : spatial diffrentiator
Gi(m,n) : gradient in the *i* th direction
G (m,n) : gradient after the compass
E (m,n) : edge map

Fig.1-b General procedure of the "Roberts" detection

Fig 2 shows the results of the "KHOROS" simulation for the detection algorithm.



Fig.2 *(a)* *(b)* *(c)* *(d)*

(a) Original image
(b) Edge map of the "classic Roberts"
(c) Edge map attained by using the first four "Roberts" operators. Some diagonal lines missing on Fig.2-b show up here.
(d) Edge map attained by using all the six "Roberts" operators. There aren't any significant differences between Fig 3-c and Fig 3-d

In fact the operation of the "Roberts" spatial convolution is the combination of subtractions of the four neighboring pixels. If the luminous signal varies slowly compared to the speed of the treatment, we can decompose the calculation in terms of time to eliminate two operations :

1/ absolute value, since the operaion of $|F_i-F_j|$ can be replaced by " max $\{(F_i-F_j), (F_j-F_i)\}$".
2/ max value, this operation is followed by a comparison with a fixed threshold, we can replace the two operations by comparing all the possible input data to the threshold successively. As long as the result of the comparison is true, "1" is writen to a memory.

So, the general procedure (Fig.1-b) can be simplified as the iterated sub-procedures with only subtraction, comparison and writing "1" in the memory (Fig.3). In this case the acquisition should be

also iterated to get all the necessary combinations of the signals. Each acquisition is immediately followed by the sub-procedure. The procedure of the detection for each cell is shown in Fig.3.

The calculation becomes "parallel and sequential". The processing time is a bit longer than the "total parallel", but the implantaion is much simpler. A compromise between the speed and the simplicity is reached.

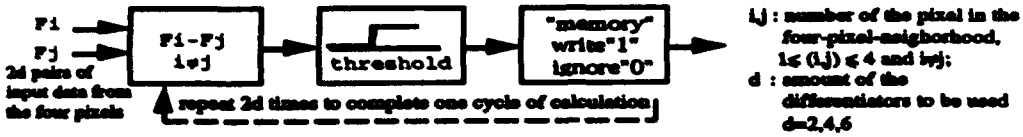


Fig.3 Simplified procedure of the "Roberts " detection for the "parallel and sequential" implantation.

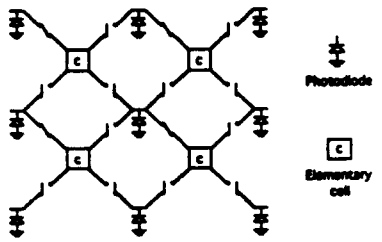


Fig.4 Pixel array

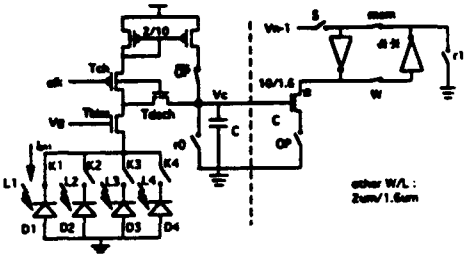
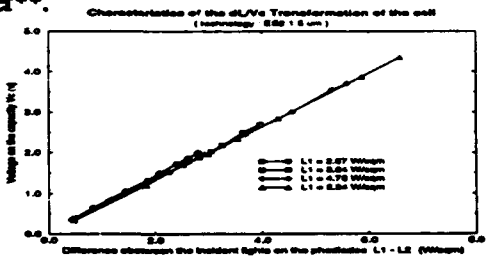


Fig.5 Scheme of a basic cell

Fig.4 shows the spatial arrangement of the pixels and Fig.5 is the scheme of a basic cell with the four neighboring photodiodes.

The left part of the cell converts the difference between incident intensities (L1-L2, for instance) into the voltage on the capacity C. By turning the four switches (K1~ K4) on or off, we can choose the data to be calculated. The control signal "clk" drives the transistors T_{ch} and T_{dech} in order for the capacity C to be charged (by means of the current mirror to change the sign of the photocurrent) then discharged by the photocurrent. Thus the voltage V_c is the function of the difference of the incident light. By choosing the value of Vg, the grid voltage of T_{bias}, we can stabilize the bias of the photodiodes, therefore improving the linearity of the transformation.

The right part of Fig.5 performs the comparison, memorisation of "1" (ignore "0"), and data shifting to the output. The value of the threshold is related to the sizes of the transistor* and the inverter**.



A prototype of the cell with four photodiodes is produced in ES2 1,5um process. The expected test results : the characteristics of the left part of Fig.5 is shown on Fig.6.

Fig.6 Test results of the linearity of the ΔL/Vc transformation

Because of the dynamic configuration of the pixel array, for each cell, the data carried by incident light on the four neighbouring photodiodes are accessible and selectable. All the basic calculations for the detection are performed by the cells, yet the order of these calculations can be simply rearranged by modifying the sequence of the control signals. So both "classic Roberts" and "modified Roberts" can be implemented in the same circuit. This allows the future users to have more flexibility to meet different needs.

We are still trying to improve the performance of the circuit, especially the linearity of the optical-electric transformation. One of the improvements in the future version of the circuit is the compensation for the imperfection of the current mirror, a critical part of the circuit. This will be done by means of an adaptive control, for example, a charge transfer or/and an analog memory.

References

(1) R. Moignard,E.Daniel, P.Cambon and J.L.de Bougrenet de la Tocnaye,"Design of a Silicon VLSI/FLC Smart Light Valve for ParallelOptical Information Processing", 8th Workshop on Optical Computing, Paris , 1992
(2) L.Guibert, G.Keryer, P.Pellat and J.L.de Bougrenet de la Tocnaye,"Compact Optical Correlator for Roadsign Recognition"
(3)William K. Pratt, "Digital Image Processing", Wiley Interscience, 1991
(4)Douglas A. Ross, " Optical Devices and Optical Imaging Techniques",1979
(5) M.Zhang, J.F.Pone, F.Devos, "Etude d'une Cellule de Mémorisation Analogique non-volatile par EFFET Tunnel en Technologie Standard CMOS 2,4um" GCIS, Grenoble Fevrier 1993
(6) Y.Ni, Y.Zhu, B.Arion, F.Devos, " Yet Another 2D Gaussian Convolver", ISCA93, Chicago, 1993

Theoretical Results on Accuracy Limitations in Analog Optical Processors

Doğan A. Tunuçin, John F. Walkup, and Thomas F. Krile

Dept. of Electrical Engineering, Texas Tech University
Lubbock, Texas 79409-3102, USA, (806) 742-3575

Abstract

A complete statistical analysis and modeling of a generic three-plane optical processor is presented. Output signal statistics are determined for a number of interesting special cases, and the fundamental theoretical accuracy limitations are established.

Summary

The most important and prominent strengths of optical processors are their speed and parallelism. However, they also suffer from some fundamental drawbacks, the most critical being low computational accuracy, that limit their application to real-world problems.

The noise sources that determine, and bound, the accuracy of an optical processor fall into two groups. On one hand, we have the system noise sources, such as diffraction, crosstalk, and background radiation, that arise from the processor architecture. On the other hand, we have the device noise sources that introduce inevitable inaccuracies associated with the physical representation and interpretation of the information-bearing signals in the system. Of particular significance are the noise in the input light intensities due to photon, excitation, and emission fluctuations, the randomness in the SLM intensity transmittances due to transmission and polarization fluctuations, and the noise in photodetection due to nonunity quantum efficiencies, gain fluctuations, shot noise, dark current, and thermal noise. Given the statistical description of these processes, one can then utilize tools from statistical optics to establish the statistics of the system output signal.[1,5] Based on these results, optimal detection- and estimation-theoretic techniques can be brought to bear on the problem in an effort to improve the accuracy of the processor, as we demonstrated earlier in proof-of-principle simulations.[2,3]

Toward this end, we first carried out a general statistical analysis of a Stanford-type optical matrix-vector multiplier under certain simplifying assumptions,[2] establishing the probability density and mutual coherence functions of the detected field intensity and the photodetector output current in terms of the statistical characteristics of the system components. We then passed to a more general and rigorous study of a generic three-plane processor, thus expanding our scope to a wider class of systems including optical correlators, optical interconnects, and optical linear algebra processors.[3,5]

We next turned to evaluating these expressions for particular cases of interest, obtaining system output statistics for various combinations of sources, modulators, and detectors.[4] Specifically, we considered classical sources such as laser diodes and LEDs, and popular photodetectors such as *p–i–n* and avalanche photodiodes. Since statistical models for most SLMs are currently unavailable, we considered hypothetical models such as a neutral device with no transmittance fluctuations and a Gaussian random amplitude/phase screen. Free-space propagation was assumed, and Fresnel-regime diffraction as well as the geometrical-optics limit were considered.

In this paper, after briefly reviewing these preliminaries, we proceed to establish the overall system output statistics for a number of interesting device combinations. We then provide a quantitative definition of accuracy for analog optical processors, first from a detection-theory perspective and then from an estimation-theory perspective. With the availability of the output signal probability density function, the maximum achievable accuracy for each special case is then found as a function of the system parameters involved. We also present theoretical results on the attributes of speed and parallelism, which are intimately related to accuracy. Finally, future work on accuracy enhancement is suggested.

References

[1] J. W. Goodman, *Statistical Optics* (Wiley, New York, 1985).

[2] D. A. Tinnuçin, J. F. Walkup, and T. F. Krile, "Accuracy enhancement in optical linear algebra processors," *OSA Tech. Digest Series* **23**, 81 (1991).

[3] D. A. Tinnuçin, J. F. Walkup, and T. F. Krile, "A decision-theoretic approach to accuracy enhancement in optical processors," *OSA Tech. Digest Series* **17**, 73 (1992).

[4] D. A. Tinnuçin, J. F. Walkup, and T. F. Krile, "Statistical analysis and modeling of analog optical processors," *Proc. SPIE* **2026**, 204-215 (1993).

[5] D. A. Tinnuçin, J. F. Walkup, and T. F. Krile, "Accuracy in analog optical processors: statistical analysis," *J. Opt. Soc. Am. A* (to appear in Feb. 1994).

Time-Integrating Correlation Using a Fiber Optic Delay Line Processor

R. A. Athale and G. W. Euliss
Department of Electrical and Computer Engineering
George Mason University
4400 University Drive
Fairfax, Virginia 22030
Phone: (703)993-1585, e-mail: rathale@gmu.edu

Abstract

A fiber optic tapped delay line correlator based on time-integration is proposed and demonstrated. Such a correlator will combine high bandwidth, large processing gain and ability to compute real-time autocorrelation functions.

Summary

Fiber optic delay lines have been suggested for use in tapped delay line architectures for performing cross-correlation operations[1,2,3]. In those systems fibers of different length implement the delay lines and a spatial\light modulator encoded the tap weights. Although attractive due to the potential for high bandwidth operation, this system suffers from two major limitations. The number of taps limits the signal length and therefore the correlation gain. Since each tap introduces signal loss, the total number of taps will be limited to a few hundred. Additionally, the system shown cannot implement real-time cross-correlations between two arbitrary signals. Similarly, calculation of the autocorrelation of a signal requires temporary storage of the signal and high bandwidth updating of tap weights.

Both of these limitations can be overcome by using an alternative design based on time-integration. Figure 1 shows a diagram of a fiber optic tapped delay line time-integrating correlator. The input signal s(t) directly modulates a laser diode. The modulated optical signal is split by a 1-to-N fiber coupler and a relative delay is introduced into each of the N channels by adjusting the length of the fibers. The second input signal r(t) is applied to a high bandwidth optical modulator. The time-delayed representations of s(t) are modulated by r(t) and imaged onto a 1-D time-integrating detector array. The output of the n^{th} detector at the end of the time-integration will correspond to:

$$c(n) = \int s(t-T_n)\, r(t)\, dt$$

where T_n is the relative time-delay in the n^{th} fiber tap and the integration is performed over time t. The correlation gain is determined by the integration time of the detector array and is independent of the number of taps. The number of taps determines the number of points computed in the correlation function. Therefore, the time-integrating architecture can accommodate a longer signal length while limiting the number of points in the cross-correlation function to the number of taps. If signals s(t) and r(t) are identical, autocorrelation results.

This architecture was experimentally demonstrated in an 8-channel correlator. A TeO_2 acoustooptic modulator A 100 MHz analog LED at 850 nm provided the light input. The output was detected on a CCD camera and digitized. Although the AO device has a 50 MHz bandwidth, the fiber outputs were focused to approximately 100 micron spot in the device leading to a transit-time limited bandwidth of only 5 MHz. The schematic diagram of the experimental setup is shown in Figure 2. The experimental results obtained on a sampled autocorrelation of a 5 MHz square wave are shown in Figure 3. The points indicate theoretical values and the continous line shows experimental results.

---

1. K. Wilner and A. P. van der Heuvel, Proc. IEEE, 64, 805 (1977).
2. R. L. Ohlhaber and K. Wilner, Electro-optical Syst. Des., 9, 33 (1977).
3. K. P. Jackson and H. J. Shaw, in "Optical Signal Processing", J. L. Horner ed., Academic Press, 1987.

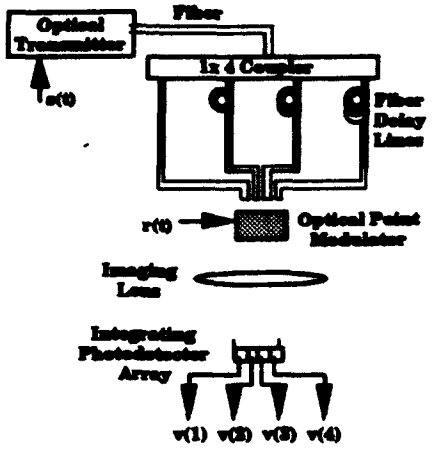


Figure 1: Schematic diagram of fiber optic time-integrating correlator

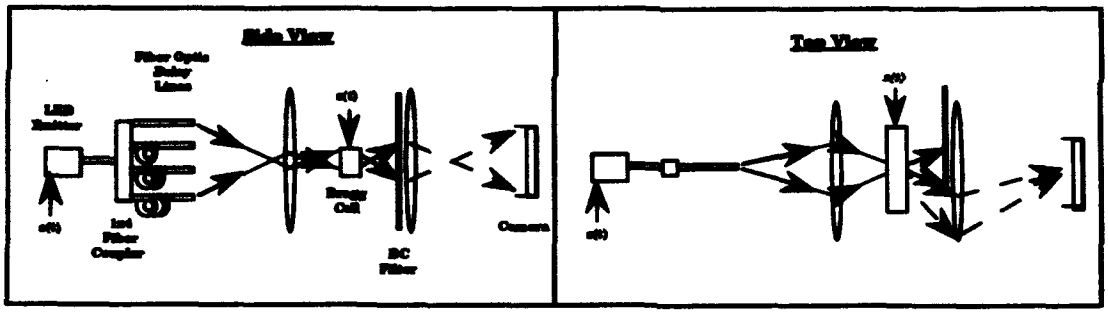


Figure 2: Schematic diagram of the experimental set up

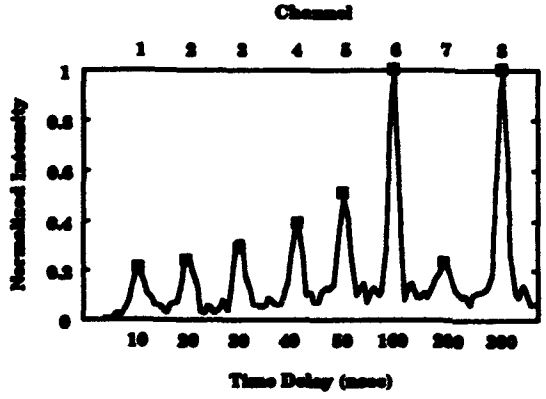


Figure 3: Experimental results of an 8-channel fiber optic time integrating correlator

Experimental implementation of a joint transform correlator providing rotation invariance

Laurent Bigué, Michel Fracès* and Pierre Ambs

Ecole Supérieure des Sciences Appliquées pour l'Ingénieur - Mulhouse (ESSAIM)
Université de Haute Alsace
12, rue des Frères Lumière
F-68 093 Mulhouse Cédex France
☎: (33) 89 59 69 34 (L. Bigué), (33) 89 59 69 30 (P. Ambs)

* ONERA-CERT
Département d'Optique
2, avenue Edouard Belin
BP 4025 F-31 055 Toulouse Cédex France
☎: (33) 61 55 71 07

ABSTRACT:

We optically experiment a joint transform correlator (JTC) where the input image is replaced by a synthetic discriminant function (SDF) filter. This latter allows us to ensure a practical invariance over a 10° range.

INTRODUCTION:

Optical correlation, and especially joint transform correlation, has been known as an efficient alternative to its electronical counterpart since the 1960's and compact implementations of joint transform correlators (JTCs) have recently been presented. But correlation is inherently rotation- and scale- variant and a traditional correlation operation cannot perform pattern recognition in most practical cases. In order to overcome this limitation, Javidi[1] has proposed and simulated a JTC using synthetic discriminant function (SDF) filters. In this paper, we provide optical experimental results.

BASIC THEORY:

The basic principle of joint transform correlation is now widely known, and we will not present it. The need of ensuring, for instance, a rotation invariance appears clearly: an in-plane rotation of one degree causes a dramatic energy loss of more than 3 dB. To achieve an invariance for such a phenomenon, we decided to use the synthetic discriminant function technique[2], a general method to achieve any invariance which in our case consists in replacing the reference image with several rotated views. The correlation peak height will be equal, provided the input view belongs to the training set. The point is to test intermediate-rotated input views, between those of the training set.

The simplest SDF filter is called pseudo-inverse SDF (PI-SDF). Its computation is straightforward because it is only a linear combination of views from the training set. Other types of filters have then been derived from it: the minimum variance SDF[3] (MV-SDF) which is noise resistant, the minimum average correlation energy[4] SDF (MACE-SDF) which sharpens the correlation peak and improves discrimination and the optimal trade-off SDF[5] (OT-SDF) which is a linear combination of the previous two filters.

SIMULATIONS:

We tested the four kinds of SDFs mentioned above, in order to verify their training ability. For each type of filter, we calculated four filters, each of them containing 6 views, with a various angular step between two consecutive views: 0.5°, 1°, 2° and 4°.

The simulations give the same results as those in the literature for the 4f architecture: the PI-SDF training ability is average: there is a marked difference between the images belonging to the training set and images of the same airplane, but not in the training set. The discrimination between the plane of the training set and another lifelike plane is unambiguous (the ratio of the

correlation peak heights is over 4). The MACE-SDF only recognizes the views it contains and so proves useless, and the MV-SDF produces a very poor discrimination, sometimes close to unity.

EXPERIMENTS:

We performed experiments on the CERT Optical Science Department demonstrator, in which SLMs are amplitude-modulating.
We tried to test the four kinds of filters previously simulated. Unfortunately, MACE-SDFs, MV-SDFs and so OT-SDFs prove unusable: they are non-positive, so produce a non-zero background on our amplitude SLM and especially their dynamic range is high. The input setup cannot display both a large dynamic range and tiny details.
We experimented 6-view PI-SDFs, with respective angular steps of 0.5°, 1.°, 2.° and 4.° between consecutive planes. For a 0.5, 1 or 2° difference, the output response is quite uniform over the angular range: +/- 7 % (see fig. 1 for the 2° step). The training ability is good: we cannot even find any difference between the images belonging to the training set and images of the same airplane which are between those in the training set. The discrimination is also good (the ratio of the peak heights is at least 1:5).
For a 4° difference, the results deteriorate dramatically (fig. 2) and are not in good agreement with the simulations.

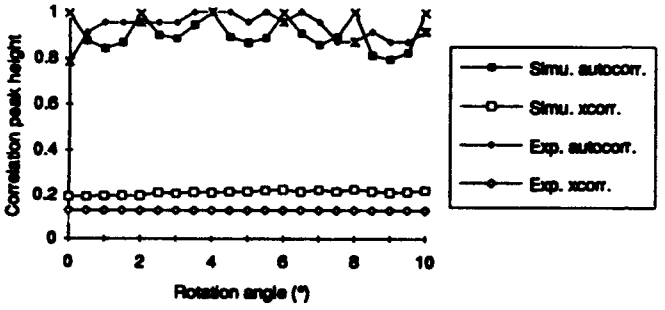


Fig. 1: simulated and experimental correlation peak heights for a SDF whose views differ from 2°. Crosses denote autocorrelation when the input view belongs to the training set

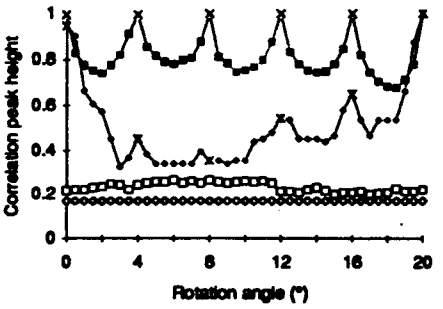


Fig. 2: simulated and experimental correlation peak heights for a SDF whose views differ from 4°. Crosses denote autocorrelation when the input view belongs to the training set

CONCLUSION:

We have implemented a joint transform correlator using synthetic discriminant function filters. The experiments proved that the MACE-SDF and the MV-SDF -and so the OT-SDF- cannot be displayed correctly on an amplitude SLM. But the PI-SDF which is correctly displayed, works. We have shown that for an in-plane rotation and provided that the angular step between the views it contains is not too high, this filter can lead to an unambiguous discrimination, for any object orientation over the filter angular range: it has shown a certain training ability and especially, that it could be optically implemented, without too much damage, into JTC architectures whose compact examples have become popular.

REFERENCES:

1. B. Javidi, "Synthetic discriminant function-based binary nonlinear optical correlator", Appl. Opt. 28 (13), 2490-2493 (1989).

2. H.J. Caulfield and W.T. Maloney, "Improved discrimination in optical character recognition", Appl. Opt. 8 (11), 2354-2356 (1969).

3. B.V.K. Vijaya Kumar, "Minimum-variance synthetic discriminant functions", J. Opt. Soc. Am. A 3 (10), 1579-1584 (1986).

4. A. Mahalanobis, B.V.K. Vijaya Kumar and D. Casasent, "Minimum average correlation energy filters", Appl. Opt. 26 (17), 3633-3640 (1987).

5. P. Réfrégier, "Optimal trade-off filters for noise robustness, sharpness of the correlation peak, and Horner efficiency", Opt. Lett. 16, 829-831 (1991).

Optimal Non Linear Filtering for Pattern Recognition and Optical Implementation

Ph. Réfrégier[1], B. Javidi[2], V. Laude[1], and J.-P. Huignard[1].
[1]: Laboratoire Central de Recherches
Thomson-CSF 91 404 Orsay cedex France. Tel.: 33 1 69 33 91 56
[2]: Univ. of Connecticut, Dept. of Electrical Engineering,
Storrs, Connecticut 06269-3157. U.S.A. Tel.: 19 1 203 486 2867.

January 19, 1994

Abstract

An optimal processor for discrimination and noise robustness is developed for pattern recognition. It leads to a natural and attractive high speed optical implementation. Furthermore, it provides theoretical insight in previous heuristic non linear filtering techniques.

Within the past decade different architectures for optical correlators have been demonstrated [1–3]. Although the spatial matched filter is optimal for noise robustness, its limitations such as broad correlation peaks, sensitivity to distortion and low discrimination capabilities are well known and different filters for optical correlation have been proposed [4–7]. On the other hand, nonlinear joint transform correlators (JTCs) [3], have shown to be very discriminant with good correlation performance. For optical correlation characterization, different criteria have been proposed [8], and among them, noise robustness and sharpness of the correlation function have been shown to be of the first interest. Furthermore, the importance of finding trade-offs between different criteria is now well established [7,8]. However, up to now, the discrimination capabilities of the filter are optimized indirectly by minimizing either the sharpness of the correlation function [7] with false objects (that is objects to be rejected) or background models to be discriminated against [9]. Here, an optimal method for discrimination capabilities which doesn't need *a priori* knowledge of the false objects or of the background is introduced.

1D notations are used for simplicity with no loss of generality. Let $r(t)$ and $s(t)$ denote respectively the reference and input image. The output of the optimum processor, $C(t) = \sum_{\xi=1}^{N} h(t+\xi)^* s(\xi)$, is the correlation between $s(t)$ and a filter function $h(t)$, where * denotes complex conjugation, and N is the total number of pixels. When the input image is the reference object (i.e., $s(t) = r(t)$), it is imposed that the filter produces the correlation peak $C(0) = C_0$.

If the input image is a modified or a distorted version of the reference image $r(t)$, one generally requires a small variation in the correlation peak. This requirement can be achieved by minimizing the mean square error, which is equivalent to the optimization of the noise robustness to input noise [10]. In order to optimize the discrimination capabilities, one may minimize the energy of the correlation function due to any input image $s(t)$: $E_s[h] = \sum_k |\hat{h}(k)|^2 \, |\hat{s}(k)|^2$.

It can be shown that the optimal trade-off between input noise robustness, discrimination $E_s[h]$, and correlation peak sharpness (see [8] for a mathematical definition of this criterion) leads to the optimum processor (in the Fourier domain):

$$\hat{C}(k) = \hat{r}^*(k)\hat{s}(k)/[\hat{S}(k) + (1-\mu)\,|\hat{r}(k)|^2 + \mu|\hat{s}(k)|^2] \qquad (1)$$

where $\hat{S}(k)$ is the spectral density of the noise model. The performances of this processor will be illustrated with numerical experiments in comparison to other well known filtering methods.

Eq. 1 is very similar to the Fourier transform of a nonlinear JTC output [3] which can be implemented optically. Indeed, both have the same Fourier phase and the amplitude modulation requires nonlinear transformation of both Fourier magnitudes of the reference function and the input function. Let us consider the case of a white noise model ($\hat{S}(k) = I_2$ which is constant). Using a photorefractive crystal in the Fourier domain, it is possible to implement optically the optimal method of Eq. 1. Indeed, if one considers a four wave mixing correlator [11] [12], the modulation index of refraction is proportional to Eq.1. This architecture is sketched in fig. 1.

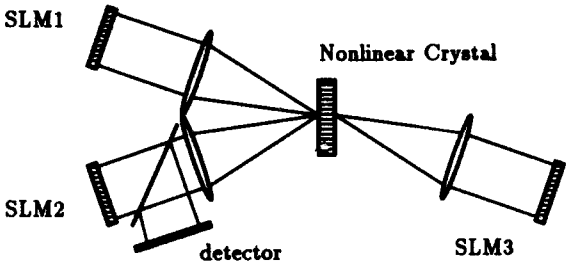


Figure 1: Schematic representation of a 4 waves mixing correlator. Input image $s(t)$ is written on SLM1, the auto-correlation of the noise model on SLM2 and the reference on SLM3.

If one considers the case for which peak sharpness in not optimized, the optimal processor is now given by: $\hat{C}(k) = \hat{r}^*(k)\hat{s}(k)/[I_2 + |\hat{s}(k)|^2]$. This can be obtained if the intensity of beam 3 is low compared to beams 1 and 2 in fig. 1. This case is very interesting since beam 3 is just reading the grating written by beams 1 and 2 (i.e. $\hat{s}(k)/[I_2 + |\hat{s}(k)|^2]$). This process doesn't require interaction in the crystal and then can be done at higher rates than the writing process of the grating (which is limited by the response time of the crystal). This property is in agreement with pattern recognition applications which, in general, need many references for a recognition in the input image.

References

[1] A. Vander Lugt, IEEE Trans. Inform. Theory, **IT-10**, p. 139 (1964).
[2] C. S. Weaver and J. W. Goodman, Appl. Opt. **5**, p. 1248 (1966).
[3] B. Javidi, Appl. Opt. **28**, p. 2358 (1989).
[4] H. J. Caulfield and W. T. Maloney, Appl. Opt. **8**, p. 2354 (1969).
[5] D. Casasent and D. Psaltis, Appl. Opt. **15**, p. 1795 (1976).
[6] J. L. Horner, Appl. Opt. **21**, p. 4511 (1982).
[7] Ph. Réfrégier, Opt. Lett. **15**, p. 854 (1990), Opt. Lett. **16**, 829 (1991).
[8] B. V. K. Vijaya Kumar and L. Hassebrook, Appl. Opt. **29**, p. 2997 (1990).
[9] L. P. Yaroslavsky, Appl. Opt. **31**, p. 1677 (1992).
[10] Ph. Réfrégier, to be published in J. Opt. Soc. Am. A (April) (1993).
[11] M.G. Nicholson, I.R. Cooper, I. McCall, and C.R. Petts, Appl. Opt. **26**, p. 586 (1987).
[12] R.C.D. Young and C.R. Chatwin. SPIE - Orlando 92, Optical Pattern Recognition - Vol. 1701, p. 239, 1992.

Rotation scale and shift invariant real time pattern recognition

Ezra Silvera and Joseph Shamir
Department of Electrical Engineering
Technion - Israel Institute of Technology, Haifa 32000, Israel

Pattern recognition using a coherent optical correlator has many advantages including high speed and parallel processing. The main problem of those systems is that usually they can not cope with the various changes of the input function such as rotation and/or scale.

We present a system which is invariant to all three distortions (rotation, scale and shift) and, at the same time, can complete the recognition process practically in real time. The overall system is composed of two parallel channels that are connected together. A schematic diagram of the system is given in figure 1.

Basically the system operate as follow: The input object is placed on the first SLM (spatial light modulator), from which it enters a correlation channel and a scale measurement channel. After the scale of the object is estimated, the correlator is adapted by changing the scale of the filter or/and the input pattern.

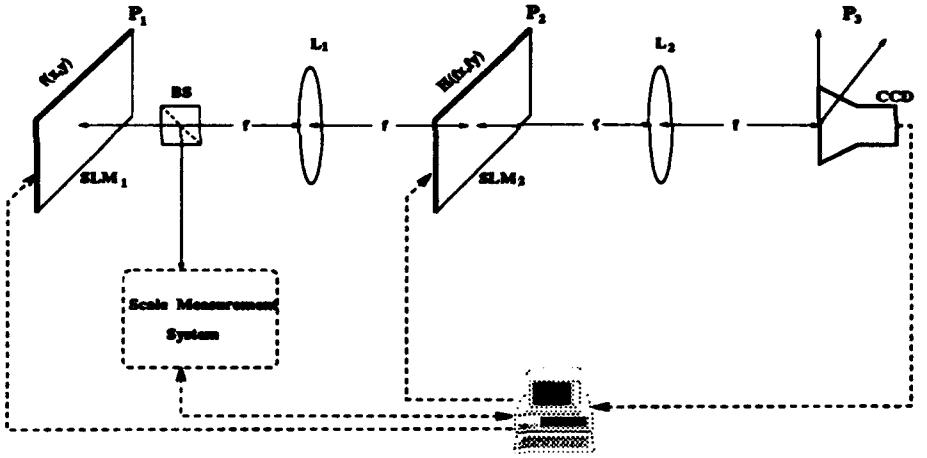


Figure 1: Schematic representation of the the overall recognition system

The scale measurement is performed at the Fourier plane where it can be easily implemented optically. Let $f(r,\theta)$ be the input function and $F(\rho,\phi)$ its Fourier transform (in polar coordinates). When the scale of the input is extended by factor a the energy ,using Parseval's theorem, becomes:

$$E_a = \int_0^{2\pi}\int_0^{\infty} \left|a^2 F(a\rho,\phi)\right|^2 \rho d\rho d\phi = a^2 E_0 \qquad (1)$$

where E_0 is the energy of the original function $f(r,\theta)$. We define the ratio between $E_a(\hat{\rho})$, the energy in the spatial frequency interval $0 < \rho < \hat{\rho}$, and the total energy E_a by:

$$T(a,\hat{\rho}) = \frac{E_a(\hat{\rho})}{E_a} = \int_0^{2\pi}\int_0^{\hat{\rho}} \left|a^2 F(a\rho,\phi)\right|^2 \rho d\rho d\phi = \frac{\int_0^{2\pi}\int_0^{a\hat{\rho}} |F(\rho,\phi)|^2 \rho d\rho d\phi}{E_0} \qquad (2)$$

Obviously $T(a, \hat{\rho})$ depends on $\hat{\rho}$ only through the integration limit, hence we can derive the scale factor a from the simple relation:

$$a = a_0 \frac{\hat{\rho}_0}{\hat{\rho}} \tag{3}$$

where $\hat{\rho}_0$ is the spatial frequency which gives the predefined T_0 for a known reference object of scale a_0.

The correlation channel is based on an adaptive 4-f correlator in which both filter and object can be modified, in real time, on the SLM's. With this approach the system is very flexible and can be easily adjusted. The filter used for the correlator was specially designed according to the system's limitation. The main requirements from the filter were:full rotation invariance, sharp and high correlation peak, good discrimination ability and, finally, a limited scale invariance. This final requirement is essential due to the errors during the scale measurement procedure. Obviously, the scale tolerance range has to be large enough in order to fully compensate for those errors.

The filter was designed using the method of projection onto convex sets (POCS). The special characteristics of the filter are achieved by applying appropriate constraints during the POCS algorithm.

Both simulation and laboratory experiments were successfully performed. Excellent results were obtained with alphanumeric characters as well as with gray scale images.

The adaptive 4-f real time correlator enable us to use the system for many related application such as iterative filter design, pattern classification etc. The double channel method, in general, can be used for a different set of distortions in a similar way.

Systems Partitioning and Placement in Optoelectronic MCM Design

J. Fan, S. H. Lee and C. K. Cheng
Dept. of ECE, University of California, San Diego
La Jolla, CA 92093-0407
(619) 534-2413

Abstract

We discuss the CAD issues for partitioning between electrical and optical interconnects and physical layout in free-space optoelectronic MCM design. The results of a design example are also presented.

Summary

1. Introduction

Free-space optical interconnections (FSOI) have been shown to have speed or power advantage over electronic interconnections for long distance interconnections[1]. By introducing FSOI into new MCM designs, it is possible to create an OptoElectronic MCM (OE MCM). However, incorporating optics into electronics presents new challenges in computer-aided design, fabrication, and packaging. To integrate optics and electronics at the system level, we need new partitioning and placement algorithms. In this paper, we first introduce the models for partitioning and placement. We have chosen the system power dissipation as the cost function to minimize in partitioning. In placement, we minimize the interconnection distance based on the constraints imposed by the fabrication limit (or cost) of the system. The models are then applied to a design example to illustrate the importance of CAD issues.

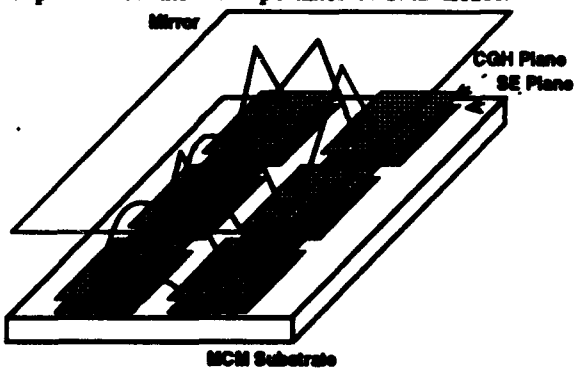


Figure 1. Schematic showing of a physical model of OE MCM package in reflective configuration. Only a few of the many actual interconnects are shown.

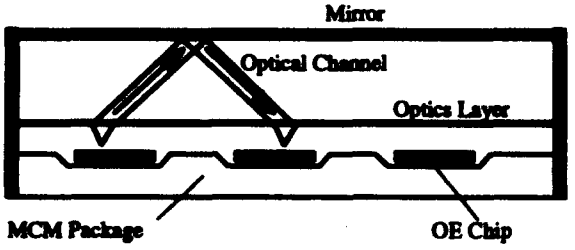


Figure 2. Cross-Section of an Opto-Electronic MCM package.

Figure 1 shows a physical model of an OE MCM. There are three layers in the packaged system. The lower layer consists of multiple chips of electronics and optoelectronic devices. Each chip contains a number of switching elements (SEs) or processing elements (PEs). The middle layer consists of diffractive optics (DOEs) or computer generated holograms (CGHs). The upper layer is a mirror. The cross section of this system is shown in figure 2. The optical transmitters, e.g. surface emitting lasers, illuminate an off-axis lens where the beam is collimated and then deflected into the desired direction. The beam then reflects off a mirror and is focused by another off-axis lens onto a receiver (detector) on another chip.

There are four aspects of optoelectronic system design that are key to the system performance: interconnection speed, heat dissipation, chip size and MCM size, and maximum optical interconnect distance. Currently in OE MCM design, optical sources (such as modulators or laser diodes and their drivers) generate heat in densities much higher than that of VLSI. Based on speed, switching energies, and power budgets, electrical and optical technologies can be compared and a break-even line length can be defined[1]. For signals that must propagate distances longer than this, optical interconnection technology is preferred, for signal propagating distances less than this, electronic interconnection technology is preferred. It can be shown that minimum feature size of the fabrication technology limits the maximum interconnect distance [2].

In the optoelectronic design process, partitioning is performed: (a) to divide the total number of PEs in the system into fewer number of chips; and (b) to choose the best technologies for each interconnect required by the netlist of a certain computing architecture. After the partitioning process, placement algorithms will perform the physical assignments of the PEs within each chips to reduce the fabrication requirement of DOEs/CGHs.

2. System Partitioning of OE MCM

To optimize the partitioning of the OE MCM design using CAD technology, a formulation must be established in terms of the technology constraints. One choice is to let three of the technology variables mentioned above be constrained and attempt to minimize the fourth. Since power dissipation of the system present a design problem, the most natural objective of the partitioning appears to be to minimize the heat dissipation while satisfying the limits placed on the speed of the interconnects, the size of the chip and OE MCM, and the optical distance.

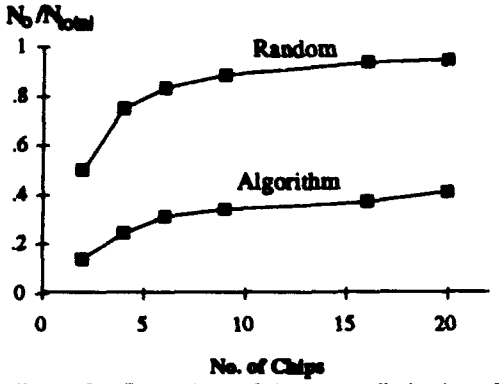


Figure 3. Comparison of the power dissipation of the interconnects between random partitioning and algorithm partitioning. Over 50% improvement can be achieved by applying the algorithm.

To solve the OE MCM partition problem, we combine an algorithm based on Burkard heuristic[3] and a modified matching algorithm based on labeling techniques[4]. The optimized partitioning is achieved by rearranging the PEs among different chips to reduce the number of interchip interconnections, and therefore to reduce the power dissipation. Figure 3 shows a comparison of the results of random partitioning with the results of the CAD algorithm on an irregular interconnection network example[5], for various numbers of chips. An improvement of over 50% is achieved in many of the cases studied.

3. PE Placement in OE MCM

In the design of optoelectronic MCM with free-space optical interconnection, it is the maximum interconnection distance that should be minimized. We investigated placement algorithms for optoelectronic systems based on iterative matching[5]. The algorithm starts with a random placement of PEs within chips and reduces the maximum interconnection distance through a fixed number of iterations by rearranging PEs within chips. Figure 4 shows the histogram results of a straight forward placement and placement by a iterative matching algorithm for comparison. The same network example used in the last section is used here. More than a 50% reduction in the maximum interconnect distance (or on the packaging volume of the system) can be achieved when we applied the algorithms to the OE-MCM design.

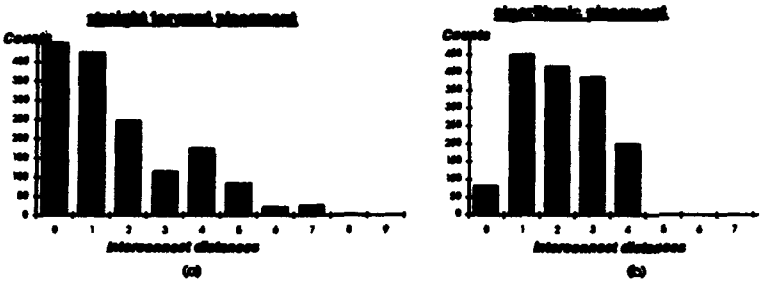


Figure 4. Comparison between two placement methods. (a) Result of the straight forward method. (b) Result after applying the placement algorithm. The maximum interconnect distance is reduced by 50%.

5. Conclusion.

In this paper, we discussed optoelectronic MCM models and algorithms for CAD partitioning and placement. Results show that more than 50% reduction in power consumption and the maximum interconnect distance can be achieved by applying these CAD algorithms to a OE MCM design.

6. Acknowledgment

We would like to acknowledge the helpful discussions with B.Catanzaro, D.Zaleta, and V.H.Ozguz. We also thank the financial support of ARPA/ONR.

7. References

1. M. R. Feldman, S. C. Esener, C. C. Guest, and S. H. Lee, "Comparison between optical and electrical interconnects based on power and speed considerations", Applied Optics, 27, 1742-1751, 1988.
2. S. H. Lee, "Diffractive optics and computer generated holograms for optical interconnects", Critical Review conference on Diffractive and Miniaturized Optics, paper CR-14, San Diego, July 1993.
3. R. E. Burkard and T. Bonniger, "A Heuristic for Quadratic Boolean Programs with Applications to Quadratic Assignment Problems", European Journal of Operational Research, 13, 372-386, 1983.
4. E. L. Lawler, "Combinatorial Optimization: Networks and Matroids", Holt, Rinehart and Winston, N.Y., Section 5.7, 1976.
5. J. Fan, D. Zaleta, C.K. Cheng and S.H. Lee, "Physical layout for computer generated holograms for optoelectronic multichip modules", Proc. IEEE MCM Conference 93, 198-203, 1993.

Architecture of a Terabit Free-Space Photonic Backplane

Ted Szymanski and H. Scott Hinton
Department of Electrical Engineering, McGill University
Montreal, PQ, Canada, H3A 2A7
email: teds@macs.ee.mcgill.ca, hinton@photonics.ee.mcgill.ca

Abstract: The architecture of a "universal" photonic backplane is described. The architecture contains a large array of "programmable" smart pixels which can be configured into three states. By setting pixel states appropriately, any network can be embedded into the backplane.

Summary: A photonic backplane consists of a large number of parallel optical channels (10,000 to 100,000) spaced a few hundred microns apart [1][2]. Each printed circuit board contains one or more smart pixel arrays, which access the photonic backplane through an "optical extender card", as shown in fig. 1 [1]. This paper proposes an attractive photonic backplane architecture which we call the "HyperPlane".

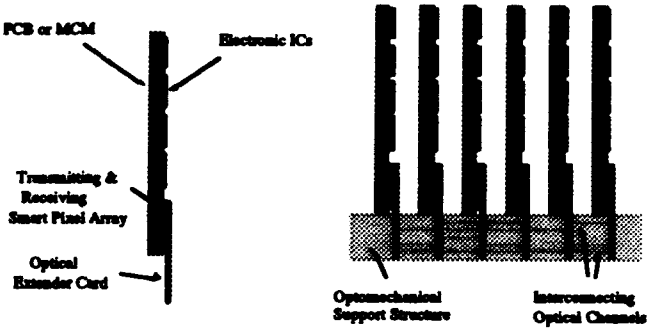


Figure 1: (a) PCBs with Optical Extender Card. (b) Photonic Backplane.

The smart pixel arrays manage access to the backplane. A smart pixel consists of an incoming window, and out-going window, a latch, two multiplexers and an address bit comparator, as shown in fig. 2. Pixels can be programmed to be in one of three states, the "idle", "transmitting" and "receiving" states, as shown in fig. 3. The state of a pixel can be changed by down-loading a bit-stream from an associated message-processor. The pixels can also be programmed to receive messages for any destination by down-loading the appropriate address bits. The pixels require 12 logic gates each. The pixels are arranged into an array as shown in fig. 4. The data for configuring the array is loaded in bit-serially; data to be transmitted enters from the top, and data being received exits from the bottom. The smart pixel arrays are being designed using AT&T's FET-SEED GaAs technology [3] and are manufacturable using existing fabrication technology.

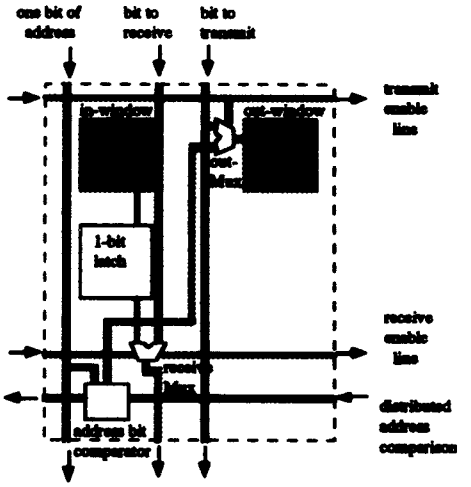


Fig. 2. Smart pixel cell with address recognition and message extraction.

The HyperPlane can embed any conventional interconnection network by programming the pixels accordingly. Optimal embeddings would minimize the length of the longest optical channel in the backplane. Optimal embeddings for linear arrays, 2D and 3D meshes, toroids, hypercubes, crossbars, orthogonal crossbars, and shuffle-based networks have been identified. Typical embeddings are shown in figures 5-6. Each box represents a node. Each vertical line represents an electrical data path within a smart pixel array. Each bold horizontal line represents an optical connection which is implemented by programming the pixels at each end as transmitters and receivers. The embeddings can be changed in real-time by down-loading appropriate control bits.

The HyperPlane architecture can also be designed to exploit transparent long distance optical transmissions. By appropriately designing the extender card, it is possible to allow long-distance optical transmissions to by-pass intermediate smart pixel arrays as they travel down the backplane [1]. This "Transparent HyperPlane" improves performance by eliminating the delays associated with passing through inter-mediate smart pixel arrays. Since the intermediate smart pixels can no

longer transmit or receive over the long-distance channels which bypass them, there may be a restriction on the types of embeddings possible.

References

[1] H.S. Hinton, Canadian Institute for Telecommunications Research - Research Program 1993-94, pp. 143-156, 1993.

[2] K. Hamanaka, "Optical Bus Inter-connection using Selfoc Lenses", Optics Letters, Vol. 16, No. 16, pp. 1222-1224, 1991.

[3] L.A. D'Asaro et al, "Batch Fabrication and Operation of GaAS-Al_x-Ga_{1-x}As Field-Effect Transistor Self-Electrooptic Effect Device (FET-SEED) Smart Pixel Arrays", IEEE Jounral Quantum Electronics, Vol. 29, No. 2, Feb. 1993, pp. 670-678.

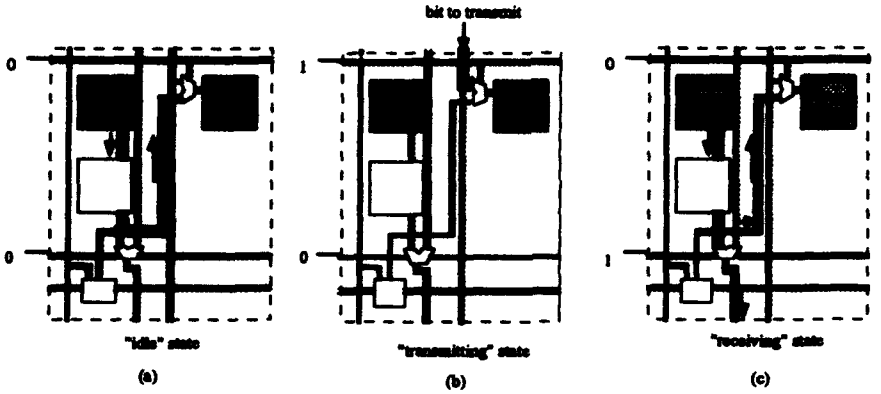


Figure 3 : (a) Cell in idle state (b) Cell in the transmitting state. (c) Cell in the receiving state.

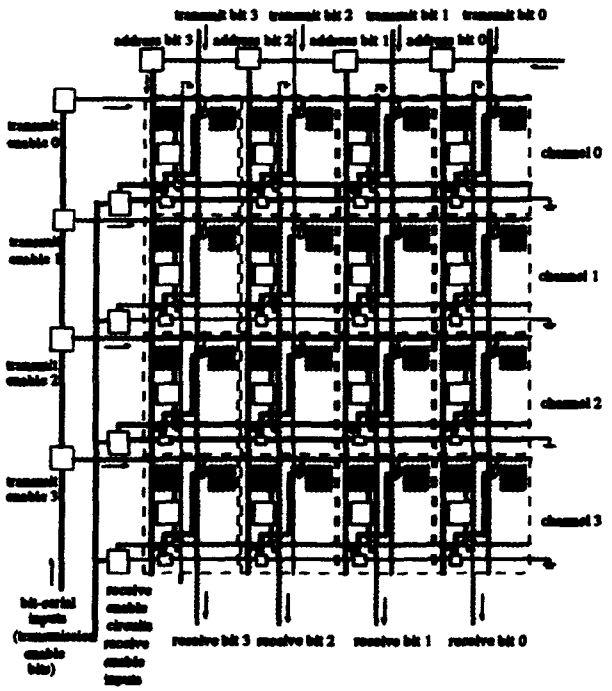


Fig. 4. Smart pixel array.

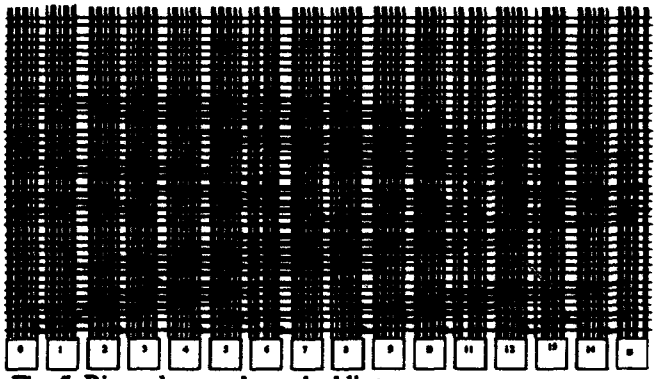


Fig. 5. Binary hypercube embedding.

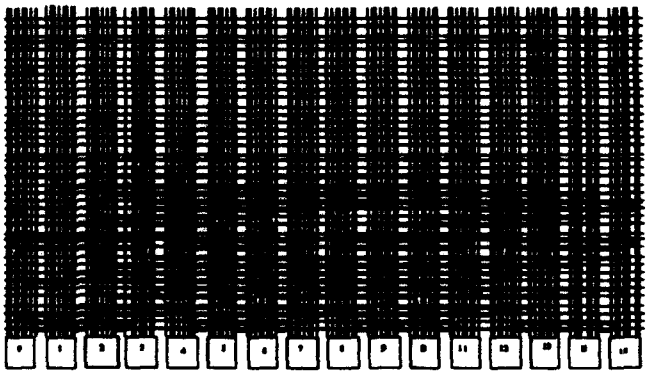


Fig. 6. 2D Mesh embedding.

A Scalable Optical Interconnection Network for Massively Parallel Computers [1]

Ahmed Louri and Hongki Sung
Department of Electrical and Computer Engineering
The University of Arizona
Tucson, AZ 85721
Phone: (602) 621 – 2318, Fax: (602) 621 – 8076

Abstract – We present a new optical interconnection network, called an Optical Multi-Mesh Hypercube, which is both size- and generation-scalable. It exhibits such properties as small diameter, fault tolerance, symmetry, constant node degree, and is highly amenable to optical implementations.

Summary – The quest for Teraflops (10^{12} floating point operations per second) supercomputers fueled by the launching of the High Performance Computing and Communication Program is putting major emphasis on exploiting massive parallelism with greater than one thousand processing elements (PEs) networked to form massively parallel computers(MPCs)[1]. An important issue in the design of MPCs is scalability. In architectural terms, scalability has two aspects; size and generation. Size-scalable parallel computers are those in which the number of nodes (or processors) can be expanded over a wide range without substantial changes in either the existing configuration or software, and the performance increases as the number of nodes increases. Generation-scalability is the adaptability of the architecture to the rapid evolution of technologies. The key to size scalability of MPCs is the interconnection network which is also a deciding factor in terms of performance and cost of the entire system. Numerous topologies have been explored for parallel computers. However, the lack of size-scalability of some of these networks (e.g., hypercube) have limited their use in MPCs despite their many other advantages. We have explored a new network topology, called *Optical Multi-Mesh Hypercube* (OMMH), which combines the advantages of both the hypercube (small diameter, high connectivity, symmetry, simple control and routing, fault tolerance, etc.) and the mesh (constant node degree and scalability) topologies, while circumventing their disadvantages (lack of scalability of the hypercube, and large diameter of the mesh). We have also developed a three-dimensional (3-D) optical implementation methodology which exploits the advantage of both space-invariant free-space and multiwavelength fiber-based optical interconnects technologies.

Definition of the OMMH network: An (l, m, n)-OMMH, where l, m, and, n are integers, network consists of $l \times m \times 2^n$ nodes and an address of a node has three components; (i, j, k), where $0 \leq i < l$, $0 \leq j < m$, $0 \leq k < 2^n$, and i, j, k are integers. The topology of an (l, m, n)-OMMH network is defined by five interconnection functions for a node (i, j, k) as follows: (1) $f_{m_1}(i, j, k) = ((i + 1) \bmod l,\ j,\ k)$, (2) $f_{m_2}(i, j, k) = ((l + i - 1) \bmod l,\ j,\ k)$, (3) $f_{m_3}(i, j, k) = (i,\ (j+1) \bmod m,\ k)$, and (4) $f_{m_4}(i, j, k) = (i,\ (m+j-1) \bmod m,\ k)$ $f_{c_d}(i, j, k_{n-1} \cdots k_{d+1} k_d k_{d-1} \cdots k_0) = (i, j, k_{n-1} \cdots k_{d+1} \overline{k_d} k_{d-1} \cdots k_0)$, for $d = 0, 1, \cdots, n-1$, where $k_{n-1} \cdots k_{d+1} k_d k_{d-1} \cdots k_0$ is a binary representation of integer k. Torus (mesh with wraparound connections in the rows and columns) connections of the OMMH network are defined by f_{m_1}, f_{m_2}, f_{m_3}, and f_{m_4}. The binary n-cube interconnection is defined by f_{c_d}, for $d = 0, 1, \cdots, n-1$. Fig.1 shows a (2,4,3)-OMMH interconnection where solid lines represent hypercube links and dashed lines represent torus links. For a network size of one million nodes, the hypercube network contains about 10.5 million links while the

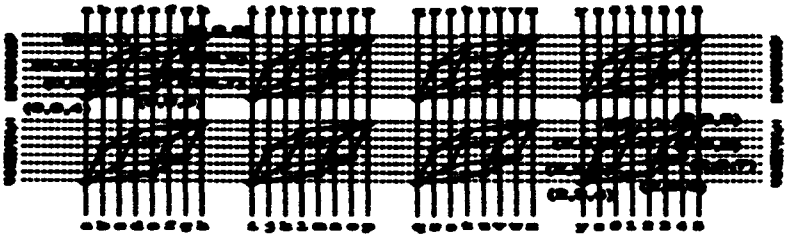


Fig. 1: An example of the OMMH network: a (2,4,3)-OMMH is shown. Labels represent wraparound connections.

$(l, m, 4)$-OMMH has about 4.2 million links and $(16, 16, n)$-OMMH has approximately 8.4 million links. Since one link implies one physical path, electrical or optical, between two nodes, the OMMH network is cost-efficient compared to the regular hypercube network in terms of hardware requirement. It should be noted that an OMMH with a constant cube as a basic building block (e.g., $(l, m, 4)$-OMMH) has constant node degree over the network size. This feature enables OMMH network to be scalable; that is, the size of the OMMH can be increased by expanding the size of the torus without changing node degree.

Optical Implementation of the OMMH network: An OMMH network is constructed from simple building blocks (hypercubes) in a modular and incremental fashion. These building blocks, once constructed, are left undisturbed when the network grows in size. The OMMH can be viewed as a two-level interconnection network: high-density, local connections for hypercube links (within a basic module), and high bit rate, low-density and long connections for the

[1]This research was supported by an NSF grant No. MIP 9113668, an NSF grant No. MIP 9310062, and a grant from USWest.

torus links connecting the basic building blocks. The optical implementation also consists of two levels: free-space space-invariant optics for the construction of basic building blocks, and multiwavelength fibers for the torus links. The breakdown of functional requirements for the OMMH network is consistent with the advantages of free-space and optical fiber technologies. The size of the OMMH can be increased by adding hypercube modules, which provides modularity and size-scalability. Generation-scalability is provided by the use of high-bandwidth wavelength multiplexed optics which would match communication bandwidth requirements of future processing elements.

The totally space-invariant optical implementation of hypercubes is provided in detail in Refs. 2 and 3. Based on these methods, an (l, m, n)-OMMH can be constructed as follows: (1) $l \times m$ n-cube modules as described in Ref. 2 and 3 are placed in a $l \times m$ matrix form. (2) $l \times m$ nodes, each of which is from the same location of the n-cube modules, are connected to form a torus of dimension $l \times m$. (3) Step 2 is repeated until every node is connected, resulting in 2^n toruses of size $l \times m$.

Now, we consider an optical implementation of the (l, m, n)-OMMH network. We use two optical components: a quadrant beam splitter (QBS) which splits a single beam into four beams (the QBS also combines four beams into one since it is bi-directional) and an i-channel wavelength multiplexor (WMUX) which multiplexes beams with i different wavelengths into a single beam (also demultiplexes since it is bi-directional). We assume that each node has two light sources; one source, S_h, to generate the required hypercube links and the second source, S_t, is coupled with an optical fiber for the torus links. A QBS is attached to every S_t to provide the four fanouts, S_{t_N}, S_{t_S}, S_{t_E}, and S_{t_W} (north, south, east, and west). A WMUX is located at both ends of each row and each column. Let each WMUX at the right end of a row be WMUX_E, each WMUX at the left end of a row be WMUX_W, each WMUX at the top of a column be WMUX_N, and each WMUX at the bottom of a column be WMUX_S. In a given row, a WMUX_E multiplexes lights from the S_{t_E} sources of that row into a single fiber which is then connected to a WMUX_W in the neighboring n-cube module. Similarly, S_{t_N}s S_{t_S}s, and S_{t_W}s are multiplexed by WMUX_N, WMUX_S, and WMUX_W, respectively. Fig.2 shows an (2,4,5)-OMMH implementation. More details will be provided at the Meeting.

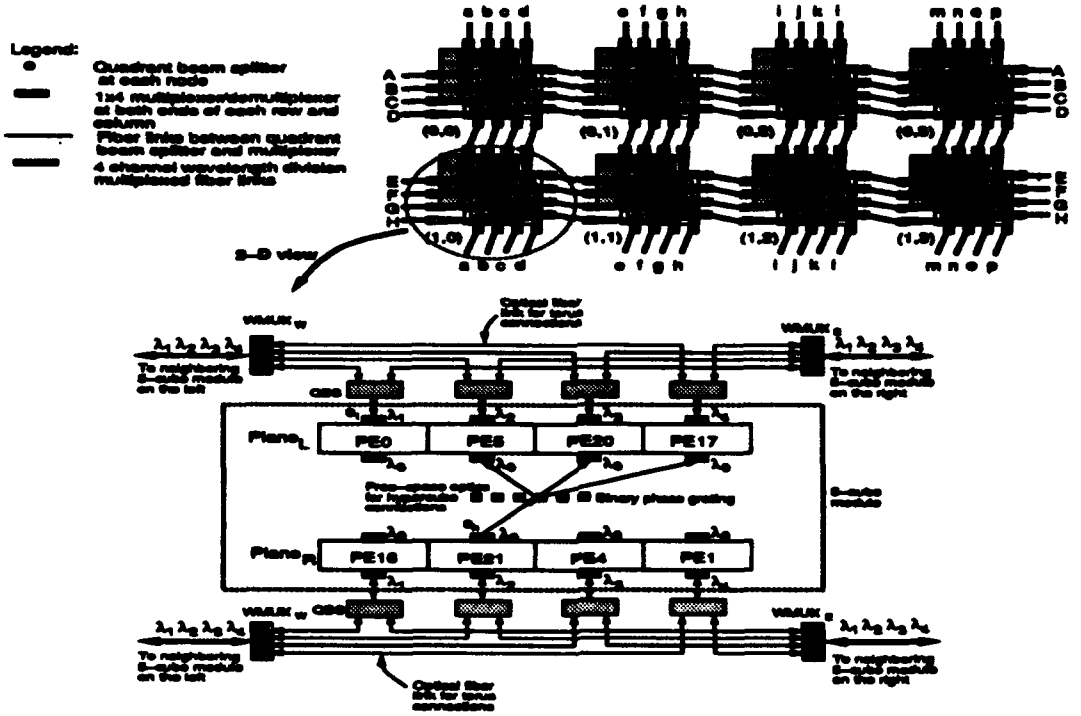


Fig. 2: (2,4,5)-OMMH implementation.

References

1. G. Bell, "Ultracomputers: A Teraflop Before Its Time", *Communications of ACM*, 35, Aug. 1992, pp. 27-47.
2. A. Louri and H. Sung, "Design Methodology for Three-dimensional Space-invariant Hypercube Networks with Graph Bipartitioning", *Optics Letters*, 18(23), 1993, pp. 2050-2052.
3. A. Louri and H. Sung, "Efficient Implementation Methology for Three-dimensional Space-invariant Hypercube-based Optical Interconnection Networks", *Applied Optics*, 32(35), 1993, pp. 7200-7209.

Demonstration of a 3D-integrated refractive microsystem

J. Moisel and K.-H. Brenner, Universität Erlangen-Nürnberg, Institut für Angewandte Optik, Staudtstraße 7/B2 91058 Erlangen, Germany, Tel. +49 9131 858378, Fax. +49 9131 13508, e-mail jm@ao.physik.uni-erlangen.de

Abstract: A 3D-integrated microsystem is presented which performs the overlay of data planes. Each channel of the microsystem consists of two gradient-index microlenses and two microprisms. The output plane is 500μm squared and contains approx. 100 Pixels.

Introduction: 3D-integrated microsystems promise a higher packaging density and complexity for optical interconnects and functional elements compared to 2D OEICs [1]. However, the additional degrees of freedom demand additional efforts for the aligning and mounting of the systems. This is critical especially for diffractive optical elements. We present a very simple refractive system performing the overlay of two data planes which is a vital step in symbolic substitution concepts for digital optical computing [2] [3].

Experimental Setup: The optical design of the system is straightforward. To perform an overlay of two data planes, imaging and deflecting elements are needed. It would also be possible to build a system containing only lenses if those are used off-axis. However, we use the lenses on-axis and shift the data planes with prisms. Again, there are two possibilities. One is to use only a single lens and pupil division, the other to use two lenses. The second option has the advantage that the whole space-bandwidth of the lens can be used. Additionally, the area where the two prism surfaces meet is not perfect (rounded) and this area is not in the center of the lens but between the lenses. In all three cases (Fig. 1) it is necessary to adjust the illumination according to the imaging conditions.

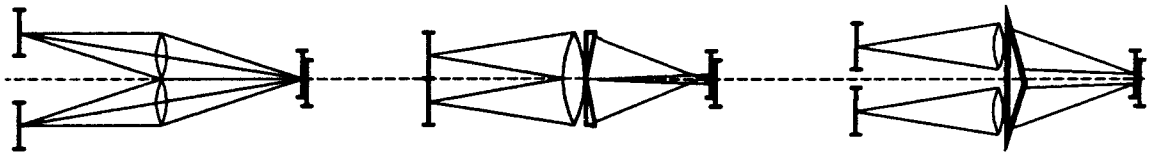


Fig.1 Three possible designs of a system performing the overlay of two data planes

The focal length of the lenses (1100μm), the pitch of the lenses (250μm) and the refractive index of the prisms (1.49) determine the prism angle (17°). In our setup, the data planes are illuminated test patterns. We use two LEDs to be able to swich the two channels independently. The LEDs are demagnified by a microscope objective and imaged in the centers of the lenses. The output plane is imaged on a CCD array by another microscope objective.

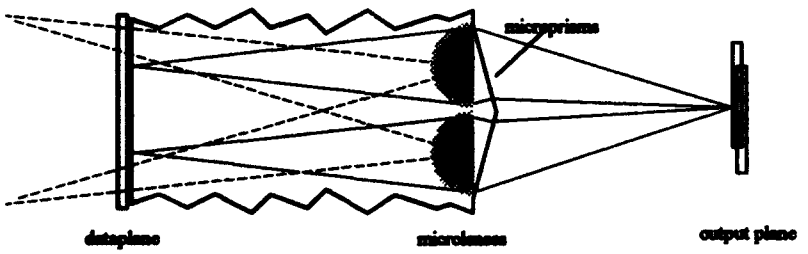


Fig.2 The experimental setup

Fabrication: The lenses were made by use of the Na-Ag ion exchange in glass [4]. The prism array was made by thermal moulding and casting [5] (Fig. 3). Firstly, a glass master of the prisms was made using standard techniques. The master was heated, embossed into a PMMA substrat and cooled down. Repeating this process

generates a regular array of negative prisms. The negative array is now used as master for the production of the final prism array. For this purpose it is filled with UV-curing glue and topped with the planar microlens array. Since the performance of the system primarily depends on the prism angle, the alignment of the negative microprism array and the microlens array is not very critical apart from a relative rotation. After curing of the glue, the negative is separated from the complete system.

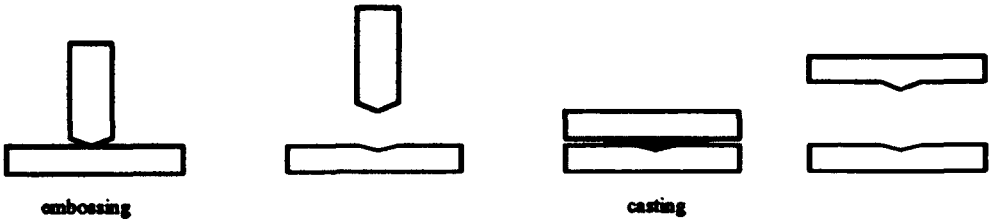


Fig.3 Fabrication of the microprism array

Experimental results: Fig. 4 shows a top view of an array of microprisms fabricated on an substrate which already is an array of planar microlenses. Fig. 5 and 6 show images of the both dataplanes independently. Fig. 7 shows the overlay of the two dataplanes.



Fig.4 Fig. 5 Fig.6 Fig.7

Acknowledgements: The microlenses were made by J. Bähr. The help of W. Eckert and W. Singer with the experimental setup is gratefully acknowledged. Parts of this work are funded by the german ministry of research and technology (BMFT) under grant TK 0585/5.

References:

[1] F.B. McCormick, *"Optical Hardware Design for Free-Space Optical Computing and Switching"*, Proceedings of 16th Congress of ICO 1993, Budapest, p. 352-356

[2] K.-H. Brenner, A. Huang, N. Streibl, *"Digital optical computing with symbolic substitution", Appl. Opt. 25(18), p. 3054-3060 (1986)*

[3] K.-H. Brenner, W. Eckert, C. Passon, *"Demonstration of a systolic array optical adder based on symbolic substitution"*, accepted by Optics an Laser Technology Jan. 1994

[4] K.-H. Brenner, J. Moisel, W. Singer, S. Sinzinger, T. Spick, M. Testorf: *"Diffusion elements in glass: comparison and optimization of the diffusion response in different substrates"*, Proceedings 1992 ICO Topical Meeting on Optical Computing, Minsk, p. 234-242

[5] K.-H. Brenner, *"Three dimensional microoptical integration techniques"*, Proceedings of 16th Congress of ICO 1993, Budapest, p. 98-104

INTEGRATION OF FREE-SPACE INTERCONNECTS USING SELFOC LENSES: OPTICAL PROPERTIES OF A BASIC UNIT

Kenjiro HAMANAKA, Kenichi NAKAMA, Daisuke ARAI, Yukihisa KUSUDA,
Takashi KISHIMOTO, and Yoshinobu MITSUHASHI
RWCP[1] Optoelectronics NSG Laboratory[2]

A vertical and horizontal integration technique of free-space interconnects using Selfoc lenses, is described. A basic unit of the optical mother board has been fabricated by slicing a Selfoc rod of 4mm in diameter.

1.INTRODUCTION

In case of integrating free-space optical systems, surface mounting techniques are preferable for fixing non-transparent devices such as surface emitting LDs and reflection-type SLMs, while transparent devices such as transparent-type SLMs and isolators must be inserted in optical paths. Therefore, it is required to develop optical mother boards for integrating free-space optical systems, which are suitable for both non-transparent and transparent devices. It is considered that "Optical bus interconnection system (OBIS) [1,2]", an optical mother board using Selfoc microlenses (SMLs) [3], is one of the promising solutions.

2.PRINCIPLES

Figure 1 shows the basic concept of OBIS. An optical mother board owning many optical I/Os on a glass substrate as well as in the substrate is composed of cascade arrays of SMLs and prisms. All the I/Os are basically conjugated each other, and as the result, two dimensional information generated at one of the I/Os is transferred into the other I/Os through the image transmission tubes composed of the SMLs. The perfectly coaxial arrays of SMLs, which are fabricated by slicing Selfoc rods using diamond blades, provide large space-bandwidth product. Non-transparent devices can be integrated horizontally at the optical I/Os on the substrate using surface mounting techniques, while transparent devices can be integrated vertically at the I/Os in the gaps. The substrate plane including the optical I/Os can also be used for electronic circuits as well as planar optical waveguides. Various interconnection networks can be realized using microlens arrays [4] or DOEs in the gaps.

3.EXPERIMENTS

A basic unit of OBIS, by means of a 4-f telecentric imaging system, was fabricated by slicing a Selfoc rod of 4mm in diameter (Fig.2). After the rod and two glass substrates with grooves were fixed using UV-resin, perpendicular gaps were fabricated using a diamond blade composed of diamond particles of 20-30μm in diameter (Fig.3). Roughness of the SML facets and the substrate planes was measured to be Rmax=2.2μm in average. The 4-f telecentric imaging system owing two optical I/Os on the substrate was formed after combining two prisms using index-matching liquid (Fig.4). The optical configuration has been designed to minimize aberration within the image height of 0.8mm, while NA of the light beams is equal to 0.1. Point sources of the corresponding NA, i.e. focusing spots of an

1) Real World Computing Partnership
2) c/o Tsukuba Research Laboratory, Nippon Sheet Glass Co. Ltd.
5-4, Tokodai, Tsukuba-City, Ibaraki 300-26, Japan
Phone:+81-298-47-8681, Fax:+81-298-47-8693

almost diffraction limited planar microlens array of NA=0.1 [5], were located at the object plane, and PSFs were observed under coherent illumination. The PSFs of 16μm in diameter in average with no critical scattering were obtained in the 1.6mm square image plane on the substrate through the reflection path (Fig.5) as well as through the transparent path.

4.CONCLUSION

A vertical and horizontal integration scheme of OBIS has been proposed and a basic unit of OBIS fabricated by slicing a Selfoc rod of 4mm in diameter has been examined.

REFERENCES

[1] K. Hamanaka, Opt. Lett. 16 (1991) 1222.
[2] K. Hamanaka, Jpn. J. Appl. Phys. 31 (1992) 1656.
[3] I. Kitano, et al., Appl. Opt. 22 (1983) 396.
[4] K. Iga, et al., Appl. Opt. 21 (1982) 3456.
[5] K. Hamanaka, et al., Appl. Opt. 29 (1990) 4064.

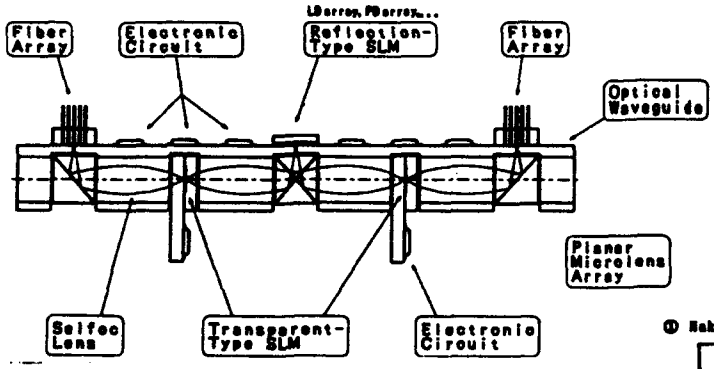


Fig.1 A vertical and horizontal integration scheme of OBIS.

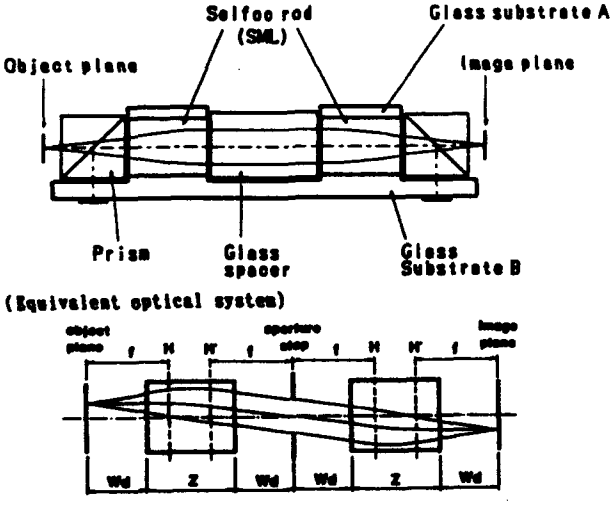


Fig.2 A basic unit of OBIS (4-f imaging system).



Fig.4 A photograph of the basic unit.

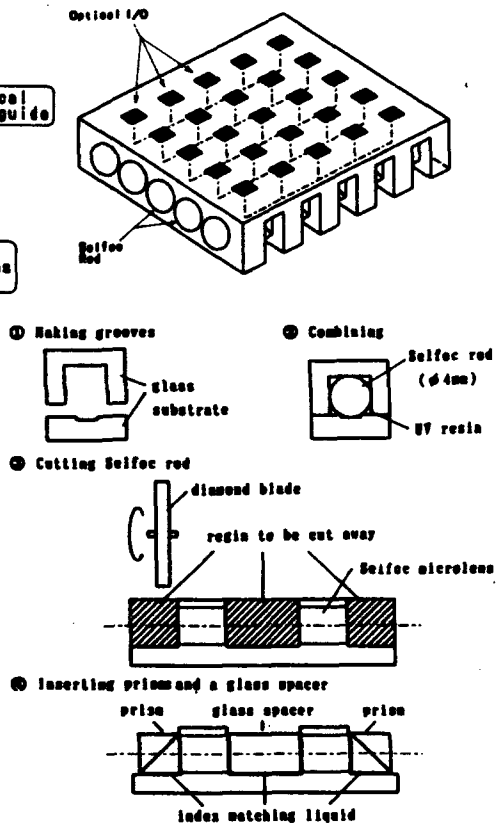


Fig.3 Fabrication procedure of the basic unit.

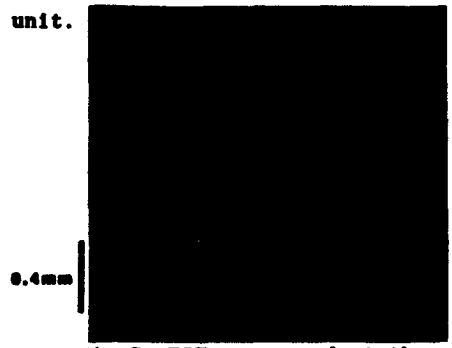


Fig.5 PSFs measured at the 4-f image plane on the glass substrate.

Fabrication of Fiber Arrays for Optical Computing and Switching Systems

Jose M. Sasian, Robert A. Novotny, Martin G. Beckman
Sonya L. Walker, Michael J. Wojcik and Stephen J. Hinterlong

AT&T Bell Laboratories
263 Shuman Blvd.
Naperville, IL 60566

Abstract

We describe a technique for assembling fiber arrays as needed in optical computing and photonic switching. A 4x8 array was manufactured with fiber ends to within 1.5 μm from their ideal position and to a pointing precision of 30 arc-minutes.

Summary

Optical fiber bundle arrays are simple to conceptualize but their fabrication has proven to be difficult when high precision positioning is required. Several fabrication techniques have been reported in the literature; for example, in the approach presented by Miller[1] a 2-D array of fibers was made by stacking a number of linear arrays of fibers supported by grooved spacers. These spacers were manufactured by the precise etching of both sides of a silicon wafer, and a polishing operation was involved after potting all the fibers in place. Recently, this technique has been used by Danzer, Kipfer, Zurl, Lindolf, and Schwider[2] to assembly a fiber array with a maximum positioning error of 10 μm. In another effort an alignment-free assembly technique has been developed by Sasaki, Baba, and Iga[3] where fiber end positioning was accomplished to within ± 8 μm. In this technique an array of fiber sockets with centering plugs were micro-fabricated to achieve fiber self-centering insertion and to expedite assembly. Koepf and Markey[4] have reported a technique involving arrays of precision holes in substrates to insert and locate optical fibers with a standard deviation of 12.6 μm. Arrays of precision holes to position fibers have also been used by Basavanhally[5] and by Proudley, Stace, and White[6] to manufacture fiber bundles. The insertion of fibers in microferrules and their stacking to create a 2-D fiber array has even been realized[7] with a mean fiber positioning error of 3 μm.

A common feature of these techniques is that fiber positioning is accomplished by referencing the fiber to a mechanical jig and this limits the ultimate precision attainable. We considered these assembling techniques but were not satisfied with their inherent errors or the processes involved. Thus we developed the assembly technique that we present which suits our photonic switching development. The basic idea around which our technique revolves is the high precision and individual positioning of each optical fiber on a substrate of large and low precision holes. Instead of relying on a mechanical substrate to reference the fiber we obtain positioning accuracy by individually locating each fiber core in the correct position. The positioning accuracy is achieved by referencing light coming from the fiber core to a lithographically made array of annuluses or doughnuts on a transparent glass substrate. Once a fiber is positioned, it is bonded in place by curing UV cement around it. The array of holes serves as the foundation for the fiber array, to achieve uniformity in fiber pointing, and to stress relieve the optical fibers.

To assemble a fiber bundle a hole array substrate is filled with UV curing cement and an array of centering doughnuts is registered on the top surface of the hole array. The centering doughnuts face the array of holes and are centered with respect to the holes. The assembly formed by the hole array and centering doughnuts substrate is placed on a microscope. Prior to the fiber insertion and alignment steps the fiber coating is stripped off and the fibers cleaved. With the aid of a fiber manipulator a fiber is grabbed and inserted through the corresponding hole in the hole array. The light that comes from the fiber core and some TV cameras make this insertion easy. The fiber can pivot on the lower rim of

the hole so that it can be aligned by horizontally moving the fiber manipulator. Then the fiber is brought into contact with the doughnut substrate. For this delicate step a piezo-electric driven mechanism is used. Once the alignment has been done a pinhole is positioned on top of the fiber core to only allow the cement in the hole of interest to be exposed to UV light. At this time the fiber position is verified and then a UV light gun is shone on top of the pinhole to cure the cement and bond the fiber to the hole and substrate. This bond holds the fiber in position and also helps to stress relieve the glued fiber end from the rest of the fiber. Other fibers are glued in a similar fashion and in an orderly way to avoid interference between the optical fibers as they are handled and moved under the hole array substrate. Physical interference between fibers is avoided by slightly bending the fibers after gluing so that all the fibers are moved out of the way of the next fiber. The elapsed time between each fiber alignment and gluing is approximately 10 minutes. Using the technique described we manufactured several fiber arrays. The most recent one has 32 single mode fibers at 1300 nm in a 4x8 array and a distance of 500 μm between fiber centers. The fiber ends were located to within 1.5 μm from their ideal position and to a pointing precision of 30 arc-minutes.

We have developed a technique for assembling fiber bundle arrays with improved fiber positioning accuracy. The technique does not depend on fiber core concentricity, on fiber dimensional uniformity, or on a final polishing step. Except for the use of lithography for fabricating the centering doughnuts all the equipment necessary to implement this assembly technique is simple and is easily obtained. We use active fiber alignment to center illuminated fiber cores within lithographically made referencing doughnuts to achieve micrometer precision in fiber end positioning. In addition, the array of centering doughnuts makes the detection of alignment errors straightforward and limited by the microscope resolution. The assembly method is very well suited for the manufacture of small arrays and for the development of optical computing and photonic switching systems where only a few fiber arrays are required but with changing requirements. Some drawbacks of the technique are the assembly time required to construct large arrays, and that it takes only one broken or mispositioned fiber to ruin an entire array. This latter drawback is common to all techniques. Thus fiber assembly reliability and yield are important figures of merit to compare assembly techniques. For future work we plan to automate the technique to decrease assembly time and increase reliability. We also plan to manufacture larger fiber arrays, study fiber array repairability, dimensional stability, and incorporate arrays of microlenses to match the numerical aperture of the fiber bundles to that of our photonic systems.

We would like to thank A. L. Lentine, R. L. Morrison, F. B. McCormick, T. J. Cloonan, R. F. Huisman, R. J. Crisci, G. M. Proudley and M. R. Taghizadeh for helpful discussions.

REFERENCES

1. C. M. Miller, "A fiber-optic-cable connector," The Bell Technical Journal, 54 (9), 1547-1555, 1975.

2. U. Danzer, P. Kipfer, K. Zarl, J. Lindolf, and J. Schwider, "High precision two dimensional fibre-array in silicon V-groove technique," Angewandte Optik, Physikalisches Institut der Universitat Erlangen, Annual Report 1992.

3. A. Sasaki, T. Baba, and K. Iga, "Pin-in microconnectors for alignment-free coupling of optical fiber array," IEEE Photonics Technology Letters, 4 (5), 908-910, 1992.

4. G. A. Koepf and B. J. Markey, "Fabrication and characterization of a 2-D fiber array," Applied Optics 23 (2) 3515-3516, 1984.

5. N. Basavanhally, "Opto-mechanical alignment and assembly of 2D-array components," Technical Digest of the IEEE Princeton Section Sarnoff Symposium, March 26, 1992.

6. G. M. Proudley, C. Stace, H. White, "Fabrication of 2-D Fibre-Optic Arrays for an Optical Crossbar Switch," Submitted to Optical Engineering.

7. K. Koyabu, F. Ohira, T. Yamamoto, and S. Matsuo, "Novel high-density collimator module," in Technical Digest, Conference on Optical fiber Communication/International Conference on Integrated Optics and Optical Fiber Communication, 1993 Technical Digest Series, Vol. 4 (Optical Society of America, Washington, D.C., 1993), pp. 2-3.

Free-space Multicast Non-blocking Interconnection Using Multidimensional Multiplexing Concepts

Yao Li, Ting Wang, Z. G. Pan
NEC Research Institute, Princeton, NJ 08540, U.S.A.

Jacob Sharony
Department of Electrical Engineering, Columbia University
New York, NY 10025, U.S.A.

ABSTRACT

Free-space optical schemes to minimize the number of switches for non-blocking multicast and broadcast interconnect applications are introduced and experimentally demonstrated based on the multidimensional multiplexing concept.

A non-blocking generalized switching network of N nodes is the one where each input can broadcast or multicast its message to any combination of output nodes without experiencing any internal blocking. In case that one input is to be multicast to j, $j < N$, outputs the remaining N-j output nodes can still be accessed by any of the remaining input nodes without experiencing internal blocking. Using this criteria, most popular point-to-point switching networks do not qualify to handle non-blocking communications for the generalized switching applications. Using the space switching concept a cross-bar network is about the only one which handles strictly non-blocking general purpose networking. A cross-bar has to use N^2 basic switches making the hardware implementation of a large network a very difficult task. The reduction of switching complexity for a general-purpose strictly non-blocking network is not possible using a purely 1D switching technique since such a network has to make available, at each of its N output nodes, all its N input signals so that any output node can independently select any input signal.

In our approach, instead of a purely 1D switching the multiple multiplexing techniques are used [1]. Here, the multiple multiplexing implies that the explicitly multiplexed signals in the time, wavelength, or space domain need to be multiplexed one on top of the other again. Let us assume for a general k-tuple multiplexed system of N nodes with $N = \mu_1 \mu_2 \ldots \mu_k$; each has a unique identity composed of k indices. Since each of the N receiving nodes receives entire inform from all the input nodes, to select an input at an output node, the receiver has to access each of the k dimensions and to select (by demultiplexing) the corresponding channels. Selecting a specific sub-channel in dimension d is equivalent to a complexity of $O(\mu_d\text{-}1)$, i.e. the number of basic 2x2 switches is $O(\mu_d\text{-}1)$, and for N users the total switch count is $O[(\mu_d\text{-}1)N)$. Thus, the total complexity of the network is $O[(\mu_1 + \mu_2 + \ldots + \mu_k\text{-}k)N]$. Since all μ_i ($i = 1,2 \ldots k$) are symmetrical, a minimum complexity will occur when all μ_i are identical. Thus, a minimum complexity of $kN(N^{1/k}\text{-}1)$ is obtained for $\mu_1 = \mu_2 = \ldots = \mu_k = N^{1/k}$. The overall complexity can be reduced by increasing k, however, since the minimum number of sub-channels in any dimension is two, no more than $\log_2 N$ dimensions can be used for a total of N signals. Thus, for $k = \log_2 N$, the complexity approaches the absolute limit of $N\log_2 N$ which ties the information lower bound pointed out by Shannon [2]. Using electronics, a $k=2$ system (time, and space) can be implemented. The use of optical fiber components allows $k=3$ with an additional wavelength dimension. When the free-space optics is used, angular dimensions in two perpendicular planes as extra degrees of freedom can be included making a $k=5$ system feasible. One additional advantage of the multiple multiplexing is that instead of squeezing all complexity into a single dimension making the system working at its extreme limit, each dimension handles its fair share of switching complexity at its comfortable range.

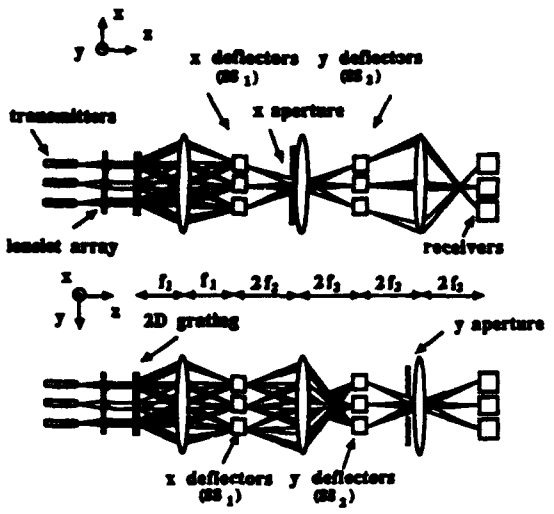


Fig.1: Top and side views of a free-space interconnect using double angular multiplexing.

To confirm the proposed multi-dimensional switching concept, an N=9, k=2 system utilizing two mutually orthogonal angular dimensions is sketched in Fig.1 for its top and side views. For the broadcast and select operations, respectively, a 2D Dammann grating and two 1D optical deflector arrays are employed. The Dammann grating splits an input beam into 9 angularly encoded beams and multiplexes them with the help of a spherical lens into 9 spatial spots to be selectively switched by the two beam deflector arrays. The first and second deflector arrays select one out three angles along the XZ and YZ planes, respectively. In this way, instead of using 81 switching states, only 2x9x3 = 54 switching states are used. The larger the N, the more savings of the switching states.

The angular selective switching can be implemented using a multichannel A-O deflector array. Since the number of angular channels is fundamentally related to spatial and frequency resolution, various technological and fundamental limitations restrict the network interconnect capacity. We have performed calculations of limitation on such a capacity based on parameters of the multichannel A-O deflectors. Fig.2 plots the network capacity limits due to the A-O deflector's time-bandwidth product, the grating's space-bandwidth product, and the interfacing numerical aperture, where the parameters are: f_1, the focal length of the lens; f_c, the central frequency of the A-O deflector; λ, the optical wavelength, z and h, the thickness and width of the transducer of each deflector, and s, the spacing between two consecutive deflectors. More than 32 angular channels can be used in each dimension making a system interconnecting more 1,024 nodes possible.

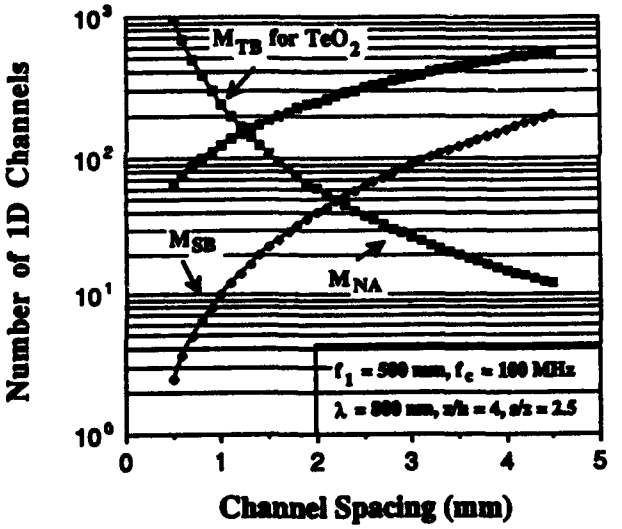


Fig.2: Interconnect capacity limit due to fundamental & technological constraints.

Experimental verification of the proposed k=2 system was performed using two 8-channel TeO_2 A-O deflector arrays fabricated by Brimrose [3]. In the proof-of-principle experiment, the N=64 system was built and tested. Experimental conditions and results will be presented at the conference.

[1] J. Sharony, T. Stern, and Y. Li "Universality of the multidimensional switching networks," *IEEE/ACM Tran. Network*, submitted.

[2] C. E. Shannon, "Memory requirements in a telephone exchange," *Bell System Tech. J.*, 29 (1950) 343-349.

[3] Y. Li, et. al., "Minimum complexity free-space optical nonblocking networks for multicast interconnect applications," *Opt. Lett.*, 19 (1994) to appear.

Parallel optical networks : interconnection patterns, physical modelling and characterisation.

S. Kocon, P. Churoux, M. Fracès, J.P. Bouzinac, D. Comte, N. Hifdi, J.Y. Rousselot.

ONERA -CERT
2, avenue Edouard Belin - B.P. 4025, 31055 TOULOUSE CEDEX
Téléphone : 61.55.71.05 - Télécopie : 61.55.70.74

We discuss interconnection networks applied to a general parallel computing architecture. Several criteria enable us to choose a specific network. An optoelectronical system, is proposed. We present an optical model and the corresponding experimental results.

Photons and matter-photons interactions are used in communications, interfaces and processing inside digital parallel computers. Parallelism involves a great number of elementary processing units (PEs) working together. Communications between these PEs or to the external world are primordial for the global efficiency of the computer. For a given number of PEs, communications have an influence on the data flow and the degree of freedom which is necessary to implement a suitable interconnection pattern.

A theorical analysis of different types of interconnection networks and the experimental results of a particular $N^2 \rightarrow N^{22}$ network are presented. In such an architecture, the applications which can be supported may be as varied as data base, image and signal processing, matrix operations.

The needs of data movements required by these applications enable us to extract a communication kernel : we discuss its compatibility with free-space optical technology. According to the optical SBWP (Space Bandwidth Product) parameter, a bidimensional optical multistage interconnection network is achievable even if the degree of parallelism is high. Moreover, one system performs all wanted communications. Multistage network is composed of several stages of fixed long link patterns combined with dynamic short link patterns (the switch element array). In our approach, the fixed long link patterns would be optical and the switch element array would be implemented with electronic technology which is efficient for neighbouring connections.

Different attractive patterns of multistage networks are compared according to the following criteria :

- _ to minimize the number of crossing through the network for the desired communications;
- _ to achieve the global reconfiguration with a SIMD process i.e. a single instruction configures all switches of a same stage.

The classical multistage networks for our applications seem not to respond to our need, so we have developed a specific one. It is a bidimensional Omega / shuffle-exchange network with additional neighbouring connections between nods in a same stage. For N^2 inputs, it consists of $\log_2(N)$ stages with all same fixed long link pattern corresponding to a bidimensional perfect shuffle.

Different network architectures were considered depending on :

- _ the network configuration process ;
- _ the alternative between a implementation with $\log_2(N)$ same physical stages or a single physical stage implementation.

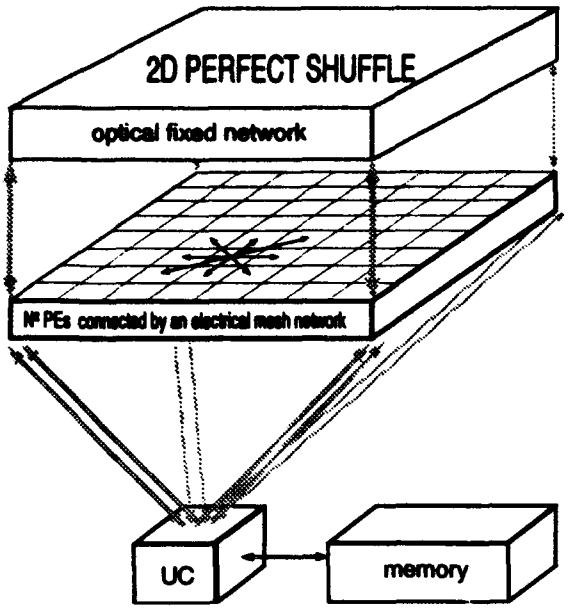


Figure 1 : our selected architecture.

We compare the different networks according to the following parameters : the network configuration time ; the data transfert time ; the number of optical connections. We take also into account the capability of the network to be bi-directional as opposed to a mono-directional ring structure. We have finally chosen the architectural option including a monostage $N^2 \rightarrow N^2$ network and a network configuration process using a fixed broadcasting $1 \rightarrow N^2$ network . In this option, PEs are interconnected with an electrical mesh network so that they simulate the switch element array. Optical 2D perfect shuffle network and the optical broadcasting $1 \rightarrow N^2$ network are connected to the processing unit array (see figure 1).

After this, we will discuss different optical means which allow to implement fixed long link patterns. Our goal was to estimate the deflection limitations of these different tecnics and verify if they are able to produce a highly parallel 2D perfect shuffle pattern.

The interfaces between the N^2 processing units and the optical fixed long link pattern is composed of source and detector arrays. The emitted beams are supposed gaussian and they are collimated and focused by microlens arrays. Refractive and Diffrative optics are possible to perform the needed deflections : a microprism array ; a micrograting array ; a CGH producing both the deflection and microlens functions (example, shifted Fresnel microlens).

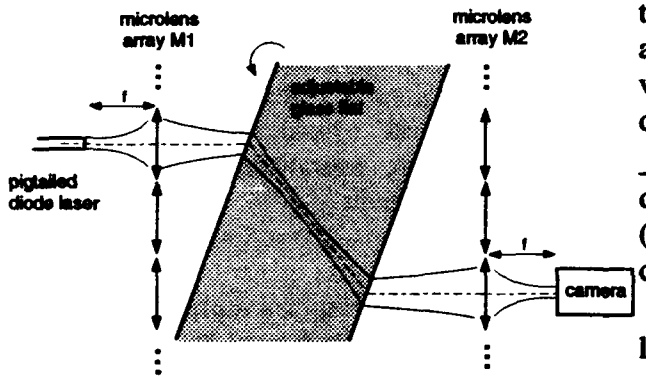


Figure 2 : basic experimental bench to study the deflection system using a microprism array.

We have analysed theoretically the deflection function based on a microprism array and implemented an experimental setup to validate this concept. The experiment, described in figure 2, consists in :

_ a pigtailed laser diode with a fiber core diameter of 5 µm to simulate a VCSEL (Vertical Cavity Surface Emitting Laser diode) ;

_ two 103x103 250 µm diameter microlens arrays ;

_ a glass flat which can be rotated to simulate different angle prisms ;

_ a CCD camera for detection.

The experimental results were in agreement with the theoretical model. The theorical results are cheering and show that a 256 x 256 perfect shuffle network could be done.

We have presented results about a deflection system using microprisms. However a refractive microprism array having a particular angle for each elementary prism seem not to be easy to produce. Diffractive elements will probably be more compatible with planar electronic integrated technology.

Design and Implementation of a Ring Array Optical Interconnect for SIMD Machines

J.-M. Wang, E. Kanterakis, A. Katz, Y. Zhang, Y. Li*

InterDigital Telecom, INC.
Division of InterDigital Communication Corp.
833 Northern Boulevard, NY 11021
Phone: 516-767 2254

*NEC Research Institute, INC.
4 Independence Way
Princeton, New Jersey 08540

Abstract: We present the design and implementation of an optical ring array free space interconnect. The system was successfully operated at a data rate of 500 MHz and with a total system throughput of 8 Gbps.

Summary: Electronic interconnections have been recognized as the bottlenecks of high performance computing systems. Because of their 3-D nature and their matched impedance, optical free space interconnects are the best alternative to electronic counterparts. Massively Parallel Machines (MPMs) require that the interconnect latency between processors be kept as small as possible. For this purpose, we have developed optical interconnects using ring topologies [1].

The principle of a Nearest Neighbor ring topology is depicted in Fig.1. Fig.1(a) shows a NN interconnect based on a rectangular grid topology. The major problem is that the interconnection length between processors is not the same on the boundary as in the central region. This unequal interconnection length will cause system latency. The problem becomes severe when the total number of processors is increased. By arranging the processors in a ring as shown in Fig.1(b), this boundary effect can be eliminated. Other rectangular grid topologies such as PM2i and Hypercube, can be implemented in a similar fashion. In addition, operations required by the ring topologies can be implemented by performing simple image rotations.

Our experimental system is shown in Fig.2. It consists of a data generator, an input ring assembly, a four-channel free space interconnect, and an output ring assembly. The input ring assembly consists of 16 laser transmitters; each being individually modulated by a 500 MHz PN data sequence generated by a data generator. In the four channel interconnect, each channel is designed to perform one of the four operations required by the NN interconnect. To demonstrate channel switching operations, Liquid Crystal (LC) switches (s1-s5) were employed in each channel. A single GaAs receiver was employed at the position of the output ring assembly. Data sequences for the four interconnect channels were received sequentially by setting the proper state of each LC switch. The received data sequence was then compared with that of the input. The experimental results showed that the data sequences corresponding to the NN interconnect were received correctly for all 16 transmitters. We also demonstrated that other topologies such as PM2i and Hypercube can be implemented by performing different rotation operations. This novel interconnect, using space invariant optical elements, having identical interconnect latency,

and allowing network reconfigurability, will be suitable for high speed Massively Parallel Machines such as SIMD machines.

References

[1] Y. Li, B. Ha, T. Wang, S. Wang, A. Katz, X. J. Lu, and E. Kanterakis, "Ring-array distribution topology for optical interconnects," Appl. Opt. 31, 5548-5558 (1992)

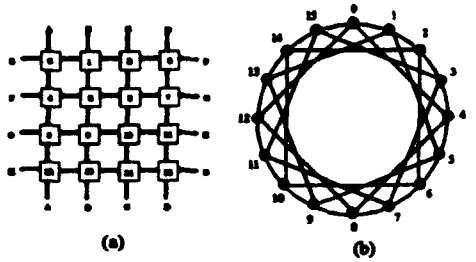


Fig.1 (a) Nearest Neighbor interconnect configured on a rectangular grid. (b) the same interconnect but with a ring topology.

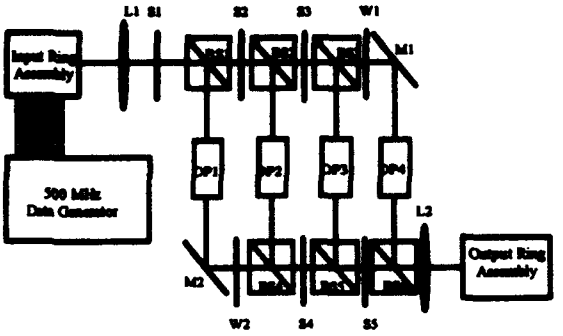
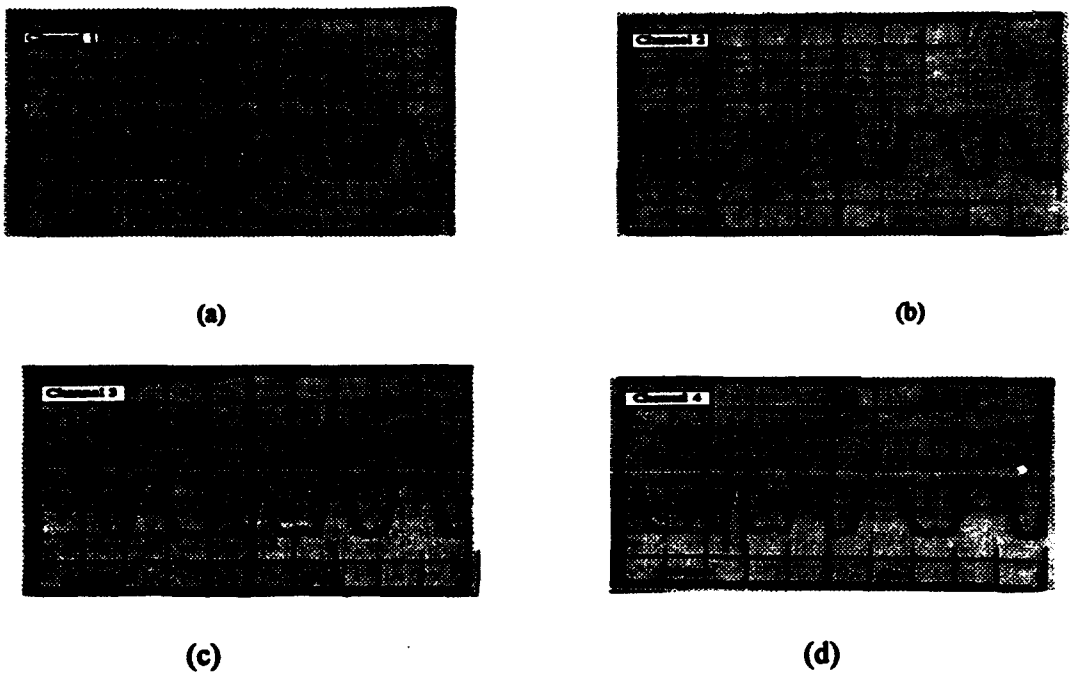


Fig.2 Schematic of the experiment setup



(a) (b) (c) (d)

Fig.3 Experimental results of the Nearest Neighbor interconnect. The pulse width is 2 ns. (a) corresponds to i+4 interconnect; (b) corresponds to i+1 interconnect; (c) corresponds to i-4 interconnect; (d) corresponds to i-1 interconnect..

Parallel Processing Architectures with Dynamic Optical Interconnections using Spatial Light Modulators

N. McArdle, J.F. Snowdon, and M.R. Taghizadeh

Department of Physics, Heriot-Watt University
Edinburgh EH14 4AS, UK
Tel. +44.31.451.3027 Fax. +44.31.451.3136

ABSTRACT

The advantages of a spatial light modulator based system for reconfigurable optical interconnections in parallel processing applications are discussed. The design of the system and experimental results are described.

1. INTRODUCTION

Optical interconnections have many advantages over electronic connections in computing and communication. In addition to these advantages a degree of programmability of the optical interconnections can provide further benefits. In this paper we concentrate on interconnections in optical computing systems using nematic liquid crystal spatial light modulators (LC-SLMs). These devices have been chosen for their low cost, easy availability, and straightforward configuration by interfacing of the drive electronics to host computers.

2. ROLE OF RECONFIGURABLE OPTICS

Reconfigurable interconnections have several advantages over fixed interconnection stages. In particular they allow the maximisation of the performance gains of non-local optical interconnections [1] over a range of algorithms inherent in practical image processing tasks. They may also be used to provide acceleration of individual algorithms by changing the processor interconnection harness during run-time of a program.

We have investigated how reconfigurable interconnects may be employed over a small range of tasks including image correlation, noise removal and enhancement, FFTs and sorting. In this study we have used such interconnects as we have experimentally configured, including nearest neighbour, next-nearest neighbour, image dilation and various shuffle connections. In particular we have built a set of optimised tasks which may be expected to run on our own demonstrator hardware containing a reconfigurable plane. This enables us to generalise the functionality of our optical processing modules while maintaining the performance advantages of the optics, thus increasing the overall performance of the system. Numerical results obtained by simulation of our reconfigurable architecture on a distributed array processor (DAP), allow comparison with non-reconfigurable computing schemes.

3. DEMONSTRATION

Optical interconnections may be classified into two categories: space-invariant and space-variant. Although both of those have useful applications, the latter is highly desirable, because

of its ability to implement arbitrary interconnections. We have already demonstrated fan-out beam array generation with a multi-level phase LCSLM [2] as well as a dynamic perfect shuffle interconnection [3]. The present system, although limited to binary phase modulation, uses a LCSLM with higher resolution and smaller pixel size than the previous device. The pixel size of 31μm is currently the smallest available for this type of device. In comparison to the minimum feature size of fixed holographic interconnections manufactured by lithographic techniques, this is relatively large. The large pixel size limits the design freedom of the phase pattern as well as producing a small diffraction angle. The consequences for the physical design of a system have previously been discussed [3,4].

We shall present results of various interconnection topologies which have been implemented in the reconfigurable optical system [5 ,6]. These topologies include simple fan-out in 1 dimension, nearest neighbour interconnections, nonlocal interconnections and array generation. Interconnection topologies such as these are required for various parallel and image processing algorithms. We shall discuss these algorithms and describe the advantages obtained by providing a degree of programmability of the interconnects.

4. ACKNOWLEDGEMENTS

Financial support from the British Council is acknowledged. The authors thank Paul Blair and Nigel Watson for assistance in providing the computed phase patterns for some of the interconnection topologies implemented.

5. REFERENCES

1 . J.F. Snowdon, A. Kashko, and B.S. Wherrett, "Design of digital optical processors", in *Optical Information Processing Systems and Architectures IV*, B. Javadi, ed., Proc. SPIE **1772**, 332-337 (1992).

2 . T.H. Barnes, T. Eiju, K. Matsuda, H. Ichikawa, M.R. Taghizadeh, and J. Turunen, "Reconfigurable free-space optical interconnections with phase only liquid crystal spatial light modulator", Applied Optics **31** (26), 5527-5535 (1992).

3 . H. Ichikawa, T.H. Barnes, M.R. Taghizadeh, J. Turunen, T. Eiju, and K. Matsuda, "Dynamic space-variant optical interconnections using liquid crystal spatial light modulators", Optics Communications **93** (3,4), 145-150 (1992).

4 . H. Ichikawa, N.M[illegible]rdle, and M.R. Taghizadeh, "The requirements for spatial light modulators for optical [illegible]nterconnection", in *Spatial Light Modulators and Applications Technical Digest,* 1993 (Optical Society of America, Washington, D.C., 1993), Vol. 6, pp74-76.

5 . H. Ichikawa, J. Turunen, J.F. Snowdon, M.R. Taghizadeh, and N. McArdle, "Application of Spatial Light Modulators in Optical Interconnections", in *Optics as a Key to High Technology: 16th Congress of the International Commission for Optics*, Gy. Akos, T. Lippenyi, G. Lupkovics, A. Podmaniczky, Editors, Proc. SPIE **1983**, pp491-492 (1993).

6 . N. McArdle, J.F. Snowdon, and M.R. Taghizadeh, "Reconfigurable Optical Interconnections for Parallel Processing", presented at *Frontiers in Information Optics: Topical Meeting of the International Commission for Optics,* Kyoto, Japan (April 1994).

A Optical Package Of Reconfigurable Free-space Optical Interconnection Network For Multiprocessor System

Mingcui Cao, Hongpu Li, Xiangjun Zhao, Fengguang Luo, Xu Jun
(National Lab of Laser Technology, Huazhong University of Science and Technology, Wuhan, 430074 P.R.China)

Ronghan Wu, Wenxi Gao
(Nation OEIC Lab, Institute of semiconductors, Chinese Academy of Science, Beijing, 100083 P.R.China)

ABSTRACT

A optical package of reconfigurable free-space optical interconnection switching network for multiprocessor system has been presented. A separated (2,2,2) node switch type consisted of two space light modulators SEEDs is presented as nodes of network system,. Optical module of one stage in optical switching network of 8 x 8 channels is demonstrated and tested.

Key Words: Optical computing, optical interconnection

SUMMARY

The interest has recently grown in reconfigurable optical interconnects and optical switching networks for multiprocessor and telecommunication system.[1]-[3] There are three free-space interconnection multistage networks for reconfigurable optical interconnection network, such as Crossover, Omega, Banyan network. We adopt crossover network as reconfigurable optical interconnection network for multiprocessor. The optical system of switching network presented in this paper comprises of optical package of Log_2N ,which optical system have same hardware components except different period of prismatic mirror arrays. The optical package of each stage consists of 4-levels phase Fresnel lenslet arrays (F) , prismatic grating mirror arrays (PG), the beam splitters (BS), the quarter waveplates, self-electro-optic-effect devices of electronic addressing(SEED) devices, and testing arrays , as show in Fig.1. The optical system based on the principle of focal plane imaging. The phase Fresnel lenslet array is used as the generation of light spots array which split one collimated laser beam with homogeneous distribution in some region into light spot array on the focal plane. It is also used as imaging lenslet array to imaging the light spot of each channel on each mesa of SEED and testing array substrates.

A switching network comprise of both link and node. A optical crossover interconnection network have $Log_2(N)+1$ node stages with N/2 node and Log_2N optical link stages with N links. The optical hardware of node stages is the first module in Fig.1, which includes F_1,BS_1,$SEED_1$,and $SEED_2$. A separated (2,2,2) node type of electronic address is presented for node switching of the system, as shown in Fig.2. In optical system, the input image is separated two image copes by BS_1. Each channel of one image copy is controlled by $SEED_1$ of electronic address to yield the straight connection. The other copy is controlled by $SEED_2$ to yield crossed connection. The $SEED_1$ and $SEED_2$ are operated at the normal-off state, or the normal-on state . The connection type of a pair of input and output ports are decided by electronic signals applied on pixels of $SEED_1$ and $SEED_2$. The optical hardware of link

stage is implemented by the second module in Fig.1, which consists of F_2, BS_2, M and PG. The straight connection is implemented by the route of F_1-BS_1-$SEED_1$-BS_1-F_2-BS_2-M -BS_2-D. The crossed connection is implemented by the route of F_1-BS_1-$SEED_2$-BS_1-F_2-BS_2-PG- BS_2-D. The testing signals are used as O/E converter for cascading electronic addressing signals of $SEED_3$ and $SEED_4$ in the next stage.

Based on the architecture detailed above, we fabricated an optical package of one stage in reconfigurable free-space optical switching network of 8x8. All channels of 8x8 are arranged in the size of 3.2 x 3.2 mm^2 when the space between adjacent channels is 0.4 mm. But the size of optical package body is 35 x 30 x 15 mm^3. It can contain 32 x 32 data channels to travel through. Due to focal length of phase Fresnel lens can be made very small, the design of optical system is very compact, in which the optical components in the first and the second modules is fixed by optical glue.The efficiency of 4-levels phase Fresnel lens array is about 63 %. The insertion losses of optical switch devices SEED estimated from the measured, the reflectivity of high state are about 1.5 dB . The switch time of SEEDs are about 10 ns, when they operate in normal-on state. the response time of testing array is about 2 ns. Some basic system operation were carried out on the optical package. A data packet which includes 8 bit of data is transmitted through one optical package of interconnection network from the input port to the output ports. The four-functions of the straight, the exchange, the upper broadcast and the lower broadcast of (2,2,2) node switching in optical interconnection network are implemented by SEED devices. The output signal from testing array are used as the input signal of the next state for cascading when input laser incident on the mesas of SEEDs. Since SEED device is the space light modulator of electronic address, so the interconnection state is controlled by electrical signals during the system operation, the processors can use more efficient. Optical package is very stable and reliab and is very easy to adjust. The optical package of reconfigurable free-space interconnection switching network suited for very high speed operation system.

Reference
[1] T Sakano et al Appl Opt., Vol.32 No.20 pp. 3690-3699 (1993)
[2] T.J.Clloonan, et al, Appl. Opt.,Vol.31, No.35, pp.7471-7492, (1992)
[3] Mingcui Cao, Hongpu Li, Fengguang Luo, Ai jun, Vol.32, No.33, (1993)

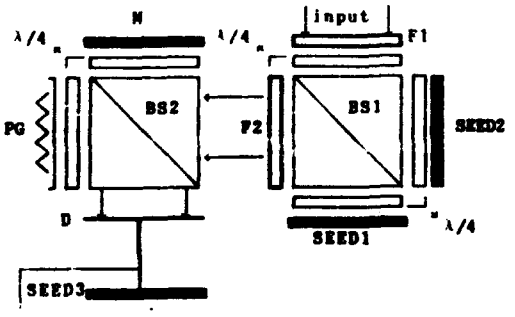


Fig.1, The optical system of one package in reconfigurable switching network.

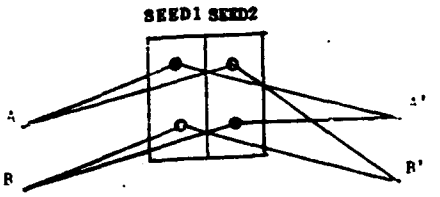


Fig.2,A separated (2,2,2) node type of electronic address.

A Distributed, Reconfigurable Free-Space Optical Interconnection Network for Massively Parallel Processing Architectures

Ian Redmond ((609)951-2718) and Eugen Schenfeld ((609)951-2742)
NEC Research Institute, Inc.; 4 Independence Way ; Princeton, NJ 08540 USA

Abstract

We present a 64-port, free-space network prototype, with communication rates of greater than 1 Gbit/Sec per port. Using today's technology, our network scales to thousands of ports and is useful for massively parallel processing architectures.

1 Introduction

The interconnection network plays an important role in the overall performance of parallel processing systems. Optics has been suggested as a potentially superior technology over electronic, for interconnecting thousands of processing elements (PEs) in a massively parallel processing system (MPP). In an MPP system, a PE may be built around a state-of-the-art, off-the-shelf processor (Digital "Alpha", MIPS R4400, etc.). To serve the interconnection needs of today's and near future processors ("Intel 2000 CPU"), that are being and will be used for building MPP systems, a high performance network is needed. Such processors, having a performance rate of one to two thousands MIPS (million instructions per second) on words of information that are 64 to 128 bits long, generate a total throughput of 128 to 256 Gbit/Sec. Not all of this traffic needs to be handled by the network. A fraction of this (e.g., 10 GBit/Sec per PE) may cause difficulties in large systems with thousands of PEs.

2 The Quest for the Ideal Network

A network can be characterized by several parameters: Number of ports; bandwidth capacity per port; the network's structure; latency delays: from one port to another, without arbitration (i.e., circuit switching or reconfigurable mode of operation); and routing and switching delays (caused by arbitration and other traffic specific issues, such as blocking, and also depends on the network structure).

It is generally accepted that for large networks (thousands of ports), optics is better than electronics in providing high bandwidth connections. However, it is also commonly accepted that today, optics cannot compete with electronics for general purpose processing because of higher cost and the immaturity of the optics technology.

3 A Reconfigurable Free-Space Network

Our proposed optical network is based on several basic principles and observations on the needs and possible tradeoffs of an optical MPP network:

1) "Logic-Less" optical operation: Optical technology is used for point-to-point high bandwidth connectivity and not to do dynamic routing or arbitration.

2) Distributed Layout and Control: No centralization in terms of one common element (e.g. a lens) or active device (e.g., one array of VCSELs). No central arbitration and control is needed. The optical network scales in proportion to the number of PEs (although for practical reasons, one would choose to use fewer, but larger active devices such as VCSELs arrays).

3) Reconfiguration is not needed very often as many parallel application exhibit switching locality: i.e., a PE will only need to communicate with a small number of other PEs for a period of time. Choosing between these PEs can be done by the electronic switches that acts as "interconnection caches" to the initial reconfiguration of the optical network.

3.1 Folded Clos Network

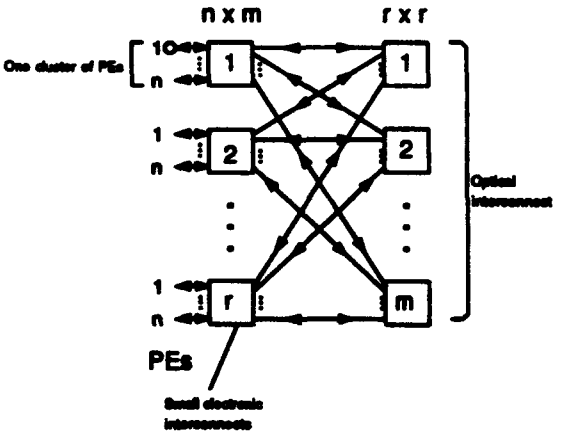


Figure 1: A folded three stage Clos network.

Figure 1 presents the structure of our network. The middle stage is the optical network, made

of "logic-less" switches (reconfigurable or circuit-switching operation) using VCSELs arrays. The first and third stages (folded into one) are made of electronic, small crossbar switches.

Such a network can be used to map parallel applications that have switching locality. We have investigated the mapping issue previously and came to a conclusion that many classical communication patterns (such as trees, 2-D and 3-D meshes, hypercubes, pyramids, mesh of trees etc.) as well as non-symmetrical communication patterns can be well embedded in our structure.

3.2 Mapping and Embedding

Figure 2 is an example of the embedding of a tree into our network. Note that the clustering means that nodes in the same cluster will be mapped to boards that share a common small electronic crossbar switch. The connections between clusters are made by reconfiguration of the optical middle layer of the Clos network.

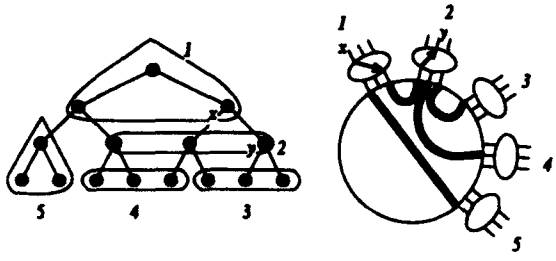


Figure 2: Embedding a binary tree into folded Clos.

4 System Overview

Figure 3 represents the overall system view. PEs are groups into boards, each having a fast electronic crossbar switch. Boards are arranged into columns that are connected using optical free-space multiple buses. Each board can be connected to few other baords (8 to 16). The selection of these boards is done by reconfiguration of the optical interconnections. This mode of operation is useful in many parallel applications that exhibit switching locality or/and have "phases" of computation with specific interconnection topologies.

We used VCSELs arrays that are arranged as 8×8 devices with access to each one of the VCSELs individually. Such an access is not needed for our architecture, but these devices where available off-the-shelf. By having access to individual VCSELs, we could used only four 8×8 devices that are subdivided into 16 separate zones each having 2×2 devices. Thus each PE can reconfigure its subdivision to connect to one of the other 3 boards.

5 Scalability and Future Issues

Future systems may have larger numbers of PEs. One critical element is the size and the electrical connections for the VCSELs arrays to be used. Our prototype is an example of the foreseen maximum needed (i.e., 16 connections per VCSELs array). We anticipate fewer electrical connections in future VCSELS arrays. Such devices can be made as an X-Y matrix or by embedding an "H-Tree" structure to control each sub-division on the array for each PE. The "leaves" of this H-Tree structure end with individual VCSELs that are selected to illuminate. By selecting a certain VCSEL, the connection to that corresponding Board, can be made by the optical layer of the Clos network. The number of high bandwidth connections that need to be made to the package of such an array, will be limited to at most 16. In addition, low speed connections used for choosing the appropriate VCSEL in each sub-division are needed. These are low speed connections since the reconfiguration is expected not to be done very often. One important issue to address is that of the power budget. Currently, we have employed "variable efficiency" holographic elements to maximize the power available. In addition to this, it may be necessary to add amplification or regeneration of the optical data, in certain location, for a high bandwidth and low noise communication. We plan to look into such problems in the future. We will attempt to build part of a larger network for connecting thousands of PEs and with bandwidth of 10 GBit/Sec per channel.

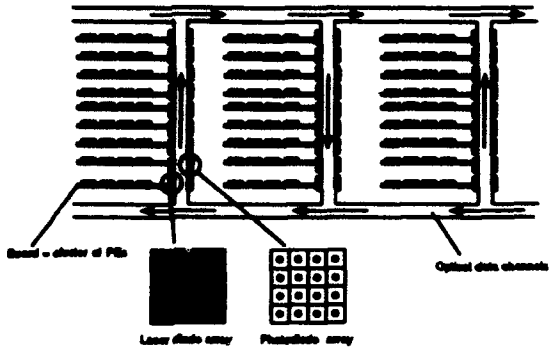


Figure 3: System View of the Optical Network.

6 Summary

We have presented the system structure of a prototype for an optical interconnection network to be used for MPP architectures. Our system benefits from the high connectivity and throughput optics can offer while limiting the processing needed for routing to electronic technology. Many parallel applications can use such a reconfigurable network as they naturally exhibit switching locality in their communication needs. We hope to extend our system in the future to accommodate thousands of PEs in a multi-Gigabit/Sec channels.

Reconfigurable Optical Interconnections in $Bi_{12}TiO_{20}$ Photorefractive Fiber

Alexei A. Kamshilin and Timo Jaaskelainen

University of Joensuu, Väisälä Laboratory, Department of Physics
P. O. Box 111, SF-80101, Joensuu, FINLAND
Phone: 358-73-151-3207, Fax: 358-73-151-3290,

Abstract

Reconfigurable optical interconnections by using double phase conjugate mirror in photorefractive $Bi_{12}TiO_{20}$ crystal are demonstrated. Phase conjugate wave reflectivity up to 7% and with a response time of 5 seconds upon pump intensity 1 mW/mm^2 was obtained at λ = 632.8 nm.

Summary

Photorefractive crystals (PRC) have been proved to be significant in parallel optical information processing owing to their real-time, high density, recyclable volume holographic recording and phase conjugation. One of the most promising and interesting effects recently discovered in PRC is double phase conjugation of mutually incoherent pump beams. For the PRC illuminated on opposite faces by two pumps, two independent counterpropagating beams build up, originating from the beam fanning. They give rise to a common grating, which is reinforced by positive feedback and finally results in the presence of a pair of phase conjugate beams through a cross-readout process[1]. This double phase conjugate mirror (DPCM) can be used as reconfigurable interconnections between two sets of fibers[2]. As an example, interconnection between one fiber and a set of three fibers is shown on the Fig.1. Light emitted from the fiber (Input 1) is focusing by the lens 1 on the PRC's face. At the same time, the light emitted from the set of fibers (Inputs 2-4) is focusing by the lens 2 on the opposite side. After a response time τ, common holographic grating is recorded in the PRC,

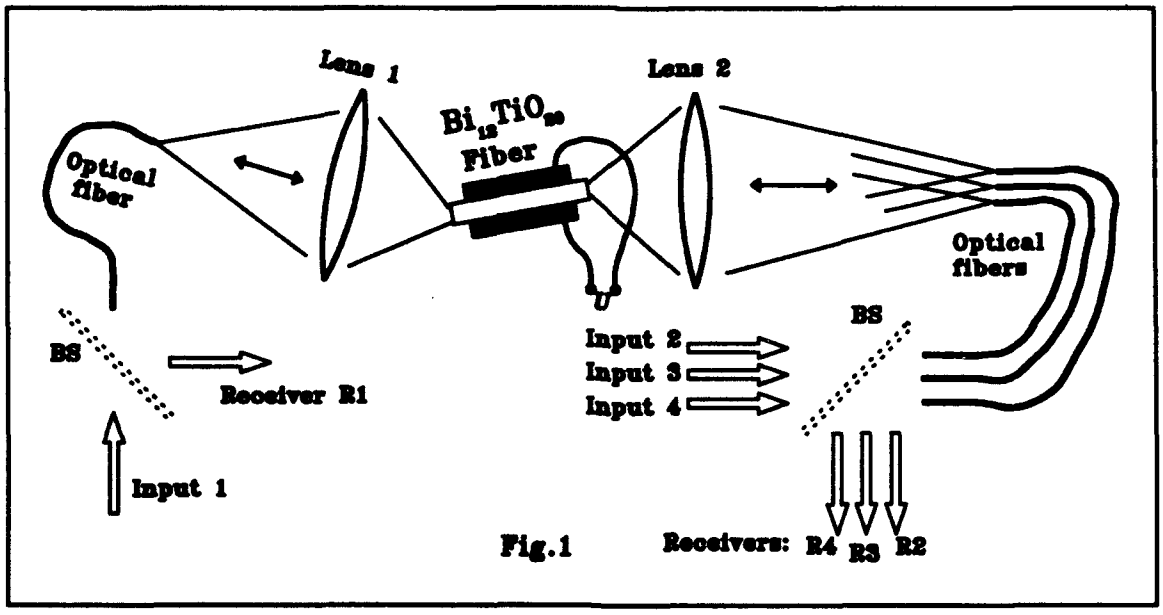


Fig.1

producing a pair of phase conjugate beams, which are automatically introduced into the fiber from one side and into the set of fibers from the other side. Phase conjugate beams can be extracted by using beamsplitters BS. Therefore, the signal from the Input 1 achieves all the Receivers R2-R4 and the sum of the signals from the Inputs 2-4 achieves Receiver R1. In this example the Input 1 is interconnected with all three Inputs 2-4. Interconnections can be simply changed by introduction of light only into two fibers 3 and 4, for example. In that case after the response time τ, a new common holographic grating will be recorded in the PRC and new interconnections between Input 1 and Inputs 3,4 will be established.

Experiments were carried out on a fiber-like $Bi_{12}TiO_{20}$ (BTO) samples. This crystal belongs to the same structural class (sillenite) as $Bi_{12}SiO_{20}$. However, BTO has larger electro-optic coefficient and lower optical activity compared with other sillenites, and is more sensitive compared with $BaTiO_3$ and SBN photorefractive crystals. The fibers were cut out from the bulk crystal along the [110] crystallographic axis and were glued between two electrodes[3]. Their length is 8-18 mm, and they have rectangular cross-section with a size of approximately 1 mm. A bipolar alternating electric field of square-wave form was applied to the fiber to improve its enhancement coefficient. Four longer faces of the fiber were optically polished, but end-faces were slightly grounded to produce a scattering of transmitted beam into the angle of approximately 4 degrees. It was especially made to introduce pump beams of complex (speckle-like) wavefront into the fiber, that allowed us to avoid conical degeneracies in the Bragg matching angle on a given volume grating[4]. Two independent linearly polarized helium-neon lasers (λ = 632.8 nm) were used to pump the BTO-fiber. The input polarization angles were chosen experimentally to produce as high phase conjugate reflectivity as possible. The fiber axis was tilted in respect to the pump beams (as shown on the Fig.1) providing at least one internal reflection for any pump from fiber faces.

Upon these experimental circumstances, the efficiency of transferring the pump beam into the phase conjugate beam up to 7% has been measured in our fiber. Note that the refractive index of BTO crystal is rather high (n_0 = 2.58 at λ = 632.8 nm) introducing big losses of light because of Fresnel reflections. Hence, the end-faces coating of the fiber by antireflection layers could increase the PC reflectivity at least twice. The response time τ is inversely proportional to the intensity of pump beams, and was measured to be 5 seconds for pump beam intensity of 1 mW/mm^2. We succeeded to obtain phase conjugate beams of complex images with spatial bandwidth up to 50 lp/mm.

Single crystal photorefractive fibers have several advantages compared to the bulk crystals. They can be assembled in a variety of configurations, isolating each stack of interconnections from other stacks in adjacent fibers. This can provide realization of great amount of interconnected fibers with a possibility of independent reconfiguration of different groups of them. Moreover, photorefractive fibers are easier to grow by using the Laser Heated Pedestal Growth Technique, that possibly diminishes the price of DPCM elements.

References:

1. P. Yeh, T. Y. Chang, and M. D. Ewbank, J. Opt. Soc. Am. B, 5, 1743 (1988).
2. S. Weiss, M. Segev, S. Sternklar, and B. Fischer, Appl. Opt., 27, 3422 (1988).
3. A.A. Kamshilin, R. Ravattinen, H.Tuovinen, T. Jaaskelainen, and V.V. Prokofiev, Optics Comm. 103, 221 (1993).
4. M. P. Petrov, S. L. Sochava, and S. I. Stepanov, Opt. Lett. 14, 284 (1989).

A compact holographically routed optical crossbar using a ferroelectric liquid-crystal over silicon spatial light modulator.

D.C.O'Brien, Douglas. J. Mcknight, Optoelectronic Computing and Systems center, Campus Box 525, University of Colorado, Boulder, CO 80309., USA. (tel 303 492 3330)

Abstract

A holographically routed crossbar interconnect is currently under development, using a ferroelectric liquid crystal over silicon spatial light modulator as a programmable hologram. Results of simulation and experiment are presented and the potential of the technique discussed.

INTRODUCTION

Reconfigurable free space interconnects have wide application in optical computing and information processing, and crossbars are a well known means to implement them: All inputs are connected to all outputs and unwanted routes are blocked. For an N channel switch this approach has an intrinsic $\frac{N-1}{N}$ fan-out loss. A programmable hologram can be used to replace the fan-out optics and blocking component, creating a dynamic fan-out element to steer the light to the desired output port [1]. This has the potential to remove the fan-out loss in shuttered geometries, and create interconnects with analogue weights using a binary device. Ferroelectric Liquid Crystal spatial light modulators (FELC SLMs) have a robust binary phase modulation scheme [2], so that a binary phase grating can be written to the SLM to create the dynamic fan-out element. In this paper we present design calculations for a 16 input 16 output holographically routed crossbar interconnect, and preliminary results for individual component performance. Full results for the system will be presented at the conference.

OVERVIEW

Figure 1 shows a schematic of the crossbar geometry. The 16 channels are arranged as a 4x4 matrix,as this makes full use of the aperture of the optical system. The SLM is divided into 16 regions, each of which is illuminated by one of the 16 sources. Each region displays a particular base hologram, designed to steer the illuminating beam to the correct output port. There are 16 base holograms, each routing to a particular output port: to route from port 1 to port 16 the correct base hologram is placed in front of source 1.

We are considering several different sources for the crossbar: The preferred option is a vertical cavity

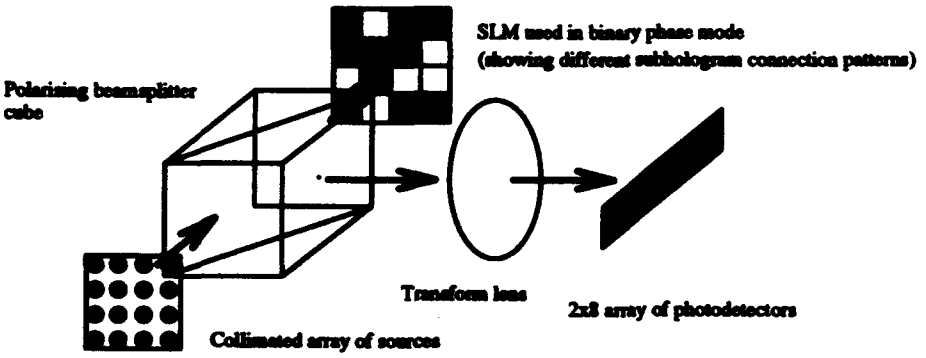


Figure 1: Schematic of holographic crossbar

surface emitting laser array emitting at 840nm , although control of polarisation across the array appears difficult.

The holograms are replayed on a 256x256 liquid-crystal over silicon spatial light modulator (SLM) [3] with a 21.6μm pixel pitch. Each hologram is 64x64 pixels and is created using a simulated annealing technique [1]. They are designed to route to a 2x8 Silicon photodiode array which forms the output of the crossbar.

The output plane is a 2x8 array of Silicon photodiodes fabricated in a 2μm n well CMOS process. These have a 200μm square active area on a 250μm pitch. The circuits have on board thresholding and CMOS output levels.

SIMULATION

The crossbar fails when the power received at a detector which is supposed to be off is greater than the lowest power level which should be detected as a one level (the detector threshold). In a holographic crossbar this is mainly caused by the holograms 'scatttering' light, which creates a uniform noise level

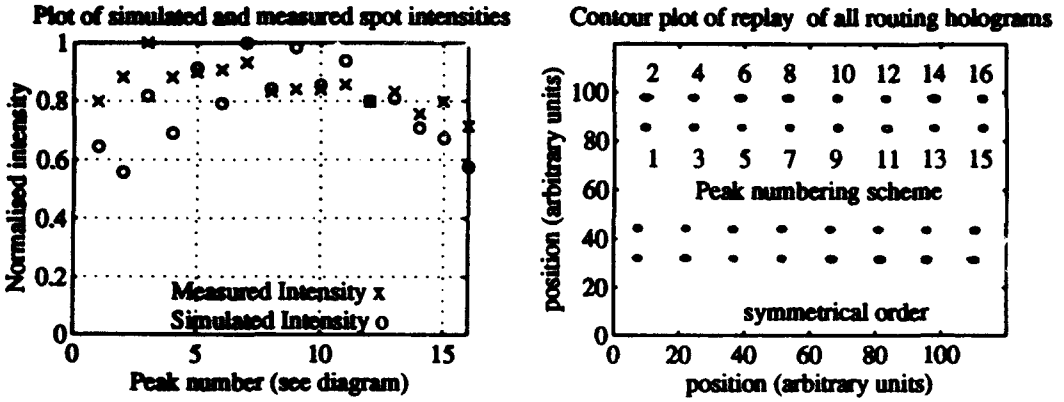


Figure 2: Performance of beamsteering holograms

over the detector plane. As more holograms are illuminated this level can build up and cause the switch to fail. In operation the outputs can either be illuminated or dark, creating a finite number of switch states, which can be simulated. In this case the worst case simulated crosstalk (highest off/lowest one) is 0.16, showing the crossbar should function with good noise margin.

MEASUREMENT

Holograms were calculated and replayed on a 64x64 pixel region (corresponding to a subhologram) of the SLM to test the performance of the device. A collimated beam ($\lambda = 633nm$ passes through a polariser and illuminates the device.The reflected wave is Fourier transformed with an achromat and passes through an analyer. Polariser and analyser are rotated to create binary (0 and π) phase modulation. A grating is created by setting alternate rows of the SLM to opposite states. This should have no central DC spot in replay if the device is binary phase, with two adjacent bright spots. The measured ratio of the bright spots to the DC spot is 33.0 $\pm$ 1.65. This compares favourably with other ferroelectric SLMs [1-2] and indicates the SLM is operating close to binary phase. In this configuration approximately 2% of the power is diffracted into each peak (excluding external losses), compared with a theoretical value of 40%. It is interesting to note that a similar shuttered crossbar would have an intrinsic transmission of 6% before real losses are taken into account- only a modest improvement in device performance is required to reach this figure, and large improvements are expected for a device with a liquid crystal layer optimised for t[illegible] wavelength.

Each of the beamsteering holograms was displayed on the SLM and the ratio of peak intensity to uniform noise intensity measured. Figure 2 shows a comparison of actual and simulated performance, and a contour plot of the replay of all the base holograms. The variation in simulated peak heights is due to the envelope caused by the pixel transmission function, which should be sinc^4 if each pixel transmits uniformly across its area. In reality the function is more complex, which creates measured peaks which are actually more uniform than predicted. The ratio of the spot intensity to the noise level in the hologram was measured for a representative hologram and was 37$\pm$10 dB. Together these results mean that the interconnect should function with a high noise margin.

CONCLUSIONS

Preliminary results indicate high quality holograms can be generated with the SLM device and that the crossbar should function with good noise margin. Overall transmission through the interconnect can be increased beyond an equivalent shadow routed crossbar with only modest improvements over these preliminary results, showing the potential of the interconnect and SLM device.

REFERENCES

(1)D.C.O'Brien, T.D.Wilkinson, R.J.Mears and W.A.Crossland. Dynamic holographic interconnects that use ferroelectric liquid-crsytal spatial light modulators.*Applied Optics.* to be published.

(2)S.E.Broomfield, M.A.A.Neill, E.G.S Paige and G.G.Yang. Programmable binary phase only optical device based on ferroelectric liquid crystal spatial light modulator. *Electronics Letters*,28(1):26-27. 1992.

(3)Douglas J. McKnight, Kristina M. Johnson and Roylnn A Serati. Electrically addressed 256x256 Liquid Crystal on Silicon spatial light modulator. *Optics Letters*,18(24):2159-2161. 1993

Optical interconnect using pixellated spatial light modulators

S.Heddle, J.Gourlay, S.Samus and D.G.Vass
Applied Optics Group, Department of Physics and Astronomy,
The University of Edinburgh, The Kings Buildings, Mayfield Road, Edinburgh EH9 3JZ
tel: 031 650 5270, fax: 031 650 5220, email: heddle@festiv...ed.ac.uk

Abstract

Two approaches to optical interconnect using pixellated spatial light modulators as reconfigurable diffractive optical elements are presented– one analytical using a low resolution SLM, the other using simulated annealing and a state-of-the-art silicon backplane device.

Summary

An analytical approach shows how simple switching may be achieved using a low resolution SLM. Previous work [1,2] has shown that the delta-function-like spikes in the power spectrum of a pixellated filter which give rise to the replication may be attenuated or removed by selection of a specific pixel pitch:size ratio, and introduction of a specific pixel position randomisation scheme which applies a displacement of the pixel centre from its regular position. This generalises the expression for the power spectrum of the Fourier plane filter ($|t(x,y)|^2$) with all pixels 'on' to

$$\langle|t(x,y)|^2\rangle = |P(x,y)|^2 \times Q^2\left[1 - |\rho(x)|^2|\rho(y)|^2 + \frac{1}{Q^2}\frac{\sin^2(\pi Q\alpha x)}{\sin^2(\pi\alpha x)}\frac{\sin^2(\pi Q\alpha y)}{\sin^2(\pi\alpha y)}|\rho(x)|^2|\rho(y)|^2\right] \quad (1)$$

where $P(x,y)$ is the Fourier transform of the single pixel transmission function, $\rho(x)$ and $\rho(y)$ are the Fourier transforms of the pixel position probability distribution functions, α is the pitch of the underlying regular array, and the array consists of $Q \times Q$ pixels. The spectral orders are placed at $(n/\alpha, m/\alpha)$, $n,m = 0,\pm1,\pm2,...$ With square pixels of side $\alpha/2$, $P(x,y) = \frac{\alpha^2}{4}\mathrm{sinc}^2(\frac{\alpha}{2}x, \frac{\alpha}{2}y)$ which has zeroes at the positions of all the even numbered spectral orders other than the zero order. Further, choosing $\rho(x) = \cos(\frac{\pi\alpha}{2}x)$ and $\rho(y) = \cos(\frac{\pi\alpha}{2}y)$, we find that the allowed displacements of the pixel from the regular position are such that each pixel can take one of four allowed positions in an $\alpha \times \alpha$ square, (figure 1) and most importantly the odd numbered spectral orders in both x and y directions are eliminated by zeroes of $\rho(x)$ and $\rho(y)$. If however we retain periodicity in either the x–direction ($\rho(x) = 1$) and/or the y–direction ($\rho(y) = 1$), the first orders on the respective axes will remain. The power in the attenuated orders is redistributed into a diffuse background $\sim 1/Q^2$ times the zero-order intensity ($\sim 0.4/Q^2$ times the first order intensity).

Thus a means exists whereby information can be routed via certain of the first order replicas, dependent on the distribution of the transmitting subpixel in each cell of the array. Figure 2 helps illustrate this.

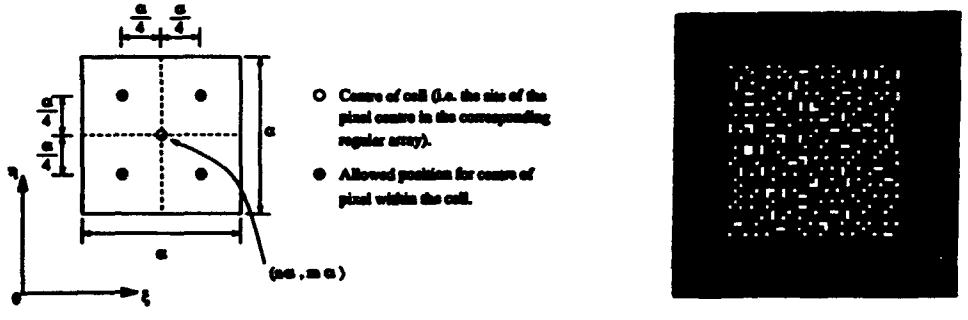


Figure 1: a) Possible pixel positions within $\alpha \times \alpha$ cell. b) A resultant 16x16 array of pixels

Using a 16x16 SLM a 2×2 block of pixels could be used to code each of the $\alpha \times \alpha$ cells, giving an 8×8 array of cells with one pixel 'on' in each cell. The SLM would be capable of routing 8x8 pixel arrays when used in the Fourier plane of a 4-f optical processor, offering the benefits of parallelism and a modest degree of image fanout. The 'on' first order replicas have the same intensity regardless of whether there are zero, two or four of them (to a good approximation): this would not be the case if the routing were achieved simply by writing stripe patterns on the SLM to approximate diffraction gratings.

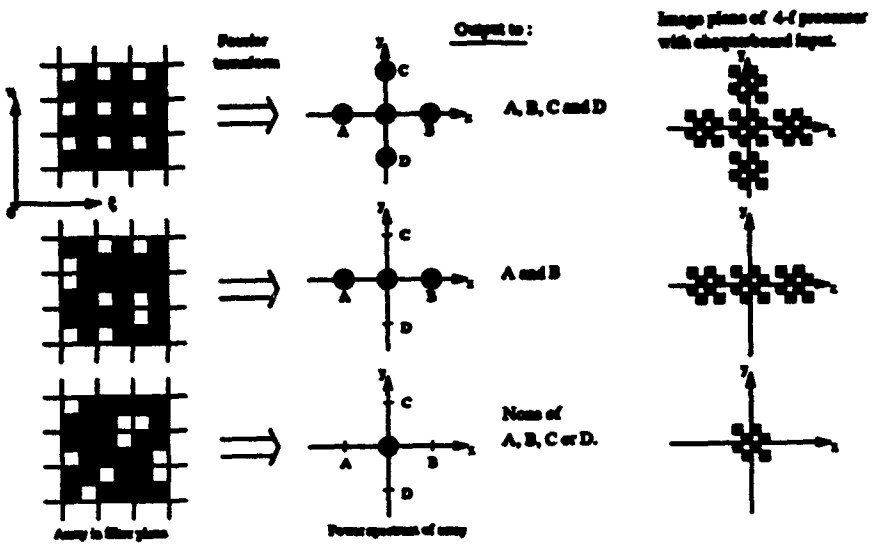


Figure 2: Selective removal of aliasing to provide selective fanout/routing

More useful adaptive optical interconnection may be achieved using binary phase Computer Generated Holograms (CGHs) displayed on SLMs. A very attractive generic type of SLM is the Ferroelectric Liquid Crystal over Very Large Scale Integration (FLC/VLSI) SLM[3]. This device has a FLC cell fabricated on top of a custom designed VLSI silicon backplane. The backplane contains an array of pixel memory elements, pixel mirrors and addressing circuitry. The controllable pixels in the SLM modulate the relative phase by exactly 0 or π due to the switchable uniaxial nature of the FLC structure.

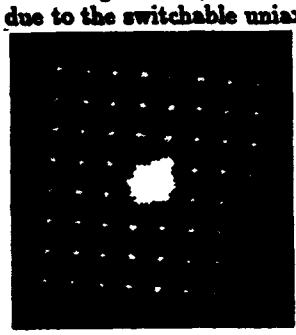


Figure 3: An 8 × 8 holographic interconnect from the SLM

Figure 3 shows an 8×8 array of spots generated using a CGH displayed on a 176× 176 FLC/VLSI SLM. The d.c. spot is very bright due to the low pixel fill factor, inherent in backplanes fabricated using commercial silicon processing with the microcircuitry located around the mirrors. The mirrors are fabricated, at present, using a standard VLSI aluminum metal layer. This layer is deposited with electrical conductivity, rather than optical flatness, as the main criterion. The mirrors are not optically flat and hence scatter light to give noise in the reconstruction. The rough surface profiles of the mirrors also prevent uniform high quality alignment of the FLC over the array.

Planarisation techniques may be used to overcome the problems associated with the VLSI fabricated circuitry and mirrors by burying them beneath a polished dielectric film, depositing high quality metal mirrors on the surface and providing small interconnection vias through the dielectric layer between the original and new metal layers[4]. This processing is expected to increase the reflection efficiency of the devices by about a factor of 2 and increase the fill factor to nearly 100%.

The improvements to the SLM performance will be presented, and comparisons of experimental and theoretical results for the high fill factor SLM, performing holographic interconnection will be discussed.

References

1. S.Heddle, D.G.Vass and R.M.Sillitto, Proc. SPIE 1772, 116 (1992).
2. S.Heddle and R.M.Sillitto, J. Mod. Opt.40(2), 299 (1993).
3. I. Underwood, D. G. Vass and R. M. Sillitto , IEE Proc. 133, Pt.J, No.1, 77 (1986).
4. A. O'Hara, J. R. Hannah, I. Underwood, D. G. Vass and R. J. Holwill , Appl.Opt. 32, 5549 (1993).

Optical Freespace Sliding Tandem Banyan Architecture for Self-routing Switching Networks

Michael W. Haney
ECE Dept., George Mason University
Fairfax, VA 22030-4444 USA
(703) 993-1571

Marc P. Christensen
Photonics, BDM Federal, Inc.
McLean, VA 22102-3204 USA
(703) 848-6909

Abstract

The optical Sliding Tandem Banyan Network permits rapid rerouting of blocked packets owing to the physical co-location of multiple switching stages. Analytical results show enhanced performance and resource savings over a VLSI Tandem Banyan architecture.

Background/Motivation

Future broadband networks will need to handle thousands of Asynchronous Transfer Mode (ATM) channels, implying a capacity in the terabit/second regime [1]. This demand may exceed the abilities of current VLSI based switching technology. In this paper, a new 3-D Optical Multi-stage Interconnection Network (MIN), called the Sliding Tandem Banyan (STB) is proposed. Banyans are useful in self routing networks because a simple destination tag routing scheme can be employed. To overcome the throughput limitation of the basic banyan, the Tandem Banyan (TB) was proposed [2]. A Tandem Banyan (TB) based on perfect shuffle interconnections is shown in Figure 1. The TB achieves low blocking probability by re-routing "blocked" packets in a sequence of banyans which successively remove remaining packets. An arbitrarily low blocking error is achieved by adding more banyans. Each stage of a shuffle-based banyan is identical, making it possible to use a single optical system based on macro-optical elements to *simultaneously* implement all stages in a pipelined configuration with spatial multiplexing of the optoelectronic I/O in a single smart pixel plane [3]. This concept assumes the smart pixels are distributed across several OEICs, on a PC board or MCM. Various implementations of this concept are possible; Figure 2 is a general schematic depiction.

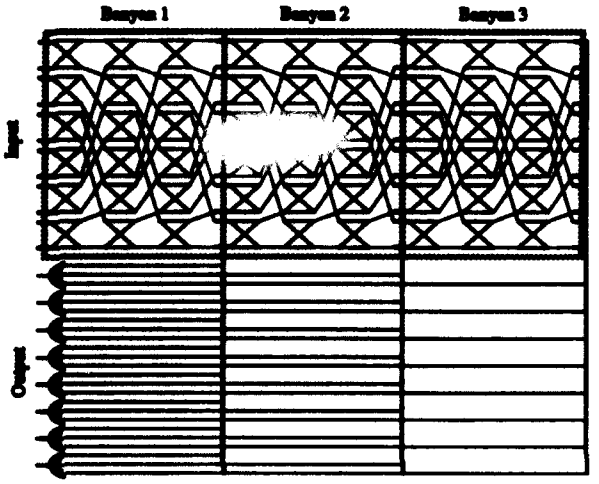


Figure 1: Shuffle based Tandem Banyan for N=8, b=2.

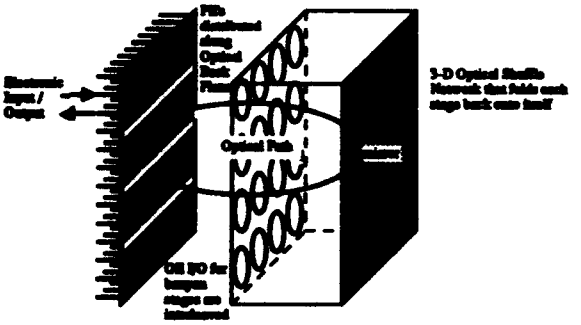


Figure 2: Optical banyan implementation that uses a single optical system to implement all stages, via spatial multiplexing of optoelectronic input/output.

Approach

For a network size of N=1024, the large SBWP of the optical system, and large area of the PE plane allow several banyans of stages to be interleaved in the optical plane before resolution or power dissipation constraints appear [3]. Therefore, a complete TB could be implemented with this scheme. However, the physical collocation of stages afforded by the 3-D optics offers an additional feature not practical with a VLSI implementation – packets may be removed from the network at *any stage*, not just at the end of a banyan. Whenever a packet's route is blocked it is misrouted once, then it begins routing immediately. If the packet is not misrouted again then it will reach its destination in $\text{Log}_2 N$ stages. This will be the end of this packets' banyan, which has slid to align with the misrouting incident, and the packet will be removed. With the STB, resources are not wasted by simply routing misrouted packets to the end of the banyan; the re-routing begins immediately. The STB concept is depicted in Figure 3. After the first banyan, packets can leave the network at any stage.

This advantage is not without some added packet coding complexity though. If packets are to be removed from the network at any stage, the packet must contain information about how far it has been correctly routed. When this number reaches $\text{Log}_2 N$, the packet is to be removed. Self routing algorithms contain a header with the destination address, and the standard TB also requires a conflict bit to determine if the packet has been misrouted. Often the destination address will be rotated by each stage as it is routed, this way the next stage need only inspect the first bit to determine the switching. For the STB the conflict bit would be replaced with a header containing the number of successfully routed stages, and the destination address would not be rotated. The number of successful stages is used to determine which bit of the destination address is to be routed on. It is a simple inspection – if the number successful stages is m, then the m^{th} bit of the destination is the determining one. Furthermore, the STB would give priority to those packets which were closest to their destination, i.e. had the highest number of successful stages in their history. This would prevent a packet which had just begun rerouting from

interfering with a packet one stage from completion. The conflict bit is replaced by this priority number. Misrouted packets simply set this number to zero, then begin routing again.

Blocking Performance Analysis

The STB concept was validated by a simulation of the network architecture. First we simulated the standard TB on a 1024 node network with a 2-D (32 × 32) separable shuffle [4] interconnection. The number of stages per banyan is $n = \log_2 1024 = 5$. The simulation tagged misrouted packets so that they would not interfere with any correctly routed packets. The traffic we chose to simulate was unity permutation traffic. In this traffic pattern every input and every output is used, exactly once, there is no output conflict. A typical plot of the number of packets remaining on the network versus the stage number is shown in Figure 4. Packets are only removed at the end of banyans, this is why the number only changes at integral numbers of 5 stages. Notice that the final banyan in vastly underutilized, it only routed 1 packet for this run. A total of 7 banyans were required to route the packets, so 35 stages were needed.

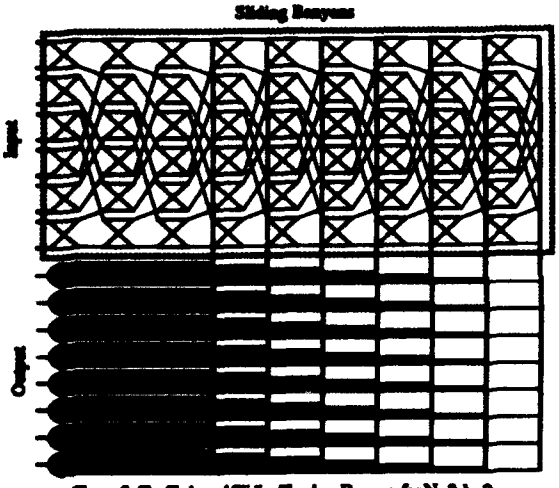


Figure 3: Shuffle based Sliding Tandem Banyan for N=8, k=2.

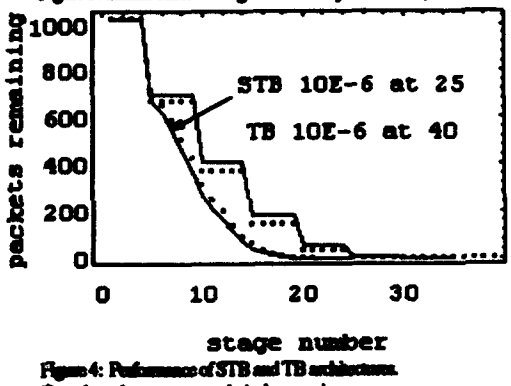


Figure 4: Performance of STB and TB architectures. Dotted graphs represent analytical expressions.

We next simulated the STB. The packets were tagged with the number of successfully routed stages, and this number was used to prioritize the routing of any conflicts that arose. The same input pattern as with the TB was used. The results are shown in Figure 4. Notice that no packets are removed before the 5th stage, but then packets are removed at every stage thereafter. The packets removed in the 6th stage are those which were misrouted in stage 1, then had 5 successful stages. The network required 21 stages to route all 1024 packets, resulting in 14 fewer stages then the standard TB. Also note that an entire banyan of stages is not utilized by the final packet, as it has already progressed towards its destination.

To estimate the blocking performance we statistically analyzed the probability of blocking in the STB and TB. This model is based on a modification to a banyan performance expression derived in [5]. The results are plotted in Figure 4, and show close agreement to the simulation results. This analysis predicts 40 stages for the TB and 25 stages for the STB. to achieve 10^{-6} clocking probability.

Resource Analysis

The number of resources needed to implement the optical STB is approximately proportional to the number of stages needed. Each stage requires N optical detectors and N/k switches (each with k^2 complexity) = Nk electronic switching resources. Additionally the STB increased the complexity of each electronic switch to $k^2 + k$ due to the ability for a packet to be removed from the network at any point. In the TB, only stages at the end of each banyan require this increased switching complexity of $k^2 + k$. The net result is the STB requires only 78% of the electronic resources and 63% of the optical resources of the equivalently performing TB.

In summary, the optical STB network described in this paper is an example of utilizing a fundamental advantage of 3-D optical interconnects over 2-D VLSI technology. The co-location of the multiple stages' switching resources makes possible a significant reduction in the resources required to achieve very low blocking probability. As a measure of resource utilization efficiency, we may compare the optical STB self-routing network with the Benes network, which is known to be the smallest network for which all permutations are realizable, but for which no pipelineable self-routing algorithm exists [5]. The equivalent Benes network requires $2\text{Log}_2 N - 1$ stages, or 9 in our example traffic above. The 25 stages for the STB needed to achieve 10^{-6} blocking is within a factor of 3 to the Benes, yet has the critical advantage of self-routing.

1. J. Hui, *Proc. of IEEE*, V 79, N 2, Feb 1991.
2. F. A. Tobagi *et al*, *IEEE J Sel. A. Comm.*, V9, N8, Oct 91
3. M. Haney, *Optics Letters*, V 17, N 4, Feb. 1992.
4. A. Lohmann, *Applied Optics* 25, N 10, 1543 (1986).
5. C. P. Kruskal *et al*, *IEEE Trans.Comp*, V C-32, N12, Dec 83.
6. F. Tobagi, *Proc of IEEE*, V 78, N 1, Jan 1990.

3-D Free-Space Transmission Polarization-Based High-Throughput Photonic Switching Systems: Architectural Issues.

V.B. Fyodorov

Scientific Computer Centre, the Russian Academy of Sciences, Leninsky pr. 32 A, Moscow, 117334, Russia. Tel: (7-095)938-6646. Fax: (7-095)938-6986.

At present, reconfigurable interconnection networks realizing data exchange between input and output ports are a bottle-neck in high-performance computers and telecommunication systems. The throughput of such switching systems (SSs) depends primarily on data capacity W of connected pairs of input-output channels and the reconfiguration time t_r. An advantage in principle of optical techniques over electrical ones offers strong possibilities to increase W by data transmitting through connected pair of channels in form of 2-D parallel binary digital code patterns with no changing of t_r. However, the specific peculiarities of optics demand architectural principle for photonic SS different from electrical one.

The architecture of a large size photonic SS, first, must make sure for 2-D flat image transmission through each pair input-output ports for any interconnect pattern, second, have great enough numerical aperture of connected optical channels, third, provide a very low crosstalk. In this report architectural decisions that satisfy these conditions are proposed for bulk multistage photonic SS of size $2N^2x2N^2$, where $N=2^r$, r = 1,2,3, ... , consisted of cascaded along K switching stages (polarization switching spatial light modulators) and K-1 routing stages, which are combined by straight optical connections.

The three types of the polarization-based building blocks with M inlets and M outlets, that can be exploited for designing of N^2xN^2 routing stages, are presented in Fig. 1. If the prism angle α satisfies the relation $cos\alpha = 2^{-0.5}(1+1/8n^2)^{0.5} + 1/4n$, where n is the refraction index of PBS, inputs and outputs with the same name are placed on the optical axis that passes through them. In the routing setup C the HWPs depicted by dashed lines can be absent if the output PBSs are turned by 90° about the horizontal axis [1]. The setup of each routing block guarantees equal optical path lengths of links between input and output ports and allows to apply optical means with the ultimate numerical aperture $u = nsin\alpha/(1+cos\alpha)M$, n/M and $n/4M$ for blocks A, B and C, respectively. The value of u for block C can be 4-fold increased if lens arrays are placed not only at inputs and outputs but also before QWPs and HWPs, as is done in [2].

In the blocks A and B *p*-polarized beams realize butterfly connections between inlets and outlets, *s*-polarized beams realize crossover connection between the ports 1, 2, ... M/2 and 1+M/2, 2+M/2, ... M. In the block C the *p*-polarized beams connect ports with the same name and the *s*-polarized beams implement crossover communication links connecting the inputs 1, 2, ... M/2 and 1+M/2, 2+M/2, ... M with the outputs M, ... 2+M/2, 1+M/2 and 1/M, ... 2, 1, respectively.

Three possible variations of 2-D nonblocking networks I, II [3] and III for an architecture of photonic SSs with straight optical interstage connections are shown in Fig. 2. It is demonstrated in the report how these networks and horizontal and vertical routing blocks A, B or C make possible the efficient interconnect architecture for $2N^2x2N^2$ three-dimensional compact high-throughput photonic nonblocking switching systems with many ports and the number of switching stages $K = 2\log N+1$, $2N+1$ or $4\log N-1$. The main characteristics of such SSs are evaluated.

1. Fyodorov V.B., *Optical Computing & Processing*, vol. 3, 1993, no. 1.
2. Jahns J.J., and Murdocca M.J., *Applied Optics*. vol. 27, 1988, no. 15.
3. Mirsalehi M.M, Shamir J., and Caulfild H.J., *Applied Optics*, vol. 28, 1989, no. 12.

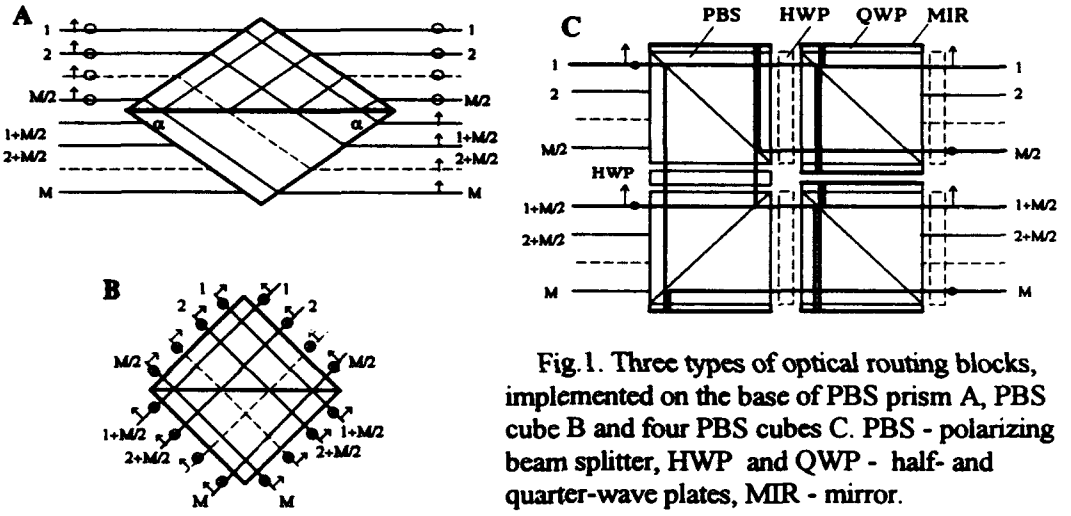


Fig.1. Three types of optical routing blocks, implemented on the base of PBS prism A, PBS cube B and four PBS cubes C. PBS - polarizing beam splitter, HWP and QWP - half- and quarter-wave plates, MIR - mirror.

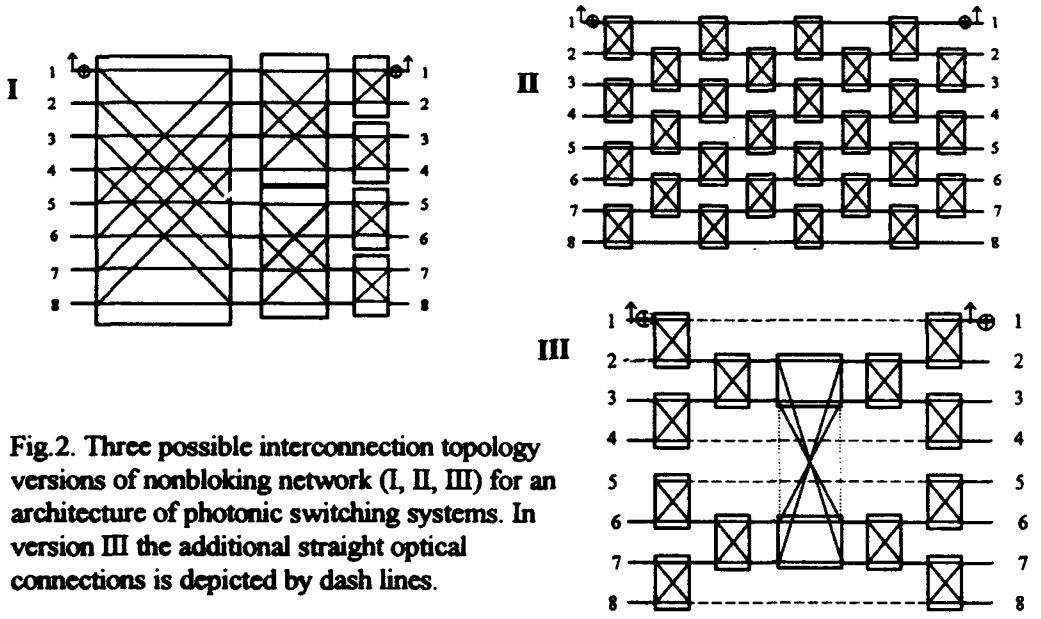


Fig.2. Three possible interconnection topology versions of nonbloking network (I, II, III) for an architecture of photonic switching systems. In version III the additional straight optical connections is depicted by dash lines.

Performance Analysis of Multistage Interconnection Networks

Igor G. Voitenko and Toyohiko Yatagai*

Institute of Applied Optics, Byelorussian Academy of Sciences
212793 Mogilev, Belarus

*Institute of Applied Physics, University of Tsukuba
Tsukuba, Ibaraki 305, Japan
Tel: +81-298-53-5334
Fax: +81-298-98-53-5205

Abstract

A holographic interconnection technique in a photorefractive waveguide formed by titanium and ion diffusion in LiNbO3 is described. A banyan network using this is designed. An integrated acoust optic switch control technique is also *discussed.*

Problems of clock distribution and data communication inside VLSI chips are solved by using optical interconnections with optical fibers and holographic techniques. Volume holograms in waveguides offer a straightforward means of interfasing dynamically reconfigurable interconnections with integrated optoelectronic devices. In this paper we consider holographic interconnections between nodes and stages for some type of the optical interconnection networks and represent experimental results for holographic interconnections in photorefractive waveguides formed by titanium and iron indiffusion in LiNbO3. We have recorded photorefractive holograms in single-mode substrates titanium and iron indiffused waveguides on nominally pure *y*-cut LiNbO3 substrates. We define the *z*-axis to the principal axis of propagation in the waveguide. Holograms were recorded from above the waveguide using light at 514 nm and the guided TE mode at 633 nm was coupled into the waveguide using a rutile and LiNbO3 prism and then used to reconstruct the holograms

We analyse the possible optical interpretations of the traditional networks, the optical interconnections between switching elements, fault detection problems of this networks and provide a new method to understand and prove the universality optical methods for application in computer systems. We demonstrate first that a bitonic sequence can be routed properly by a banyan network using integrated-optic holographic interconnections. First, the architecture and the working principle of the integrated acousto-optic space switch control, functional and topological equivalence this networks on basis of the optical interconnections are described.

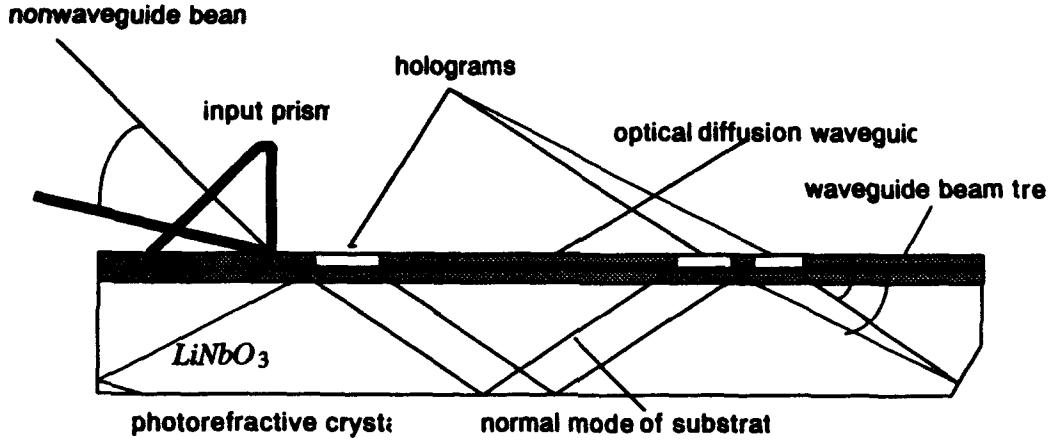


Fig. Example of Holographic Interconnection in Photorefractive Waveguide.

Diagnostic techniques for investigating free-space photonic switching systems

R. L. Morrison, F. B. McCormick, T. J. Cloonan, A.L. Lentine, R. A. Novotny,
J. M. Sasian, M. G. Beckman, M. J. Wojcik, F. A. P. Tooley*, E. Kerbis and S. J. Hinterlong
AT&T Bell Laboratories, Naperville, IL 60566
*Heriot-Watt University, Edinburgh, Scotland, U.K.

Over the past few years, we have designed and assembled five free-space switching photonic system demonstrators[1,2,3]. Our goal is to investigate and develop the technology of free-space digital optics as a framework for exploring high throughput interconnection architectures. Since the status of this evolving technology is often contrasted against the capabilities of a more mature electronic field, it is important to understand the operation of the demonstrators in order to promote advanced features in each new prototype. In addition, the feedback obtained provides a foundation for gauging the future potential of the technology.

The integration of novel opto-mechanical frameworks, diffractive optics, opto-electronic device arrays, and high power semiconductor lasers requires the development of a unique array of diagnostics tools that are not typically commercially available. In this talk, we describe a number of tools that we have implemented for characterizing components and systems. These tools have proven essential in the development of these complex demonstrators.

The process of designing diagnostic hardware for research systems ranges from careful and deliberate planning, where the tool is craftily integrated into the system, to the quick assembly of equipment to investigate unforeseen effects. Typically, the first instance of a diagnostic tool relies on the user to diligently align the opto-mechanic framework and measurement apparatus, and then manually record and analyze the measurements. As our knowledge of the critical issues increases, diagnostic tools have been directly integrated into the system during the design phase. Computer applications are also increasingly important for automating complex measurements, monitoring long term stability tests, and analyzing experimental results. Our experience ranges from designing custom applications for exercising the system fabric to using commercial software applications for coordinating test equipment.

Component diagnostic tools

Beam array generation holograms: Phase gratings have been fabricated that generate from two to over two thousand uniform intensity spots. Intensity variations are primarily due to limitations of the fabrication process. A computer controlled microstage aligned pinhole and detector is used to characterize smaller arrays. For larger arrays, a custom CCD imaging system coordinated with image processing software characterizes the arrays (see figure 1.) This tool has also been used to measure optical signal uniformity throughout the system.

Laser optical power supplies: The current demonstration system employs six high power, current modulated, frequency stabilized, semiconductor lasers to provide optical power beams at the device modulator windows. It is crucial that lasers be tuned to within 0.5 nm of the 850 nm operating point and that they maintain this wavelength at a variety of modulation speeds. Characterizing the lasers requires standard testing systems such as monochromators, optical power meters, beam profilers, and high speed photodetectors. A LabView™ application was used to coordinate several of the tests.

Device arrays: An automated multiple quantum well modulator characterization setup measures modulator reflectivity and photocurrent as a function of voltage, wavelength, spot position and optical power. In addition, each smart pixel array is tested to assure that the cells operate at the design speed.

Polarization beam splitters: Polarization beam splitters are used in the system to combine beam arrays. They must operate uniformly over an angular range of several degrees, a more stringent requirement than is typical for beam splitters. A software application was used to control the diagnostic equipment and then analyze the data.

Optical components: Twyman-Green and radial shearing interferometers were built to operate at 850nm to examine the quality of optical components. A commercial fringe analysis application was used to analyze the results.

System diagnostic tools

Fabric control: The current system[2] is a five stage banyan interconnection network connecting 32 inputs with 16 outputs. A total of 512 path combinations exist. Control information for establishing the data routes must be optically

injected into the system and latched within each smart pixel at the appropriate time, at rates of up to 155Mbits per second. A computer based control system is used for both initializing the system and presenting a nonthreatening user interface. A DOS based PC with a custom written C program was designed.

Multichannel analysis: Currently, proper operation is assured during assembly by examining optical channels at every stage by aligning an avalanche photodetector with the magnified image of the data modulated spot array.

Fabric analyzer: A program that controls a mechanical fiber switch, a sampling oscilloscope, and the system fabric was developed to scan each of the 512 possible paths (see figure 2.) A secondary application analyzes the data to determine if the data matches the expected bit value sequence and then identifies faulty nodes.

Stability: Commercial applications of free-space digital optical technology will require long term mechanical stability. A software application was developed to monitor positioning, ambient and system temperature, detector photo-currents, laser wavelength and optical power fluctuations.

Alignment: The current smart pixel array is approximately 1000 μm square and the spot arrays must be aligned to within about 1 μm. A high magnification viewport was designed that is nonintrusive (i.e., it does not adversely affect normal operation or require repositioning of components), removable (since light sampled for diagnostics is stolen from normal operation), and include an auxiliary light source for illuminating the device array.

In the future, we will also concentrate on further development of bit error rate characterizations, long-term stability and lifetime measurements, and a two-dimensional multi-channel optical sampling oscilloscope.

In this paper, we have discussed diagnostic tools developed by this group. We would also like to acknowledge the extensive device testing effort of our colleagues at Bell Laboratories facilities in Holmdel, Murray Hill and the Solid State Technology center, and the micro-optic characterization by colleagues at the Engineering Research Center.

References

1. F. B. McCormick, T. J. Cloonan, F. A. P. Tooley, A. L. Lentine, J. M. Sasian, J. L. Brubaker, R. L. Morrison, S. L. Walker, R. J. Crisci, R. A. Novotny, S. J. Hinterlong, H. S. Hinton, and E. Kerbis, "A Six-Stage Digital Free-Space Optical Switching Network Using S-SEEDs," Applied Optics 32 (23), 1993.

2. F. B. McCormick, T. J. Cloonan, A. L. Lentine, J. M. Sasian, R. L. Morrison, M. G. Beckman, S. L. Walker, M. J. Wojcik, S. J. Hinterlong, R. J. Crisci, R. A. Novotny, and H. S. Hinton, "A 5-Stage Free-Space Optical Switching Network Using FET-SEED Smart Pixel Arrays," accepted in Applied Optics, Information Processing, special issue on Optical Computing, 1994.

3. F. B. McCormick, J. M. Sasian, R. J. Crisci, R. L. Morrison, F. A. P. Tooley, E. Kerbis, "Fabrication and testing issues in free-space digital optical switching and computing," in Intn'l Symposium on Optical Fabrication, Testing, and Surface Evaluation, J. Tsujiuchi, ed., Proc. SPIE 1720, 553-572, (1992).

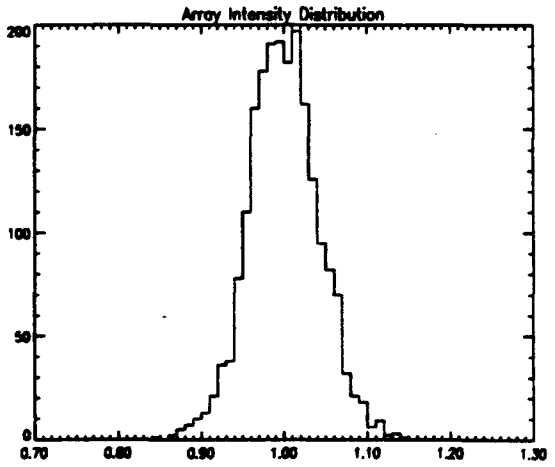


Figure 1: Intensity distribution of a 64x32 spot array.

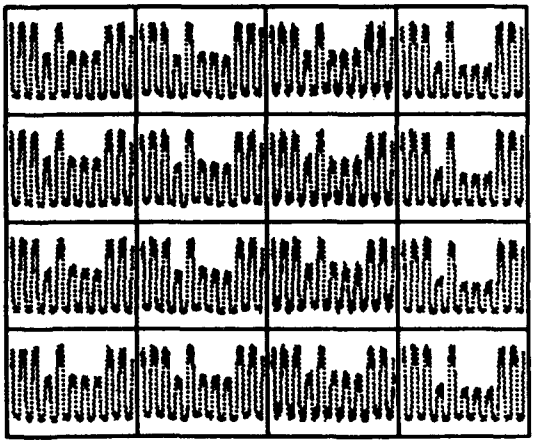


Figure 2: Array of oscilloscope scans showing a portion of the 512 paths.

A cell-based algorithm for designing beam array generators

Rick L. Morrison and Mike J. Wojcik
AT&T Bell Laboratories
Naperville, IL 60566

Current free-space digital optical systems require optical power supplies that generate two dimensional arrays of uniform intensity light beams[1]. One method for creating these uniform intensity beam arrays is to illuminate a computer designed Fourier hologram using a collimated, high power laser source. These surface relief gratings, also referred to as multiple beamsplitters, are designed using scaler diffraction theory via a computer optimization process. The quality of the hologram is quantified by its diffraction efficiency and the relative uniformity of the beam intensities.

We present a new algorithm that uses a pixelated, discrete phase level representation of the hologram to examine and modify only those cells that form the boundary between phase transitions, thereby substantially reducing processing requirements. An additional feature of the algorithm is the capability to increase the spatial bandwidth of the hologram during the design process. Using this algorithm, we have designed holograms with up to 4096x4096 phase cells per period that couple light into arrays containing up 16,000 spots. We have fabricated a number of smaller designs for use in our free-space photonic switching program.

The algorithm presented here is similar in nature to the IDO (iterative discrete on-axis) encoding algorithm[2]. In the basic IDO algorithm, one period of the two-dimensional Fourier-plane hologram is divided into an array of rectangular cells where each cell imparts one of two fixed phase delays to the incident wavefront. The contribution of each cell to an order intensity is independent of the other cells, thus, each test requires calculation of only a small fraction of the full set of diffraction equations. During a series of iterations, each cell phase is reversed and this new value is retained based on its contribution to the merit function and a probabilistic simulated annealing process.

It is the locations of the level transitions that determine the order intensities. Therefore, in the this new algorithm, it is necessary to examine and modify only cells along phase transition boundaries. The result is a significant reduction in processing since only a fraction of the cells are tested during each iteration. An additional feature is the ability to increase the spatial resolution of the phase array during the optimization process. When the merit function value stagnates, each phase cell is subdivided into 4 parts with each new cell given the original cell's phase value.

Scaler diffraction theory is used to calculate the complex amplitude of the nth order in the mth row as given by the sum of the contributions from each of the JxK phase cells,

$$A_{m,n} = B_{m,J} \cdot B_{n,K} \cdot \sum_{j=0}^{J-1} \sum_{k=0}^{K-1} F_{m,j,J} \; F_{n,k,K} \cdot exp\,(i\theta_{j,k}),$$

where, θ_{jk} is the phase delay associated with cell (j,k), and,

$$B_{m,J} = \frac{1}{2\pi m} \cdot \sin\,(2\pi \frac{m}{J}) \cdot exp\,(-i\pi \frac{m}{J}), \quad \text{and} \quad F_{m,j,J} = exp\,(-2\pi i \frac{mj}{J}).$$

The intensity of the order is given by the complex square of $A_{m,n}$.

The quality of this solution is measured using a merit function that is a combination of the diffraction efficiency and the deviation of the order intensities from their target values. Uniform intensity arrays as well as those containing suppressed orders and arbitrary orders can be designed by selecting the proper form for the merit function. The parametrization of this function has been observed to significantly influence the design time.

First, a two dimensional data array is defined that contains the JxK pixel phase values of one period of the hologram. This array is filled with a random distribution of multilevel or binary phase values. We have also included the ability to load the phase array with values generated by a separate application based on the Gerchberg-Saxton [GS]

algorithm[3]. In this case, the GS program generates a rudimentary solution. This significantly reduces the design time and avoids the stagnation problem that can occur with binary level designs in the GS program. A further reduction in processing effort is achieved by integrating symmetries into the design[4].

Next, the amplitude of each designated order is calculated. The algorithm then examines cells with the objective of improving the merit function value. A series of four comparisons are performed where all phase values, $\theta_{j,k}$, are compared against $\theta_{j+1,k}$, $\theta_{j,k+1}$, $\theta_{j-1,k}$, and then $\theta_{j,k-1}$ respectively. If the two phase values are equal, no action is taken. If the phase values differ, the neighbor's value is used and its contribution to the merit function is calculated. If the merit value is improved, the new phase value is inserted into $\theta_{j,k}$.

The algorithm repeats the cell examination and update sequence until either a termination condition is met or the optimization stagnates. To proceed with the optimization, the phase array is subdivided such that each cell is replaced by four equivalent cells. The search process is then revisited. When the program terminates the phase array is stored in a data file which is later used to create the lithographic mask(s) that transfers the pattern into an optical surface.

Uniform intensity, binary phase array generators producing an 8x8 spot array were designed in about 12 seconds on a SUN Sparcstation 10. An equivalent 16 phase level 8x8 generator required about 18 seconds. A 32x32 spot array binary phase design with a final size of 512x512 cells per quadrant took 42 minutes to generate. When the Gerchberg-Saxton application was used to create an initial phase distribution, the design time for the total optimization was reduced to 16 minutes. Typically, binary phase solutions had a diffraction efficiency of about 75%. Figure 1 shows the hologram designed used to generate an irregularly spaced spot array used in a free-space photonic switching system. A picture of the resulting spot array from a fabricated grating is shown in figure 2.

In summary, this new algorithm, in conjunction with the application of design symmetries, substantially reduces processing time making the design of moderate size array generators feasible. The algorithm accomplishes this goal by selectively examining only cells located adjacent to a phase transition. In addition, the spatial resolution is increased as needed allowing the design to begin from a much simpler initial distribution.

References

1. R. L. Morrison, S. L. Walker, and T. J. Cloonan, "Beam array generation and holographic interconnections in a free-space optical switching network," Appl. Optics 32 2512-2518 (1993).
2. M. R. Feldman and C. C. Guest, "Iterative encoding of high-efficiency holograms for generation of spot arrays," Optics Letters 14, no. 10, 479-481 (1989).
3. R. W. Gerchberg and W. O. Saxton, "A practical algorithm for the determination of phase from image and diffraction plane pictures," Optik 35, no. 2, 237-246 (1972).
4. R. L. Morrison, "Symmetries that simplify the design of spot array phase gratings," J. Opt. Soc. Am A 9 (3), 464-471 (1992).

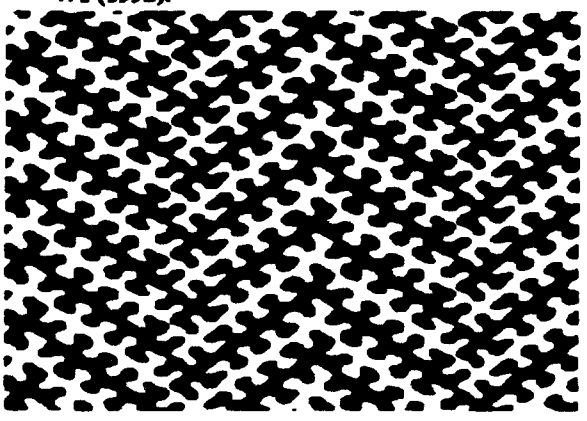


Figure 1. Nonseparable design used to generate

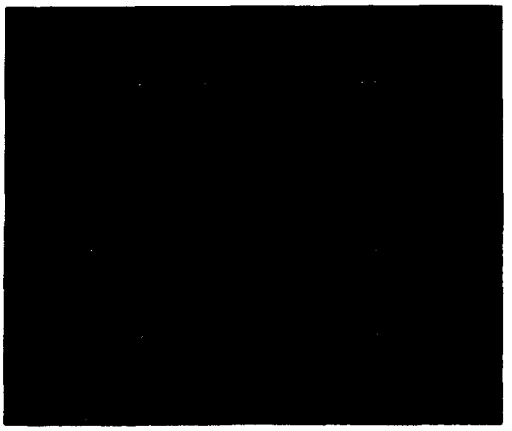


Figure 2. Picture of spot array generated by grating

Multilevel diffractive phase elements with trapezoidal shaped pulses

P. Blair, H. Luepken[*], *M. R. Taghizadeh and F. Wyrowski*[#]

Department of Physics, Heriot Watt University, Edinburgh, Scotland.

[*] Department of Physics, Universitat Essen, Essen, Germany.

[#] Department of Diffractive Optics, Berlin Inst. of Optics, Germany.

Summary

Digital optics and material processing encourages research into the design of diffractive phase elements (DPEs) that split an incoming light beam into an array of prescribed intensity light spots. To achieve this several design concepts using different modulation schemes have been proposed. Of these the optimisation technique of simulated annealing (SA), allied with a trapezoidal shaped surface-relief phase profile, realised some of the highest diffraction efficiencies seen for binary DPEs to date[1]. Binary elements were initially designed as the process for fabricating multilevel phase profiles (i.e. microlithography) introduced an unacceptable non-uniformity in the desired signal wave[2] despite the increase in the diffraction efficiency. Presently electron-beam lithography's direct-write capability can be used to overcome the alignment problem intrinsic to microlithography. Thus fabrication of a multilevel trapezoidal shaped phase structure with acceptable fabrication error becomes a possibility.

The design of a multilevel trapezoidal shaped phase structure with optimised diffraction efficiency is more difficult than for the binary case. To overcome this we offer a design concept that is embedded in the theoretical framework of design theory of diffractive elements[3].

As only the intensity of the desired diffraction pattern, which we call the desired signal wave, is specified within the signal windows W, the phase is a free parameter. The first design step is an optimisation of the signal phase with respect to the upper bound of the diffraction

efficiency, as a function of the number of phase levels allowed for the element. This step furnishes information about the maximum diffraction efficiency achievable for the specified number of phase levels. Thus, if a specific diffraction efficiency is required for an application, this step gives information about the minimum number of phase levels the design has to have in order to achieve the desired efficiency. To optimise the diffraction efficiency upper bound, an iterative Fourier Transform algorithm is employed.

The projection of the spectrum of the phase optimised signal wave onto the allowed phase levels provides a set of phases for a sampled quantised phase hologram. As this is a sampled data set, a parameterisation of the projection is needed. We use a parameterisation that leads to trapezoidal shaped pulses. This step yields an set of initial parameters that are already optimised with respect to diffraction efficiency. A non-linear optimisation of the initial set of parameter is then performed in order to increase the uniformity, which worsens as a result of parameterisation.

This design concept contributes detailed instructions on how to design a phase grating with optimised diffraction efficiency as a function of a specified number of phase levels. Assuming that a specified minimum diffraction efficiency is required for an application, the first step in the design concept gives information about the lowest number of phase levels required to achieve this. The following steps result in a initial distribution for a non-linear optimisation that is near the desired solution.

References

1. A. Vasara, M. R. Taghizadeh, J. Turunen, J. Westerholm, E. Noponen, H. Ichikawa, J. M. Miller, T. Jaakkola and S. Kuisma, "Binary surface relief gratings for array illumination in digital optics", *Appl. Opt.* **31**, 3220-3336 (1992).
2. J. M. Miller, M. R. Taghizadeh, J. Turunen and N. Ross, "Multilevel-grating array generators: fabrication error analysis and experiments", *Appl. Opt.* **32**, 2519-2525 (1993)
3. Hermann Luepken and Frank Wyrowski, "General design concept for periodic and non-periodic diffractive phase elements", *Soc. Photo-Opt. Instr. Eng.* OELASE 94 (in press.)

Demonstration and discussion of an interlaced fan-out interconnect

N. Collings

Institute of Microtechnology, Rue A.-L. Breguet 2, University of Neuchâtel, CH-2000 NEUCHATEL, Switzerland. (Tel: +41.38.205.489)

Abstract
2D fully interconnected processing systems where the output array is smaller than the input array can use a fan-out interconnect where the extra channels are accomodated within the repeat spacing of the input array.

Introduction

A commonly used 2D fan-out (fan-out **A**), where the input array is replicated at neighboring spatial locations which are located at distances of at least the array size from the original array, is illustrated in Fig.1.



Fig.1 Conventional 2D array fan-out.

A complementary fan-out is illustrated in Fig. 2 (fan-out **B**). It is complementary in the sense that, whereas **A** is useful when the subsequent fan-in is to an array of larger size repeat spacing than the input, **B** is useful when the output array is of smaller repeat spacing. This can be useful in cascaded interconnect systems, for example.



Fig.2 Interlaced 2D array fan-out.

A further advantage of **B** is that it allows lower resolution fan-out gratings to be used than **A**. This in turn eases the fabrication tolerances of the grating. The reduced fan-out angle also allows more compact systems to be envisaged.

Demonstration of interlaced fan-out

The layout of the optical system is shown in Fig. 3. Collimated light of 6 mm diameter from a HeNe laser beam is incident on a 8 x 1 Dammann grating of 690 μm period, which was fabricated at the Paul Scherrer Institute, Zürich. A lenslet array of 45 mm focal length and 1.15 x 1.4 mm repeat spacing acts as an array of Fourier Transform lenses to form multiple fan-outs in the focal plane of the lenslets. Provided that the grating is not placed at the focal plane of the lenslet array, the multiple fan-outs can be fanned-in to an 8 x 1 array using a simple lens, in this case of focal length 80 mm. The spot separation at the output is determined by the distance between the grating and lenslets. In this case, it was about one half the focal length of the lenslets. Figure 3 shows the beam paths for one of the diffracted beams, which produces a single point at the output.

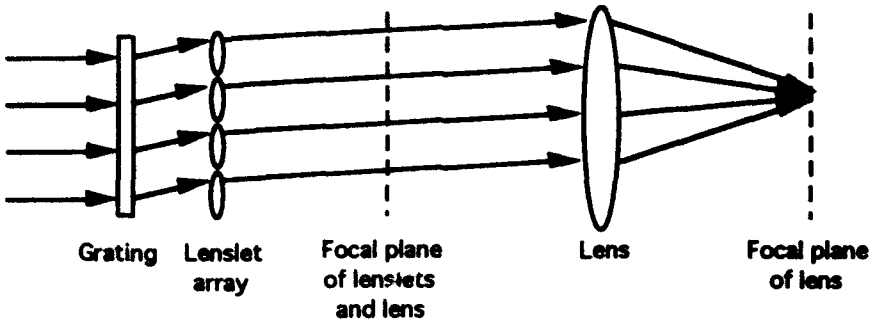


Fig.3 Component layout of interlaced fan-out.

Results and discussion

The focal plane of the lenslets contains spatially multiplexed 8 x 1 arrays on the repeat spacing of 1.15 x 1.4 mm (Fig. 4a). The spot size within the array is variable between one row and another of the lenslet array. However, some rows produce the calculated spot size, which is about one half of the repeat spacing within the area, since there are approximately two grating periods per lenslet. In the focal plane of the lens there is just a single 8 x 1 array with a 140 μm repeat spacing and 20 μm spot size (Fig. 4b).



Fig. 4. Focal plane of lenslets (a), and rear focal plane of lens (b).

This type of fan-out can form the basis of a compact interconnect structure because the input channels are well separated at the start and the demands on the optical components are not high. In the demonstrated arrangement, one can envisage placing a liquid crystal television screen in the focal plane of the lenslets where the repeat spacing of the spots in each array is 80 μm. Smaller focal length lenslets with a smaller period grating would give a sharper spot size in this plane. Shorter focal length (16 mm) microlens arrays have already been used for multiple Fourier transforms [1]. Since both the lenslets and lens work at small field angles, no special lens design features are required. In order to apply this interconnect in a real system, better quality lenslets are required.

References

[1] K. Hamanaka and T. Kishimoto, "Multiple imaging and multiple Fourier transformation using microlens arrays", Jap. J. Appl. Phys. **29**, L 1277-1280 (1990).

Considerations for free space microoptical systems in layer architecture

W. Eckert, K.-H. Brenner, C. Passon, Universität Erlangen-Nürnberg, Institut für Angewandte Optik, Staudtstr. 7/B2, 91058 Erlangen, Germany, Tel. +49 9131 858377, Fax +49 9131 13508

Abstact: Architectural concepts for micro-integrated digital optical data processing systems are presented. From these concepts a microoptical system consisting of stacked layers of micro-components is derived.

Introduction: Microoptical systems for digital optical information processing impose a series of requirements on the optical realization. Light efficiency is necessary to achieve low bit-error rates with the available optical power. For constructing complex systems from standardized parts, the system also has to be designed in a modular way. As interfaces between these modules and for space variant operations, real images of the data planes must exist, where e.g. masks can be placed. For space invariant operations on data planes, an optically generated Fourier plane is necessary, where beam forming and beam deflecting components can be inserted.

Fourier stages: Single lens $2f$ Fourier stages (fig. 1) exhibit certain disadvantages when used in microoptical setups consisting of arrays of identical components. A lens diameter of two times the pupil diameter is necessary to avoid vignetting. In an integrated system, the $2f$ configuration requires an additional spacer in order to place the lens in the center. From the fabrication point of view it would be more desirable to place the lenses at the substrate's surface. A more general two-lens configuration is shown in fig. 2, which is identical to the $2f$ system when b becomes zero. This setup is chosen symmetrically, because the space-bandwidth product reaches a maximum, as was shown in [1]. Assuming symmetric configurations, the number of resolvable pixels is maximal when $b = f$ and $a = 0$ [2]. This represents the 'light pipe' configuration. In practical implementations, a small distance a is often required for technological reasons. With microoptical systems, space-bandwidth is a critical parameter. The distance b should therefore be chosen close to f to obtain maximal resolution.

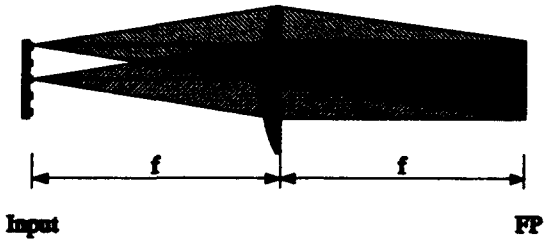


Figure 1: $2f$ system

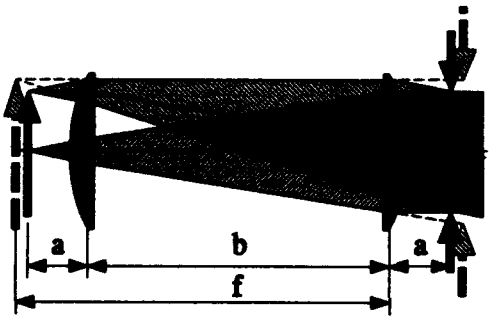


Figure 2: Two-lens Fourier setup

Pupil division: Digital optical systems often require the generation of multiple copies of a data- plane and the superposition of different dataplanes. For these split and join operations pupil division is most advantageous since the join operation can be performed almost lossless for an arbitrary number of joins. Pupil division may be performed either by splitting the aperture of a single lens or by using a lens for each channel in the pupil plane. In microoptical setups, multi-lens pupil division is preferable, because the full space-bandwidth product of the light pipe is available in all channels. Additionally, multi-lens pupil division can also be used for space invariant nearest neighbor interconnections.

Layer architecture: A transfer of these considerations to a micro-integrated system is shown in fig. 3. This layer architecture consists of two modified lightpipes with multi-lens pupil division. Precise alignment can be achieved if each layer is produced with lithographic precision. The light pipes can be realized on one substrate with microlens arrays on both sides. Mask layers are introduced on additional spacers. The prism layers, realized by embossing, perform space invariant split and join operations. Since for thermal and practical reasons, active devices should be located at the system surfaces. In most cases active devices on one surface are sufficient. Cascading of several stages is then realized by placing a mirror layer on the top system surface, as shown in fig. 4. The performance and typical dimensions of these layer architectures will be discussed in the presentation.

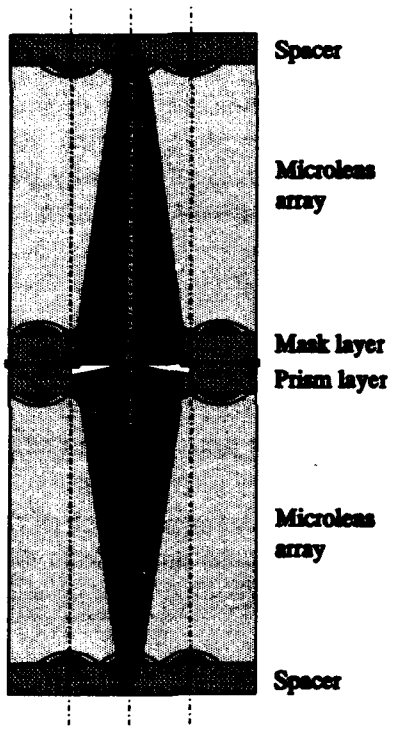


Figure 3: Microsystem in layer architecture

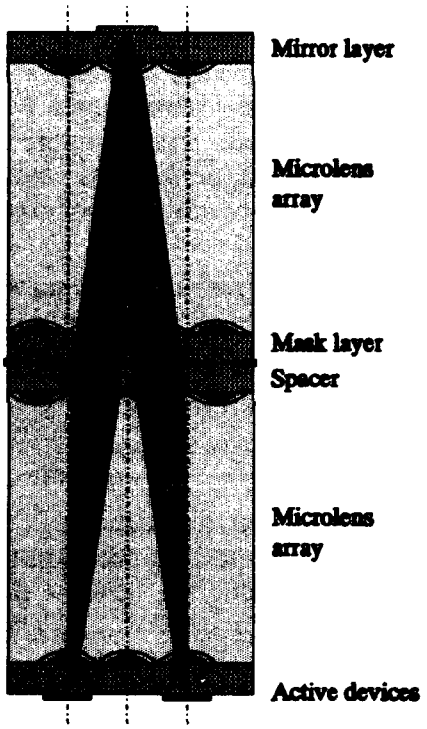


Figure 4: Cascading with active devices

Acknoledgements: The authors want to thank J. Bähr, J. Moisel and M. Testorf for many fruitful discussions and suggestions. This work was partially founded by the German ministry of research and technology (BMFT) under grant BV 225/9.

References:

[1] A. Lohmann, *Image formation of dilute arrays for optical information processing.* Optics Comminications 86 (1991) 365-370

[2] K.-H. Brenner, W. Eckert, C. Passon: *Demonstration of an optical pipeline adder and design concepts for its microintegration.* Opt. Laser Technol. , Special issue on optical computing, accepted.

An Approach to Active Alignment of Free-Space Optical Interconnects

G.C. Boisset, B. Robertson, and H. S. Hinton

Department of Electrical Engineering, McGill University, 3480 University Street, Montréal, Québec, Canada H3A 2A7
email: boisset@photonics.ee.mcgill.ca

Abstract

An active alignment system is demonstrated. The error between the actual and desired spot location on a quadrant detector is used to compute the angular displacement required for two Risley Prisms to centre the spot.

Summary

Free-space optical interconnects hold the promise of alleviating the communication bottlenecks which will arise in future connection-intensive electronic systems. A separable interconnect offering the massive connectivity of free-space optics will greatly increase the data throughput between multi-chip-modules and/or printed circuit boards on an optical backplane.

A key issue facing free-space photonic circuit design is that of alignment. For a system to be of practical use, it must be capable of operating continuously over long periods of time, unaffected by external vibrations and by temperature changes.

At least two approaches exist to overcome alignment drift:

1) Design an extremely rigid system which will not drift over time. This can be performed by removing as many degrees of freedom as possible[1] and by improving pre-alignment.

2) Implement active alignment, a process in which system parameters such as throughput or error in spot position are monitored and fed back to a controller which realigns the system by altering the state of the optics. Such simple feedback loops exist in CD players[2].

An example of active alignment we are currently investigating involves a simple closed feedback loop which centres a spot on a quadrant detector. The control loop has the following characteristics:

Input: Light intensity incident on a quadrant detector generates differential photo-currents from which the spot position can be determined.

Output: The controller outputs the desired angle of rotation to two stepper motors which rotate two Risley Steerers located at the focal plane of a lens. The rotational displacement of the steerers imparts an angular displacement to the beam which creates a lateral displacement of the spot on the quadrant detector.

Controller: An error signal, which is the difference between the ideal spot position and the detected spot position, is fed back into the controller algorithm. Given the error signal and the current rotational position of the steerers, the algorithm computes the new rotational position of both Risley Steerers which will centre the spot on the quadrant detector.

Embedded in the control algorithm is a transform (CtoR transform), which maps a Cartesian (x,y) displacement to a Rotational displacement of two steerers (θ_A, θ_B). A CtoR transform which is based on first order optics can be expressed as follows:

$$\theta_A = \theta_l + \theta_a$$
$$\theta_B = \theta_l - \theta_a$$

where

θ_1 = Arctan (y / x) (modified to give an angle between 0 and 2π).

θ_a = Arccos[Sqrt (x^2+y^2) / (2r)]

2r = 2f tan (n - 1) δ, the maximum displacement imparted by Risley steerers of wedge angle δ, index n, and located at the focus of a lens with focal length f.

θ_A and θ_B are conventional geometric angles: they are zero on the positive x axis and increase in a counterclockwise direction. For example, point (x, y) = (2r, 0) will map to (θ_A, θ_B) = (0,0) and point (x, y) = (0, 2r) will map to (θ_A, θ_B) = (π/2, π/2). Given the physical nature of the optics, there are two different (θ_A, θ_B) values for any given (x, y) ($x \neq 0$ and $y \neq 0$). The above transform is thus only one of a family which will perform the desired mapping. Finally, it should be noted that from a control perspective, this system is nonlinear since multiplying the input error signals by a scalar k will not correspondingly multiply the control outputs by k.

The experimental demonstration features two 40 mm lens and two Risley Steerers each with a 15 minute wedge and n = 1.509. A simple beamsplitter and viewing system are used to directly view the spot on the detector. The maximum possible spot displacement for our system is of the order of 2r = 177 μm. The incremental rotation of the Risley Steerers required to move a spot by Δx = 1 μm depends on the spot position, but is usually of the order of 0.65°. The setup is shown in Figure 1.

The controller was implemented on a Macintosh computer. Inputs are obtained in two different ways: 1) by focusing the spot on a CCD camera, using a frame grabber to define a virtual quadrant detector on the digitized CCD image and extracting the spot centre from the digitized CCD image 2) by focusing the spot on an actual silicon photodetector and measuring the resulting photocurrents. Outputs to the stepper motors are sent out on serial electrical lines from the computer.

Acknowledgment

This work was supported by the Canadian Institute for Telecommunications Research and the McGill NT/BNR-NSERC Industrial Chair in Photonic Systems

References:

[1] F. B. McCormick, T. J. Cloonan, A. L. Lentine, J. M. Sasian, R. L. Morrison, M. G. beckman, S. L. Walker, M. J. Wojcik, S. J. Hinterlong, R. J. Crisci, R. A. Novotny, and H. S. Hinton, "A 5-stage embedded-control EGS network using FET-SEED smart pixel arrays" *Topical Meeting on Photonics in Switching, Postdeadline paper PD5,* Palm Springs, Palm Springs, CA, March 15- 17, 1993.

[2] W. H. Lee, "Optical technology for compact disk pickups", *Lasers & Optronics*, Vol. 6, No. 9, 1987.

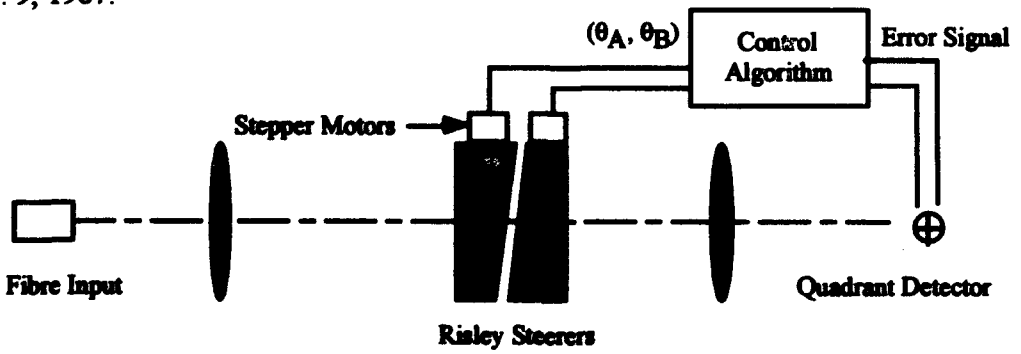


Figure 1: Optomechanical setup and control loop

Design of a Lenslet Array Based Free-Space Optical Backplane Demonstrator

B. Robertson, G. C. Boisset, H. S. Hinton, Y. S. Liu, N. H. Kim, M. R. Otazo, D. Pavlasek, D.V. Plant

Department of Electrical Engineering, McGill University, 3480 University Street, Montreal, Quebec, Canada H3A 2A7. (Tel 514-398-4470)

W. M. Robertson

National Research Council, Institute for Information Technology, Montreal Road, Ottawa, Ontario, Canada K1A OR6 . (Tel 613-991-6839)

Abstract

The optical and optomechanical design of a representative portion of a lenslet array based free-space photonic backplane is described. Issues relating to the optical performance, optomechanical layout and alignment tolerances will be discussed.

Summary

The following paper will consider the optical and optomechanical design of a representative portion of an experimental free-space photonic backplane. The system uses FET-SEED modulators and receivers to transmit the data and multi-level diffractive lenslets to interconnect the two device planes. This work forms part of a project aimed at developing terabit capacity photonic backplane technology.

Integrating free-space optics directly into a backplane is a challenging problem for a number of reasons. Current electronic backplanes have a board-to-board spacing of only about one inch (the card pitch for Futureboard+ modules, for example, has been set at 30mm [1]). Any competitive optical backplane must therefore be compact enough to fit within this space. In addition, the system must be arranged such that it is possible to remove and insert circuit boards while maintaining a high degree of alignment between the optical signal beams and the transmitter and receiver arrays. This places exacting demands on the optomechanical design of the backplane.

The optical design of the backplane demonstrator is shown in Fig. 1. Linear polarized light from a Ti-Sapphire laser operating at 850nm enters the system via a single mode polarization preserving fiber. A periodic binary-phase grating (BPG) is used to generate an array of optical beams which are collimated by the first lenslet array and reflected by the polarizing beam splitter/quarter waveplate assembly onto the modulator array. The BPG utilizes a non-separable grating design and has a theoretical diffraction efficiency of 77.3%. The modulated signal beams pass through the PBS (the polarization of the light having being rotated by the quarter waveplates) and onto the receiver array. As the system uses dual-rail logic, the signal channels were designed to handle two signal beams, one for each FET-SEED window (the FET-SEED windows have dimensions of approximately 25μm×25μm). A 4-f optical layout was therefore chosen to ensure a high optical throughput and improve the tolerance of the system to misalignment errors. Implementing a photonic backplane using lenslet arrays has several advantages; it can be made compact enough to fit within the limited space available, it does not suffer from field dependent aberrations and it will not be affected by the angular dependence of polarizing beam-splitters [2]. The photonic backplane demonstrator which we shall describe has a channel spacing of 600 microns, a device plane separation of just over 30mm and was designed to initially interconnect a 2x2 array of optical channels. The alignment tolerances required by this system include a focal length accuracy for f_1 of ±0.25%, a lenslet array positional accuracy of ±20μm, a defocus error of ±50μm, a device plane tilt of ±0.5°, and a device plane roll (with respect to the lenslet arrays) of better than 0.25°. A full discussion of the alignment tolerances will be given.

The mechanical layout of the backplane is shown in Fig. 2. The optical components are mounted in steel cylinders, prealigned and positioned using a magnetic slot channel arrangement [3]. The

baseplate was fabricated from Magnesium AZ31B tooling plate due to the material's high flatness tolerance, lightness and the ease with which it can be machined. The magnets are mounted on top of steel bars which have the effect of increasing the restraining force on the components. A chamfered groove structure was chosen to reduce wear and tear and improve alignment tolerances.

Acknowledgments

The authors would like to thank M. R. Taghizadeh and the diffractive optics group at Heriot-Watt University for fabricating the lenslet arrays. This work was supported by the Canadian Institute for Telecommunications Research and the McGill BNR-NT/NSERC Industrial Chair in Photonics Systems.

1) IEEE Standard 896.2 - 1991 (Profiles A and B).
2) F. B. McCormick, F. A. P. Tooley, T. J. Cloonan, J. M. Sasian, H. S. Hinton, K. O. Mersereau, A. Y. Feldblum, "Optical Interconnections Using Microlens Arrays", Optical and Quantum Electronics, Vol. 24, No. 4, April 1992, pp. 265-477.
3) F. B. McCormick, F. A. P. Tooley, J. L. Brubaker, J. M. Sasian, T. J. Cloonan, A. L. Lentine, R. L. Morrison, R. J. Crisci, S. L. Walker, S. J. Hinterlong, and M. J. Herron, "Optical Applied Science and Engineering", SPIE Proc. Vol. 1 1533, paper 12 (1991).

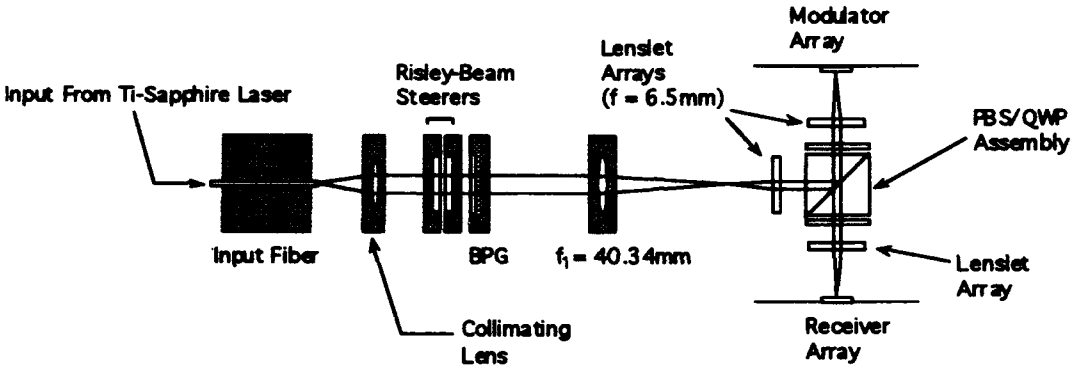


Fig 1. Optical design of system.

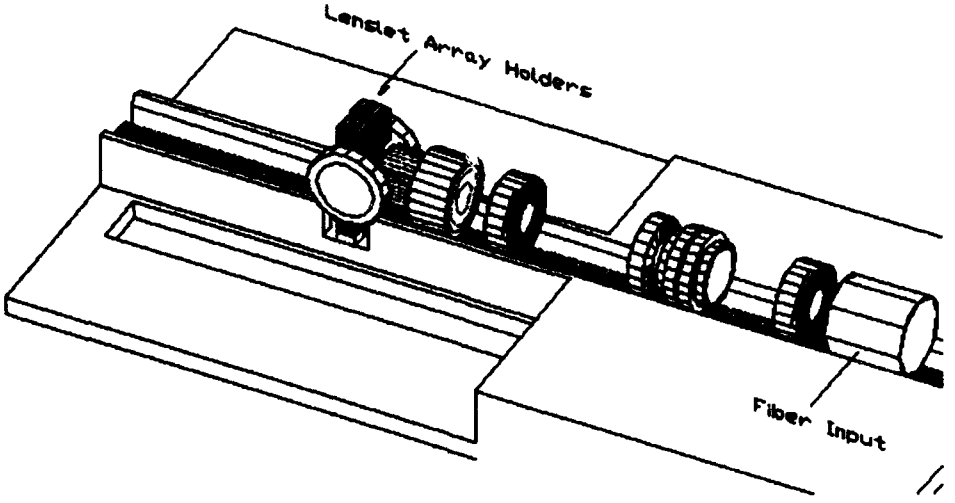


Fig 2. Optomechanical layout of backplane.

Hybrid lens implemented using an afocal microlens doublet

Simon M. Prince, Frank A. P. Tooley and M.R. Taghizadeh

Department of Physics, Heriot-Watt University, Edinburgh, U.K.
031 451 3065, physmp@uk.ac.hw.clust

Abstract

The design, manufacture and assessment of a hybrid lens for an optical computing demonstrator will be discussed. A comparison will be made of the performance of the microlens singlets and doublets used.

Summary

Microlens arrays have been proposed as components that will enhance the performance of conventional optics through the exploitation of their small diameter and focal length. Such features lead to compact optics that can be readily integrated with semiconductor devices. Hybrid lenses (figure 1) have been proposed [1]. These devices exploit the large field of view of slow, conventional lenses with the small spot size that can be achieved by microlenses. An f/5 lens was designed which images over a ±5° field angle and produces spots with 99% of the energy coupled into a 15μm spot. This spot is imaged by an afocal telescope composed of f/3 and f/1 microlens doublets. The doublets work at infinite conjugates. The first doublet collimates the light and the second, faster microlens doublet focuses the light into a small spot. The hybrid lens creates an array of small spots over a large field (7mm). These hybrid lenses will be used to interconnect two S-SEED arrays. S-SEEDs comprise two 5μm windows which are separated by 20μm. Imaging two spots with each microlens requires that they be used off-axis.

Code V has been used to model the performance of the hybrid lens. The performance is evaluated by the calculation of the encircled energy. The spot size is dependent on the speed of the final microlens doublet and the amount of spherical aberration introduced by the afocal pair. The diameter of the collimated beam is determined by the f/# of the conventional lens and the focal length of the first microlens doublet. The aberrations that the second microlens doublet introduce are determined by the size of this collimated beam.

The microlenses doublets have been produced in-house in our micro-fabrication facility. The microlenses are made from melted photoresist on 100μm thick substrates. With this technique we can fabricate microlens arrays with f-numbers ranging from f/2 to f/8 and individual lens diameters ranging from 50 to 250μm. Thin substrates are required as the afocal relay has a working distance of 150μm and the focus must be outside of the glass to permit the imaging of S-SEEDs. The microlens array doublets are assembled using our mask aligner which is equipped with a stereo microscope. A spacer layer (~20-30μm thick) is placed between the two microlens arrays, and the doublets are secured in place using UV curing optical cement. Our measurements have shown that an alignment accuracy of better than 1μm is routinely achievable.

Interferometric analysis has been performed on the microlens doublets and afocal pairs. A Mach-Zehnder interferometer with fringe analysis software is used to analyse the aberrations introduced by the microlenses. The off-axis performance is evaluated by changing the angle of the beam at the aperture stop of the bulk lens. This shifts the focused spot across the microlens enabling off-axis measurements to be made. Measurements will be presented of the performance of hybrid lenses including the achieved spot sizes and interferograms showing the aberrations introduced into the beam by the hybrid lens (figure 2).

[1] McCormick F.B., "Free-Space Interconnection Techniques," Chapter 15 in "Photonics in Switching," ed. by J.E. Midwinter, Plenum (1993).

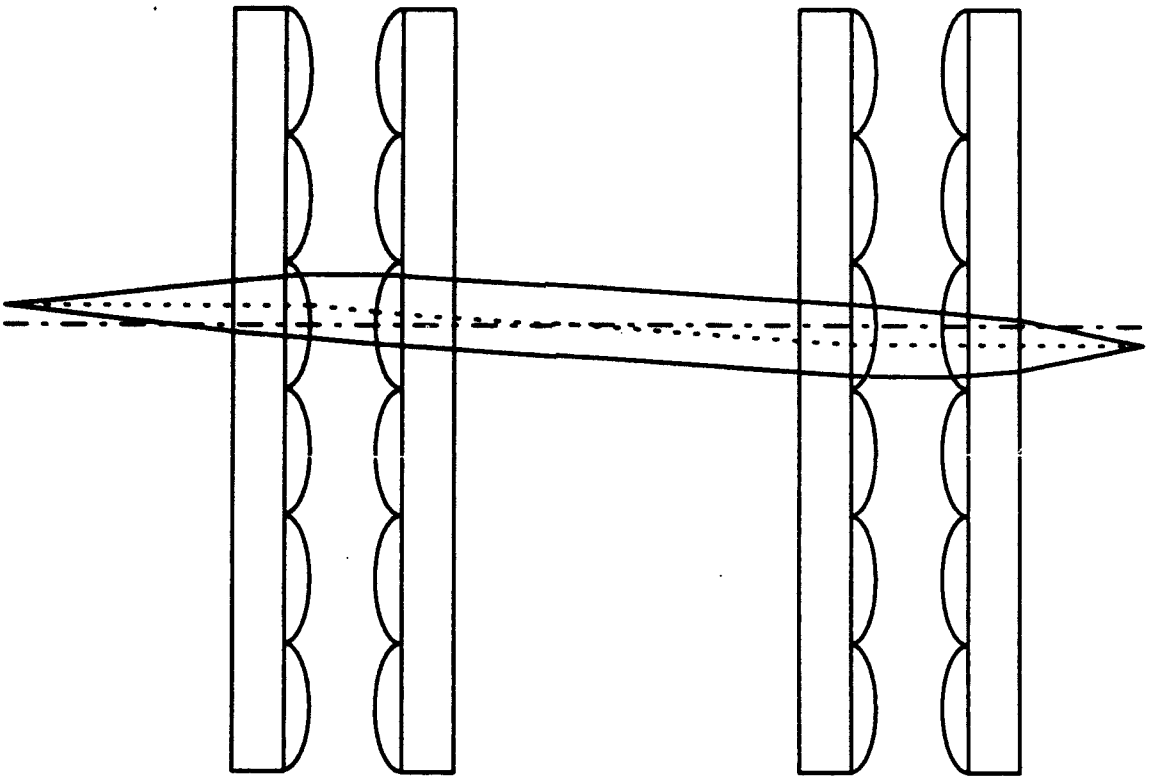


Figure 1: Pairs of doublets relaying and magnifying off-axis input spot.

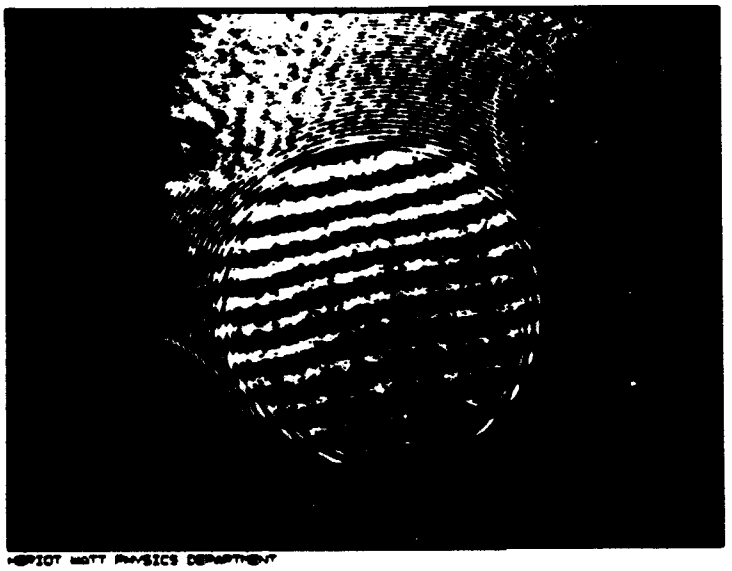


Figure 2: Microlens interferogram of f/2, 110μm diameter microlens.

Microlens array for perfect shuffling fabricated by laser writing system

Seok Ho Song and Sang-Don Jung

Electronics and Telecommunications Research Institute, Research Department
P.O.Box 106, Yusong, Taejon 305-606, Republic of Korea
(tel)+82-42-860-6033, (fax)+82-442-860-5033, (e-mail) shsong@ard.etri.re.kr

Abstract

By use of a laser writing system, an array of four off-axis microlenses for perfect shuffle interconnections and the toric microlenses for planar optical imaging have been fabricated.

I. Introduction

In the fields of communication and optoelectronic processing, microoptical interconnections make a potential to improve the degree of system integration and stability. Microoptical components for focusing, imaging, branching, combining, and so on, have progressed beyond prototypes by the fabrication techniques of PR melting, ion exchange, deposition, e-beam writing, and laser writing. The writing technique using e-beam or laser beam makes it possible to produce an arbitrary surface profile, such as the continuous surface-relief grating for spot array generators or a set of diffractive and/or refractive components on a same substrate[1-2]. In this work, the laser writing technique is described to make an array of four microlenses specially designed for perfect shuffle interconnections, as well as toric microlenses for planar optical imaging.

II. Laser writing system

Figure 1 shows the laser writing system which consists of air-cooled Ar^+ laser (λ=458nm, 4mW), acousto-optic modulator, XY positioning stage with a moving resolution of 0.1μm, and CCD camera for monitoring the focusing of the incident beam on the sample substrate. The sample substrate of a 10 μm thick positive-PR (AZ4562) layer coated onto glass substrate was

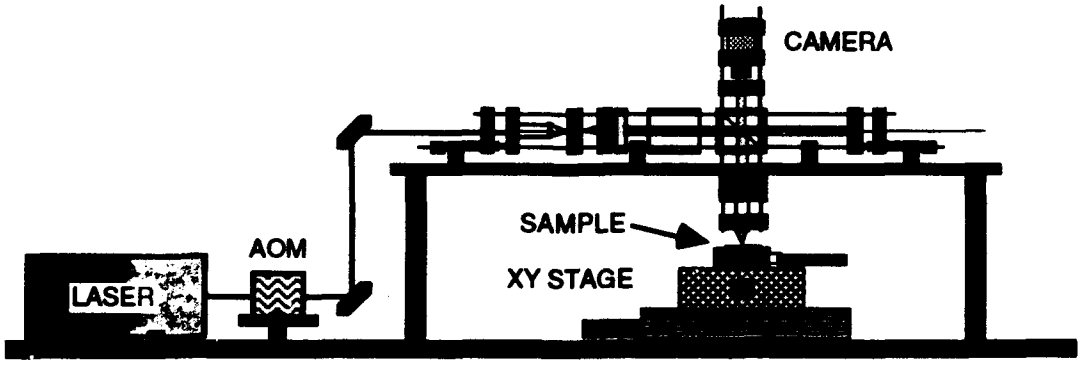


Figure 1. Scheme of laser writing system

exposed by the raster scanning process, and developed with the solution of AZ500MIF. Based on the gamma curve of the PR layer, any surface-relief micro-structure can be fabricated as it was designed. The spot size of the incident beam focused on the PR layer was measured by

2.3μm. Therefore this system would be more useful for refractive microoptics with larger dimensions than for diffractive ones.

III. Results

We have fabricated a set of four off-axis microlenses for the application of perfect shuffle interconnections. Figure 2(a) shows the interferogram of the microlenses obtained by the Mach-Zehnder interferometer. The dimension of one microlens was $(d=100\mu m)^2$ and the axis was shifted toward the center of four lenses with the amount of $d/4 = 25\mu m$. This configuration enables to implement the perfect shuffling of the 2-D arrays of input signals at four quadrants. Figure 2(b) shows the four spots with the $d/4$ spacing generated by the four off-axis microlenses, and one of the wavefronts after passing through the microlenses is depicted in Fig.2(c). There are some of microlenses with a spherical shape of Fig.3(a) shown as an interferogram and an aspherical (toric) shape of Fig.3(b). Further detail characteristics including optical aberrations of the microlenses in Fig.2 and Fig.3, will be discussed in the presentation.

References

1. M. T. Gale, M. Rossi, H. Schutz, P. Ehbets, H. P. Herzig, and D. Prongue, Appl. Opt., 32, 2526(1993).
2. T. Shiono and H. Ogawa, Opt. Lett., 17, 565(1992).

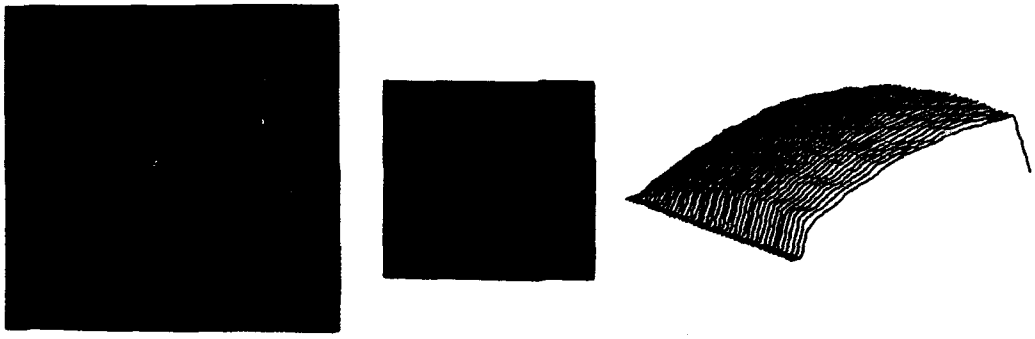


Figure 2. Array of four off-axis microlenses for perfect shuffling. (a); interferogram, (b); focused spots, and (c); wavefront after passing through one of the microlenses.



Figure 3. Interferograms of the fabricated microlenses with a spherical shape in (a) and an aspherical (toric) shape for imaging an input with oblique incident angle of 30 deg. in (b).

Integration of Microlens and Fiber Holder Arrays by Deep Proton Irradiation

Maria Kufner, Stefan Kufner, Philippe Lalanne, Pierre Pichon, Pierre Chavel

Institut d'Optique, Centre Scientifique d'Orsay, Bât. 503, 91403 Orsay, France
Tel. ++33-1-69416846, Fax. ++33-1-69413192

ABSTRACT

We describe the fabrication of self aligned arrays of microlenses and fiber holders on the same PMMA substrate using a suitable deep proton irradiation.

SUMMARY

For almost all fiber applications the combination of fibers and microlenses is of evident relevance. A microlens can couple light from a source into a fiber and collimate light coming out of a fiber. In both cases the longitudinal and the lateral displacement between fiber and lens have to meet strict tolerances. Also of interest is the alignment between arrays of fibers and arrays of microlenses, which is of particular relevance to optical interconnects and optical computing. Problems arise from the fact that conventional methods of fabricating fiber holder and microlens arrays are fairly distinct. This is not the case for a technology called deep proton irradiation[1,2]. With this technique it is possible to fabricate lenses on the top side of a polymethyl methacrylate (PMMA) layer and fiber holder holes on the back side. The PMMA layer can have a thickness of several hundred µm up to more than 1 mm. This results in high holder aspect ratios for a standard fiber (125 µm) having for example a 500 µm deep holder hole. A simulation of the dose deposition in a 500 µm thick PMMA layer irradiated with $2*10^{12}$ protons/cm^2 of 7 MeV is shown in fig. 1. The figure shows the lines of equal dose deposition in a side view to the irradiated PMMA substrate. As can be seen from this figure in the shadow region (left hand side) the dose distribution shows fan shaped lines caused by the straggling of the incident protons after multiple collisions. This can be used to achieve fan shaped fiber holders which facilitates the fiber positioning and tightening. The alignment between a microlens array and a fiber holder array can be obtained by irradiation of two PMMA layers through the same mask, one layer for a microlens array the other for the fiber holder array. After irradiation the two layers are handled separately in different processes and then recombined. More sophisticated is the use of only one PMMA layer with only one exposure and a separate handling of the two sides. Then the microlenses are placed directly above the fiber holder holes and are therefore best aligned to the hole. An approach to a monolithic solution using the longitudinal dose distribution (fig. 1 right hand side, irradiated region) is in progress. Experimental results like in fig. 2b will be discussed.

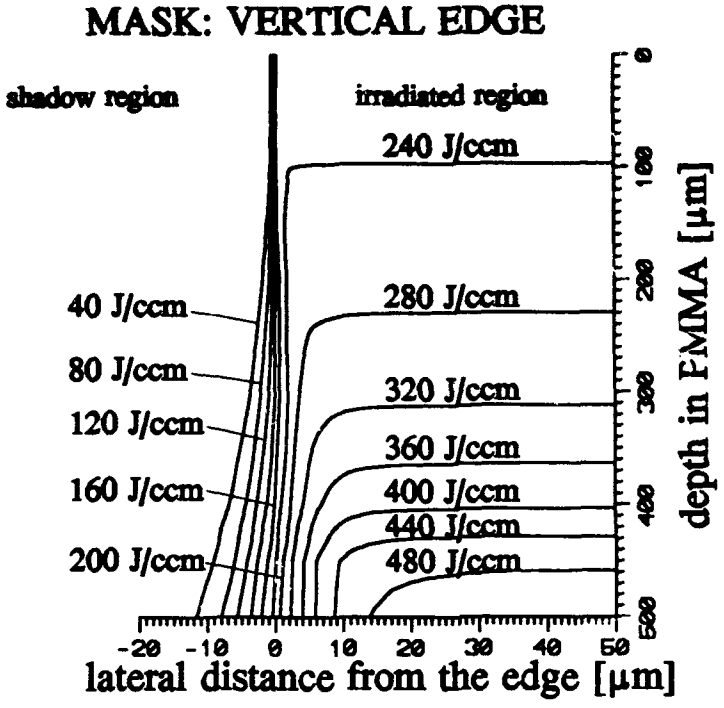


Fig. 1 Dose distribution in PMMA under a vertical edge after irradiation with a dose of $2*10^{12}$ protons/cm^2

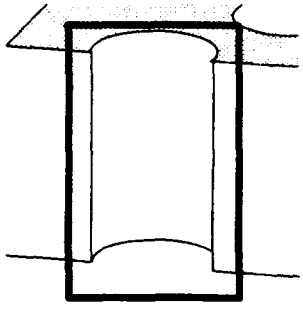


Fig. 2a Scheme of fig. 2b

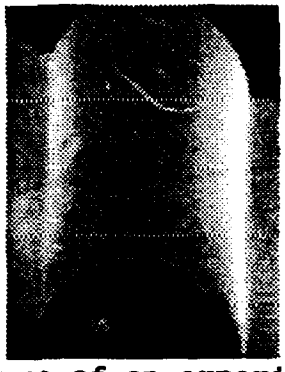


Fig.2b SEM picture of an experimental result, 1st step: side view of a fan-shaped hole in PMMA. Top diameter: 250 µm, bottom diameter: 270 µm.

1) M. Kufner, S. Kufner, M. Frank, J. Moisel, M. Testorf: "Microlenses in PMMA with high relative aperture: A parameter study", Pure Appl. Opt. 2, 9-19, 1993.
2) S. Kufner, M. Kufner, M. Frank, A. Müller, K.-H. Brenner: "3D integration of refractive microoptical components by deep proton irradiation", Pure and Appl. Opt. 2, 111-124, 1993.

Direct laser writing of planar Fresnel elements for optical interconnects

M.T. Gale, M. Rossi and R.E. Kunz
Paul Scherrer Institute, Badenerstrasse 569, CH-8048 Zurich, Switzerland
Tel. +41-1-492 6350 Fax +41-1-491 0007

G.L. Bona
IBM Research Center, Säumerstrasse 4, CH-8803 Rüschlikon, Switzerland
Tel. +41-1-724 8111 Fax +41-1-724 1789

Phase-matched Fresnel elements have been fabricated for laser array to fibre-cable coupling and for fan-out operations. The continuous-relief planar microoptical elements are produced by direct laser writing in photoresist and copied by replication techniques.

1. Introduction

Parallel optical links are attracting increasing interest in the fields of data communications and optical computing. Typical applications include lens arrays for light source to fibre array coupling and fan-out elements for parallel, high-speed, high-capacity interconnects for optical processors and data links. The paper will describe progress in the realisation of Phase-Matched Fresnel Elements (PMFEs [1]) for such applications. These computer-generated Diffractive Optical Elements (DOEs) are fabricated as surface-relief microstructures by direct laser writing in photoresist and can be reproduced by replication techniques. PMFEs can be produced with very high numerical aperture, arbitrary aperture shape and as large area, close-packed arrays. Examples of laser diode to fibre imaging lens arrays with high numerical aperture and of focusing Nx1 fan-out elements will be described.

2. Fabrication

The fabrication of Phase-matched Fresnel elements with continuous-relief surface profiles represents a challenging area of modern optical fabrication technology, in particular for high aperture lenslets with segment sizes in the order of micrometers. Laser writing (Fig. 1) offers a highly flexible approach for the fabrication of such DOEs. Technology for direct laser writing in photoresist has been developed over a number of years at the Paul Scherrer Institute in Zurich. The system, described in more detail elsewhere [2], uses a HeCd laser to expose a photoresist coated substrate which is raster scanned under the focused beam using a high precision xy-stage. In this paper we will present latest results for PMFEs fabricated using this technique and discuss the limitations in microstructure resolution and lenslet numerical aperture as determined by current technology.

PMFE microstructures can be characterised by the maximum relief depth and the minimum segment size. In laser writing technology, the maximum depth is given by the resist layer thickness, typically ~ 5 μm. The minimum segment size at the perimeter of the lenslet area is determined by the numerical aperture (NA) of the lenslet, together with the phase (height) step at the segment boundary. The maximum aperture of Fresnel lenslets is determined by the size of a segment in which the continuous-relief profile can be reasonably attained using the writing spot size; for a relief depth of 5 μm, this typically corresponds to a maximum lenslet aperture of NA ~ 0.5 (phase step of 8π). Lenslets with this NA have a dominantly diffractive behaviour and function best with monochromatic (laser) or narrow band (LED) illumination.

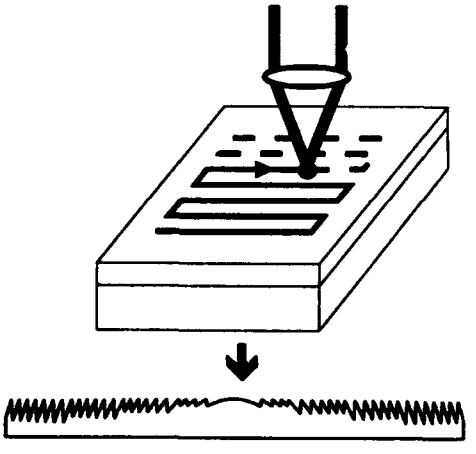


Fig. 1. Continuous-relief Fresnel elements are fabricated by direct writing in photoresist.

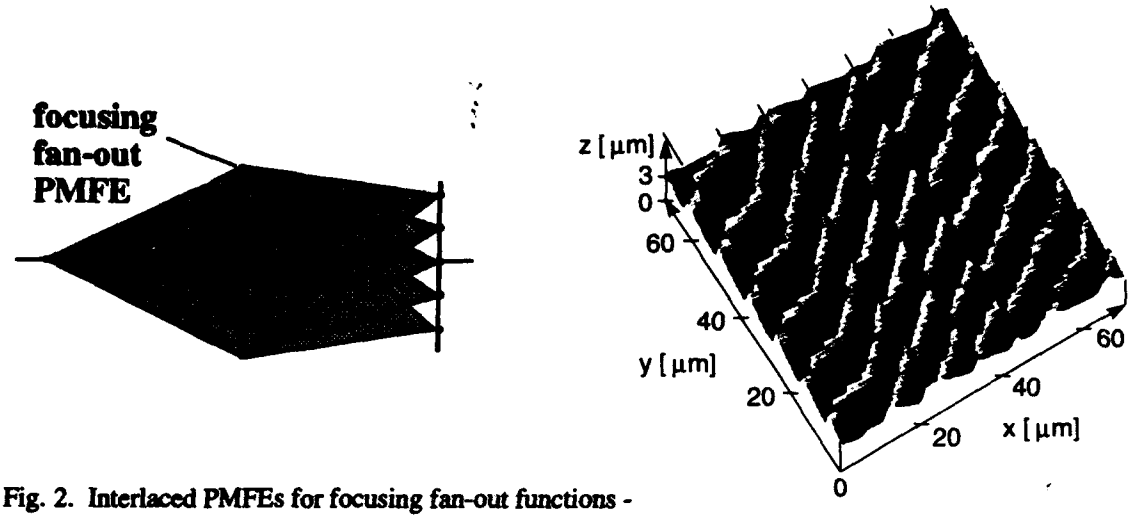


Fig. 2. Interlaced PMFEs for focusing fan-out functions - schematic and AFM image of a fabricated microstructure.

Resist surface-relief microstructures are electroformed to a Ni shim and reproduced by replication in plastic or epoxy materials. Replication technologies which are commercially available and currently under investigation include hot embossing, injection moulding and uv-replication techniques.

3. Fresnel lens arrays for laser to fibre coupling

High numerical aperture, planar microstructures and flexible design in shape and array formats are attractive features for the application of PMFEs in the coupling of laser diode arrays to fibre ribbon cable. An example will be presented of a PMFE array designed for coupling an array of laser diodes (λ = 831 nm) into a ribbon of 12 fibres. The laser diodes each emit an astigmatic beam with divergence angles $\theta_{\perp}$ = 8° and $\theta_{//}$ = 28° (FWHM) in the horizontal and vertical planes. The MT-connector compatible ribbon cable consisted of 12 multimode fibres with 0.21 NA and 50 μm core diameter. The PMFE fabricated achieved a measured efficiency of 60% with a laser to fibre separation of 1.65 mm.

4. Spatially interlaced lenses for fan-out applications

Novel PMFE structures have been designed to perform focusing fan-out functions (see Fig. 2.) in a single planar microoptical element. The desired fan-out function is implemented by combining different PMFEs (e.g. one for each interconnection channel) in a special area sharing arrangement. Each PMFE is divided into a subarray structure, leading to an array of focused diffraction orders centred around the focal point of the basic PMFE. The period of the different subarray structures is chosen such that the diffraction orders coincide with and are coherently superimposed upon the desired image points. Simple and fast procedures have been developed for optimising such fan-out PMFEs, based upon a low number of well-defined physical-optical parameters. The concept can easily be extended for realising 2D fan-out elements.

Such fan-out elements have been fabricated by direct laser beam writing in photoresist. The splitting and spatial interlacing procedures are performed in real-time during the writing process. A major advantage of the PMFE fan-out approach is the large tolerance with respect to fabrication errors. In a series of experiments in which depth scaling errors over a range of ±20% were introduced, PMFE fan-outs showed a uniformity error of < 5%. This is much superior to the performance of conventional surface relief fan-out elements for which a uniformity reduction of 10% typically results from a depth scaling error of only a few percent. Latest results will be presented in the paper.

[1] R.E. Kunz and M. Rossi., "Phase-matched Fresnel elements", Opt. Comm. **97**, 6-10 (1993).

[2] M.T. Gale, M. Rossi and H. Schütz, "Fabrication of continuous-relief microoptical elements by direct laser beam writing in photoresist," Proc. SPIE, **2045** (1994).

This work was supported in part by the Swiss Priority Program OPTIQUE.

Strategies for realising large computer generated holograms from the calculation of sub holograms

by

R. I. Young, A. E. MacGregor and C.W. Slinger

Abstract

Several schemes that decrease the calculation time of a computer generated hologram through utilising sub holograms are presented. The applicability of these schemes to differing encoding schemes and design criteria is discussed.

Summary

The design of computer generated holograms (CGH) is an optimisation calculation in a solution space given by all the possible pixel configurations for the hologram[1]. Generally the assessment of the replay of a CGH involves evaluating all the sampling points simultaneously. This leads to calculations involving large arrays. Shortening the calculation time is achievable by reducing the number of pixels in the CGH needing revaluation. One possibility for doing this is to only calculate certain pixel values by an updating methodology[2].

This paper presents three strategies that allow Fourier CGH design by calculating sequentially small regions of solution space, i.e. sub sections of the desired hologram. The common feature of these schemes is a decrease in the time taken to realise the final hologram by reducing the size of data requiring Fourier Transforming during the calculation. Additionally convergence time of the algorithm falls rapidly with decrease in pixel number. Of these schemes the expansive and partitioning methodologies are novel whilst the Interlaced Technique (IT) has appeared in the literature[3].

The effects of sub hologram size upon encoding errors, replay fidelity, convergence time and number of iterations are given. The manipulation of solution space is demonstrated for two well-known CGH design algorithms, the Iterative Fourier Transform Algorithm (IFTA) and Direct Binary Search (DBS).

The applicability of manipulating solution space to CGH design involving differing design criteria (e.g. complex amplitudes or intensities) for the evaluation of replay fidelity is also discussed.

A comparison of the performance of all three methodologies is made with respect to each other and also to the equivalent single large calculation. While the new schemes all converge quicker than the single calculation, they introduce a redundancy of information into the CGH leading to poorer replays. It is shown how redundancy

arises within these schemes and how a further iterative design can circumvent some of these problems.

From these assessments, possible cases and applications where the manipulation of solution space is beneficial in comparison with a single calculation are given.

References

1 Digital holography as part of diffractive optics. Wyrowski F & Bryngdahl, O. Rep Prog Phys, 54, Pg. 1481-1571, 1991.

2 Efficient design of DBS CGH. Jennison BK, Allebach JP & Sweeney DW. J Opt Soc Am A, 8(4), Pg 652-660, April 1991.

3 Iterative interlacing approach for synthesis of CGH. Ersoy OK, Zhuang JY & Brede J. Applied Optics, 31(32), Pg 6894-6901, Nov1992.

Authors

Robert I. Young. DRA, St Andrews Road, Malvern, Worcs. WR14 3PS.

Tel 44-(0)684-894907.

Dr Alastair E. MacGregor. Dept EEEP, Northumbria University at Newcastle, Ellison Place, Newcastle upon Tyne. NE1 8ST. Tel 44-(0)91-2273652, e-mail: PHU1@uk.ac.unn.

Dr Chris W. Slinger. DRA, St Andrews Road, Malvern, Worcs. WR14 3PS.

Tel 44-(0)684-895670, e-mail: Slinger@signal.dra.hmg.gb.

Optical Implementation of Crossover Optical Interconnect Network using Dammann Grating with 65×65 Spot Arrays

Luo Fengguang, Cao Mingcui, Li Hongpu, Ai Jun, Xu Jun, Li Zaiguang
(The National Laboratory On Laser Technology, Huazhong university of science and technology, wuhan 430074, tel. 027701541-4096)

Abstract

Dammann grating with 65×65 spot arrays has been optimized using SAT-GRG optimized algorithm and fabricated. Crossover optical interconnect network of 64×64 pixel arrays with Dammann grating has been performed.

1. Introduction

Dammann grating is binary phase grating that can be used to generate equal intensity spot arrays.[1] Resently, the interest in Dammann grating has been stimulated by the development of optical computing. In optical computing system, the sizes N of arrays as high as 64 ×64, or more are required. Due to complexity of optimization in the case of large spot arrays, application of Dammann grating will be limited[2]. In order to optimize Dammann grating, we present a efficient optimized algorithm: simulated annealing -tempering-generalized reduced gradient algorithm (SAT-GRG). Dammann grating with 65×65 spot arrays is fabricated and used in crossover optical interconnect network.

2. Optimization and fabrication for Dammann grating

The principle of Dammann grating is based on Fraunhofer diffraction theory. Dammann grating is illuminated by plane wave from a laser source. The output pattern appears in the back focal plane of a Fourier converging lens. For the optimization, we define an objective function:

$$\text{Merit}=\sum [I_m(x)-I]^2 \qquad (1)$$

$I_m(x)$ is the diffraction intensity of m-th order, I is the mean value of all intensity. Simulated annealing algorithm (SA) is one of optimization, but its shortage is that it requires large quantity of calculation for large spot arrays. in order to reduce the calculation quantity and enchance the calculation efficiency, we add a tempering process to the SA algorithm. SAT algorithm avoids too much stay at the local minimum magnitude of merit function. Furthermore, on the base of SAT algorithm we add a generalized reduced gradient algorithm(GRG) with much higher precision solution. With SAT-GRG algorithm, the structure of 65×65 array of Dammann grating with non-uniformity of 0.4% and diffraction efficiency

of 82% is obtained. In order to fabricate Dammann grating with 65 × 65 spot arrays, the VLSI technique is used in our experiment, by Si_3N_4 film deposition on quartz glass substarte, photolithographic and reactive ion etching, the phase structure of Dammann grating is transfer onto the Si_3N_4 film. the Dammann grating of 65×65 spot arrays is achieved.

3. Optical implemention of crossover network with 64×64 pixel arrays

The optical setup of one stage of crossover network is shown in fig. 1. The beams from laser is projected onto Dammann grating(D) through combination lens(L1). a mask with character 'E' is placed on the focal plane of lens(L2) where a input pattern of character 'E' with 64 × 64 pixels is produced. The beamsplitter(BS) split the input pattern into two diferent paths. The path E-P2-CCD with a mirror in P2 plane implements straight connection. The path E-P1-CCD implements cross connection. The output pattern of i=0 stage for cross connection can be achieved by placing a reflecting 90° prism in P1 plane. For implemention output pattern of i-stage cross connection, we can place a prism grating with the period of 2^i in the plane of P1. Using six such setup, we can complete crossover network with 64×64 spot arrays.

4. conclusion

Dammann grating with 65×65 spot arrays has been optimized using SAT-GRG algorithm and fabricated. Crossover optical interconnect network of 64 ×64 spot arrays with Dammann grating has been performed. This setup has the advantage of equal optical path length and no light energy loss.

Reference

[1] Dammann H, Gortler K, Opt. Commun., 1970, 3: 312-315.

[2] Jahns J. et al., Opt. Eng., 1989, 28 (12): 1267.

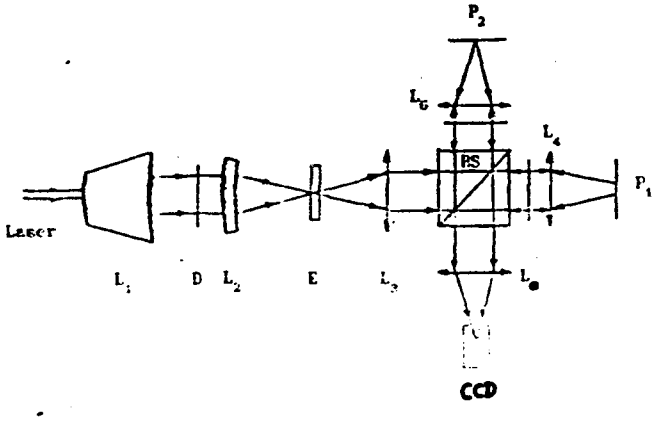


Fig. 1. Optical setup of one stage of crossover network

Three dimensional distribution of light generation by a diffractive element

Rafael Piestun and Joseph Shamir

Department of Electrical Engineering
Technion - Israel Institute of Technology, Haifa 32000, Israel

In many laser and optics applications it is necessary to govern the wavefront (WF) propagation through long distances. These include storage and display of information, spatial distribution of energy, optoelectronic interconnections, precision measurements and alignment. Fourier and Fresnel computer generated holography, do not provide this capability. Most of the known techniques can be used only to generate a desired field intensity distribution over a specified transversal plane and sometimes on a limited depth of field.

The problem, in its most general form, can be stated as follows: 'Given a known WF incident on a diffractive element, design this element to obtain a desired intensity distribution within a given three-dimensional domain.' It is obvious that physics does not allow a solution for any arbitrary distribution but it does in many cases of practical interest. Moreover, if a solution does not exist, it still may be valuable to derive the closest solution to our constraints. This is clearly an optimization problem for which many known algorithms can be applied. In our approach we consider a region of space behind the diffractive element where we want to control the beam propagation, and in this region we impose the necessary constraints on sufficiently close transversal planes.

Consider a given WF incident on a diffractive element at the input plane of the system in Fig. 1 which then propagates in free space a distance d_1 towards the region D. Certain conditions on the field intensity distribution are to be imposed in this region, up to a distance d_2 from the input.

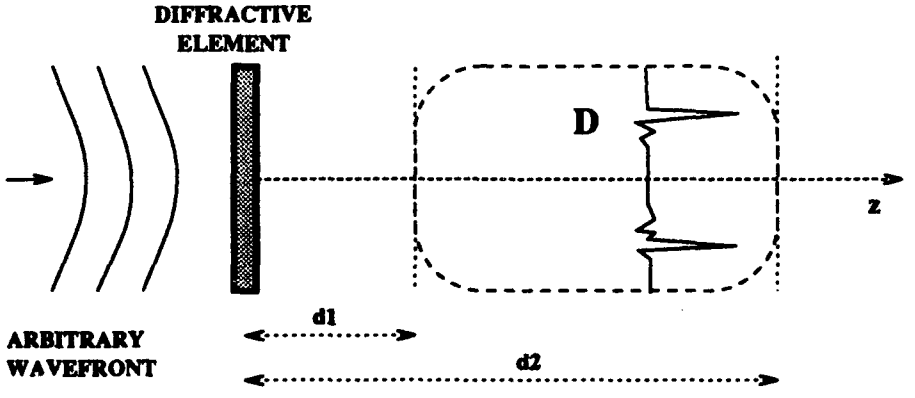


Figure 1: The basic scheme for WF synthesis in the region D.

The complex amplitude over a plane at a distance z can be described by the Fresnel transform,

$$F(\xi, \eta, z) = \mathbf{FrT}\left(f(x, y)\right) \tag{1}$$

The constraints prescribed on this plane can be transformed into constraints on the field at $z = 0^+$ and represented as C_z.

Using the iterative algorithm of projections onto convex sets we can associate with each constraint, C_z, a projection operator $\mathcal{P}_z$. By definition, $g = \mathcal{P}_z f$ is the projection of f onto C_z if

$$\|f - g\| = \mathbf{inf}_{x \in C_z} \|f - x\| \tag{2}$$

where $\|f\| = \sqrt{(f, f)}$ is the norm of f, and $(f, g) = \int |f||g| dx dy$. If C_z is closed, $g \in C_z$ and if it is convex, the projection is unique.

Given a function f describing the input field, we find its projection onto the constraint C_z by calculating the field at the distance z, projecting this function onto the constraints of that plane and finally performing the inverse FrT to obtain the corresponding field at the input:

$$g = \mathcal{P}_z f = \mathbf{FrT}^{-1}\left\{\bar{\mathcal{P}}_z \mathbf{FrT}\left(f\right)\right\} \tag{3}$$

where $\bar{\mathcal{P}}_z$ represents the projection operator on the plane at the distance z. This is possible since the FrT satisfies Parseval's theorem.

If we take n planes we have a set of constraints $C = C_1 ... C_n$. In the problem under consideration, a function f is searched, which lies simultaneously in all sets C_i $(i = 1...n)$,

$$f \in C = \bigcap_{i=1}^{n} C_i \tag{4}$$

It is not possible to perform the projection onto C directly, but in the case of convex sets the problem can be solved by a recursive process using the composite operator $\mathcal{T} = \mathcal{P}_n \mathcal{P}_{n-1} ... \mathcal{P}_1$:

$$f_m = \mathcal{T}^m f_0 = \mathcal{T} f_{m-1} \qquad m = 0, 1, 2... \tag{5}$$

where f_0 is an arbitrary initial function.

We assume that the intensity pattern does not change substantially between adjacent constraint planes. Therefore, the maximal local axial frequency must be taken into account to choose the distance Δz between these planes:

$$\Delta(z) = 2\pi \frac{z^2}{kr^2 + 4\pi z} \tag{6}$$

Preliminary experiments indicate that the proposed approach leads to efficient solutions for various problems. As examples, "nondiffracting beams" and "nondiffracting beam" arrays were demonstrated. These "nondiffracting" arrays can be useful for optical interconnections, precision alignment and measurements.

The procedure adapts the design to the available space bandwidth and to the imposed constraints. As the method is not restricted to incident plane waves, the design of diffractive elements can be adapted to any WF such as Gaussian beams coming directly from laser sources.

Evaluation of a Fast Access Phase Encoded Photorefractive Memory

Clara Alves, Gilles Pauliat, Gérald Roosen.
Institut d'Optique Théorique et Appliquée, Unité Associée 14 au Centre National de la Recherche Scientifique, Centre Scientifique d'Orsay,
B.P. 147, 91403 Orsay Cedex, France.
Tel.: 33/1 69416855; Fax: 33/1 69 41 68 92

Abstract

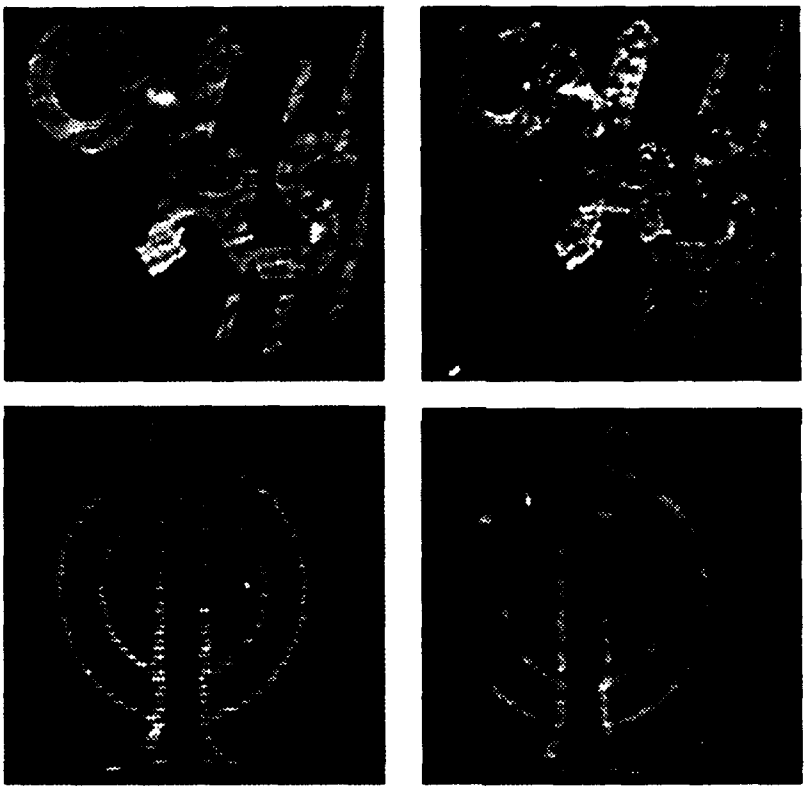
64 images of 128x128 pixels each, have been multiplexed in a same volume of a $BaTiO_3$ photorefractive crystal with the deterministic phase encoding technique. We compare the performances of that memory with the theoretical predictions.

Summary

We have implemented a dynamic holographic memory with a capacity of 64 images[1]. During the recording process, the images are impressed on the image beam with a binary ferroelectric modulator of 128x128 pixels. The holograms are multiplexed in the same volume of a $BaTiO_3$ photorefractive crystal by using the deterministic phase encoding of the reference beam[2]. In that technique, each of the N=64 images is recorded by interfering the image beam with all N=64 reference beams. The same N reference beams are used to record all images. However, the set of relative phases (0 or π) between the reference beams and the image beam is changed for each image. It represents the image address. These images are reconstructed by reading out the holograms with the whole set of reference beams carrying the phase code corresponding to the image one wants to retrieve. In theory if the phase codes are well chosen[2,5] (i.e. if the crosscorrelations of the different sets of reference beams are zero) the images can be retrieved without any crosstalk. Experimentally a given amount of crosstalk arises from imperfections of optical components and especially from the non equal intensities of the reference beams and from imperfect 0-π phase shifts.

We have optimized our set up trying to reduce these sources of crosstalk as follows. The 64 reference beams of equal intensities are produced by splitting a single beam into 64 beamlets with a computer generated fan out hologram. It was realized by King's College London in the frame of the POPAM project[1]. All intensities are equal within σ=8%. These 64 beams are phase modulated by the 64 pixels of a spatial light modulator. In order to achieve very accurate 0-π phase shifts, we implemented the phase modulation from a polarization modulator[5]. We utilized a binary ferroelectric liquid crystal SLM acting as an array of 64 half wave plates. The input beams are linearly polarized along the bisector of the two possible states of the fast axis of the liquid crystal. After passing through it, the beams have one of the two possible linear polarizations. An output polarizer set at 90° of the input polarization state (i.e. at 90° of the

bisector of the two output polarization states), transforms the polarization modulator into a phase modulator. Because the polarizer can be precisely adjusted, an exact phase shift is obtained. In our set up, the phase shifts are equal to 0-π with an error less than 6.10^{-4} *radian*. The fast random access time of this modulator allows to retrieve any of the images in 150µs.
We completely characterized our set up. For instance, we found that the crosstalk in one image due to all other 63 images is always lower than 1:20. Examples of images transmitted by the crystal before storage and the same images retrieved after storage are shown in the figure.
We will discuss in more details the influence of set up imperfections on the memory capacity by comparison of theory and experiments conducted on our set up on which we have intentionally added some defects.



Transmitted (left) before storage and retrieved (right) images (2 among 64).

References:

1-Parallel Optical Processors And Memories (POPAM) project funded by the Commission of the European Community under the ESPRIT Programme for Research and Development.

2-Y. Taketomi, J. E. Ford, H. Sasaki, J. Ma, Y. Fainman, S. H. Lee, Opt. Lett., **16**, pp. 1774-1776, 1991.

3- C. Denz, G. Pauliat, G. Roosen, T. Tschudi, Opt. Comm., **85**, pp. 171-176, 1991.

4-C. Denz, G. Pauliat, G. Roosen, T. Tschudi, Appl. Opt., **31**, pp. 5700-5705, 1992.

5-D. Psaltis, E. G. Paek, S. S. Venkatesh, Opt. Eng., **23**, pp. 698-704, 1984.

A Novel Information Storage Device Utilizing Photostimulated Luminescence in Eu-Doped KCl Phosphors

Hidehito NANTO, Fumitaka ENDO[1], Yoshiaki HIRAI[1], Mitsuo IKEDA[1], Shouichi NASU[2] and Nozomu TAKEUCHI[3]
[1]Electron Device System Research Laboratory, Kanazawa Institute of Technology Ishikawa, Japan
(Tel.No. 0762/48-1100, Fax.No. 0762/48-6189)
[2]Department of Electrical Engineering, Kanazawa Institute of Technology, Ishikawa, Japan
[3]Faculty of Technology, Kanazawa University, Ishikawa, Japan

Abstract

A intense photostimulated luminescence (PSL) at about 420 nm was observed when the UV-light irradiated Eu-doped KCl (KCl:Eu) phosphor was stimulated with 580 nm light at room temperature (RT). The PSL phenomenon in KCl:Eu phosphor is applicable to an erasable and rewritable optical memory.

A new type of optical memory based on the photostimulated luminescence (PSL) phenomenon in electron trapping phosphor materials for optical storage have been studied in the fields of optical associative memory, optical parallel Boolean logic operations and optical neural networks. The electron trapping phosphor materials can emit different output photons that correlate spatially in intensity with input photons.[1] [2] Consequently, the phosphor materials can be used to store optical information as trapped electrons and the information stored can be read out by a laser beam scanning of the phosphor materials. The unique features of the electron trapping phosphor materials that exhibit the PSL phenomenon provide the potential for high bit storage densities, high data transfer and fast recovery speeds. Important characteristics of a good electron trapping phosphor materials for optical memory are high PSL brightness for low noise, short luminescence lifetime for minimum readout time and low light scattering for high bit storage densities. Especially, the electron trapping phosphor materials using transparent single crystal or thin film provide an efficient PSL and low light scattering.

As a results of surveying many possible transparent phosphor materials such as alkali halide, II – VI compound and oxide phosphors in order to obtain a novel electron trapping phosphor material with high PSL brightness and low light scattering, we found that transparent Eu-doped potassium chloride (KCl:Eu) crystals exhibit an efficient PSL for

optical stimulation with visible light after ultraviolet (UV)-light excitation. In this work, we report PSL characteristics of KCl:Eu storage phosphor for optical memory.

An intense PSL peak at about 420 nm was observed when the UV-light irradiated sample was stimulated with 560 nm light at room temperature (RT). A typical PSL emission spectrum (solid line) as well as stimulation spectrum (dashed line) for the 420 nm PSL peak from 240 nm UV-ray irradiated sample is shown in Fig.1. Excitation spectrum (dotted line) for the 420 nm PSL peak is also shown in Fig.1. Using the PSL phenomenon in KCl:Eu phosphor, stored UV (KrF laser) write-in information can be read-out using visible-emitting laser such as He-Ne or Ar^+ ion laser.

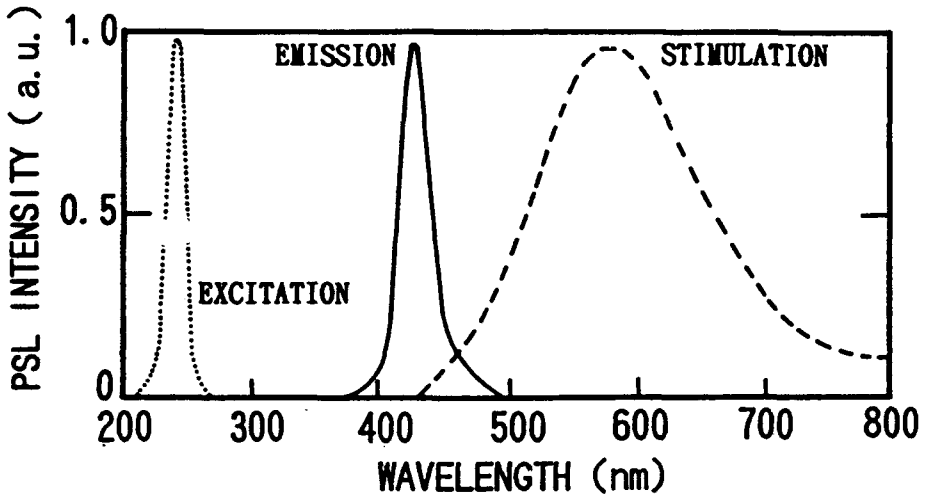


Fig.1

References

1) S.Jutamulia, G.M.Storti, J.Lindmayer and W.Seiderman, Appl. Opt., 30(1991)1786.
2) H.Nanto, Kotai Butsuri, 28(1993)49.

Holographic Associative Memory Using Learning Pattern Method

Ho Hyung Suh, Chong Hoon Kwak, Jong-Sool Jeong, and El-Hang Lee

Research Department, Electronics and Telecommunications Research Institute
P.O. Box 106, Yusongku, Taejon, Korea
Tel: +82-42-860-6033, Fax: +82-42-860-5033, E-mail: hhsuh@ard.etri.re.kr

We have developed a new holographic associative memory (HAM) that uses learning patterns derived from an adaptive learning rule. The principle of learning pattern method (LPM) and simulation result of the present HAM are presented.

1. Introduction

Although the optical implementation of an associative memory such as the Hopfield model can be done easily with vector-matrix multiplications[1] or holographic systems[2-3], the performance may be limited due to the practical difficulties of having pseudo-orthogonality in memory patterns and the existence of undesirable stable states. The LPM utilizes the high performance of adaptive learning by using the simple outer-product learning implementation in HAM.

2. Principle of LPM

Let b^m be the m-th memory pattern to be stored, then the error function E is defined as

$$E = \frac{1}{2}\sum_{m}^{N}\sum_{i,j}^{N}(o_{ij}^m - t_{ij}^m)^2 . \qquad (1)$$

where o^m and t^m is the actual output state and its desired state, respectively.

$$o_{ij} = \sum_{k,l}^{N} W_{ijkl} b_{kl}^m , \qquad (2)$$

$$t_{ij}^m = \gamma b_{ij}^m . \qquad (3)$$

We have adopted gradient-descent algorithm to get the optimal interconnection weight W.

$$\Delta W_{ijkl} \propto -\frac{\partial E}{\partial W_{ijkl}} . \qquad (4)$$

The above algorithm is modified so as to obtain the interconnection matrix of discrete and positive elements.[3] Then the matrix can be expressed as the liner combination of new matrices T^s as follows:

$$W = \sum_{s=1}^{S} a_s T^s = \sum_{s=1}^{S} \alpha_s u^s (v^s)^T . \qquad (5)$$

where α_s is the constant coefficient and the matrix T^s is the outer product between learning vectors u^s and v^s with binary elements (1,0).

3. Holographic Implementation of LPM

The three two-dimensional binary patterns L, P, and M are selected as the memory patterns as shown in Fig.1, and they can be written in the form of 25(5×5)-bits vectors as follows:

(L) : b^1 = (1000010000100001000011111),
(P) : b^2 = (1111010001111101000010000),
(M): b^3 = (1000111011101011000110001).

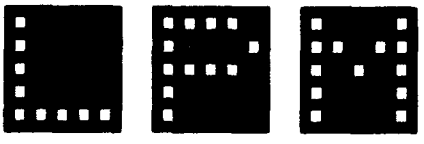


Fig. 1 Three two-dimensional memory patterns

```
21110200012111020000211 11
03330000000303000000000 0
03330000000303000000000 0
03330000000303000000000 0
00003030300000300003000 00
21110200012111020000211 11
00003030300000300003000 00
00000000000000000000000 00
00003030300000300003000 00
02222020240242200002000 00
21110200012111020000211 11
03330000000303000000000 0
02222020240242200002000 00
03330000000303000000000 0
00003030300000300003000 00
21110200012111020000211 11
00000000000000000000000 00
00000000000000000000000 00
00000000000000000000000 00
00003030300000300003000 00
21110200012111020000211 11
00000000000000000000055 50
00000000000000000000055 50
00000000000000000000055 50
00002020200000200002033 35
```

Fig. 2 The interconnection matrix W obtained from the adaptive learning rule.

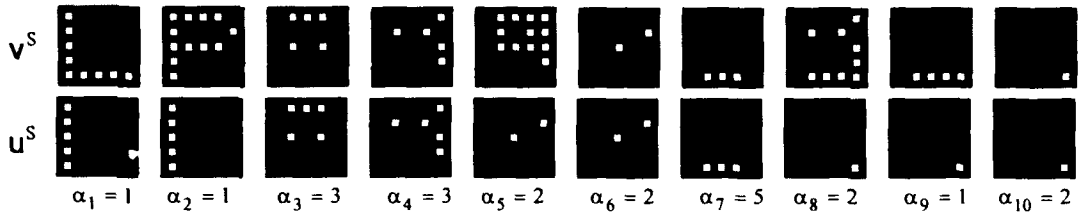


Fig. 3 Ten learning pattern pairs (v^s,u^s) and their coefficients α_s (s=1,2,...,10).

Figure 2 illustrate the 25×25 interconnection matrix obtained by using the algorithm in Sec. 2. We can derive ten pairs of learning pattern pairs (v^s,u^s) and their coefficients α_s out of the matrix W after simple algebra (Fig.3). As shown in Fig. 4, the interference patterns between the collimated beam passing through the pattern v^s and the scattered beam from the pattern u^s and ground glass construct holographically the outer-product between v^s and u^s.[3,4] The coefficients α_s controls the exposure time. The energy function U is defined as follows:

$$U = -\frac{1}{2}\sum_{ij}^{N}\sum_{kl}^{N} W_{ijkl} b_{ij}^{s} b_{kl}^{s} + \lambda (N_0)^2 . \quad (6)$$

where N_0 is the number 1's of input $b^s$and λ is a constant. It is important to use appropriate value of λ, because the stable state of energy and the input-dependent threshold level depend on it. Figure 5 shows the simulation results of the LPM for the various values of λ. The recognition probability is defined as the number of correction recognition per total number of the inputs. The simulations were repeated over 300 randomly generated inputs of each Hamming distance ($0 \sim 15$), and the results are averaged for the three memory vectors L, P, and M. We could get best results in the range of $0.6 \le \lambda \le 0.7$. Figure 6 represents one of the correctly reconstructed output. In summary, all memory patterns can be stored in stable state when we use these learning patterns using LPM.

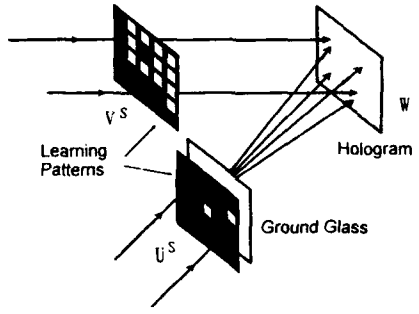


Fig. 4 Schematic diagram of recording the outer-product of learning patterns holographically.

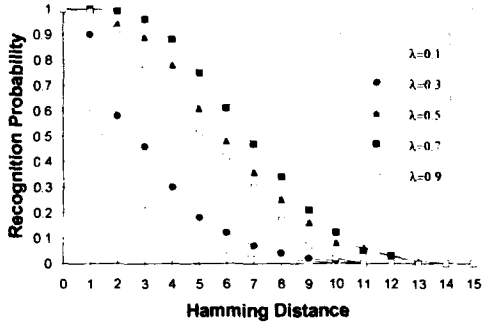


Fig. 5 Recognition probability versus Hamming distance of input patterns with various constant scale factors λ.

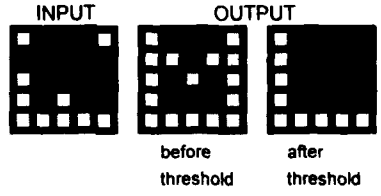


Fig. 6 A result of recognizing the erroneous input pattern.

References

1. N. H. Farhat, D. Psaltis, A. Prata, and E. Paek, Appl. Opt. **24**, 1469-1475 (1985).

2. J. S. Jang, S. W. Jung, S. Y. Lee, and S. Y. Shin, Opt. Lett. **13**, 248-250 (1988).

3. H. H. Suh and S. S. Lee, Appl Opt. **31**, 199-204 (1992).

4. H. H. Suh, C. H. Kwak, and S. S. Lee, Japanese J. Opt. (KOGAKU), **22**, 721-726 (1993).

Optical associative memory with bipolar edge-enhanced learning

Xu-Ming Wang, Trevor J. Hall and Jian Wang

Department of Physics, King's College London, Strand, London WC2R 2LS, England

Abstract

An optical associative memory with bipolar edge-enhanced feature learning by using a ferroelectric liquid crystal spatial light modulator and a barium titanate crystal is presented. A high discrimination ability of input stimuli is achieved.

SUMMARY

In an associative memory the recalled output can be understood as the weighted summation over the stored patterns. The weight is determined by the similarity of the input stimulus and the stored patterns. To achieve a better association we increase the wanted weight and suppress the unwanted ones. We can find the same objective in optical correlation pattern recognition where we seek better discrimination ability of a correlator. Therefore techniques used in pattern recognition can be applied to the optical implementation of associative memories. The phase-only filter (POF) has been known for its optimal discrimination. Investigations revealed that the magnitude squared of the impulse response of the optical correlation system using a POF is the edge outline of the original reference and the histogram of the impulse response consists of both positive and negative values; the positive part lies predominantly inside the outline while the negative part lies predominantly outside the outline. According to this property of the POF filter we can produce ternarily valued edge-enhanced versions of the patterns to be stored by the associative memory. In the bipolar edge-enhanced version of a pattern, pixels are assigned values of 1 and -1, respectively, if their positions in the original pattern are adjacent to the outline of the object and are inside and outside the object, respectively, while the other pixels are given the value of 0. The bipolar edge-enhanced pattern has nearly equally distributed positive and negative pixels besides the zero valued pixels, which meet the equal-distribution requirement for an associative memory.

We set up an optical associative memory which uses a barium-titanate photorefractive crystal as the memory recording medium, a ferroelectric SLM as the programmable input device and a charge coupled device camera as the output detector. The use of a photorefractive crystal enables the interconnect hologram to be recorded into the material in real-time, which also introduces reconfigurability into the system. The use of the SLM permits a programmable system. A 33×33 fanout computer generated hologram is used to project the laser beam onto the SLM. The use of a CGH in this experiment is two-folded. One is to pixelate the pattern displayed on the SLM in order to increase the displaying contrast ratio. The other purpose is to take the function of a ground glass as used in some reports. In the optical system performing the bipolar edge-enhanced feature learning, both the original patterns and their bipolar edge-enhanced versions are displayed on a binary SLM with the edge enhanced and the original corresponding to the input and output, respectively. The ternary modulation is realized in the following way: Three pictures, A, B and B', respectively, are simultaneously displayed on

the SLM. The fan-out beams of the CGH illuminate patterns A and B. Beams passing through B will be reflected and coincidedly imaged pixel-wise onto B'. Polarizers are so placed that light passing through A and B is binarily amplitude modulated while light passing back through B' is binarily phase modulated. Therefore light passing through both B and B' is ternarily modulated. The light interferes at the crystal and forms a volume hologram within it. Patterns are memorized by being input into the SLM in turn. For optical demonstration, five 13 × 13-pixel Chinese characters, four as the memory patterns and one as the false input stimulus are chosen.

For associative recall of an original pattern, its incomplete version or the edge-enhanced version can be used as the input stimulus, in place of B or B'. The weights of the weighted output are determined by the inner products of the input stimulus and the corresponding edge-enhanced patterns. If one of the stored memories has the largest similarity with the input the weight for that stored pattern will be much larger than the other weights. Hence high discrimination amongst the stored patterns is achieved and then the association performance is improved. We have calculated the weights for the original bipolar Hopfield model (BH), where the input stimulus takes bipolar binary form, and the corresponding values for the bipolar edge enhanced model (EE). An average improvement of discrimination from 73% (BH) to 80% (EE) is achieved. Here discrimination is defined as the average ratio of difference in the weights of an expected memory and an unexpected memory to the weight of the expected memory which is used as the input stimulus. It is equivalent to a high order nonlinear system with an order of 1.3. There is a dramatic drop in the output energy, normalized to the input energy, when a nonstored pattern is input into the system. This implies that the system has a strong discrimination among the stored and nonstored patterns. It also suggests that this phenomenon can be used as a measure to decide whether the input is a memory of the system. Partial information addressability is also investigated. The results show that the system can also perform the partial association except for a slight decrease of the output signal to noise ratio. When the edge-enhanced versions are used as the input stimuli the output is better than in the first two cases.

We also perform a computer simulation to evaluate the retrieval error of the proposed learning algorithm. Most of the performance evaluation of a neural network is statistically carried out by computer simulation where the stored patterns are randomly generated. But a random pattern might be meaningless in practical applications, where most of the patterns involved are obtained from the real world. So the storage capacity will be lower than the simulation prediction. Here we choose the frequently used chinese character set, which consists of 3755 characters in a 16×16 bitmap format. We simulate the relationship between the retrieval error averaged over 200 independent simulations and the number of the stored patterns, where stored patterns were selected randomly from the 3755 character library. We calculate the cases for the Hopfield model (HM), its bipolar counterpart, the BH, and EE. Computer simulations show the retrieval error for EE is much smaller than those of HM and BH. When the stored pattern number is 9, the error for the three are 6.99% (EE), 17.8% (BH) and 33.5% (HM), respectively. We also test a modified EE algorithm (ME), where the edge-enhancement is so carried out that for a 1-valued pixel its value will be reset to be the number of its 0-valued nearest neighbour pixels, and for a 0-valued pixel its value will be reset to the negative of its 1-valued nearest neighbour pixels. With the same simulation as above we find the corresponding retrieval error is now 0.732%.

Self-routing using an Pulse Interval Coded Optical Content Addressable Memory

Subrat Kar[1]

Abstract

At multi-gigabaud data rates, the unacceptable overheads of O/E-E/O conversion may be avoided by self-routing of optical data streams. We discuss a scheme by which data may be self-routed through a optical switch using an optical content addressable memory. The integrated optic realization of this element and its application to a synchronous time slot interchanger are also discussed.

Introduction

A novel self-routed slot-switching scheme using an integrated optic directional coupler is outlined using a pulse interval coded optical content addressable memory (PICOCAM). The integrated optic devices required for its implementation are also outlined. This bit-switching approach avoids the bottleneck in speed imposed by the electronic drive circuitry in electro-optic switches.The scheme achieves bit-wise self-routing in a 2x2 two-wavelength c n multiplexing photonic element - an integrated optic directional coupler (IODC) or the -mode interferometer (TMI) structure.

Principle

We use a four-port (2x2) optical switching device which switches its inputs as a function of their wavelength. Thus, input data presented on one of two wavelengths λ_1 and λ_2 would cross over to the other waveguide if presented on wavelength $\lambda 1$ and would remain in the same waveguide if present on wavelength $\lambda 2$. Therefore, assuming broadcast states as forbidden, the two-state functionality of the switch is preserved. By avoiding the associated drive circuitry, the scheme allows data throughput at near optical rates. Further, the switching scheme is inherently real-time i.e. the response time of the switch is less than the data bit width. The responsibility of presenting the data to the switch with the appropriate wavelength now devolves on the input - the data must be recognized and converted to the appropriate wavelength *before* it is input to the switch.

We assert that, in any non-faulty rearrangeably non-blocking PSA, if the routing architecture is known, the set of connections η between any set of inputs and outputs is deterministic. Further, this assertion implies that if I_n is the set of inputs and O_n is the set of outputs, then for all $\eta \in I_n \times O_n$, the set of states S_s^{η} of every switch σ_n is known. For instance, in a 3x3 switch with two-state switches (through/cross) the number of possible connections are given by the following six sets: S1 = (0, 0), (1, 1), (2, 2); S2 = (0, 1), (1, 0), (2, 2); S3 = (0, 2), (1, 0), (2, 1); S4 = (0, 0), (1,2), (2, 1); S5 = (0, 1), (1, 2), (2, 0); S6 = (0, 2), (1, 1),(2, 0) We note that, for some connections (represented by the set S_T), the switch is in the through state while, for other connections (represented by the set S_X), it is in the cross state. Furthermore, for each switch, the sets S_T and S_X are predetermined and $S_T = \{I_n \in O_n\} \setminus S_X$ In switch 1, for instance, S_T = {S1, S2, S3, S4 } and S_X = {S5, S6}.

---

[1]Laboratory for Lasers & Optical Fibers, International Center for Theoretical Physics, I-34100 Trieste, Italy Tel: ++39 (40) 2240322 FAX: +39 (40) 224559 email:subrat@ictp.trieste.it

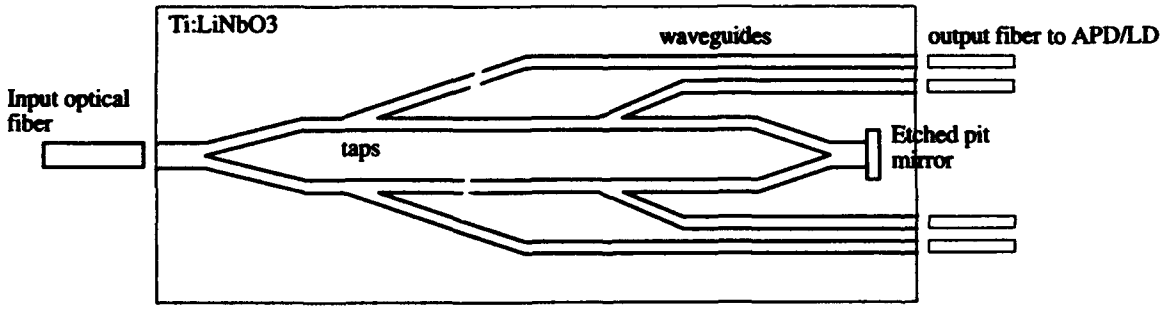
The routing function can be obtained by the considering each switch as a optical content addressable memory (CAM) whose output is 1 if it contains the required data and 0 (null) if it does not. The recognition of the data at the switch is done using a pulse-interval coded optical CAM (PICOCAM). The set of possible destinations D (i.e. *two* sets of destinations for a single switch) of a data bit is split into two sets S_T and S_X as shown in the table below.

Switch No.	ST	SX
1	1,2,3,4	5,6
2	1,4	2,3,5,6
3	1,2,5	3,4,6

A data bit bound for a destination $d \in S_T$ (Case I) requires the PSE to be in the through state and must be presented on wavelength λ_1. Similarly, a data bit going to a destination $d \in S_X$ (Case II) requires the PSE to be in the cross state and must be presented on a wavelength λ_2. Each data bit is encoded in the PICOCAM format as follows: each bit is translated into an equivalent header consisting of n+1 slots (S_0,...,S_n) of duration T each where n is the number of destinations with a guard delay E between each slot (for a single switch, n = 2).

We discuss the realization of this CAM structure using fiber optic delay lines. Also the monolithic integration of this device onto a Lithium Niobate substrate is discussed. The calculated data rate, therefore, is determined by the largest pulse interval -- for the fiber optic delay line structure we discuss, this is 506 picoseconds - which corresponds to a fixed data throughput of 1.97×10^9 Hz or nearly 2 Ghz. Since this routing scheme requires no switching in the electronic domain, the throughput expected is high and at the speeds defined largely by the optical inputs and the response times of the opto-electronic components used.

As an application of the PICOCAM element, we also discuss the implementation of a self-routing synchronous time slot interchanger based on the PICOCAM element -- a stream of time slots is manipulated to achieve an interchange of time slots in such a way that the i^{th} input slot occupies the j^{th} output slot if input i is to exchange data with output j. The destination of each slot is slot-coded into a part of the slot using spread spectrum codes with sorting achieved using coincidental pulse techniques. A suggestion for an all-optical implementation of the proposed scheme is also given.



The PICOCAM element

Use of Multiplexing Diffraction Gratings and Holographic Lens Arrays in Optical Associative Memories

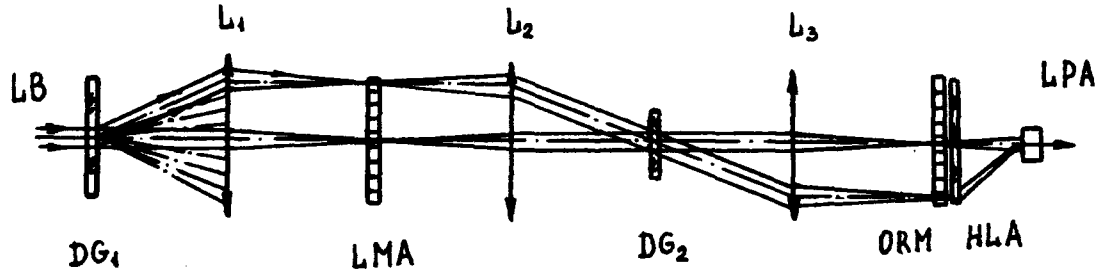
V.F.Yarmolitskij, A.I.Bogdanovich, A.M.Polikanin, V.I. Polyakov

Institute of Electronics, Academy of Sciences of Belarus
22 Lagoiski Trakt, Minsk-90, 220841 Republic of Belarus
Tel. (0172) 65 34 38, Fax. (0172) 65 35 41

ABSTRACT. The paper discusses the design and operation of an optical associative memory (OAM) in which effective optical coupling between memory elements is realized by using phase diffraction gratings and holographic lens arrays made by specially developed technology. Experimental results are presented corroborate a promising potential of the OAM variant under consideration.

One of the problems arising in implementing an optical associative memory (OAM) structure concerns provision of an effective illumination of light-modulating and light-recording elements of the OAM [1]. This study concentrates upon the possibility of solving the above-mentioned problem by using a set of diffraction gratings (DG) and 2-D holographic lens arrays (HLA) as multiplexing and demultiplexing elements of the OAM.

The following figure illustrates an optical circuit of the OAM.



In associative search of information, a laser beam is split by a DG_1 into n rays of equal intensities and illuminates a linear modulator array (LMA) having n channels. Then, the search-word modulated rays are divided by the grating DG_2 into m rays in orthogonal plane. The raster of $n \times m$ rays (where n is the number of paraphasing bits search words, m is the number of search words stored in the memory) simultaneously illuminates all cells of an operative recording medium (ORM). The search word code is compared with the corresponding inverted code of the searched data in accordance with the total mismatch principle, and the result of

comparison is projected to a linear photodetector array (LPA) by means of an HLA consisting of n x m holographic lenses.

The peculiarity of the optical circuit proposed is that it ensures telecentrical path of rays which minimizes abberrations and gives the possibility of arranging active elements (LMA, ORM, LPA) in the regions of laser beam waists, resulting in lower circuit sensitivity to distortions in the light raster and reducing crosstalk.

In the prototype version of the OAM, we used phase diffraction gratings made of dichromated gelatin (DCG) layers by a specially developed method using multiple contact replication of metallized master grating with 20 μm spacing and rectangular slits. Owing to nonlinearity-build up effect, nonuniformity of the energy distribution over diffraction orders of the gratings was within about 10% up to the ± 5th order, the energy efficiency of the grating being 80%. Maximum deviation from equidistant position of diffraction maxima was not greater than 4%. The holographic lens arrays used in the prototype was made on DCG layers in laboratory conditions. The array contained 10^2 holographic lenses with average diffraction efficiency of 60% and the diffraction efficiency nonuniformity over the array field of 5%.

Taking into account losses in multichannel DKDP-based light modulators [2] used as LMA and ORM, the integrated light efficiency of the proposed scheme was about 35%, which, in our opinion, makes it promising for use in optical associative memory structures.

References

1. V.S. Burtsev, V.B. Fyodorov. Kvantovaya Elektronika. 1992, Vol.19. N 8. P. 795-803 (in Russian).
2. V.A. Pilipovich, V.I. Polyakov. SPIE, Vol. 1807 Photonic Switching (1992), P. 361-365.

Optical Learning Neural Network with Reversal Input Superimposing Technique

Masahiko Mori, Masaru Kondo[1], Yoshio Hayasaki[2],
Ichiroh Tohyama[1] and Toyohiko Yatagai[1]

Electrotechnical Laboratory, 1-1-4 Umezono, Tsukuba, 305 Japan
Telephone: +81-298-58-5623 E-mail: e8612@etlrips.etl.go.jp

[1]University of Tsukuba, 1-1 Tennodai, Tsukuba, 305 Japan
[2]The Institute of Physical and Chemical Research, 19-1399, Koeji, Nagamachi, Aoba-ku, Sendai, 980 Japan

ABSTRACT

Reversal input superimposing technique is applied to an optical learning neural network. Optical neural networks introduced the technique are not necessary to use negative weights and subtraction, and inherently constructed all optical systems.

1. Introduction

In general neural network models, the synaptic weights and the weighted sum are the finite real values. It means that some of them have minus values. In the other hand, to implement optical neural networks, usually the output of neurons and the values of weights are represented by optical intensities, transmittances or refrectivities. It is hard to realize minus values under these representations. Therefor, in some optical neural network systems, the twice weights, separated plus and minus weights are used. After each weighted sum operation, these values are subtracted by electronic circuits[1,2]. In this approach, twice pixels of weight matrix and electronic subtract circuits are required and the system speed is limited by these circuits. In another case, the weights are added with a bias and the thresholds of each neuron are changed according to the total values of inputs. In this case special hardwares to realize controlling the each threshold are needed, and an all optical system is impossible.

We proposed the reversal input superimposing technique (RIST) to avoid above problems[3,4]. In this paper, we report an optical learning neural network with RIST. The optoelectronic neural system based on RIST is implemented and learning capability is realized by using a Pockels readout optical modulator (PROM) device[5].

2. Principle of RIST

Consider general discrete neural network models consisting of M neurons, which receive the same input signals $X = \{x_1,\ldots,x_p\ldots,x_N\}$ from N input neurons, and emit respective output signals $V = \{v_1,\ldots,v_p\ldots,v_M\}$. Let w_{ji} be the synaptic weight from the i-th input neuron to j-th output neuron. The j-th weighted sum of input signals u_j and the output v_j are written as

$$u_j = \Sigma_j w_{ji} x_i - h_j \qquad (1)$$

and

$$v_j = f(u_j), \qquad (2)$$

where h_j is the j-th value of a set of the thresholding values $H = \{h_1,\ldots,h_j,\ldots,h_M\}$ and f is a nonlinear output function. Introducing a constant α, Eqs.(1) and (2) are rewritten as

$$u'_j = \Sigma_i (w_{ji} + \alpha) x_i + \alpha \Sigma_i (1 - x_i) \qquad (3)$$

and

$$v_j = f'(u'_j), \qquad (4)$$

where $f'(y) = f(y - N\alpha)$. The thresholding values $H = \{h_j\}$ are neglected because they can be treated as same as the synaptic weights. The constant α is a bias of the weights w_{ji} and is determined to $\alpha > -\min(w_{ji})$, where $\min(w_{ji})$ denotes the minimum values of a set of the weights $W = \{w_{ji}\}$. Hence, the biased synaptic weights $\{w_{ji}+\alpha\}$ of the first term in Eq.(3) are necessary to be positive. The input x_i is ranged from 0 to 1 in many neuron models. In these case, $\{1-x_i\}$ of second term in Eq.(3) are the reversal values of the inputs x_i in the range of 0 to 1, and positive. Under these conditions all terms of Eq.(3) are all positive and easily realized by optical techniques. f' is

the nonlinear function with the thresholding value which is slid the constant Nα from f in Eq(2).

3. Optical Implementation and Experiments

The experimental system of an optoelectronic neural network is shown in Fig.1. He-Ne laser light (633nm) is used at the recalling process. Input signals of neurons are polarization encoded by a liquid crystal TV (LCTV) panel which has not an analyzer. The upper path (PATH1) of the system performs a weighted sum operation which is the first term of Eq.(3) with input signals. The lower path (PATH2) realizes reversal inputs of the second term. And these calculated results are superimposed and detected by a CCD camera. The balance of these signals are adjusted by the angel of a half wave plate in PATH2. To achieve the learning capability on the system, a PROM device is located in PATH1. The PROM is written or erased by white light according to the values which displayed on the LCTV. Therefor it is not necessary to align the weight matrix on the PROM and input signals on the LCTV. The modification values of the weights are calculated from the teaching signals and the recalling results by a computer.

On the experimental system, 8 input and 8 output neurons system is realized. 3 input patterns of 8 bits are stored by the system. The weights on the PROM start from random values nearby the constant α which is the half value of the dynamic range of the device. The learning curves are shown in Fig.2. By 13 iterations, the weights went to right values and the error went down to 0.

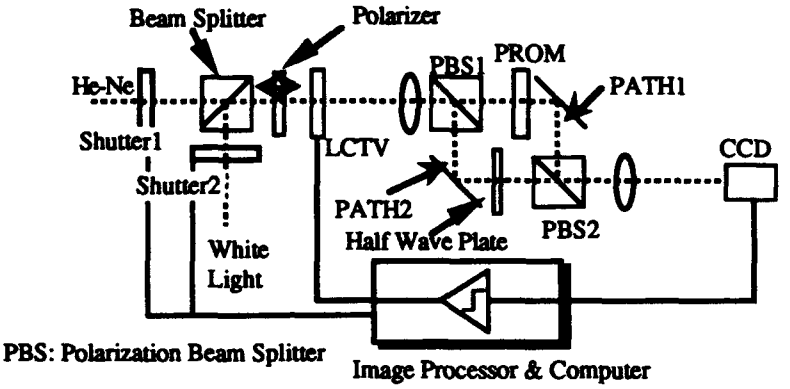


Figure 1 Experimental Setup of Optical Learning Neural Network with RIST

4. Conclusion

Reversal input superimposing technique is applied to an optical learning neural network. Optical neural networks introduced the technique are not necessary to use negative weights and subtraction. The learning capability was applied to the optoelectronic system using a PROM device and verified at the performance with an 8-8 neurons network.

The authors thank S.Ishihara, H.Yajima and T.Hidaka of Electrotechnical Laboratory for useful discussions and encouragements. Thanks are also due to Y.Osugi of NGK Insulators, Ltd. for providing the PROM.

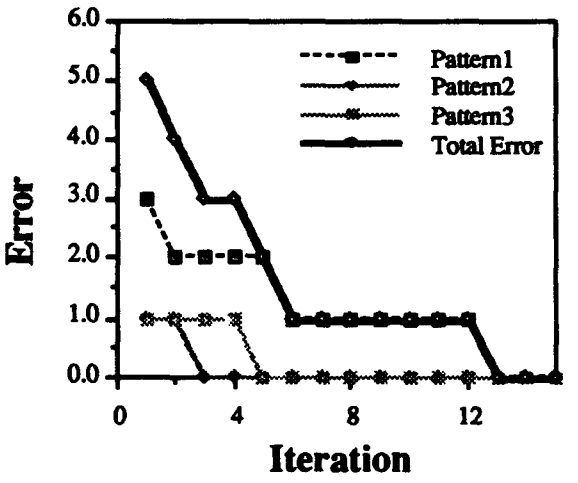


Figure 2 Learning curves of each stored pattern and the total error

References

[1] J.Ohta, S.Tai, M.Oita, K.Kuroda, K.Kyuma and K.Hamanaka, Opt. Lett., 14,844 (1989).
[2] N.Kasama, Y.Hayasaki, T.Yatagai, M.Mori and S.Ishihara, Jpn. J. Appl. Phys., 29. L1565 (1990).
[3] Y.Hayasaki, I.Tohyama, T.Yatagai, M.Mori and S.Ishihara, Tech. Digest OC'93 (Palm Springs, USA), 140 (1993).
[4] Y.Hayasaki, I.Tohyama, T.Yatagai, M.Mori and S.Ishihara, Appl. Opt., to be published.
[5] Y.Osugi, H.Abe, A.Honda, A.Hamajima and S.Toyoda, Conf. Record of OC'90 (Kobe, Japan), 21 (1990).

Optoelectronic Fuzzy Control of an Inverted Pendulum Using Light-Emitting-Diode Arrays and Position-Sensing-Devices

Hideo ITOH, Bruno HOUSSAY and Seiji MUKAI
Optoelectronics Div., Electrotechnical Lab.
1-1-4, Tsukuba, Ibaraki, 305 JAPAN
Phone: +81 298 58 5622 Fax: +81 298 58 5627 Internet: itoh@etl.go.jp
Tatsuya YAMADA and Shinichiro UEKUSA
School of Sci. and Technol., Meiji Univ.

Abstract

For the first time real-time optoelectronic fuzzy control of an inverted pendulum is realized. The system uses arithmetic product-sum-gravity method with Gaussian-like membership functions. Membership functions and center-of-gravity operations are realized using LEDs and position-sensing-devices.

1.Introduction

High-speed optoelectronic analog fuzzy inference technique has been proposed[1] using beam-scanning laser diodes (BSLDs)[2] and position-sensing-devices (PSDs). The inference process uses an arithmetic PRODUCT-SUM Gravity method with Gaussian membership functions and the controllability of the inference method is better than conventional MIN-MAX Gravity method with triangle membership functions[3]. The inference speed of the system will be more than several tens of MFLIPS (Mega Fuzzy Logical Inference Per Second) using high-speed operation of the beam scanning laser diodes. However, a real system control using the BSLDs has not been yet realized because of the present low resolution of their far-field pattern.

In this paper, configurations of optoelectronic antecedent and consequent fuzzy operation units using an LED array and a PSD are proposed. Furthermore, the first optoelectronic control system using the consequent unit is realized and its usefulness is demonstrated using an inverted pendulum.

2. Optoelectronic analog antecedent and consequent units

Figure 1 shows a schematic configuration of a fuzzy antecedent grade evaluation unit, which calculates the satisfaction of a fuzzy antecedent rule. In this figure, 1, 2 and 3 serially-wired LEDs are connected with the input in parallel. 1, 2 and 3LEDs start emission in turn with increasing the applied voltage. Because a PSD can detect a center-of-gravity of the radiation pattern, Gaussian-like membership function is realized by position and emitting characteristics of the LEDs. Figure 2 shows a schematic result of several membership functions. Peak position of the function is controlled by value of the resistors and level-shift-diodes.

Figure 3 shows a schematic configuration of an optoelectronic fuzzy consequent operational unit. Unified output membership function by superposition of LED radiations and defuzzification of the radiation patterns are realized by an LED array and a position sensing device. Figure 4 shows an example of defuzzification of the unit. Unequal interval of each PSD output reflects the separation of each LED of the array.

3. Inverted pendulum control system

Figure 5 shows a schematic configuration of optoelectronic fuzzy inverted pendulum control system. A 50cm-long free-rotating inverted pendulum is on a stepping-motor-driven cart. Input data for the fuzzy control are angle of the pendulum, which is measured by a rotary encoder, and angle velocity, which is calculated by the difference of measured angles. Consequent fuzzy inference processes are realized by the optoelectronic operation unit and antecedent fuzzy inference processes are simulated by a personal computer. Figure 6 shows schematic experimental results of various experimental conditions. Angle of a controlled inverted pendulum after initial perturbation (40cm/sec, 0.3sec) is displayed as a function of time. Cases of optoelectronic control (0.015 sec/cycle) and pure electronic fuzzy control (0.08 sec/cycle) are shown in the figure. Difference of the cycle time are from introduction of optoelectronic processing. Control gain of HIGH in the figure is 4.5 times than that of LOW. The results show the superior controllability of the optoelectronic system.

4.Conclusion

First real-time control of an inverted pendulum is realized based on an optoelectronic analog fuzzy inference system. Both antecedent and consequent parts of the fuzzy inference is realized

by LED arrays and position-sensing-device arrays.

The authors thank I.Yokoyama, M.Mori, M.Watanabe, T.Hidaka and H.Yajima for technical support and fruitful discussions.

References

[1]H.Itoh, M.Watanabe,S.Mukai,and H.Yajima,"Optoelectronic fuzzy inference system using beam scanning laser diodes", Proceedings of Topical Meeting on Optical Computing '93, OWD5, pp.123-126, Palm Springs (1993).

[2]S.Mukai, M.Watanabe, H.Itoh, H.Yajima, Y.Hosoi, and S.Uekusa,"Beam scanning and switching characteristics of twin-striped lasers with a reduced stripe spacing", Opt. and Quantum Electron, 17, pp.431-434 (1985).

[3]H.Itoh, T.Yamada,B.Houssay, S.Mukai and S.Uekusa,"Stability Evaluation of Inference Methods for Optoelectrionic Fuzzy Inference System", Abstract of the Topical Meeting of the International Commission for Optics '94 -Frontiers in Information Optics-, 5-B2-19, Kyoto (1994).

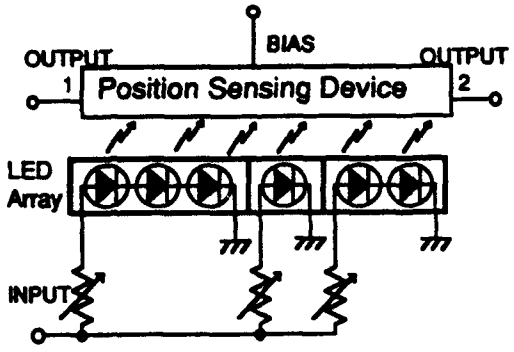


Fig.1 Optoelectronic antecedent grade evaluation unit using a LED array and a PSD

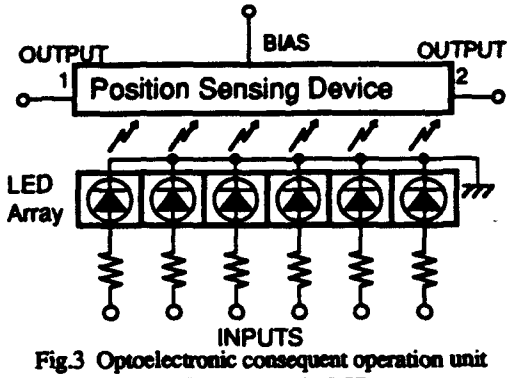


Fig.3 Optoelectronic consequent operation unit using a LED array and a PSD

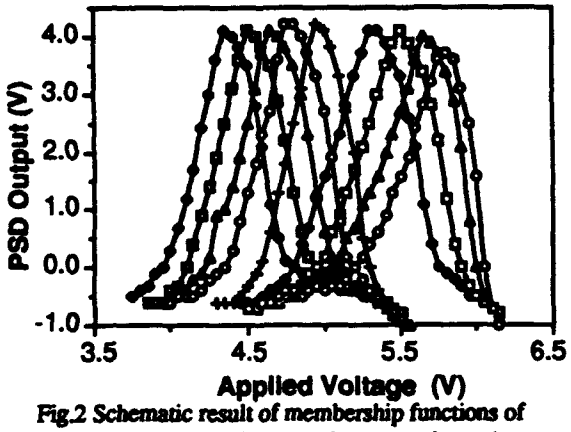


Fig.2 Schematic result of membership functions of an optoelectronic antecedent operation unit.

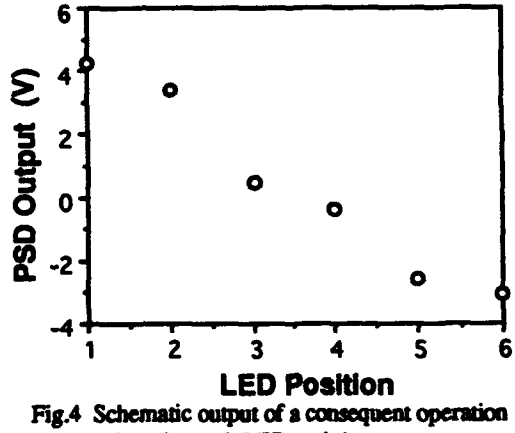


Fig.4 Schematic output of a consequent operation unit under each LED emitting

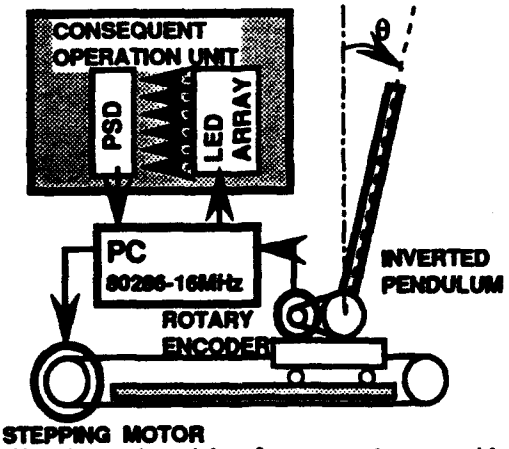


Fig.5 Inverted pendulum fuzzy control system with an optoelectronic antecedent grade evaluation unit

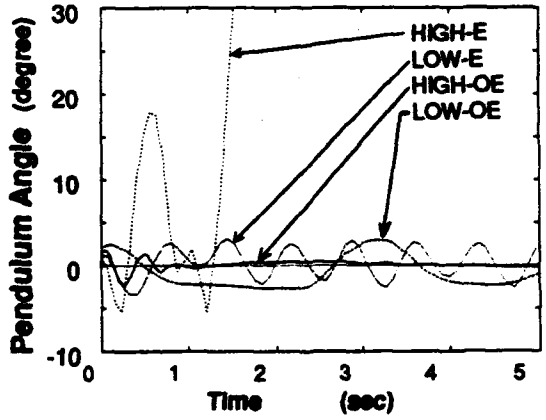


Fig.6 Traces of the angle of an inverted pendulum controlled by optoelectronic systems and electronic systems

Smart Pixel Optical Neural Networks : Design and Simulation.

Andrew J. Waddie & John F. Snowdon

Department of Physics, Heriot-Watt University,
Riccarton, Edinburgh, EH14 4AS, Scotland,UK
Tel : UK 31 451 3068 E-mail : andrew@phy.hw.ac.uk

Abstract

Hybrid analogue/digital optoelectronic devices allow implementation of practical optical neural networks. A smart pixel design to perform a unique learning algorithm is presented. Network simulations reveal the advantages of high contrast receivers/transmitters/neurons.

Motivation for Implementation of Optical Neural Network.

A major strength of optical computing architectures is the high degree of parallelism which can, theoretically, be exploited. However the actual implementation of such highly parallel systems can be problematic with non-uniformity of the processing elements being a major drawback. A fault-tolerant neural processor may be used to overcome these non-uniformities at the cost of more individual thresholding elements and greater in-unit complexity. However the large fan-in/fan-out requirements of such networks prevent the full realisation of the potential of the neural paradigm in conventional silicon electronics. Indeed the extension of neural (or hybrid analogue/digital) processing to more complex tasks requires a novel approach to algorithm design that exploits the dynamics and physical characteristics of the technology of the implementation. Optics is a natural medium in which to conceive neural processor design due to the high communication bandwidth available. A topology for such a hybrid implementation of a simple perceptron-like neural network [1] is presented in Figure 1.

Implementation of an Optical Neural Network.

The devices used in the neural plane of this network are S-SEEDs although a similar network has been simulated using the *NLIF* class of device. [2] The behaviour of the S-SEED is well modelled [3] and is potentially suited for use as a thresholding neuron. The dual-rail nature of the device permits dynamic alteration of the threshold level of each neuron. The learning algorithm used by the network is designed to exploit the dual-rail and dynamic thresholding behaviour of the S-SEED neurons.

The network presented here has been simulated on a digital array processor for a 32 unit network and a number of simple problems tackled. These include pattern recognition, composite Boolean functions and simple arithmetic. The number of presentations required to learn a particular function is shown to be dependent upon the optical characteristics and dynamics of the devices employed. For example for optimal operation a higher contrast ratio than currently acheivable with S-SEEDs is desireable, therefore the basic S-SEED may not be the ideal device to deploy in the neural plane. Two avenues currently being explored to produce higher contrast ratio neuronal devices are AFPMs [4] and smart pixel neurons [5].

Smart Pixel Design for the S-SEED Optical Neural Network.

The integration of optical modulators with electronics allows units to be designed which can

calculate the changes in the weight matrices produced by the optical outputs from the neural plane. The hybrid technology can also be used to perform the multiplication of each optical input by the appropriate weights. By utilising an assymmetrically clamped S-SEED the voltage input into the circuit can be linearly dependent upon the optical power incident upon the one of the windows of the S-SEED. This allows the weight update circuitry to be simple and to perform its task with the minimum of propagation delay.

In general the simulation of the complete network allows us both to optimise the algorithms and to evaluate the effectiveness of particular device/architecture combinations.

References

[1] D.E.Rumelhart & J.L.McClelland, Parallel Distributed Processing, 1986, *MIT Press*, pps 318-362

[2] J.F.Snowdon, 1992, *Proceedings of Int. Symp. on Opt. Appl. Sci. & Eng., SPIE 1773*

[3] B.S.Wherrett, M.P.Y.Desmulliez & J.F.Snowdon, 1993, *Optical Computing and Processing*, Vol. 3, 1 , 19-38

[4] K-K Law , J.L. Merz & L.A. Coldren, 1992, *IEE J. Quantum Electronics*, Vol.29, 2 , 727-739

[5] S.Lin, A. Grot, J. Luo & D. Psaltis, 1993, *Applied Optics*, Vol. 32, 8 , 1275-1289

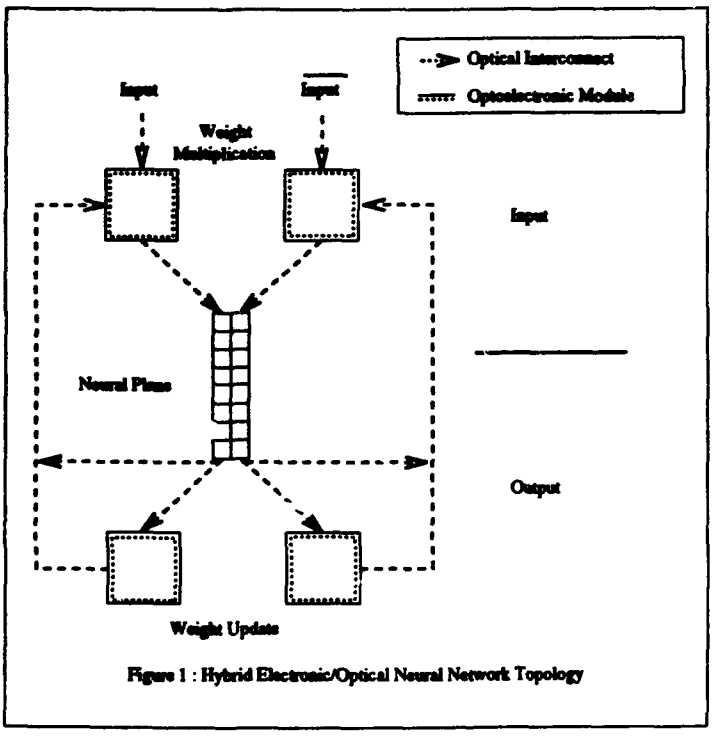


Figure 1 : Hybrid Electronic/Optical Neural Network Topology

An Optoelectronic Neural Network With On-Line Learning

D. Pignon, T.J. Hall, L.Q. Xu, K.B. Russ[1], S.R. Cherry[1],
N.C. Roberts[2], P. Prewett[3], P. Hallowell[3]

King's College London, [1]Pilkington Group Research, [2]BAe Sowerby Research Centre,
[3]Rutherford-Appleton Laboratory UK

Abstract

An optoelectronic implementation of a multi-layer perceptron with on-line learning is presented. Results obtained from two demonstrator systems are reported.

Summary

An optoelectronic implementation of a multi-layer perceptron with on-line learning is presented. Results obtained from a transmissive design demonstrator and a simpler, more compact, reflective design demonstrator will be reported. The basic design philosophy, which is the same for both systems, is presented.

Both demonstrators exploit an optical matrix-matrix multiplier with a spatial light modulator shutter array and computer generated holograms and refractive micro-lens arrays providing the required fan-out and fan-in functions. The latest system consists of a reflective architecture whereby different areas of the same spatial light modulator (SLM) are used simultaneously for the input to the system and for weighting the interconnect, thus facilitating a significant reduction in the size and hardware cost of the system (compared to the two SLM transmission architecture).

The implementation technology places constraints on the network model not found in software simulations such as the need to accomodate hard thresholds and quantised weight values. Unfortunately, the most sucessful learning algorithms involve the evaluation of a gradient which is not possible to calculate in this case. We report on how successful on-line learning may still be achieved using either a heuristic self-optimisation algorithm or a rigorous stochastic approximation algorithm. For the classification of nine 64 pixel binary patterns containing up to 16% pixel errors using a system with 16 quantised weight levels, classification accuracy was increased from 93% to 97.6% with the application of self optimisation.

Results of a demonstration of the system configured as a back propagation neural network is presented and comparisons are made between results obtained from transmissive and reflective architectures.

D. Pignon, Physics Department, King's College London,
Strand, London WC2R 2LS
Telephone: 071-836 5454 Ext. 3718
Fax: 071-836 1799
E-mail: dp@uk.ac.kcl.ph.ipg

Optical Implementation of Signal Feed-forward and Error Back-propagation with a Ground Glass

Hyuck-Jae Lee, Soo-Young Lee, and Sang-Yung Shin
Department of Electrical Engineering, Korea Advanced Institute of Science and Technology
373-1 Kusong-dong, Yusong-gu, Taejon 305-701, Korea, Fax : +82-42-869-3410

Abstract : Both signal feed-forward and error back-propagation paths for adaptive learning of TAG neural network model are implemented by a single ground glass, which provides much higher diffraction efficiency and interconnection density.

Introduction : Our goal has been to find solid compact optical architectures for large-scale implementation of artificial neural networks with adaptive learning capability. We had proposed a new adaptive neural network architecture, TAG(Training by Adaptive Gain)[1], which consists of the random fixed global interconnections and local adaptive gain-controls. The TAG neural network model is suitable for large-scale optical implementation owing to much less adaptive elements. The fixed global interconnections may be implemented by multifacet hologram[1,2], volume hologram[3], or ground glass[4], while the adaptive gains are done by spatial light modulators(SLMs). The fixed global interconnections are predetermined randomly or obtained from any learning algorithm for standard patterns. The ground glass is more advantageous for random interconnections with much higher diffraction and interconnection density. In this paper, the optical signal feed-forward architecture with ground glass[4] is extended to incorporate error back-propagation. Both signal feed-forward and error back-propagation paths are implemented by a single ground glass, and adaptive learning has been demonstrated for hetro-associative memory.

TAG neural network architecture : Number of adaptive elements for synapses is a major limiting factor for practical large-scale implementation of neural networks. As shown Fig. 1, TAG model consists of fixed global interconnections and local adaptive gain-controls, which results in much less adaptive elements and becomes advantageous for image classification with large number of pixels. In mathematical notations output y_{ij} is represented as

$$y_{ij} = S(\hat{y}_{ij}) , \quad \hat{y}_{ij} = \sum_{k,l} v_{ij} T_{ijkl} w_{kl} x_{kl} \tag{1}$$

where x_{kl} and y_{ij} denote activations of klth input neuron and ijth output neuron, respectively. $S(.)$ is a Sigmoid function. To train the TAG model, we have adopted gradient-based least-square-error minimization algorithm. And the total error E is defined as $E = \sum_s \sum_{i,j} (y^s_{ij} - t^s_{ij})^2/2$, where s is an index for each class (input-output pairs), y is the actual state of an output neuron, and t is its desired state. The learning rule is based on the error back-propagation. By applying chain rule, the partial derivatives of E with repect to the local gain-controls v_{ij} and w_{kl} are obtained as

$$\frac{\partial E}{\partial v_{ij}} = \sum_s \delta^s_{ij} \hat{y}^s_{ij}/v_{ij} , \quad \frac{\partial E}{\partial w_{kl}} = \sum_s \gamma^s_{kl} x^s_{kl}/w_{kl} , \tag{2}$$

where $\hat{y}^s_{ij}$ is argument of the Sigmoid function in Eq. (1) with input x^s_{kl}. The δ^s_{ij} and γ^s_{kl} are output and input errors, respectively, and defined as

$$\delta^s_{ij} = (y^s_{ij} - t^s_{ij}) S'(\hat{y}^s_{ij}) , \quad \gamma^s_{kl} = \sum_{i,j} \delta^s_{ij} v_{ij} T_{ijkl} w_{kl} \tag{3}$$

The single-layer TAG may be cascaded for multi-layer architecture, and still error back-propagation is applicable for training of the local gain-controls.

Optical implementation using ground glass : For the fixed global interconnections multifacet hologram(MFH) may be used. However for very large scale implementations the MFH shows limited interconnection density and low diffraction efficiency. We had developed the optical implementation of TAG model for only the forward signal path using cheap ground glass[4], while error back-propagation was performed by a personal computer(PC). But, learning in a conventional computer is often a very time-consuming because of (transpose matrix)-vector multiplication for the error back-propagtion.

In Fig.2, a schematic illustration of optical implementation for single-layer TAG model with both signal feed-forward and error back-propagation paths using a single ground glass is shown. As described in

Ref. [5], a single SLM with multifacet hologram architecture may be used for both forward and backward(transpose) path with N^4 weighted interconnections, and now replaced by a cheap ground glass for random interconnections. For forward signal path, the local gain-control w_{kl} is combined with input $x_{k,}$, and displayed at CRT with gray levels. Uniform laser beam incident at the mirror side of the LCLV generates a 2-D optical patterns corresponding to $w_{kl}x_{kl}$'s, which is multiplied with random fixed global interconnections T_{ijkl}'s by the ground glass. The diffracted lights at the LCD panel plane become $\hat{y}_{ij}/v_{ij} = \sum_{k,l} T_{ijkl} w_{kl} x_{kl}$. When all pixels of LCD panel are set clear, this diffracted lights, reflected by the beamsplitter(BS) and passing through relay lenses L1 and L2, can be detected by Detector1(CCD-Camera). The output gain-controls v_{ij}'s, the sigmoid operation, and calculations of errors δ_{ij}'s at output neurons may be performed by a personal computer. In case of error back-propagation, all pixels of LCLV are set clear, and the combined error $v_{ij}\delta_{ij}$ is displayed at the LCD panel. The lights collected by the Detector2 are products of the form $\delta_{ij} v_{ij} T_{ijkl}$ by aid of Lens L3 with SLMs. The adaptive local-gain changes for w_{kl} and v_{ij} are implemented by a personal computer. The personal computer in this experiment may be easily substituted by 2-dimensional arrays of smart pixels consisting of photodiodes and appropriate electronic circuits. The simplicity of this architecture with cheap ground glass is a big advantage over existing architectures using volume holograms, lenslet array with SLMs, or multifacet holograms.

In the experiment, to simulate bipolar synapses, difference between two neuron values are used. And bipolar input patterns are handled by a time-multiplexing technique. This optical system is currently trained to classify six 5×7 number patterns.

Conclusion : We have demonstrated the feasibility of optical implementation for the signal feed-forward and the error back-propagation by a single ground glass. Provided 2-dimensional arrays of photodiodes and electronic circuits were available, this TAG with ground glass may come up with compact solid electro-optic artifical neural networks.

Acknowlegement : This research was supported by Korea Science and Engineering Foundation.

References

[1] H.J. Lee, S.Y. Lee, S.Y. Shin, and B.Y. Koh, "TAG : A neural network model for large-scale optical implementation," Neural Computation, Vol. 3, pp. 135-143, 1991.

[2] H.J. Caulfield, "Parallel N^4 weighted optical interconnections," Appl. Opt., Vol. 26, pp. 4039-4040, 1987.

[3] D. Brady, X.G. Gu, and D. Psaltis, "Photorefractive crystals in optical neural computers," Proc. SPIE 882 Neural Network Models for Optical Computing, pp. 132-136, 1988.

[4] H.J. Lee, S.Y. Lee, and S.Y. Shin, "Random interconnections with ground glass for optical TAG neural networks," OSA Topical Meeting Optical Computing, pp. 104-107, 1993.

[5] J.S. Jang, S.Y. Lee, and S.Y. Shin, "Parallel N^4 weighted optical interconnections : Comments," Appl. Opt., Vol. 27, p. 4364, 1988.

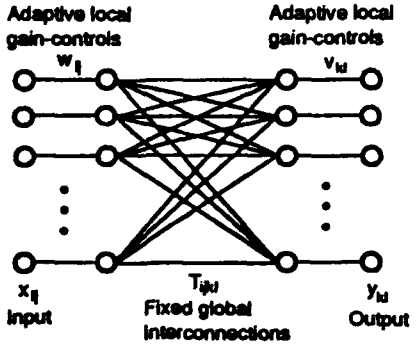


Fig. 1 Single-layer TAG architecture

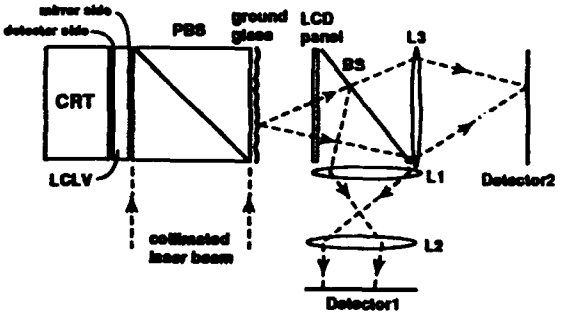


Fig. 2 Schematic illustration for the experiment of optical TAG neural network with signal feed-forward and error back-propagation path.

Feature Extraction Preprocessing and Optical Neural Network

Ichiroh Tohyama, Masaru Kondoh, Toyohiko Yatagai,
Institute of Applied Physics, University of Tsukuba,
1-1 Tennoudai, Tsukuba, 305, Japan
Telephone: +81-298-53-5217 Fax: +81-298-53-5205

Masahiko Mori,
Electrotechnical Laboratory, 1-1-4 Umezono, Tsukuba, 305, Japan

Yoshio Hayasaki
The Institute of Physical and Chemical Research,
19-1339 Koeiji, Nagamachi, Aoba-ku, Sendai, 980 Japan

Abstract:
A new architecture combined with an optical Fourier transform processor and a three-layer optical neural network is proposed. This hybrid system can reduce a number of neural elements.

Optical neural network computing is of interest in terms of massively parallel computing. Many optical neural network systems based on the matrix-vector multiplication architecture,[1] however, are limited in a scale of parallelism, because of spatial resolution of optical systems and spatial light modulators. Besides, when the bipolar synaptic weights are represented by optical intensity, they are divided into positive unipolar weights and negative unipolar weights[2],[3]. This means that twice number of the synaptic weights are needed. To solve these problems, as an alternative method, we introduce optical feature extraction techniques. The feature extraction can map the data onto a new feature space. The data on the feature space are subjected to input data for an optical neural system. If we can design a suitable mapping system, the ability , the function, and the size of the optical neural system could be reduced.

We propose here a new type of neural computing with a preprocessor for feature extraction to reduce the number of neural units. A variety of optical feature extraction techniques have been discussed, which include analog[4] and digital methods[5]. The Fourier transform, the Hough transform, the polar coordinate transform, the scale-invariant transform and so on are typical examples of analog methods.

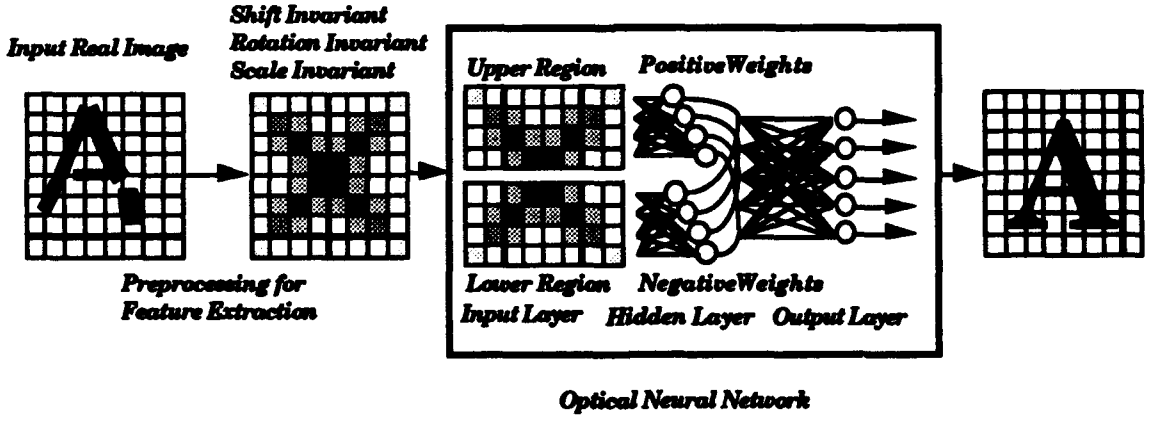


Fig. 1 Concept of a hybrid optical neural computing.

Figure 1 shows a concept of a hybrid optical neural network using the Fourier transform which is one of feature extraction preprocessing. We note that a Fourier transform of a real object is shift invariant and point-symmetrical. A half region of the Fourier transform is connected with positive synaptic weights, the other region negative synaptic weights. This procedure reduces half the number of weights to display on a spatial modulator.

Computer simulation for the feature extraction preprocessing and the neural network with the back-propagation learning algorithm is performed. We consider a three-layers neural network consisting of 64x64 input layer neurons, 64 hidden layer neurons, and 5 output neurons, to recognize 26 alphabet characters of 64x64 pixels. At first we calculate Fourier transforms of input images. Because of point symmetry of Fourier transform images, the half of transformed images are used. Figure 2 shows the change of the squared sum error of 26 characters vs iteration times of learning iteration in the cases when inputs for the neural network are;

(1) original character images without Fourier transforming,
(2) Fourier transformed images
(3) half of Fourier transformed images.

We have estimated the recognition ability for non-shift and for shifted input images using the value of the weights and offsets when the learning is completed. Figure 3 shows the error rates of recognition for each input pattern with and without random shift within 4 pixels. The results indicate reduction of the error rates due to shift invariance of the Fourier transform. The feature extraction preprocessing has two advantages; reduction of the number of neuron units and shift-invariance for input patterns.

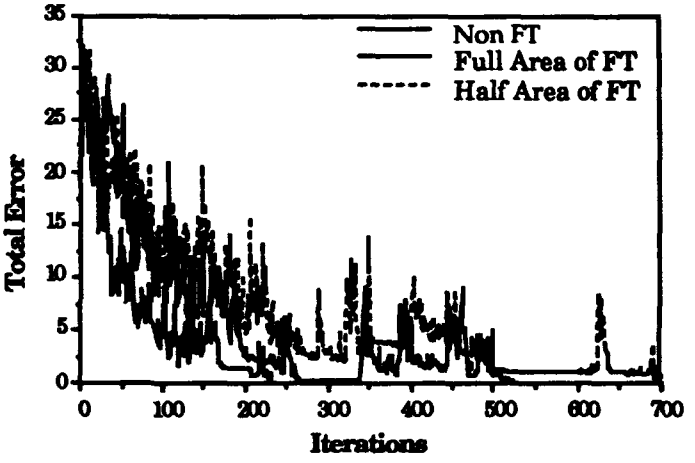


Fig. 2 Change of the squared-sum error

The authors thank S.Ishihara, H.Yajima and T.Hidaka of Electrotechnical Laboratory for their useful discussions and encouragements

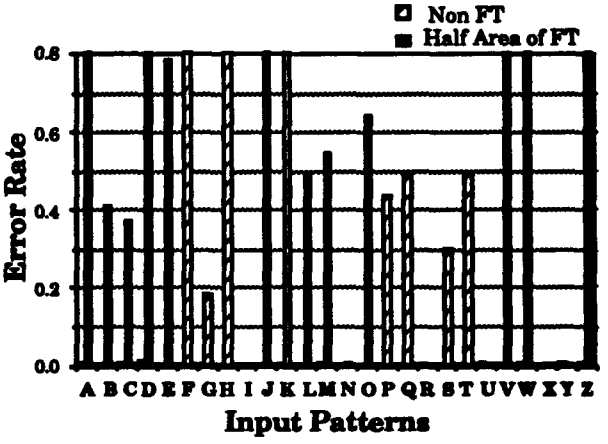


Fig.3 Error rates for the shifted each input

References

[1]N. Farhat, D. Psaltis, A. Prata and E. Peak, Appl. Opt., 24 (1985) 1469.
[2]N. Kasama, Y. Hayasaki, T. Yatagai, M. Mori and S . Ishihara, Jpn. J. Appl. Phys., 29 (1990)1565.
[3]I. Tohyama, Y. Hayasaki, T. Yatagai, M.Mori, and S. Ishihara, Proc. SPIE 1806 (1992) 271-278.
[4]K. Sasaki, D. Casasent and S. Natarajan, Proc. SPIE, 1384 (1990) 228-233
[5]T. Yatagai, Opt. Lett., 11 (1987) 270-272

Optical Digit Recognition based on Kohonen Maps

Michel BARGE, Raymond CHEVALLIER, Eugene CURATU# and Alain MARUANI

Télécom-Paris département Images 46 rue Barrault 75634 Paris cedex 13 France,
tel : +33-1-45-81-73-20
#Polytechnical Institute of Bucharest Applied Optics Laboratory Spl. Independentei No.313
R-77206 Bucharest Romania

Abstract

We present an optical implementation of the recognition stage of a Kohonen-like neural network based on a supervised learning algorithm. The set-up includes diffractive optical elements to both store and address the weights.

1. Introduction

Our work involves the study of optical implementation of neural networks. We describe the optical implementation of the recognition stage of a neural network based on Kohonen's feature maps. Indeed, this stage can be understood as a multichannel correlation and thus is well suited to an optical implementation.

2. Learning algorithm

We use a supervised learning algorithm, based on Kohonen self-organizing feature maps, for pattern recognition. While in the classical Kohonen algorithm the map is self organized by the inputs according to their probability density function, pattern recognition applications need some supervision to map together similar stimuli in terms of their context and not in terms of a known vector distance metric. We adopt here an idea previously used for semantic map organization [1] adapted to pattern recognition [2]. The basic motivation is to organize the map by the patterns and their association targets simultaneously. A by-product of this process is that the class labelling of neurons on the map emerges during the learning phase, while in the classical Kohonen maps the labelling is achieved after the learnig stage.

3. Numerical studies

The algorithm and its application for handwritten digit recognition have been numerically implemented. More precisely, two points relevant to an optical implementation were studied. For classical Kohonen feature maps, the selection of a neuron is made by minimizing a distance between the input and the weights. For an optical version, it is easier to maximize an inner product, which is strictly equivalent to minimizing a distance under the condition that the weights and the inputs used for the learning stage are normalized. Another point of matter is to study the influence on the results during the recognition stage when using a binary hologram instead of an actual weights map.

4. Experimental work

For our set up, the size of the inputs is 16x16 pixels and the Kohonen map has 8x8 neurons so that 256x64 weights must be coded using a hologram of 1024x1024 binary pixels. This set up is a slightly improved version of a previously-used one for the implementation of an associative memory [3,4]. It is specifically designed to achieve a multiplexing of connection holograms involving a special coding scheme for the weights matrix, that we called Frequency Multiplexed Raster (F.M.R.). It leads to standard spatial filtering set up except that the inputs must be sampled in a special manner and the holographic filter contains the F.M.R. coded synaptic array. An holographic element (microlens array or Dammann gratings for instance) enables the achievement of the sampling scheme of the inputs.

This component and the connection hologram consist of a silicon substrate processed by traditionnal means : contact-lithography using e-beam designed masks and reactive ionic etching (R.I.E.).

The output image diffracted by the connection hologram is detected using a CCD camera. This image shows the activation of the neurons. For the classical Kohonen algorithm, a special kind of non-linearity called "winner-takes-all" is used, which means that only the most active neuron is retained. In our case, the difference between neurons activation is first emphasized by quadratic detection. The decision is then made by a micro-computer and suitable software.

5. Conclusion

As a conclusion, we present results for the three steps of an optical implementation : software implementation for the learning algorithm, numerical simulation of the optical implementation and preliminary experimental optical implementation. We are still working on the experimental part of this work in order to improve, in terms of dynamic range, the quality of the storage of data for the connection hologram.

References

[1] S. Midenet and A. Grumbach " Supervised learning based on Kohonen's self-organizing feature maps" Proceedings of INNC Paris, pp773-776 (july 1990).

[2] Y. Idan and R. Chevallier " Handwritten Digits Recognition by a Supervised Kohonen-Like Learning Algorithm" Proceedings of IJCNN'91 (Singapore), pp 2576-2581.

[3] R.Chevallier "Associative memory for image classification : new interleaved coding of 4-dimensional information in a plane" International Journal of Optical Computing, Vol.1, 71-87 (1990).

[4] K.Heggarty and R.Chevallier "Optical implementation of an improved Hopfield-like retrieval algorithm" Optics Communications Vol.88 91-95 (1992)

TWO-LAYERED BIDIRECTIONAL OPTICAL NEURAL NETWORK BASED ON THE HOLOGRAPHY CORRELATOR: VARIATION OF THE ATTRACTOR POSITION TO ACHIVE NEW SOLUTION TYPES

A.V.Pavlov

Laboratory of Optical Pattern Recognition & Neural Networks,
Research Centre "S.I. Vavilov State Optical Institute",
12, Birgevaya line, St. Peterburg, 199034, Russia
Fax: (812) 350-44-78

ABSTRACT

Optical Neural Network formed by placing the holography correlator into the linear resonator is discussed. Variation of the attractor position by means of inhibitory optical interconnections to achive new solution types is proposed. The experimental results are presented.

Optical Neural Network (ONN) under consideration consists of two neuron layers - image I and correlation C, which are coincide to the image and correlation planes of Van der Lught correlator. In these layers there are the phase-conjugating mirrors, forming the linear resonator. Interconnection matrix which associating the pair of the learning vectors - reference image R in layer I and δ-function in layer C is realized as holography filter.

Usially, this architecture is considered as the bidirectional associative memory only [1,2]. The reason for this is that this NN has unique attractor in the space of the network states and this attractor corresponds to the pair of the learning vectors [1].

However, other solution types were demonstrated on this ONN - associative processing with common or different parts of the input and reference images restoration [3,4]. These experimental results contradict the conventional optical associative memory theory. In this paper the approach based on the anilysis of the interconnection massive and network state space is proposed to explain these results.

To achive these new solution types (except associative memory) the position of the attractor in the network state space must be changed. Associated pair R $\leftrightarrow$ δ must be replaced by the pair, including the common part of the reference and object images R' in the layer I. To do this, the neurons in layer I (I-neurons), corresponding to the vector (R-R'), are inactivated by the inhibitory interconnections involving.These inhibitory interconnections were absent in the original matrix, activating interconnections only were presented. And the interconnection matrix must not be changed phisically (i.e. the hologramm must not be rewrited) because R' is not

known *a'priori*. Therefore, the matrix changing is adaptive to the input vector, but no new learning occurs.

The second vector (in layer C) of the new pair, which is associating by holography filter, is (R⊕R') and the inhibitory interconnections from C-neurons corresponding to the (R⊕R') sidelobe are used. But the interconnections using themselves is impossible due to realization them by hologramm and this hologramm must not be rewriting. That is why the problem is solved in layer C. C-neurons activated by R' only must be used to suppress (R-R'), but it is impossible because part of C-neurons are activated by both R' and B, where B is the part of input vector, that $B \cap R = \emptyset$. The impossibility of the separation of the interconnections C→R' from C→B results in activating of the I-neurons corresponding to B , but this result is neither B nor R', but the noise is. This noise depends on the alignment and allocation of R' and B in I. The number of activated C-neurons is optimused to decrease this noise in the output vector by proposed for this aim power criterion.

Unlike the activating interconnections δ→R, the inhibitory interconnections are not invariant to the angular displacement of the restorating beam in C-layer. This determines conditions on the ONN devices accuracy. The number of inhibitory interconnections depends on the number of the C-neurons activated by (R'⊕R) sidelobe and it determines conditions on the information capability of the processing images .

The experimental results of the restoration of the identical part of images for various numbers of activated C-neurons are presented.

Therefore, the potential for ONN under discussion is wider then only associative memory. The algorithms of the restoration of the identical and nonidentical parts of the images are possible. These algorithms are realised by involving the inhibitory interconnections to change the attractor position.

REFERENCES

1. B.Kosko, "Adaptive Bidirectional Associative Memories", Apple.Opt., 1987, v.26, #23, p.4947-4960.
2. Y.Owechko, "Nonlinear Holographic Associative Memories", IEEE Journal of Quant. Electr., 1989, v.25, #3, p.619-634.
3. A.V.Pavlov, E.I.Shubnikov, "Revealing of Different and Common Features in Images on Holographic Correlator", Opt.& Spectr., 1987, v.63, #3, p.589-593.
4. A.V.Pavlov, "Possible Image Processing Algorithms in Optical Neural Networks Based on the Van der Lught Correlator", Opt. Mem. & Neural Networks, 1992, v.1, #2, p.153-156.

OPTOELECTRONIC SORTING NEUROCHIP

V.R.Grigor'ev and S.P.Naumov

Scientific Research Institute "Quant", 15, 4-th Likhachevsky Lane, 125438, Moscow, Russia.

Abstract. A new sorting algorithm on the adaptive neural network is offered. It is proved that algorithm can be implemented in one step irrespectively of the sorted succession. The features of 3D optical neuralchip construction, realizing adaptive sorting algorithm, are discussed. A neural hardware realization complexity estimations are given.

Summary. Parallel sorting algorithm elaboration is a classical task which practical importance is the creation of parallel programs and devices capable of providing effective sorting of big data massives on modern and respective multiprocessing computing systems. In this connection this operation on the algorithms and hardware level is very actual.

In this paper a new sorting algorithm on the adaptive neural network is offered. The time and value complexity is evaluated $O(1)$ and $O(n^2)$ accordingly. It is proved that the algorithm can be implemented in one step irrespectively of the sorted succession. As far as the time complexity is concerned the aquired results proved the best in comparison with the previously known results of the same volume complexity.

The pecularities of the three dimensional optoelectronic neuralchip having the hardware implementation of the given neural network algirithms have been studied. The practical realization is oriented to the three dimensional integral optic neuralchip advanced manufacturing technology, which was worked out at the Automatic and Electrometry Institute [The Sibirian Branch of the Russian Academy of Sience] [1]. The research which has already been made, demonstrates the way of creating of multilayer multichannel integral structures with the optical communication channels in the third dimension according to the compatible with the VLSI technology inserted.

It is shown that realization of the parallel sorting algorithm is possible on the single chip of the given type depending on the size of the photodetector array (256×256 or 512×512) 256 or 512 numbers accordingly. The sorting neurochip throughtput will be here about 10^8 - 10^9 op/sec.

Thus, the creation of neuralchip on the three dimensional integral optical chip basis will make it possible to reduce grately the time spent on sorting in various applied computer and information systems. The comparative evaluation of the neural chip parameters with the submitted algorithm transputer realization characteristics is applied.

References

[1] Egorov V.M., Kostsov E.G. Integral optical digital computers// Appl. Opt.-1990.-29, N8.-P.1178.

Photorefractive Implementation of Neural "Self-Correcting" Learning Algorithms

Tigran Galstyan, Gilles Pauliat, André Villing, Gérald Roosen
Institut d'Optique Théorique et Appliquée, Unité de Recherche Associée 14 au Centre National de la Recherche Scientifique (CNRS), Centre Scientifique d'Orsay
Bât. 503, B.P. 147, 91403 Orsay Cedex, France
Tel.: 33/1 69416855; Fax: 33/1 69413192

Abstract

Some "self correcting" learning laws are compared with photorefractive dynamics. Possible optical implementations of neural basic units with photorefractive crystals are proposed and the key characteristics, required for self organizing network realization, are experimentally demonstrated.

Summary

Modification laws of neural interconnects govern their processing capabilities. The learning process is called "supervised" when, for each input signal, a classification code is known a priori and the learning process is an iterative updating of weight vector components to approximate this code. So, at each updating step, we deal with an error correction controlled by an external "teacher" (the a priori known code). Some learning algorithms, however, allow to get feature extraction in a stochastic set of input signals and selectively self-adapt to provide neuron maximal activation for signals exhibiting the same features. The learning is conducted by comparing the input signal with the weight vector in which are stored the common features extracted by the algorithm during the learning of previously processed signals. This mismatch is considered as an effective error. The learning process of the current input then results in a correction of this error by updating the weight vector components proportionally to that mismatch. So, the algorithm itself finds the classification code (i.e. the weight vector coefficients) from the real time inputs.

Digital simulations are mostly used to get such kind of algorithms and only the simplest versions of algorithms are implemented (by means of discrete time formalism) because of the complexity of the others.

However, the fundamental dynamics of hologram creation in some nonlinear optical materials appears to be perfectly fitted to implement these algorithms. In this work we show, theoretically and experimentally, that different learning algorithms can be implemented by taking advantage of the kinetics of photorefractive holograms. In the first part of the work some of the most

important neural learning algorithms, widely used in Self-Organizing Neural Networks, will be described and demonstrated by digital simulations. The theoretical model analysis will be presented in the second part. An holographic analogy for a neural basic unit will be described. In this scheme, the neural interconnects are represented by the elementary holographic gratings. The weights of interconnects are the diffraction efficiencies of these gratings and the input signal components are angularly multiplexed beams. So the result of holographic readout (diffracted light amplitude) represents the neural output.

The dynamics of photorefractive hologram creation will then be presented and the analogy with the above mentioned learning laws will be outlined. Some possible ways of optoelectronic implementation of error self-correcting learning laws, based on the photorefractive dynamics, will be discussed. The third part of the work describes the experimental realization of a single neural basic unit based on these learning laws and the comparisons with digital simulations. The discrete time formalism is used in our experiments similarly to computer simulations.The mismatch of each input signal with recorded earlier information is detected as readout amplitude value and the neural weights are then updated with an holographic exposure, corresponding to the measured error. An electronic circuit through a personal computer is used to generate stochastic input signals, to perform the desired neuron transfer function and the feedback. The interconnect updating is fully based on the photorefractive dynamics. Key capabilities, such as competitive learning, selective adaptation and feature extraction in a stationary stochastic set of input signals are demonstrated. These characteristics are in good agreement with the theoretical models.

A proposal for a massive architecture of an Optoelectronic Self-Organizing "Kohonen Map" Network, based on these neural basic units, and corresponding estimations of its processing capabilities will be presented.

Neural Networks with Unipolar Weights and Normalized Thresholds

Jan Stanisław Bródka and Bohdan Macukow

Institute of Mathematics Warsaw University of Technology
Pl.Politechniki 1, 00-661 Warsaw Poland
phone/fax (+48 2) 621 93 12

Abstract

The method of the replacement of the neural network by the other, equivalent network with nonnegative or uniform weights is described. This simplification yields much easier implementation of a network.

Summary

This paper is concerned on problem of simulation of one neural network by the other one. Simulating network may have *different structure* (*i.e. different number of neurons* and different connection weights) from the initial one, but it proceeds *in the same way* as a initial network.

Neural network is formally defined as the triple (V,E,P), where V is the set of network nodes (neurons); E: $V \times V \rightarrow R$ is connection weight function (i.e. $E(x,y)$ is connection weight from neuron x to neuron y); and P: $V \rightarrow R$ is threshold function (i.e. $P(x)$ is a threshold of node x).

Simulation is defined by indication of correspondence of nodes in both networks and correspondence of instant in both networks proceedings. This means, that functions g i h are defined. Function g establishes correspondence of nodes and function h establishes correspondence of instants. More intuitively, we can say: the network S is simulated by network S' if the condition *neuron x is active in network* S *in the instant k if, and only if, neuron g(x) is active in network* S' *in the instant h(k)* is satisfied for all neurons x and any instant k.

Definition of network, simulation and related notions are precisely formulated in the full version of this paper. They can also be generalized to continuous neuron model.

Two theorems are proved. The first one shows, that each neural network can be simulated (replaced) by a neural network with non-negative connection weights only. Proof of this theorem gives algorithm to construct simulating network. Idea is based on the replacement of each node of original network by a pair of two nodes in the constructed network. Connection weights and the node thresholds are also appropriately defined. Constructed network has only two times more nodes and non-zero connection weights that the original network.

The second theorem shows, that each neural network can be replaced by a neural network with the connection weights equal to zeros and ones. Proof of this theorem also gives algorithm for the construction of simulating networks. Detailed proof of both theorem will be described in the full version of this paper.

Experimental investigation of the performance of the two-layer neural network based on optical vector-matrix multiplier.

Nikolay N. Evtihiev, Rostislav S. Starikov, Boris N. Onyky,
Vadim V. Perepelitsa, Igor B. Scherbakov

Dept. 37, Moscow Engineering Physics Institute, Kashirskoe
shosse 31, Moscow 115409 RUSSIA. Phone 324-97-55.

ABSTRACT

The paper presents the obtained results of learning of the two-layer (64x8) neural network (TLNN), the results of tolerant noising of weight matrixes and results of hardware implementation. The unperfectness of optics satisfies the margin requirements of TLNN model.

SUMMARY

Different types of neural networks (NN) are under careful investigation now. Creating of the working models of NN, including optical models, is most useful and promising. One of the most interesting is the two-layer NN (TLNN), which can be easily made on the basis of proposed optical matrix-vector multiplier (OVMM). OMVM has extremely high information processing capabilities. Computing in such TLNN is performed sequentially in OVMM, high performance speed is available due to the implementation of the acoustooptic spatial light modulator (Bragg cell). Large time-bandwidth product acoustooptic devices are the fastest up-to-date spatial light modulators.

As a base devices for OVMM we propose to implement high-speed high dynamic range spatial light modulator namely the multichannel multifrequency acoustooptic Bragg cell (MAOM), laser array and CCD (charge-coupled device) array in well-known orientation of OVMM. Traditionally the DMAC (digital multiplication via analog convolution) algorithm is used for obtaining high accuracy in optical calculations. The algorithm we propose (fig.1) is similar to DMAC, and the only difference is concerned with ability to use frequency coding in MAOS. Due to this fact we can obtain the whole vector-matrix multiplication in one step with speed about frame rate of MAOS. In this case the vector is inputed into the laser array in bit-serial order - time-sequentially bit by bit of vector components in corresponded to this component laser. The matrix is entered into MAOS - each element in each window, but each element is represented in binary code. Bits of each element is frequency multiplexed. The CCD operates in shift-and-add mode. Shift velocity corresponds to bit loading velocity of lasers. At the end of lasers expositions the CCD will contain sequence of data (output vector components) in presentation, similar to DMAC. The supporting electronic (personal or specific computer) is responsible for converting the presentation of this data from mixed to hex format, the thresholding, the synchronization etc.

The TLNN simulation software program was designed. Simulated NN contains 64 neurons in the first layer and 8 neurons in the second. The network was trained with gradient and stochastic algorithms. The ability of trained network allows to recognize binary images of all 26 alphabet letters. Each image consists of 8x8 pixel.

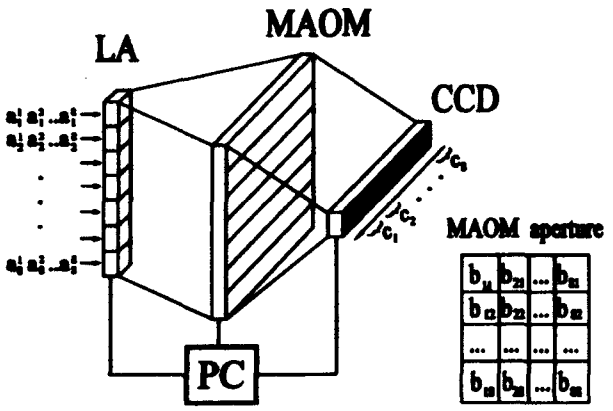


Fig.1. Optical vector-matrix multiplier.

The trained network has stable recognition of images with amount of inverted pixels up to 15-20%. Gradient learning was performed in 300 iterations. The velocity of stochastic method is less.

The tolerant noise simulations was carried out. The ratio of tolerant noising in weight matrix and input vector was defined. The recognition ability of TLNN decreases on 1% for 10% noise ratio in the TLNN parameters. This fact allows to cover the unperfectness of the OVMM and became the implementation possible.

The paper presents mathematical description of TLNN, learning methods overview, optical architecture and software and hardware simulation results.

Features of application of holographic memories in PC networks and optical neuralcomputers

V.N.Shahgedanov

Moscow Scientific and Research
Institute of Instrument Engineering

34 Kutuzov Avenue, Moscow 121253, Russia
phone: (095) 249 34 52, fax: (095) 148 79 96

ABSTRACT

The characteristics of experimental prototypes of disc holographic memories 1,5 Gbytes with data reading rate 16 Mbit/sec are given.

The features of interfacing these devices and personal computers based on data holographic recording are discussed as well as the question on application of the data recorded in holographic disc as a command matrix for neuralcomputer.

SUMMARY

The efficiency of optical memory systems is determined higher than the efficiency of the traditional methods using, it is conditioned by recording density and information capacity, by high speed recording and reading as well as by parallel calls. Holographic memories on one -dimensional holograms realize the following :

-possibility to increase by order or more the density of

data recording due to capacity increase;

-relative simplicity for realization of multichannel systems and, therefore, the possibility to realize high speed recording and reading the information from parallel channells;

-increased reliability of recording based on holographic method where every information bit "is spread" over the entire area of hologram and, so the level of reading signal weakly depends on small defects of the carrier.

In our days the prototypes of devices 1,5 Gbytes with information selection rate 16 Mbit/sec are constructed. These paramcters are achieved by using the unique lines of avalanhce photodiodes with high sensitivity and speed as a photodetector. Howerer, these photodetectors require a specific order of information organization caused by absence of constant component in signal. Therefore, the application of holographic systems as a fixsed memory for PC and PC networcs requires the construction of special coders and decoders. The function specific of coders is the interpretation of income information into balanced code limiting in data flow the continuous sequence of nulls and units (not more 3 units or nulls in order).

The similar problem appears when developing the architecture of optoelectronic neuralcomputer based on disc holographic memory as a matrix of synaptic links recorded in disc can contain any information. The developed method of information organisation and constructed coders and decoders allow to realize the neural modulus for processing the synaptic matrix as the information entering and to develop microsoftware for performing adjustment both the neural modulus and demonstration task.

High-voltage CMOS array for liquid crystal on silicon spatial light modulators

C. C. Mao and K. M. Johnson
The Center for Optoelctronic Computing Systems
University of Colorado at Boulder
Boulder, CO 80309-0425, USA
Phone: 303-492-1835, Fax: 303-492-3674

The design and test results for a 64 x 64 high-voltage CMOS array which can provide voltages as high as 30 V to switch liquid crystals are described.

I. Introduction

Very-large-scale-integration/ferroelectric-liquid crystal (VLSI/FLC) spatial light modulators (SLMs) have a great variety of applications, including image display, optical processing, and optical optical pattern recognition. With the standard CMOS process, typical transistor voltages available to modulate the liquid crystals are approximately 5 V. These voltages result in slow FLC response times, ranging between 50 us to 200 us.[1-3] It is also difficult to switch the analog electroclinic LCs with such low voltages. To reduce the FLC switching times and activate the analog switching chiral smectic electroclinic LCs, volatges higher than typical CMOS voltages are required at each pixel. In this paper, we describe a novel CMOS 64 x 64 array which can provide voltages as high as 30 V to switch liquid crystals.

II. High-voltage CMOS array design

The maximum voltage a transistor can operate is limited by the junction breakdown voltage. Transistor junction breakdown voltages are inversely proportional to the impurity concentrations of their deffusion regions. This implies that using a lower doping concentration for the transistor drains should extend their voltage handling capacity. This approach is applied to the structure shown in Fig. 1. The n-fet uses the n-well as its drain, which has lower doping than n-diffusion, and the p-fet uses p-base as its drain, which has lower doping than p-diffusion. The n-well has a breakdown voltage of approximately 70 V and the p-base implants breaks down to the n-well at a voltage arround 35 V. These voltages are well above the voltages required to switch 2 um of the chiral smectic liquid crystals. However, the poly silicon gates significantly decrease the breakdown voltages. Our measurement results show that the highest voltages the n-fet can accomodate is 30 V, while the p-fet voltage is limited only to 15 V. To make the circuit provide a voltage higher than 15 V to switch liquid crystal, we may drop the voltage across several such transistors in series. A high-voltage addressing circuit including four high-voltage p-fets and two high-voltage n-fets is designed to provide 30 V to switch FLCs. The voltages applied drop across two p-fets, so each p-fet operates with 15 V.

We have designed and fabricated a 64 x 64 high-voltage VLSI backplane array to rapidly switch FLCs. The array, including bonding pads, is 4.4mm x 6.6 mm. Each pixel contains one high-voltage n-fet transistor and a metal modulating pad. The pixel is 48 um in x and y dimensions. The row and column addressing circuits consist of common CMOS transistors and high-voltage

addressing circuits as described in the above paragraph. The high-voltage addressing circuits convert TTL-level voltages to high voltages.

III. Experimental results

A liquid crystal on silicon (LCOS) high-voltage electrically addressed spatial light modulator (EASLM) was assembled and tested. The liquid crystal used is the British Drug House smectic C^* ferroelectric liquid crystal SCE-13. In the operation, metal modulating pads in the pixels are provided with 25 V or 0 V and the common electrode on the cover glass is applied with 12.5 V. When a uniform light beam is incident upon the device, the reflected light from VLSI/FLC interface is polarization modulated. Using an analyzer in output optical path will display an intensity image. Fig. 2 shows an intensity modulated pattern displayed on the high-voltage EASLM. We also tested the response times and ON/OFF contrast ratio of the SLM with an applied voltage of 25 V. The 10% - 90% rise time is approximately 25 us and the 90% - 10% fall time is 30 us. The meaured ON/OFF contrast ratio for four rows is 10:1.

IV. Conclusions

We have designed, fabricated, and tested a 64 x 64 high-voltage VLSI/FLC spatial light modulator. The SLM has a 10% - 90% rise time of 25 us and a 90% - 10% fall time of 30 us. The measured ON/OFF contrast ratio is 10:1. We also designed a VLSI array using high-voltage transistor inverters instead of six-transistor addressing circuit to convert TTL signal to a voltage of 15 V. The results will be presented at the conference.

References

1. K. M. Johnson, I. Underwood, D. M. McKnight, IEEE J. Quant. Electron. **29** , 699 (1993).
2. D. J. McKnight, K. M. Johnson, and R. A. Serati, Opt. Lett. **18** , 2159 (1993).
3. C. C. Mao, K. M. Johnson, and Z. Y. Huang, OSA Annual Meeting Technical Digest, pp. 165, Oct. 3-8, 1993, Toronto, Canada.

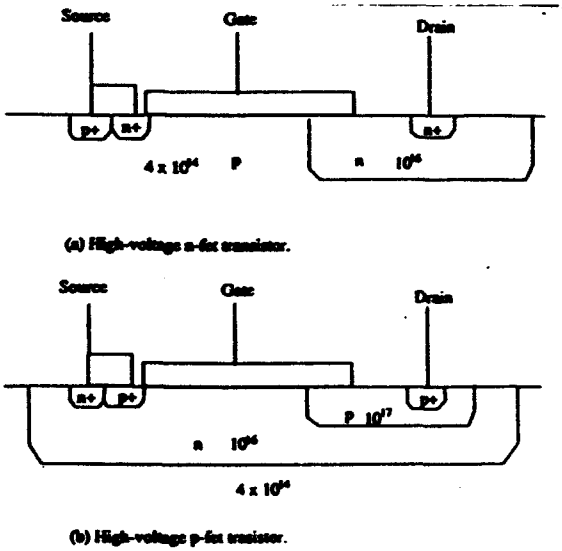


Figure 1. Structure of high-voltage transistors.

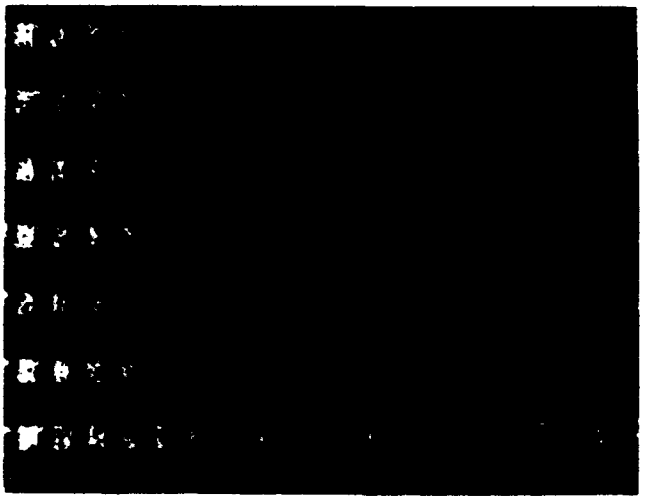


Figure 2. Intensity pattern displayed by the high-voltage VLSI/FLC device.

Saturation effects and wavelength optimization of quantum well modulators in Smart Pixels

G. D. Boyd[a], L. M. F. Chirovsky[b], A. L. Lentine[c], G. Livescu[b],
AT&T Bell Laboratories [a] 908 949 6492
Holmdel[a], NJ 07733, Murray Hill[b], NJ 07974, Naperville[c], IL 60566

ABSTRACT

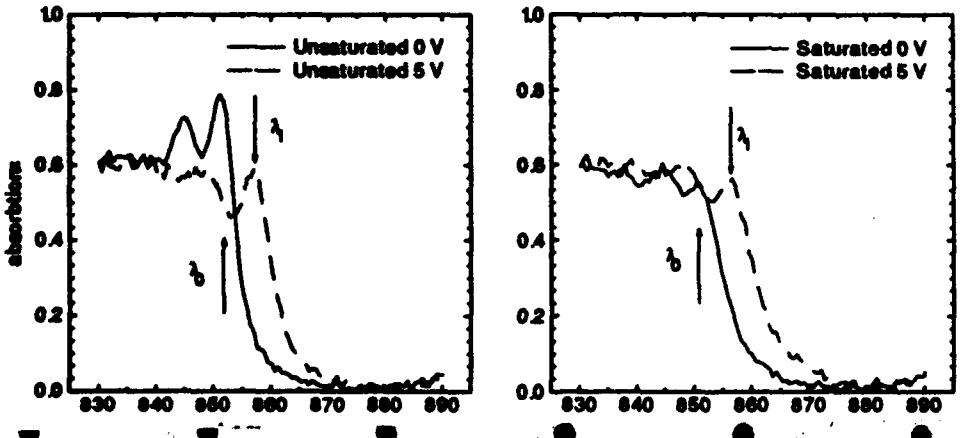
We describe the selection of the operating wavelength of field effect transistor self-electrooptic effect devices (FET-SEEDs) in order to minimize saturation effects, as well as to optimize the photonic switching circuit figure of merit.

It is desirable to operate optical processing systems using FET-SEEDs [1], at greater than 100 MHz clock rate. These smart pixels incorporate multiple quantum well (MQW) modulators and field effect transistors. Average optical powers on individual modulators, in excess of 100 μW may be required to achieve this data rate, leading to saturation of the absorption of the modulators. It has been recently recognized that reduced switching energies and faster switching may result from using short pulses, such as those generated by a mode locked (ML) laser, instead of quasi-continuous wave (CW) operation [2]. The use of short pulses may compound the saturation problems because all the energy is supplied before the carriers can escape from the wells. We define λ_0 as the heavy hole wavelength location with zero applied field and λ_1 as the shifted heavy hole wavelength with an applied field determined by the number of quantum wells and the applied modulator voltage V. In this paper we compare CW operation at λ_0 and λ_1 and then compare the saturation of CW (long pulse) Vs ML (short pulse) operation at λ_1 so as to minimize saturation effects. We then define a circuit figure of merit, to minimize the incident optical read energy required on a device to switch another down stream device. This optimizes the selection of operating wavelength λ_1 and the number of quantum wells in a modulator design.

The absorption coefficient (arbitrary units) of an AlGaAs MQW modulator versus wavelength as measured with a CW tuneable laser at low (unsaturated) power levels is shown in Fig. 1 and when saturated in Fig. 2 at two different voltages levels [3]. This demonstrates that a modulator operating at λ_0 is degraded by saturation much more than operating at λ_1 and is to be preferred since bistability is not required with FET-SEEDs. A figure of merit for the modulator and detector can be defined by

$$Fm = \delta R\,(1 - R_{off}) \qquad (1)$$

where δR is the difference between the on (high) and off (low) reflectivity states at λ_1. In Fig. 3 we plot the measured Fm versus the energy in the ML pulse which is the product of average power with a 13 μs repetition period (76 MHz). The exciton, λ_0, was shifted to 843 nm in this sample. The CW Reflection curve is the saturation results at a power level such that the energy in a 13 μs period is the same as the ML experiment. The curves in Fig. 3 show the difference in saturation behavior between the situation in which the energy is supplied in a period much greater than typical carrier sweep out times of 100 ps (quasi CW case), and when the energy is supplied as a ML (approximately 2 ps) pulse much shorter than sweep out times. If we speculate on a smart pixel optical processing system operating at a 1.6 ns repetition period with the energy inputted in a 25% duty cycle of 400 ps, then the CW saturation conditions should be expected to prevail. The "0.4 ns CW" curve shown is a shifting of the CW Reflection curve such that the same amount of energy is integrated in 400 ps to be compared with the ML measurement. For receiver switching energies greater than 0.1 pJ, the



modulator read power should be greater than 0.5 pJ due to array to array coupling losses, and Fig. 3 indicates that there will be some saturation penalty for our focused beam of 3.5 μm diameter.



Fig. 3

Having decided on λ_1 operation, it is useful to determine the optimum shift $\delta\lambda_1 = \lambda_1 - \lambda_0$ and the optimum number of quantum wells N each of width L_s (μm). A better figure of merit which includes the capacitance of the MQW detector which effects the switching energy is

$$FM(\lambda_1) = Fm\ NL_s = \delta R\ (1 - R_{off})\ NL_s \qquad (2)$$

For a given operating voltage V one can calculate, using our previous modeling efforts [4], δR and R_{off}. The number of quantum wells N is adjusted at each λ_1, as shown in Fig. 4.

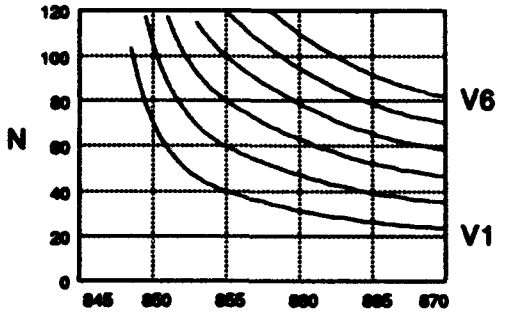


Fig. 4

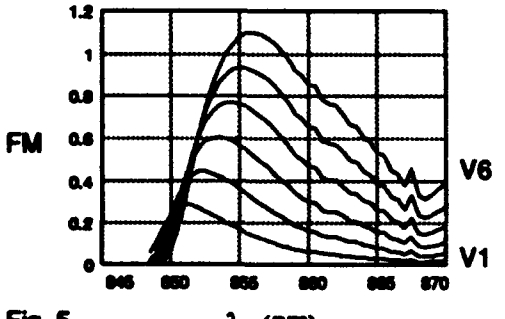


Fig. 5

$FM(\lambda_1)$ is shown in Fig. 5, at various fields and the corresponding V (voltages V1 = 2.5 through V6 = 15 volts in steps of 2.5 volts). From these calculations we conclude that for 10 volt operation across the modulators that $\delta\lambda_1 = 7$ nm and N = 95 maximizes the figure of merit FM. Fig. 6 shows calculations for N = 95 quantum wells of Fm (solid curve) with two independent experimental measurements shown as the broken curves.

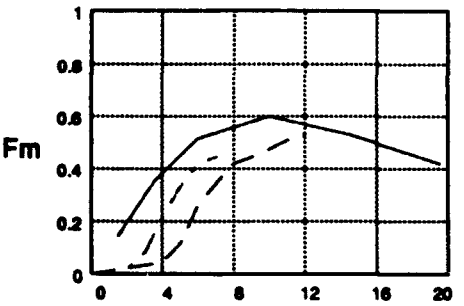


Fig. 6

References:

1. L. A. D'Asaro, L. M. F. Chirovsky, E. J. Laskowski, S. S. Pei, T. K. Woodward, A. L. Lentine, R. E. Leibenguth, M. W. Focht, J. M. Freund, G. G. Guth, L. E. Smith, "Batch fabrication and operation of GaAs-Al_xGa_{1-x}As field-effect transistor-self-electrooptic effect device (FET-SEED) smart pixel arrays". IEEE J. Quantum Electronics, 29, 670-677 (1991).
2. A. L. Lentine, L. M. F. Chirovsky, T. K. Woodward, "Optical energy considerations for diode-clamped smart pixel optical receivers". IEEE J. Quantum Electronics, to be published.
3. G. D. Boyd, J. A. Cavailles, L. M. F. Chirovsky, D. A. B. Miller, "Wavelength dependence of saturation and thermal effects in multiple quantum well modulators", Appl. Phys. Letts. 63, 1715-1717 (1993).
4. G. D. Boyd, G. Livescu, "Electro-absorption and refraction in Fabry-Perot quantum well modulators: A general Discussion", Optical and Quantum Electronics 24, S147-S166 (1992).

DYNAMIC STUDIES OF GaAs/AlGaAs MULTIPLE QUANTUM WELL MODULATORS USING PHOTON-COUNTING TECHNIQUES

Gerald S. Buller, John S. Massa, Stuart J. Fancey and Andrew C. Walker
Department of Physics, Heriot-Watt University,
Riccarton, Edinburgh EH14 4AS,
United Kingdom
Tel. (0)31-451-3069

Abstract *Photon-counting measurements of carrier sweep-out in biased multiple quantum well p-i-n diodes are presented. These results are compared with switching characteristics of symmetric-SEEDs, which were measured using an adapted pump-probe technique.*

Summary A key component of several opto-electronic devices (eg modulators, SEEDs, detectors, etc.) is the reverse-biased p-i-n multiple quantum well (MQW) structure. A fundamental limitation on the speed of such devices is the carrier sweep-out time. We present measurements and analysis of the carrier dynamics in such biased modulators using picosecond time-resolved photoluminescence techniques. The measurements were performed with an adapted optical microscope, and using a passively Q-switched picosecond laser diode as the excitation source. A small-area silicon single-photon avalanche diode detector, with a rise-time of <20ps, was used in conjunction with the time-correlated single-photon counting technique. Key features of this approach include: (a) the high spatial resolution possible (>=0.5μm); (b) the detection sensitivity which allows analysis of carrier densities as low as ~ $10^{14}cm^{-3}$; and (c) good temporal resolution, permitting decay times as short as 10ps to be measured. Figure 1 shows PL decays from a GaAs/AlGaAs multiple quantum well modulator as a function of reverse bias electric field . Numerical modelling of these decays which take account of carrier drift, Coulomb screening, tunnelling and thermionic emission, will be presented. A discussion of the implications of such results on electro-absorption saturation will also be given.

A notable device which utilises two such MQW p-i-n diodes connected in series is the Symmetric-SEED (S-SEED). The switching speed of this is limited by a combination of RC electrical time constants and the above MQW carrier transport effects. By using an adapted pump-probe technique, the single-photon detection system was used to probe the reflection from one window of an S-SEED and hence measure its switch speed. Such a detection system meant that switching times as short as ~20ps could be resolved using this instrument. Figure 2 shows an example of the dynamic switching characteristics of an S-SEED at three different bias voltages. Discussions on the instrumental performance (eg temporal dynamic range, spatial resolution, etc.) will be presented, as well as the application of such techniques to other SEED derivatives, such as FET-SEEDs. The relevance of the above TRPL measurements to S-SEED dynamics will also be discussed.

Acknowledgements This work was funded by SERC, through the Scottish Collaborative Initiative on Optoelectronic Sciences, and the Royal Society Paul Instrument Fund. The authors acknowledge useful discussions and assistance from Dr. FAP Tooley and Dr. S Wakelin.

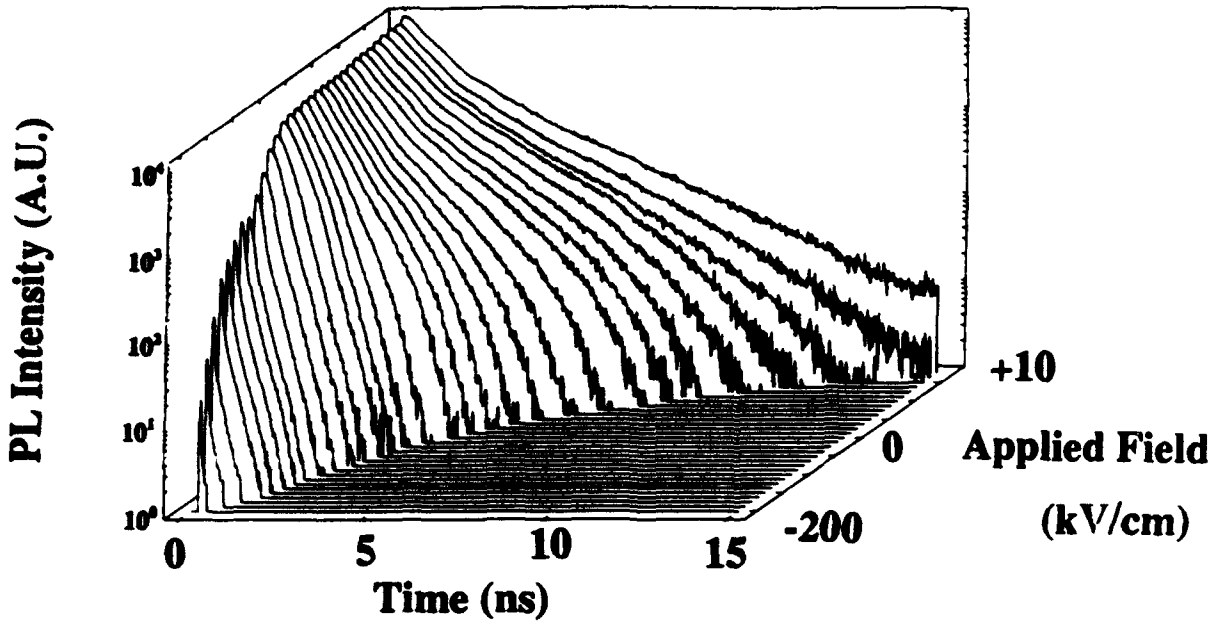


Fig. 1 Time-resolved photoluminescence decays of a GaAs/AlGaAs MQW modulator under different bias conditions.

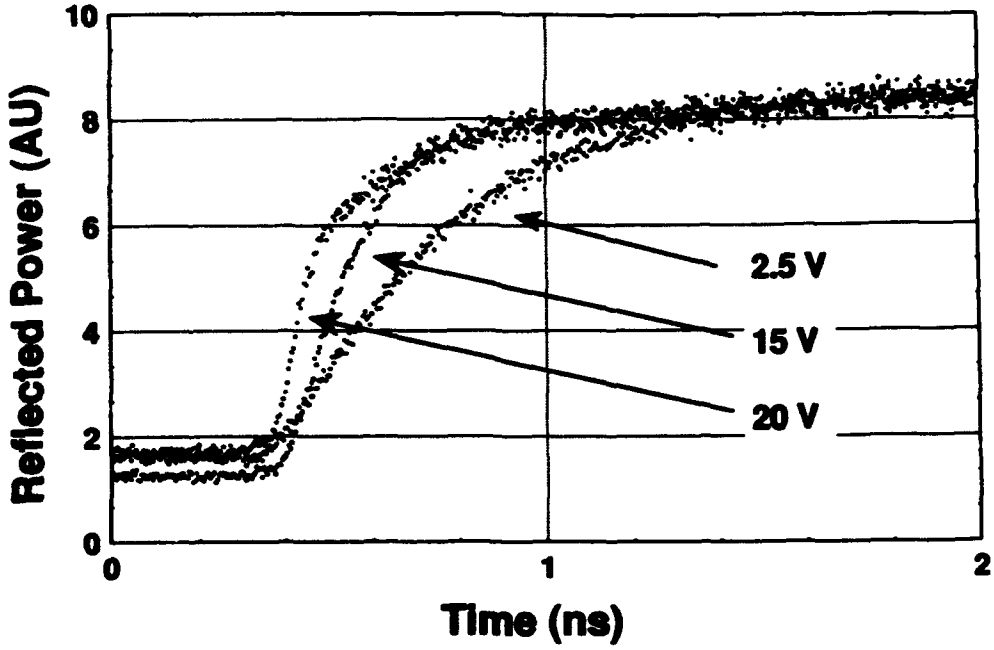


Fig. 2 Time-resolved switching characteristic of an S-SEED, at applied reverse bias of 2.5V, 15V and 20V.

The Monolithic Integration of Quantum-Well High Electron Mobility Field Effect Transistors, and Asymmetric Fabry-Pérot Optical Modulators

Garrett O'Sullivan[1], Tomás Aherne[1], Eithne Mc Cabe[1], John Hegarty[1], Paul Horan[2], Brian Corbett[3]

Abstract

We will discuss a novel high speed smart pixel structure which integrates a high electron mobility transistor with an asymmetric Fabry-Pérot optical modulator. Its use in an optoelectronic amplifer circuit will be also described.

Summary

Monolithic integration of electronic components with optical elements provides a means whereby practical optoelectronic data processing may become a reality. Following recent interest in smart pixels [1,2,3,4] we have developed a novel wafer structure (figure 1) which combines an AlGaAs p-i-n detector/modulator structure and a quantum-well high electron mobility transistor (QW-HEMT) structure.

The complete configuration is that of a modified asymmetric Fabry-Pérot modulator (AFPM) allowing high contrast reflection modulation and efficient photodetection. We grow the QW-HEMT layers inside the AFPM cavity on top of an undoped back mirror. This design avoids the presence of a p-n junction under the QW-HEMT which would otherwise result in backgating [1]. Backgating reduces the output optical contrast ratio and gives rise to a gradual switching action. It arises when a continuous p-layer under more than one n-channel device is held at a fixed voltage. A more complex solution involves the insulation of selected areas of this layer with proton bombardment and contact formation with Be implantation [3].

The QW-HEMT contacts the quantum well region directly. A deep etch uncovers the QW-HEMT surface for processing. This leaves the p-i-n detectors and modulators as mesas. The structure is flexible in that it permits etching of the front surface in order to adjust the optical resonance. Alternatively it would be possible to grow an additional front mirror to increase the contrast ratio of the output modulation. This approach also facilitates the optimisation of the high speed performance of the AFPM [5]. This, married with the high bandwidth offered by the QW-HEMT, holds great potential for high speed smart pixels.

The fully integrated circuit in figure 2 demonstrates the basic utility of this structure. Both the detector and the modulator are formed from the same wafer layers. The QW-HEMT structure is designed to be normally-on (depletion mode). The circuit accepts an optical input beam via a p-i-n diode. In the configuration shown the diode acts as a capacitor being charged by the photocurrent. The upper QW-HEMT is connected as an active load. The charge developed in the diode modulates the gate voltage of the lower QW-HEMT. This allows the gate voltage change to induce a larger output voltage shift which is applied to the underside of the output AFPM thereby controlling its reflectance. The circuit may thus function as an optical amplifier since a low power input may control the modulation of a higher power optical output.

---

[1] *Dept. of Physics, Trinity College, Dublin 2, Ireland, +353-1-7022221*

[2] *Hitachi Dublin Lab., O'Reilly Institute, Trinity College, Dublin 2, Ireland, +353-1-6798911*

[3] *NMRC, LEE Maltings, Prospect Row, Cork, Ireland, +353-21-276871 extn. 4820*

References

1. T.K. Woodward et al.," Operation of a fully Integrated GaAs-AlGaAs FET-SEED: A basic optically addressed integrated circuit", IEEE Photon. Tech. Letts., 4 (6), June 1992.
2. T.K. Woodward et al.," GaAs/AlGaAs FET-SEED smart pixels with several transistors", IEEE LEOS Summer Topical Meeting on Smart Pixels, Santa Barbara, CA (IEEE, New York, NY, 1992), paper no.TUC3, pp. 61-62, August 1992.
3. L.A. D'Asaro et al.,"Batch Fabrication and testing of FET-SEED smart pixels arrays", as [2], paper no. TUC4, pp. 63-64.
4. B.F. Aull et al.,"Monolithic optoelectronic transistor: A new smart-pixel device", Appl. Phys. Lett. 63 (11), September 1993.
5. C.C. Barron et al.,"High-Speed Design of Asymmetric Fabry-Perot Modulators", as [2], paper no. WB2, pp. 89-90.

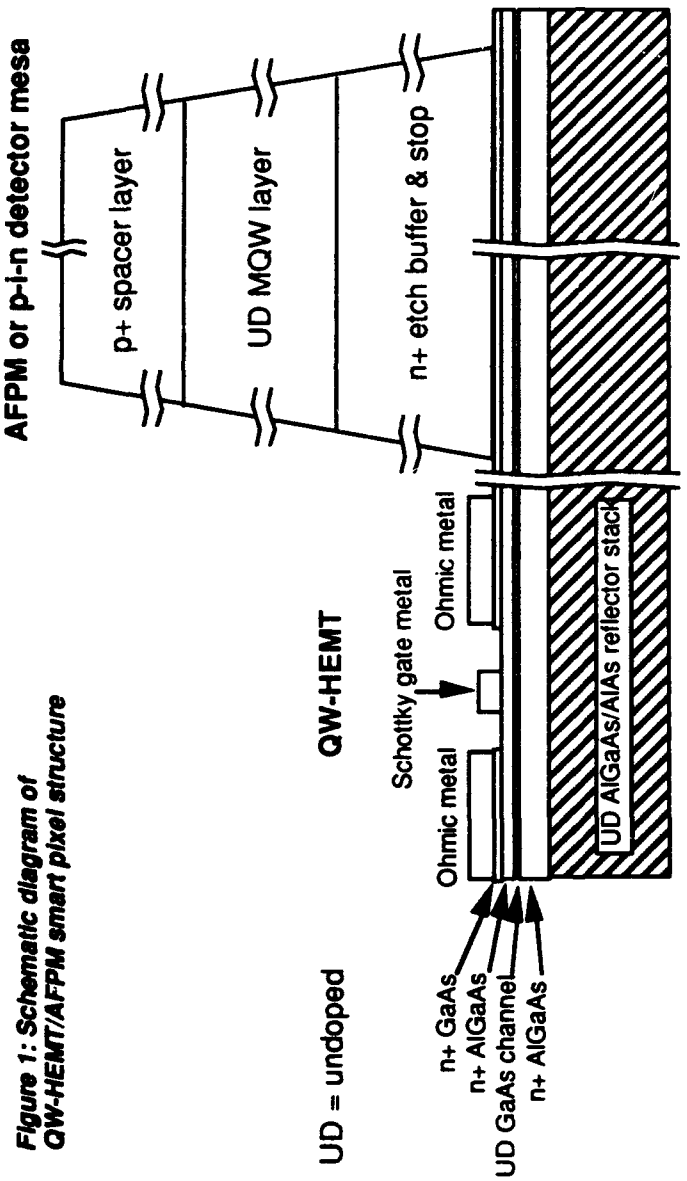


Figure 1: Schematic diagram of QW-HEMT/AFPM smart pixel structure

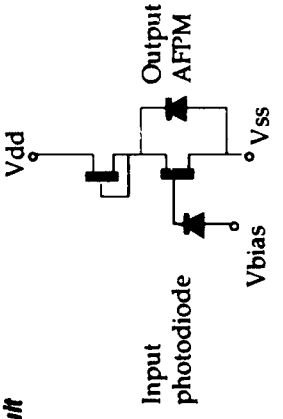


Figure 2: Optical amplifier circuit

Contactless Quantum Confined Stark Modulator Based on GaAs/AlAs Quantum Filters

N.T.Pelekanos[a], B. Deveaud-Plédran[b], P. Gravey, F. Clérot, J. M. Gérard[*]

France Télécom, CNET-Lannion, BP 40, 22301 Lannion, France
[*] France Télécom, CNET-Bagneux, BP 107, 92225 Bagneux, France

Telephone: 49-711-6891320

Abstract

We demonstrate a novel all-optical Quantum Confined Stark modulator. The necessary electric field is switched-on optically, by exploiting strongly asymmetric carrier transfer in GaAs/AlAs layers. In an unoptimized sample, we measured 9 meV exciton redshift at 850nm with optical excitation of only a few W/cm^2 of He-Ne laser at 633 nm.

Summary

In this report, we present preliminary results on a light modulator based on the Quantum Confined Stark Effect (QCSE) [1] but for the first time operating all-optically. The principle of operation of the device is as follows: every period of the heterostructure contains three quantum wells (QWs) designed in such a way that following above bandgap photoexcitation a large fraction of the photogenerated electrons and holes tend to separate and accumulate in the exterior QWs, creating a local space-charge field having its maximum in the region in between and acting via the QCSE on the exciton resonance of the central QW.

In **Figure 1**, we show a schematic band diagram of one period of the heterostructure. The three QWs are enumerated from left to right. QW1 is $\approx$ 25Å of GaAs, surrounded by a graded AlGaAs (x=36 – 42%, 800Å) and an AlAs barrier (100Å). The combination of a narrow GaAs QW adjacent to an AlAs layer is the key aspect of the device. Following photoexcitation resonant with the AlGaAs barriers or QW1 ($\lambda_{write} \approx 620nm$ or $700nm$, respectively), this layer combination functions as a one-way "quantum filter" for the photocarriers of QW1, by blocking the holes out but allowing the electrons transfer rapidly into QW2. This is due to the fact that, for sufficiently thin GaAs layer thicknesses, the electron energy level at the Γ-point in the GaAs QW is higher than the one at the X-point in the AlAs layer. $\Gamma-X$ electron transfer times in the subpicosecond regime have been measured in thin GaAs/AlAs superlattices [2]. QW2 is 150Å of GaAs and QW3 100Å of InGaAs (x=10%). The electrons that pass through the quantum filter leaving behind holes, are able to subsequently tunnel through a thin ($\leq$ 50Å) AlGaAs barrier into QW3. The resulting space-charge electric field acts upon the excitonic resonance of QW2 ($\lambda_{read} \approx 850nm$).

In **Figure 2**, we show the transmission spectra of one of our samples in the region of the QW2 exciton, with and without photoexcitation by 1W/cm^2 of He-Ne laser operating at 633nm. The distinct heavy (HH) and light hole (LH) exciton features clearly redshift under the effect of illumination. Redshifts up to 9 meV were registered with a few W/cm^2 of optical excitation. This corresponds

to an effective electric field of nearly 30 KV/cm. Optimization of our structure parameters is under way.

Presently:[a] Max-Planck-Institute, Heisenbergstr.1, 70569 Stuttgart, Germany.
[b] Ecole Polytechnique Fédérale Lausanne, CH 1015 Lausanne, Switzerland.
[1] Miller et al, PRB 32, 1043 (1985) [2] Feldmann et al, PRB 42, 5809 (1990).

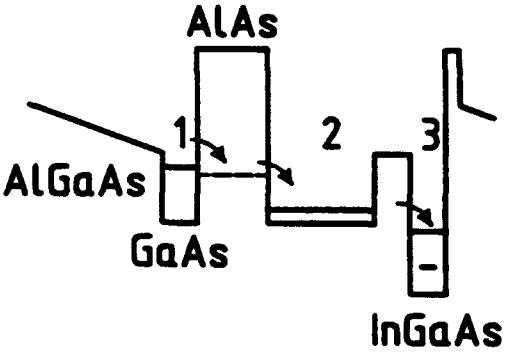
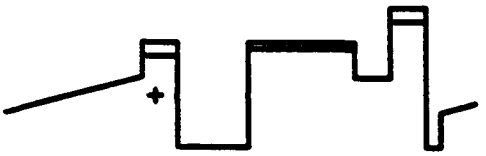


Figure 1: Schematic band diagram of one period of the heterostructure and photogeneration of electric field by rapid electron transfer from QW1 to QW3. The QW energy levels at the Γ point are denoted by full lines whereas the X point energy level in the AlAs layer by a dotted line.



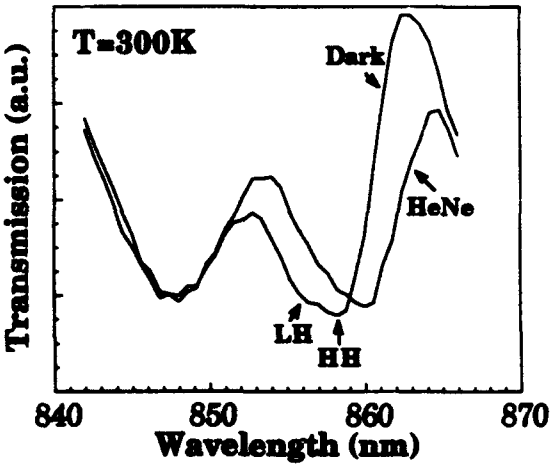


Figure 2: Redshift of the QW2 heavy (HH) and light (LH) hole excitons observed in room temperature transmission spectra, with (HeNe) or without (Dark) photoexcitation by $1 W/cm^2$ of HeNe laser.

Sensitivity transition of LAPS-SLM and its application for optical neural network

Naoki Kato,
Nobuyuki Kasama, Rieko Sekura, Katsuki Matsusita,
Yasuyuki Mitsuoka and Tadao Iwaki

Corporate R & D department, Seiko Instruments Inc.
563 takatsukashinden, Matsudo, Chiba 271, Japan

Phone: +81-473-92-7825, Fax: +81-473-92-2026

ABSTRACT

We present the sensitivity transition characteristics of LAPS-SLM. Furthermore, optical neural network that is using the LAPS-SLM as a thresholding device will be presented.

Utilizing these characteristics to the optical neural network, the memory effect similar to the brain is realized.

SUMMARY

We present the sensitivity transition characteristics of LAPS-SLM, which is incorporating a hydrogenated amorphous silicon photoconductor and ferroelectric liquid crystal modulators, and its application for the optical neural network.

In the past, we reported the gray scale expression characteristics of the LAPS-SLM in SPIE Electronic Imaging Science and Technology '91, moreover we reported the two threshold characteristics of LAPS-SLM and its application for digital optical processing in SPIE's 1992 International Symposium on Optical Applied Science and Technology. (1) (2) (3) (4) (5)

This time, we evaluated the sensitivity transition characteristics of LAPS-SLM. Fig. 1 shows the relation between write light intensity and sensitivity transition. Sensitivity transition of LAPS-SLM is occurred by continuous writing, and is controllable by write, read or bias light intensity.

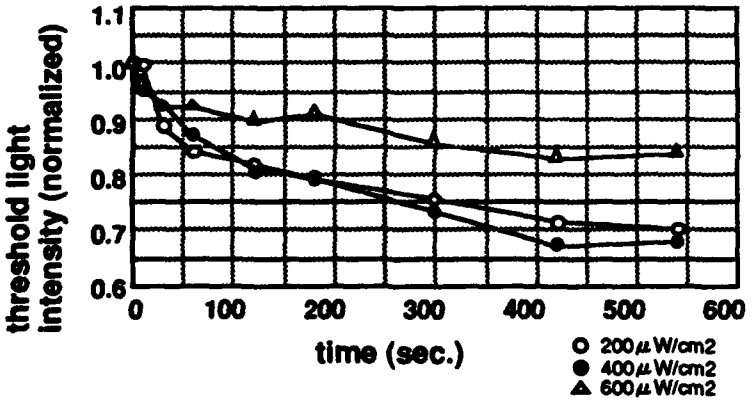


Fig. 1 : Relation between write light intensity and sensitivity transition

Sensitivity transition is also controllable by driving voltage, pulse width, and writing or neglecting time. Control range of sensitivity transition is from 10% to 40% on threshold intensity of write light.

Fig. 2 shows the relaxation after 10 minutes continuous action.

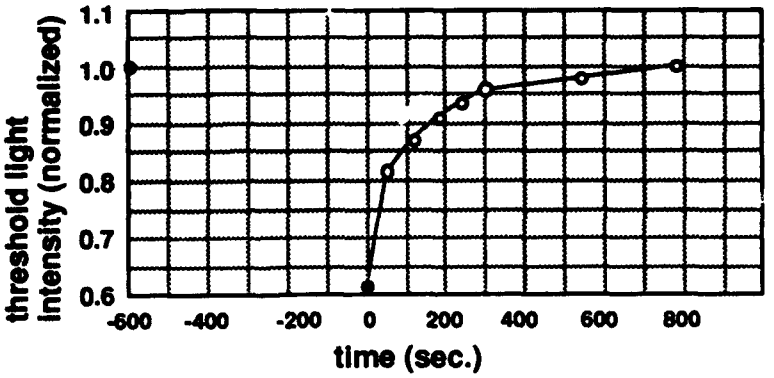


Fig. 2 : Relaxation after 10 minutes continuous action

These characteristics realize the memory effect similar to the brain as it was applied to the optical neural network. If the LAPS-SLM is used as a thresholding device in an optical neural network system, lower of threshold light intensity was namely lower of neuron's excitement threshold level. Therefore the accumulation effect shown in Fig.1 corresponds to the memorization in the function of brain, because the repeat of writing gives the lower of threshold light intensity. Similarly, the relaxation effect shown in Fig.2 corresponds to lose of memory in the function of the brain.

These functions are realized in parallel by purely optical means using LAPS-SLM. LAPS-SLM also exhibits higher performance in the system as resolution (over 100 lp/mm, max. 380 lp/mm), contrast ratio (over 400:1) and frame rate (over 1 KHz). Therefore, performance of the optical neural network becomes very high.

References

1. S. Yamamoto, R. Sekura, J. Yamanaka, T. Ebihara, N. Kato and H. Hoshi, "Optical pattern recognition with LAPS-SLM (1) / Light addressed photoconductor and smectic C* liquid crystal spatial light modulator," Proceedings SPIE, vol. 1211, pp. 273-283, (1990).
2. T. Iwaki and Y. Mitsuoka, "Optical pattern recognition by a joint transform correlator using a ferroelectric liquid crystal spatial light modulator," Optics letters, **15**, pp. 1218-1220, (1990).
3. N. Kato, R. Sekura, J. Yamanaka, T. Ebihara, and S. Yamamoto, "Characteristics of a ferroelectric liquid crystal spatial light modulator with a dielectric mirror," Proceedings SPIE, vol. 1455, pp. 190-205, (1991).
4. N. Kato, R. Sekura, T. Ebihara, T. Iwaki and S. Yamamoto, "Threshold characteristics of an OASLM using a a-Si:H photoconductor and a SSFLC modulator," Proceedings SPIE, vol. 1773, pp. 275-283, (1992).
5. N. Kasama, Y. Mitsuoka, T. Iwaki and S. Yamamoto, "Effects of nonlinear parameters in feedback joint transform correlator," Proceedings SPIE, vol. 1772, pp. 51-62, (1992).

The Nonuniformity Tolerance of FET-SEED Smart Pixel Arrays

L. M. F. Chirovsky[a], *A. L. Lentine*[b], *T. K. Woodward*[c], *G. Livescu*[a], *and G. D. Boyd*[c]
AT&T Bell Laboratories, [a]Murray Hill, NJ 07974, [b]Naperville, IL 60566, [c]Holmdel, NJ 07733

ABSTRACT

We quantify the nonuniformity tolerance of FET-SEED circuit arrays, show its dependence on optical output contrast and speed, and describe a single-ended mode of operation whose nonuniformity tolerance compares well with that of differential operation.

Although a particular kind of FET-SEED Smart Pixel circuit may have acceptable performance for a given application, one cannot assume immediately that all the Smart Pixels in a large array can exhibit the same performance in a system. Neither the circuits nor their concomitant optical beams can be identical even if designed to be so. There will be variations or nonuniformities due to many different causes. Thus the circuit and system designs should be such as to, first of all, minimize possible variations, then to minimize the effect of remaining variations, and finally, failing that, to be tolerant to the lingering effects of nonuniformities, so that all pixels operate properly under one global set of conditions. In recent years, as sources of nonuniformity were identified, iterative redesign has significantly reduced the size of variations which occur in FET-SEED circuits and the associated system hardware [1,2]. The use of "dynamic latching" greatly dissipates the effects of many of the nonuniformities not eliminated [3,4]. The remaining variations can be analytically dealt with as if due solely to differences in the amount of optical power in the beams incident on the modulators in the FET-SEED circuits, hereafter called the "read beams". The principal issue is to guarantee that the two possible digital signals (logical "1" and "0") are correctly recognized as such, as data is optically transmitted from pixel to pixel, despite the fact that the read beam powers, P_r, are not all equal. Recall that data is optically transmitted by a FET-SEED circuit when a read beam impinges on an output modulator, that is either in a high reflectivity state, R_{HI}, for one logic state, or a low reflectivity state, R_{LO}, for the other logic state. The output signals are then either $R_{HI}P_r$ or $R_{LO}P_r$. Their ratio, $K_O = R_{HI}/R_{LO}$, is often called the modulator output contrast.

A mode of FET-SEED circuit operation, where optical data encoding is done with transmitters which use only one modulator is called single-ended. If R_{LO} is not zero, and K_O is finite (as is usually the case for SEED modulators) then one can intuitively see that for single-ended operation, a nonuniformity problem can arise when $P_{ri} \neq P_{rj}$, where i,j denote the ith, jth pixel in an array. For instance, when $P_{ri} >> P_{rj}$, then either $R_{LO}P_{ri}$ becomes too large for one logic state or $R_{HI}P_{rj}$ becomes too small for the other logic state, as one tries to globally adjust all the P_r powers together. To date, this problem has usually been dealt with in systems using FET-SEED circuit arrays by operating in a mode where the data encoding is differential. Each transmitter has two modulators, configured to settle into complementary states, and receives two read beams, P_{ri1} and P_{ri2}. The two digital states are thus represented by complementary signal pairs ($R_{HI}P_{ri1}$, $R_{LO}P_{ri2}$) and ($R_{LO}P_{ri1}$, $R_{HI}P_{ri2}$). The optical receivers, already having dynamic latching for its benefits, are then designed to respond to the difference in power in a signal pair, so that the two logic states are registered by ($R_{HI}P_{ri1} - R_{LO}P_{ri2}$) or ($R_{LO}P_{ri1} - R_{HI}P_{ri2}$). If there is local uniformity (where $P_{ri1} \approx P_{ri2} \approx P_{ri}$, $P_{rij} \approx P_{rj2} \approx P_{rj}$) and only global non-uniformity ($P_{ri} \neq P_{rj}$), then in differential operation the digital signals become $P_{ri}(\Delta R)$ or $P_{ri}(-\Delta R)$; $P_{rj}(\Delta R)$ or $P_{rj}(-\Delta R)$; etc., where $\Delta R = R_{HI} - R_{LO}$. Then, once all P_r are made large enough, all digital signals will be correctly recognized even if $P_{ri} >> P_{rj}$ or vice-versa. Thus differential operation is generally considered much more nonuniformity tolerant than single-ended operation and essentially dependent on ΔR rather than K_O.

Some of the assumptions underlying the above assertion do not hold steadfastly under close scrutiny. The two principal ones are that there is local uniformity ($P_{ri1} \approx P_{ri2}$, *etc.*) and that the P_r's can be made as large as necessary. Recent measurements of beam powers in a real system [2] showed that, effectively, the local and global variations, as defined above, are about the same. Saturation and heating effects in the modulators as well as limited laser source power, for read beams, conspire to set an upper limit on the P_r's. The consequences of these facts can be quantified with the following analysis.

When a FET-SEED receiver has a switching energy, E_{sw}, to deliver E_{sw} through a transmitter, a source laser must launch an energy, E_ℓ. These two energies can be related by an operation mode's figure of merit, (FM), by the equation:

$$E_{sw} = (FM)E_\ell \ . \tag{1}$$

(FM) is the efficiency with which launched energy is converted to switching energy. This (FM) is reducible to the one discussed in [5]. For differential operation $(FM)_d$ is given by:

$$(FM)_d = \frac{\alpha_1 \alpha_2 (R_{HI}P_{\ell i1} - R_{LO}P_{\ell i2})}{2\,P_\ell} \ ; \tag{2}$$

where P_ℓ is the average laser launched power per beam, α_1 is the attenuation factor, due to system optics, between the laser and a transmitter's modulator and α_2 is the attenuation factor, due to system optics, between transmitters

and receivers. (Note that by these definitions $P_{d} = \alpha_1 P_{\ell 1}$, etc.).

Let the beam powers vary such that over N pixels, $$(1-x)P_\ell \le P_{\ell i_a} \le (1+x)P_\ell \,, \tag{3}$$

where x is a fraction ≤ 1, i = (1, 2, $\cdots$ N) and a = 1,2.

Also define the nonuniformity tolerance margin, M, by $$M = (1+x)/(1-x) \,. \tag{4}$$

(Note that M is the ratio of the largest over the smallest beam power.) Then, for the worst case, which governs the array performance, $$(FM)_d = \frac{\alpha_1 \alpha_2 R_{HI}(1-x)}{2}\,(1-M/K_0) \,. \tag{5}$$

Thus even for differential operation, the contrast ratio, K_0, is important, as was pointed out before in [6]. Error-free performance is not possible unless $K_0 > M$, and then $(FM)_d$ remains small until $K_0 >> M$ (or at least $K_0 \ge 3M$). A very small $(FM)_d$ means a very large E_ℓ is needed, which implies a much reduced data rate, f, or the need for very high power laser beams, since $P_\ell = fE_\ell$. In a system application, there will be an upper available limit on P_ℓ and a lowest acceptable limit on f, setting an upper limit on E_ℓ and a lower limit on $(FM)_d$. Without a sufficiently large K_O, the allowable x and M become small and the nonuniformity tolerance of differential operation evaporates. A similar analysis shows that standard methods of single-ended operation fare even worse. Is there an alternative?

The answer is possibly yes, in an unusual form of single-ended operation, we call Asynchronous Reset On Every Bit, or AROEB-ic for short. The operating procedure requires pulsed optical data and dynamically latching receivers with a sharp switching threshold. (We will show experimental data). Of the two types of digital logic signal (logical 1 or 0) pulses, one should deliver E_{sw} and the other no more than a threshold energy, E_{th}, which causes no switching. Interleaved in time between the signal pulses are informationless reset pulses which return the receiver to a preset state. Being asynchronous with signal pulses, the reset pulses create no contention with the signal pulses. This fact allows the signals to be smaller than in other operating modes, and removes the upper bound from the reset pulses that reference signals would have. The receiver then has a required input contrast ratio, K_{RI}, obviously ≥ 1, such that $$K_{RI} = E_{sw}/E_{th} \,. \tag{6}$$

The AROEB-ic mode of operation has two figures of merit, $(FM)_{a1}$ and $(FM)_{a2}$ such that:

$$E_{sw} \le (FM)_{a1} E_\ell \quad \text{and} \quad E_{th} \ge (FM)_{a2} E_\ell \,. \tag{7}$$

For the worst cases, which govern array performance,

$$(FM)_{a1} = \alpha_1 \alpha_2 (1-x) R_{HI} \quad \text{and} \quad (FM)_{a2} = \alpha_1 \alpha_2 (1+x) R_{LO} \,. \tag{8}$$

Error free performance is not possible unless, (from eqs. 6, 7, 8)

$$(FM)_{a1}/FM_{a2} \ge K_{RI} \quad \text{i.e.} \quad K_O \ge MK_{RI} \,, \tag{9}$$

and $(FM)_{a1}$ satisfies the constraints imposed on E_ℓ by P_ℓ and f. Note that $(FM)_{a1}$ exceeds $(FM)_d$ by a factor of $2/(1-M/K_O)$. For receivers with $K_{RI} = 2$ (which should not be impossible), and with a not very large K_O of 4, a very respectable M=2 is allowed and $(FM)_{a1} = 4(FM)_d$. So, such an AROEB-ic operation would be four times faster than the differential mode or alternatively could be done with four times less laser power. From a different perspective, one can also deduce that when a system application demands a high data rate with limited laser power, the single-ended AROEB-ic mode of operation can have greater nonuniformity tolerance than the differential mode of operation. On the other hand, with a very relaxed data rate requirement, the differential mode will work with a lower K_O, by a factor of K_{RI}, than the AROEB-ic mode would.

In summary, we present a simple method of analysis which quantifies nonuniformity tolerance in FET-SEED circuit arrays by relating it to easily measurable parameters, so that reasoned choices can be made when such arrays are incorporated into systems.

[1] A. L. Lentine, R. A. Novotny, T. J. Cloonan, L. M. F. Chirovsky, L. A. D'Asaro, G. Livescu, S. Hui, M. W. Focht, J. M. Freund, G. D. Guth, R. E. Leibenguth, K. G. Glogovsky, and T. K. Woodward, "4×4 arrays of FET-SEED embedded control 2×1 optoelectronic switching nodes with electrical fan-out" submitted to IEEE Photonics Tech. Lett. (1994).

[2] F. B. McCormick "Design issues for free-space photonic switching demonstrators", OC '94 invited talk.

[3] L. M. F. Chirovsky, "Dynamic Operation of Quantum Well SEED's", MRS Symp. Proc., V. 261, pp. 27-32 (1992).

[4] A. L. Lentine, L. M. F. Chirovsky, and T. K. Woodard, "Optical energy considerations for diode-clamped smart pixel optical receivers", to be published IEEE JQE (1994).

[5] G. D. Boyd, L. M. F. Chirovsky, A. L. Lentine, and G. Livescu, "Saturation effects and wavelength optimization of quantum well modulators in smart pixels", submitted for an OC '94 talk.

[6] A. L. Lentine and F. A. P. Tooley, "The relationships between speed and tolerances for self electro-optic effect devices", to be published, Appl. Optics, special issue on Optical Computing.

Logic and layout design of arrays of optically interconnected exchange/bypass self-routing node arrays

Marc P.Y. Desmulliez, Frank A.P. Tooley, Graham J. Crowder
Department of Physics, Heriot-Watt University,
Riccarton, Edinburgh, EH14 4AS, Scotland, UK
Tel : UK 31 451 3068 E-mail : marc@phy.hw.ac.uk

Patrick W. Foulk, Scott Ashcroft, Martin Coy
Department of Computing and Electrical Engineering, Heriot-watt University

Abstract

The design and implementation of optically interconnected self-routing exchange/bypass modules arrays is described. The nodes are laid out using silicon and gallium arsenide based technologies. Performance metrics of the pixels are analysed.

Motivation

Sorting remains one of the most commonly performed tasks in any computation [1]. The parallel implementation of this function using space-variant non-local optical interconnects such as the perfect shuffle [2] has been shown to provide a bonus factor compared to its electronic counterpart [3]. This bonus factor could be increased by two orders of magnitude if dedicated hardware (smart pixel) is provided to reduce the computational part of the sorting [3]. Consequently self-routing exchange/bypass modules have been designed and laid out using 1.5 μm CMOS and AT&T FET-SEED monolithic integration [4]. The smart pixels arrays will be used in a time multiplexed multi-stage interconnection network (MIN) [5] in which the bitonic sort is implemented with perfect shuffle interconnects [6].

The enhanced exchange/bypass module .

The smart pixel is designed to latch at the first difference in the significant bit of the two optical input data streams A and B. It remains in the state set until a electrical reset signal R is activated at the end of the word. This ensures that the output signal C exhibits either the maximum or the minimum of the two input signals depending on the state of the control signal P. An additional signal S may be activated to allow the output data C and D to be the "straight through" inputs at certain stages of the sorting. The module is clocked by the signal CLK. The logical design of this circuit is shown in figure 1. It is intended to add to the logic circuitry a storage unit which consists of a 4-bit shift register.

The module is implemented in European Silicon Structures (ES2) 1.5 μm CMOS, n-well double metal technology via Eurochip (similar to US MOSIS). This allows the design to be debugged and the process to be demonstrated economically. The layout of 4x4 array of pixels is shown in figure 2. The optical interconnects come into the silicon chip via metal pads from a GaAs chip which has the transmitters and receivers. The two chips will be flip-chip bonded together [7]. Assuming that the common clock and reset signals can be electrically connected and that dual rail logic is implemented ten optical input signals per pixel are hence to be considered. A similar design using FET-SEED monolithic integration technology is currently under study. Electrical characteristics of a 4x4 array of such pixels will be presented.

References

[1] D.E. Knuth, 1973, *The Art of Computer Programming*, Vol. 3, Addison-Wesley, Reading, Ma.

[2] H.S. Stone, 1971, *IEEE Trans. Computers*, Vol. C-20, 2 , 153.

[3] B.S. Wherrett and al., 1992, *SPIE Proceedings on Optical Computing*, Vol. 1806. 333.

[4] A.L. Lentine and D.A.B. Miller, 1993, *IEEE J. Quantum Electron.*, Vol. 29. 2 , 655.

[5] F.A.P. Tooley and al., 1994 *submitted to Optical Computing, Endinburgh. U.K.*.

[6] C.W. Stirk and R.A. Athale, 1988, *Appl. Opt.*. Vol. 27. 9 , 1271.

[7] M.J. Goodwin et al, 1991, *J. Light. Techn.*, Vol. 9. 9 , 1639.

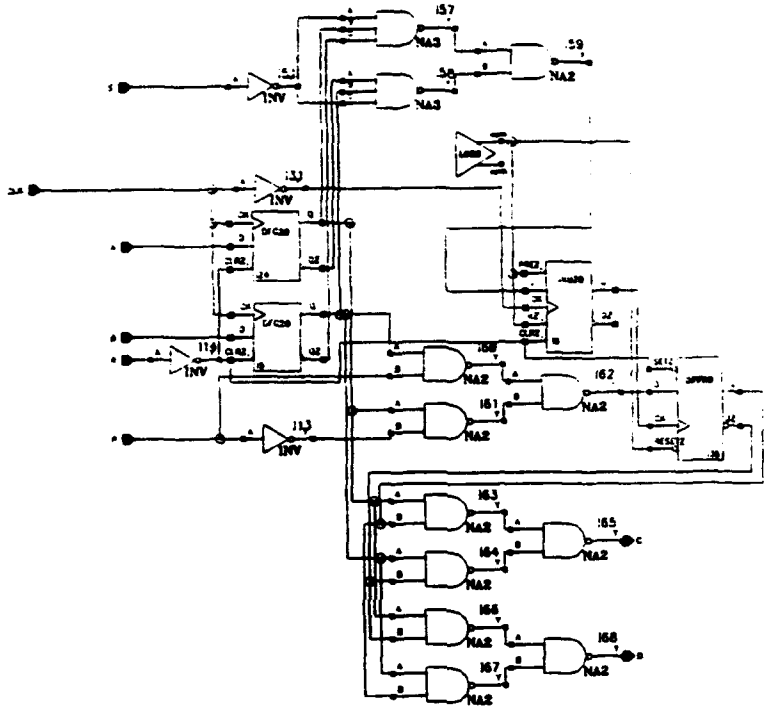


Figure 1

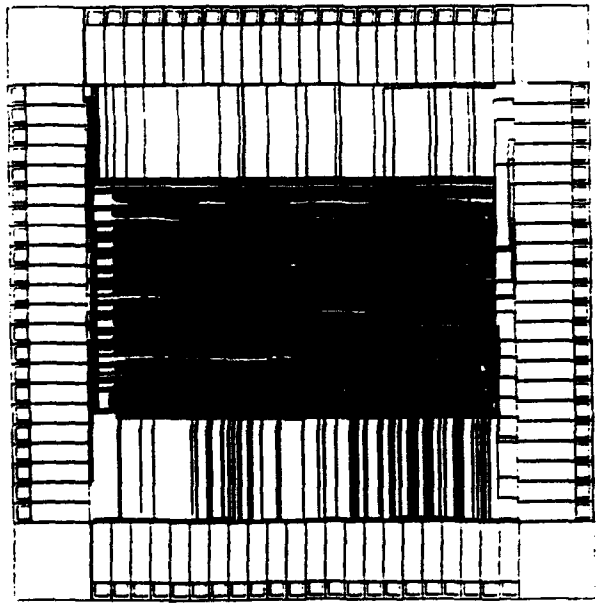


Figure 2

Optoelectronic Gain of Phototransistor/Surface Emitting Laser Smart Pixel Logic Gates

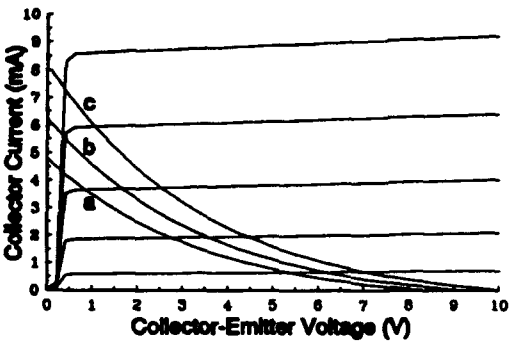
S.A. Feld, F.R. Beyette, Jr., K.M. Geib,
R.D. Snyder and C.W. Wilmsen

Optoelectronic Computing System Center and
Department of Electrical Engineering
Colorado State University
Fort Collins, Colorado 80523 USA 1-303-491-7577

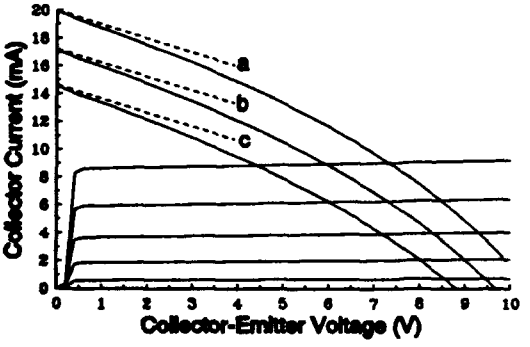
Abstract: The maximum optical P_{out}/P_{in} ratio of phototransistor/surface emitting laser smart pixel logic gates has been analyzed in terms of device and circuit parameters. Cascading gate experiments have been performed.

Heterojunction phototransistor/vertical cavity surface emitting laser (HPT/VCSEL) smart pixel arrays hold great promise for parallel optoelectronic processing systems and other applications [1-3]. The implementation of many of these systems requires beam splitters, holograms and lenses. These passive elements, along with misalignment and beam spreading, greatly reduce the magnitude of the optical signals as they propagate from one stage to another. To overcome these losses and insure that the arrays are cascadable, the HPT/VCSEL pixels must have sufficient optical gain. Unfortunately, the optical output power of a VCSEL is not a continuous linear function of the current above threshold, but rather reaches a maximum and then decreases rapidly as the drive current is increased further. Therefore, logic gate pixels formed with VCSELs and either HPTs or FETs will have a maximum gate gain (defined as the maximum P_{out}/P_{in} ratio) that depends upon the optoelectronic gain of the transistors and the characteristics of the VCSELs.

This paper presents an analysis of the maximum gate gain of HPT/VCSEL logic gates and the variation of this gain with transistor optoelectronic gain (G_{op}), maximum VCSEL power out (P_{max}), threshold current (I_{th}) and I_{max} (the current at P_{max}). We have applied load line analysis and numerical simulation to determine the gate gain of inverting, e.g. NOR and NAND, and non-inverting, e.g. AND and XOR logic gates for various device parameters (note:the XOR gate has both inverting and non-inverting components). In addition, we have experimentally demonstrated three cascaded HPT/VCSEL stages and have set up a demonstration of an AND gate driving an XOR gate. The results of both the analysis and experiments will be presented in the paper. Figures 1a and 1b illustrate the common emitter I_c vs. V_{ce} characteristics of an HPT with three super-imposed VCSEL load lines, for inverting and non-inverting logic gates respectively. Figures 2a and 2b show the P_{out} vs. P_{in} curves resulting from these load lines. These plots demonstrate that there is an optimum supply voltage required in order to achieve

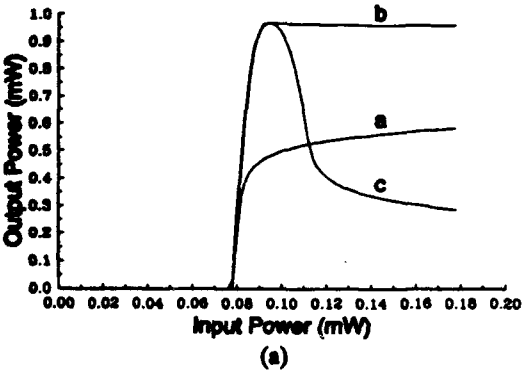


(a)

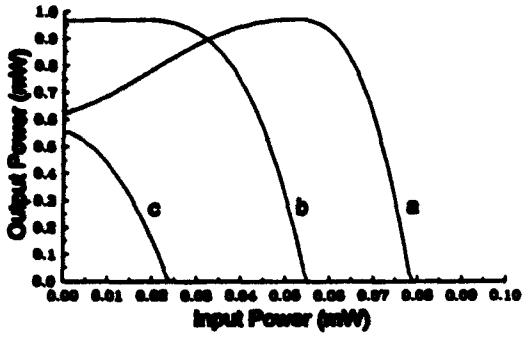


(b)

Figure 1. a) Load-line curve for non-inverting gate. b) Load-line for inverting gate.



(a)



(b)

Figure 2. Power input-output relationship for a) non-inverting gates, and b) inverting gates.

the maximum output from the logic gate over the widest input range. Determining the effects of changing various VCSEL and HPT parameters requires numerical calculation and we have developed empirical expressions to fit our HPT and VCSEL data. Two VCSEL designs with different efficiencies as summarized in Table I were used in this analysis.

Table I			
Experimental VCSEL characteristics			
VCSEL	I_{th}	I_{max}	P_{max}
VCSEL1 High Efficiency	4.0mA	5.5mA	1.0mW
VCSEL2 Low Efficiency	5.0mA	14mA	0.5mW

Some of the results of these calculations are shown in Figs. 3 and 4. These figures illustrate the effect of VCSEL threshold current on the gate gain for the two VCSEL designs and a HPT optoelectronic gain of G_{op} = 50A/W. It is seen that the gate gain is only a weak function of I_{th} and thus small changes in I_{th} across an array should not effect the over-all performance. However, it is also clear from this figure that reducing I_{th} of the low efficiency VCSEL does not significantly increase the gate gain. Thus, while reducing I_{th} decreases the power dissipation, it does not increase the cascadability of the array. Even with the more efficient VCSEL, the gate gain does not increase dramatically until I_{th} becomes very small.

Summary: The gain of optoelectronic logic pixels has been shown to critically depend upon the bias applied to the circuit and to be proportional to the gain of the transistors and the maximum output power of the VCSELs. The gate gain was found to be only a weak function of the VCSEL threshold but is strongly dependent upon I_{max}-I_{th}, the efficiency of the VCSELs.

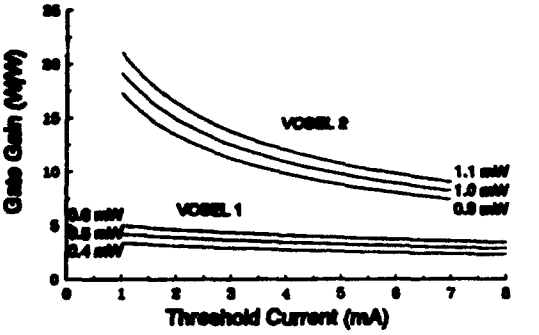


Figure 3. Gate gain vs threshold for non-inverting gates.

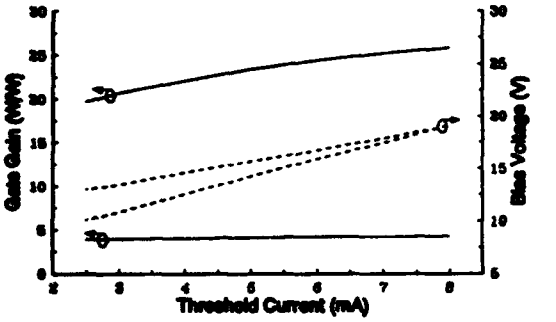


Figure 4. Gate gain vs threshold current for inverting gates.

Acknowledgement: This work has been supported in part by the Optoelectronic Computing System Center which is sponsored by NSF/ERC grant ECD9015128 and by the Colorado Advanced Technology Institute.

Bibliography

1. J. Cheng, P. Zhou, S.Z. Sun, S. Hersee, D.R. Myers, J. Zolper, G.A. Vawter, "Surface-Emitting Laser-Based Smart Pixels for Two-Dimensional Optical Logic and Reconfigurable Optical Interconnections", IEEE J. Quantum Electron., Vol. 29, No. 2, pp. 741-756, Feb. 1993.
2. J.I. Song, Y.H. Lee, J.Y. Yoo, J.H. Shin, A. Scherer, R.E. Leibenguth, "Monolithic Arrays of Surface-Emitting Laser NOR Logic Devices", IEEE Photon. Technol. Lett., Vol. 5, No. 8, pp 902-904, Aug. 1993.
3. P.A. Mitkas, L.J. Irakliotis, F.R. Beyette, Jr., S.A. Feld, C.W. Wilmsen, "An Optoelectronic Data Filter for Selection and Projection", To be published in Appl. Optics 1994.

Photothyristor smart pixels in M.I.M.D. optical computing architectures

T. Van de Velde and H. Thienpont
Vrije Universiteit Brussel, Applied Phys. Dept.
Pleinlaan 2, B-1050 Brussels, Belgium

We describe the application of vertical-to-surface transition electrophotonic devices to Multiple Instruction, Multiple Data parallel optical information processing and in particular the development of smart pixels based on photothyristors - the basic elements for M.I.M.D. machines.

Recently a new and very promising generation of active bistable vertical-to-surface transition electrophotonic devices was developed to perform chip-to-chip optical interconnects - the PnpN photothyristors. When used in the configuration of the differential pair, these multilayer III-V semiconductor (GaAs) structures have been shown to be capable of emitting binary optical signals, receiving 50 fJ optical inputs together with a set-on-set-off-cycle time of 10 ns [1].

Making use of these exceptional optical signal receiving and emitting abilities, we will present a method in five distinct steps to extend the functionality of the differential pair of optical thyristors with a Si integrated electronic control cell, which converts the incoming optical signals into TTL- or CMOS- compatible electronic signals and vice versa. If digital logic and memory is implemented inside each of these control cells, we obtain smart pixels for Multiple Instruction Multiple Data optoelectronic processors, where *different* operations can be executed on different pixels at the same time.

The first step consists of applying a common voltage sequence to the whole array of differential pairs of optical thyristors. During the *receiving level* (0 V), optical inputs create charge carriers in the central junctions of one or both thyristors of the differential pair. At *set-on level* (e.g. +6 V) the decision is made whether the first (logic '1') or the second (logic '0') thyristor received the largest optical input - this one switches on while the other remains off. At set-off level (e.g. -10 V), charge carriers are extracted from both central junctions by punch-through.

In step 2 the differential pair achieves the conversion of electronic to optical signals and vice versa is achieved in step 2. The first operation requires that an electronic control cell is able to select which of both thyristors is switched on at set-on level (independently of any optical input), the latter to determine which of both thyristors is on after having received an optical input. We present several solutions to these problems; one of these is the use of GaAs transistors parallel to each thyristor, decreasing the amount of charge carriers in this thyristor (electronic to optical data conversion), together with a Si integrated voltage comparator to determine which of both is on (optical to electronic data conversion). The GaAs and Si chips are electrically linked to each other by solder bumping.

Step 3 is the synchronisation of the common voltage sequences of different arrays in the system, making use of a system of alternating light beams to transmit system clock pulses. At step 4 we propose an elementary Si-integrated control module (individual to each differential pair) to translate the set of required and measured voltages (at times given by the local synchronization circuit of the array) into the higher-level command lines DATA, SEND and CLOCK. Finally, step 5 is the implementation of Si-integrated digital logic and memory, allowing the smart pixels to exchange and store information at application level, including shifting, pattern recognition, or general purpose M.I.M.D. computing.

A promising approach to M.I.M.D. computing is the Tse concept [2], which provides a simple way to make several optoelectronic processing units (several logic planes of smart pixels) work together to implement the intricate M.I.M.D. processing task. 'Tse' is the Chinese word for 'icon' or 'small image element'. And indeed, the binary images that can be processed by this machine are divided into image elements of e.g. 4 bits each. An instruction image, containing

the different 4 bit instructions X (e.g. X = AND, NOT, ...) to be executed on the different image elements, and one or several data images are applied to all processing units. If the processing unit X recognises the instruction X in some image elements of the instruction image, the instruction X is executed on corresponding image elements in the data images. The result image is obtained by combining (OR-ing) the partial results of the different processing units X,Y,Z,... which can perform logic operations as well as shifting operations, allowing data to be transferred between different image elements of a same image. The global aim of these principles is to execute different programs on different image elements while letting these programs exchange results.

Compatibility of the optoelectronic Tse M.I.M.D. concept with the classic S.I.S.D. operation of an electronic personal computer can be achieved if the format of the image element is chosen according to the registers of the CPU of the computer under consideration. A single image element could then consist of an instruction field, data fields, the status register, data and address registers. A parallel memory plane (an array of smart pixels with memory) is used to deliver the image with the instructions in the instruction fields. Each processing unit (an array of smart pixels with digital logic) compares the contents of the instruction fields to a specific value to determine the image elements on which the instruction will be executed - which causes the register values of that image element to be altered. Finally, the processing units put the addresses of the next instructions in the instruction fields of the result image, which is then sent back to the parallel memory plane, after which a new image with instructions is sent to the processing units, etc. In addition to the original computer instruction set, data transfer instructions as well as global image processing functions can be implemented in a modular and flexible way.

References : [1] P. Heremans, M. Kuijk, R. Vounckx, G. Borghs, *Appl. Phys. Lett.* 61, 1326 (1992)
[2] D.H. Schaefer, J.P. Strong III, 'Tse computers', *Proc. IEEE* 65(1), p. 129, 1977

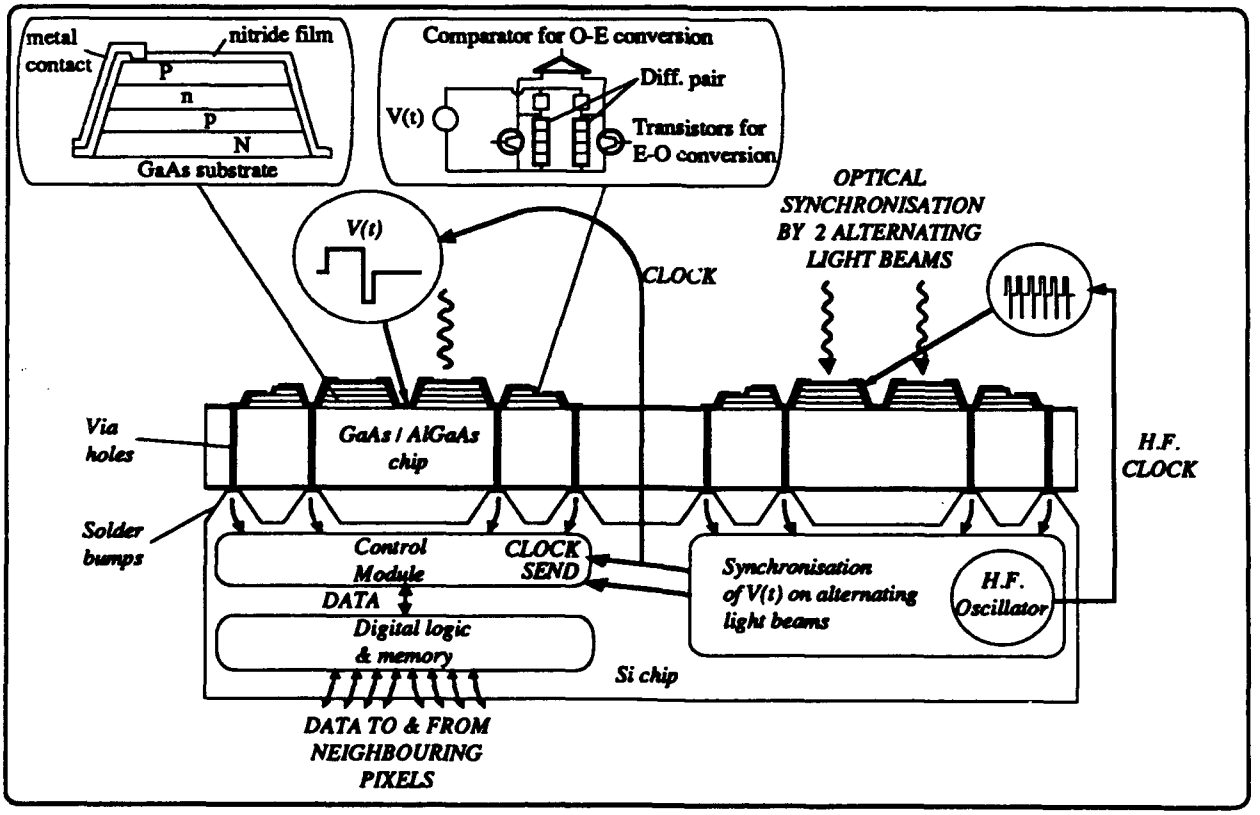


Fig. 1 : Extension of the functionality of the differential pair of optical thyristors to a smart pixel by adding control, logic, memory and synchronising Si integrated circuitry

A normalizing detector array for an adaptive neural network

J. Sharpe
I. Bar-Tana
K. Johnson

University of Colorado
Optoelectronic Computing Systems Center
Boulder, CO 80309-0525
U. S. A.
email: sharpe@boulder.colorado.edu
Tel: (303) 492 3260. Fax: (303) 492 3674

1 Abstract

An optoelectronic smart pixel array for incorporation in an optical neural network is considered. The circuit, based on the ART memory of Tsay and Newcombe comprises photodetectors, modulators and normalization and winner-take-all circuitry.

2 Summary

There has recently been considerable interest in the optical implementation of adaptive resonance theory (ART) [1] neural networks [2] [3]. Part of this interest arises from the ART matching metric being an inner product between the input pattern and stored templates. This can be implemented optically, either as the zeroth lag in an optical correlator or as a vector matrix multiplier system. However, the details of the ART algorithm call for normalization steps and the selection of maximum outputs in order to decide on the best match. Conventionally one would read the optical signals out of the system and into an electronic computer where the required manipulations would be performed. This leads to a substantial bottleneck in the processing. Recently Caudell proposed a system based on the optical vector matrix multiplier which uses smart pixels on several planes in order to obtain the required functionality [2]. Light from the input array illuminates the matrix columns and this light is collected on the detector array. Depending on the outcome of this calculation the stored vectors on the matrix rows may be either updated via an ANDing operation with the input vector or a new row is added. Caudell explains the operation of the system in schematic terms and recently we have implemented the matrix array using liquid crystal on silicon (LCOS) technology [4]. Each pixel of this two dimensional array comprises a photodetector, a memory element (flip-flop) and a modulating element and measures 75 μm on a side.

The matrix element is thus relatively simple. However, the output array has considerably more functionality since we require the following mathematical operations.

$$\frac{T \cdot I}{\alpha + |T|} \stackrel{?}{\geq} \frac{|I|}{\alpha + N} \tag{1}$$

and

$$\frac{T \cdot I}{|I|} \stackrel{?}{\geq} \rho \tag{2}$$

The numerators on the left hand side of both these equations are, of course, implemented optically. If the normalizations were to be implemented "directly" we would need analog memory and division circuitry. A more compact way however is to adapt the circuitry discussed in [5]. Consider the circuit shown in figure 1 where the current I which flows through voltage controlled resistors R1 and R2 is

$$I = \frac{V_d}{\frac{1}{K_a V_a} + \frac{1}{K_b V_b}} \tag{3}$$

where $K_a V_a$ and $K_b V_b$ are the conductances of R1 and R2 respectively. Then the voltage V_{sig} measured at the junction of R1 and R2 is (after a little manipulation)

$$V_{sig} = I \times \frac{1}{K_b V_b} = \frac{V_d V_a}{V_a + K_b V_b / K_a} \tag{4}$$

Thus if we can make the template moduli proportional to V_b and the inner products between the inputs and templates proportional to V_d we can perform calculations of the form required for equations 1 and 2. A problem however is the storage of the template moduli while the inner products are being calculated. We get round this problem using the circuit of figure 2 at each pixel. The operation of this circuit is as follows. Light first falls on the photodetectors from the template modulus calculation, generating photocurrent. V_i is pulsed high, letting the gate of T_1 charge up. The final voltage on T_1 is determined by the amount of photocurrent and the time that V_i goes high. V_i now goes low, trapping charge on the gate of T_1. Light now falls on the photodetector from the inner product calculation. If the voltage V on transistor T_2 is now set to a small value, we see that the circuit is identical to that of figure 1 and the required calculation of equation 3 can be read as V_{sig}. Once the signal is read off V_i and V_0 are set high to discharge the gate of T_1 in preparation for the next calculation.

There are several other operations that need to be implemented for the ART algorithm. One of these is the selection of the maximum output from equation 1. This can be effected using a winner-take-all circuit, as described in [6]. The implementation and testing of the circuitry will be presented at the conference.

References

[1] Carpenter, G. A. and S. Grossberg. A massively parallel architecture for a self organizing neural pattern recognition machine. Computer vision, graphics and image processing 37 (24), (1987)

[2] Caudell, T. P. A hybrid optoelectronic ART1 neural processor. Applied Optics 31(29) 6220, (1992).

[3] Kane, J. S. and M. J. Paquin. POPART: partial optical implementation of adaptive resonance theory 2. IEEE Transactions on Neural Networks 4(4) 695-702 (1993).

[4] Sharpe, J. P. et al. A smart pixel SLM for incorporation in an optpoelectronic neural network. Report to Boeing Computer Services. Contract W-301569, 1993.

[5] Tsay, S. W. and R. Newcomb. VLSI implementation of ART1 memories. IEEE Transactions on Neural Networks 2(2) 214-221 (1991).

[6] Lazzaro, J. at al Winner-take-all networks of O(n) complexity. Advances in Neural Information Processing Systems, Touretsky (Ed), Morgan Kauffman 1989.

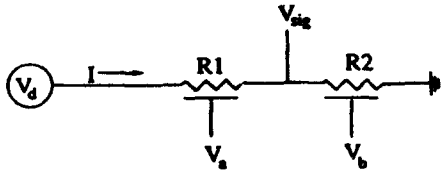


Figure 1.

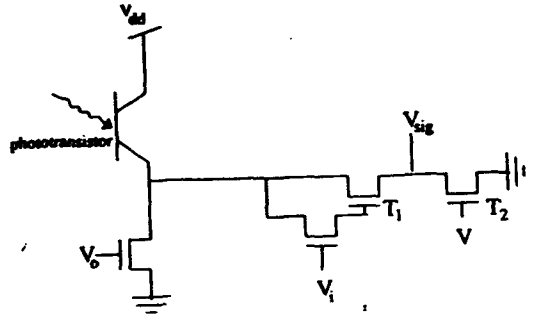


Figure 2.

The Completely Depleted *PnpN* Optoelectronic Switch

Paul Heremans*, Maarten Kuijk•, Roger Vounckx•, Gustaaf Borghs*

* Interuniversity Micro Electronics Center (IMEC)
Kapeldreef 75, B-3001 Leuven, Belgium, tel: 32 - 16 - 281521

• Vrije Universiteit Brussel, Appl. Phys. Dept. (TONA)
Pleinlaan 2, B-1050 Brussel, tel: 32 - 2 - 6412990

Abstract: A novel double-heterojunction optical *PnpN* switch is presented which can be reset from its on-state to its *equilibrium* state in a few nanoseconds. We show the unique potential of this device as fast and sensitive optoelectronic switch.

Latching devices like thyristors are ill reputed for their slow turn-off. In a *PnpN* device, the reset operation requires the removal of the excess free carriers in the center *n* and *p* layers. For device integration in arrays, it is elegant to use *two-terminal PnpN* devices, and perform carrier extraction by applying a negative anode-to-cathode voltage pulse (V_{AK}). Furthermore, it is also important to realize that carrier extraction on its own is not sufficient: for the switch to operate uncritically and with optimum sensitivity, it is imperative that *all* free carriers of the center layers be extracted. *No previously reported PnpN device allows complete carrier extraction*, because of breakdown of one or both of the outer junctions under negative V_{AK}.

The key to *PnpN* layer structures allowing complete carrier extraction was revealed by numerical simulations (Figure 1). The number of free carriers (per unit area) in the center *n* and *p*-layers during turn-on (between 0 to 2 ns) and turn-off (from 2 to 10 ns) are shown for 3 cases. Case A has too highly doped center layers: a negative pulse of -10 Volt is not sufficient for complete carrier removal. Case B has low enough doping in the center layers: within 1.5 ns all carriers are extracted, and the voltage across the device V_{AK} drops to the applied -10 V. Case C shows that without negative pulse, carrier decay is extremely slow.

Next, we have fabricated *PnpN* switches which allow complete carrier extraction. Dopings and layer thicknesses are chosen such that the center *n* and *p* layers are already *completely depleted at equilibrium*, as shown in Fig. **2a**. A switch can be reset from its carrier-flooded on-state (Fig. **2b**) to the zero-carrier equilibrium state by means of a negative pulse lasting less than 10 ns (detailed measurements show 3 ns) ! Figure **3** shows the static I-V characteristics of such device. Figure **4** shows that after reset to equilibrium by means of a negative pulse beyond -8 V (region C), our *PnpN* devices can be pulsed to any positive voltage smaller than the static breakover voltage (2.69 V) in nanoseconds without unintentional switch-on. In other words, our thyristors are completely immune to dV/dt triggering! If the extraction pulse is not sufficient to reset the device (less than -8V), dV/dt immunity is not complete in nanoseconds (Fig 4), but necessitates milliseconds (Figure **5**). This is typically always the case with *PnpN* devices described so far in literature.

Our novel *PnpN* device has a unique potential as high-performance optoelectronic switch (as *e.g.* demonstrated in differential configuration in [1]). Amongst all *PnpN* devices, it is the only one to permit the *combination of high speed and excellent optical sensitivity:*

High speed operation is possible. The reset speed is intrinsically limited by drift and diffusion of the carriers being extracted, and even faster reset than the demonstrated 3 ns is expected to be possible. After reset, the thyristor is completely immune to dV/dt triggering. It can therefore be switched to any voltage close to the break-over voltage in nanoseconds (instead of the usual micro- to milliseconds) without unintentional switch-on.

Optical Sensitivity is optimum: Independently of the detection principle used, highly-sensitive light-reception requires to have a well-defined number of carriers present at the start of the incoming light pulse: if any uncertainty exists on this value, the light pulse must *at least* contain an equivalent number of photons to overcome the unknown carrier content. Our switch provides *ideal* and most reproducible control over the residual carrier density, since this residue is *zero*.

[1] M. Kuijk *et al.*, "Optoelectronic switch operating with 0.2 fJ/μm^2 at 15 MHz", abstract sent in to Optical Computing '94, Edinburgh, August 1994.

Figure 1:

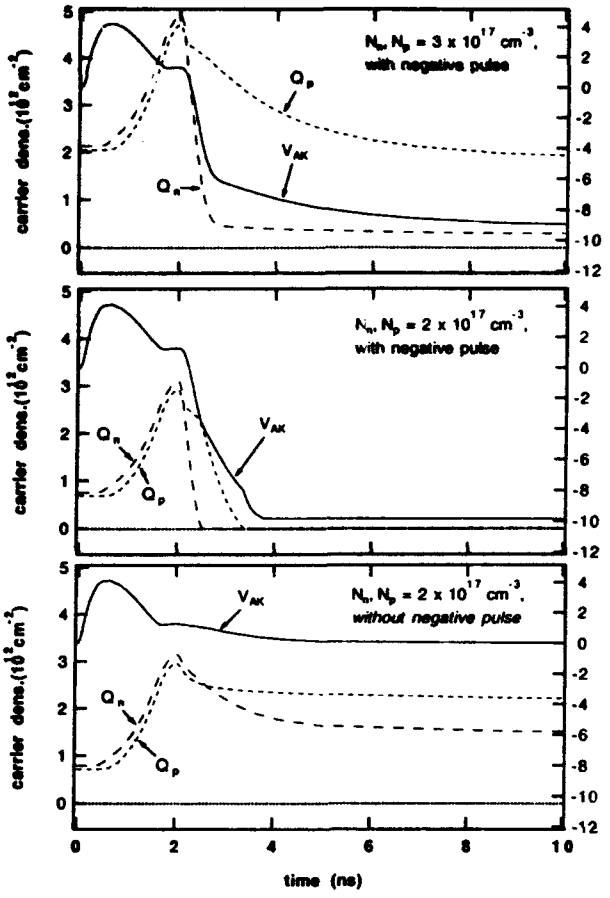


Figure 2:

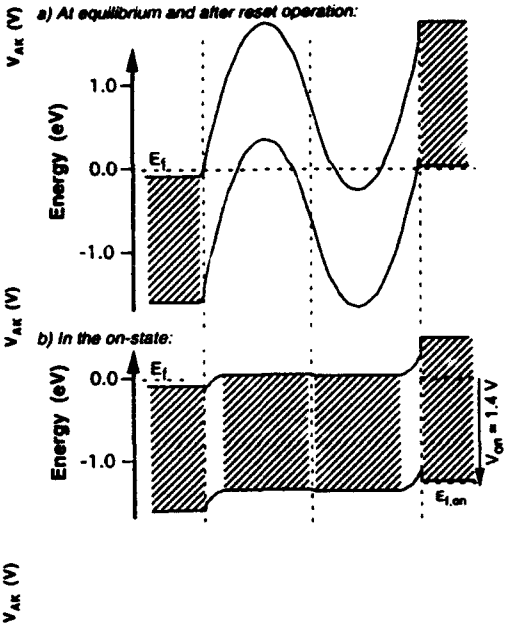


Figure 3:

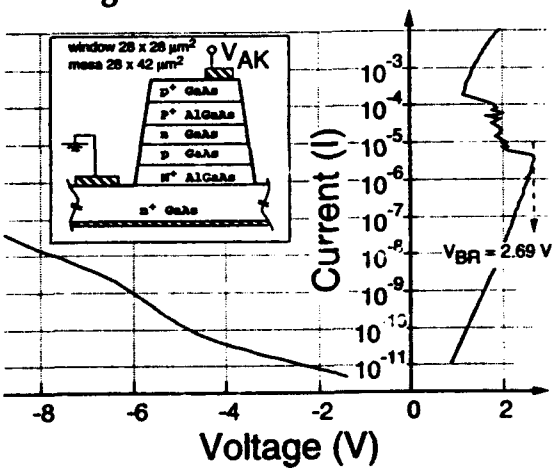


Figure 4:

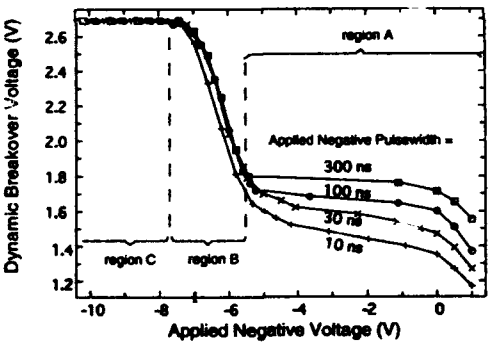
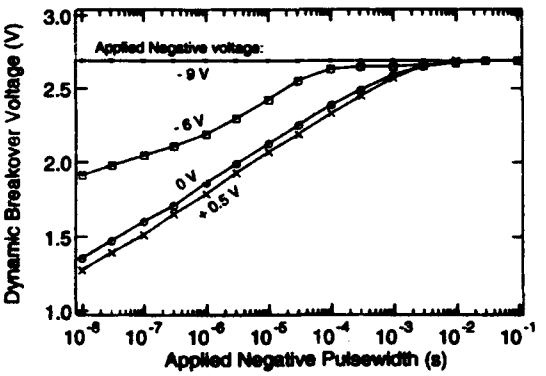


Figure 5:



Resonant-tunneling Triangular-barrier Optoelectronic Switch (R-TOPS) for Optical Logic

H. Sakata, K. Utaka and Y. Matsushima

KDD R&D Laboratories
2-1-15 Ohara, Kamifukuoka-shi, Saitama 356, Japan
Phone:+81-492-66-7831 FAX:+81-492-66-7516

Abstract - We report a novel optical bistable device, which consists of a double-barrier resonant-tunneling diode and a triangular-barrier phototransistor. Clear negative differential resistance and optical bistability with high contrast and high sensitivity are demonstrated.

An optical bistable device is a key for optical computing, and a lot of devices have been studied so far for this purpose. As a photodetecting element in the devices several kinds of structures such as a conventional heterostructure phototransistor (HPT) have been studied [1]. As another candidate, a triangular-barrier phototransistor (TBP) with a very thin gate layer, which has been developed in GaAs / AlGaAs [2], is very promising from a view point of high speed and high sensitivity. On the other hand, a resonant-tunneling diode (RTD) has a potential to give a rise to unique functions attributed to its negative differential resistance (NDR). In this paper, we propose a novel bistable device, resonant-tunneling triangular-barrier optoelectronic switch (R-TOPS), in which a TBP and a double-barrier RTD (DB-RTD) are integrated.

Figure 1 shows a band diagram of the device fabricated. It was composed of InGaAs / InAlAs for 1.5 μm wavelength range operation. The TBP had n^+-i-δp^+-i-n^+ structure, and in the DB-RTD a well layer and barrier layers were InGaAs and AlAs, respectively. The device was grown on an n^+-InP substrate by gas source MBE and was etched into a mesa with 60 μmϕ. Figure 2 shows a schematic load-line graph for R-TOPS. A thick curve is the characteristic of the DB-RTD, and three thin curves are the ones of the TBP at different input-light powers P_1,P_2 and P_3, which show exponential-like dependence of current upon voltage due to thermionic emission. By changing the input-light power, the intersection varies as shown in Fig.2. Experimental I-V characteristics at different input-light powers are shown in Fig.3. The substrate side was normally positively biased at V_b, and the wavelength of input-light was 1.55 μm. Clear NDR with bistability was observed as predicted in Fig.2 , and a peak-valley ratio was 3.6 . These properties show that both TBP and DB-RTD worked well. The bistability in the relation between input-light power and output-current was obtained as shown in Fig.4. It operated at the input-light power as small as 50 μW or even smaller, and the output-current change was about 10 mA, which was large enough to drive other optical devices such as a laser diode. Figure 5 shows the optical bistability at different bias voltages, which was obtained by connecting the device and a laser diode. Clear optical bistability and sharp optical NDR property with high contrast and low input-light power was

observed. An intrinsic optical gain was estimated to be larger than 6 dB from fiber to fiber. These characteristics show the possibility of XOR logic operation as well as optical memory.

In conclusion, we fabricated a novel R-TOPS, and clear NDR and optical bistability were obtained. The device is expected to play an important role for optical computing.

[1] Y.Kawamura et al. IEEE J. Quantum Electron., QE-28, 308 (1992)
[2] C.Y.Chen et al.,Appl.Phys.Lett. 39, 340 (1981)

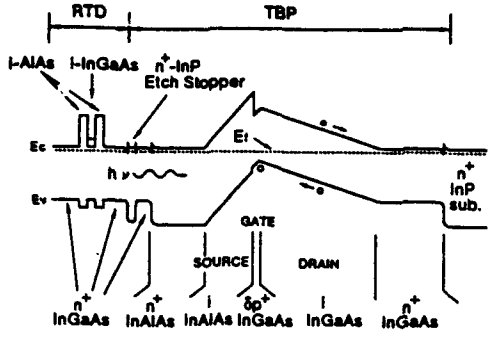


Fig.1 Band diagram

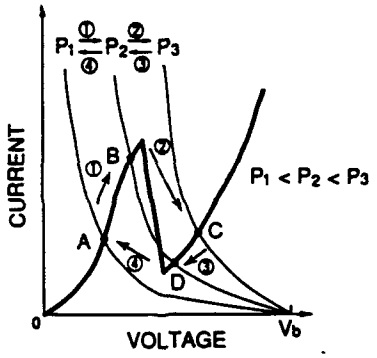


Fig.2 Schematic load-line graph for R-TOPS

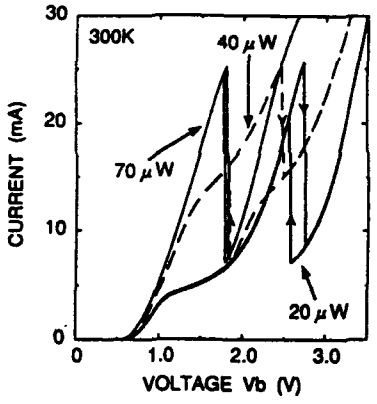


Fig.3 I-V characteristics at different input-light powers

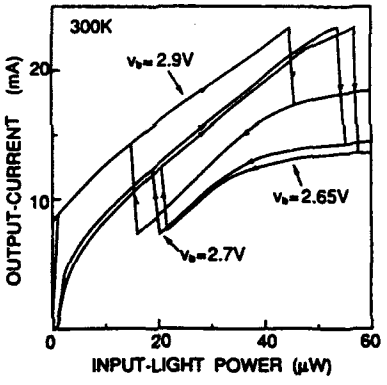


Fig.4 Output-current vs. input-light powers at different bias voltages

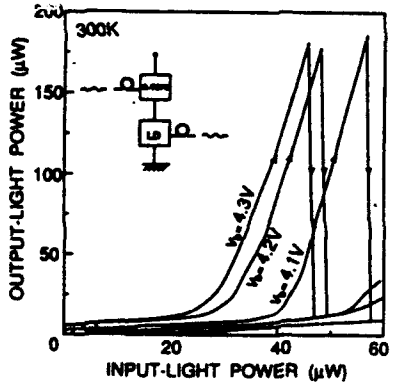


Fig.5 Optical bistable characteristics at different bias voltages

Silicon IMplanted OXide-based optical logic gates for use in silicon smart pixel circuitry: device characterisation, modeling and optimization.

Werner PEIFFER[1], Hugo THIENPONT[1], Irina VERETENNICOFF[1],
Cathleen DE TANDT[2], Willy RANSON[2], Roger VOUNCKX[2], Alain KOSTER[3]

1 Lab for Photonic Computing and Perception, Applied Physics Department (TW/TONA)
Vrije Universiteit Brussel, Pleinlaan 2, B-1050 Brussel, Belgium
tel. ++ 32 2 641 35 67, e-mail: wpeiffer@vnet3.vub.ac.be
2 Lab for Microelectronics and Technology, Applied Physics Department (TW/TONA)
Vrije Universiteit Brussel, Pleinlaan 2, B-1050 Brussel, Belgium
3 Institut d'Electronique Fondamentale, CNRS UA22, Université Paris-Sud
Bat. 220, 91405 Orsay, France

Abstract

We simulate heat transfer in hybrid Silicon IMplanted OXide optical logic gates and link it to their static and dynamic behaviour. We compare our simulations with experimental data and draw conclusions for optimization. The potentialities of the device in view of its compatibility with VLSI circuitry are discussed.

Summary

In this paper we report on the progress which has been made in the fabrication and use of 2-D optical logic planes consisting of silicon Hybrid Electrically Assisted Thermo-Optic Resonators (HEATORs) [1].

The HEATOR-structure combines a pixellated nonlinear microresonator with the properties of a pin-photodiode. When reverse biasing the device it can be used as logic gate [2], while a forward bias turns it into a high-speed spatial light modulator [3]. Moreover we believe it is possible to extend its functionality by providing both active intrapixel and interpixel MSI, LSI and even VLSI circuitry, thanks to the unique combination of both the hybrid character of the device and its silicon nature. The present-day devices might therefore evolve to more sophisticated smart pixels. The ability to store data at a pixel can be used to implement memory functions (although this might be done exclusively with electronic circuitry). Furthermore, HEATORs integrated with Si-photodetectors or HEATORS used as photodetectors can lead to on-chip sensors. In combination with electronic circuitry, the HEATORs can be used to perform intrapixel processing with low level processing capabilities such as signal amplification, thresholding, summation and logical operations that can be performed on input and stored data. Finally, since the HEATORs also feature SLM properties, they can be used to optically output data and to provide interpixel communication via local and global interconnects.

In the past we developed and characterized two types of HEATORs: the first generation was fabricated with double-sided polished Si substrates, the second generation used silicon-on-sapphire substrates (SOS) [2]. The second generation, relying on an epitaxially grown silicon layer, overcomes the thickness nonuniformity of the first type. Moreover, the mesa-like shape of the second generation resonators prevents lateral heat diffusion, lowering switching power and eliminating interpixel thermal cross-talk. The second generation prototypes display optical bistability at much lower input powers than the first generation, but still need mW-switching powers.

We now have fabricated a third HEATOR type with a Silicon Implanted Oxide (SIMOX) substrate that overcomes the second-generation shortcomings [3]. The device structure that is depicted in figure 1 is obtained by implanting an oxide layer (D=0.43 μm) in a silicon substrate such that the Si-SiO_2-Si interface acts as a mirror with a reflectivity of R=0.55. Then three Si epilayers (layer 1: 10000Å p^+ 10^{18}-10^{19} cm^{-3}, layer 2: 45000Å non doped, layer 3: 5000Å n^+ 10^{18}-10^{19} cm^{-3}) are grown and we etch the mesa with RIE and standard lithographic techniques. Finally, a reflective dielectric coating (R=0.8) is deposited on top of the pixel thus increasing the finesse of the resonator cavity to F=3.3. If we etch the Si substrate right down to the SiO_2 layer, we can deposit on the bottom a coating with a reflective coefficient R=1, and on the top side a coating with R=0.9. In that case the finesse of the resonator would be F=12.2.

An efficient operation of these devices requires a high increase of the resonator's temperature

ΔT when illuminated. In order to gain insight into the temperature distribution within this structure and to optimize the temperature rise ΔT, we have developed a simulation program in which we use a finite-difference method to solve the partial differential equations that describe the heat transfer in the device. Besides the dynamical build up of the temperature in the resonator cavity (figure 2) the program also calculates at any instant the optical output of the device for a variable optical input. To that end it takes into account all the characteristics of the resonator. In our paper we show, using the heat transfer model, that these devices can display bistability at multi-microwatt optical bias power and that, when adequately dimensioned, cross-talk can be avoided such that they can be packed into dense arrays. Furthermore, we demonstrate that an appropriate geometrical design of the structure combined with proper heat sinking allows microsecond switching times. We compare experimental data with the results that follow from the numerical modeling and show that the scaling down of the resonator dimensions considerably decreases the required switching power. We investigate on phenomena such as critical slowing down and discuss the further improvements that can be made to these devices from the viewpoint of switching times, biasing powers and switching energies. We will show with experimental data that the use of thin Si-resonators allows the operation of these devices from 400nm to 1100 nm leading to a true wavelength-flexible, spectral linewidth tolerant operation. Finally, we will discuss the potentialities of this device as a smart pixel, when considering its integration with silicon LSI, MSI and VLSI circuitry.

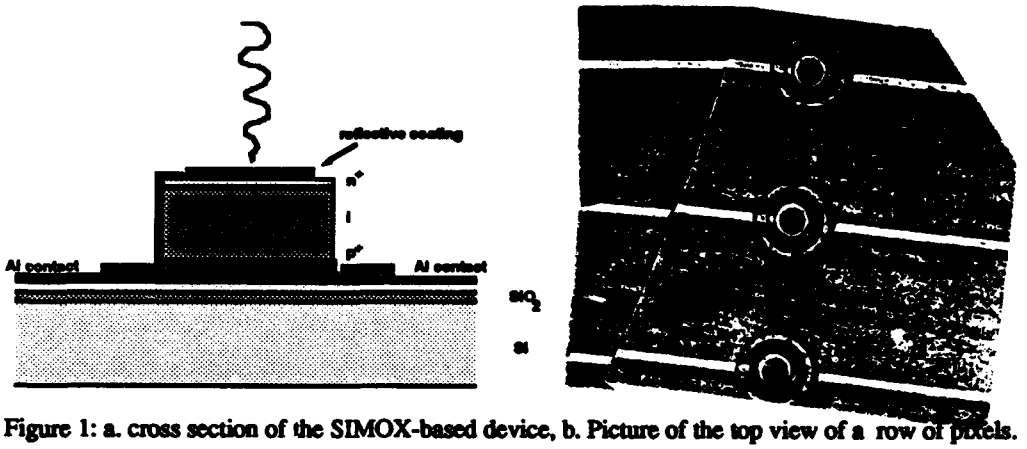


Figure 1: a. cross section of the SIMOX-based device, b. Picture of the top view of a row of pixels.

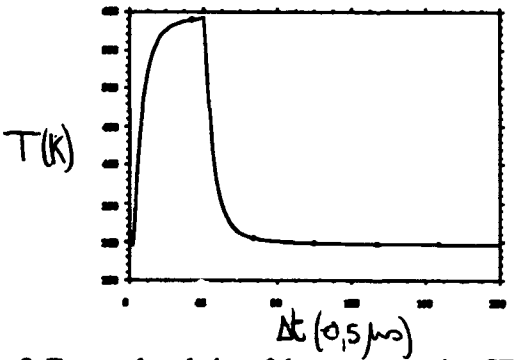


Figure 2: Temporal evolution of the temperature in a SIMOX-device.

[1] H. Thienpont, I. Van De Voorde, I. Verbesselt, W. Ranson, C. De Tandt, R. Vounckx and I. Veretennicoff, "Hybrid Electrically Assisted Thermo-Optic Resonators for Prototype Digital Optics: from element to array", *Optical Computing and Processing*, 1(2), pp. 145-155 (1991).
[2] H. Thienpont, W. Peiffer, N. Nieuborg, I. Veretennicoff, H. Dupont, R. Fernandez, Y. Bertic, W. Ranson, C. De Tandt, R. Vounckx, A. Koster, A. Laval, "Optical information processing planes with silicon technology", *International Conference on Optical Information Processing*, *SPIE* 2051, pp. 180-192 (1993).
[3] X.Xiao etal, IEEE Phot. Tech. Lett. ,Vol 3, No 3, 1991.

Photonic Devices Based on Nonlinear Excited-State Absorption

Chun-Fei Li, Lei Zhang, Rui-Bo Wang
Department of Physics, Harbin Institute of Technology
Harbin 150001, China

Summary

All-optical logic devices are imperative for the development of optical computing. Although semiconductor devices using resonant nonlinearity usually exhibit large Δn, their large linear absorption may cause low device throughput and undesirable thermal effects. Here we suggest a new kind of devices based on nonlinear excited-state absorption, which are advantageous for their low linear absorption, fast response and mirrorless structure. C_{60} and some metal-organic materials are employed to demonstrate the principle of such photonic devices.

A six-level model for organic molecule is proposed as shown in Fig.1. Photons with frequency ν off the peak of ground-state absorption are simultaneously absorbed by molecules in S_0, S_1, S_2 and T_1. Populations of n_0, n_1, n_2, n_T in S_0, S_1, S_2, T_1, and the photonic flux ϕ can be obtained from following equations:

$$(\partial/\partial t)n_1=\sigma_0\phi n_0-\sigma_1\phi n_1-K_{10}n_1-K_{ST}n_1+K_{21}n_2 \quad (1)$$
$$(\partial/\partial t)n_2=\sigma_1\phi n_1-\sigma_2\phi n_2-K_{21}n_2 \quad (2)$$
$$(\partial/\partial t)n_T=-\sigma_T\phi n_T-K_{T0}n_T+K_{ST}n_1 \quad (3)$$
$$N=n_0+n_1+n_2+n_T \quad (4)$$
$$(\partial/\partial z)\phi=(\sigma_0 n_0+\sigma_1 n_1+\sigma_2 n_2+\sigma_T n_T)\phi \quad (5)$$

where K_{ij} are transition probabilities, $\phi=I/h\nu$. Assume that $I=I_m(z)f(t)$, here $I_m(z)$ is the peak intensity at z, f(t) is temporal function of the pulse. In above equations n_2 can be neglected for ns laser pulses and n_T can be neglected for ps laser pulses.

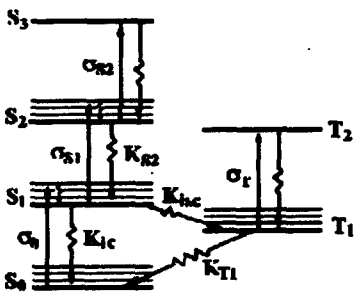


Fig.1 Energy-level structure

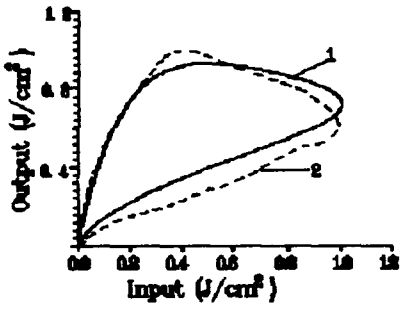


Fig.2 Transient absorptive optical bistability

Assume that a laser pulse with 15ns width (large than intersystem-crossing time constant) at 532nm are employed as the light source. For a copper phthalocyanine solution, we simulated the characteristics of transient absorptive optical bistability and the curve of output I(t,L) versus input I(t,0) by using Eq.(1)-(4). The calculated results are consistent with experimental data as illustrated in Fig.2.[1]

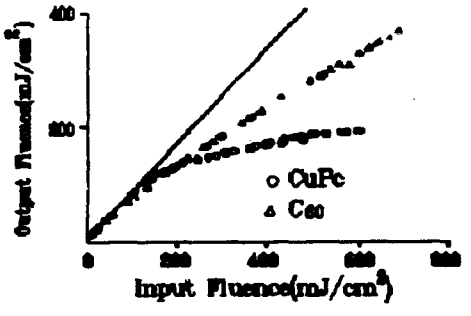


Fig.3 Characteristic curves of optical limiters

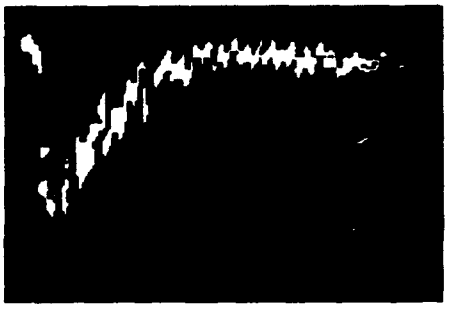


Fig.4a Experimental results for all-optical switching

Simulation of optical limiting in C_{60} solution, and transmission $T=F_L/F_0$ versus input fluence F_0 by using Eq.(1)-(5), are also consistent with experimental data (Fig.3)[2].

When a pulse laser with 15ns at 532nm pumps a C_{60} solution of toluene, a large population can be accumulated in T_1. If in the same time a CW laser diode beam at 747nm (coincides with absorption peak wavelength of excited state T_1) passes through the sample, photons of which will be intensively absorbed. So that the output intensity switches off. This all-optical switching process is shown in Fig.4 (a). The simulation can be made by using Eq.(1)-(4) for pump beam and Eq.5 for probe beam, as shown in Fig.4 (b)[2].

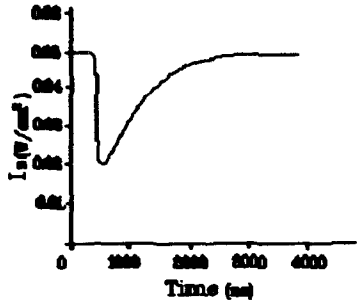


Fig.4b Calculated results for switching process in C

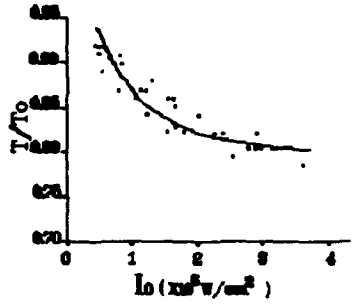


Fig.5 Relative transmission versus peak intensity of pumping beam

Fig.5 gives the simulated and experimental results of optical modulation and relative transmission of probe beam T/T_0 versus peak pumping intensity I_0. A design for "Exclusive AND" and "Exclusive OR" gates based on this characteristics is shown in Fig.6.[3].

When using 8ps pulses at 532nm to act on a cadmium texaphyrin solution we observed that reverse saturable absorption was exhibited only at low fluences. At high fluences, however, saturable absorption was appeared, as illustrated in Fig.7. The reason is that lifetimes of S_1 and S_2 in cadmium texaphyrin are comparable to laser pulse width, so n_2 can not be neglected, and $\sigma_2 < \sigma_1$[4]. The simulated results of T versus F_0 by using (1)-(5) agree well with experimental data. This kind of curve may be useful for optical logic operations in optical computing.

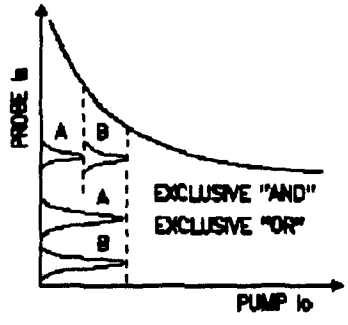


Fig.6 Principle of logic operations

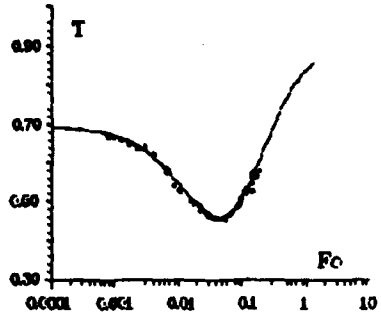


Fig.7 Experimental and theoretical results for cadmium texaphyrin

Reference

[1] Chun-Fei Li, Lei Zhang, Miao Yang, Hui Wang, and Yu-Xiao Wang, Physical Review A, 49, (1994).

[2] Chun-Fei Li, Yu-Xiao Wang, Feng-Yun Guo, Rui-Bo Wang, and Lei Zhang, ACTA PHYSICA SINICA, 42, 1236 (1993).

[3] Chun-Fei Li, Miao Yang, Feng-Yun Guo, Yu-Xiao Wang, and Kunu Tada, International Journal of Nonlinear Optical Physics, 2, (1993).

[4] Jin-Hai Si, Miao Yang, Yu-Xiao Wang, Lei Zhang, and Chun-Fei Li to be published.

Polychromatic all-optical gate based on second-order nonlinearity

V.P. Torchigin and A.E. Kobyakov

Scientific Computer Center, Russian Academy of Sciences, Moscow, Leninsky pr. 32A, 117334, Russia, tel. (095)-938-1893, fax (095)-938-6986, e-mail user@comcp.msk.su

A possibility of using known quasi-phase-matched second-harmonic generators as the main components of an all-optical gate for performing logical operations on WDM signals is considered. The main parameters of the gate are estimated.

The proposed approach enables the unique possibility of development of polychromatic all-optical gates for processing wave-division multiplexed (WDM) signals so that the overall rate of signal processing can coincide with the maximal bit-rate in a short optical communication line.

A schematic diagram of the proposed gate is shown in Fig.1. The horizontal nonlinear integrated-optics lightguide has several identical periodical domain inverted structures (PDIS), which are usually used in a well-known quasi-phase-matched second-harmonic generator (QPM SHG) [1]. Optical power enters in the input of the lightguide in the form of a periodical sequence of pulses with a carrier ω_p. The frequency selective directional couplers (DC) are used both for entering the logical signals *A*, *B*, and *C* with carriers ω_s ($\omega_s<\omega_p$) and for extraction of the result signals *X*, *Y*, and *Z* with the same carriers. The cross-transmission coefficient of the DC is close to one for the signals with the carrier ω_s and to zero for the signals with the carrier ω_p. In such a device the pump ω_p, signal ω_s, and idle ω_i carriers satisfy the following conditions of quasi-phase-matching:

$\Delta k=2\pi/\Lambda$ (1), $\omega_p=\omega_s+\omega_i$ (2), where $\Delta k=(n(\omega_p)\omega_p-n(\omega_s)\omega_s-n(\omega_i)\omega_i)/c$ (3),

$n(\omega)$ is an effective refractive index of the lightguide, Λ is the period of PDIS in the lightguide, *c* is the velocity of light in vacuum. In the particular case when $\omega_s=\omega_i=\omega_p/2$ equation (1) represents the QPM condition for an SHG.

As the waves with the carriers ω_p, ω_s and arbitrary phases enter the PDIS lightguide the interaction mentioned manifests itself in appearing the idle wave with the carrier ω_i and increase in the intensity of the waves with the carriers ω_s and ω_i and in decrease in the intensity of the wave with the carrier ω_p [2]. In this case the PDIS lightguide is used as an optical parametric traveling wave amplifier (OPTWA). The intensity of the wave with the carrier ω_p vanishes on some distance. The length of the OPTWA is chosen equal to this distance, so that there is no wave with the carrier ω_p at its output. This situation takes place if a small control signal with the carrier ω_s enters in the input of the OPTWA.

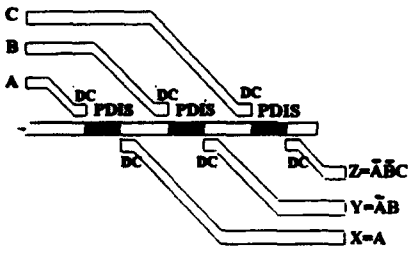


Fig. 1 Schematic diagram of the gate

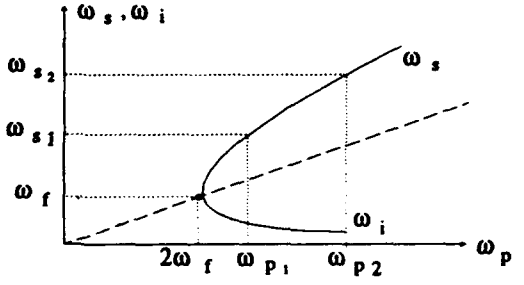


Fig. 2 Dependence of the carriers ω_s and ω_i of signal and idle waves on the carrier ω_p of pump in an OPTWA if the QPM condition is satisfied

The signal with the carrier ω_s is present at the output X only when the control signal A with the carrier ω_s exists at the input A, i.e., the output signal corresponds to the input one amplified by power. Analogously, the signal with the carrier ω_s presents at the output Y only in the absence of the signal A and presence of the signal B, i.e., the result signal at the output Y corresponds to the logical function $\bar{A}B$. Generally, the gate can have N logical inputs $A,B,C,...$ for control signals and N logical outputs for result signals $X,Y,Z,...$ The result signals correspond to the following functions: $X=A$, $Y=\bar{A}B$, $Z=\bar{A}\bar{B}C$,... It is easily seen that even the gate which has only two logical outputs is boolean complete.

The usual well-known DCs can be used for physical realization of the gate. Because localization of light wave field in a cross-section of a lightguide decreases on lower carriers, the beating length L_s for a wave with the carrier ω_s can be obtained essentially smaller than L_p for a wave with the carrier ω_p. The DC length is chosen equal to $L_s/2$ so that the cross transmission coefficient is equal to one for the wave with the carrier ω_s. As $L_s<<L_p$, for a wave with the carrier ω_p this coefficient is close to zero.

One more essential advantage of the gate is its capability of simultaneous processing several sets of signals. Actually, QPM condition (1) can be satisfied at the same time for several sets of signals ω_p and ω_s, which can be chosen so that Δk be constant. Therefore, several signals ω_{sj} (j=1, 2, ..., N) can be simultaneously amplified. In other words, any SHG with $\omega_s=\omega_p/2$ for which equation (1) is satisfied can be used as an OPTWA with other values of ω_p and ω_s for which (1) is also valid.

In the particular case when $n(\omega)$ is a linear function of ω, dependence of ω_s and ω_i on ω_p is shown in Fig.2. The carrier ω_f corresponds to the fundamental harmonic when an OPTWA is used as an SHG, for $\omega_p>2\omega_f$ each value of ω_p corresponds to the only value of ω_s and vice versa. One should note that for pairs ω_{pj} and ω_{sk} ($j\neq k$) QPM condition is not satisfied and the average effect of their interaction is equal to zero.

The power gain of the gate is equal approximately to that of an OPTWA and can exceed 20-30 dB. The contrast ratio of the gate is larger than its power gain by the value of losses in the PDIS lightguide. The bit rate F_1 is determined by the difference in group velocities of pulses with the carriers ω_p and ω_s in an OPTWA and by its bandwidth. Assuming that the difference in velocities is equal to 8% [3] and the bandwidth of an OPTWA having the length of about 1 cm is ~0.2 nm [3], we obtain $F_1\cong 25$ GHz. The maximal value of N is determined by the expression $N=F_t/F_1$, where F_t is the total bandwidth of an OPTWA for various pumps. In this case $N\cong 10^3$. The pump power for 1 cm-length-OPTWA is equal to several Watts, the control signal power is 20-30 dB less.

References

1. Arvidsson, G., Laurell, F., and Webjorn, J.: 'Compact light sources based on frequency conversion in lithium niobate and other nonlinear optical crystals', Proc. of the 6-th European Conf. on Integr. Optics ESIO-93, Apr. 18-22, 1993, Neuchatel, Switzerland, pp. 3-23 - 3-25

2. Bloembergen, N.: 'Nonlinear optics' (W. A. Benjamin, Inc. New York-Amsterdam, 1965)

3. Yamamoto, K., Mizuuchi, K., and Taniuchi, T.: 'Quasi-Phase-Matched Second Harmonic Generation in a LiTaO Waveguide', IEEE Journ. of Quant. Electron., 1992, 28, 9, pp. 1909-1914

All-optical Bistable Devices (ORION) using Laser Diodes coupled to Interference Filters of Narrow Spectral Bandwidth

Yoshinobu MAEDA

Light and Material Group, PRESTO, Research Development Corporation of Japan (JRDC).
Department of Information and Control Engineering, Toyota Technological Institute,
2-12-1 Hisakata, Tempaku, Nagoya 468, Japan. Phone: 81-52-802-1111

Abstract: All-optical bistable devices were demonstrated by using the longitudinal mode hopping of the laser diode and the narrow transmission spectrum of an interference filter. Optical switch-on and -off were confirmed by directly injecting a dye laser.

Optical bistability in laser diodes (LDs) is a most interesting subject because of its many advantages; for example, such diodes have optical gain, can provide large fan-out and can have operating times less than a sub-nano second. Bistable optical devices were confirmed by using the longitudinal mode hopping of the laser diode and the narrow absorption band of erbium in an yttrium aluminum garnet crystal (Er:YAG), and referred to as ORION (Optical logic devices using the Red shift of a laser diode and Inversion in Optical absorbers (or filters) of a Narrow spectral bandwidth).[1-3] However, when using an absorber such as an Er:YAG crystal as reported earlier, no absorption wavelength can be utilized other than that specific to the absorber. Furthermore, there was a disadvantage that ceramics like YAG hardly conform to semiconductor. This paper shows that the ORION device was successfully demonstrated by using an artificial dielectric interference filter in place of the natural absorber such as the Er:YAG. By using the interference filters in this study, it becomes possible to use an arbitrary wavelength and form the filter on semiconductors using vacuum evaporation with ease. The optical switch-on and -off phenomena were observed by direct injection of an external dye laser beam into the LD.

The light source was a high power AlGaAs laser diode operating in the single transverse mode. The threshold current is 50mA, the operating current at optical output of 30mW is 100mA and the slope efficiency is 0.6mW/mA. Its oscillation wavelength was kept stable by adjusting the temperature of the laser-head. The dielectric interference filter was formed by vacuum evaporating 11 layers of 866Å of TiO_2 and 1335Å of SiO_2 alternately on a glass substrate heated to 300°C, then placing 2670Å of SiO_2 as a spacer, and adding another 11 layers of TiO_2 and SiO_2 alternately with the same thicknesses. The refractive indices of TiO_2 and SiO_2 films were 2.25 and 1.46, respectively. Optical waveforms were determined with a digital oscilloscope with a bandwidth of 1GHz and a photodetector with a rise time of 90psec. An external dye laser excited with a nitrogen (N_2) laser was injected through a beam splitter into the LD. The dye laser produced a

beam with a central wavelength of 546nm, a spectral width of 2nm and a pulse width of 500psec.

Figure 1 shows relationship after transmission through the interference filter between the laser power and the injection current of the LD in continuous operation measured with an optical power-meter. It was observed that the bistable curve fell rapidly at 82mA as the injection current increased, and in contrast, rose rapidly 78mA when it decreased.

Figure 2(a) exhibits the optical intensity variation after transmission through the filter when the pulsed dye laser in Fig.2(b) was injected into the LD during continuous oscillation at an injection current of 79mA (Point A in Fig.1). The optical switch-on and -off are observed when the trigger light pulse of Fig.2(b) is applied. The rise and fall time are around 1nsec and these are limited by the bandwidth of the oscilloscope.

In summary, since a hysteresis characteristic exists in the relationship between the wavelength and the injection current of the LD, an optical bistability was observed in this system. In addition, the optical switch-on and -off phenomena were observed by directly injecting a pulse 500psec wide into an external dye laser. It was confirmed that the device could convert changes in the wavelength of the LD into changes in intensity transmitting it through the filter.

References:

1) Y. Maeda, Rev. Laser Eng., 21, *577 (1993).*

2) Y. Maeda, Tech. Digest in Conference on Laser and Electro-Optics, 11, *CThS62 (1993).*

3) Y. Maeda, Appl. Phys. Lett., 62, *3393 (1993).*

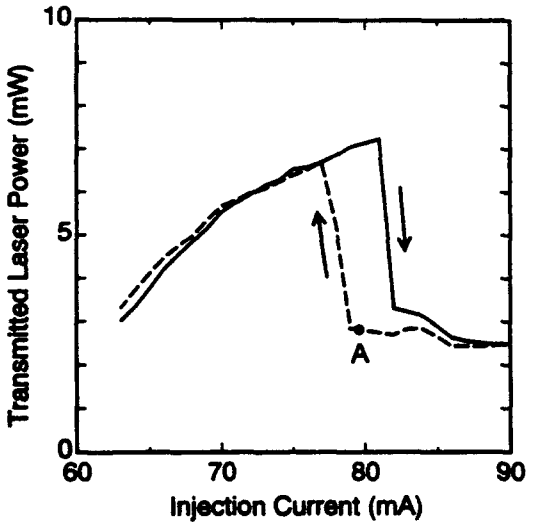


Fig.1 Laser intensity after transmission through the filter versus injection curren' of the laser diode characteristics sh' hysteresis.

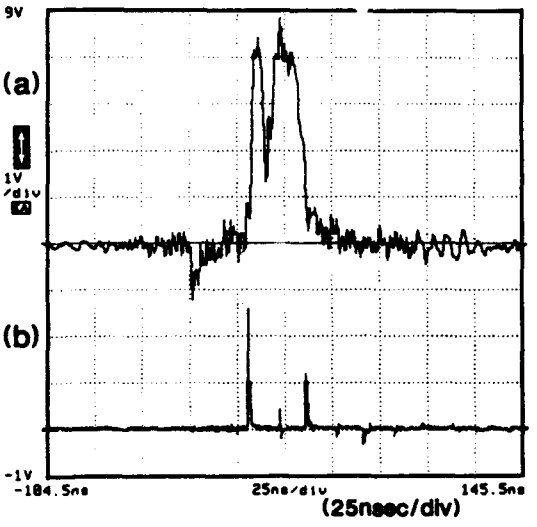


Fig.2(a): Optical intensity variation after transmission through the interference filter by applying the trigger light pulse into the laser diode. (b): Trigger light pulse of dye laser.

Large Reduction of Saturation Carrier Densities by Strain in InGaAs/AlGaAs Quantum Wells

M H Moloney and J Hegarty
Optronics Ireland Research Centre, Department of Pure and Applied Physics, Trinity College, Dublin 2, Ireland
Tel : +353-1-7021569 Fax : +353-1-6711759

L Buydens and P Demeester
I.M.E.C., Rijkuniversiteit Gent, Sint-Pieternieuwstraat, 41, B9000 Gent, Belgium

Abstract: *The carrier densities needed to saturate excitons in strained $In_xGa_{1-x}As$ /GaAlAs quantum wells decreases with increasing x and hence with increasing strain. A factor of 10 reduction for x = 0.11 compared to x = 0 occurs. Implications for nonlinear devices are discussed.*

The viability of all-optical computing depends critically on finding a material structure with strong enough nonlinearity for array devices along with an optimised architecture. Semiconductor quantum wells have shown good promise due to excitonic enhancement at resonance near the bandedge. While the densities of carriers necessary to saturate the excitons at room temperature are low, there is still need for much lower densities. In this paper, we show that almost an order of magnitude reduction in saturation densities can be achieved by introducing strain into the quantum well. We show that for 0.11 In in InGaAs/GaAlAs fully strained wells, the saturation density is $< 1 \times 10^{17}$ cm^{-3} compared to $\sim 8 \times 10^{17}$ cm^{-3} in unstrained GaAs wells. Previously only factors of 2 reduction have been observed in this system [1, 2].

Samples of $In_xGa_{1-x}As$/GaAlAs quantum wells were grown by MOVPE with x = 0, 0.03, 0.11 and 0.15, the latter three labelled S_1 to S_3, respectively in Figure 1. Ten periods of 8 nm/8 nm wells/barriers were grown in each sample. Samples with x = 0.03 and 0.11 were fully strained, while the x = 0.15 sample was partially strain relieved, as shown by cross-hatching under a Nomarskii microscope. Al was used in the barrier to increase the well depths. The carrier lifetimes in these InGaAs wells with AlGaAs barriers have been shown to be uniformly short [3], about 0.5 nsec, and independent of In concentration or strain relief. We attribute the effect to defects in the AlGaAs barriers. To probe the effect of the strain on the nonlinearity, we measure and calculate the saturation carrier density instead of saturation intensity, since the latter also includes lifetime effects. To do this, we measure the absorption spectra near the exciton resonance in each sample as a function of input optical intensity I, and from the absorption coefficient $\alpha(\lambda, I)$ we can calculate the carrier density $N(\lambda, I) = \alpha(\lambda, I)\,\tau / E(\lambda)$ where τ is the measured carrier lifetime independent of intensity over the range used, and $E(\lambda)$ is the photon excitation energy. The saturation of the absorption at the exciton peak follows $\alpha(I) = \alpha(o) / (1 + N/N_{sat})$ where N_{sat} is the saturation carrier density. This equation is only valid when far from intensities at which absorption switches over to gain. Figure 1 shows a plot of N_{sat} against In concentration for the four samples measured. N_{sat} for x = 0 is within the range of values measured by other groups and the x = 0.03 is similar to this. A large decrease of a factor of 8 in N_{sat} occurs between x = 0.03 and 0.11 showing that strain has a dramatic effect on nonlinearity as expected from

modification of the valence band density of states by strain. The 0.15 sample is similar to the 0.11 sample and this can be attributed to the partial strain relief of this sample. Also shown is a value of N_{sat} derived from a previous experiment [1] on an asymmetric Fabry-Perot modulator with a large number (30) of x = 0.1 In wells. The large value for N_{sat} is explained by the significant measured strain relief in that sample. The value of N_{sat} reported in Ref 2 for a sample similar to S_2 is only about a factor of 2 less than in GaAs wells indicating possible strain relief in that sample also.

In summary, a reduction of almost a factor of 10 in the saturation carrier densities for excitons in InGaAs by strain has been observed. This is expected from the reduced density of hole states at the valence band edge by strain and consequently an enhancement of the effect of phase space filling for exciton saturation. The data indicate that, for higher In concentrations and full strain, N_{sat} may keep on decreasing. This would have a large impact on devices based on exciton saturation and increase their attractiveness for optical computing architectures. To avail of this large effect, however, the problem of short carrier lifetime with AlGaAs barriers because of defects will need to be resolved. For higher In concentrations, on the other hand, GaAs barriers may be used without significant thermal activation of the carriers over the barrier occurring, and hence without deleterious effects on carrier lifetime and sample heating.

References:

1. M H Moloney, J F Heffernan, J Hegarty, R Grey and J Woodhead, Applied Physics Letters 63, 435 (1993).
2. R Jin, K Okada, G Khitrova, H M Gibbs, M Pereira, S W Koch and N Peyghambarian, Applied Physics Letters 61, 1745 (1992).
3. M H Moloney, J Hegarty, L Buydens, P Demeester, R Grey and J Woodhead, Applied Physics Letters 62, 3327 (1993).

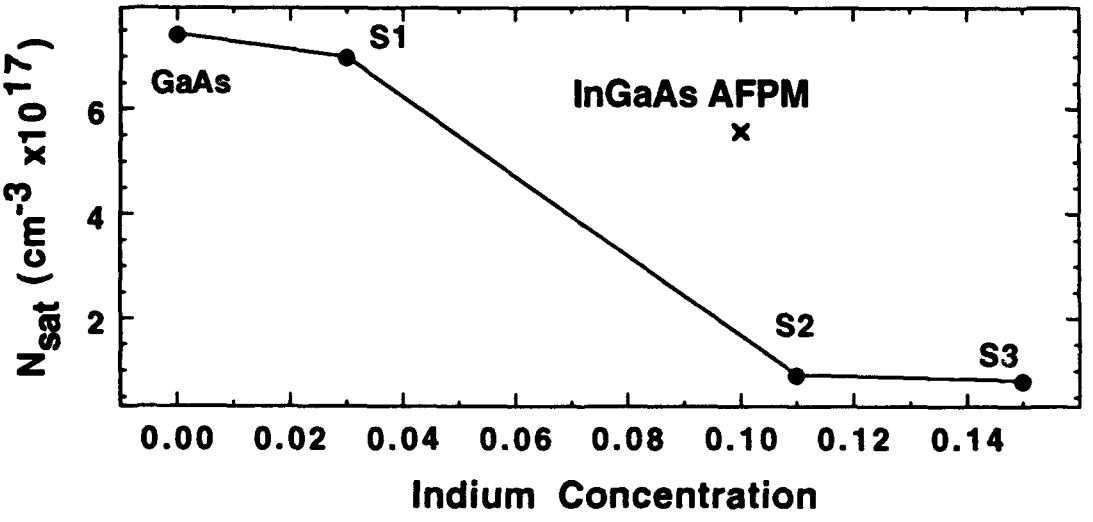


Figure 1: Plot of saturation carrier density against Indium concentration x for x=0.03 (S_1), 0.11 (S_2) and 0.15 (S_3).

Strong Optical Nonlinearities of Semiconductor Quantum Dots and Wires.

V. Dneprovskii, V. Karavanskii*, V. Klimov, D. Okorokov, Ju. Vandyshev.
Physics Faculty, Moscow State University, 119899 Moscow,Russia, Tel:(095)9393731
**Institute of General Physics, 117942 Moscow, Russia, Tel:(095)1328226*

Strong and fast optical nonlinearities were detected in CdSe, CdSSe nanocrystals and porous silicon. The observed phenomena were explained in terms of filling of quantum well energy levels by carriers excited by picosecond laser pulses.

Nonlinear optical properties of semiconductor nanocrystals and wires of nanometer scale size (quantum dots - QD and quantum wires - QWr) are of significant interest in view of their possible applications in optical computing , as well as from the fundamental point of view. The spatial confinement of carriers in these objects results in the drastic modification of the energy spectrum (the quasi-continuous spectrum of bulk semiconductor is replaced by the discrete one) and supposedly leads to the enhancement of optical nonlinearities. We have studied nonlinear optical transmission spectra of CdSe, CdSSe nanocrystals and porous silicon wires using time-resolved pump-probe technique. Powerful picosecond (20 ps) pulses of the second harmonic of a mode-locked Nd-YAG laser excited the samples; the delayed pulses of picosecond continuum were used to probe the transmission.

The investigated samples of CdSe, CdSSe nanocrystals embedded in glass matrix (semiconductor doped glasses - SDG) were prepared by the method of secondary heat treatment and contained crystallites of the average radius R less than 10nm. Free-standing porous silicon layers were prepared by electrochemical etching of n-type (111) Si wafers; the films were removed from the substrate by applying a short electrical pulse. Atomic force microscopy data indicates that our porous Si samples contain thin silicon wires of 3-5 nm diameter. The absorption edge in CdSe,CdSSe QD and Si QWr is shifted relatively to the absorption edge of the corresponding bulk semiconductor due to the quantum size effect.

Photoexcitation resulted in the significant bleaching above the absorption edge of quantum dots and wires. Up to three bleaching bands have been observed in the nonlinear transmission spectra of CdSe,CdSSe nanocrystals. We could resolve the thermalization of carriers (transitions from higher energy levels to the lower one seen as the changes of the relative amplitude of the bleaching bands) followed by the recombination of electrons and holes. A sufficient cuttoff of the intraband relaxation time compared with the bulk semiconductor was observed. The spectral position of bleaching bands and their kinetics allowed to attribute this bleaching to the filling of energy levels of spatially confined electrons and holes by photoexcited carriers: saturation of 1S-1S, 1P-1P and even higher transitions was clearly seen. It is important that these bands could not be resolved in the linear absorption spectra (probably because of the strong inhomogeneous broadening due to the size distribution of nanocrystals).

The obtained values of $\chi^{(3)}$(10^{-9}-10^{-10}esu) for SDG samples are much greater than for "classical" nonresonant nonlinearities.

The bleaching bands corresponding to the transitions between the levels of size quantization were observed in the nonlinear transmission spectra of porous crystalline Si wires while the linear absorption spectra had no perculiarities dealt with space confinement probably because of strong inhomogeneous broadening caused by size dispersion of wires.

The induced decrease of absorption was explained by filling of the size-quantized energy levels with nonequilibrium carriers (saturation effect). Instead of the indirect gap of crystalline bulk silicon, the band structure of the wires exhibits a direct gap - the projections of four valey minima of bulk silicon oriented along (100) and (010) directions onto the wire axis are at the zone center. The energies of two bleaching bands correspond to that of size-quantized wire with about 3x3 nm^2 cross section (the lowest transitions E^h_{11}, E^l_{11} for electrons with effective mass in (110) and ($\bar{1}10$) confinement directions and heavy and light holes). Probably only part of the wires with proper cross section (proper energy spectra) were resonantly excited by the laser beam. The E^l_{11}-band could be seen only at zero delay of the probe pulse; the relaxation time of E^h_{11}-band for porous Si (300 K) was about 40 ps.

The values (~10^{-8}esu) and dispersion of imaginary part of third order nonlinear susceptibility $\chi^{(3)}$ of porous Si were obtained.

The observed strong and fast nonlinearities in Si quantum wires and CdSe, CdSSe quantum dots make possible future applications of these materials for high speed optical switching.

Carrier Heating Induced Optical Bistability in Degenerate Semiconductors and Quantum-Well Structures

V.I. Tolstikhin[1], and M. Willander

Department of Physics and Measurement Technology, Linköping University S-581 83, Linköping SWEDEN.
Tel.: +46-013-282473, Fax.: +46-013-137568, E-mail: vit@ifm.liu.se

Abstract. *Carrier heating induced suppression of band filling has been shown as an effective mechanism of optical nonlinearity in bulk and quantum well III-V semiconductor structures, which leads to both absorption and dispersion types of optical bistability and all-optical switching in a picosecond time-scale.*

Photonic switching in III-V heterostructures in the spectral region near the fundamental absorption edge attracts much attention because of its great capability for optical computing and information processing [1]. An important line of activity in the field is a search for novel physical mechanisms of optical nonlinearity (ON), those can improve characteristics of related digital systems, in particular their speed. Here we discuss the carrier heating induced suppression of band filling as such a mechanism in both bulk semiconductors (BS) and quantum-well structures (QWS), that leads to all-optical switching in a picosecond time-scale.

The nature and the main features of this ON may be explained as follows. Consider degenerate n-type BS or QWS with thermalized 3D or 2D electron gas and Fermi quasilevel Φ well above the conduction band edge or bottom of the ground subband, respectively. The optical absorption is determined by both intraband and interband radiative transitions. For photon energy $\hbar\omega$, related to direct interband transition into the state a little bit below Fermi quasilevel, exciton effects play no role and the absorption coefficient A_ω may be written as:

$$A_\omega = \sigma_\omega N + \alpha_\omega [1 - f(\varepsilon_\omega)].$$

Here σ_ω is the cross-section (per one electron) of intraband absorption, N is the carrier concentration, α_ω is the interband absorption coefficient when degeneracy is lifted, f is the Fermi-Dirac distribution function, $\varepsilon_\omega = (\mu/m)(\hbar\omega - \varepsilon_g)$, where μ and m are the reduced mass of electron-hole pair and effective mass of electron, respectively, ε_g is the energy bandgap. In a case of QWS A_ω, N, and α_ω all are thought as being averaged over the period of a structure, while ε_g - as the energy gap between extrema of ground electron and hole subbands. Usually $\alpha_\omega \gg \sigma_\omega N$ and so interband transitions give the main contribution if $f \to 0$, i.e. in the absence of degeneracy. Otherwise, if Fermi quasilevel Φ satisfies inequalities:

$$\Phi - \varepsilon_\omega > T \ln\left(\frac{\alpha_\omega}{\sigma_\omega N}\right) > T,$$

where T is the effective temperature of carriers, $f(\varepsilon_\omega) \to 1$, i.e. interband absorption gets weakened by band filling, and $A_\omega \approx \sigma_\omega N$. However, intraband transitions lead to generation of energetic carriers and under the thermalization conditions, those are typical for a high-density degenerate electron gas, they give rise to increase in temperature of a Fermi sea as a whole. The larger intensity of light, the stronger carrier heating and when $T > \Phi - \varepsilon_\omega$ the ultimate case of $f(\varepsilon_\omega) \to 0.5$ and $A_\omega \approx 0.5\alpha_\omega$ is achieved. Thus, we have an ON with increasing absorption caused by carrier heating suppression of band filling and characterized by a nearly step-

---

[1]V.I. Tolstikhin is on leave from the Institute of Radio Engineering & Electronics of the Russian Academy of Sciences, 11 Mokhovaya, Moscow 103907 RUSSIA.

function dependence of absorption coefficient A_ω on light intensity I_ω. Its value needed for switching from weak (intraband) to strong (interband) absorption may be estimated as:

$$I_\omega \cong \zeta \frac{T_0}{\sigma_\omega \tau_T} \ln\left(\frac{\alpha_\omega}{2\sigma_\omega N}\right),$$

where T_0 and τ_T are the dark temperature and characteristic cooling time of carriers, ζ is numerical parameter, different in cases of BS and QWS. The last one is more attractive from the power point of view, because of quantum confinement makes possible the direct intraband transitions (from ground to continuum state, for example) and so enhances the free-carrier absorption. For a typical *GaInAsP/InP* QWS parameters ($\sigma_\omega \approx 10^{-15}\,cm^2$, $\tau_T \approx 3\,ps$, $N \approx 3 \cdot 10^{17}\,cm^{-3}$, and $\alpha_\omega \approx 10^4\,cm^{-1}$) we find that at room temperature switching from weak to strong absorption occurs at $I_\omega \cong 10^6\,W/cm^2$. Even this value, related to full eliminating of band filling effect, seems to be not an extremely large, but really only the partial suppression of band filling is needed for optical switching. The speed of switching from weak to strong absorption is determined by thermalisation of energetic carriers, while the speed of a back switching is limited by the rate of cooling of a Fermi sea. Under the actual conditions both processes lead to a time delay in a few picoseconds only and so described mechanism of ON allows to improve speed of switching compared to any ones involving bipolar generation and accompanying slow recombination processes [1].

To justify the adduced qualitative scenario we performed the detailed theoretical study and numerical simulation of carrier heating induced ON and optical bistability (OB) in doped *GaInAsP/InP* BS and QWS. In a case of BS the impurity-assistant indirect transitions are assumed as being responsible for intraband absorption. They are described under the second order of perturbation theory, and arbitrary degeneracy as well as plasma screening are taken into account. In a case of QWS the direct radiative transitions from ground subband to continuum are considered as a reason for intraband absorption. For their description the convenient envelope function approximation is employed, but spatial variations of a longitudinal effective mass and quantum-size effects in the continuum states also are involved into consideration. The results of numerical calculations are presented in the form of photon energy and carrier temperature dependencies of material absorption coefficient and refractive index (determined trough the Kramers-Kronig transformation). They show that the main features of temperature ON in degenerate narrow-gap semiconductors as *n*-type *GaInAsP/InP* (both BS and QWS) – the red-shift of fundamental absorption edge and the nearly step-function variation of $A_\omega(T)$ – are analogous (with interchange of T and N) to the features of well-known concentration ON in undoped wide-gap semiconductors of the type *CdS* [2]. At the same time, carrier temperature induced ON is faster than carrier concentration induced ON in the recombination to cooling times ratio, i.e. approximately in three orders of magnitude.

Carrier heating induced OB in BS and QWS is studied in vertical and waveguide geometry, respectively (the radiation in a waveguide is assumed TM polarized). So far as generation of nonequilibrium carriers is unimportant under the actual conditions and both absorption coefficient and propagation constant are determined by carrier temperature only, the self-consistent treatment of a nonlinear light-carrier interaction is based on the coupled set of electron thermal conductivity and light propagation equations. Also the nonequilibrium phonon effects are taken into account as leading to a lag in the energy relaxation of a dense electron gas and so having substantial influence on carrier temperature. Then, two ultimate cases in the conditions for appearance of OB are distinguished, those relate to resonatorless OB due to increasing absorption and dispersion type OB in nonlinear asymmetric resonator. The numerical simulation is carried out for each of which, that shows the occurrence of hysteresis in the power transmission characteristics and the possibility of all-optical switching in a picosecond time-scale. It is found, that the lowest required intensity of the incident light corresponds to the case of dispersion type OB in a QWS asymmetric waveguide resonator.

References. 1. S.W. Koch, N. Peghambarian, and H.M. Gibbs. *J. Appl. Phys.*, **63**, R1 (1988).
2. S.W. Koch, H.E. Schmidt, and H. Haug. *Appl. Phys. Lett.*, **45**, 932 (1984).

Diffraction kinetics of electronic and thermal transient gratings in GaAs epilayers and GaAs/GaAlAs multi-quantum wells.

N. Gouaichault, L. Legratiet, E. Bedel, C. Fontaine, J.L. Iehl,
R. Grac, M. Pugnet and J.H. Collet,
Laboratoire d'Automatique et d'Analyse des Systèmes
du Centre National de la Recherche Scientifique,
7, Avenue du Colonel Roche- 31077 - Toulouse Cedex- France

Abstract:
Diffraction kinetics of transient gratings in GaAs epilayers and GaAs/GaAlAs multi-quantum wells at room temperature are reported. Samples are prepared by lift-off epitaxy. The results are interpreted in terms of time separation of the electronic and thermal contributions .

SUMMARY

The aim of this work was to study the subnanosecond diffraction capabilities of GaAs epilayers and GaAs/GaAlAs multi-quantum wells at room temperature. The epitaxial structures were grafted onto glass slides by means of the lift-off epitaxy technique. Diffraction kinetics of transient gratings were measured using the first order diffraction in the Raman-Nath configuration.

Experimental set-up: Pulses were generated directly at the wavelength 1.064 μm by an actively mode-locked Nd:YAG laser. Pulses at the wavelength 0.532 μm were generated by frequency doubling in KDP crystals. The duration of the pulses was approximately 30 ps. These pulses synchronously pump a dye laser operating in the range (825-850 nm). The duration of the pulses was approximately 15-20 ps.Two equal energy pump pulses at the wavelength 0.532 μm (P1 and P2) interacted inside the sample to produce transient gratings. The external angle between these two pump beams was $2\theta = 0.1$ radian, corresponding to a grating period Λ of 10 μm. The grating was then read by a probe pulse (T) generated by the dye laser and directed in normal incidence to the sample surface. The probe pulse was delayed with respect to the pump pulses P1 and P2. The pump and probe beam sections were limited by a circular diaphragm stuck on the sample. The diameter of the hole was 1mm.The pump pulses energy was varied in the range 1-10 mJ/cm^2 . The probe pulse energy was lower than 0.1 mJ/cm^2.We measured the energy of the first order diffracted pulse versus the probe delay. A diffraction kinetics is reported in Fig.1.

Samples preparation:
Active multi-quantum well epitaxial structures on transparent substrates were achieved in two steps. First, the structures were grown on GaAs substrates by molecular beam epitaxy. They consist of 80 periods of alternating GaAs wells and (Ga,Al)As barriers, whose thicknesses are 9.6 nm and 13 nm respectively. Second, the epitaxial structures were removed from their substrates and grafted onto glass slides by means of the lift-off epitaxy technique.

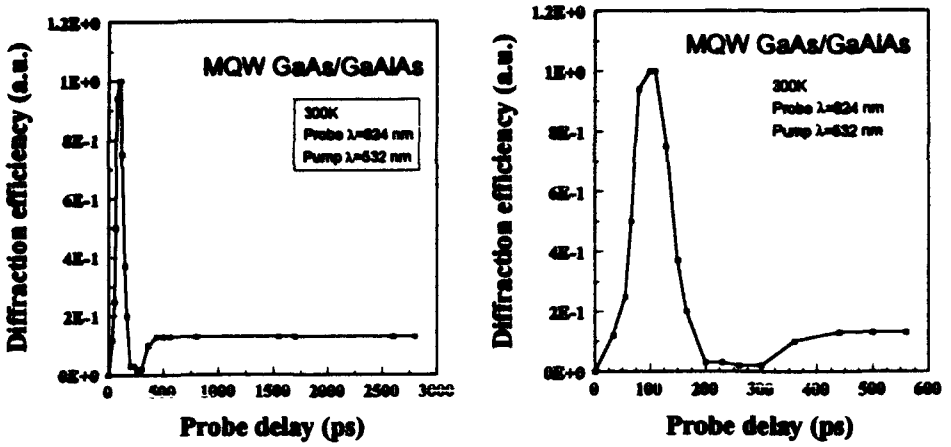


Fig. 1: Diffraction kinetics in the first order Raman-Nath configuration measured on multi-quantum wells GaAs/GaAlAs. The pump pulse energy for P1 and P2 are respectively 4 mJ/cm^2 and 2 mJ/cm^2 .

Experimental results:

The diffraction kinetics exhibit a peak during the first 200 ps and then a minimum within the interval 200-300 ps. The diffracted pulse is very unstable in this late interval due to the competition between several opposite processes (each reported data point has been averaged over 20 pulses). After 300 ps the energy of the diffracted pulse rises up to a stable value.

Interpretation:

The peak in the curve of Fig.1 is due to an electronic process. The presence of the electron-hole plasma induces a decrease of the optical index in the illuminated fringes. For long delays, the thermal contribution is dominant and produces an increase of the optical index in the illuminated fringes. The interval (200-300 ps) corresponds to the change of sign of the optical index. A model will be presented to support this interpretation.

In present work, differents wavelengths for the pump pulses are used in order to vary the penetration depth of the pump.

These results are only a part of a more general study developped in our laboratory in order to use GaAs epilayers and GaAs/GaAlAs multi-quantum wells for all-optical interconnects.

Absorption and refractive nonlinearity in heavily-doped GaAs and InP below the fundamental absorption edge

I.A. Utkin, V.L.Malevich, F.V.Karpushko

Division for Optical Problems in Information Technologies
Academy of Sciences of Belarus
P.O.Box No.1, 220072, Minsk, Belarus
0172/39 58 82 (tel), 0172/32 45 53 (fax)
E-mail: dopit%bas02.basnet.belpak.minsk.by@demos.su

Abstract. Optical nonlinearity in the vicinity of fundamental absorption edge in heavily-doped n-GaAs and n-InP has been experimentally investigated in details. The theoretical analysis concerning the possible mechanisms of nonlinearity observed is presented.

By an earlier date it was reported [1-3] that heavily-doped semiconductors A^3B^5 exhibited high potentiality for use in bistable Fabry-Perot switching devices. The nonlinear optical properties of such semiconductors need to be understood in details. In this paper we report the results of our further experimental investigations and some theoretical considerations of the optical nonlinearity in heavily-doped bulk samples of GaAs and InP (the concentrations of shallow donors $n \approx 10^{18} cm^{-3}$) in the vicinity of fundamental absorption edge. This spectral region is of particular interest because of the maximum of the nonlinear response observed. We have used both the technique of saturation absorption (to determine nonlinear absorption changes) and self-diffraction experiments (to determine refractive index changes). The experiments have been carried out by using 8 ns laser pulses, generated by a tunable color-center laser. All of the experiments were conducted at room temperatures.

i. The transmission spectra of the semiconductor samples at incident light power varied from 10^3 to 10^6 W/cm^2 were measured. The effect of optical bleaching below the band edge has been observed. This effect is much greater in samples with high concentration of impurity ($n \geq 10^{18}$ cm^{-3}) as compared with medium and slightly doped ones. The nonlinear response in absorption decreases with the increasing of a wavelength. For instance, in n-InP:Sn sample ($n \approx 10^{18} cm^{-3}$) the saturation intensity increases from 0.17 MW/cm^2 at wavelength 935 nm to 0.88 MW/cm^2 at 955 nm). To the contrast, in semi-insulating samples the increase of absorption has been observed in the same spectral region.

ii. The self-diffraction measurements have been carried out at the

conditions of the Raman-Nath diffraction. In most experiments the multy-order diffraction (up to the fourth diffraction order) took place. The spectral and energy dependencies for the 1st, 2d and 3d diffraction orders were measured for a number of doped semiconductor samples. It has been found that the self-diffraction efficiency reaches the maximum at wavelengths slightly below the band edge. Our estimates give the value of nonlinear refraction index change of about 0.002 at incident power of 200 KW/cm^2 for InP:Sn ($n=10^{18}cm^{-3}$).

iii. Theoretical analysis of possible mechanisms that are responsible for the nonlinear optical absorption observed is presented. The nonlinearity considered is assumed to involve the following effects: band filling, band gap shrinkage and screening of randomly distributed impurity potential, as a result of optically generated electron-hole plasma. It is supposed that the nonlinear optical absorption can be analyzed on the basis of the theory of linear interband optical absorption in case of disordered potential [4], by taking into account the dependencies of semiconductor parameters, such as band gap energy, electron and hole Fermi quasi-levels and screening length, on the density of photogenerated carriers. This method enables us to consider the absorption edge broadening caused by both the Franz-Keldysh effect in the internal field of randomly distributed ionized impurity atoms and inhomogeneous band gap shrinkage. In Numerical simulation of the process of a nonlinear interaction of laser pulses with semiconductor samples we use preliminary calculated dependencies of the absorption coefficient on the concentration of the photoinduced plasma. The comparison of calculated and experimentally measured spectral and energy dependencies of transmission allows to clarify the contribution of different mechanisms in nonlinearity observed.

References

1. F.V.Karpushko, S.A.Bystrimovich, A.M.Goncharenko, S.A.Porukevich, G.V.Sinitsyn, I.A.Utkin, J.Mod.Opt., v.39, No 7, pp.1593-1998, 1992.

2. S.A.Bystrimovich, F.V.Karpushko, I.A.Utkin, SPIE vol.1807 Photonic Switching, p.51, 1992.

3. D.G.Goodwill, F.V.Karpushko, S.D.Smith, A.S.Walker, in Optical Information Technology, ed. S.D.Smith and R.Neal, Springer-Verlag, Berlin-London, p.203, 1993.

4 V.L.Bonch-Bruevich, Phys.Stat.Sol., v.42, p.35, 1970.

Title : Design Example of Wavelength Conversion and Filtering Components

Author : Jun-ichi Mizusawa
Affiliation : NTT Telecommunication Networks Laboratories
Address : 3-9-11, Midori-cho, Musashino-shi, Tokyo 180, Japan
Tel : +81 422 59 2551
Fax : +81 422 59 2552
E-mail : mizu@tnlab.ntt.jp

Abstract

Two key components for future photonic networks using wavelength multiplexing are designed using commercially available popular technologies. These components handle wavelength conversion and filtering. Design parameters and design results are introduced.

1. Introduction

The first step towards a photonic switching network will probably be the introduction of frequency multiplexing into a subscriber access fiber line. Most research level devices are not adequate yet because they are too expensive, not reliable enough and hard to find. This paper describes two key components for wavelength conversion and filtering designed using currently available technologies. The components are experimental products, therefore it is assumed that further improvements will be needed by having evaluation result such as applying new device technologies. The design specifications were :

(a) Wavelength band : 1.1 - 1.6 μm
(b) Number of multiplexed waves : eight
(c) Minimum Wavelength spacing : 20 nm
(d) Fiber mode : Multi-mode (50 μm core diameter)
(e) Maximum signal speed (design target) : 622 Mbps (>1GHz)
(f) Transmission distance (design target) : 5 - 10 km

Selected LD (Laser Diode) wavelengths were 1175-1190, 1210-1225, 1275-1285, 1305-1310, 1330-1340, 1505-1525, 1545-1550, 1570-1580μm .

2. Wavelength Conversion Component

This converts a signal of one wavelength to one of another wavelength, under instructions from wavelength selection port. The incoming signal is detected by a photodiode, the electronic signal is amplified, a LD driver activates an appropriate LD out of eight, and the output light is guided to the output fiber through a coupling device.

(a) Input signal level : > -30 dBm (using an InGaAs-APD)
(b) Amplifier gain : 30 dB
(c) Modulation transparency : digital / analogue (by bias selection)

(d) LD output signal level : 0 dBm (using a commercially available Fabry Perot resonator type LD bare chip)
(e) Fiber output signal level : -10 dBm
(f) Signal selection port : TTL level (selecting one out of eight)
(g) Size : 120x66x40 mm (excluding connectors and pigtails)
(h) Power : +5, -5, +80 volts
(i) Others : power feed connector, channel selection monitor LED, input signal monitor LED.

3. Filtering Component

This receives a signal with eight wavelengths multiplexed on it, and separates out and guides the signal at each wavelength to an output port for that wavelength. It has no active device. The input light signal from the fiber is converted into concurrent beams by several lenses. Each time the beam arrives at a filter, it is divided into signals of two different wavelengths, one passes through to the output port and the others is reflected to the next filter. The output ports have a lens circuit which guides the light to an output fiber.
(a) Number of new lens designs : eight
(b) Filter fabrication : dielectric multi-coated filter
(c) Number of filter types : 16
(d) Insertion loss : less than 10 dB (design target)
(e) Size : 26x26x18 mm (excludes connectors and pigtails)

4. Design Evaluation

The performance was measured and results will be introduced at the conference. More than forty of each component were produced. Their cost was reasonable.

Eight wavelengths is an adequate number at presents. If the number increases, it will be difficult to purchase commercially available LD , and the loss of the coupling device will also increase.

There is a technical bottleneck at connection between LD and coupling device. Variations in LD alignment cause a loss of more than 10 dB. A simple solution to this problem is required.

Optical multichannel heterodyne communication line

V.V.Firsov*, N.V.Kravtsov*, O.E.Nanii*, M.Yu.Nikol'skii, I.A.Shcherbakov, E.V.Zharikov

General Physics Institute of Russian Academy of Sciences
117942 Moscow, Vavilov str., 38, Russia
*M.V.Lomonosov State University, 117234, Moscow, Russia

ABSTRACT

We present a new multichannel heterodyne optical communication line based on a family of high-stable monolithic neodymium mini-lasers pumped by the single laser.

Introduction

Diode lasers emission spectra demonstrate far from full accordance with neodymium ions absorption spectra. Moreover, strong temperature dependence of the form and width of emission spectrum of the semiconductor laser ($\Delta\lambda/\Delta T \sim 0.3$nm/K) makes it necessary to use thermostabilizing devices, which complicates the design of laser and decreases total efficiency. For pumping with diode arrays the additional aspects of the variation in the central wavelength and bandwidth from stripe to stripe must be considered. Variation of neodimium absorption line center wavelegth in various laser materiales complicate simultaneousl pamping of a number of different lasers using only one laser[1].

Recently we demonstrated[2] the possibility to pump via Cr^{3+} a family of various neodymium doped laser hosts using the only one laser. A set of such mini-lasers is useful in multichannel optical communication lines. The comparative performance of a set of laser-pumped mini-lasers based on Nd^{3+}, Cr^{3+}:REG (Rare-Earth Garnets) are presented. The prototype of a new multichannel communication line with information transfer rate estimated to be of 1000 Gbit/sec is described.

Experimental results

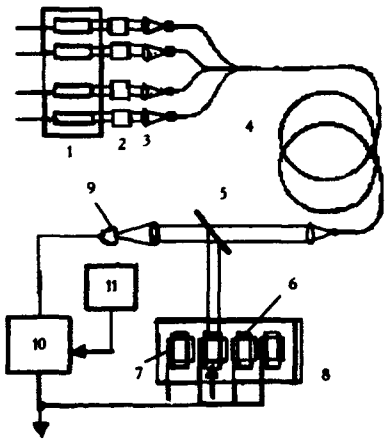
Different semiconductor AlGaAs lasers or argon laser were used pump sources of different Nd, Cr-codoped crystals: GGG (λ = 1062.1 nm), GSGG (λ = 1061.2 nm), YSGG (λ = 1058.5 nm), GSAG (λ = 1060.2 nm) and several garnet mixtures (GSGG/GSAG and YSGG/GSAG type)[3].

We have tested the following active elements: GGG:Cr,Nd ; GSGG:Cr,Nd; YSGG:Cr,Nd; GSAG:Cr,Nd. Cr^{3+} and Nd^{3+} ions concentration in the crystals can be varied from $1x10^{20}$ to $5x10^{20}cm^{-3}$ depending on the absorption efficiency of radiation pumping.

A set of four linear monolithic mini-lasers united in one block and simultaneously or separately pumped by the only one argon laser was created. The frequency shift (ΔF_L) between different lasers was ~ 100 GHz. On the base of this block of the lasers the model of optical-fiber communication line was developed. The scheme of such optical-fiber

communication line is shown in Fig. The emission of four lasers is independently modulated by high-frequency modulators.

The modulated emission was inserted through the optical connectors in one optical fiber. The radiation emitting from optical fib distant end is mixed with the emission of a similar discrete-tuned laser. The discrete-tuned laser is a laser-heterodyne, which consists of the same set of solid state mini-lasers. Due to the mixing of the laser-transmitter beam with the laser-heterodyne beam on the broad-band photodiode the beat frequency signal is formed. The beat signal carries useful information. Used photodiode band width ΔF_{pd} was approximately equal to ~ 5 GHz, that is considerably less than the difference between frequencies of the separate lasers ΔF_L. The photodiode selects the information from only one channel, which matches with the frequency of the laser-heterodyne optical frequency. Thermal tuning of the laser-heterodyne was used to get optical frequency to operate at nearly the same frequency as a laser-transmitter made of the material of the same composition. The monolithic linear lasers bandwidth was less than 5 kHz. The heterodyne feed-back signal is used for the automatic thin tuning of frequency of the laser-heterodyne. Information transfer rate using such multi-channel communication line with the family of solid state mini-lasers on the base of GSAG/YSGG solid mixtures ($\Delta\lambda_{Nd}$ ~ 3 nm) has the order of 10^{12}bit/sec.



Emitting (1) and heterodyne (6) mini-laser families;
RF modulators (2);
optical fiber connectors (3);
optical fiber line (4);
optical mixer (5);
piezzo elements (7);
temperature stabilizer (8);
broad-band photodetector (9);
RF heterodyne (10);
tunable RF oscillator (11)

Acknowledgments. The authors wish to thank Dr. G.B.Lutts, Dr. A.I.Zagumennyi, and Dr. I.A.Ivanov (ELMA- firm) for the laser crystals growing for our work.

References

1. V.V.Firsov, N.V.Kravtsov, O.E.Nanii, M.Yu. Nikol'skii, I.A.Shcherbakov, E.V.Zharikov. Optical materials, v.1, n4, 307 (1992).
2. V.V.Firsov, N.V.Kravtsov, O.E.Nanii, M.Yu. Nikol'skii, I.A.Shcherbakov, E.V.Zharikov. OSA Proceedings on Advanced Solid-State Lasers, 1993, v.15, p.96.
3. C.Pfistner, V.G.Ostroumov, et. al., Optical Materials, v.1, n2, 101, (1992).

Photoconducting Organic Media in Liquid Crystal Light Valves

Vladimir Mylnikov, Olga Kosheleva

Institute of Cinema & Television
Pravda str.I3, St.-Petersburg,
I9II26 Russia, Tel: 8I2-3I5-7285

ABSTRACT. Photoconducting polyimides, phthalocyanines and its polymer dispertions have been studied as a photosensitive elements for liquid crystal spatial light modulators. High resolution, low active losses and excellent physico-mechanical properties are the main advantages of the light valves investigated.

SUMMARY. Organic photoconductors are promising materials for optoelectronic processes and devices (I,2). Photosensitive characteristics of polyimides, phthalocyanines and its polymer dispertions in various polymer matrixes were investigated by photoconductivity, photoelectromotive force and electrophotographic methods. The diverse types of sensitizers were used for expantion the photosensitivity to the red and near infrared regions of spectrum. The best results were obtained with phthalocyanine type sensitizers with sensitivity up to IOm^2/J. Phthalocyanine dispertions in nonphotoconducting matrixes were also studied with photosensitivity in the visual and near infrared regions of the spectra. The photosensitivity in such systems is mainly due to the photoelectronic processes in molecules and aggregated forms of the pigment. The traces of the solvent have strong influence on the photosensitivity spectra. All the systems investigated may be successfully used in optically addressed liquid crystal spatial light modulators as photosensitive elements and matrixes for dispersed liquid crystals.

The liquid crystal light valves with organic photoconducting films which investigated had high spatial resolution, low active losses and excellent physico-mechanical properties. All the results obtained are discussed as applied to the photonic information processing.

I.V.Mylnikov, A.Slusar., Mol. Cryst. Liq. Cryst., I992, v.222, p. I25

[2]V.Mylnikov., Photoconductivity of polymers., Leningrad, Chimia, I990

New Optical Effects Stimulated by Influence of Anisotropy in Optical Information Processing Schemes

A.M.Goncharenko[1)], N.A.Khilo[1)], N.N.Korneyev[1)]
V.N.Belyi[2)] , A.G.Khatkevich[2)]

[1)] Division for Optical Problems in
Information Technologies,
Academy of Sciences of Belarus ,
P.O.Box No.1, 220072 Minsk Belarus
[2)] Laboratory of Crystallooptics, Institute of Physics
Academy of Sciences of Republic of Belarus
Fr.Scaryna ave.,70, Minsk, 220072, Belarus

Abstract *The possibility of self-focusing and diffractionless propagation of light beam in linear biazial gyrotropic crystal has been shown. Asymmetrical components of Kerr-like nonlinearity tensor being taken into account may lead to instability of slow component of fiber mode and also to self-rotation of polarization plane of linearly-polarized incident light.*

An account of anisotropy is essential in various kinds of linear and nonlinear schemes of Optical Information Processing. Here we study forming of spatial structure of light beam in linear medium with anisotropy of a specific kind and nonlinear interaction of modes in a fiber with Kerr-like nonlinearity.

1. For focusing or diffractionless propagation of light beams negatively or sero curved wave vectors surface is necessary. Biaxial gyrotropic crystals are unique media in this respect. For qualitative description of these effects we use the following expansion for the wave vector $\vec{k} = k_z(\vec{q})\vec{n} + \vec{q}$, $k_z(\vec{q}) = k_0 n_0 - \vec{u}\vec{q}/v - \vec{q}w\vec{q}/2$, where $k_z(\vec{q})$ - projection of wave vector of parcial wave on beam axis direction $\vec{n}$, $\vec{u}$ is the vector of group velocity, w - curvature tensor of wave vectors surface, $v = \vec{u}\vec{n}$, n_0 - phase velocity and refraction index in the direction of beam axis.

From Maxwell equations with anisotropy and gyrotropy being taken into account one may obtain the following expressions for principal values of curvature

$$w_1 = w_2 = \frac{c^2}{2vw}\Phi, \quad \Phi = \varepsilon_1^{-1} + \varepsilon_3^{-1} \pm \frac{\varepsilon_0^{-2}}{G}, \quad \varepsilon_0^{-2} = (\varepsilon_3^{-1} - \varepsilon_2^{-1})(\varepsilon_2^{-1} - \varepsilon_1^{-1}), \tag{1}$$

$\varepsilon_{1,2,3}$- principal values of tensor of dielectric perceptibility.

The aberrations described by the following division term in expansion for the wave vector $\vec{k}$ have been appreciated. They limit angular aperture θ_m of a spherical part. For $\alpha - HIO_3$ crystal and for $\lambda = 10^{-6}m$, length $L = 10^{-2}m$ the estimation gives $\theta_m = 7.1 * 10^{-3}$ rad.

Diffraction properties of light in crystalls like $\alpha - HIO_3$ are considered at gaussian beam example. Calculation gives the following expressions for its width and radius of curvature:

$$w^2(\bar{z}) = \left(1 + \left(\frac{2\bar{z}}{kw_0^2}\right)^2\right), \quad R(\bar{z}) = n_0\bar{z}\left(1 + \left(\frac{kw_0^2}{2\bar{z}}\right)^2\right), \tag{2}$$

where $\bar{z} = z_1 + n_0 z_2 \Phi/2$, z_1 is the distance from caustic to the front face of the crystal, z_2 is the distance passed by light inside the crystal. From (2) one can see if $\Phi = 0$ beam trapping and if $\Phi < 0$ beam focusing occurs. In the last regime, in dependence on Φ, z, L - relationship, may take place focusing either at output face of the crystal or inside the one or double focusing both inside and outside the crystal.

Note considered effects of focusing may occur for $\alpha - HIO_3$ crystal for which $\Phi = -0.175$.

2. Interaction of orthogonal linearly polarised modes in nonlinear fibers has been considered with asymmetrical components of χ_3 tensor being taken into account. E.g., for D_{2h} symmetry with χ_{12}^a getting into account we obtain

$$-i\frac{da}{dz} = (\chi_{12}^{c} + i\chi_{12}^{a})a^{*}b^{2} + (2\chi_{66} \mid b \mid^{2} + \chi_{11} \mid a \mid^{2} + k)a, \tag{3-a}$$

$$-i\frac{db}{dz} = (\chi_{12}^{c} - i\chi_{12}^{a})b^{*}a^{2} + (2\chi_{66} \mid a \mid^{2} + \chi_{22} \mid b \mid^{2} - k)b, \tag{3-b}$$

where k is proportional to linear anisotropy. Questions concerning stability of slow mode are studed below.

We introduce both the parameters of anisotropy $\Delta_{11} = (\chi_{22} - \chi_{11})/2$, $\Delta_{12} = 2\chi_{66} + \chi_{12} - (\chi_{11} + \chi_{22})/2$ and parameter x_0^2, characterising relative level of excitation of orthogonally-polarised modes. When $x_0^2 = 0$, slow mode is excited, which used to be stable without the account of Kerr-type anisotropy [1,2]. Now it losses stability when $(2\bar{k} - \Delta_{11})/\Delta_{12} < 1$, where $\bar{k} = k/\alpha_0^2, \alpha_0^2$ - the total intensity.

Under self-coordinate change of x_0^2 and α_0^2, when

$$x_0^2 = \frac{1}{2}\left(1 + \frac{\Delta_{11} - 2\bar{k}}{\Delta_{12}}\right), \tag{4}$$

slow mode keeps the stability while intensity increases either. Polarisation of mode is elliptical and is changed from linear one on Y-axe (polarisation of slow mode) when $2\bar{k} = \Delta_{11} - \Delta_{12}$ to linear one on X-axe when $2\bar{k} = \Delta_{11} + \Delta_{12}$.

The account of χ_{16}^{a} is also carried out in the study presented. In that case nonlinear interaction of two circular polarised modes doesn't change their amplitudes, but affects only their phase difference $\Psi = \varphi_{+} - \varphi_{-}$:

$$\frac{d\Psi}{dz} = -\chi_{12}\left(\mid a_{+} \mid^{2} - \mid a_{-} \mid^{2}\right) + \chi_{16}\left(\mid a_{+} \mid^{2} + \mid a_{-} \mid^{2}\right). \tag{5}$$

As appears from (5), nonlinear phase shift and, therefore, self-rotation of polarisation plane, in comparison with the case of $\chi_{16} = 0$, occurs *for* linearly-polarized incident light either.

References

[1] H.G.Winful. *Appl. Phys. Lett.*, 47, 213 (1985).

[2] S.Trillo, S.Wabnitz, R.H.Stolen, G.Assanto, C.T.Seaton, G.T.Stegeman. *Appl. Phys. Lett.*, 49, 1224 (1986).

Experimental Results of a 64 Channel, Free-Space Optical Interconnection Network for Massively Parallel Processing

Ian Redmond ((609)951-2718) and Eugen Schenfeld ((609)951-2742)
NEC Research Institute, Inc., 4 Independence Way, Princeton, NJ 08540 USA

Abstract

We report the experimental results of a 64 channel, high data rate, free-space interconnection network for massively parallel processing architecures. It uses VCSEL arrays, photodetector arrays and a passive optical routing network.

1 Introduction

In considering the massively parallel computers of the future, it is apparent that there are significant difficulties in using electrical interconnection methods. Peak data rates in excess of 100 Gbit/sec are typical for a single processor with a 64 or 128 bit wide word. Inter-processor data rates are presently in the range of 1-10 Gbit/Sec, although clearly this will increase with higher processor speeds. Coping with such data speeds over inter-board distances, whether in single channel or word-wide buses, is becoming increasingly difficult with electrical interconnections.

2 Goals

Our goal is to develop a system capable of achieving:
1) Interconnection of 10,000 processors in an interconnection cache architecture.
2) Processor-to-processor data rates of 1-10Gbit/sec.

Many optical interconnection schemes have been suggested, but often have difficulties of very demanding optics (SEED systems), or require diffractive elements (and hence wavelength control), or use large central switches (such as SLMs and photorefractive crystals) which do not scale well. We have attempted to make the best use of the optical and electronic components currently available. The optics is used only as an efficient method for communication, while signal generation, routing and detection is all done using electronics. Beam combination and splitting is done by simple mirror surfaces (no space-variant redirection), and relaying is done by simple optics, on-axis wherever possible, to reduce the build-up of aberrations.

3 System Overview

Our experimental system (figure ??) presents the one-way paths of the optical channels. All possible routings to a the target detector are shown. The experiment has 4 'columns' each with one simulated 'board' of 16 processors driving an 8x8 element VCSEL array. Data is received at the board by a 4x4 photodiode (PD) array. Note that in the largest possible system, each *processor* would have one VCSEL array and a single photodiode (and the passive optics would have to be replicated as many times as there are processors on a board).

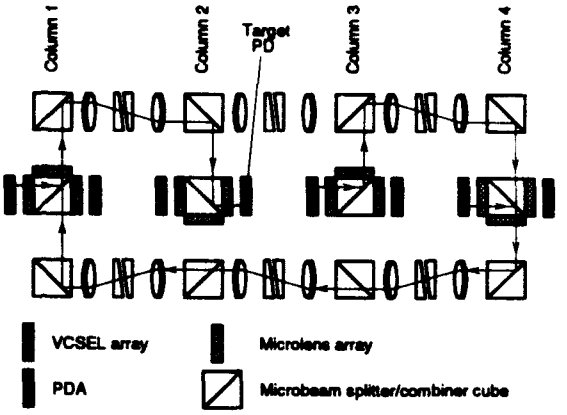


Figure 1: Schematic of the optical system.

Data is carried on arrays of parallel slow-gaussian beams from the VCSELs and relayed by microlens and micromirror arrays and simple bulk lenses. The experimental system is constructed on a 'slot-rail' system which allows modular assembly, minimal alignment and good stability, similar to slot-plate systems already demonstrated.

Each optical channel is fixed and terminates at the receiving photodiode of one processor, so that there are N channels for N processors. Each processor selects, via an electronic switch, the appropriate laser that transmits onto the channel of the target receiver PD.

Since a large number of processors must have access to the same PD, an optical fan-in problem exists. Fan-in occurs at each beamsplitter cube. To optimize the fan-in power efficiency, the reflectivity at each beamsplitter must be controlled, so that, beginning at the most distant processor from the target, the coupling efficiencies onto the chan-

nel are 1, $\frac{1}{2}$, $\frac{1}{3}$, .. $\frac{1}{M}$, for a fan-in of M. This gives a $\frac{1}{M}$ efficiency for every connection. However, because all the channels within a combining cube are generally at different distances from their targets, the coupling efficiencies for each channel within a single cube are also different. Hence, micromirror arrays are used at the center of each cube, the channels are kept spatially separate. Th the main reason for the slow-gaussian microb approach.

The key advantages of this system are:
1) Distributed nature - no central switch or control needed.
2) The microbeam approach is scalable.
3) Only one laser per LDA is on, so low LDA power dissipation, reliable.
4) Speed limited by LD/PD technology, electronic drivers and amplifiers.

4 Scaling

To scale up the experimental system, M boards (e.g. $M = 10$'s) are to be added in each column, giving a column channel efficiency of $\frac{1}{M}$. 20 boards results in a 5% efficiency, sufficient for our target data rates with 1mW lasers. However, whole columns must also be cascaded to get the target processor numbers. Therefore channel efficiency drops rapidly as columns are added. This, along with the difficulty of maintaining alignment and aberration means that 'repeaters' will be necessary every few columns. These may be arrays PD/LD hybrids, devices with gain (such as VSTEPS) or solid state amplifiers.

5 Optics

Diffraction limits the dimensions and hence the total number of distinct microbeams that can be supported within a cube. The relation giving this maximum number, N_{max}, is

$$N_{max} = \frac{\pi n D}{4\lambda m^2} \qquad (1)$$

where n is the cube refractive index, D the cube dimension and m the multiplier for beam pitch $2mr_0$ (where r_0 is the $\frac{1}{e^2}$ radius) at the cube surface. Figure ?? shows the relation between N_{max} and λ for $m = 1.5$ at various cube sizes. It illustrates the high numbers of channels that can be used with compact ($\leq$30mm) optics.

In our experiment, the 850nm beams emitted from VCSEL arrays have a 250μm pitch, and are collimated by ion-exchange planar microlenses. Some micromirror arrays are conformal HOEs made in dichromated gelatin, with controlled efficiencies and optimized for 850nm, and some are evaporated patterned metal.

Board-to-board relaying (20-50mm) within a column is done by $f = 14$mm, 16 level diffractive microlens arrays with a typical efficiency of 90%.

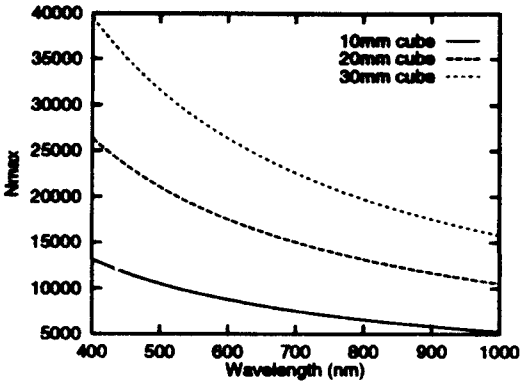


Figure 2: Max. number of channels for $m = 1.5$.

The microlens arrays are bonded to the surface of each cube. The distance from column to column is larger ($\approx$ 300mm for a board width), and conventional bulk [illegible] can be used in a 4-f imaging arrangeme[illegible] Individual beams have extremely smal[illegible] numerical apertures (NAs), easing imaging requirem[illegible]ts

The theoretical aberrations of this system are very low, because NAs are very low (< 0.01), and much of the imaging is on-axis. Exact ray-tracing simulations around the worst case path of the experimental system shows negligible aberrations (strehl ratio ≈ 1). The telecentric 4-f bulk lens imaging system adds only significant spherical aberration, which, in our case, results in a beam pointing and position error. Simulations show that for our standard 40mm lenses at full 7mm field, the pointing error is only 0.025° and position 0.69μm. For a full size system using 80mm lenses and 20mm cubes, full 15mm field has only 0.028° and 2.1μm errors. After 8-f errors are 0.057° and 8.6μm, indicating repeaters could be placed every 2 or 3 columns. Optimized lenses would give improved performance, potentially allowing greater separation.

Current experimental results will be reported.

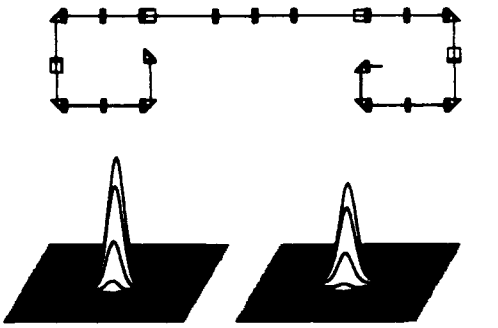


Figure 3: OSLO model of system, and longest path PSFs at 1.4 (operating) and 5mm field (1.4mm patches).

Performance of an Optical Free-Space Crossbar

H.J.White[1], G.M.Proudley[1], C.Stace[1], N.A.Brownjohn[1], A.C.Walker[2], M.R.Taghizadeh[2], B.R.Robertson[2], C.P.Barrett[2], W.A.Crossland[3], J.R.Brocklehurst[4], M.J.Birch[4], M.Snook[5], D.Vass[5]

1 British Aerospace Sowerby Research Centre, PO Box 5 Bristol BS12 7QW, UK. Tel. 0272 363532. 2 Dept. of Physics, Heriot-Watt University, Riccarton, Edinburgh, UK. Tel. 031 451 3036. 3 Engineering Department, University of Cambridge, Trumpington Street, Cambridge, CB2 1PZ, UK. Tel. 0223 330264. 4 THORN EMI CRL. Smectic Technology, Dawley Road, Hayes, Middlesex, UN3 1UK. Tel. 081 848 6445. 5 Dept. of Physics, Edinburgh University, The King's Buildings, Mayfield Road, Edinburgh, EH9 3JZ, UK. Tel. 031 650 1000.

Abstract

Initial results on the performance of a 64 input 64 output free-space optical crossbar are reported. The components of the compact and ruggedised system are described.

The use of free-space optics to perform high bandwidth connections for computing applications has been widely discussed in the literature. In this paper we present the practical results from a 64×64 free-space optical crossbar switch which has been developed as part of a collaborative project entitled OCPM [1].

Figure 1 shows the layout of the 64×64 system. A matrix-matrix crossbar design has been used and data inputs to the switch are provided by 790nm laser diodes pigtailed to polarisation preserving fibres. To create the most compact system, the design uses one-to-one imaging and hence the input fibres are arranged in an array that matches the pixel spacing of the SLM. These are 80μm cladding diameter Hi-Bi fibres which are arranged in an 8×8 square array with a 120μm pitch. Each fibre has its polarisation axes orientated in the same direction. This fibre array was fabricated in an array of holes formed by excimer laser material ablation of a Kevlar substrate [2]. The light from the input array is fanned out by means of a binary phase grating based on a non-separable two-dimensional design. A half-wave plate is used to align the polarisation of the channels with the liquid crystal axes of the SLM.

The relay lenses have effective focal lengths of ~40mm and a 16° full field of view. Code-V has been used to design and optimise the system and predicts that 90% of the input falls within 10.5μm diameter circles after two relay stages [3]. The contrast ratio of the polarising beam splitter limits the possible signal to crosstalk ratio of the switch. Due to the large range of working angles it was necessary to incorporate a second polariser in the output arm of the crossbar. Alignment of the components is achieved by means of accurate positioning of the optics within cylindrical mounts which are held in place by magnetic strips within channels machined into the baseplate. Beam-steering prisms are used in the output arm of the crossbar to provide fine adjustment of the optical axis.

The 64×64 SLM is currently being fabricated for inclusion in the system at a later date. This device will have ~70μm square pixels on a 120μm pitch. It will use a chiral smectic C* liquid crystal, operating in the binary latching bookshelf structure. This will be an active backplane device with DRAM pixel circuitry and a switching speed of ~10 – 25μs is expected. Until this device becomes available, initial system tests are being performed with an SLM of the same dimensions but containing just 64 pixel stripes.

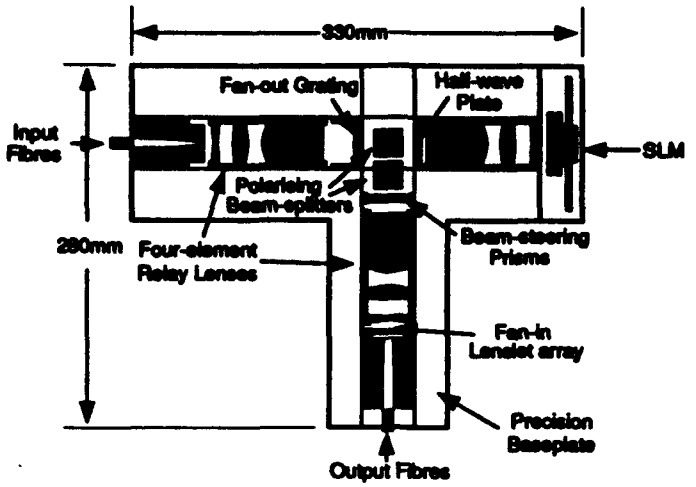


Figure 1: Lay-out of the 64×64 crossbar baseplate and optics

The fanning-in of the light into the output fibres is performed by two lenslet arrays. These have been combined to form a single high efficiency holographic element. To increase the collection efficiency of the fanning-in to the output fibres, 300μm core diameter fibre is used. These fibres are formed into a square 8×8 array with a 960μm pitch using an array of holes that are anisotropically etched in silicon.

The technology for fabricating compact, high bandwidth, non-blocking free-space optical crossbar switches capable of full broadcast and multi-cast has been developed and demonstrated. The performance of this 64×64 crossbar for switching data up to a bandwidth of 1Gbit/s is to be evaluated and the subsequent results will be presented at the conference.

References

[1] H.J.White J.R.Brocklehurst W.A.Crossland I.M.McLaren D.M.Monro and A.C.Walker. Optically Connected Parallel Machines. Proc. of the JFIT Technical Conference. Keele University UK, March 1993.

[2] G.M.Proudley C.Stace and H.J.White. Fabrication of 2-D fibre-optic arrays for an optical crossbar switch. To be published in Optical Engineering, Feb 1994.

[3] C.P.Barrett A.C.Walker D.T.Neilson B.R.Robertson. Optical Design For Crossbar Systems. Submitted to International Optical Design Conference Sponsored by OSA Rochester NY, June 6-9 1994.

The authors would like to acknowledge the invaluable work of D.J. McKnight, I. Redmond, G. Smith and D. Neilson in the development of the crossbar switches. The OCPM project (Optically Connected Parallel Machines) is a collaboration between British Aerospace (Sowerby Research Centre), BNR Europe, Heriot-Watt University, the University of Bath and THORN EMI CRL. The project is coordinated by British Aerospace and is funded in part by the DTI and SERC.

A FET-SEED Based Optical Backplane Demonstrator

by

D.V. Plant, B. Robertson, H.S. Hinton, W. M. Robertson*, G.C. Boisset,
N. H. Kim, Y. S. Liu, M.R. Otazo, A. Z. Shang, and L. Sun
Department of Electrical Engineering
McGill University
Montreal, Canada
H3A 2A7
(514) 398-2989

Abstract

We demonstrate a representative portion of an optical backplane using free-space optical channels to interconnect printed circuit boards which employ FET-SEED based smart pixel arrays. Results of system demonstrator performance will be presented.

Introduction

Free-space optical interconnects represent a solution to the needs of future connection-intensive digital systems such as ATM switching systems, and massively parallel processing computer systems. These systems will require the large board-to-board connectivity provided by an optical backplane created with two-dimensional arrays of passive, free-space, Parallel Optical Channels (POCs) to optically interconnect electronic Printed Circuit Boards (PCBs) and/or Multi-Chip Modules (MCMs). Such a backplane could be capable of supporting terabit/second aggregate capacities with connectivity levels on the order of 10,000 input/output channels per PCB.

FET-SEED Transmitter/Receiver circuits

We have developed the optics and optomechanics to demonstrate these high bit rate optical backplanes. As part of this program, we have constructed a representative portion of an optical backplane capable of interconnecting two printed circuit boards which utilize FET-SEED based smart pixel transceiver arrays.(1) Figure 1a shows a schematic of the transmitter circuit, including the optical diodes and the FETs used to modulate the optical input. Figure 1b is a schematic of the receiver circuit, including the optical input windows, clamping diodes for voltage control, the differential amplifier section of the circuit, and the power FETs which are designed to drive 100 ohm transmission lines on the PCBs. Both the 4 x 4 transmitter and receiver array optical windows are 25 x 25 μm, separated by 50 μm, with the pixel to pixel pitch being set at 200 μm. These circuits are designed to run at 155 MBits/sec in parallel. Figure 2 shows the results of a Spice simulation of the receiver circuit indicating a cut-off frequency of 1.4 GHz. Experimentally

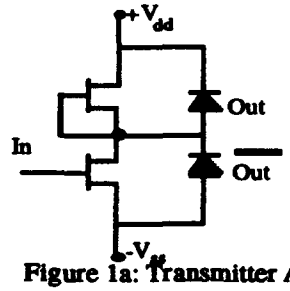


Figure 1a: Transmitter Array

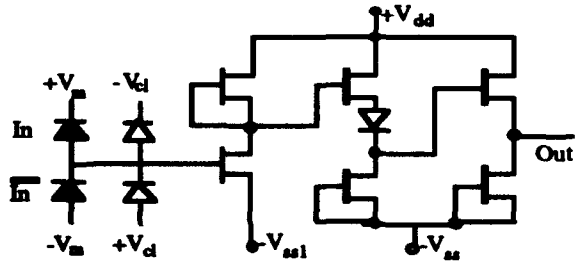


Figure 1b: Receiver Array

measured device and circuit parameters will be presented including measurements of not only individual pixel performance but also the 4 x 4 array speed and efficiency. These results will be compared to the simulator results to confirm the accuracy or our models.

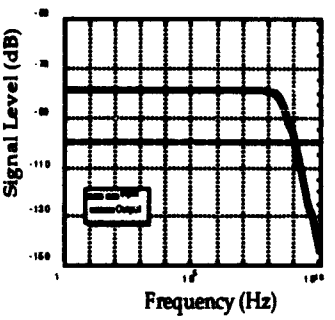


Figure 2: Receiver Circuit Response

Optical System Design and Characterization

The board-to-board interconnection will be accomplished using a two-sided optical backplane approach, shown in Figure 3.(2) This first demonstrator is capable of interconnect two PCBs using the 4 x 4 smart pixel arrays described above. Specifically, light from the output of an argon laser pumped Ti:Sapphire laser is delivered and collimated using single mode fibers and collimating optics. A binary phase grating is used to provide spot array generation for illuminating the smart pixel array optical windows. Vertically polarized light is reflected off the polarization beam splitter, directed through a quarter waveplate, and focused onto the transmitter array. The transmitter circuit modulates the light, reflecting the light back towards the adjacent printed circuit board through the polarizing optics. The modulated light is detected by the receiver smart pixel photodiodes, and amplified using power FETs. These signals are then directed onto the PCB for appropriate processing. The optomechanics for this first demonstrator is based on a modified AT&T baseplate approach.(3) The baseplate is made from Magnesium to insure extreme flatness tolerances. The baseplate design is capable of implementing both a bulk optics approach, and a lenslet array based approach for creating the passive optical channels used to interconnect the PCBs. Tolerancing issues such as optical component alignment and PCB optomechanics will be discussed.

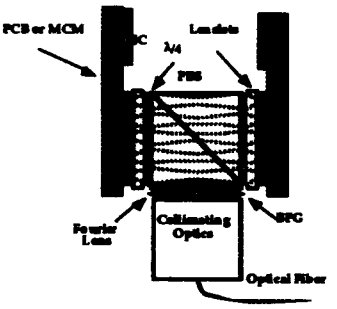


Figure 3: Demonstrator Schematic

Results of system measurements will be presented and discussed. These measurements include characterization of optical throughput, the associated optical efficiency, and spot array uniformity. In addition optical crosstalk and bit error rates will be presented. Finally, short and long term stability will be described with an emphasis being placed on the ultimate manufacturablity of this approach being addressed.

Acknowledgments

This work was supported by the Canadian Institute for Telecommunications Research and the McGill NSERC/BNR Industrial Chair in Photonics Systems.

*Permanent address: National Research Council of Canada, Instate for Information Technology, Ottawa, Canada.

References:

1) L.A. D'Asaro et. al., IEEE Journal of Quantum Electronics, QE-29, no 2, pp. 670-677,1993.
2) H.S. Hinton, Canadian Institute for Telecommunications Research, Research Program 1993-94, pp. 143-156, 1993
3) F.B. McCormick et. al., Applied Optics, vol. 32, no. 26, pp. 5153-5171, 1993.

High Speed Parallel Switching of Symmetric Self-Electrooptic Effect Devices(S-SEEDs)

Dominic Goodwill, Douglas A.Baillie and Frank A.P.Tooley

Physics Dept., Heriot-Watt University, Edinburgh, UK.

(44) 31 451 3053 phydjg1@vaxa.hw.ac.uk

Abstract

An S-SEED switching experiment has been designed and constructed to investigate operation at 5-50 MHz using powers of 1 mW/device over a 512 device array. Details of the implementation and experimental results will be presented.

Summary

Arrays of optically interconnected self-electrooptic effect devices (SEEDs) have been proposed for use in optical computing systems to overcome the problems encountered in high speed electronic systems; e.g. clock-skew, limited interconnect possibilities, cross-talk, etc. Individual S-SEED devices have been switched at 150 MHz [1] and the degradation in their performance that occurs at high powers has been measured[2]. Large arrays have only been operated at below 1 MHz[3]. It is important to demonstrate the system capabilities of these devices by combining these two: operation of a large array at high speeds. This investigation into the implementation of high speed, highly parallel switching has revealed the practical difficulties described below.

We have used a 1 W cw, argon ion pumped Ti-sapphire laser operated at 850 nm and an electro-optic modulator to switch a single 16 by 32 array of GaAs/GaAlAs symmetric-SEEDs (S-SEEDs)[4]. The set-up used is shown in the figure and photograph. The optics in this system are kinematically mounted on a custom slot baseplate. The electro-optic modulator (EOM) and two polarising beamsplitters define separate routes for the s and p polarisations, producing the set and reset beams. These two angularly separated beams pass through a 16 by 32 binary phase grating array generator and are relayed to the 8.4 mm focal length objective lens that focuses the beams into 5 μm spots on the device windows. The design is telecentric. A fast avalanche photodiode system and high bandwidth oscilloscope were required to detect the reflected beams from the SEED devices.

The requirement for high power in a single mode precludes the use of an easily modulated diode laser, necessitating the use of an externally modulated large frame laser. The external modulator had the highest optical power handling and speed specification available. It could rotate the polarisation to produce a pseudo-square wave at 50 MHz, which resulted in a contrast ratio for the beams incident on the SEEDs of 6:1. However, even with a beam as large as the 1 mm aperture allowed, significant photo-refractive damage accumulated, producing a strong focusing effect.

Signal encoding is a major issue that is best addressed by directly modulating the laser itself. Current development of master oscillator power amplifier (MOPA) devices[5] is resulting in compact lasers with high power single mode performance that should soon be configurable for high speed modulation. Our experience confirms that the problems of beam drift, cavity alignment and the difficulties of modulation exclude the practical use of gas lasers for this type of system demonstration. This laser was discovered to operate multi-longitudinal mode with beats at multiples of 250 MHz, which clearly diminishes the visibility of high frequency switching. Any misalignment of the cavity degrades the beam profile and introduces transverse mode beating at 80 MHz as well as misaligning the modulator and hence lowering the contrast ratio.

Operation to date has been limited by the EOM and laser. Half of the array has been observed switching at 5 MHz (1.25 Gbit/s) and individual pixels at 10 MHz. Operation at up to 50 MHz is anticipated.

Acknowledgements

The authors would like to thank G. Smith for the design and construction of the baseplate and M.R.Taghizadeh for providing the binary phase grating. This work was funded by the UK Science and Engineering Research Council (SERC) under the Scottish Collaborative Initiative in Optoelectronic Sciences (SCIOS).

References

[1] A.L.Lentine, L.M.Chirovsky and L.A.D'Asaro, "Photonic ring counter using batch fabricated symmetric self-electrooptic effect devices." *Opt Lett.*, vol. 16 pp. 36-38. 1991

[2] G.D. Boyd, J.A. Cavailles, L.M.F.Chirovsky and D.A.B. Miller, " Wavelength dependence of saturation and thermal effects in multiple quatum well modulators." *Appl.Phys. Lett.* vol. 63 no. 13 p. 1715 1993
[3] F.B. McCormick, F.A.P.Tooley, J.M.Sasian, J.L.Brubaker, A.L.Lentine, T.J.Cloonan, R.L. Morrison, S.L.Walker and R.J. Criaci, "Parallel interconnection of two 64 x 32 symmetric self-electrooptic effect devices." *Electron. Lett.* vol. 27 p. 1869 1991
[4] Commercially available from AT&T Microelectronics.
[5] D.F.Welch, R.Parke, D.Mehuys, A.Hardy, R.L.Ang, S.O'Brien and S.Scifres, "1.1 W cw diffraction limited operation of a monolithically integrated flared-amplifier master oscillator power amplifier." *Electron. Lett.* vol. 28 no. 21 pp 2011-2013 1992

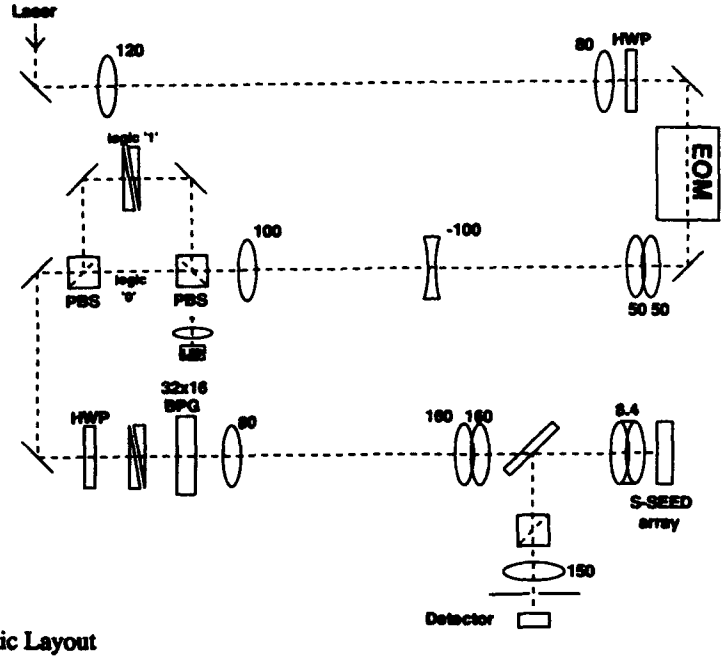


Figure 1 Schematic Layout

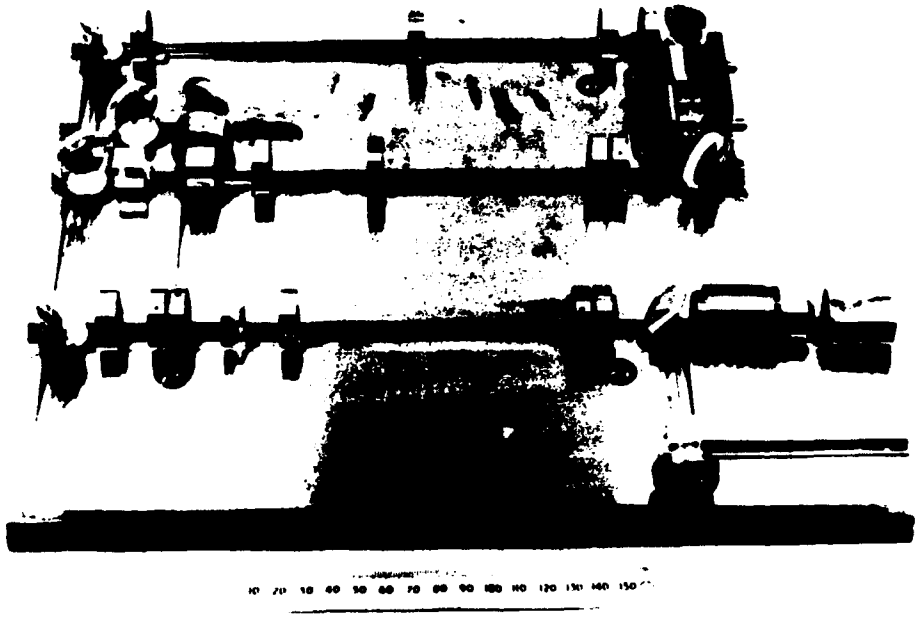


Figure 2 Photograph of baseplate and optics

Arrays of Field Effect Transistor-Self Electrooptic Effect Device (FET-SEED) Differential Transimpedance Amplifiers for Two Dimensional Optical Data Links

R.A. Novotny, M.J. Wojcik, A.L. Lentine
AT&T Bell Laboratories, 263 Shuman Blvd, Naperville, IL 60566, USA
(708) 713-5419, FAX (708) 713-7951

L.M.F. Chirovsky, L.A. D'Asaro
AT&T Bell Laboratories, 600 Mountain Ave., Murray Hill, NJ 07974, USA

M.W. Focht, G. Guth, K.G. Glogovsky, R. Leibenguth, M.T. Asom, J.M. Freund
AT&T Bell Laboratories, SSTC, 9999 Hamilton Blvd, Breinigsville, PA 18031, USA

ABSTRACT

Two dimensional (4x18) arrays of Field Effect Transistor-Self Electrooptic Effect Device transimpedance receivers have been fabricated for application in massively parallel optical data links. Up to 100Mbps/channel was demonstrated. Test results are discussed.

SUMMARY

Architectures for large switching systems are constrained by the limitations of available interconnections at the chip and board level.[1] [2] Two Dimensional Optical Data Links (2D-ODLs)[3] [4] could provide a low cost, high bandwidth, high density, interconnection scheme and would open up new avenues to architects of these systems. Key components used to construct 2D-ODLs are a modulator or source array, a 2D-fiber bundle,[5] and a receiver array. This talk describes the design, and experimental results of 4x18 differential transimpedance receiver arrays (Figure 1) fabricated in the Field Effect Transistor-Self Electrooptic Effect Device (FET-SEED)[6] technology. The FET-SEED technology consists of multiple quantum well (MQW) reflection detectors/modulators[7] [8] monolithically integrated with doped channel MIS-like Field Effect Transistors (DMTs).

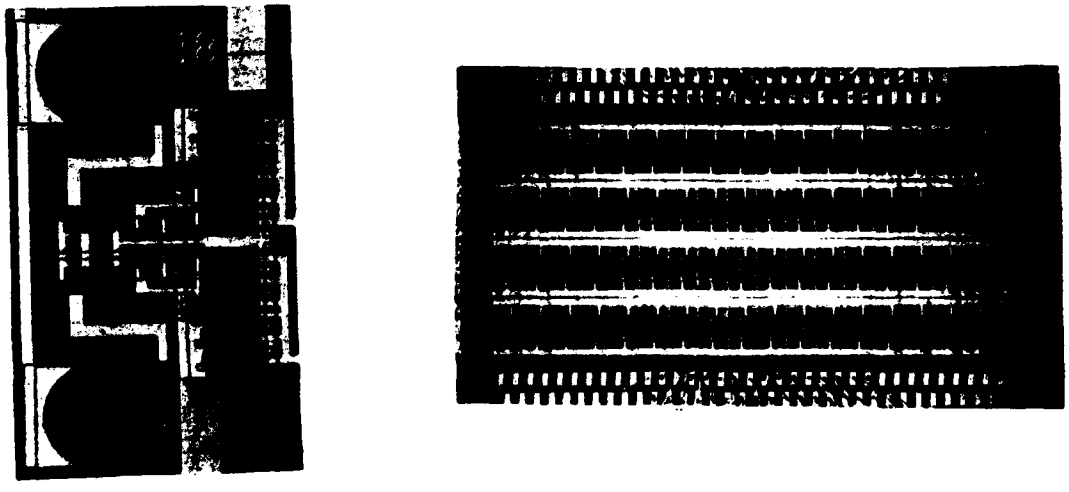


Figure 1. Photomicrographs of 4x18 FET-SEED differential receiver circuit and array

The receiver schematic and amplifier response histogram are shown in Figure 2. Several 4x8 FET-SEED transimpedance receiver arrays were tested and displayed a mean response of -0.7mV/μW, and were capable of >100Mbps per channel operation. Eye diagrams for 40Mbps and 100Mbps operation is shown in Figure 3. The mean receiver sensitivity for a BER of $<10^{-9}$ at the design rate of 40Mbps was -25dBm, and was found to incur a 1/f noise penalty. These receiver arrays were successfully used in a demonstration of a Small Computer System Interface (SCSI) fully differential parallel optical data link. In this talk, we will compare the measured bit error rate, crosstalk, and noise to theoretical values, and discuss the limitations in fabricating large arrays of DC coupled receivers.

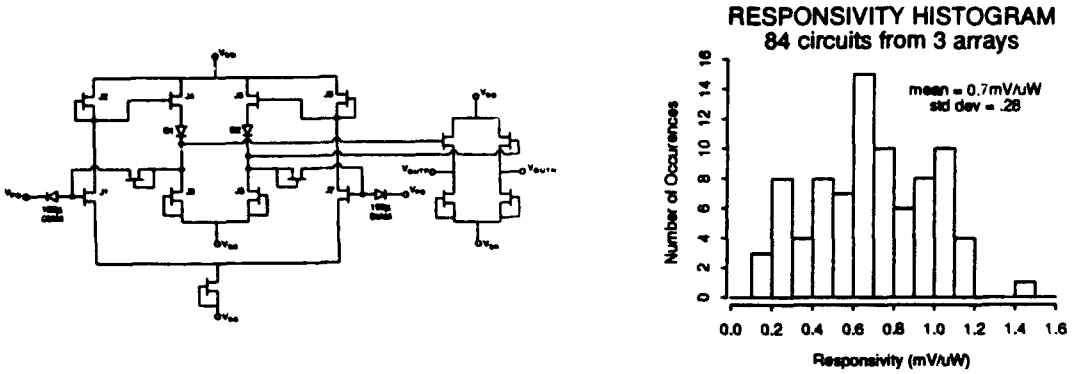


Figure 2. Differential transimpedance amplifier schematic diagram, and responsivity histogram

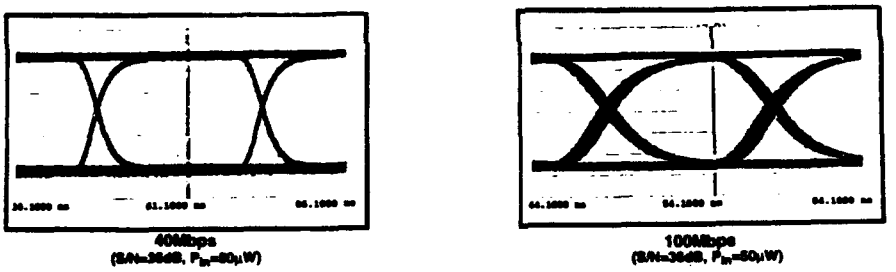


Figure 3. Eye diagrams for 40 and 100Mbps operation

ACKNOWLEDGEMENT

This work was partially funded by the National Communication System Contract DCA100-91-C-0153.

REFERENCES

[1] T. J. Cloonan, "A comparative study of optical and electronic interconnection technologies for large ATM packet switching applications", accepted for publication in Optical Engineering.

[2] R.A. Nordin, A.F.J Levi, R.N. Nottenburg "A Systems Perspective on Digital Interconnection Technology," Journal of Lightwave Technology, V10, N6, p811-827, 1992.

[3] R.A. Novotny, E. Kerbis, J.L Brubaker, N. Basavanhally, J. Freund, "Two-Dimensional Fiber Optical Data Link using Self-Electrooptic Effect Device Modulators and OEIC Detectors," 1991 OSA Annual Meeting, November 1991.

[4] G. Hasnain, R.A. Novotny, J.D. Wynn, R. Leibenguth, "Thirty-six Channel Parallel Optical Data Link using Monolithic 2x18 Arrays of Fiber-Pigtailed GaAs Vertical Cavity Lasers and PIN Photodetectors," 1992 Conference on Lasers and Electro-Optics, May, 1992.

[5] N. Basavanhally, ASME Winter Annual Meeting, EEP Vol2, 11/92.

[6] L.A. D'Asaro, et al, "Batch Fabrication and Structure of Integrated GaAs-AlGaAs Field-Effect Transistor-Self Electro-optic Effect Devices (FET-SEEDs)," IEEE EDL, V13, N10, October 1992.

[7] D.A.B. Miller, "Quantum-well Self-Electro-optic Effect Devices," Optical and Quantum Electronics, V22, S61-S98, 1990.

[8] A.L. Lentine, H.S. Hinton, D.A.B. Miller, J.E. Henry, J.E. Cunningham, L.M.F. Chirovsky, "Symmetric Self- Electrooptic Effect Device (S-SEED): Optical Set-Reset Latch, Differential Logic Gate, and Differential Modulator/Detector," IEEE Journal of Quantum Electronics, Vol.25, No. 8, Aug 1989.

The Optical Computing of National 863 High Technology Program in China

Yi-mo Zhang*

**Group of Optoelectronic Devices and Integration,
National 863 High Technology Program,
Beijing 912 Mail Box, 100083, Beijing P.R.China**

Abstract: Some of the achievements of National 863 High Technology Program in China are summarised.

1. Introduction

The national 863 High Technology Program, which was proposed and drew up by scientists, has been implemented in China since March 1986. Under the program there are several groups according different scientific fields. There is Optical Computing in the Group of Opto-electronic Devices and Integration, which incorporates more than twenty universities and institutes that have made achievements in optical computing. The several areas of optical computing are being implemented as follows.

2. Devices

The S-SEED and S-SEED Array have been made and applied to optical computing. Devices as Multiple Quantum-Well-Based Lasers(MQW), Top Surface Emitting Vertical Cavity Diode Laser, Multi-Channel-Splinder, Micro Lens Array and the related materials (include semiconductor and crystal) for these devices have been also developed.

In the research on real time Spatial Light Modulators(SLM), the Liquid Crystal Light Valve (LCLV) and Electrically Addressed SLM that closely coupled with CRT, Ferro electric Liquid Crystal Valve and Pockel-Read Optical Modulators(PROM) have been implemented.

3. Architecture and System

The optoelectronic hybrid processor's array consists of three 2DPAs (2-D Processors Array), which has 3-D architecture. A programmable, electrically addressed optical-fiber inter-connection network has been employed between each two 2DPA. This system can be used for parallel processing.

In the research on Morphological processors, the varied operations in image algebra are realised by means of hardware, which have been applied to image processing. The demonstration of image processing in real time has been made by Optical Cellular Array processors developed.

The adaptive processors that based on the multi-Channel JTC System and optical disc memory system have been developed to carry out the image correlation processing.

* Please contact with the address: Yi-mo Zhang, Institude of Optoelectronics and Precision Engineering, Tianjin university, Tianjin 30072, P.R.China

The modules of interconnection and parallel processing system based on S-SEED will be used as the demonstration system of opto-digital computing and a kind of special-purpose system.

4. Neural Network Processors

In the research on optoelectronic hybrid neural network, more than 1000 neural cells have been reached for optical computing, where the threshold is done by electrical computers to implement varied kinds of operations.

In the studies of optoelectronic hybrid associative memory, the storage devices are made up with the new kind of Crystal, KNSBN, a Liquid Crystal screen with changeable thresholds is employed as a device of threshold and gain. Associativity of the system is as high as 75%. The studies of associative storage system with multi-channels are going on to increase the processing speed.

5. The Fiber Network of Computers

The optical fiber network of multiple micro computers has been studying and been in progress. The products of this kind of system with the resources shared by multi-computers will be developed soon.

6. Conclusions

(1)under the united organisation all the studies are cooperately going on.

(2)There are some differences between the National Nature Academic Fund, which mainly supports the studies of areas such as the new ideas, new architecture's and new kinds of devices etc., and National 863 Program, which lays particular emphasis on the creative researches in practical applications.

(3)The first stage of this program will end by 2000. When the time comes, there will be some available optical computing systems.

Parallel Optoelectronic Processing Systems and Applications

Masatoshi Ishikawa

Faculty of Engineering, University of Tokyo
Bunkyo-ku, Tokyo 113, Japan
e-mail: ishikawa@k2.t.u-tokyo.ac.jp

I. INTRODUCTION

Integrated optical devices such as surface emitting laser array, photo detector array and OEICs promise high performance parallel processing. Although these devices have two-dimensional parallelism for pattern information processing, their potential capabilities are not utilized in conventional parallel processing systems. The "I/O bottleneck" between processing element (PE) array and I/O devices sets the limit to the processing speed.

In order to overcome the I/O bottleneck, two-dimensional interconections between them are required. The interconnections, however, can not be implemented by using conventional macro-scale wiring technology even if the integrated optical devices are used. Only the integrated wiring technology that is VLSI technology can implement the interconnections. It means that the processing element should be so compact to be implemented with integrated optical devices. Integrated PE and optical device array realizes fully parallel processing with high computing performance.

In this paper, architectures of compact PE array and experimental systems, some experimental results on the system performance for applications, and a design of an intergrated one chip parallel processing system are shown.

II. PARALLEL OPTOELECTRONIC PROCESSING SYSTEMS

A. Design of processing element

Conventional microprocessors can not be used as the PE of the system, because the number of gates is too large that many PEs cannot be implemented into small area on VLSIs. Keys of the design are how generality of processing is kept by using small number of gates and how integration and high speed processing is performed.

Ishikawa et al. have proposed a compact PE architecture with general purpose and programable functionality and implemented a scale-up model [1]. A conceptual diagram based on the architecture with optical interconnection is shown in Fig.1.

The architecture of the PE has following features to be compact; 1) direct connection between PE and optical I/O, 2) SIMD type parallel processing, 3) controlled by microinstruction, 4) bit serial processing, 5) restricted electrical interconnections (4 neibours).

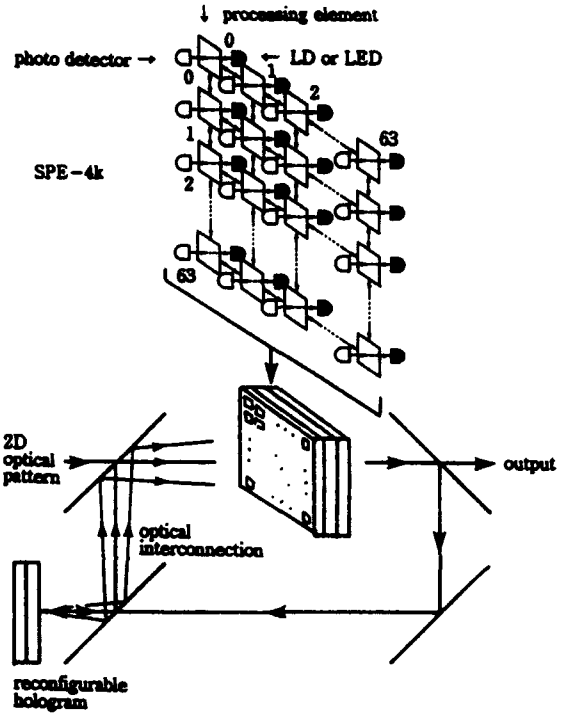


Fig. 1. Parallel optoelectronic processing system

Each PE has three 8bit registers, one arithmetic logical unit (ALU, 1bit), one 4bit multiplier as shown in Fig. 2. Although bit serial processing is slow in comparison with bit parallel processing, it is so compact to realize the integration and variable bit length processing.

In the result, the PE is implemented by using 337 gates. The number of the gates is quite small.

B. Scale up model : SPE-4k

An experimental optoelectronic processing system which has matrix positioned $64 \times 64 = 4096$ (4k) PEs is implemented by using gate array technology. The system is named SPE-4k (sensory processing elements - 4k) and is designed as a scale up model of integrated one chip optoelectronic processing systems shown in Fig. 1. The system uses LEDs and PTRs for optical I/O.

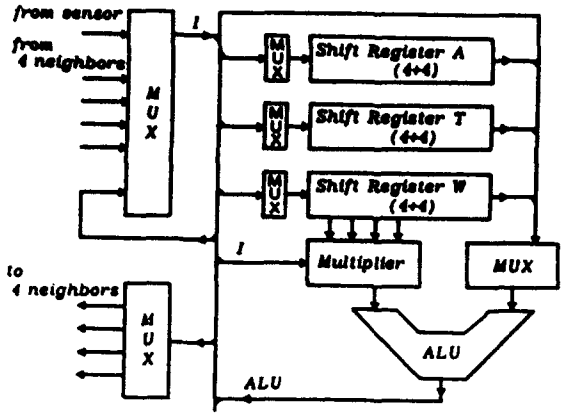


Fig. 2. Block diagram of processing element

TABLE I
PROCESSING TIME OF APPLICATIONS

Processing	Steps	Time
Edge detection (binary) (EXOR with 4 neighbours)	33	3.3μs
Skeltonization (iteration, 4 neighbours)	149	149.0μs
Gaussian	111	11.1μs
Matched Filter (binary)	89	8.9μs
Optical flow (iteration)	672	13.44ms
Poisson's equation (iteration)	125	2.5ms

The cycle time of the system is 100ns. Considering the 8bit integer addition as a basic operation of processing for the evaluation of the speed of SPE-4k, 3.2GOPS (Giga Operations Par Second) at the maximum speed of the system are obtained.

C. Reconfigurable optical interconnection

Shift-invariant and reconfigurable optical interconnection between the PEs of SPE-4k using Fourier plane computer generated hologram (CGH) has been proposed and demonstrated by using a parallel aligned nematic liquid crystal (PAL) saptial light modulator (PALSLM) by Kirk et al. [2]. Since the CGH is optimized and the PALSLM is a phase modulation type spatial light modulator, high diffraction efficiency and accuracy have been obtained.

Recently a laser diode array for integration of the optical interconnection and Fourier plane hologram for real-time generation of the interconnection kernel are examined and practical algorisms using optical interconnection for parallel processing operations such as prefix calculation and vector-matrix multiplication are also examined.

D. One chip system

The number of transisters can be reduced by using full custom VLSI design rule. Yamada and Ishikawa have designed and implemented one chip version of PE array with photo array [3]. In their chip, 3600 PEs with the same number of photo detectors are integrated as shown in Fig. 3.

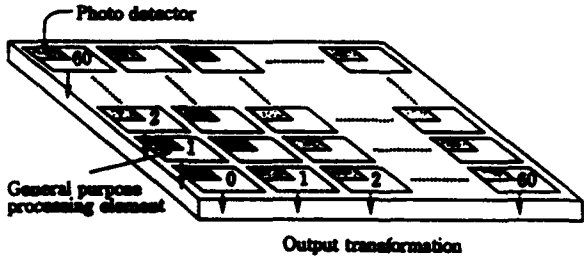


Fig. 3. One chip optoelectronic system

III. APPLICATIONS

This type of parallel processing is matched with early stage of visual information processing. In order to evaluate processing performance of the SPE-4k, some applications have been carried out on the system. The processing time of the applications is shown in Table I.

In principle, input pattern is binary and calculation is in fixed point. A few applications in Table I use iterative algorism, so in such applications, the processing time depends on the iteration.

IV. CONCLUSION

Optoelectronic processing architectures for realizing a integrated optoelectronic systems and some experimental results are shown.

In the SPE-4k, compact processing elements realize general early vision processing and high speed visual feedback. In addition, it is shown that 3600 PEs with the same number of photo detectors can be implemented into one chip.

REFERENCES

[1] M.Ishikawa, et al., "Massively Parallel Processing System with an Architecture for Optoelectronic Computing, *Technical Digest of Optical Computing 1993 (Optical Society of America, Washington, D.C.)*, Vol.7, pp.272-275 (1993)

[2] A.Kirk, et al., "Design of an optoelectronic cellular processing system with a reconfigurable holographic interconnect," *Appl. Opt.*, (in press)

[3] Y.Yamada and M.Ishikawa, "VLSI parallel processing vision sensor," (to appear)

Free Space Holographically Interconnected Counter

R.J. Feuerstein, D.C. O'Brien, A. Fedor, M.C. Chang, L.H. Ji
Optoelectronic Computing Systems Center
University of Colorado
Boulder, CO 80309-0525
303-492-7077

Abstract: We have constructed a simple 4-bit counter using holographic interconnects, microlens arrays, vertical cavity lasers, and a CMOS detector array chip. Performance of this prototype system will be discussed.

We are working on various architectures for three-dimensional optoelectronic computers. They all share free space holographic interconnects from one optoelectronic processing board to another. We will describe the results of an experiment to construct a system using this technology. This is also the first step in the development of a testbed for evaluation of source and detector arrays, holograms and the necessary optomechanics.

Figure 1 is a schematic of the experiment. The system implements a simple 4-bit counter with the right (left) half of the system counting the odd (even) numbers. For the top beams, there are four pairwise optical OR's performed by the receiver detectors. The electronics are a few discrete TTL gates that are used to implement the Boolean expressions for the four bits of a counter. On each clock signal the right (left) counts 1, 3, 5, 7, 9, 11, 13, 15, 1... (0, 2, 4, 6, 8, 10, 12, 14, 0...) etc.

A pair of Vertical Cavity Surface Emitting Laser arrays(VCSELs), a 1x8 and a 1x4, emitting at 842 nm, are the sources. The VCSEL output powers vary from 550 μW to 900 μW, with bandwidths in the GHz. The VCSEL is cooled by a thermoelectric cooler to control the wavelengths.

A Nippon Sheet Glass company microlens array (μLA) with a 560 μm focal length is glued directly to the VCSEL package while actively monitoring the beam outputs. The μLA collimates the Gaussian output beams of the VCSELs.

Each of the 4 or 8 channels illuminates a separate computer generated hologram (CGH), which creates the desired interconnect pattern. These are designed using a modified Gerchberg-Saxton algorithm. Two types of elements are produced from this: the first is a standard etched binary (two level) phase grating in quartz. The second is a phase copy of the amplitude mask recorded at 514 nm in Dupont photopolymer. The performance characteristics of these approaches will be presented. The hologram array (HA) is glued to the μLA while actively monitoring the beam outputs.

The transform lens is a standard laser diode lens anti-reflection coated for 830 nm.

Standard 2 μm process CMOS chips made by the MOSIS chip fabrication service are used as 2x8 pn diode detector arrays with 200x200 μm^2 detection area. Each channel has amplifiers and a TTL level output driver. The receivers require optical pulse power >40 μW to generate an electrical output pulse. These outputs are wired to the TTL chips.

All array elements are on a 250 μm pitch.

The components are mounted with Spindler and Hoyer microbench parts with the VCSEL/μLA/HA component mounted on a slug held by the standard x-y adjustable stage and similarly for the receiver chips. There are two independent optical paths as shown in the figure.

The system speed is limited by the minimum power required for the receiver chips to generate an output pulse. This in turn depends on the efficiency of the holograms, and the VCSEL output powers. Another issue relating to speed is the absorption depth of the light. We measured the speed and sensitivity of the detector chips at both 830 nm and at 670 nm to separate the circuit speed limitations from the diffusion time delay for carriers absorbed deep inside the silicon substrate. The implications of these interconnected factors will be discussed in terms of the requirements placed on each element for reliable system design.

The complete system performance and implications for larger systems will be discussed.

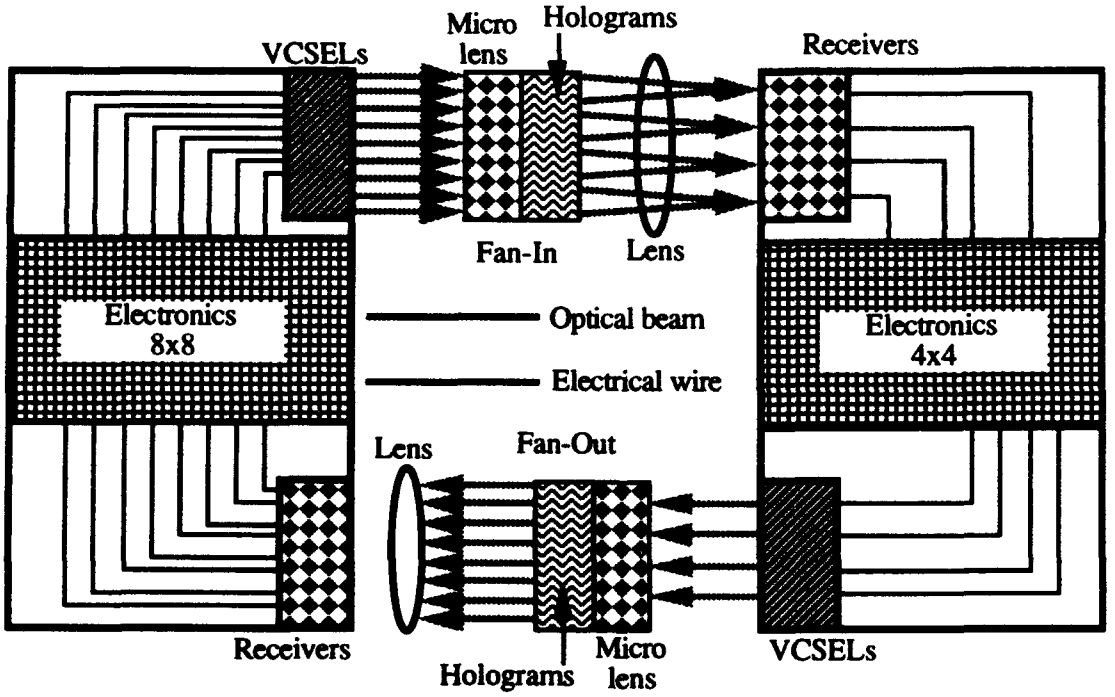


Figure 1. Experimental schematic.

This work was supported by the National Science Foundation, Engineering Research Center program, and the Colorado Advanced Technology Institute.

Versatile Compact Image Processor with Optical Feed-Back using Photopolymer and Ferroelectric Liquid Crystal on Amorphous Silicon

Pierre Cambon*
GOSC, Télécom Bretagne, Département d'Optique
BP 832, 29285 Brest Cedex, France.
Fax 98 00 10 25, E-Mail: cambon@gosc.enst-bretagne.fr

John Sharpe and Kristina M. Johnson
Optoelectronic Computing Systems Center
University of Colorado, Boulder, Colorado, 80309-0525
Phone (303) 492 3260, Fax (303) 492 3674

1 Abstract

An optical image processor with optical feedback and gray scale capability compactly organized around bistable binary amorphous silicon and ferroelectric liquid crystal devices and a one lens correlator using reflective multiplexed photopolymer hologram is presented.

2 Summary

A broad class of efficient and widely used low level image processing operations are the non-linear filters such as rank-ordered filtering and morphological operations. They can be performed on binary images by convolving with a binary or gray scale kernel and thresholding the output. Extension to gray scale images is performed by considering them as a finite collection of binary slices, processing each slice as previously and finally summing the processed slices to obtain the processed gray scale image [1].

As they involve mainly a correlation, these processes may be advantageously implemented optically with thresholding binary optoelectronic devices. As even the simplest processes involve many sequential basic operations, a strictly parallel optical feedback is necessary. Pipelining of optical processors quickly becomes very expensive and using electronic feedback introduces an IO bottleneck which destroys the advantage of optics. The correlator must be multiplexed or quickly reconfigurable. The 2D optoelectronic devices must have memory capability to control the data flow in the optical loop, cascadable and able to perform a sharp thresholding at a programmable level. Additionally, the processor must be compact and inexpensive. Under such stringent constraints, very few realistic solutions have been found. Here we propose a system using recently available devices.

Optically addressed spatial light modulators (OASLM) using Ferroelectric Liquid Crystal (FLC) are considered here. Although FLC and silicon VLSI based smart pixel [2] arrays allow an interesting versatility at the pixel level, the processor considered here is based on equivalent resolution but higher optical quality and lower cost devices which use a hydrogenated amorphous silicon (aSi:H) continuous thin film as substrate.

The device is a mosaic of nine independently driven aSi:H/FLC bistable OASLMs with fixed high threshold [3] (250 $\mu W/mm^2$ at 633 nm and 2.5 kHz frame rate) realized on the same optical flats. It is illuminated on both sides through the polarizing beam splitters CBS and FBS (see figure). The aSi:H/FLC

*Pierre Cambon is with Opt. Comp. Sys. Center, Univ. of Colorado. phone (303) 492 5605 until May 31, 1994. phone: (303) 492 5605, E-mail: cambon@ilka.colorado.edu

interface is reflective (pixelated aluminium). The central OASLM faces in the opposite direction compared to the peripheral ones. The right side performs the feedback by using a lens (FL), a plane facet mirror (FM) and independently controlled feedback laser diodes (Fld). The left side performs correlation from the central OASLM to the peripheral one's by using a power source (PS) and variable light biasing (Tld) for threshold control and erasing. The filter is a multiplexed reflective hologram recorded in-situ using recent Du Pont photopolymer materials[4].

The gray level input image (In) is formed by input lens (IL) on the central OASLM. A biasing light (from Tld through the mirror FM) is incoherently added to the image to determine the threshold level and the result thresholded and stored as a binary image in the FLC. Using the power source (PS) this slice is convolved simultaneously with the eight kernels recorded in hologram (RMH) chosen for the application. One or a few of the convolved images are stored on a peripheral OASLM while the previously stored images on the other OASLMs are retained. The other slices of the images are successively formed and processed in the same way and stored in peripheral OASLMs. The final summing operation is performed by illuminating simultaneously with the feed-back diodes the OASLMs where the previously processed slices are stored. The input image is obstructed using the shutter SH. The gray level output image is directed onto the "Out" plane by activating a quarter wavelength FLC plate (QP) which rotates the polarization of the reflected beam. Binary image processing can be performed in the same way and operations are easily cascaded by using the feedback diodes.

Design, scaling, power budget and technology are presented. Performance simulations, partial experiments and controlling programs exemplified by a cytology diagnosis application requiring only four slices of 256 X 256 images are shown.

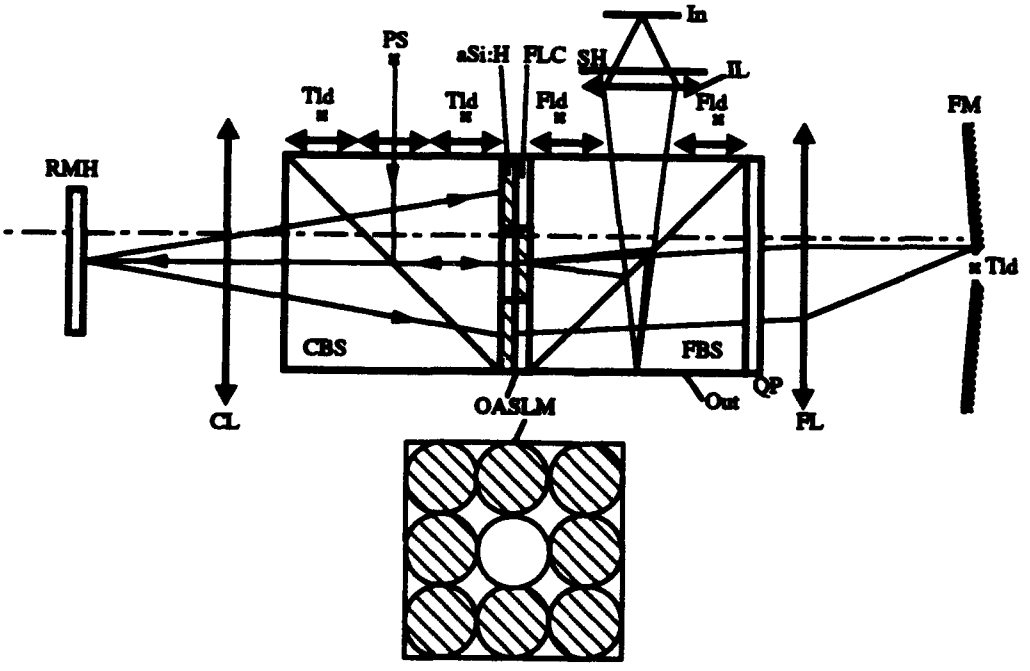
References

[1] J.W. Hereford, W.T. Rhodes *"Non linear optical image filtering by time-sequential threshold decomposition"* Optical Engineering, vol 27, No 4, (1988), pp 274

[2] K.M. Johnson, D.J. McKnight and I. Underwood *"Smart spatial light modulators using liquid crystal on silicon"* IEEE J. of Quantum electronics, vol 29, No 2, (1993), pp 699

[3] J.B. Chevrier, P. Cambon, R.C. Chittick, B. Equer *Use of nipin aSi:H structure for bistable OASLM"* J. of Non-Crystalline Solids, 137 and 138, (1991), pp 1325-1328.

[4] R.W. Brandstetter, N.J. Fonneland *"Photopolymer elements for an optical correlator system"* Proceedings SPIE on Photopolymer device physics, chemistry and applications II (1991) vol 1559, pp 308.



Digital Optical Computing Demonstration Systems

Frank Tooley, Simon Prince, Douglas Baillie, Dominic Goodwill, Marc Desmulliez and Mohammed Taghizadeh
Physics Dept., Heriot-Watt University, Edinburgh, UK.
031 451 3065, phyfapt@clust.hw.ac.uk

Abstract

Details of the implementation of two optical computer demonstrators will be presented: a 64-channel S-SEED cellular logic image processor with a dynamic interconnect and a sorting module implemented by interconnecting smart pixels with a shuffle.

Summary

Dynamic interconnect O-CLIP: This is a demonstration of a 8x8 channel, S-SEED optical cellular logic image processor using hybrid lenses and a dynamic interconnect. Two arrays of S-SEEDs are used and are interconnected to each other as shown schematically in the photograph (figure 1). The interconnect used is an electrically-addressed Seiko Epson phase modulator(not shown in photo). For optimum efficiency, it is essential that the CGH period is an integer multiple of the SLM pixel pitch (46 μm). The pixel pitch of the microlens/S-SEED was therefore chosen to be 160 μm and a 41.9 mm focal length lens was used. The interconnect can i) map one-to-one, ii) fan-out by 3 horizontally to straight on and two nearest neighbours(460 μm period), iii) fan-out to next nearest neighbours and straight(230 μm). With these reconfigurable interconnects it is possible to create a compact system with interesting processing capabilities.

One point of the demo is to show that a low-power high-field macrolens in combination with a high-power low-field microlens produces the high-power high-field hybrid lens which is required to interface with a large array of widely separated smart pixels with small windows. The microlens needs to have field of 30 μm to allow both dual-rail beams required to read and set the state of a S-SEED to pass through a single microlens. A singlet microlens is inadequate so an afocal relay consisting of f/3 and f/1 doublets has been fabricated. This is also required for the magnification step between the 15μm spot produced by the low power lens and the sub-5μm spot required for the S-SEED. The in-house macrolens used is a f/5 triplet with a 10 degree full-field (7.3mm). Full details will be presented of the characterization of system components and its operation.

Sorting Module: Another demonstration system currently under construction is a system which performs the bitonic sort algorithm using smart pixels interconnected by a 2-D perfect shuffle (figure 2). The perfect shuffle module is based on an approach adapted from Cloonan[1] which uses a 2x2 fan-out grating followed by a 2x telescope. The smart pixels required for this system consist of an array of pixels with the following functionality: a self-routing exchange/bypass node with a latch, optically programmable to sort the higher or lower of the two inputs to either output or allow a straight connection with no comparison, optical clock, and 4-bit shift registers at both outputs. A FET-SEED smart pixel has been designed to perform this function. A similar but less powerful F-SEED has been fabricated and results of tests on it will be presented. In addition, a CMOS version of this smart pixel has been designed and is currently being fabricated. A SPICE simulation has shown that it should operate at 100MHz. Results will be presented of a hybrid smart pixel array which will be fabricated by bonding an InGaAs modulator array to a CMOS circuit.

[1] T. J. Cloonan et al, "A complexity analysis of smart pixel switching nodes for photonic EGS switching networks," IEEE J. QE 29 619 (1993)

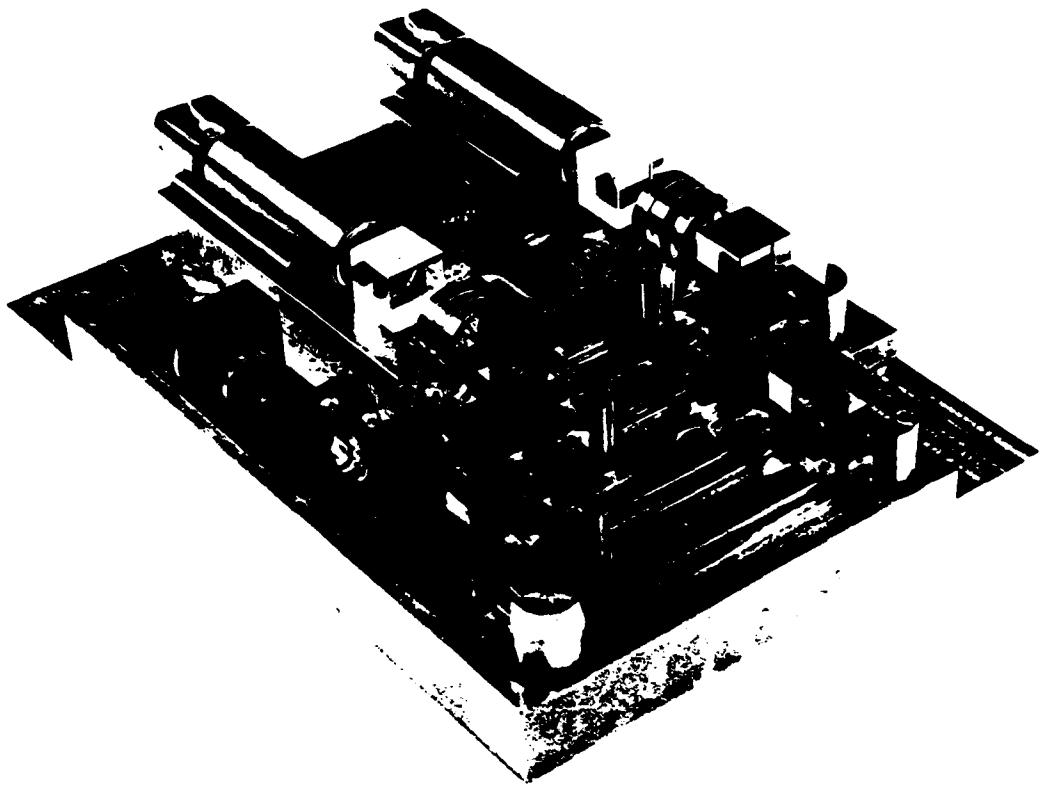


Figure 1: Dynamic interconnect O-CLIP

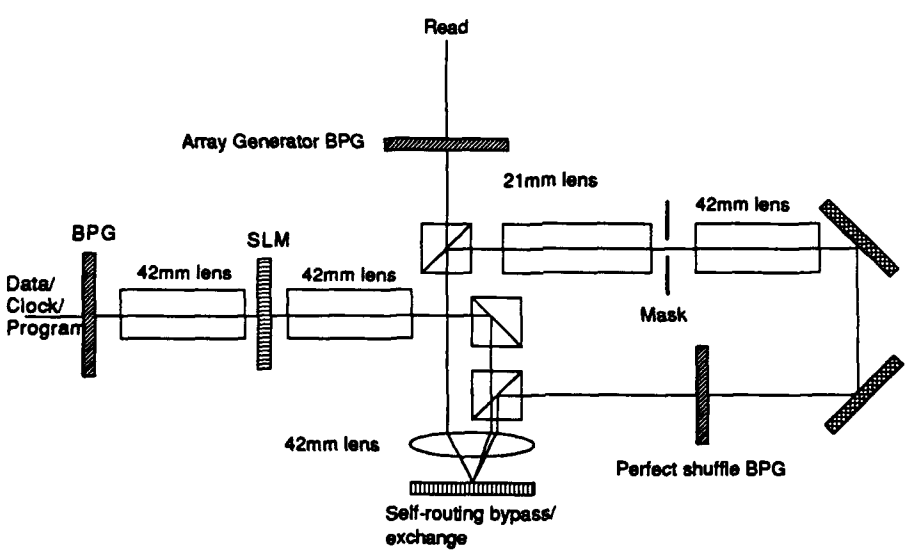


Figure 2: Sorting Module

NOTES

AUTHOR INDEX

Aherne T. WP49
Ahouzi E. MP20
Alam M.S. MP49
Alves C. WP27
Ambs P. WC4
Apanasevich S.P. MP24, MP44
Arai D. WD5
Ashcroft S. WP53
Asom M.T. ThA5
Athale R.A. WC3

Baillie D.A. ThA4, ThB4
Balkarey Y.I. MP41, MP42
Bar-Tana I. WP56
Barge M. WP39
Barrett C.P. ThA2
Barshan B. TuA2
Bashlakov A.U. MP54
Battiato J. WB2
Beckman M.G. WD6, WP13
Bedel E. WP66
Belyi V.N. WP71
Ben V.N. MP18
Berger D. WB2
Bernardo L.M. MP16
Bertolotti M. MP64
Beyette F.R. MP28, MP32, WP54
Bigué L. WC4
Birch M.J. ThA2
Birjukov V.A. MP54
Blair P. WP15
Blair S. TuC6
Bogdanovich A.I. WP32
Boisset G.C. ThA3, WP18, WP19
Bona G.L. WP23
Borghs G. TuC1, WB5, WP57
Bosch S. MP14
Bougrenet de la Tocnaye J.L. TuB6
Bouzinac J.P. WP2
Boyd G.D. WP47, WP52
Brenner K.-H. MP35, WD4, WP17
Brocklehurst J.R. ThA2
Bródka J.S. WP43
Brooks P. MP55
Brownjohn N.A. ThA2
Buller G.S. WP48
Burns D.C. MC6
Bussjager R. WB2
Buydens L. WP63

Cambon P. ThB3
Campos J. MP13, MP14, MP19, MP20
Cao M. WP5
Carcolé E. MP19
Carnicer A. MP3
Casasent D. TuA1
Caulfield H.J. MP26
Chang M.C. MP30
Chau K.K. WB4
Chavel P. MA3, MP22, MP36, WB1, WP22
Chen Y. MP7
Cheng C.K. WD1
Cherry S.R. WP36
Chevallier R. WP39
Chirovsky L.M.F. MB4, ThA5, WP47, WP52
Christensen M.P. WP10
Churoux P. WP2
Clérot F. WP50
Cloonan T.J. WP13
Cohen A.S. MP42
Cohen N. MP21
Collet J.H. WP66
Collings N. WP16
Comte D. WP2
Constad C.G. MA2
Corbett B. WP49
Crossland W.A. MP1, TuB2, ThA2
Coy M. WP53
Crowder J.G. WP53
Curatu E. WP39

D'Asaro L.A. MB4, ThA5
Daalen M. TuB2
Daniel O. MP6
Datta A.K. MP40
Demeester P. WP63
Derstine M.W. WB4
Desmulliez M.P.Y. MC1, MP38, ThB4, WP53
Deveaud-Plédran B. WP50
Devos F. WC1
Dines J.A.B. MC2
Dinev S. MP61
Dneprovskii V. WP64
Döhler G.H. TuC3
Dreischuh A. MP61
Duvillier J. TuB6
Dykman M.I. MP25

Ebeling K.J. MB2
Eckert W. MP35, WP17
Elinson M.I. MP41, MP42
Endo F. WP28
Esman A.K. MP59
Eugenieva E. MP61
Eulss G.W. WC3
Evtihiev N.N WP44
Evtikhov M.G. MP42

Fan J. WD1
Fancey S.J. WP48
Fedor A. MP30
Fedorov A.V. MP60
Fedorov S.V. MP60
Feld S.A. MP28, MP32, WP54
Fengguang L. WP25

AUTHOR INDEX

Fernandez J. WB5
Feuerstein R.J. MP30
Firsov V.V. WP69
Focht M.W. MB4, ThA5
Fontaine C. WP66
Foulks P.W. WP53
Fracès M. WC4, WP2
Freund J.M. MB4, ThA5
Fyodorov V.B. WB6, WP11

Gale M.T. WP23
Galstyan T. WP42
Gao W. WP5
Garzia F. MP64
Gelb K.M. MP32, WP54
Gérard J.M. WP50
Ghanta S. MP51
Gillies B.R. MP38
Glogovsky K.C. ThA5
Glogovsky K.G. MB4
Golubev G.P. MP25
Goncharenko A.M. WP71
Goncharenko I.A. MP59
Gonzalez-Marcos A. MP52, MP53
Goodwill D.J. MB3, ThA4, ThB4
Gouaichault N. WP66
Gourlay J. MC6, WP9
Grac R. WP66
Gravey P. WP50
Greger E. TuC3
Grigor'ev V.R. WP41
Grot A.C. MA2
Guilfoyle P.S. ThB2
Guizani M. MP50
Gulden K.H. TuC3
Guth G.D. MB4, ThA5

Hackbarth T. MB2
Halim S.A. MP63
Hall T.J. TuB2, WP30, WP36
Hallowell P. WP36
Hamanaka K. WD5
Haney M.W. WP10
Hatch J.A. MP31
Hayasaki Y. WP33
He X. MP39
Heer J.P. MP34
Heddle S. WP9
Hegarty J. WP49, WP63
Hegarty K. TuB6
Heremans P. MP36, TuC1, WB5, ThB2
Hessenbruch J.M. ThB2
Hifdi N. WP2
Hinterlong S.J. WD6, WP13
Hinton H.S. WD2, ThA3, WP18, WP19
Hirabayashi K. MC4
Hirai Y. WP28
Höfler A. TuC3
Holland M.C. MB3
Hongpu L. WP25
Horan P. TuB4, WP49
Houghton A.W. MP4, MP5
Houssay B. WP34
Hui S. MB4
Huignard J.-P. WC5

Ichioka Y. MP57, WB3
Iehl J.L. WP66
Inoue TuC5
Ikeda M. WP28
Iraklidis L.J. MP27, MP32
Ishida T. MP29
Ishikawa M. MP29, ThB1
Itoh H. WP34
Itoh K. MP57
Itoh M. MP9
Ivakin E.V. MP18
Iwaki T. WP51

Jaaskelainen T. WP7
Jäger D. TuC2
Jang J.-S. MP15
Javidi B. WC5
Jeong J.-S. WP29
Jeong S.I. MP15
Ji L.H. MP30
Johnson K.M. MC5, ThB3, WP46, WP56
Johnson W.H. MP42
Jonathan J.-M.C. MP6
Jukov E.A. MP25
Jun A. WP25
Jun X. WP5, WP25
Jung S.-D. WP21
Juvells I. MP3, MP13, MP19

Kakuda N. MC3
Kamshilin A.A. WP7
Kanetake T. TuC5
Kanterakis E. WP3
Kar S. WP31
Karasik Y.B. MP11, MP12
Karavanskii V. WP64
Karpushko F.V. MA4, MP24, MP43, WP67
Kasama N. WP51
Kato N. WP51
Katz A. WP3
Kaufman I.K. MP25
Kehrli U. MC1
Kerbis E. WP13
Khatkevitch A.G. WP71
Khilo N.A. MP62, WP71
Khodova G.V. MP60
Kiesel P. TuC3
Kim N.H. WP19, ThA3
Kirk A. MP29, WB5
Kishimoto T. WD5
Klimov V. WP64
Kneissl M. TuC3
Knigge S. TuC2
Knüpfer B. TuC3

AUTHOR INDEX

Kobyakov A.E. WP61
Kocon S. WP2
Kohda S. MC3
Kondo M. WP33
Kondoh M. WP38
Koppa P. WB1
Korneev N.N. WP71
Korolkov A.V. MP8
Kosheleva O. WP70
Koster A. WP59
Kotzer T. MP21
Kravtsov N.V. WP69
Krile T.F. WC2
Kufner M. WP22
Kufner S. WP22
Kuijk M. MP36, TuC1, WB5, WP57
Kunz R.E. WP23
Kusuda Y. WD5
Kuszelewicz R. WB1
Kwak C.H. WP29

Lafi A.O. MP51
Lalanne P. MP36, WP22
Laude V. MP22, WC5
Lebreton G. TuB1
Lee E.-H. WP29
Lee H.-J. WP37
Lee S.-Y. TuB5, WP37
Lee S.H. WD1
Legratiet L. WP66
Leibenguth R.E. MB4, ThA5
Leier H. MB2
Leipold D. MC1
Lentine A.L. MB4, WP13, WP47, WP52, ThA5
Li C. MP7, WP60
Li D. MP7
Li G. MP46, MP48
Li H. WP5
Li Y. WA2, WP1, WP3
Liu L. MP46, MP47, MP48
Liu W. MP39
Liu Y.S. WP19, ThA3
Livescu G. MB4, WP47, WP52
Lohmann A.W. WA2
Louri A. MP31, WD3
Luchinsky D.G. MP25
Luepken H. WP15
Luo F. WP5
Lyakhnovich A.V. MP24, MP44

Mao C.C. WP46
MacGregor A.E. WP24
Macukow B. WP43
Maeda Y. WP62
Malevich V.L. WP67
Manykin E.A. MP45
Marinho F.J. MP16
Martín-P[illegible]ez E. MP3
Martin-Pereda J.A. MP53
Maruani A. WP39
Massa J.S. WP48
Matoba O. MP57
Matsuoka K. MP1, MP2
Matsushima Y. WP58
Matsuura K. WP51
Mazurenko Y.T. MP23
McArdle N. WP4
McCabe E. WP49
McClintock P.V.E. MP25
McCormick F.B. WA3, WP13
McElhinney M. MB3
McKnight D.J. MC5
McKnight D.J. WP8
McLeod R. TuC6
Mears R.J. MB1, MP10
Mendlovic D. TuA2
Mikaelian A.L. TuA4
Miller D.A.B. MA1
Mingeui C. WP25
Mitkas P.A. MP27, MP28, MP32
Mitsuhashi Y. WD5
Mitsuoka Y. WP51
Mizusawa J. WP68
Moisel J. WD4
Mokuno Y. MP1
Möller B. MB2
Moloney M.H. WP63
Moneo J.T. MP13
Montes-Usategui M. MP13, MP14
Mori M. WP33
Morozov V.N. MP37
Morrison R.L. WP13, WP14
Mosyakin Y.S. MP8
Mukai S. TuC4, WP34
Murdocca M. WB2
Mylnikov V. WP70

Nakama K. WD5
Nanii O.E. WP69
Nanto H. WP28
Nasu S. WP28
Naumov S.P. WP41
Nelson S. WA1
Nishimura TuC5
Nikol'skii M. WP69
Novotny R.A. MB4, WD6, WP13, WP53, ThA5

O'Brien D.C. MP30, WP8
O'Hara A. MC6
O'Sullivan G. WP49
Okamura M. MC3
Okorokov D. WP64
Onyky B.N. WP44
Otazo M.R. WP19, ThA3
Oudar J.L. WB1
Ozaktas H.M. TuA2

Pan Z.G. WP1

AUTHOR INDEX

Passon C. MP35, WP17
Patterson B.D. MC1
Paulat G. WP27, WP42
Pavlasek D. WP19
Pavlov A.V. WP40
Peiffer W. WB5, WP59
Pelekanos N.T. WP50
Pellat-Finet P. MP34
Peng H. MP47
Perepelitsa V.V. WP44
Perov P.I. MP42
Petrov M.P. TuA3
Pichon P. WP22
Piestun R. WP26
Pignon D. WP36
Pilipovich V.A. MP59
Plant D.V. WP19, ThA3
Pochelle J.P. WB1
Polikanin A.M. WP32
Polyakov V.I. WP32
Posedko V.S. MP59
Pottier F. MB3
Prémont G. MP36
Prewett P. WP36
Prince S.M. WP20, ThB4
Proklov V.V. MP54
Pronkin G.I. MP8
Proudley G.M. ThA2
Przybylek G. MB4
Psaltis D. MA2
Pugnet M. WP66

Ranson W. WP59
Rao S.B. WA2
Redmond I. WA2, WP6, ThA1
Reeve C.D. MP4,MP5, MP55
Refregier P. MP22, WC5
Reingruber K. TuC3
Riel P. TuC3
Roberts N.C. WP36
Robertson B. WP18, WP19, ThA2, ThA3
Robertson W.M. ThA3
Roosen G. MP6, WP27, WP42
Rosanov N.N. MP60
Rosi M. WP23
Rousselot J.Y. WP2
Rubanov A.D. MP18
Russ K.B. WP36
Ryvkin B.S. MB3

Sakata H. WP58
Sallent J. MP14
Samus S. WP9
Sasian J.M. WD6, WP13
Schenfeld E. WP6, ThA1
Scherbakov I.B. WP44
Schnell J.P. WB1
Schweizer H.P. MC1
Seitz P. MC1
Sekura R WP51
Serati R.A. MC5
Serikawa T. MC3
Seth M. MP40
Shahgedanov V.N. WP45
Shamir J. MP21, WC6, WP27
Shandarov V.M. MP58
Shang A.Z. ThA3
Shao L. MP46
Sharony J. WP1
Sharp G.D. MC5
Sharpe J. WP56,ThB3
Shawe-Taylor J.S. TuB2
Shcherbakov I.A. WP69
Shenoy K.V. MA2
Shin S.-Y. WP37
Shirai S. MC3
Sibilia C. MP64
Silvera E. WC6
Sinitsyn G.V. MP24, MP43, MP44
Slinger C.W. TuB3, WP24
Smirnov V.A. MP60
Smith J.S. TuC3
Snook M. ThA2
Snowdon J.F. MC2, MP38, WP4, WP35
Snyder R.D. MP32, WP54
Soares O.D.D. MP16
Solonovich I.F. MP59
Song S.-H. WP21
Stace C. ThA2
Stanley C.R. MB3
Starikov R.S. WP44
Stein N.D. MP25
Stevens W. WB5
Stocks N.G. MP25
Stone R.V. ThB2
Stone T. WB2
Suh H.H. WP29
Sun D. MP39
Sun L. ThA3
Sung H. WD3
Szymanski T. WD2

Tabata T. MP29
Taghizadeh M.R. WP4, WP15, WP20,ThA2, ThB4
Tai J.-W. MP17
Takeuchi N. WP28
Tanaka S. TuC5
Tandt C. WP59
Tanida J. WB3
Taniguchi M. MP1, MP2
Thelen K. MC1
Thienpont H. WB5, WP55, WP59
Tian R. MP9
Timucin D.A. WC2
Tohyama I. WP33, WP38
Tolstikhin V.I. WP65
Tooley F.A.P. WP13, WP20, WP53, ThA4, ThB4

AUTHOR INDEX

Torchigin V.P. WP61

Uekusa S. WP34
Underwood I. MC6
Urey H. TuA2
Utaka K. WP58
Utkin I.A. WP67

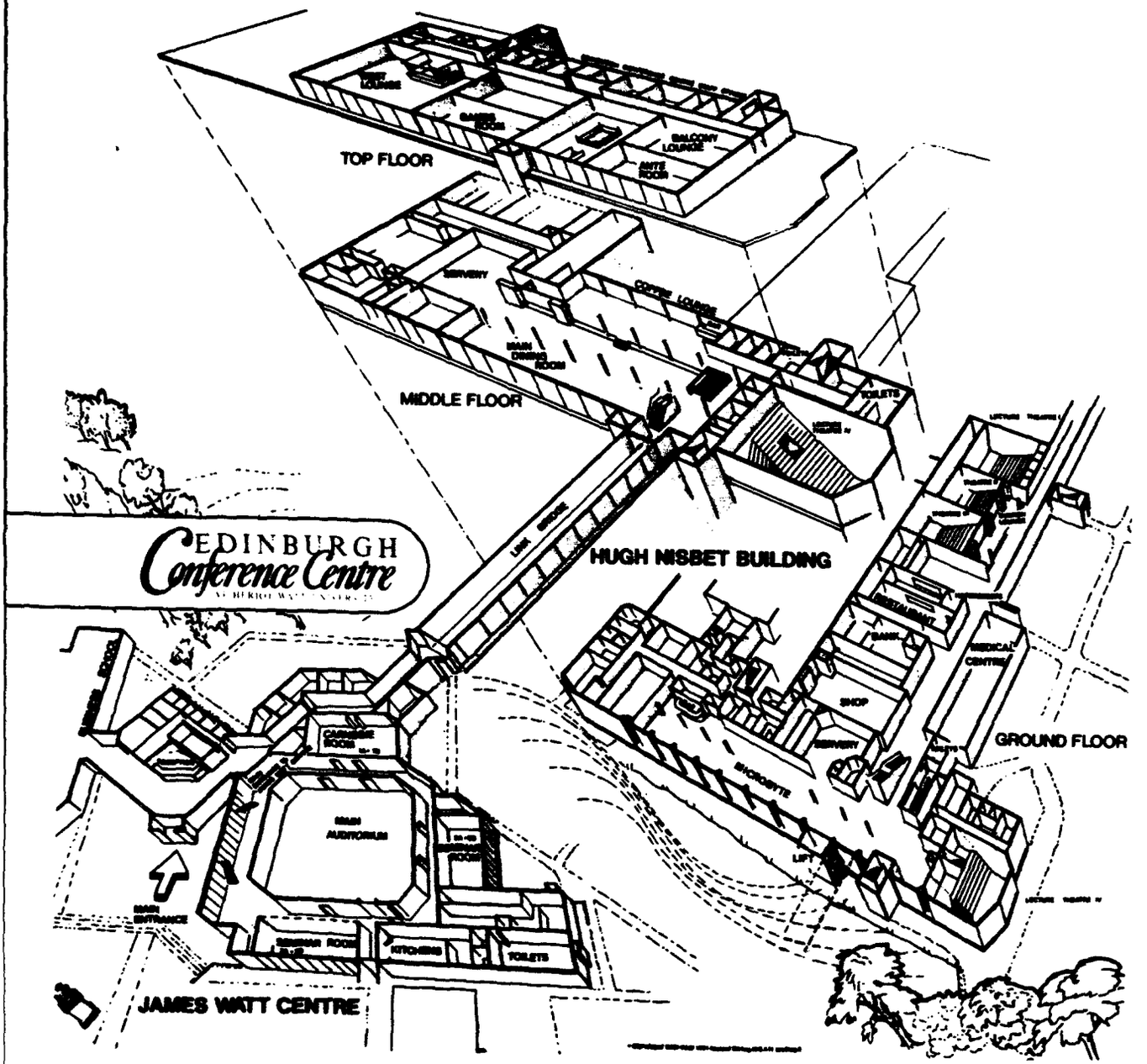
Valimitjana S. MP3
Van de Velde T. WB5, WP55
Vandyshev J.V. WP64
Vass D.G. MC6, ThA2, WP9
Veretennicoff I. WB5, WP59
Villing A. WP42
Vogele B. MB3
Voitenko I.G. MP56, WP12
Vounckx R. TuC1, WB5, WP57, WP59
Vyssotina N.V. MP60

Waddie A.J. WP35
Wagner K. MP33, TuC6
Wahiddin M.R. MP63
Wakelin S. WB4
Walker A.C. MB3 , ThA2, WP48
Walker S.L. WD6
Walkup J.F. WC2
Wang T. WA2
Wang C. WC1
Wang D.-X. MP17
Wang J. WP30
Wang J.-M. WP3
Wang R. WP60
Wang T. WP1
Wang X.-M. WP30
Wang Y. MP39
Wang Z. MP48
Warr S.T. MB1
Watanabe M. TuC4
Wherrett B.S. MC2, MP38
White H.J. ThA2
Wicke M. TuC2
Wilkinson T.D. MP10
Willander M. WP65
Wilmsen C.W. MP28, MP32, WP54
Wojcik M.J. WD6, WP13, WP14,ThA5
Woodward T.K. WP52
Wu R. WP5
Wu X.X. TuC3
Wyrowski F. WP15

Xu L.Q. WP36

Yajima H. TuC4
Yamada T. WP34
Yamaguchi M. MC4
Yamamoto T. MC4
Yamauchi N. MC3
Yarmolitskij V.F. WP32
Yatagai T. MP9, MP56, WP12, WP33, WP38
Yin Y. MP47
Young R.I. WP24
Yzuel M.J. MP20

Zaiguang L. WP25
Zakharov S.M. MP45
Zeeb E. MB2
Zhang L. WP60
Zhang Y. MP7
Zhang Y. MP39, ThA6
Zhang Y. WP3
Zhao X. WP5
Zharikov E.V. WP69
Zheng S. MP7
Zhou G. MP39


TOP FLOOR
BALCONY LOUNGE
MIDDLE FLOOR
MAIN DINING ROOM
TOILETS
EDINBURGH
Conference Centre
HUGH NISBET BUILDING
GROUND FLOOR
SHOP
MAIN AUDITORIUM
MAIN ENTRANCE
KITCHENS
TOILETS
JAMES WATT CENTRE